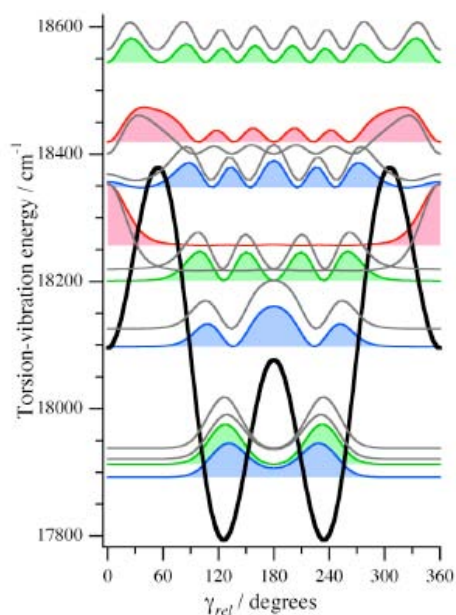
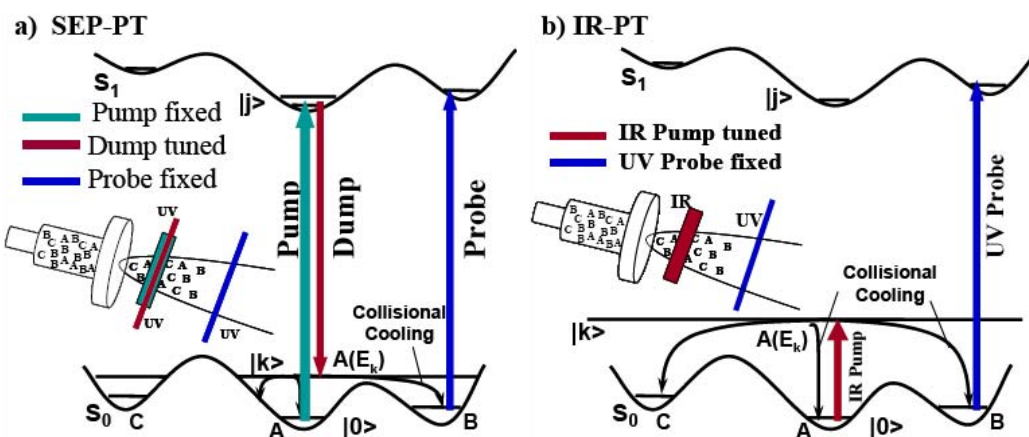
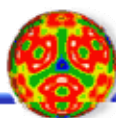


29th Annual Combustion Research Conference



Airlie Conference Center
Warrenton, Virginia
May 27 – May 30, 2008



Office of Basic Energy Sciences

Chemical Sciences, Geosciences & Biosciences Division

29th Annual Combustion Research Conference

DOE Contractors' Meeting Program and Abstracts

Airlie Conference Center
Warrenton, Virginia
May 27 – May 30, 2008

Chemical Sciences, Geosciences, and Biosciences Division
Office of Basic Energy Sciences
Office of Science
U.S. Department of Energy

Cover Graphics:

Top: Schematic diagrams for investigating the dynamics of conformational isomerization via: (a) stimulated emission pumping-population transfer (SEP-PT) spectroscopy and (b) infrared population transfer (IR-PT) spectroscopy. Taken from "Experimental Characterization of the Potential Energy Surfaces for Conformational and Structural Isomerization in Aromatic Fuels," Timothy S. Zwier, pg. 307 of this book.

Bottom: A diabatic effective torsional potential of the local $\nu_{\text{CH}} = 5$ stretch of methanol is shown as the heavy black curve. The fully coupled torsional probability distributions (color) are compared with the approximate diabatic probability distributions (grey). Taken from "The dynamics of large-amplitude motion in energized molecules," David S. Perry, pg. 223 of this book. This was adapted from J. Phys. Chem. A 2008, 112, 215-223.

This document was produced under contract number DE-AC05-06OR23100 between the U.S. Department of Energy and Oak Ridge Associated Universities.

The research grants and contracts described in this document are supported by the U.S. DOE Office of Science, Office of Basic Energy Sciences, Chemical Sciences, Geosciences and Biosciences Division.

Foreword

This abstract booklet provides a record of the twenty-ninth U.S. Department of Energy contractors' meeting focused on gas-phase chemical physics. The reports appearing in this volume present work in progress in basic research contributing to the development of a predictive capability for combustion processes. The work reported herein is supported by the Department of Energy's Office of Basic Energy Sciences (BES) and, in large measure, by the chemical physics program. The long-term objective of this effort is the provision of theories, data, and procedures to enable the development of reliable computational models of combustion processes, systems, and devices.

The objective of this meeting is to provide a fruitful environment in which researchers with common interests will present and exchange information about their activities, will build collaborations among research groups with mutually reinforcing strengths, will identify needs of the research community, and will uncover opportunities for future research directions. The agenda consists of an invited keynote talk and oral presentations by program PIs. Approximately one third of the PIs in the program speak each year in rotation. With ample time for discussion and interactions, we emphasize that this is an informal meeting for exchange of information and building of collaborations; it is not a review of researchers' achievements or a forum to define the future direction of the program.

During the past year, and a number of preceding years, this program benefited greatly from the leadership and insights of Dr. Frank Tully and Dr. Richard Hilderbrandt. We are grateful for their service to this community. We appreciate the privilege of serving in the management of this research program. In carrying out these tasks, we learn from the achievements and share the excitement of the research of the many sponsored scientists and students whose work is summarized in the abstracts published on the following pages.

We thank all of the researchers whose dedication and innovation have advanced DOE BES research and made this meeting possible and productive. We hope that this conference will help you will build on your successes and we look forward to our assembly next year for our 30th annual meeting.

We thank Diane Marceau of the Chemical Sciences, Geosciences and Biosciences Division, and Margaret Lyday and Camella Mitchell of the Oak Ridge Institute for Science and Education for their important contributions to the technical and logistical features of this meeting.

Michael Casassa
Larry A. Rahn
Wade Sisk

29th Annual Combustion Research Conference
U.S. Department of Energy
Office of Basic Energy Sciences

Agenda

Tuesday, May 27, 2008

3:00 pm *Registration*
5:00 pm *No-host Reception at The Whistling Swan Pub*
7:00 pm *Dinner*

Wednesday, May 28, 2008

7:00 am *Breakfast*
Session I
David Chandler, Chair

8:00 am Welcome and Introduction, Michael Casassa

8:15 am **Keynote Speaker** *“All About Molecular Hydrogen,”*
Richard N. Zare, Stanford University1

9:15 am *“The Dynamics of Large-amplitude Motion in Energized Molecules,”*
David S. Perry.....223

9:45 am *“Chemical Dynamics in the Gas Phase: Quantum Mechanics of Chemical Reactions,”* Stephen K. Gray.....75

10:15 am *Break*

Session II
Tomas Baer, Chair

10:45 am *“Hydrocarbon Radical Thermochemistry: Gas-Phase Ion Chemistry Techniques,”* Kent M. Ervin.....55

11:15 am *“Determination of Accurate Energetic Database for Combustion Chemistry by High-Resolution Photoionization and Photoelectron Methods,”* C.Y. Ng.....211

11:45 am *“Theoretical Studies of the Reaction and Spectroscopy of Radical Species Relevant to Combustion Reactions and Diagnostics,”* David R. Yarkony303

12:15 pm *Lunch*

5:00 pm *Dinner*

Wednesday, May 28, 2008

Session III

Terry Cool, Chair

6:00 pm	<i>“Theory and Modeling of Small Scale Processes in Turbulent Flow,”</i> Alan R. Kerstein.....	127
6:30 pm	<i>“Investigation of Non-premixed Turbulent Combustion,”</i> Stephen B. Pope.....	231
7:00 pm	<i>“Large Eddy Simulation of Turbulence-Chemistry Interactions in Reacting Multiphase Flows,”</i> Joseph C. Oefelein.....	215

7:30 pm *Break*

Session IV

Don Trular, Chair

8:00 pm	<i>“Intermolecular Interactions of Hydroxyl Radicals on Reactive Potential Energy Surfaces,”</i> Marsha I. Lester.....	151
8:30 pm	<i>“Wave Packet Based Quantum Statistical Model for Complex-forming Reactions,”</i> Hua Guo.....	83

Thursday, May 29, 2008

7:00 am *Breakfast*

Session V

Michael Frenklach, Chair

8:00 am	<i>“Computational and Experimental Study of Laminar Flames,”</i> Marshall B. Long.....	263
8:30 am	<i>“Chemical Kinetic Modeling of Combustion Chemistry,”</i> William Pitz.....	227
9:00 am	<i>“Multiple-time-scale Kinetics and Combustion Modeling,”</i> Michael Davis.....	47

9:30 am *Break*

Thursday, May 29, 2008

Session VI

Joel Bowman, Chair

10:00 am	<i>“Kinetics and Dynamics of Combustion Chemistry,”</i> David L. Osborn219
10:30 am	<i>“Theoretical Modeling of Spin-forbidden Channels in Combustion Reactions,”</i> Anna I. Krylov139
11:00 am	<i>“Theoretical Chemical Dynamics Studies of Elementary Combustion Reactions,”</i> Donald L. Thompson279
11:30 am	<i>“Experimental Characterization of the Potential Energy Surfaces for Conformational and Structural Isomerization in Aromatic Fuels,”</i> Timothy S. Zwier.....307
12:00 pm	<i>Lunch</i>

Session VII

Amy Mullin, Chair

5:00 pm	<i>“Time-resolved Infrared Absorption Studies in Radical Reactions,”</i> R. Glen Macdonald.....163
5:30 pm	<i>“Photodissociation of the propargyl and propynyl radicals,”</i> Daniel M. Neumark.....207
6:00 am	<i>Break</i>

Session VIII

Greg Hall, Chair

6:30 pm	<i>“Advanced Nonlinear Optical Methods for Quantitative Measurements in Flames,”</i> Robert Lucht159
7:00 pm	<i>“Picosecond Nonlinear Optical Diagnostics,”</i> Thomas B. Settersten255
7:30 pm	<i>Cash Bar</i>
8:00 pm	<i>Dinner</i>

Friday, May 30, 2008

7:00 am	<i>Breakfast</i>	
	Session IX	
	<i>Jim Muckerman, Chair</i>	
8:15 am	<i>“Theoretical Studies of Potential Energy Surfaces and Computational Methods,” Ron Shepard</i>	259
8:45 am	<i>“Dynamics of Product Branching in Elementary Combustion Reactions,” Laurie J. Butler</i>	19
9:15 am	<i>“Chemical Accuracy from ab initio Molecular Orbital Calculations,” Martin Head-Gordon</i>	103
9:45 am	<i>Break</i>	
10:00 am	<i>“Theoretical Studies of Elementary Hydrocarbon Species and Their Reactions,” Wesley Allen</i>	251
10:30 am	<i>Closing Remarks</i>	
11:00 am	<i>Lunch</i>	

Table of Contents

Table of Contents

Foreword	iii
Agenda	v
Table of Contents	ix
Abstracts	1
Richard N. Zare - All About Molecular Hydrogen.....	1
Tomas Baer - Threshold Photoelectron Photoion Coincidence (TPEPICO) Studies: The Road to 0.1 kJ/mol Thermochemistry	3
Robert S. Barlow - Turbulence-Chemistry Interactions in Reacting Flows.....	7
Joel M. Bowman - Theoretical Studies of Combustion Dynamics.....	11
Nancy J. Brown - Combustion Chemistry.....	15
Laurie J. Butler - Dynamics of Product Branching in Elementary Combustion Reactions.....	19
David W. Chandler - Production and Study of Ultra-cold Molecules Produced by Kinematic Cooling.....	23
Jacqueline H. Chen - Terascale Direct Numerical Simulation and Modeling of Turbulent Combustion.....	27
Robert E. Continetti - Dynamics and Energetics of Elementary Combustion Reactions and Transient Species.....	31
Terrill A. Cool - Studies of Flame Chemistry with Photoionization Mass Spectrometry.....	35
F.F. Crim - Dissociation Pathways and Vibrational Dynamics in Excited Molecules and Complexes.....	39
H. Floyd Davis - Bimolecular Dynamics of Combustion Reactions.....	43
Michael J. Davis - Multiple-time-scale kinetics and combustion modeling.....	47
Frederick L. Dryer - Comprehensive Mechanisms for Combustion Chemistry: Experiment, Modeling, and Sensitivity Analysis.....	51
Kent M. Ervin - Hydrocarbon Radical Thermochemistry: Gas-Phase Ion Chemistry Techniques.....	55
Robert W. Field - Spectroscopic and Dynamical Studies of Highly Energized Small Polyatomic Molecules.....	59
George Flynn - Scanning Tunneling Microscopy Studies of Chemical Reactions on Surfaces.....	63
Jonathan H. Frank - Quantitative Imaging Diagnostics for Reacting Flows.....	67
Michael Frenklach - Mechanism and Detailed modeling of Soot Formation.....	71
Stephen K. Gray - Chemical Dynamics in the Gas Phase: Quantum Mechanics of Chemical Reactions.....	75
William H. Green - Computer-Aided Construction of Chemical Kinetic Models.....	79
Hua Guo - Wave packet based quantum statistical model for complex-forming reactions.....	83

Gregory E. Hall and Trevor J. Sears - Gas-Phase Molecular Dynamics: Experimental Studies of the Spectroscopy and Dynamics of Transient Species	87
Nils Hansen - Flame Chemistry and Diagnostics.....	91
Ronald K. Hanson and Craig T. Bowman - Spectroscopy and Kinetics of Combustion Gases at High Temperatures.....	95
Lawrence B. Harding - Theoretical Studies of Potential Energy Surfaces.....	99
Martin Head-Gordon - Chemical Accuracy from Ab-Initio Molecular Orbital Calculations ..	103
John F. Hershberger - Laser Studies of Combustion Chemistry.....	107
Ahren W. Jasper - Non-Born–Oppenheimer Molecular Dynamics and Theoretical Chemical Kinetics	111
Philip M. Johnson - Ionization Probes of Molecular Structure and Chemistry.....	115
Ralf I. Kaiser - Probing the Reaction Dynamics of Hydrogen-Deficient Hydrocarbon Molecules and Radical Intermediates via Crossed Molecular Beams.....	119
Michael E. Kellman - Dynamical Analysis of Highly Excited Molecular Spectra.....	123
Alan R. Kerstein - Theory and Modeling of Small Scale Processes in Turbulent Flow	127
J. H. Kiefer - Kinetics of Combustion-Related Processes at High Temperatures	131
Stephen J. Klippenstein - Theoretical Chemical Kinetics.....	135
Anna I. Krylov - Theoretical modeling of spin-forbidden channels in combustion reactions..	139
Stephen R. Leone - Synchrotron Studies of Photofragmentation, Radical Reactions, and Aerosol Chemistry Related to Combustion	143
William A. Lester, Jr. - Theoretical Studies of Molecular Systems.....	147
Marsha I. Lester - Intermolecular Interactions of Hydroxyl Radicals on Reactive Potential Energy Surfaces.....	151
M. C. Lin and M. C. Heaven - Kinetics of Elementary Processes Relevant to Incipient Soot Formation.....	155
Robert P. Lucht - Advanced Nonlinear Optical Methods for Quantitative Measurements in Flames.....	159
R. G. Macdonald - Time-Resolved Infrared Absorption Studies of Radical Reactions.....	163
Alexander M. Mebel - Theoretical studies of chemical reactions related to the formation and growth of polycyclic aromatic hydrocarbons and molecular properties of their key intermediates.....	167
Joe V. Michael - Flash Photolysis-Shock Tube Studies	171
H. A. Michelsen - Multiphase Combustion Diagnostics Development.....	175
James A. Miller - Chemical Kinetics and Combustion Modeling.....	179
Terry A. Miller - Detection and Characterization of Free Radicals Relevant to Combustion Processes.....	183
T.J. Mountziaris, P. R. Westmoreland - Probing Flame Chemistry with MBMS, Theory, and Modeling.....	187
James T. Muckerman and Hua-Gen Yu - Gas-Phase Molecular Dynamics: Theoretical Studies in Spectroscopy and Chemical Dynamics.....	191
Amy S. Mullin - Dynamics of Activated Molecules.....	195

Habib N. Najm - Reacting Flow Modeling with Detailed Chemical Kinetics.....	199
David J. Nesbitt - Spectroscopy, Kinetics and Dynamics of Combustion Radicals.....	203
Daniel M. Neumark - Radical Photochemistry and Photophysics.....	207
C. Y. Ng - Determination of Accurate Energetic Database for Combustion Chemistry by High-Resolution Photoionization and Photoelectron Methods.....	211
Joseph C. Oefelein - Large Eddy Simulation of Turbulence-Chemistry Interactions in Reacting Multiphase Flows.....	215
David L. Osborn - Kinetics and Dynamics of combustion Chemistry.....	219
David S. Perry - The dynamics of large-amplitude motion in energized molecules.....	223
William J. Pitz and Charles K. Westbrook - Chemical Kinetic Modeling of Combustion Chemistry.....	227
Stephen B. Pope - Investigation of Non-Premixed Turbulent Combustion.....	231
S.T. Pratt - Optical Probes of Atomic and Molecular Decay Processes.....	235
Hanna Reisler - Photoinitiated Reactions of Radicals and Diradicals in Molecular Beams.....	239
Klaus Ruedenberg - Accurate Calculations and Analyses of Electronic Structure, Molecular Bonding and Potential Energy Surfaces.....	243
Branko Ruscic - Active Thermochemical Tables – Progress Report.....	247
Henry F. Schaefer III and Wesley D. Allen - Theoretical Studies of Elementary Hydrocarbon Species and Their Reactions.....	251
Thomas B. Settersten - Picosecond Nonlinear Optical Diagnostics.....	255
Ron Shepard - Theoretical Studies of Potential Energy Surfaces and Computational Methods.....	259
M. D. Smooke and M. B. Long - Computational and Experimental Study of Laminar Flames.....	263
John F. Stanton - Quantum Chemistry of Radicals and Reactive Intermediates.....	267
Arthur G. Suits - Universal and State-Resolved Imaging Studies of Chemical Dynamics.....	271
Craig A. Taatjes - Elementary Reaction Kinetics of Combustion Species.....	275
Donald L. Thompson - Theoretical Chemical Dynamics Studies of Elementary Combustion Reactions.....	279
Robert S. Tranter - Elementary Reactions of PAH Formation.....	283
Donald G. Truhlar - Variational Transition State Theory.....	287
Wing Tsang - Chemical Kinetic Data Base for Combustion Modeling.....	291
Peter M. Weber - Dynamics on Multiple and Single Electronic Surfaces: Isomerization and Conformerization.....	295
Curt Wittig - Photoinitiated Processes in Small Hydrides.....	299
David R. Yarkony - Theoretical Studies of the Reactions and Spectroscopy of Radical Species Relevant to Combustion Reactions and Diagnostics.....	303
Timothy S. Zwier - Experimental Characterization of the Potential Energy Surfaces for Conformational and Structural Isomerization in Aromatic Fuels.....	307
Participant List.....	311

Abstracts

All About Molecular Hydrogen

Richard N. Zare

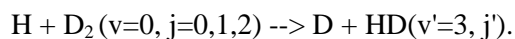
Chair, Department of Chemistry, Stanford University

Stanford, CA 94305-5080

zare@stanford.edu

I hope in this talk to share with you some recent work on studying the H + D₂ collision system and dreams of what might be done next.

I will report on the comparison of fully quantum calculations and experiment for the reactive scattering process:



I will also present a new mechanism for energy transfer which will be illustrated by the inelastic scattering process:



Finally, I will also show how to prepare aligned or oriented molecular hydrogen using stimulated Raman pumping for future scattering studies.

Annual Progress report April 2008
**Threshold Photoelectron Photoion Coincidence (TPEPICO) Studies:
The Road to ± 0.1 kJ/mol Thermochemistry**

Tomas Baer (baer@unc.edu)
Department of Chemistry
University of North Carolina
Chapel Hill, NC 27599-3290
DOE Grant DE-FG02-97ER14776

Program Scope

The threshold photoelectron photoion coincidence (TPEPICO) technique is utilized to investigate the dissociation dynamics and thermochemistry of energy selected medium to large organic molecular ions. The reactions include parallel and consecutive steps that are modeled with the statistical theory in order to extract dissociation onsets for multiple dissociation paths. These studies are carried out with the aid of molecular orbital calculations of both ions and the transition states connecting the ion structure to their products. The results of these investigations yield accurate heats of formation of ions, free radicals, and stable molecules. In addition, they provide information about the potential energy surface that governs the dissociation process. Isomerization reactions prior to dissociation are readily inferred from the TPEPICO data.

The TPEPICO Experiment

The threshold photoelectron photoion coincidence (TPEPICO) experiment in Chapel Hill is carried out with a laboratory H₂ discharge light source. Threshold electrons are collected by velocity focusing them into a 1.5 mm hole on a mask located at the end of the 12 cm drift tube. Some hot electrons pass through a 2x5 mm opening located next to the central 1.5 mm hole. In this fashion, two TPEPICO spectra are simultaneously collected, one for threshold and one for hot electrons. Hot electron free data are obtained by subtracting a fraction of the hot from the threshold TPEPICO data. The ion TOF is either a linear version or a reflectron for studying H loss processes. The electrons provide the start signal for measuring the ion time of flight distribution. When ions dissociate in the microsecond time scale, their TOF distributions are asymmetric. The dissociation rate constant can be extracted by modeling the asymmetric TOF distribution. A high-resolution version of this experiment with a molecular beam source and an electron imaging detector at the Swiss Light Source (SLS) has been constructed and is beginning to collect data as of the end of April, 2008. Because of the high photon flux, we have implemented the first multi-start multi-stop coincidence scheme using a master clock as the time base. When combined with coincidence ion detection, the results will permit the measurement of ion dissociation limits to within 1 meV or 0.1 kJ/mol.

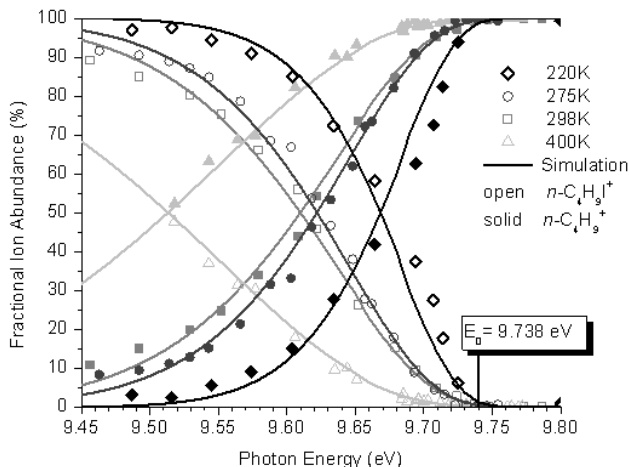
Recent Results

Dissociation dynamics of sequential ionic reactions: Heats of formation of tri-, di- and monoethyl phosphine: The sequential ethylene (C₂H₄) loss channels of energy-selected ethyl phosphine ions have been studied using threshold photoelectron photoion coincidence (TPEPICO) spectroscopy in which ion time-of-flight (TOF) distributions are recorded as a function of the photon energy. The ion TOF distributions and breakdown diagrams have been modeled in terms of the statistical RRKM theory for unimolecular reactions, providing 0K

dissociation onsets, E_0 , for the ethylene loss channels. Three RRKM curves were used to model the five measurements, since two of the reactions differ only by the internal energy of the parent ion. This series of dissociations provides a detailed check of the calculation of the product energy distribution for sequential reactions. From the determined E_0 s, the heats of formation for sequential reactions. From the determined E_0 s, the heats of formation of several ethyl phosphine neutrals and ions have been determined: $\Delta_f H^\circ_{298K}[\text{P}(\text{C}_2\text{H}_5)_3] = -152.7 \pm 2.8$ kJ/mol, $\Delta_f H^\circ_{298K}[\text{P}(\text{C}_2\text{H}_5)_3^+] = 571.6 \pm 4.0$, $\Delta_f H^\circ_{298K}[\text{HP}(\text{C}_2\text{H}_5)_2] = -89.6 \pm 2.1$, $\Delta_f H^\circ_{298K}[\text{HP}(\text{C}_2\text{H}_5)_2^+] = 669.9 \pm 2.8$, $\Delta_f H^\circ_{298K}[\text{H}_2\text{PC}_2\text{H}_5] = -36.5 \pm 1.9$, $\Delta_f H^\circ_{298K}[\text{H}_2\text{PC}_2\text{H}_5^+] = 784.0 \pm 1.5$ kJ/mol. These values have been supported by G2 and G3 calculations using isodesmic reactions. Coupled cluster calculations have been used to show that the C_2H_4 loss channel, which involves a hydrogen transfer step, proceeds without a reverse energy barrier.

Modeling Ionic Unimolecular Dissociations from a Temperature Controlled TPEPCIO Study on $I\text{-C}_4\text{H}_9\text{I}$ Ions:

We have constructed a new temperature controlled inlet system for the study of gas phase unimolecular reaction dynamics. Temperatures in the range of 220K to 400K can be achieved, with a deviation of less than 5K over the course of a 48 hour experiment. Iodine loss from energy selected I -butyl iodide ($I\text{-C}_4\text{H}_9\text{I}$) ions was studied at four temperatures, 220K, 275K, 298K and 400K. The fractional ion abundances, in the form of breakdown diagrams are presented. Particular attention is paid to the slopes of the molecular and daughter

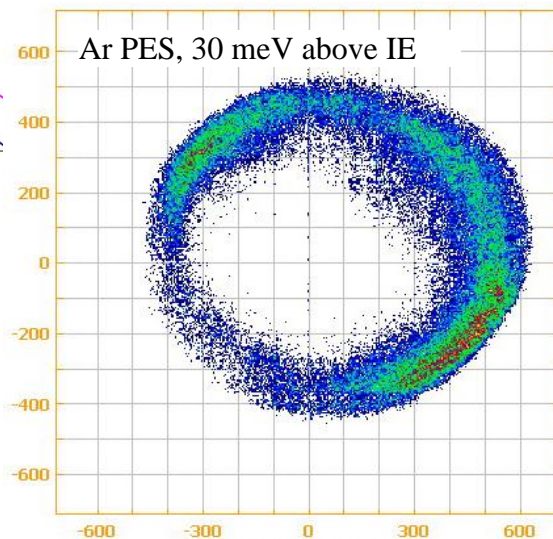
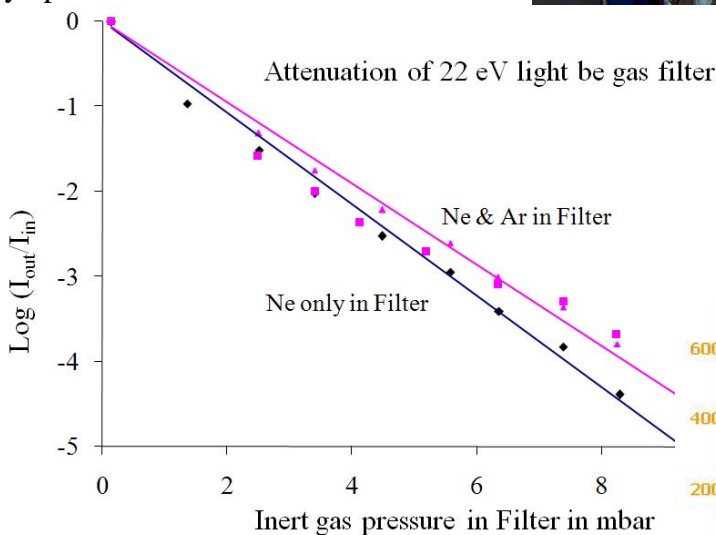
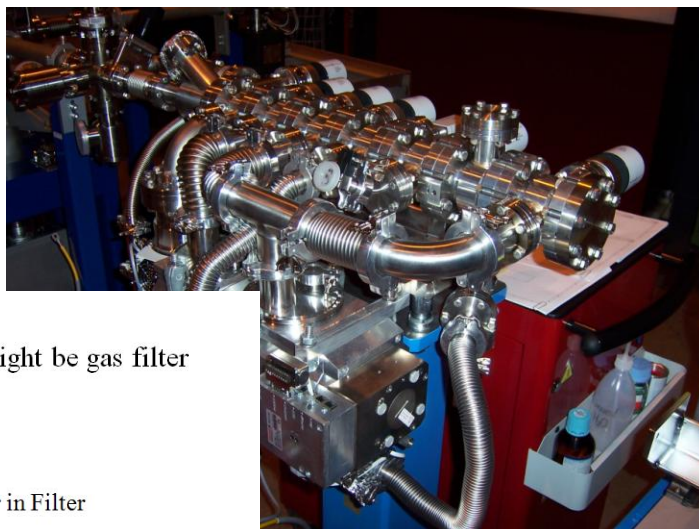


ion abundances in crossover region of the breakdown curve since they are governed solely by the internal energy distribution, $P(E)$, of the neutral precursor. $P(E)$ is a function of both the temperature and vibrational frequencies of the neutral precursor. From the four experimental measurements, the E_0 for the production of the $2\text{-C}_4\text{H}_9^+$ ion was determined to be 9.738 ± 0.015 eV. The simulated solid curves use a set of calculated vibrational frequencies to model the molecule's thermal energy distribution. It is interesting these data provide a direct measure of the molecule's thermal energy distribution. This temperature controlled inlet at low temperatures is now in routine use to help sharpen up dissociation onsets.

Data acquisition schemes for continuous two-particle time-of-flight coincidence experiments:

In preparation for the high flux experiments at the Swiss Light Source, we undertook a theoretical study of three data acquisition schemes for two-particle coincidence experiments with a continuous source. These are single-start single stop (SSSS), single start multi stop (SSMS) and multi start multi stop (MSMS). We found that the SSSS method associated with a time-to-pulse-height converter breaks down severely at high count rates. The single-start/multiple-stop setup, based on a time-to-digital converter (tdc), and the first choice in today's coincidence experiments, although significantly better at high count rates, is hampered by missing many starts, especially for long ion flight times and a variable false coincidence background. These predictions have now been verified by the recent (04/28/08) results at the SLS, where the MSMS experiment increased the signal by a factor of 5 over the SSMS and yielded a much smoother background signal.

Performance of a new gas filter design at the Swiss Light Source: The SLS VUV bending magnet beamline uses a grazing incidence monochromator to achieve a best resolution of 1 meV at 12 eV. The higher orders are suppressed by a rare gas suppression filter (see picture) that employs 6 stages of differential pumping to restrict the rare gas flow into the synchrotron ring. It is pumped by four 70 L/s turbomolecular pumps. As is evident from the plot of light intensities versus inert gas pressure, the filter easily suppresses the higher orders by up to 10^5 .



Electron Imaging Detector at the SLS: The new iPEPICO set up at the SLS incorporates electron imaging with a Roentek delay line detector. The first images for Ar, 30 meV above the IE have been obtained (see picture at right) and look very good. Alignment problems of the grating have so far limited the resolution to 6 meV, but this should be fixed soon so that we will have the ultimate resolution of 1-2 meV

Work in Progress

A paper on the thermochemistry of vinyl halides is currently in press in *J.Phys.Chem-A*. The heats of formation of vinyl chloride, bromide and iodide have been measured to ± 3 kJ/mol. Halobenzene ion dissociation rate constants measured over a 5 order of magnitude range are being analyzed by VTST, and heats of formation of HCCl_3 , HCCl_2Br , HCClBr_2 , HCBBr_3 and the $\text{H}_2\text{CCl}^\bullet$ radical have been measured and a paper is in the preparation stage.

Publications from DOE supported work 2006 – 2008

A.F. Lago and T. Baer, A Photoelectron photoion coincidence study of the vinyl bromide and tribromoethane ion dissociation dynamics: Heats of formation of C_2H_3^+ , $\text{C}_2\text{H}_3\text{Br}^+$, $\text{C}_2\text{H}_3\text{Br}_2^+$ and $\text{C}_2\text{H}_3\text{Br}_3^+$, *J. Phys. Chem. A*. **110**, 3036-3041 (2006)

- M. Hochlaf, T. Baer, X.-M. Qian, and C.Y. Ng, A vacuum ultraviolet pulsed field ionization-photoelectron study of cyanogen cation in the energy range of 13.2-15.9 eV, *J. Chem. Phys.* **123** 144302 (2005)
- A. Bodi, B. Sztaray, and T. Baer, Dissociative Photoionization of Mono-, Di- and Trimethylamine Studied by a Combined Threshold Photoelectron Photoion Coincidence Spectroscopy and Computational Approach, *Phys.Chem.Chem.Phys.* **8**, 613-623 (2006)
- H. Koizumi, J. Davalos, and T. Baer, Heats of Formation of GeH₄, GeF₄ and Ge(CH₃)₄, *Chem. Phys.* **324** 385-392(2006)
- A. Lago and T. Baer Dissociation dynamics and thermochemistry of chloroform and tetrachloroethane molecules studied by threshold photoelectron photoion coincidence, *Int. J. Mass Spectrom.* **252** 20-25 (2006)
- James P. Kercher, Bálint Sztáray, and Tomas Baer, On the dissociation of 2-Pentanone ions by threshold photoelectron photoion coincidence spectroscopy, *Int. J. Mass Spectrom.* **249-250** 403-411 (2006)
- Juan Z. Dávalos and Tomas Baer, Thermochemistry and Dissociative Photoionization of Si(CH₃)₄, BrSi(CH₃)₃, ISi(CH₃)₃, and Si₂(CH₃)₆ Studied by Threshold Photoelectron-Photoion Coincidence Spectroscopy, *J.Phys.Chem. A* **110** 8572-8579 (2006)
- Juan Z. Dávalos, and Hideya Koizumi, and Tomas Baer, Threshold Photoelectron-Photoion Coincidence Spectroscopy: Dissociation Dynamics and Thermochemistry of Ge(CH₃)₄, Ge(CH₃)₃Cl, and Ge(CH₃)₃Br, *J. Phys. Chem. A* **110**, 5032-5037 (2006)
- Agnes Revesz, Csaba I. Pongor, Andras Bodi, Balint Sztaray, and Tomas Baer, Manganese-Chalcarbonyl bond strengths from threshold photoelectron photoion coincidence spectroscopy, *Organometallics* **25**, 6061-6067 (2006)
- Andras Bodi, Curtis Bond, Patcharica Meteesatien, James P. Kercher, Balint Sztaray, and Tomas Baer, Photoion Photoelectron Coincidence Spectroscopy of Primary Amines RCH₂-NH₂ (R = H, CH₃, C₂H₅, C₃H₇, *i*-C₃H₇): Alkylamine and Alkyl Radical Heats of Formation by the Means of Isodesmic Reaction Networks, *J. Phys.Chem. A* **110**, 13425-13433 (2006)
- James P. Kercher, Zsolt Gengeliczki, Bálint Sztáray, and Tomas Baer, Dissociation dynamics of sequential ionic reactions: Heats of formation of tri-, di- and monoethyl phosphines, *J. Phys. Chem. A* **111**, 16-26 (2007)
- James P. Kercher, Will Stevens, Zsolt Gengeliczki, and Tomas Baer, Modeling Ionic Unimolecular Dissociations from a Temperature Controlled TPEPCIO Study on *I*-C₄H₉I Ions, *Int. J. Mass Spectrom.* **267**, 159-166 (2007)
- Zsolt Gengeliczki, László Szepes, Bálint Sztáray, and Tomas Baer, Photoelectron spectroscopy and thermochemistry of tert-butylisocyanide substituted cobalt tricarbonyl nitrosyl, *J. Phys. Chem. A* **111**, 7542-7550 (2007)
- Andras Bodi, Bálint Sztáray, Tomas Baer, Melanie Johnson and Thomas Gerber, Data acquisition schemes for continuous two-particle time-of-flight coincidence experiments, *Rev. Sci. Instrum.* **78**, 084102/1 – 7 (2007)

Turbulence-Chemistry Interactions in Reacting Flows

Robert S. Barlow
Combustion Research Facility
Sandia National Laboratories, MS 9051
Livermore, California 94550
barlow@sandia.gov

Program Scope

This program is directed toward achieving a more complete understanding of turbulence-chemistry interactions in flames and providing detailed measurements for validation of combustion models. In the Turbulent Combustion Laboratory (TCL) at the CRF, simultaneous line imaging of spontaneous Raman scattering, Rayleigh scattering, and two-photon laser-induced fluorescence (LIF) of CO is applied to obtain spatially and temporally resolved measurements of temperature, the concentrations of all major species, mixture fraction, and reaction progress, as well as gradients in these quantities in hydrocarbon flames. The instantaneous three-dimensional orientation of the turbulent reaction zone is also measured by imaging of OH LIF in two crossed planes, which intersect along the laser axis for the multiscale measurements. These combined data characterize both the thermo-chemical state and the instantaneous flame structure, such that the influence of turbulent mixing on flame chemistry may be quantified. Our experimental work is closely coupled with international collaborative efforts to develop and validate predictive models for turbulent combustion. This is accomplished through our visitor program and through the TNF Workshop series. Although the past emphasis has been on nonpremixed combustion, the workshop and this program are in the process of expanding their scope to address a broad range of combustion regimes, including premixed and stratified flames. Within the CRF we collaborate with Joe Oefelein to use highly-resolved large-eddy simulations (LES) of our experimental flames in order to gain greater fundamental understanding of the dynamics of multi-scale flow-chemistry interactions. We also collaborate with Tom Settersten and Jonathan Frank to refine our quantitative LIF methods and to apply complementary imaging diagnostics to selected turbulent flames.

Recent Progress

New Line-Imaging Detection System

The use of spontaneous Raman scattering to measure major species concentrations in turbulent flames has a long history at the CRF. Still, the need for simultaneous, single-shot measurements of the state of mixing, the progress of reaction, and gradients in scalar quantities, with both high precision and good spatial resolution, provides motivation to push these methods toward the physical limits imposed by optics, mechanical systems, and available lasers. Such advances are particularly important for measurements of scalar dissipation in turbulent reacting flows and for investigations of premixed or stratified flames in which the reaction zones are very thin.

A new detection system for multiscale measurements in flames was recently brought on line in the Turbulent Combustion Laboratory. As illustrated in Fig. 1, this system brings cameras for line imaging of Raman scattering, Rayleigh scattering, and two-photo laser-induced fluorescence of CO into a single unit, which maintains very stable alignment. It combines commercial camera lenses with a custom high-efficiency transmission grating (theoretical efficiency above 90% at the center wavelength) and two motor-driven shutter wheels that are

locked in frequency and phase. The spatial resolution and overall throughput of the Raman system are significantly improved, such that single-shot measurements of temperature and all major species are now obtained with 104- μm spacing, compared to 220- μm spacing previously. The measured blur spot varies with wavelength and off-axis position, but is well under 100 microns across most of the Raman detector. Measurement precision in calibration flames, as listed in Table 1, is nearly as high as for the previous system. The high-speed shutter wheel (21,000 rpm) provides temporal gating of 3.9 μs for the Raman measurements, compared to 9.2 μs with the previous system. This improves the rejection of flame luminosity when using a non-intensified, low-noise CCD detector with high quantum efficiency.

Table 1. Representative values of the precision (rms noise) of measurements at 104 μm spacing in combustion products over a premixed CH₄/air flat flame are listed below.

Scalar	Precision, σ	Premixed flame	Scalar	Precision, σ	Premixed flame
T	0.75%	$\phi = 0.97, T = 2185$	CO	4.5%	$\phi = 1.28, T = 2045$
N ₂	0.7%	"	H ₂	7.5%	"
CO ₂	3.2%	"			
H ₂ O	2.4%	"			
ϕ	2.2%	"			

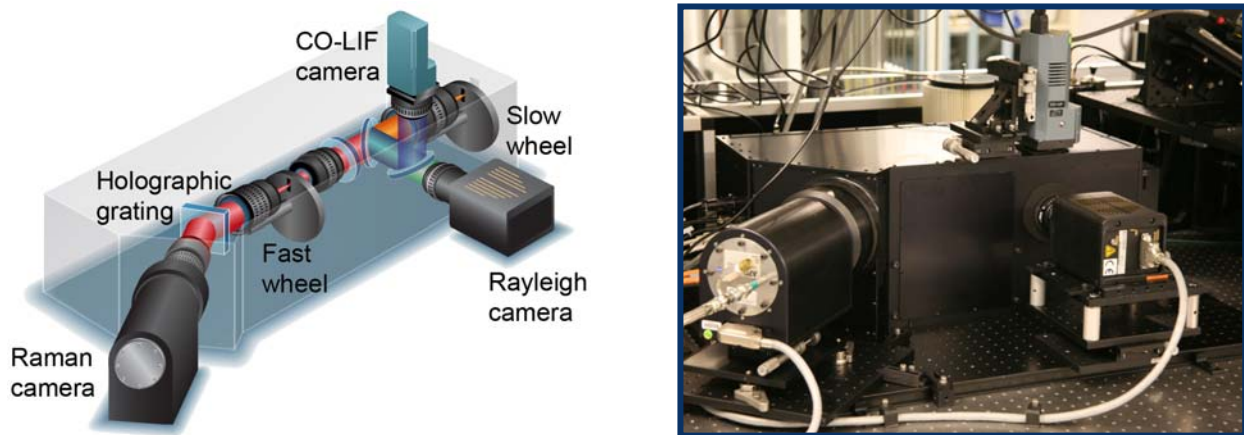


Figure 1. Schematic (left) and photograph (right) of the new Raman/Rayleigh/CO-LIF line-imaging detection system in the Turbulent Combustion Laboratory.

Stratified V-Flame Experiments

In stratified combustion a turbulent flame propagates through a nonuniform mixture of fuel and oxidizer. This mode of combustion is common on practical systems but is not well understood, and it represents a significant challenge for combustion models. Stratified combustion is also challenging for laser diagnostics because high precision in the measurement of the local equivalence ratio, ϕ , is required and the thin reaction zones demand high spatial resolution. In collaboration with Cambridge University, we have investigated the scalar structure of stratified CH₄/air flames using the new multispectral detection system in combination with crossed planar LIF imaging of OH. As shown in Fig. 2, the burner has a simple slot geometry, in which one leg of a rod-stabilized V-flame burns through a turbulent mixing layer formed between two streams of different equivalence ratio. Single-shot profiles of equivalence ratio, CO mole fraction, and temperature illustrate the resolution of the measurements relative to the flame thickness. This sample profile of ϕ also demonstrates that significant gradients in ϕ can exist within the thin

flame structure. The crossed OH image pair includes the detected flame edges (black curves) and corresponding 2D and 3D normal vectors. These data allow for determination of flame-normal gradients in reaction progressed variable, based on temperature and the local equivalence ratio, which means that it should be possible to extract mean and conditionally averaged result for the full (3D) dissipation of the reaction progress variable. As for the mixture fraction dissipation in nonpremixed combustion, dissipation of the reaction progress variable is an important modeled quantity in stratified flames. To our knowledge, there are no such measurements in the literature and no other systems capable of performing them.

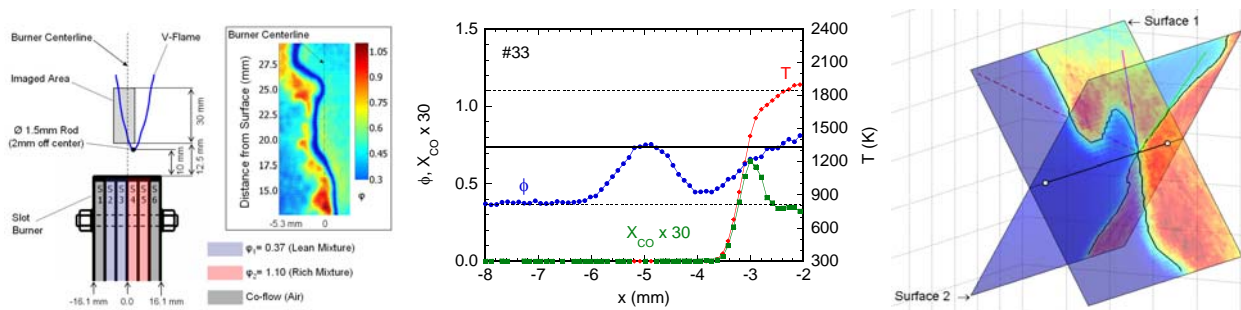


Figure 2. Cambridge stratified slot burner: Burner diagram and example of combined acetone and OH PLIF imaging performed at Cambridge (left), single-shot profiles of equivalence ratio, CO mole fraction, and temperature (center), and example crossed OH PLIF images (right).

Future Plans

The demonstrated performance of new Raman/Rayleigh/LIF detection system opens two significant new research paths. Both are closely coupled with planned collaborative research thrusts under the framework of the TNF Workshop. The first is to extend our work on stratified combustion to flames with higher levels of turbulence. This is being done in collaboration with the Technical University of Darmstadt (Germany) and the University of Cambridge (UK). In both cases, burner designs emphasize the establishment of well-defined boundary conditions for turbulent combustion models, such that unambiguous comparisons of measured and modeled results may be achieved. A second aspect of the ongoing stratified combustion work is to evaluate the accuracy of measurements of dissipation of the reaction progress variable and develop optimized methods of data analysis.

The second new thrust for this program will be to extend multiscale measurements to flames of more complex fuels. This will be pursued by developing polarization separation Raman spectroscopy as a quantitative single-shot diagnostic technique. A second three-camera, line-imaging detection system is currently being built for this purpose. Exploratory measurements on flames of various gaseous fuels will be conducted during the next year in order to gain understanding of the accuracy and limitations of the approach.

BES Supported Publications (2006 - present)

J.C. Oefelein, R.W. Schefer, R.S. Barlow, "Toward Validation of Large Eddy Simulation for Turbulent Combustion," *AIAA J.* **44**, 418-433 (2006).

R.S. Barlow, "Laser Diagnostics and Their Interplay with Computations to Understand Turbulent Combustion," invited plenary paper, *Proc. Combust. Inst.* **31**, 49-75 (2007).

D. Wang, C. Tong, R.S. Barlow, A.N. Karpetis, "Experimental Study of Scalar Filtered Mass Density Function in Turbulent Partially Premixed Flames," *Proc. Combust. Inst.* **31**, 1533-1541 (2007).

G.H. Wang, R.S. Barlow, N.T. Clemens, "Quantification of Resolution and Noise Effects on Thermal Dissipation Measurements in Turbulent Non-premixed Jet Flames," *Proc. Combust. Inst.* **31**, 1525-1532 (2007).

G.H. Wang, A.N. Karpetis, R.S. Barlow, "Dissipation Length Scales in Turbulent Nonpremixed Jet Flames" *Combust. Flame*, **148**, 62-75 (2007).

R.P. Lindstedt, H.C. Ozarovsky, R.S. Barlow, A.N. Karpetis, "Progression of Localised Extinction in High Reynolds Turbulent Jet Flames," *Proc. Combust. Inst.* **31**, 1551-1558 (2007).

A.R. Masri, P.A.M. Kalt, Y.M. Al-Abdeli, R.S. Barlow, "Turbulence-Chemistry Interactions in Non-Premixed Swirling Flames," *Combust. Theory Modelling*, **11**, 653-673 (2007).

G.H. Wang, N.T. Clemens, R.S. Barlow, P.L. Varghese, "A System Model for Assessing Scalar Dissipation Measurement Accuracy in Turbulent Flows" *Meas. Sci. Technol.* **18**, 1287-1303 (2007).

G.H. Wang, N.T. Clemens, P.L. Varghese, R.S. Barlow, "Turbulent Time Scales in a Nonpremixed Turbulent Jet Flame by Using High-Repetition Rate Thermometry," *Combust. Flame*, **152**, 317-335 (2008).

T.G. Drozda, G.H. Wang, V. Sankaran, J.R. Mayo, J.C. Oefelein, R.S. Barlow, "Scalar Filtered Mass Density Functions in Nonpremixed Turbulent Jet Flames," *Combust. Flame*, accepted.

R.S. Barlow, G.H. Wang, P. Anselmo-Filho, M.S. Sweeney, S. Hochgreb, "Application of Raman/Rayleigh/LIF Diagnostics in Turbulent Stratified Flames," *Proc. Combust. Inst.*, accepted.

M.J. Dunn, A.R. Masri, R.W. Bilger, R.S. Barlow, G.H. Wang, "The Compositional Structure of Highly Turbulent Piloted Premixed Flames Issuing into Hot Coflow," *Proc. Combust. Inst.*, accepted.

Web-Based Information

<http://www.ca.sandia.gov/CRF/staff/barlow.html>

<http://www.ca.sandia.gov/TNF>

Theoretical Studies of Combustion Dynamics (DE-FG02-97ER14782)

Joel M. Bowman

Cherry L. Emerson Center for Scientific Computation and
Department of Chemistry, Emory University
Atlanta, GA 30322, jmbowma@emory.edu

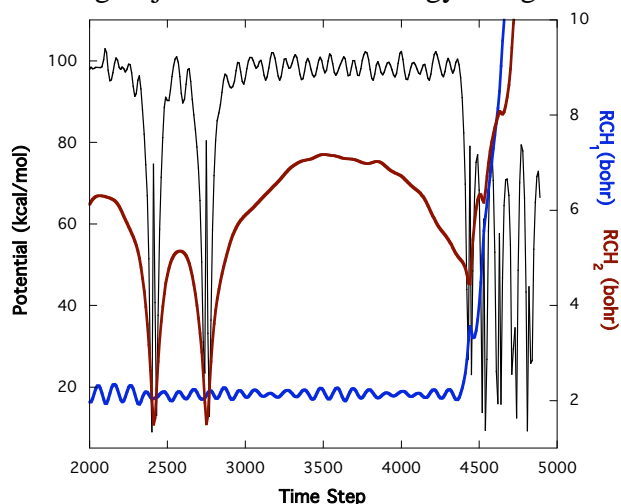
Program Scope

This research supported by the Department of Energy is to develop and apply rigorous computational methods to model and gain insight into chemical and physical processes of importance in combustion and issues related to combustion. Our focus recently has been on developing methods to obtain global potential energy surfaces that are fits to tens of thousands or more of *ab initio* energies using special polynomial bases that are manifestly invariant with respect to any permutation of like nuclei. Dynamics on these potentials, which may contain multiple minima and saddle points, can be done for long times and can reveal new pathways and mechanisms of chemical reactions. The choice of reaction system to study is always motivated by experiments that challenge and ultimately advance basic understanding of combustion reaction dynamics.

Recent Progress in “Roaming” Dynamics

H₂CO photodissociation

We have continued our collaboration with Arthur Suits and co-workers to elucidate the details of the “roaming” dynamics in the photodissociation of H₂CO to form the molecular products H₂ + CO.^{P1-P4} In agreement with a recent calculation of a “roaming” transition state by Harding and co-workers,¹ we have determined that the apparent threshold for the roaming pathway is very slightly below the energetic threshold for the formation of the H+HCO radicals. This determination was made by examining roaming trajectories and the energy along them. One example of such a trajectory is



shown where the two CH bond distances are plotted for the portion of trajectory where one H atom is roaming with respect to the HCO and where the potential is oscillating (due to the HCO vibration) about a value somewhat below 100 kcal/mol. At about time step 4300 the H₂ is formed, the potential drops precipitously and then oscillates greatly reflecting mainly the high internal energy of the H₂. We estimate that the threshold for the roaming is roughly only 50-100 cm⁻¹ below the radical threshold in

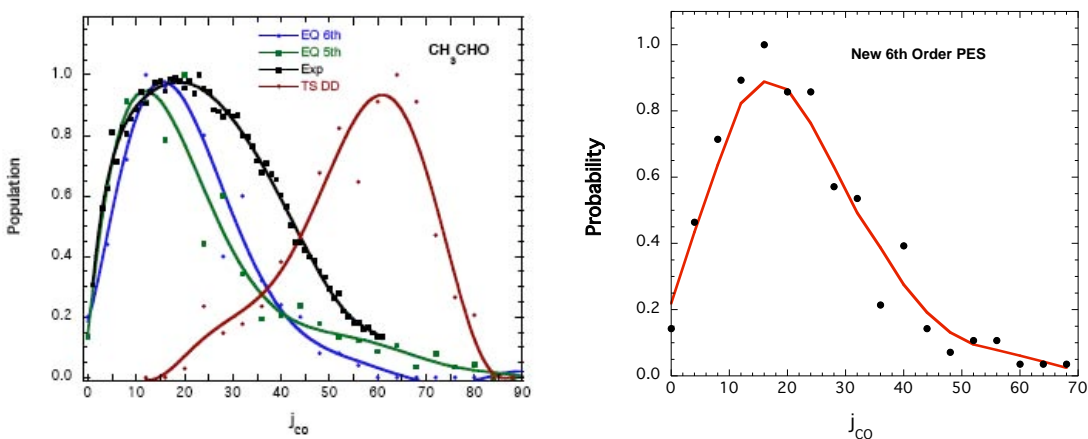
quite good accord with Harding *et al.* calculation based on the energy of the roaming TS.¹

CH₃CHO Photodissociation

We have begun dynamics calculations of the photodissociation of CH₃CHO, which in an initial focus on 308 nm, the photolysis wavelength of earlier experiments of Houston and Kable² and also new experiments in by Scott Kable and David Osborn.³ Houston and Kable speculated, based on the CO rotational distribution and CH₄-CO kinetic energy distribution, that a roaming mechanism is at play here analogous to the one in H₂CO photodissociation. The earliest joint theoretical experimental on this photodissociation was done by Bershon and co-workers,⁴ who reported the CO rotational distribution resulting from photolysis at 248 nm and also a determination of the molecular elimination saddle point.

Our work, which has resulted in a Letter thus far, has been to develop a global potential energy surface that described the many possible intermediates and product channels of the this system.^{P8} This is quite a daunting task given that CH₃CHO is far more complex in this respect than H₂CO. Without going into the details here we have been able to do this by fitting roughly 256 000 CCSD(T)/cc-pVTZ electronic energies in the single-reference regions of the potential and augmenting those energies with accurate CCSD(T)/cc-pVTZ and aug-cc-pVTZ energies for many fragments, e.g., CH₄+CO, CH₃+HCO, CH₂CO+H₂, C₂H₂+H₂O, etc. We have dealt with the multi-reference regions by an expedient, up to now, i.e., we interpolate through those regions by using reliable single reference energies for the complex regions and the fragments. Then we check the reliability of the potential in these regions by doing MRCI calculations. This procedure may miss flat, floppy saddle points if they are multireference in character; however, based on our dynamics calculations to date and comparison with experiment (see below) these are not yet a concern.

The first set of calculations is aimed at the HK experiments and the new Kable-Osborn experiments which have determined the internal energy distribution of the CH₄ product. Here we compare calculations done on several versions of PESs, based on different ways to fit the *ab initio* data and also based fitting just 135 000 electronic energies of the CO rotational distribution. We also present the results from a “Direct-dynamics” trajectory calculations initiated at the molecular TS done using MP2/cc-pVDZ energies and gradients. These are shown in figures below where EQ 6th and EQ



5th refer to two different fits to 135 000 energies and where “New 6th Order PES” refers to

a new fit to 256 000 energies. First note the poor agreement between experiment and the TS dynamics. By contrast there is good agreement for the “EQ” trajectories, which were run on the various PES starting at the CH₃CHO equilibrium. Also note the improved agreement with the new PES based on many more energies. The poor agreement with the standard saddle-point TS dynamics clearly suggests that the pathway(s) taken to the molecular products either deviates substantially from the molecular saddle point or perhaps arrives at it with a very non-standard internal energy distribution. We have examined the EQ trajectories and have determined that the former is the case, analogous to the roaming dynamics in H₂CO. Comparison with the Kable-Osborn experiments on the CH₄ internal energy distribution, not shown here, dramatically confirm the non-molecular TS dynamics in this system.

Reaction Dynamics of C+C₂H₂ → *linear, cyclic* C₃H+H, C₃+H₂

Work is continuing on the above reactions. We have reported a calculation of the threshold ionization potentials of *c*-C₃H and *l*-C₃H.^{P10} The goal of this work is to develop a means to directly distinguish these two isomers experimentally.

Future Plans

We have begun dynamics calculations of the C+C₂H₂ reaction including spin-orbit coupling of singlet and triplet PESs in hopes of sorting out the various issues still outstanding about this reaction. Mebel and co-workers have recently has done a nice analysis based on RRKM theory with electronic transitions;⁶ however, some of those results are at variance with our dynamics calculations and this needs to be resolved.

References

1. L. B. Harding, S. Klippenstein, and A. Jasper Phys. Chem. Chem. Phys. **9**, 1 (2007).
2. P. L. Houston and S. H. Kable, Proc. Natl. Acad. Sci. USA, **103**, 16079 (2006).
3. S. Kable and D. A. Osborn, private communication.
4. B. F. Gherman, R. A. Friesner, T-H. Wong, Z. Min and R. Bersohn, J. Chem. Phys. **114**, 6128 (2001).
5. R. I. Kaiser, A. M. Mebel, and Y. T. Lee, J. Chem. Phys. **114**, 231 (2001).
6. F. Leonori, R. Petrucci, E. Segoloni, A. Bergeat, K. M. Hickson, N. Balucani, and P. Casavecchia, J. Phys. Chem. A **112** 1363 (2008).
6. A. M. Mebel, V. V. Kislov, M. Hayashi, J. Chem. Phys. **126**, 204310 (2007).

PUBLICATIONS SUPPORTED BY THE DOE (2006-present)

1. Energy dependence of the roaming atom pathway in formaldehyde decomposition, S. A. Lahankar, S. D. Chambreau, X. Zhang J. M. Bowman, A. G. Suits, J. Chem. Phys. **126**, 044314 (2007).
2. The roaming atom pathway in formaldehyde decomposition, S. A. Lahankar, S. D.

- Chambreau, D. Townsend, F. Suits, J. Farnum, X. Zhang, J. M. Bowman, and A. G. Suits, *J. Chem. Phys.* **125**, 044303 (2006).
3. Phase Space Analysis of Formaldehyde Dissociation Branching and Comparison with Quasiclassical Trajectory Calculations, J. D. Farnum and J. M. Bowman, *J. Phys. Chem. A* **111**, 10376 (2007).
 4. Formaldehyde photodissociation: Dependence on total angular momentum and rotational alignment of the CO product, J. Farnum, X. Zhang and J.M. Bowman, *J. Chem. Phys.* **126**, 134305 (2007).
 5. Skirting the transition state, a new paradigm in reaction rate theory [Commentary], J. M. Bowman, *PNAS* **103**, 16061 (2006).
 6. New insights on reaction dynamics from formaldehyde photodissociation, J. M. Bowman and X. Zhang. *Phys. Chem. Chem. Phys.*, invited review, **8** 313 (2006).
 7. Signatures of H₂CO photodissociation from two electronic states, H.M. Yin and S.H. Kable, X. Zhang and J.M. Bowman, *Science*, **311**, 1443 (2006).
 8. Quasiclassical Trajectory Calculations of Acetaldehyde Dissociation on a Global Potential Energy Surface Indicate Significant Non-transition State Dynamics, B.C. Shepler, B. J. Braams, J. M. Bowman, *J. Phys. Chem. A (Letter)*; **111**; 8282 (2007).
 9. Quasiclassical trajectory calculations of the reaction $C + C_2H_2 \rightarrow l-C_3H, c-C_3H + H, C_3 + H_2$ using full-dimensional triplet and singlet potential energy surfaces, W. K. Park, J. Park, S. C. Park, B. J. Braams, C. Chen, and J. M. Bowman, *J. Chem. Phys.* **125**, 081101 (2006).
 10. Combined Experimental and Computational Study on the Ionization Energies of the Cyclic and Linear C₃H Isomers. R. I. Kaiser, L. Belau, S. R. Leone, M. Ahmed, Y. Wang, B. J. Braams, and J. M. Bowman, *Chem Phys Chem* **8**, 1236 (2007).
 11. *Ab initio*-Based Potential Energy Surfaces and Franck-Condon Analysis of Ionization Thresholds of cyclic-C₃H and linear-C₃H, Y. Wang, B. J. Braams, and J. M. Bowman, *J. Phys. Chem. A* **111**, 4056 (2007).
 12. An *ab initio* potential surface describing abstraction and exchange for H+CH₄, X. Zhang, B. Braams, J. M. Bowman, *J. Chem. Phys* **124**, 021104 (2006).
 13. Potential Energy Surface and Reaction Dynamics of the OH+NO₂ Reaction, C. Chen, B. Schepler, B. Braams, J. M. Bowman, *J. Chem. Phys.* **127**, 104310 (2007).
 14. Quasiclassical trajectory study of the reaction of fast H atoms with C-H stretch excited CHD₃, Z. Xie, J. M. Bowman, *Chem. Phys. Lett.* **429**, 355 (2006).
 15. Quasiclassical trajectory study of the reaction $H + CH_4(\nu_3=0,1) \rightarrow CH_3 + H_2$ using a new *ab initio* potential energy surface, Z. Xie, J. M. Bowman, and X. Zhang, *J. Chem. Phys.* **125**, 133120 (2006).
 16. Termolecular kinetics for the Mu+CO+M recombination....J, J. Pan, D. J. Arseneau, M. Senba, D. M. Garner, D. G. Fleming, Ti. Xie and J. M. Bowman, *J. Chem. Phys.* **125**, 014307 (2006).

COMBUSTION CHEMISTRY

Principal Investigator: Nancy J. Brown

Environmental Energy Technologies Division

Lawrence Berkeley National Laboratory

Berkeley, California, 94720

510-486-4241

NJBrown@lbl.gov

PROJECT SCOPE

Combustion processes are governed by chemical kinetics, energy transfer, transport, fluid mechanics, and their complex interactions. Understanding the fundamental chemical processes offers the possibility of optimizing combustion processes. The objective of our research is to address fundamental issues of chemical reactivity and molecular transport in combustion systems. Our long-term research objective is to contribute to the development of reliable combustion models that can be used to understand and characterize the formation and destruction of combustion-generated pollutants. We emphasize studying chemistry at both the microscopic and macroscopic levels. To contribute to the achievement of this goal, our current activities are concerned with three tasks: Task 1) developing models for representing combustion chemistry at varying levels of complexity to use with models for laminar and turbulent flow fields to describe combustion processes; Task 2) developing tools to probe chemistry fluid interactions; and Task 3) modeling and analyzing combustion in multi-dimensional flow fields.

RECENT PROGRESS

Task 1: Developing models for representing combustion chemistry at varying levels of complexity to use with models for laminar and turbulent flow fields to describe combustion processes in collaboration with Tonse and Day. We have developed DYSSA, the dynamic steady state approach, for reducing the computational burden associated with solving complex rate equations in models of laboratory scale flames. DYSSA, because it can be implemented in a straightforward fashion, offers the potential for more widespread use in the combustion community. It requires optimization and automation to achieve this. The chemistry portion of combustion models requires the largest percentage of computational burden. Two factors contribute to DYSSA's accuracy/efficiency trade-off. First and most significant is the computational burden associated with the solution of chemical rate equations for the non-steady state species—the larger their number, the larger the burden. A key target for efficiency is creating a reduced mechanism that has a computational burden equal to that of other processes in the reactive CFD simulation so that solving the chemical rate equations is no longer rate limiting. Our recent analysis indicates that there are species in steady state that are not being identified by the species time scale criteria that we are using. The second is concerned with partitioning of chemical composition space. There is a trade-off between accuracy and efficiency that favors accuracy and penalizes efficiency as the number of hypercubes is increased and which has the opposite effect when it is decreased. Optimizing of this trade-off requires further refinement. We have improved DYSSA's

efficiency while maintaining its accuracy at a high level that can be pre-selected. We continue to improve our criteria for identifying FnL species, our steady state species that also have low concentrations. We devised a new error determination scheme in DYSSA to assess the relative error in the reduction scheme. The accuracy of the reduced system is determined at the time of the initial call for each hypercube. This is accomplished by making a reduced call using the same non-FnL (non-fast and low) initial concentrations, temperature and timestep as were used for the full, unreduced system, and calculating the relative errors of the non-FnL species with respect to the unreduced system. A hypercube which does not meet the user-defined relative error requirement is noted, and the full unreduced ODE system is used on subsequent visits to the hypercube. The relative error determined in this manner correlates strongly with the relative error obtained by comparison with pure ODE simulations. A typical value for the user-specified relative error is less than 2%.

Task 2. A review of transport property formalisms and their underlying parameterizations is being prepared (Brown). Coupling between transport and chemistry is responsible for flame propagation. In combustion modeling, profile shapes, flame velocities, and pollutant production are all affected by values of transport properties. The combustion modeling community has focused considerable effort on improving the chemical descriptions of the combustion and has recently made substantial advances in treating the chemistry of moderately complex fuels and flow fields.

It is important to describe properly the transport of species, momentum, and energy in flames. Transport coefficients required for the quantification of these processes are diffusion, viscosity, and thermal conductivity coefficients. Our recent sensitivity studies have demonstrated the importance of transport properties and the potential parameters that underlie them in the development of chemical mechanisms and on combustion modeling. Transport property importance varies according to the dependent variable considered and the flame type. As an important step in improving the representation of transport in combustion modeling, we are comparing calculated values of properties derived using different formalisms with experimentally determined values for conditions required for combustion modeling. We are focusing on properties required for modeling H_2 and CH_4 combustion. This effort also contributes to the PrIME collaboration.

We are writing a review paper that summarizes the evaluation of transport properties within the context of the currently used theoretical and experimental measurements archived in the literature, e.g., NIST data by Lemmon et al. We examine the consequences and limitations of the various approximations that underlie the different approaches. Issues discussed are: the intermolecular potential and their supporting molecular parameters, the interpretation of corresponding states, the various approaches to evaluating collision integrals, the combination rules that yield pair molecular parameters for unlike species from like species, mixture approximations, and the suitability of different types of experimental data for evaluating the accuracy of the transport parameters. We focus on the approaches that might be used for the calculations of transport properties suitable for combustion modeling, and pay particular attention to the data needs associated with them. The importance of orientation dependent forces for molecular pairs where one member of the pair has a dipole moment is often emphasized. Orientation dependent forces have often been treated incorrectly with averaging done improperly. Supporting data like dipole moments and polarizabilities are often lacking,

and do not benefit from more recent state-of-the-art measurements. When calculating properties of mixtures, interactions of both like and unlike pairs of molecules are required. Combination rules are the formulae by which we infer the interactions between molecules in an unlike pair from those in like pairs. Familiar examples are Lorentz rules for collision diameters that is exact for hard spheres, and the geometric mean rule or Berthelot rule for wells depths. Unfortunately, there have been insufficient data to verify their accuracy. When well depths calculated using the Berthelot rule are compared with those derived from molecular beam experiments, the former are too large, and this affects the temperature dependence of the transport properties. In light of these errors in potential parameters, the considerable efforts associated with some mixture approximations may not be warranted.

FUTURE PLANS

We will also extend the data set associated with the potential parameters that support the evaluation of transport properties for species important for H₂ and CH₄ combustion. We will improve the accuracy of transport properties important for supporting H₂ and CH₄ combustion. We will work with Michael Frenklach as part of PrIME (<http://primekinetics.org>), an international collaboration concerned with developing reaction models for combustion, which includes kinetics, thermochemistry, and transport. We will collaborate with Michael Frenklach on the homogeneous nucleation of carbon nanoparticles, and focus on collisions of aromatic-aliphatically-linked hydrocarbon compounds.

REFERENCES

M.S. Day, and J.B. Bell, Numerical Simulation of Laminar Reacting Flows with Complex Chemistry. *Combust. Theory and Modeling*, 4(4), pp 535-556 (2000). Also LBNL Report 44682.

M.S. Day, <http://seesar.lbl.gov/CCSE/Software> (2003).

J.B. Bell, N.J. Brown, M.S. Day, M. Frenklach, J.F. Grcar, and S.R. Tonse, "Effect of Stoichiometry on Vortex-Flame Interactions," *Proceedings of the Combustion Institute* 28, 1933-1939 (2000). Also Lawrence Berkeley National Laboratory Report No. LBNL-44730.

Q.V. Nguyen, and P.H. Paul, "The Time Evolution of a Vortex-Flame Interaction Observed in Planar Imaging of CH and OH," 26th Symp. (Intl.) on Combustion, the Combustion Inst., Pittsburgh, PA, 1996, pp 357-364.

N.J. Brown and Revamp, K.L., "Comparative Sensitivity Analysis of Transport Properties and Reaction Rate Coefficients". *International Journal Chemical Kinetics*, 37, pp 538-553 (2005). Also LBNL Report No. 55671

PUBLICATIONS

Tonse, S.R., M.S. Day, and N.J. Brown. Dynamic Reduction of a CH₄/Air Chemical Mechanism Appropriate for Investigating Vortex Flame Interactions. *International Journal of Chemical Kinetics* 39, pp 204-220, 2007. Also LBNL Report No. 59750

Dynamics of Product Branching in Elementary Combustion Reactions

Laurie J. Butler

The University of Chicago, The James Franck Institute
5640 South Ellis Avenue, Chicago, IL 60637
L-Butler@uchicago.edu

I. Program Scope

The elementary reactions that determine the performance of a combustion system range from direct H-atom abstraction reactions to complex reactions involving competing addition/elimination mechanisms. The reaction rate and the branching to multiple product channels can evidence a strong temperature and pressure dependence. While the total rate constant for many elementary reactions is well-characterized, understanding the product branching in complex reactions presents a formidable challenge. To gain an incisive probe of such reactions, our experiments supported by DOE directly probe the dynamics of the product channels that arise from long-lived radical intermediates along the bimolecular reaction coordinates. The work uses the methodology developed in my group in the last seven years, using both imaging and scattering apparatuses. The experiments generate a particular isomeric form of an unstable radical intermediate along a bimolecular reaction coordinate and investigate the branching between the ensuing product channels of the energized radical as a function of its internal energy under collision-less conditions. They probe the reaction from each radical intermediate to the competing product channels and determining the energetic barriers in both the entrance and the product channels. When one of the competing product channels produces a heavy and a light co-fragment, such as in the acrolein + H product channel from the O + allyl reaction described below, the experiments offer a direct measurement of the microcanonical rate, $k(E)$, of that product channel relative to the other competing product channels resulting from an addition mechanism.

The experiments use a combination of: 1) measurement of product velocity and angular distributions in a crossed laser-molecular beam apparatus, with electron bombardment detection in my lab in Chicago or 2) with tunable vacuum ultraviolet photoionization detection in collaboration with Jim Lin at Taiwan's National Synchrotron Radiation Research Center (NSRRC), and 3) velocity map imaging using state-selective REMPI ionization and single photon VUV ionization of radical intermediates and reaction products. Our work for DOE in the past three years¹⁻⁵ is referenced below. We describe in detail our work on the O + allyl reaction, focuses on probing the product channels that result from addition of the O atom at an end carbon atom. The other work referenced has been described in prior DOE abstracts and is in the literature. We finish with our new efforts, some in collaboration with Steve Pratt, to investigate the reaction dynamics formed in the addition channel of OH with ethylene. In summary, the results develop insight on product channel branching in such reactions and provide a key benchmark for emerging electronic structure calculations on polyatomic reactions that proceed through unstable radical intermediates.

II. Recent Progress

Our work this year focused on the complex dynamics of the O + allyl reaction. We submitted one paper on this work and a second is in preparation. The experimental work includes imaging experiments and scattering experiments in our lab at Chicago, CCSD(T)

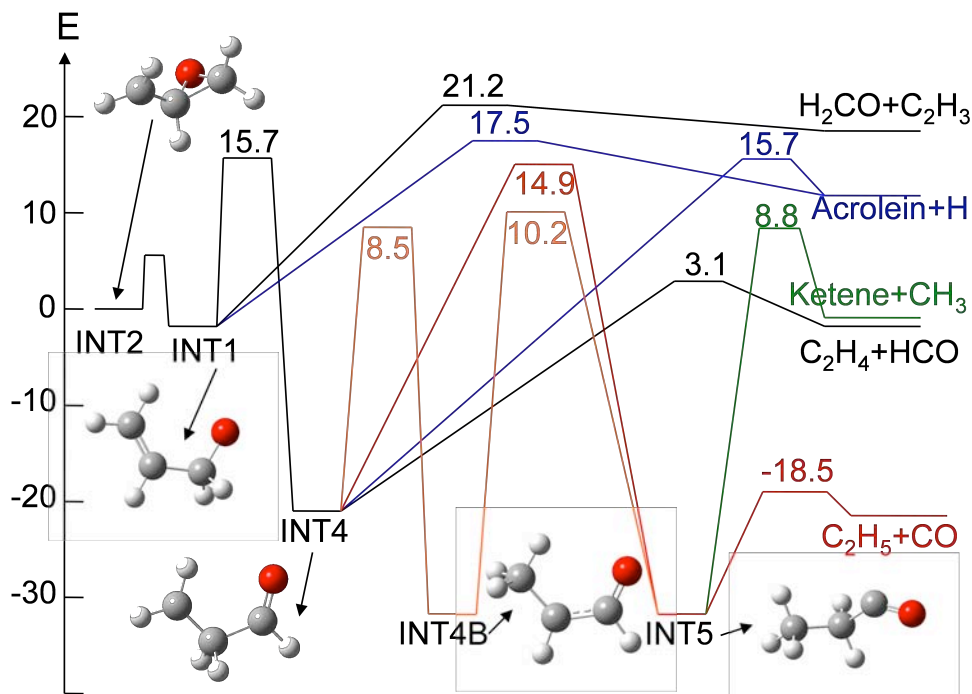
calculations on the relevant radical intermediates and transition states on the path to the energetically allowed product channels, and extensive scattering experiments at the NSRRC in Taiwan in collaboration with J. J. Lin on the product channels accessed from the radical intermediate formed when the O atom adds to an end C atom. We took data at the synchrotron (in April 2006 and Nov. 2007) to identify all the product channels accessed from that radical intermediate and to experimentally determine the product branching fractions. (The latter requires measuring the relative signal levels and calibrating, in separate experiments, the photoionization cross sections of some of the detected radical and molecular products with respect to Cl atoms or standards like ethene at the photoionization energies used.)

Before our work, a few key studies on the O + allyl reaction had attempted to probe the product branching and dynamics of this reaction. The early bulk kinetics work of Gutman et al (J. Phys. Chem. 94, 3652 (1990)) identified only the acrolein + H product channel as a primary one, putting a <20% upper limit on the H₂CO + C₂H₃ product channel. Later crossed molecular beam experiments by Choi et al (J. Chem. Phys. 116, 2675 (2002); 117, 2017 (2002); 120, 7976 (2004)) focused on detecting only OH and H atom products; they also computationally characterized (J. Chem. Phys. 119, 8966 (2003)) the multiple reaction pathways that can result from the addition of O atoms to an end vs. the central C atom. The experimental work evidenced OH products, attributed to direct abstraction and a competing addition channel forming OH + allene, as well as H atoms, consistent with Gutman's acrolein + H channel. Most recently, Casavecchia et al (Phys. Chem. Chem. Phys. 9, 1307 (2007)) used soft-electron impact ionization in a crossed-molecular beams experiment to try to identify all the product channels. The data evidenced that acrolein + H is a major product channel, but they were unable to definitively assign the product channels resulting in their signal at m/e=29 and 27, concluding that "one or more C-C fission product channels" contribute to the product branching.

Our experiments photolytically generated the radical intermediate formed when an O atom adds to the end C atom of allyl and then resolved all three major product channels resulting from this radical intermediate. The photodissociation of epichlorohydrin at 193 nm produces chlorine atoms and c-OCH₂CHCH₂ radicals; these undergo a facile ring opening to the OCH₂CHCH₂ radical intermediate. State-selective REMPI detection resolves the velocity distributions of ground and spin-orbit excited state chlorine independently, allowing for a more accurate determination of the internal energy distribution of the nascent radicals. We obtain good agreement detecting the velocity distributions of the Cl atoms with REMPI, VUV photoionization at 13.8 eV, and electron bombardment ionization; all show a bimodal distribution of recoil kinetic energies. The dominant high-recoil-kinetic-energy feature (87% of the total) peaks near E_T=33 kcal/mol and produces nascent radical intermediates with internal energies ranging from about 20 to 50 kcal/mol (relative to the zero-point-level of the O-bridged intermediate (INT2) in the figure below). The minor channel (13%) produces higher internal energy radicals that are likely electronically excited, formed in a concerted bond fission/ring-opening process.

To elucidate the product channels resulting from the OCH₂CHCH₂ radical intermediate, the crossed laser-molecular beam experiment uses VUV photoionization and detects the velocity distribution of the possible products. The data identifies the three dominant product channels as acrolein + H, ethene + HCO, and H₂CO + C₂H₃. A small signal from ketene product is also detected. The measured velocity distributions and relative signal intensities at m/e = 27, 28, and 29 at two photoionization energies suggest that the most exothermic product channel, C₂H₅ + CO, does not contribute significantly to the product branching. The higher internal energy onset of the acrolein + H product channel, detected in the velocity measurements of the acrolein

product, is consistent with the relative barriers en route to each of these product channels calculated at the CCSD(T)/aug-cc-pVQZ level of theory, though a clean determination of the barrier energy to H + acrolein is precluded by the substantial partitioning into rotational energy during the photolytic production of the nascent radicals. The measured branching fraction to the H + acrolein product channel of 18% is roughly half that predicted using RRKM theory and the calculated transition states. This suggests that the barrier for the 1,2 H-atom shift en route to the ethene + HCO product channel calculated at the CBS-QB3 and CCSD(T) levels of theory is too high (this isomerization competes with the acrolein + H and $\text{H}_2\text{CO} + \text{C}_2\text{H}_3$ product channels).



Our second paper on this system focuses on the dynamics of the C-C fission product channels and their branching fractions. Interestingly, the electronically excited radicals formed in the precursor's minor C-Cl fission channel do not dissociate to acrolein + H. We can determine the branching fraction to the $\text{H}_2\text{CO} + \text{C}_2\text{H}_3$ product channel from the measured signal intensity at $m/e=27$, C_2H_3^+ , dividing by the total number of radicals formed, determined by detecting the momentum-matched Cl atoms, and correcting for the appropriate kinematic factors and photoionization cross sections of each. (The photoionization cross section for vinyl radicals measured by Neumark et al, J. Chem. Phys. 119, 5311 (2003) is key here.) The relative signal intensities at $m/e=28$ and $m/e=35$ similarly allow us to determine the branching fraction to the ethene + HCO product channel (using photoionization cross sections measured by Person and Nicole, J. Chem. Phys. 49, 5421 (1968), and put on an absolute scale by Cool et al., Int. J. Mass Spectrom. 247, 18 (2005)). This analysis is underway.

III. Future Work

Our next experiments focus on the product branching from the radical intermediate formed when an OH radical adds to ethene. There has been extensive experimental and theoretical work on the OH + ethene reaction: thirteen prior theoretical studies and a shocking thirty-eight prior experimental studies, many focusing on the temperature and pressure dependence of the total rate constant. The experiments evidence stabilized radical adduct at

high pressure and low temperatures, but become dominated by the H atom abstraction channel to form $\text{H}_2\text{O} + \text{vinyl}$ at high temperatures. Our work focuses on the pathways opened by the addition of OH to the C=C bond of ethene, forming the HOCH_2CH_2 radical intermediate. Upon forming this adduct, one can expect a competition between collisional stabilization of the adduct in the bulk and, if the adduct is formed with high enough internal energy, its direct dissociation to ethenol + H, and its isomerization, via H-atom transfer, to a second radical intermediate, OCH_2CH_3 . This second radical intermediate leads to the formaldehyde + CH_3 and acetaldehyde + H product channels. Interestingly, there has been two recent reports (Taatjes et al, *Science* **308**, 1887 (2005) and *J. Phys. Chem. A* **110**, 3254 (2006) and Cool et al, *J. Chem. Phys.* **119**, 8356 (2003)) of ethenol production in ethene flames; this observation is attributed to the ethenol + H product channel in the OH + ethene reaction.

We have investigated the photolytic generation of the HOCH_2CH_2 radical intermediate from the photodissociation of 2-chloroethanol, but the small absorption cross section at 193 nm precludes investigating the product branching from the nascent radicals. Thus we are switching to 2-bromoethanol, which requires additional imaging experiments with state selective detection of the Br atom spin orbit state to accurately determine the internal energy distribution of the nascent radicals. Our first goal is to probe the relative energies of the isomerization barrier to the OCH_2CH_3 radical, which leads to the formaldehyde + CH_3 and acetaldehyde + H product channels, and the barrier for direct dissociation of the HOCH_2CH_2 radical intermediate to ethenol + H. The most recent theoretical work (Senosiain et al, *J. Phys. Chem. A* **110**, 6960 (2006)) predicted the barrier to ethenol + H is higher by 1.2 kcal/mol than the isomerization barrier. In contrast other recent theoretical work by M. C. Lin et al (*Chem. Phys. Lett.* **408**, 25 (2005)) predicts the barrier to isomerize to OCH_2CH_3 is higher than the barrier for the HOCH_2CH_2 radical intermediate to dissociate to ethenol + H by 2.1 kcal/mol, not lower. They conclude that the ethenol + H product channel would be the only significant product channel to compete with the direct abstraction reaction that forms $\text{H}_2\text{O} + \text{C}_2\text{H}_3$. Thus, our first experiments are designed to determine the barrier energies for the HOCH_2CH_2 radical adduct to dissociate to ethenol + H and to isomerize to OCH_2CH_3 .

IV. Publications Acknowledging DE-FG02-92ER14305 (2006 or later)

1. The photodissociation of propargyl chloride at 193 nm, L. R. McCunn, D. I. G. Bennett, L. J. Butler, H. Fan, F. Aguirre, and S. T. Pratt, *J. Phys. Chem. A* **110**, 843-850 (2006).
2. Unimolecular dissociation of the CH_3OCO radical: An intermediate in the $\text{CH}_3\text{O} + \text{CO}$ reaction, L. R. McCunn, K. -C. Lau, M. J. Krisch, L. J. Butler, J. - W. Tsung, and J. J. Lin, *J. Phys. Chem. A* **110**, 1625-1634 (2006).
3. Unimolecular dissociation of the propargyl radical intermediate of the $\text{CH} + \text{C}_2\text{H}_2$ reaction, L. R. McCunn, B. L. FitzPatrick, M. J. Krisch, L. J. Butler, C. -W. Liang, and J. J. Lin, *J. Chem. Phys.* **125**, 133306 (2006).
4. Characterization of the Methoxy Carbonyl Radical Formed via Photolysis of Methyl Chloroformate at 193.3 nm, M. J. Bell, K.-C. Lau, M. J. Krisch, D. I. G. Bennett, L. J. Butler and F. Weinhold, *J. Phys. Chem. A*, **111**, 1762-1770 (2007).
5. Investigation of the of the O + allyl addition/elimination reaction pathways from the $\text{OCH}_2\text{CHCH}_2$ radical intermediate, B. L. FitzPatrick, K. -C. Lau, L. J. Butler, S. -H. Lee, and J. J. Lin, submitted to *J. Chem. Phys.* (2008).

Production and Study of Ultra-cold Molecules Produced by Kinematic Cooling

David W. Chandler
Combustion Research Facility
Sandia National Laboratory
Livermore, CA 94551-0969
Email:chand@sandia.gov

Program Scope:

My research focuses on the field of chemical dynamics of gas phase molecular species. Chemical dynamics is the detailed study of the motion of molecules and atoms on potential energy surfaces in order to learn about the details of the surface as well as the dynamics of their interactions. We have recently produced measurable amounts of cold molecules using a unique crossed molecular beam scattering technique. The routine production of samples of ultracold molecules will provide a potent new tool for the study of many aspects of molecular interactions that are difficult to study with current technologies. For instance, studies of ultracold atomic species have already been able to refine the long range potentials of alkali diatomics from the determination of the energy of the highest vibrational state supported in the intermolecular potential by determination of the Feshbach resonance energies. This success motivates similar sorts of experiments utilizing molecule-atom interactions or molecule-molecule interactions to directly measure the density of quantum states near a dissociation threshold of a polyatomic species.

We define ultracold as the temperature range where the deBroglie wavelength (h/mv) of the molecule is of the same order of magnitude as its size. When molecules are cooled to these temperatures, several characteristics of the interaction both with each other and with external fields become observable. We are particularly interested in those new observables that enable new studies of chemical dynamics, both unimolecular and bimolecular. Three important properties of the interactions of molecules with each other and with their environment become important when molecules are cooled to ultra-low translational energies. These are the ability to interact with a single molecule for long periods of time, the ability to better manipulate matter with external fields, and, as the DeBroglie wavelength of the particles becomes large, the possibility to interact with the molecules as waves as well as particles. Each of these properties enables new experiments and new precision measurements. For example, the ability to interact with single molecules for long periods of time enables ultra-high resolution spectroscopy for studies of fundamental physics and the direct counting of the density of states for large molecules. The ability to manipulate matter with an external field allows one to orient molecules, shift energy levels, and to trap them for long periods of time in order to study their collisional interactions. Orientation of a molecule before subsequent photodissociation reduces the averaging associated with photon absorption by a randomly oriented molecule. New detail observed in the angular distributions of the photofragments will reveal underlying dynamics of the photodissociation process. A large DeBroglie wavelength makes it possible to perform unique interferometric studies with molecules,

such as the separation of mixtures of clusters by diffraction through a transmission grating. Additionally, the formation of interesting states of matter such as molecular Bose Einstein Condensates, degenerate Fermi gasses, and dipolar crystals have all been proposed.

The study of bimolecular collisions will be enhanced in several ways by the development of ultracold molecule sources. The appropriate utilization of ultracold molecules will enable the study of barrierless reactions, the study of non-adiabatic transitions between closely lying states (transition between tunable Stark states, for example), the study of tunneling resonances in relaxation and reactivity phenomena (for example, both shape and Feshbach type resonance are expected to contribute), and the study of collisions of oriented molecules. In order to study collisions between cold molecules, techniques need to be developed to make and store significant densities of ultracold molecules. No general technique is presently developed for the routine production and utilization of ultracold molecules. This proposal is to further the development of our process of kinematically cooling molecules by a single collision with an atom for the production of ultracold molecules and for the utilization of those molecules in scattering and bimolecular interaction experiments. Collisions can be studied either by trapping molecules and holding them for long periods of time or directing them toward each other using guiding fields. Both variations will be investigated here.

Progress Report:

The kinematic cooling method does not rely on any specific physical property of either colliding species except their masses, because production of a zero velocity sample is a consequence of the experimentally selectable energy and momenta of the collision pair. Moreover, this technique can be used to prepare a single, selectable ro-vibronic quantum state for trapping. We demonstrate this technique using inelastic collisions between NO molecules in one beam and Ar in the other, specifically $\text{NO}(^2\Pi_{1/2}, j=0.5) + \text{Ar} \rightarrow \text{NO}(^2\Pi_{1/2}, j'=7.5) + \text{Ar}$. We have now been able to make samples of NO7.5 that persist in our observation volume for 150 microseconds after they have been formed; see Figure 1. By modeling this fly out time we determine the temperature to be around 30 milliKelvin. We have built a magnetic trap utilizing permanent magnets for trapping NO in the $^2\Pi_{3/2}$ state. We are able to build a 300 milliKelvin deep trap for these molecules and are working at detecting molecules in this trap.

We have recently begun cooling NH_3 and ND_3 with collision with Ne because Ne has the same mass as ND_3 . This mass match means that the elastic and near elastic collisions will be the ones cooled and the 11 state and 22 state are the best ones to try to trap with electrostatic traps. We show a series of images of ND_3 after collision with Ne in Figure 2. Cold ND_3 can be observed for 40 μsec after the molecular beams. Figure 3 shows the existing electrostatic trap we are utilizing in our efforts to trap and detect the ultracold ND_3 molecule using the first order Stark effect. Because the ND_3 is lighter than the NO it moves more quickly for a given temperature and therefore leaves our viewing volume more quickly. The volume is also much reduced as we use 2+1 REMPI detection to detect the ammonia molecules and 1 + 1 REMPI for the NO molecules.

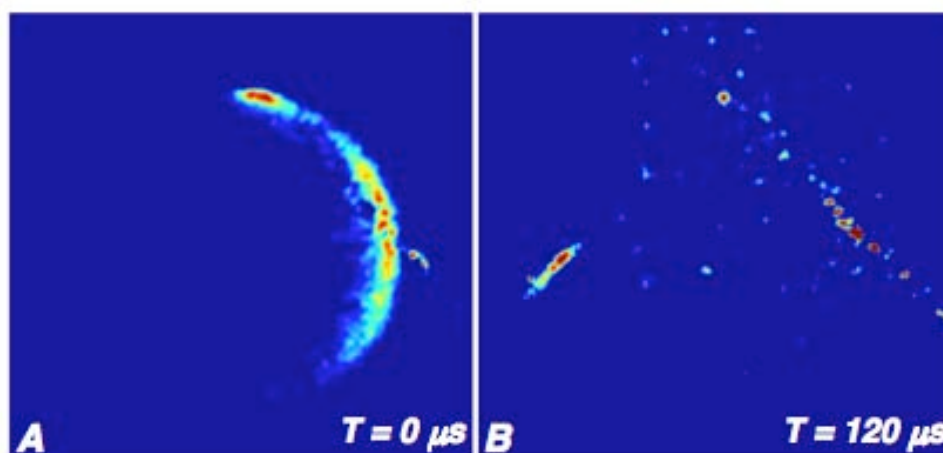


Figure 1: Image on the left is a velocity mapped ion image of the NO(X)7.5 quantum state at the peak of the scattering between NO and Ar. All velocities produced during the collision process are visible. The image on the right is taken 120 microseconds later. We observe that only the cold molecules, spot on centerline of image, persist.

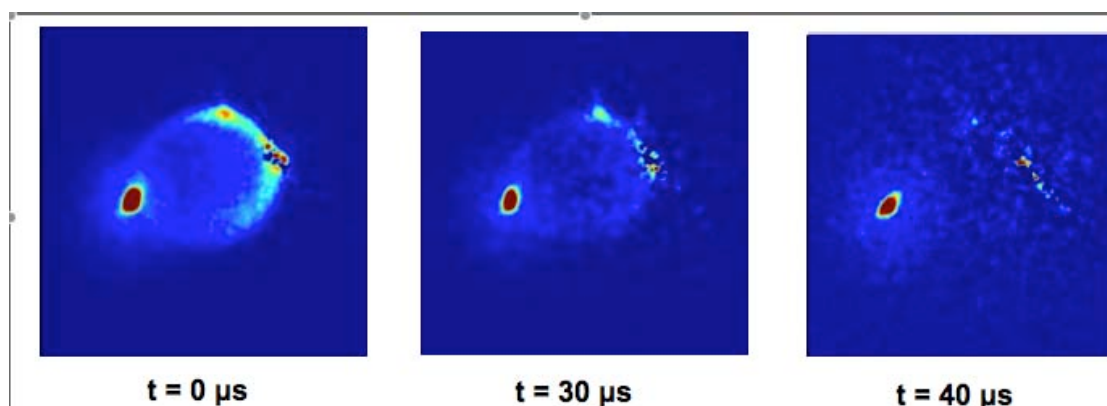


Figure 2: Images of ND₃ J=2, K=2 during and after scattering from Ne. The ND₃ is seeded in krypton to slow its velocity to shift the Newton Sphere such that forward scattering is more aligned with the laboratory zero.

Proposed Work:

Over the next year we anticipate to further develop our collisional cooling technique to produce colder samples and better quantify the velocity distribution we form in the crossed molecular beam apparatus. Additionally, we propose to take advantage of our ability to collisionally cool molecules in a crossed molecular beam apparatus in several ways. First, we will demonstrate the ability to trap cold molecules at the intersection region of the molecular beams with either electrostatic, magnetic or optical fields. Second, we will produce counter-propagating pulses of slowly moving molecules from the atom/molecular beam intersection region into a hexapole guide as they exit the interaction region for production of a molecular fountain. Third, we are building an

atomic magneto-optical trap (MOT) for the collisional cooling and trapping of molecules by collision with an ultracold atom of the same, or similar, mass.

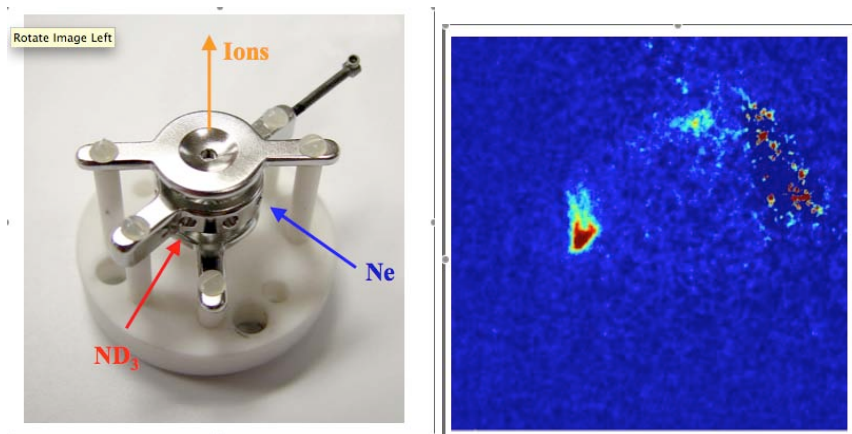


Figure 3: The image on the left is the electrostatic trap that the molecular beams collide inside of to make cold molecules. On the right is the image of ammonia at a 30 μ sec delay that is taken through the opening on the top of the trap.

Publications 2006-2008

Modification of the velocity distribution of H_2 molecules in a supersonic beam by intense pulsed optical gradients “Ramirez-Serrano J., Strecker K.E., Chandler D.W.” *Phys. Chem. Chem. Phys.* Volume: 8 Issue: 25 Pages: 2985-2989 (2006).

Probing spin-orbit quenching in $Cl(P_2)+H_2$ via crossed molecular beam scattering, Parsons B.F., Strecker K.E., Chandler D.W., *European Phys. J. D*, Volume: 38 Issue: 1 Pages: 15-20 2006.

Inelastic Energy Transfer: The NO-rare gas system, David W. Chandler and Steven Stolte, in *Gas Phase Molecular Reaction and Photodissociation Dynamics*, Editors K. C. Lin and P. D. Kleibert, Transworld Research Network, India. 2008.

Kinematic Cooling of Molecules, David W. Chandler and Kevin Strecker, World Scientific, editor IWM Smith. 2008.

Kinematic Production of Isolated milliKelvin molecules, K. E. Strecker and D. W. Chandler, *Phys. Rev. A*. Accepted for publication 2008.

Imaging of NO(A) products formed via the bound-bound A-X transition of NOAr van der Waals complexes W. G. Roeterdink, Kevin E. Strecker, Carl C. Hayden, Maurice H.M. Janssen and David W. Chandler, *J Phys. Chem.* Accepted for publication 2008.

Terascale Direct Numerical Simulation and Modeling of Turbulent Combustion

Jacqueline H. Chen (PI), Ed Richardson, David Lignell, and Chun Sang Yoo

Sandia National Laboratories, Livermore, California 94551-0969

Email: jhchen@sandia.gov

Program Scope

In this research program we have developed and applied terascale three-dimensional (3D) direct numerical simulation (DNS) of simple laboratory scale flows that reveal fundamental turbulence-chemistry interactions in combustion. The simulation benchmarks are designed to expose and emphasize the role of particular physical subprocesses in turbulent combustion. The simulations address fundamental science issues associated with chemistry-turbulence interactions that underly all practical combustion devices: extinction and reignition, stratified premixed flame propagation and structure, flame stabilization in autoignitive flows, autoignition under homogeneous charge compression ignition (HCCI) environments, and differential transport of soot in turbulent jet flames. In addition to the new understanding provided by these DNS, the data are being used to develop and validate predictive models.

Recent Progress

In the past year, significant computer allocations from 2007 and 2008 DOE INCITE grants have enabled us to perform terascale 3D DNS of turbulent flames with detailed chemistry. These studies focused on fundamental understanding and modeling of: 1) Stabilization of lifted autoignitive turbulent jet flames; 2) Extinction/reignition in turbulent hydrocarbon jet flames; 3) Lower-dimensional approximations to scalar dissipation rate; 4) Differential soot transport in a turbulent sooting jet flame; and 5) Effect of NO and H₂O addition on extinction/reignition in unsteady laminar strained flames. Highlights of some of our accomplishments are presented below, followed by a summary of future research directions.

Stabilization of Lifted Turbulent Hydrogen Jet Flames in Heated Coflow and Analysis of CMC Model

In many modern combustion systems such as diesel engines and gas turbines, fuel is injected into an environment of hot gases, and a flame may be stabilized through the recirculation of hot air and combustion products. DNS of the near field of a 3D spatially-developing turbulent lifted jet flame in heated coflow was performed with a detailed hydrogen-air mechanism to determine the stabilization mechanism [1]. The DNS was performed at a jet Reynolds number of 11,000 with over 900 million grid points. The results show that auto-ignition in a fuel-lean mixture immediately upstream of the flame base is the main source of stabilization of the lifted jet flame. Hydroperoxy intermediate is found to be a good marker of ignition. The flame stabilizes at a preferred fuel-lean mixture fraction where the scalar dissipation rate is low and the ignition delay is shortest. At the lifted flame base, heat release predominantly occurs through non-premixed combustion. Further downstream, both rich premixed and non-premixed flame modes emerge. In addition to auto-ignition, Lagrangian tracking of the flame base reveals the passage of coherent jet structures and their correlation with the flame base. Notably, the coherent jet structure induces a cyclic motion of the flame base about a mean stabilization height. This is confirmed by Lagrangian tracking of key scalars, heat release rate, and velocity at the stabilization point.

The DNS data set for the lifted hydrogen jet flame [1] was subsequently used to analyze the Conditional Moment Closure (CMC) approach in the autoignitive regime [2]. The timing and location of autoignition can be highly sensitive to turbulent fluctuations of composition. Therefore, second-order CMC equations, which provide transport equations for conditional fluctuations in turbulent reacting flows, were extended accounting for compressibility and differential diffusion. From the DNS data analysis of the CMC equations it was found that second-order moments are required to accurately model the conditional reaction rates; however it was demonstrated that the majority of the second-order reaction rate component was obtainable with a small subset of the species-temperature covariances. The balance of the second-order CMC equation reveals that transport due to turbulent flux between fluids with differing histories is responsible for the initial generation of conditional variances.

Lower-Dimensional Approximations to the Scalar Dissipation Rate from DNS of Plane Jet Flames

The difficulty of experimental measurements of the scalar dissipation rate in turbulent flames has led to many researchers approximating the true 3D scalar dissipation rate from 1D or 2D gradient

measurements. In doing so, some relationship must be assumed between the true values and their lower dimensional approximations. Previous theory is extended to develop these relationships solely as functions of the pdf of the angle to the measurement direction or plane. Assuming a form for this pdf enables analytical relationships between the pdfs of true and approximated scalar dissipation rate to be developed. As a consequence, in the case of a log-normal true pdf, new analytical relationships between the lower dimensional moments and those of the true pdf were derived. The true pdf is also reconstructed from the lower-dimensional approximations, and, significantly, the joint pdf of the scalar dissipation and any other scalar, such as chemical species or temperature. DNS of turbulent plane jet flames [3] were used to examine the statistics of scalar gradient alignment and verify our assumptions [4]. The theoretical relationships between the lower-dimensional and true moments were validated. A comparison of pdfs reconstructed from lower dimensional gradient projections with the true values show excellent agreement for a 2D measurement and also for a 1D measurement perpendicular to the mean flow variations. Comparisons of pdfs of thermal dissipation from DNS with those obtained via reconstruction from 2D experimental measurements by Kaiser and Frank show a very close match, indicating a universal character of this pdf. Reconstructed pdfs of the conditional mean of the hydroxyl mass fraction are compared with the true values and excellent agreement is obtained.

Extinction and reignition in 3D DNS of Turbulent Ethylene-air Jet Flames

A parametric study of flame extinction and reignition in turbulent nonpremixed temporally-evolving planar ethylene jet flames was performed using DNS. The simulation configuration and Reynolds number is very similar to a previous CO/H₂ parametric study in which the Reynolds number was varied [3], allowing direct comparison between the fuels. The objective is to understand the mechanism by which flames reignite following local extinction events. The simulations were performed at constant jet Reynolds number, but varying the Damköhler number. This was accomplished by varying the fuel and oxidizer stream compositions to affect the extinction scalar dissipation rate. As a result, the extent of peak flame extinction achieved was 35%, 70%, and nearly 100% in the three cases. The varying levels of flame extinction affect the degree of premixing of fuel, oxidizer, and combustion products, prior to the reignition event. The relative importance of reignition via auto-ignition through chemical chain branching and via flame propagation both normal and tangential to the stoichiometric surface was assessed. For the case that exhibits the greatest extent of extinction (near blowout conditions), significant premixing of fuel and oxidizer occurs in the absence of flames, and nearly complete reignition occurs in a premixed flame mode. Preliminary results suggest that the lowest extinction case reignites primarily through edge flame propagation, while mixed modes are evident in the medium extinction case. Moreover, it was found that the degree of extinction, and hence burning flame surface area, has a strong impact on scalar mixing and the overall heat release rate in the flames.

3D DNS of Soot Formation in a Turbulent Ethylene-Air Jet Flame and CMC Model Validation

DNS of soot formation in a nonpremixed, temporal ethylene jet flame was performed using a reduced, 19-species ethylene mechanism, and a four-step, semi-empirical soot model using the method of moments. The simulation extends previous work in two-dimensional decaying turbulence [5] to a three-dimensional jet flame [6]. The analysis centered on the importance of differential diffusion between soot and the mixture fraction, in which flame strain and curvature play dominant roles in transporting soot into or out of reaction zones. The 3D study has provided statistics of the soot and flame dynamics, and generally confirms the 2D results. However, the effect of flame-normal diffusion was significantly more important in the 3D simulation than in the 2D simulation due to the greater extent of mixing between the fuel and oxidizer streams.

The DNS database was subsequently used to analyze the conditional moment soot transport equation. The CMC model has the potential to capture unsteady soot growth and transport of soot in the mixture fraction coordinate and has been successfully applied. A new CMC model developed by Hewson et al. [7] was evaluated by comparing exact terms in the conditional moment equation to modeled closures of these terms [8]. Good agreement was found for the model for the differential diffusion of soot, which was shown in the 2D and 3D DNS to be important in describing soot formation and transport.

Future Plans

Next-generation alternative-fuel internal combustion engines will operate in nonconventional, mixed-mode, turbulent combustion under previously unexplored ‘turbulence-chemistry’ regimes. Compared to current engines, combustion in next-generation engines are likely to be characterized by higher pressures, lower temperatures, higher levels of dilution and/or excess air (fuel-lean). Combustion processes in these environments, combined with new physical and chemical fuel properties associated with non-petroleum based fuels, results in complex interactions that are unknown even at a fundamental level. Therefore, we propose to perform the following petascale DNS that capture some of these ‘turbulence-chemistry’ interactions, and in particular, capture and discriminate the effects of variations in fuel composition.

Flame Stabilization in Turbulent Lifted Autoignitive Jet Flames

This simple laboratory configuration enables the study of flame stabilization mechanisms in an autoignitive, heated coflow. The roles of autoignition, flame propagation, and large-eddy structure at the lifted base will be identified. A range of fuels – ethylene, methanol, ethanol, and n-heptane – exhibiting a wide range of ignition characteristics representative of oxygenated fuels and multi-stage ignition fuels will be considered. A parametric study with co-flow temperature and ambient pressure will be performed. Of particular interest is the influence of turbulent transport on the slower, rate-limiting chemical reactions that occur in the negative temperature coefficient regime of multi-stage ignition fuels such as n-heptane at high pressure. This chemical kinetic-turbulent transport coupling may have a significant effect on the ignition timing, and hence, stabilization position.

HCCI Combustion with Thermal and Concentration Stratification

A major challenge posed by HCCI engine combustion is to control the heat release rate, suppressing the occurrence of a rapid rate of pressure rise. One possible control strategy is to introduce inhomogeneities in the temperature or mixture composition in order to produce the desired heat release. Moreover, incomplete turbulent mixing and temperature stratification between the bulk gases and the cylinder wall lead to spatial nonuniformities that also contribute to a range of combustion modes that are distinct from homogeneous autoignition. Therefore, a better understanding of autoignition of an inhomogeneous charge at constant volume is crucial in the development of control strategies for HCCI engines. We propose to study the influence of temperature and, independently, concentration stratification on characteristics of ignition and subsequent combustion in an HCCI-like environment, and to provide information relevant to the modeling of HCCI combustion. Fuels ranging from n-heptane to ethanol will be considered. Issues addressed include: dependence of mode of combustion (deflagrative versus sequential ignition front propagation; premixed versus nonpremixed) on thermal and concentration stratification, and heat-release rate and emissions dependence upon the distribution of the different modes of combustion.

Turbulent Stratified Turbulent Jet Flames

In stratified combustion, the fuel and oxidizer are neither completely mixed nor completely segregated prior to combustion, and therefore traditional modeling approaches based on pure ‘premixed’ or ‘nonpremixed’ burning modes are inadequate. An example of this is found in aero-gas turbine engines where fuel and secondary air are injected at different spatial locations, resulting in a nonuniform equivalence ratio at the flame front. Therefore, the objective of the proposed DNS is to determine the combustion efficiency and emissions characteristics (*i.e.* NO and CO) resulting from initially stratified distributions of fuel and oxidizer in a turbulent slot Bunsen flame configuration. The flame structure and burning velocity under stratified conditions will be compared to the equivalent uniformly premixed case. 3D DNS with detailed methane and ethanol chemistry will be performed in a stratified turbulent slot jet Bunsen flame configuration. A parametric study will be performed varying the integral scale of the reactant stratification and the range of equivalence ratios in the stratification at the slot burner exit. The parameters will be chosen such that combustion occurs in the thin-reaction zones to broken reaction zones regimes.

References:

1. C. S. Yoo, J. H. Chen, and R. Sankaran, “3D Direct Numerical Simulation of Turbulent Lifted Hydrogen/Air Jet Flame in Heated Coflow,” submitted to *Combust. Flame* (2008).

2. E. S. Richardson, C. S. Yoo, and J. H. Chen, "Analysis of Second-Order Conditional Moment Closure Applied to an Autoignitive Lifted Hydrogen Jet Flame," to appear *Proceedings of the Combustion Institute*, **32** (2008).
3. E. Hawkes, R. Sankaran, J. Sutherland, and J. H. Chen, "Scalar Mixing in DNS of Temporally-Evolving Plane Jet Flames with Detailed CO/H₂ Kinetics," *Proc. of the Combustion Institute*, **31**:1633-1640, (2007).
4. E. R. Hawkes, R. Sankaran, J. H. Chen, S. Kaiser, and J. H. Frank, "An Analysis of Lower-Dimensional Approximations to the Scalar Dissipation Rate using DNS of Plane Jet Flames," to appear *Proceedings of the Combustion Institute*, **32** (2008).
5. D. Lignell, J. H. Chen, P. J. Smith, T. Lu and C. K. Law, "The effect of flame structure on soot formation and transport in turbulent nonpremixed flames using DNS," *Combust. Flame* 151:2-28 (2007).
6. D. Lignell, J. H. Chen, P. J. Smith, T. Lu and C. K. Law, "The effect of flame structure on soot formation and transport in turbulent nonpremixed flames using DNS," submitted to *Combust. Flame* (2006).
7. J. Hewson, A. Ricks, S. Tieszen, A. Kerstein, R. Fox, "Conditional Moment Closure with Differential Diffusion for Soot Evolution in Fire, Center for Turbulence Research," *Proceedings of the Summer Program*, 2006.
8. D. Lignell, J. C. Hewson, and J. H. Chen, "Apriori Analysis of Conditional Moment Closure Modeling of a Temporal Ethylene Jet Flame with Soot Formation using DNS," to appear *Proceedings of the Combustion Institute*, **32** (2008).

BES Publications (2006-2008)

1. J. H. Chen, E. R. Hawkes, R. Sankaran, S. D. Mason, and H. G. Im, "DNS of Ignition Front Propagation in a Constant Volume with Temperature Inhomogeneities, Part I: Fundamental Analysis and Diagnostics," *Combust. Flame*, **145**: 128-144. (2006).
2. E. R. Hawkes, R. Sankaran, P. Pebay, and J. H. Chen, "DNS of Ignition Front Propagation in a Constant Volume With Temperature Inhomogeneities, Part II: Parametric Study", *Combust. Flame*, **145**: 145. (2006).
3. S. Liu, J. C. Hewson, and J. H. Chen, "Nonpremixed *n*-heptane autoignition in unsteady counterflow, " *Combust. Flame*, **145**: 730-739, (2006).
4. R. Sankaran, E. R. Hawkes, J. H. Chen, T. Lu, and C. K. Law, "Structure of a Spatially-Developing Lean Methane-Air Turbulent Bunsen Flame," *Proc. of the Combustion Institute*, **31**:1291-1298, (2007).
5. E. Hawkes, R. Sankaran, J. Sutherland, and J. H. Chen, "Scalar Mixing in DNS of Temporally-Evolving Plane Jet Flames with Detailed CO/H₂ Kinetics," *Proc. of the Combustion Institute*, **31**:1633-1640, (2007).
6. D. J. Cook, H. Pitsch, J. H. Chen, and E. R. Hawkes, "Flamelet-Based Modeling of Autoignition with Thermal Inhomogeneities for Application to HCCI Engines," *Proc. of the Combustion Institute*, **31**: 2903-2911, (2007).
7. J. C. Sutherland, P. J. Smith, and J. H. Chen, "A quantitative method for apriori evaluation of combustion reaction models," *Combust. Theory and Modelling*, **11**, 287-303, (2007).
8. D. Lignell, J. H. Chen, P. J. Smith, T. Lu and C. K. Law, "The effect of flame structure on soot formation and transport in turbulent nonpremixed flames using DNS," *Combust. Flame* 151:2-28 (2007).
9. D. Lignell, J. H. Chen, and P. J. Smith, "Three-dimensional DNS of Soot Formation and Transport in a Temporally-Evolving Non-premixed Ethylene Jet Flame," to appear *Combust. Flame* (2008).
10. C. S. Yoo, J. H. Chen, J. H. Frank, "A Numerical Study of Transient Ignition and Flame Characteristics of Diluted Hydrogen Versus Heated Air in Counterflow," submitted to *Combust. Flame* (2007).
11. N. Chakraborty, E. R. Hawkes, J. H. Chen, and S. Cant, "The Effects of Strain Rate and Curvature on Surface Density Function Transport in Turbulent Premixed Methane-Air and Hydrogen-Air Flames, a Comparative Study," to appear *Combust. Flame* (2008).
12. F. Bisetti, J. Y. Chen, E. R. Hawkes, and J. H. Chen, "Probability Density Function Treatment of Turbulence-Chemistry Interactions during the Ignition of a Temperature-Stratified Mixture for Application to HCCI Engine Modeling," submitted to *Combust. Flame* (2007).
13. E. R. Hawkes, R. Sankaran, J. H. Chen, S. Kaiser, and J. H. Frank, "An Analysis of Lower-Dimensional Approximations to the Scalar Dissipation Rate using DNS of Plane Jet Flames," to appear *Proc. of the Combustion Institute*, **32** (2008).
14. E. S. Richardson, C. S. Yoo, and J. H. Chen, "Analysis of Second-Order Conditional Moment Closure Applied to an Autoignitive Lifted Hydrogen Jet Flame," submitted to *Proc. of the Combustion Institute*, **32** (2008).
15. U. D. Lee, C. S. Yoo, J. H. Chen, and J. H. Frank, "Effects of H₂O and NO on Extinction and Reignition of Vortex-Perturbed Hydrogen Counterflow Flames," to appear *Proc. of the Combustion Institute*, **32** (2008).
16. D. Lignell, J. C. Hewson, and J. H. Chen, "Apriori Analysis of Conditional Moment Closure Modeling of a Temporal Ethylene Jet Flame with Soot Formation using DNS," submitted to *Proc. of the Combustion Institute*, **32** (2008).
17. F. Bisetti, J. Y. Chen, E. R. Hawkes, and J. H. Chen, "Differential Diffusion Effects During the Ignition of a Thermally Stratified Premixed Hydrogen-Air Mixture Subject to Turbulence," submitted to *Proc. of the Combustion Institute*, **32** (2008).
18. T. Lu, J. H. Chen, and C. K. Law, "On-the-fly Stiffness Removal for DNS," submitted to *Proc. of the Combustion Institute*, **32** (2008).
19. C. S. Yoo, J. H. Chen, and R. Sankaran, "3D Direct Numerical Simulation of Turbulent Lifted Hydrogen/Air Jet Flame in Heated Coflow," submitted to *Combust. Flame* (2008).
20. T. Lu, C. S. Yoo, J. H. Chen, and C. K. Law, "Analysis of a Turbulent Lifted Hydrogen/Air Jet Flame from DNS with Computational Singular Perturbation," submitted to *Combust. Flame* (2008).

Dynamics and Energetics of Elementary Combustion Reactions and Transient Species

Grant DE-FG03-98ER14879

Robert E. Continetti
Department of Chemistry and Biochemistry
University of California San Diego
9500 Gilman Drive
La Jolla, CA 92093-0340
rcontinetti@ucsd.edu

April 4, 2008

I. Program Scope

This research program focuses on the preparation and study of transient neutral species and collision complexes relevant to combustion phenomena. In the past year, we have brought to fruition significant aspects of our studies of the HOCO and DOCO free radicals that play essential roles as intermediates in the $\text{OH} + \text{CO} \rightarrow \text{H} + \text{CO}_2$ reaction. We have also extended our studies of oxygenated organic species to include several small carboxyl radicals, including the propyloxy, isobutyroxy and pyruviloxy radicals. Information on the energetics and reaction dynamics of species like these is critical to evaluating the roles they may play in combustion and the validation of theoretical approaches to predicting the dynamics of combustion reactions. The experimental approach taken to these studies uses photodetachment of precursor anions. The technique of photoelectron-photofragment coincidence (PPC) spectroscopy on a mass-selected negative ion beam allows the preparation of mass- and energy-selected neutral species. The dissociation pathways of unstable neutral products can then be measured using translational spectroscopy. In addition, the employment of large-solid-angle imaging techniques enables measurement of the angular distributions for both the photoelectrons and photofragments, providing further insights into the dissociative photodetachment (DPD) dynamics. A major initiative is currently underway to construct a cryogenically cooled (10K) ion trap that will allow radiative cooling of the ions to remove any uncertainty in the parent anion internal energy.

II. Recent Progress

A. Probing the $\text{OH} + \text{CO} \rightarrow \text{HOCO} \rightarrow \text{H} + \text{CO}_2$ reaction by photodetachment of HOCO^-

In the past year we have published three manuscripts focusing on characterization of the HOCO free radical and the potential energy surface governing the important $\text{OH} + \text{CO} \rightarrow \text{H} + \text{CO}_2$ reaction. These experiments extend our earlier work on this system at a photon energy of 4.80 eV,¹ and allow the identification of photodetachment processes leading to the production of stable HOCO free radicals and both the $\text{H} + \text{CO}_2$ and $\text{OH} + \text{CO}$ dissociation channels on the neutral surface, in coincidence with the detached electron. The first of these focused on isotope effects in the product energy distributions and branching ratios obtained by the dissociative photodetachment (DPD) of HOCO^- and DOCO^- at a photon energy of 3.21 eV. These experiments confirmed that the $\text{H} + \text{CO}_2 + e^-$ channel is open below the calculated dissociation barrier,² indicating that quantum mechanical tunneling is important for this channel even near the bottom of the HOCO well. Furthermore, it appears at all wavelengths that the $\text{OH} + \text{CO}$ product channel is observed at and below the calculated energetic limit. In this case, tunneling is not possible and the most likely explanation are hot bands in the HOCO^- anion, assuming the quantum chemical calculations on the energetics of this system are accurate. Isotopic substitution by deuterium in the parent ion was found to reduce the product branching ratio for the $\text{D} + \text{CO}_2$ channel, consistent with tunneling playing a role in this dissociation

pathway. These results can be compared with recent six-dimensional quantum dynamics simulations of the DPD of HOCO^- by Gray, Goldfield and co-workers.³ There is good qualitative agreement with the theory, with the exception of the absence of significant tunneling in the $\text{HOCO} \rightarrow \text{H} + \text{CO}_2$ pathway on the LTSH potential energy surface⁴ used in the calculations. Given that this surface was optimized for reproducing kinetic data, and thus has a relatively poor description of the HOCO well and the barrier between the well and the $\text{H} + \text{CO}_2$ product channel, this may not be a major surprise. A refined potential energy surface for both the neutral and the parent anion are required for more accurate quantum dynamics predictions. Experimentally, the outstanding issue is better characterization of the parent anion vibrational temperature, in particular in light of the $\text{OH/OD} + \text{CO}$ product channel results. This critical issue will be experimentally addressed with the new cryogenic ion trap currently under construction.

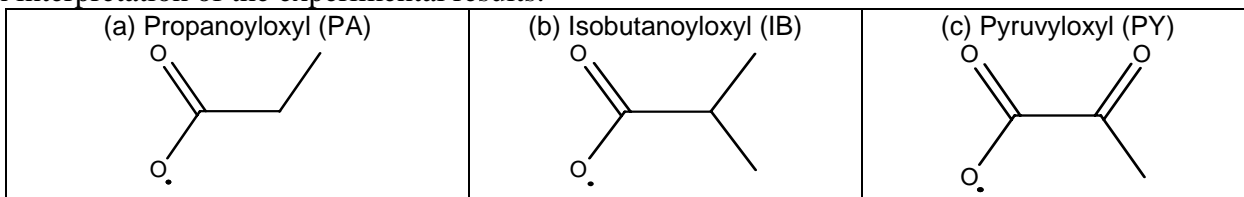
This study was extended by examining the photoelectron-photofragment angular correlations in a manuscript in press in the journal *Molecular Physics*.⁵ Anisotropic photofragment angular distributions were observed in the $\text{HOCO}^-/\text{DOCO}^- + h\nu \rightarrow \text{OH/OD} + \text{CO} + e^-$ channel. The anisotropy parameters were obtained for the laboratory frame (LF) angular distributions of photoelectrons of all three DPD channels and photofragments $\text{OH} + \text{CO}$. The photoelectron angular distributions (PAD) were also studied within the photofragment recoil frame (RF) using the coincidence data. The comparison of LF- and RF-PAD in the $\text{OH} + \text{CO} + e^-$ channel shows the latter one is more isotropic, indicating that the lifetime of the neutral HOCO free radicals that dissociate into $\text{OH} + \text{CO}$ is commensurate with the molecular rotational period. The radical lifetime was examined as a function of the orientation of the transition dipole, with upper limits of 9×10^{-13} sec and 1.3×10^{-12} sec estimated for HOCO and DOCO lifetime for dissociation into $\text{OH/OD} + \text{CO}$, respectively.

Experiments were also performed near the threshold for photodetachment of HOCO^- at a photon energy of 1.60 eV as reported in *Physical Review Letters*.⁶ In this work, a striking two-photon process was observed, yielding a very anisotropic photoelectron angular distribution (PAD) consistent with a strong molecular alignment in absorption of the first photon. A quantitative analysis of the PAD reveals this is associated with a temporary anion formed by a *p*-wave shape resonance and the PAD in the two-photon signal is a result of interfering *s*- and *d*-partial waves within the atomic approximation. The extracted intensity and phase shift of the partial waves were found to be consistent with the Wigner threshold law for photodetachment. Use of a continuum resonance for alignment has, to the best of our knowledge, not been observed before. These results were confirmed by the photoelectron-photofragment angular correlations reported in ref. 5 concerning the two-photon DPD of HOCO^- , showing that when the photon energy is near the photodetachment threshold, a molecular anion like HOCO^- can be effectively aligned through a continuum shape resonance.

B. Stability of oxygenated reactive intermediates: simple carboxyl radicals

Oxygenated organic radical species, including carboxyl radicals, are known to play important roles in complex atmospheric and combustion phenomena (e.g., likely component of propionic acid, $\text{CH}_3\text{CH}_2\text{CO}_2\text{H}$, being observed in propane flames).⁷ Studies of carboxyl radicals and their corresponding anions can provide insights into the energetics and dynamics of these types of reactive species. Photodetachment of anions generated by three carboxylic acids and the dissociation dynamics of the subsequent carboxyl radicals have been studied using photoelectron-photofragment coincidence technique at 258 nm (4.80 eV). The results show that the propanoyloxyl (PA, $\text{CH}_3\text{CH}_2\text{CO}_2^\cdot$) radical completely dissociates on the μs timescale of the experiment, yielding ethyl radicals (29 amu) and CO_2 products (44 amu), with a kinetic energy release peaking at 0.5 eV. The lack of a stable PA radical product stands in contrast to the smaller acetyloxyl radical that was previously found to produce both stable and dissociative

radicals.⁸ These studies have also been extended to the branched and substituted isobutanoyloxy (IB, $\text{CH}_3\text{CH}_2\text{CHCO}_2$) and pyruviloxy (PY, CH_3COCO_2) radicals, respectively. In these more complex species, results similar to acetyloxy radical were found, with detection of a stable neutral component (~90%) with ~10% dissociating. The dissociation pathways in these cases were found to product $\text{CH}_3\text{CHCH}_3 + \text{CO}_2$ in the case of IB and $\text{CH}_3\text{CO} + \text{CO}_2$ in the case of PY. The kinetic energy release from dissociation of these radicals was found to peak around 0.25 eV, much lower than the alkyloxy radicals. This probably is a result of the stabilization of the more substituted radicals. Density Functional Theory (DFT) calculations are currently underway to aid in interpretation of the experimental results.



C. Cryogenically cooled linear ion beam trap

Preparation for the construction of a cryogenic linear ion trap is nearing completion, and assembly is about to begin. The vacuum chamber should be delivered by the end of April, 2008. This trap will enable the study of internally cold ions, leading to more precise determinations of

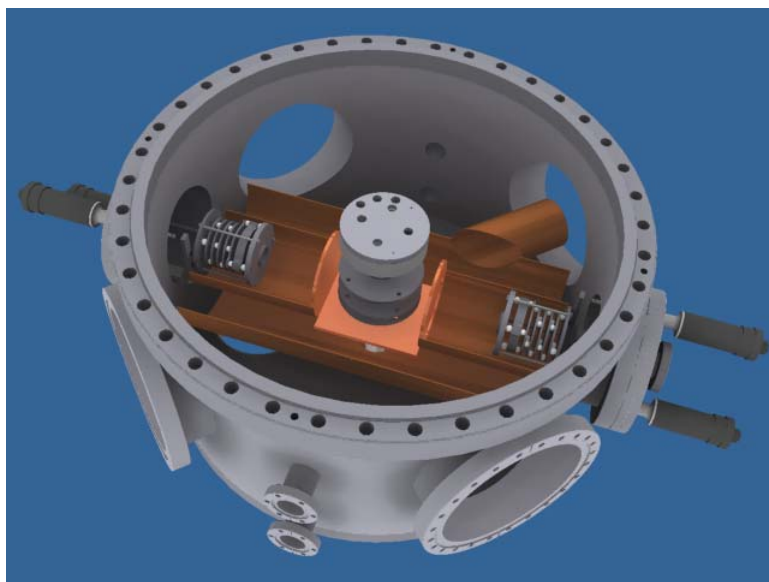


Figure 1. Assembly view of the cryogenically cooled linear ion beam trap with magnetic and cryo-shielding cut away to show the photoelectron detector.

the energies of molecular dissociation processes and the internal states of various species, as well as remove ambiguities in dissociation processes due to potential internal excitation.⁹ In addition, by monitoring the energy spectra as a function of trapping time, the radiative cooling rates for complex molecular ions can be studied.

This type of trap consists of two electrostatic mirrors which will reflect bunches of ions along a central axis, analogous to an optical resonator.¹⁰ Ions oscillating in the trap have well defined and consistent momenta, which makes it ideal for the DPD experiments carried out in this lab.

The design also features a large field-free region at the center of the resonator which will serve as the interaction point between the laser pulse and the ion packet. This interaction produces an electron which will be detected by a full solid angle, velocity mapped imaging, time-and-position sensitive detector placed at the center of the cavity, and multiple neutral products that will continue downstream along the center-of-mass trajectory and impact another full solid angle multiparticle time-and-position sensitive detector.¹¹

The resonator will be surrounded by cryogenically cooled shields and components: the electrostatic mirrors and most of the resonator length will be held at approximately 10 K. The middle of the resonator contains the electron detector and a magnetic shield that will be 50 K, as

will be a second shield surrounding the entire assembly to reduce the heat load on the 10 K parts. The ions will spend practically no time in the 50 K environment and will have no exposure to room temperature radiation, ensuring that they can radiatively cool to the ground vibrational and electronic state and low rotational states as well.

III. Future plans

In the coming months we are focusing our efforts on construction and testing of the cryogenic linear ion trap. The chamber has already been commissioned and other components are being designed and built currently. The trap will be installed on a second apparatus in the laboratory, and thus we are planning to also extend our studies of the HOCO system prior to trap completion by examining simultaneous one- and two-photon excitation pathways to see if interference phenomena can be used to affect the overall photoelectron spectrum and product branching ratios. The studies of carboxyl radicals will continue as well, and should lead to a publication in the coming year. Efforts to study other hydroxyl radical reactions with organic species will also be pursued by forming precursor cluster anions such as hydroxide – acetone (OH^-)(CH_3COCH_3) and others.

IV. DOE Publications: 2006 – 2008

1. Z. Lu, Q. Hu, J.E. Oakman and R.E. Continetti, “Dynamics on the HOCO potential energy surface studied by dissociative photodetachment of HOCO^- and DOCO^- .”, *J. Chem. Phys.* **126**, 194305-1 – 194305-11 (2007).
2. Z. Lu and R.E. Continetti, “Alignment of a molecular anion via a shape resonance in near-threshold photodetachment.”, *Phys. Rev. Lett.* **99**, 113005-1 – 113005-4 (2007). Featured in the Virtual Journal of Ultrafast Science, vol. 6, No. 10, 2007. <http://www.vjulfrafast.org/>
3. Z. Lu, J.E. Oakman, Q. Hu and R.E. Continetti, “Photoelectron-photofragment angular correlations in the dissociative photodetachment of HOCO^- .”, *Molec. Phys.* (in press, 2008).

V. References Cited

-
1. T.G. Clements, R.E. Continetti and J.S. Francisco, *J. Chem. Phys.* **117**, 6478 (2002).
 2. H.-G. Yu, J.T. Muckerman and T. Sears, *Chem. Phys. Lett.* **349**, 547 (2001).
 3. S. Zhang, D. M. Medvedev, E. M. Goldfield, and S. K. Gray, *J. Chem. Phys.* **125**, 164312 (2006).
 4. M. J. Lakin, D. Troya, G. C. Schatz, and L. B. Harding, *J. Chem. Phys.* **119**, 5848 (2003).
 5. Z. Lu, J.E. Oakman, Q. Hu and R.E. Continetti, *Molec. Phys.* (in press, 2008).
 6. Z. Lu and R.E. Continetti, *Phys. Rev. Lett.* **99**, 113005 (2007).
 7. E. Zervas, *Environmental Engineering Science* **22**, 651 (2005).
 8. Z. Lu and R.E. Continetti, *J. Phys. Chem. A* **108**, 9962 (2004).
 9. Z. Lu, Q. Hu, J. E. Oakman, and R. E. Continetti, *J. Chem. Phys.* **126**, 19305 (2007).
 10. M. Dahan, R. Fishman, O. Heber, M. Rappaport, N. Altstein, D. Zajfman, and W. J. van der Zande, *Rev. Sci. Instrum.* **69**, 76 (1998).
 11. K.A. Hanold, A.K. Luong, T.G. Clements, and R.E. Continetti, *Rev. Sci. Instrum.* **70**, 2268 (1999).

Studies of Flame Chemistry with Photoionization Mass Spectrometry

Terrill A. Cool
School of Applied and Engineering Physics
Cornell University, Ithaca, New York 14853
tac13@cornell.edu

Project Scope

Studies of the flame chemistry of oxygenated fuels or fuel additives (dimethyl ether, ethanol, alkyl esters), proposed as clean burning alternatives to conventional liquid hydrocarbon fuels derived from petroleum, are principal themes of our current research. Kinetic model development for these reaction systems requires direct measurements of the absolute concentrations of combustion intermediates in laboratory flames chosen to reveal underlying reaction mechanisms. While jet-stirred reactors, shock tubes, flow reactors, laminar flame speed measurements and non-premixed counter-flow diffusion flames offer many advantages for modeling studies under conditions close to those encountered in practical combustion devices, low pressure burner-stabilized premixed flames provide the spatial resolution needed for the examination of detailed reaction pathways.

Photoionization mass spectrometry (PIMS) using monochromated synchrotron radiation, applied to the selective detection of reaction intermediates in low-pressure premixed flat flames, is uniquely suited for the development and testing of kinetic models of combustion chemistry. A flame-sampling PIMS instrument, developed at the Advanced Light Source (ALS) of the Lawrence Berkeley National Laboratory is leading to major advances in the detection of reaction intermediates in laboratory flames and the measurement of their concentrations. These advances yield improved kinetic models for the combustion of the major classes of modern fuels and fuel blends, including biofuels. They also enable measurements of fundamental properties (photoionization cross sections and ionization energies) of selected reaction intermediates. This instrument is the first to use easily tunable vacuum ultraviolet synchrotron radiation for PIMS studies of flame species.

Recent Progress

A. Isomer-specific influences on the composition of reaction intermediates in dimethyl ether/propene and ethanol/propene flames, Juan Wang, Ulf Struckmeier Bin Yang, Terrill A. Cool, Patrick Oßwald, Katharina Kohse-Höinghaus, Tina Kasper, Nils Hansen, Phillip R. Westmoreland

This work provides experimental evidence on how the molecular compositions of fuel-rich low-pressure premixed flames are influenced as the oxygenates dimethyl ether (DME) or ethanol are incrementally blended into a propene base fuel. Ten different flames with a carbon-to-oxygen ratio of 0.5, ranging from 100% propene ($\phi = 1.5$) to 100% oxygenated fuel ($\phi = 2.0$), are analyzed with flame-sampling molecular-beam mass spectrometry employing electron- or photoionization. Absolute mole fraction profiles for flame species with masses ranging from $m/z = 2$ (H_2) to $m/z = 80$ (C_6H_8) are analyzed with particular emphasis on the formation of harmful emissions. Fuel-specific destruction pathways, likely to be initiated by hydrogen abstraction, appear to lead to benzene from propene combustion and to formaldehyde and acetaldehyde through DME and ethanol combustion, respectively. While the concentration of acetaldehyde

increases ten-fold as propene is substituted by ethanol, it decreases as propene is replaced with DME. In contrast, the formaldehyde concentration rises only slightly with ethanol replacement but increases markedly with addition of DME. Allyl and propargyl radicals, the dominant precursors for benzene formation, are likely to be produced directly from propene decomposition or via allene and propyne. Benzene formation through propargyl radicals formed via unsaturated C₂ intermediates in the decomposition of DME and ethanol is negligibly small. As a consequence, DME and ethanol addition lead to similar reductions of the benzene concentration.

B. Composition of reaction intermediates for stoichiometric and fuel-rich dimethyl ether flames: photoionization mass spectrometry and modeling studies,

Juan Wang, Bin Yang, Terrill A. Cool, Marcos Chaos, Fredrick L. Dryer, Tina Kasper, Nils Hansen, Patrick Oßwald, Katharina Kohse-Höinghaus, Phillip R. Westmoreland

Molecular-beam synchrotron photoionization mass spectrometry (PIMS) is used for measurements of species mole fraction profiles for low-pressure premixed dimethyl ether (DME) flames with equivalence ratios ranging from near-stoichiometric conditions ($\Phi=0.93$) to fuel-rich flames near the limits of flat-flame stability ($\Phi=1.86$). The results are compared with predictions of a recently modified kinetic model for DME combustion [Zhao et al., *Int. J. Chem. Kinetics*, **2008**, *40*, 1-18] that has been extensively tested against laminar flame speed measurements, jet-stirred reactor experiments, pyrolysis and oxidation experiments in flow reactors, species measurements for burner-stabilized flames and ignition delay measurements in shock tubes. Comparisons of measurements of the composition of reaction intermediates with predictions over this broad range of equivalence ratios are uniquely sensitive to the details of the reaction mechanisms incorporated in the model. Excellent agreement between measurements and predictions is found for all major and intermediate species with the exception of the methanol intermediate. These discrepancies and measurements of mole fractions for ethyl methyl ether, a species not included in the model, suggest directions for further evolution of the DME flame model.

C. Near-threshold Absolute Photoionization Cross Sections of some Reaction

Intermediates in Combustion, Juan Wang, Bin Yang, Terrill A. Cool, Nils Hansen, Tina Kasper

The use of photoionization mass spectrometry for the development of quantitative kinetic models for the complex combustion chemistry of both conventional hydrocarbon fuels and oxygenated biofuels requires near-threshold measurements of absolute photoionization cross sections for numerous reaction intermediates. Near-threshold absolute cross sections for molecular and dissociative photoionization for 20 stable reaction intermediates (methane, ethane, propane, *n*-butane, cyclopropane, methylcyclopentane, 1-butene, *cis*-2-butene, isobutene, 1-pentene, cyclohexene, 3,3-dimethyl-1-butene, 1,3-hexadiene, 1,3-cyclohexadiene, methyl acetate, ethyl acetate, tetrahydrofuran, propanal, 1-butyne, 2-butyne) are presented. Previously measured total photoionization cross sections for 9 of these molecules are in good agreement with the present results. The measurements are performed with photoionization mass spectrometry (PIMS) using a monochromated VUV synchrotron light source with an energy resolution of 40 meV (fwhm) comparable to that used for flame-sampling molecular beam PIMS studies of flame chemistry and reaction kinetics.

D. A detailed chemical reaction mechanism for oxidation of four small alkyl esters in laminar premixed flames,

Charles K. Westbrook, William J. Pitz, Phillip R. Westmoreland, Fredrick L. Dryer, Marcos Chaos, Patrick Oßwald, Katharina Kohse-Höinghaus, Terrill A. Cool, Juan Wang, Bin Yang, Nils Hansen, Tina Kasper

A detailed chemical kinetic reaction mechanism has been developed for a group of four small alkyl ester fuels, consisting of methyl formate, methyl acetate, ethyl formate and ethyl acetate. This mechanism is validated by comparisons between computed results and recently measured intermediate species mole fractions in fuel-rich, low-pressure, premixed laminar flames. The model development employs a principle of similarity of functional groups in constraining the H atom abstraction and unimolecular decomposition reactions in each of these fuels. As a result, the reaction mechanism and formalism for mechanism development are suitable for extension to larger oxygenated hydrocarbon fuels, together with an improved kinetic understanding of the structure and chemical kinetics of alkyl ester fuels that can be extended to biodiesel fuels. Variations in concentrations of intermediate species levels in these flames are traced to differences in molecular structure of the fuel molecules.

Future Plans

Flame chemistry of alkyl esters (biodiesel). Studies of diesel engine emissions for both neat biodiesel fuels and for blends of oxygenated additives with petroleum diesel show pronounced fuel-specific trends in the composition of emitted pollutants. We are studying the influences of fuel structure on the composition of reaction intermediates in the combustion of 12 selected methyl and ethyl ester surrogates for biodiesel fuels:

methyl and ethyl formate	methyl 2-methylpropenoate
methyl and ethyl acetate	methyl butanoate
methyl and ethyl propanoate	methyl isobutanoate
methyl and ethyl propenoate	methyl crotonate

The broad objective of this work is to define the reaction pathways that account for fuel-specific differences in the production of aldehydes, ketones, CO, prompt CO₂, and the unsaturated hydrocarbon precursors to PAH and soot.

These 12 fuels have been selected using three different criteria intended to identify fuel-specific effects on the flame chemistry. First, comparison of the flames of structural isomers allows detailed analysis of the influence of functional groups on the fuel consumption pathways. Similar overall combustion characteristics (e.g., temperature profiles, equivalence ratios, C/O ratios, and major species composition) are often achievable for isomeric fuels, which assists quantitative analysis of flame chemistry. Differences in initial fuel destruction reactions and comparisons of the composition of reaction intermediates highlight the influences of fuel structure on the kinetic mechanism. Secondly, esters differing only in the alkoxy group (methoxy vs ethoxy) may be compared to isolate those changes in the compositions of reaction intermediates directly attributable to the ester function. Finally, the selected molecules possess important structural differences including the degree of unsaturation and the effects of branched chains, which are expected to influence the respective compositions of reaction intermediates. These molecules have relatively simple structures compared with the long hydrocarbon chains (up to 16-18 carbon atoms) of the component fatty acid esters of practical biodiesel fuels, which are precluded for use in laboratory flame studies because of their low volatility. Nevertheless, these molecules are well-suited for the proposed studies because they contain all of the structural functional groups expected to account for fuel-specific effects and their structural simplicity enables comprehensive quantitative kinetic modeling (supplemented with quantum calculations of energy barriers, transition states and thermochemical parameters).

Measurement of photoionization cross sections. To date, we have completed measurements absolute cross sections for molecular and dissociative photoionization for nearly 50 key reaction intermediates found in the combustion of simple hydrocarbons and oxygenates,

which contribute to a growing database of critical importance for applications of PIMS to flame chemistry. These molecules include alkanes, alkenes, alkynes, alcohols, ketones, ethers, esters, aldehydes, carboxylic acids, and aromatics. We plan to measure cross sections for 24 additional molecules selected to support our studies of the flame chemistry of oxygenated and nitrogenous biofuels. A paper reporting cross section measurements for 12 alkyl esters is in preparation.

DOE Publications, 2006-present

1. J. Wang, U. Struckmeier, B. Yang, T. A. Cool, P. Oßwald, K. Kohse-Höinghaus, T. Kasper, N. Hansen, P. R. Westmoreland, "Isomer-Specific Influences on the Composition of Reaction Intermediates in Dimethyl Ether/Propene and Ethanol/Propene Flames", *J. Phys. Chem. A*, in press
2. N. Hansen, S. J. Klippenstein, P. R. Westmoreland, T. Kasper, K. Kohse-Höinghaus, J. Wang, T. A. Cool, "A Combined *ab-initio* and Photoionization Mass Spectrometric Study of Polyyne in Fuel-Rich Flames", *Phys. Chem. Chem. Phys.*, **10**, 366-374 (2008).
3. J. Wang, B. Yang, T. A. Cool, N. Hansen, T. Kasper, "Near-threshold Absolute Photoionization Cross Sections of some Reaction Intermediates in Combustion", *Int. J. Mass Spectrom.*, **269**, 210-220 (2008).
4. C. A. Taatjes, N. Hansen, D. L. Osborn, K. Kohse-Höinghaus, T. A. Cool, P. R. Westmoreland, "Imaging' Combustion Chemistry via Multiplexed Synchrotron-Photoionization Mass Spectrometry", *Phys. Chem. Chem. Phys.*, **10**, 20-34 (2008)
5. N. Hansen, T. Kasper, S. J. Klippenstein, P. R. Westmoreland, M. E. Law, C. A. Taatjes, K. Kohse-Höinghaus, J. Wang, T. A. Cool, "Initial Steps of Aromatic Ring Formation in a Laminar Premixed Fuel-Rich Cyclopentene Flame", *J. Phys. Chem. A*, **111**, 4081-4092 (2007).
6. P. Oßwald, U. Struckmeier, T. Kasper, K. Kohse-Höinghaus, J. Wang, T. A. Cool, N. Hansen, P. R. Westmoreland, "Isomer-Specific Fuel Destruction Pathways in Rich Flames of Methyl Acetate and Ethyl Formate and Consequences for the Combustion Chemistry of Esters", *J. Phys. Chem. A*, **111**, 4093-4101 (2007).
7. T. A. Cool, J. Wang, N. Hansen, P. R. Westmoreland, F. L. Dryer, Z. Zhao, A. Kazakov, T. Kasper, K. Kohse-Höinghaus, "Photoionization Mass Spectrometry and Modeling Studies of the Chemistry of fuel-rich Dimethyl Ether Flames", *Proc. Combust. Inst.*, **31**, 285-293 (2007).
8. M. E. Law, P. R. Westmoreland, T. A. Cool, J. Wang, N. Hansen, C. A. Taatjes, T. Kasper, "Benzene Precursors and Formation Routes in a Stoichiometric Cyclohexane Flame", *Proc. Combust. Inst.*, **31**, 565-573 (2007).
9. K. Kohse-Höinghaus, P. Oßwald, U. Struckmeier, T. Kasper, N. Hansen, C. A. Taatjes, J. Wang, T. A. Cool, S. Gon, P. R. Westmoreland, "The Influence of Ethanol Addition on a premixed fuel-rich Propene-Oxygen-Argon Flame", *Proc. Combust. Inst.*, **31**, 1119-1127 (2007).
10. N. Hansen, J. A. Miller, C. A. Taatjes, J. Wang, T. A. Cool, M. E. Law, P. R. Westmoreland, "Photoionization Mass Spectrometric Studies and Modeling of Fuel-Rich Allene and Propyne Flames", *Proc. Combust. Inst.*, **31**, 1157-1164 (2007).
11. N. Hansen, S. J. Klippenstein, J. A. Miller, J. Wang, T. A. Cool, M. E. Law, P. R. Westmoreland, T. Kasper, K. Kohse-Höinghaus, "Identification of C₅H_x Isomers in Fuel-Rich Flames by Photoionization Mass Spectrometry and Electronic Structure Calculations", *J. Phys. Chem A*, **110**, 4376-4388 (2006).
12. N. Hansen, S. J. Klippenstein, C. A. Taatjes, J. A. Miller, J. Wang, T. A. Cool, B. Yang, R. Yang, L. Wei, C. Huang, J. Wang, F. Qi, M. E. Law, P. R. Westmoreland, "Identification and Chemistry of C₄H₃ and C₄H₅ Isomers in Fuel-Rich Flames", *J. Phys. Chem. A*, **110**, 3670-3678 (2006).
13. C. A. Taatjes, N. Hansen, J. A. Miller, T. A. Cool, J. Wang, P. R. Westmoreland, M. E. Law, T. Kasper, K. Kohse-Höinghaus, "Combustion Chemistry of Enols: Possible Ethenol Precursors in Flames", *J. Phys. Chem. A*, **110**, 3254-3260 (2006).

Dissociation Pathways and Vibrational Dynamics in Excited Molecules and Complexes

F.F. Crim
Department of Chemistry
University of Wisconsin–Madison
Madison, Wisconsin 53706
fcrim@chem.wisc.edu

Our research investigates the chemistry of vibrationally excited molecules. The properties and reactivity of vibrationally energized molecules are central to processes occurring in environments as diverse as combustion, atmospheric reactions, and plasmas and are at the heart of many chemical reactions. The goal of our work is to unravel the behavior of vibrationally excited molecules and to exploit the resulting understanding to determine molecular properties and to control chemical processes. A unifying theme is the preparation of a molecule in a specific vibrational state using one of several excitation techniques and the subsequent photodissociation of that prepared molecule. Because the initial vibrational excitation often alters the photodissociation process, we refer to our double resonance photodissociation scheme as *vibrationally mediated photodissociation*. In the first step, fundamental or overtone excitation prepares a vibrationally excited molecule, and then a second photon, the photolysis photon, excites the molecule to an electronically excited state from which it dissociates. Vibrationally mediated photodissociation provides new vibrational spectroscopy, measures bond strengths with high accuracy, alters dissociation dynamics, and reveals the properties of and couplings among electronically excited states.

We have used our new ion imaging capabilities to follow the adiabatic and nonadiabatic dissociation pathways in ammonia and to make new measurements on the vibrationally mediated photodissociation of the hydrogen bonded dimer of formic acid. Most recently, we have extended our ion imaging studies of the dynamics at conical intersections to the phenol molecule. Phenol is particularly interesting because of well-characterized one-photon photodissociation dynamics and clear theoretical predictions about changes arising from vibrational excitation prior to dissociation. In each of these cases, the goals are understanding and exploiting vibrations in the ground electronic state, studying the vibrational structure of the electronically excited molecule, and probing and controlling the dissociation dynamics of the excited state.

Ammonia

Ammonia is a famously well-studied molecule that holds interesting opportunities for vibrationally mediated photodissociation experiments because it has both a nonadiabatic dissociation to yield ground state $\text{NH}_2 + \text{H}$ and an adiabatic dissociation to form excited state $\text{NH}_2^* + \text{H}$. We have demonstrated that NH_2^* is the primary product from vibrationally mediated photodissociation through the antisymmetric N-H stretching state (3^1) because the vibrational excitation preferentially drives the system along the adiabatic dissociation path. Ion imaging has allowed us to detect the rotational structure of the products and to identify the electronically excited fragment.

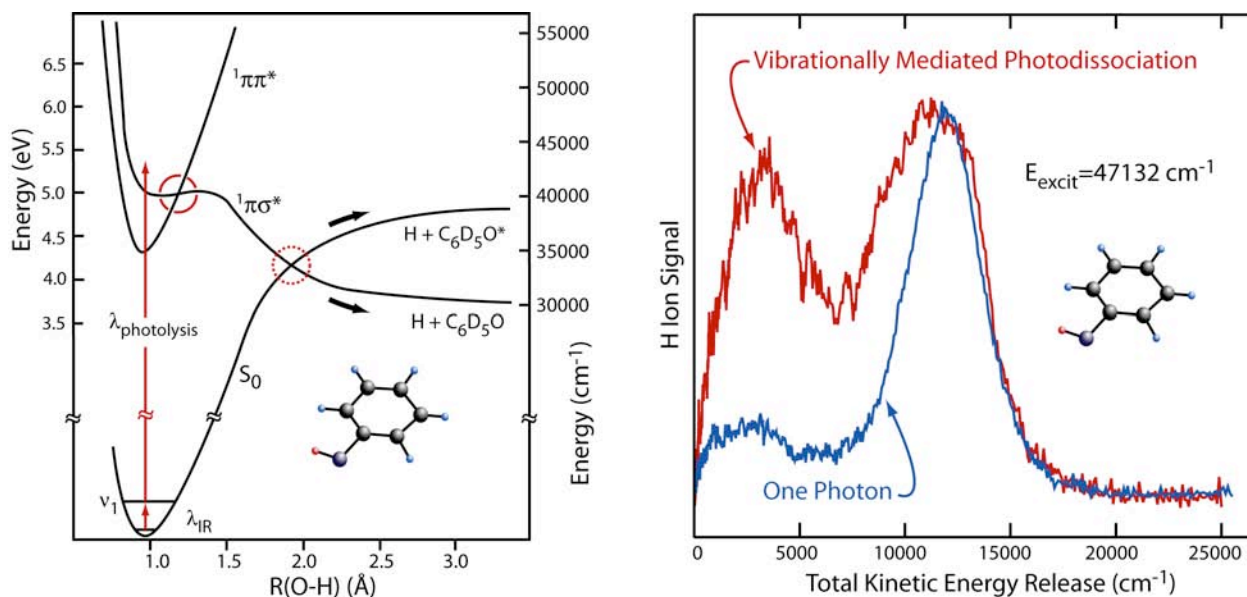
The ion imaging experiments also provide the angular distributions of the recoiling fragments, and we have recently completed the analysis for the ground state NH_2 product from photodissociation through the excited symmetric N-H stretch (1^1) and through the excited antisymmetric N-H stretch (3^1). The angular

distribution for the first case qualitatively resembles that for dissociation through the origin (0^0) and shows both parallel and perpendicular components depending on the rotational excitation in the NH_2 product. In general, the two-photon excitation scheme introduces higher order terms in the initial alignment, and the consequences are particularly clear in the NH_2^* products from dissociation through the antisymmetric (3^1) N-H stretching state. In that case, the first (vibrational) excitation step has a transition moment that is perpendicular to the C_3 axis of ammonia, and the second (electronic) excitation step has a parallel transition moment. The consequence is angular distributions that reflect these two alignments as well as the dynamics of the dissociation.

Phenol

Phenol is one of several heteroaromatic molecules that has multiple conical intersections that are accessible at different excitation energies. Our goal in studying phenol is to discover the influence that vibrational excitation has on the passage through or around these crossings. We perform both one-photon and vibrationally mediated photodissociation ion imaging experiments to extract the recoil energy distributions.

The left-side of the figure shows schematically diabatic potential curves for the ground (S_0) and first two excited states ($^1\pi\pi^*$ and $^1\pi\sigma^*$). The development of the wave function of the system as it passes through both intersections, $^1\pi\pi^*-^1\pi\sigma^*$ (solid circle) and $^1\pi\sigma^*-S_0$ (dotted circle), determines the branching at the second intersection to form either ground state phenoxyl by nonadiabatic dissociation or excited state phenoxyl by adiabatic dissociation. The right-hand side of the figure shows the recoil energy distributions obtained from the images of one-photon dissociation (blue curve) and vibrationally mediated photodissociation (red curve) at the same total energy. The vibrationally mediated experiments use an infrared photon to excite the O-H stretching vibration in $\text{C}_6\text{D}_5\text{OH}$ prior to electronic excitation.

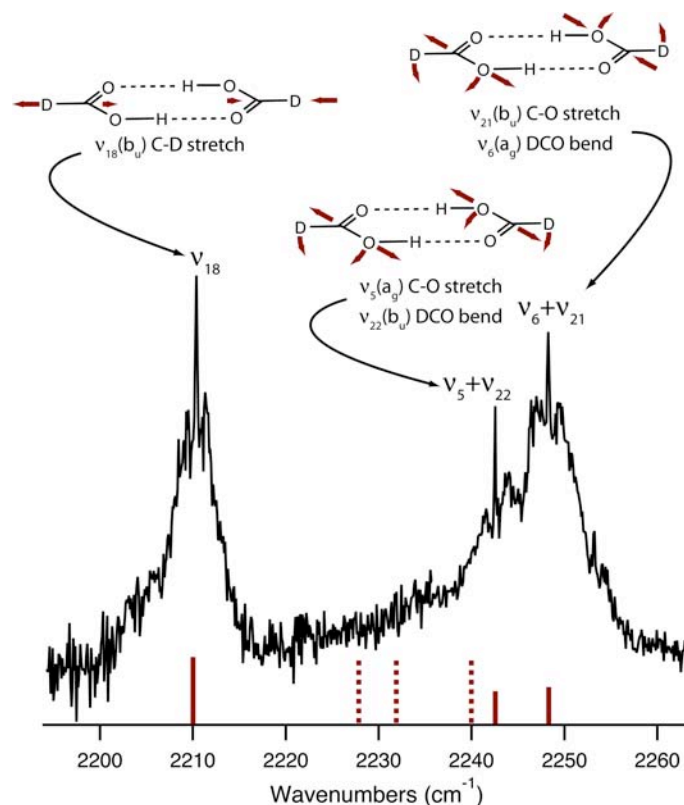


Comparing the recoil energy distributions of the fragments from one-photon dissociation of phenol- d_5 with those from vibrationally mediated photodissociation shows that initial vibrational excitation strongly influences the disposal of energy into relative translation. Dissociation of phenol- d_5 molecules initially excited in the O-H stretching region produces significantly more fragments with low recoil energies than does one-photon dissociation at the same total energy. The difference appears to come from the increased probability of adiabatic dissociation in which the initially vibrationally excited molecule passes around the conical intersection between the dissociative state and the ground state to produce electronically excited phenoxy- d_5 radicals. The additional energy deposited in electronic excitation of the radical reduces the energy available for relative translation, causing the H atoms from adiabatic dissociation to recoil slowly. These observations are qualitatively consistent with theoretical calculations of the role of vibrations in the dissociation of phenol (Domcke and coworkers, *J. Chem. Phys.* **122**, 224315 (2005)).

Formic Acid and Formic Acid Dimers

Another primary goal of our work is understanding the dissociation dynamics in vibrationally excited dimers, and we have applied our newly developed capabilities to studying formic acid and its hydrogen bonded dimer. We have developed schemes for distinguishing the monomer from the dimer in both one-photon dissociation and vibrationally mediated photodissociation. Exciting either the O-H or C-H stretch while observing the H-atom product from the undeuterated dimer gives vibrational action spectra that agree with the absorption spectrum in a supersonic expansion. Using the partially deuterated molecule and exciting the C-D stretch while detecting the D atom product gives the first vibrational spectrum of the cold partially deuterated dimer.

The spectrum in the region of the C-D stretch shows three features arising from the interaction of the antisymmetric C-D stretch with two different combinations of the C-O stretch and the DCO bend, each having the proper symmetry to interact with the infrared active b_u -symmetry C-D stretch. These combination states gain transition probability from their interaction with the C-D stretching vibration. The action spectrum of the cooled dimer reveals a Fermi resonance between the C-D stretch and two antisymmetric combination states formed from the C-O stretch and DCO bend. A three-state deperturbation analysis shows that there is a relatively strong coupling between the fundamental vibration and each of the combination vibrations (13 cm^{-1}) as well as between the combination states themselves (7 cm^{-1}). The stick spectrum in the figure shows the unperturbed line positions (dotted lines) and the predicted positions of the eigenstates (solid lines) from the three state analysis. The strong Fermi resonance interaction in $(\text{DCOOH})_2$ contrasts with that for the action spectrum of $(\text{HCOOD})_2$, where the C-H oscillator is isolated and not strongly coupled



to other states. It appears that the couplings that are present in the monomer dominate the interactions and that dimerization primarily shifts the C-O stretching and DCO bending vibrations into resonance with the C-D stretch.

FUTURE DIRECTIONS

Our experience with phenol, ammonia, and formic acid dimers prepares the way for our studies of the influence of an adduct on dissociation pathways and dynamics in vibrationally excited molecules. Because complexes can influence bimolecular reactions, our vibrationally mediated photodissociation studies potentially provide insights with consequences beyond excited state dissociation. We plan to study one-photon dissociation in complexes containing molecules such as ammonia and phenol, where we know conical intersections are important, in order to determine the influence of the adduct on the nonadiabatic dynamics. There are experimental studies of the structures and, in some cases, of the vibrational spectroscopy of the complexes as well as theoretical predictions about excited state dissociation. The one-photon studies lead to vibrationally mediated photodissociation experiments on complexes, combining the influences of an adduct and initial vibrational excitation.

PUBLICATIONS SINCE 2006 ACKNOWLEDGING DOE SUPPORT

Vibrationally Mediated Photodissociation of Ammonia: The Influence of N-H Stretching Vibrations on Passage through Conical Intersections, Michael L. Hause, Y. Heidi Yoon, and F. Fleming Crim, *J. Chem. Phys.* **125**, 174309 (2006).

Vibrational Action Spectroscopy of the C-H and C-D Stretches in Partially Deuterated Formic Acid Dimer, Y. Heidi Yoon, Michael L. Hause, Amanda S. Case, and F. Fleming Crim, *J. Chem. Phys.* **128**, 084305 (2008).

Dynamics at Conical Intersections: The Influence of O-H Stretching Vibrations on the Photodissociation of Phenol, Michael L. Hause, Y. Heidi Yoon, Amanda S. Case, and F. Fleming Crim, *J. Chem. Phys.* **128**, 104307 (2008).

Bimolecular Dynamics of Combustion Reactions

H. Floyd Davis
Department of Chemistry and Chemical Biology
Baker Laboratory, Cornell University, Ithaca NY 14853-1301
hfd1@Cornell.edu

I. Program Scope:

The aim of this project is to better understand the mechanisms and product energy disposal in elementary bimolecular reactions fundamental to combustion chemistry. Using the crossed molecular beams method, a molecular beam containing highly reactive free radicals is crossed at right angles with a second molecular beam. The angular and velocity distributions of the products from single reactive collisions are measured, primarily using Rydberg tagging methods.

II. Recent Progress:

i. Search for a Second OH* + D₂ Reactive Quenching Channel and Photodissociation of OH

We have previously studied the reactive quenching process $\text{OH} (A^2\Sigma^+) + \text{D}_2 \rightarrow \text{HOD} + \text{D}$ in crossed molecular beams.¹ A competing channel, $\text{OH} (A^2\Sigma^+) + \text{D}_2 \rightarrow \text{HOD}_2 \rightarrow \text{H} + \text{D}_2\text{O}$, is intriguing, as it involves formation of two new OD bonds with simultaneous fission of the original OH moiety. This channel may be mediated by short-lived HOD₂ complexes trapped on the upper adiabatic well associated with the conical intersection thought to be important in the reactive quenching processes.² The commonly-used source of OH radicals, involving photodissociation of HNO₃ at 193 nm, leads to significant HONO production, ultimately contributing to significant H atom signals that interfere with our measurement of the H + D₂O channel. We therefore employed an alternative approach, involving photolysis of N₂O/H₂ mixtures at 193 nm.³ The nascent O(¹D) produced by photolysis of N₂O, upon coexpansion with H₂, yields a relatively intense OH beam free of interfering contaminants.

During our study, we observed highly structured HRTOF signals that were attributable to photodissociation of OH radicals. Analysis of the TOF spectra revealed contributions from photolysis at 121 nm (*i.e.*, the Lyman- α used in Rydberg tagging), and at 212nm (*i.e.*, from residual UV from VUV generation). Although the photodissociation of OH has been extensively studied, most investigations were restricted to wavelengths around 300 nm where the A² Σ^+ state undergoes predissociation. Relatively little is known about the VUV photodissociation of OH and OD, although there has been some work on the two-photon excitation at the same total energy, in part due to interest in developing ionization schemes for OH detection.⁴ In 1974, Douglas concluded that the OH Rydberg D ² Σ^- state is responsible for the strong ($\sim 1 \times 10^{-17}$ cm²) absorption near 120 nm.⁵ Energetically, photodissociation at 121nm can lead to formation of H with the counterfragment in any of three electronic states, O(³P_{1,2,3}), O(¹D₂) or O(¹S₀). We observe all three channels. In addition, a number of peaks associated with photodissociation of OH at 212 nm involve absorption by vibrationally excited OH radicals ($v = 1, 2, 3$) produced in the O(¹D) + H₂ reaction employed for OH production. Parallel experiments have also been carried out on OD.

ii. Production and Characterization of Simple Hydrocarbon Free Radicals

As a first step towards studies of bimolecular reactions of hydrocarbon radicals with O₂, we have evaluated the performance of a number of different approaches for preparation of intense pulsed hydrocarbon radical beams. The beams were characterized using both electron impact ionization with quadrupole mass spectrometry, as well as by photoionization TOF spectroscopy at several different wavelengths, ranging from 118 to 140 nm. For small radicals such as methyl, ethyl, *etc.*, we have found that UV photolysis of stable precursors, either an alkyl halide or a carbonyl, in a 1 mm ID quartz tube attached to a supersonic pulsed molecular nozzle, produces the most intense radical beams. For larger species (*e.g.*, phenyl), carbon deposition on the inner walls of the quartz tube led to gradual heating and ultimate destruction of the tube. In such cases, photolysis in free space directly in front of the nozzle orifice led to the most intense and stable beams.

While the phenyl radical (C₆H₅) has been characterized previously by VUV photoionization and by cavity ringdown absorption spectroscopy, there is only one brief report of LIF detection in the literature.⁶ Since fluorescence detection might be a valuable and generally-applicable method for phenyl radicals, we will evaluate the feasibility of this approach using the weak ²B₁ ← ²A₁ bands in the visible.

iii. Stimulated Raman Pumping of D₂

We have constructed and optimized performance of a home-made narrow band optical parametric oscillator (OPO) for studies of reactions involving vibrationally-excited molecules in crossed beams. The OPO⁷ is based on the use of KTP (potassium titanyl phosphate), and facilitates production of high energy pulsed light in the 700 – 900 nm range, as well as at 1.4 – 4.0 μm. Following the approach of Lucht and coworkers,⁸ we have been able to obtain near transform-limited pulses through injection seeding with narrow bandwidth distributed feedback (DFB) diode lasers. We employ the tunable narrowband near IR radiation from this device, along with the fundamental from an injection seeded Nd:YAG laser, for SRP of D₂. Vibrationally excited D₂ is employed in our crossed beam studies with OH. By seeding at the idler wavelength using a DFB laser operating at 1.55 μm, the 532 nm pumped nonresonant oscillator produces several mJ of near-transform-limited 807 nm radiation as the signal. This 807 nm light is amplified to produce ≈ 50 mJ/pulse of near-transform-limited radiation. To date, we have characterized the SRP process by photoionization spectroscopy of D₂. Studies of the OH + D₂ (v=1) → HOD + D reaction are in progress.

iv. VUV generation using 4-wave mixing methods.

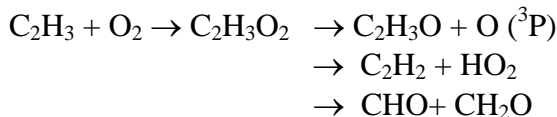
High-n Rydberg TOF spectroscopy involves excitation of atomic products (H, D, or O) resulting from photodissociation or bimolecular reaction to high-n Rydberg levels. This process typically involves a two-color excitation, where the first photon is in the VUV and the second in the UV. Production of light at 121 nm (H or D atoms) or 130 nm (O atoms) at intensities sufficient for photodissociation experiments can be achieved by simple frequency-tripling of a single laser beam in an inert gas. However, for crossed beam reactive scattering, it is generally necessary to increase the VUV intensity by employing resonance enhanced four wave mixing of two laser beams, with one laser tuned to a two-photon resonance (*e.g.*, 212 nm for Kr). The

presence of residual 212 nm light is of no consequence for simple systems, *e.g.*, F + H₂, since both reactants are transparent. However, in studies of more complex chemical systems, the 212 nm light usually leads to very strong interfering signals due to unintentional photodissociation. We have recently devoted considerable effort to spatially separating the VUV from the fundamental UV and visible laser beams in our crossed beams apparatus. Several different approaches, including the use of a LiF prism and noncollinear phase matching have been explored. While these approaches do increase the complexity of alignment, the vastly decreased background levels so produced greatly expands the range of systems that can be studied.

III. Future Work:

i. Crossed Beam Reactions of Atomic and Hydrocarbon Radicals with O₂

The reaction of free radicals, R (*e.g.*, H, CH₃, C₂H₅, C₂H₃, C₆H₅ *etc.*) with O₂ is initiated by addition, forming peroxy radicals (RO₂) which subsequently undergo unimolecular rearrangement and/or decomposition. While the O(³P) channel is thermodynamically closed for some systems (*e.g.*, CH₃), in many cases this channel, while relatively high in energy, is dynamically favorable, as it involves simple O-O bond fission within the initially-formed complex. It thus likely plays an important role in combustion at higher temperatures. Other competing reaction pathways involving more complex rearrangements are also likely. In the case of vinyl radical, C₂H₃, the most likely reaction pathways are:



There has been very little work on this family of elementary reactions using crossed molecular beams. The ORTOF method will be used to first study the O atom channels directly. The O atom product angular distributions provide insight into the timescales for decomposition of the peroxy radical, and the TOF spectra provide information about the internal energy distribution of the RO counterfragment. Kaiser's group recently demonstrated that in reaction of phenyl radicals (produced by pyrolysis of C₆H₅NO) with O₂, the O atom channel is likely dominant at high collision energies.⁹ The lifetimes of the C₆H₅O₂ intermediates were shorter than their rotational periods at E_{coll} = 107 kJ/mol, suggesting a stripping-type mechanism. Due to the presence of a deep well (≈200 kJ/mol relative to reactants) and large number of vibrational degrees of freedom, the lifetime must increase substantially at lower collision energies. While electron impact ionization of products is less sensitive than photoionization or Rydberg tagging, it has the advantage that multiple competing processes can be studied. Furthermore, it may be possible to calibrate the detection sensitivity for competing channels, facilitating the determination of product branching ratios. After characterizing the O atom channel directly, we will search for other product channels using universal mass spectrometric detection.

ii. Studies of OH + HD, OH + H₂, and OH + D₂ (v = 1).

The OH + D₂ reaction is important in combustion, and is the simplest member of the family of abstraction reactions involving OH. It involves a substantial potential energy barrier, leading to a small reaction cross section even at relatively high collision energies. The OH moiety acts much like a spectator, and is not appreciably excited in the product HOD. On the other hand, the D-D bond in D₂ is broken during the course of the reaction; vibrational excitation of this reactant

will strongly enhance reactivity.¹⁰ We are presently investigating the OH + D₂ (v=1) reaction using SRP of D₂ (discussed above) and DRTOF spectroscopy.

Finally, the substantial reduction of interfering signals achieved by spatially removing the UV and VUV lasers from the interaction region should make it possible for us to carry out studies of related reactions such as OH + HD and OH + H₂. We will also further investigate the competing reactive pathways in the OH* quenching processes.

IV. Publications since 2006:

1. Reaction Dynamics of CN + O₂ → NCO + O(³P₂), Mark F. Witinski, Mariví Ortiz-Suárez, and H. Floyd Davis, *J. Chem. Phys.*, **124**, 094307 (2006).
2. Reactive Quenching of OH (A ²Σ⁺) + D₂ Studied by Crossed Molecular Beams, Mariví Ortiz-Suárez, Mark F. Witinski, and H. Floyd Davis, *J. Chem. Phys.* **124**, 201106 (2006).

V. References:

-
1. Mariví Ortiz-Suárez, Mark F. Witinski, and H. Floyd Davis, *J. Chem. Phys.* **124**, 201106 (2006).
 2. M. W. Todd, D.T. Anderson, and M.I. Lester, *J. Phys. Chem. A* **105**, 10031 (2001).
 3. B. Zhang, W. Shiu, J.J. Lin, and K. Liu, *J. Chem. Phys.* **122**, 131102 (2005).
 4. a) M. P. J. van der Loo and G. C. Groenenboom, *J. Chem. Phys.* **123**, 074310 (2005); b) M. E. Greenslade, M. I. Lester, D.C. Radenovic, A.J. A. van Roij and D.H. Parker, *J. Chem. Phys.* **123**, 074309 (2005).
 5. A.E. Douglas, *Can. J. Phys.* **52**, 318 (1974).
 6. P. Misra, X. Zhu, M.M. Kamal, A. H. Nur, and H.L. Bryant, Jr. *Proc. Int. Conf. on Lasers*, **16**, 326 (1993).
 7. W.R. Bosenberg and D. Guyer, *J. Opt. Soc. Am. B* **10**, 1716 (1993).
 8. W.D. Kulatilaka, T.N. Anderson, T.L. Bougher, and R.P. Lucht, *Appl. Phys. B* **80**, 669 (2005).
 9. X. Gu, F. Zhang, and R.I. Kaiser, *Chem. Phys. Lett.* **448**, 7 (2007).
 10. M. J. Lakin, D. Troya, G. Lendvay, M. Gonzalez and G.C. Schatz, *J. Chem. Phys.* **115**, 5160 (2001).

Multiple-time-scale kinetics and combustion modeling

Michael J. Davis

Chemistry Division
Argonne National Laboratory
Argonne, IL 60439
Email: davis@tcg.anl.gov

For most of the last three years, research in this program has focused on model reduction in reactive flows, with applications to transient reaction-diffusion systems and steady flames. The main goal of the research has been to understand if model reduction is a natural consequence of the dynamics of the systems. Another important aspect of this research has been the investigation of the interaction of transport and chemistry in reactive-flow systems. This project is near completion and the focus of the effort is shifting to combustion modeling.

Recent Progress

There are many methods used to reduce the effort in kinetic modeling and the modeling of reactive flows. From a dynamical-systems perspective the effectiveness of model reduction depends on two features: 1) there is relaxation and 2) there is a separation of scales. The first feature leads to reduction and the second feature leads to *effective* reduction. Depending on the type of system studied the separation of scales refers to: 1) time scales, 2) spatial scales, or 3) spatio-temporal scales.

Recent progress in this program has focused on the dynamics of reactive-flow systems. The systems studied can be divided into two categories: 1) steady systems, such as steady flames, and 2) transient systems such as reaction-diffusion equations and transient flames. The investigation of transient systems has been divided into two categories, short-to-intermediate time dynamics and intermediate-to-long time dynamics. A project has been completed in the latter category and two papers were published. In the steady category, a project with Alison Tomlin (Leeds) on steady, one-dimensional burner-stabilized premixed H_2/O_2 flames has been completed and two papers have been submitted. In collaboration with Tomlin and James Miller (Sandia) a project on lean methane flames was initiated and is near completion.

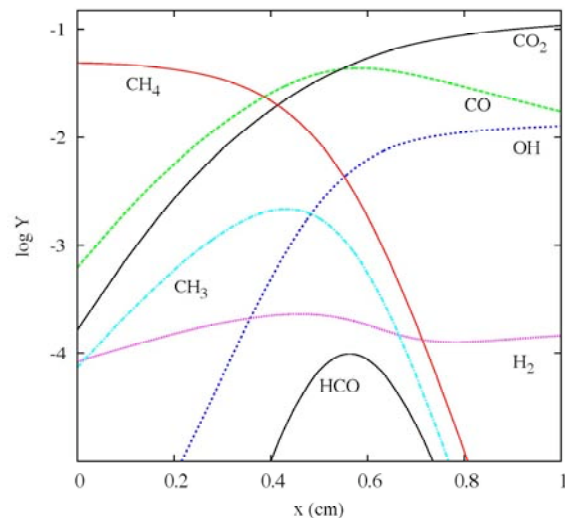


Fig. 1

Several results for H_2/O_2 flames were presented in the abstract of the previous Contractors meeting. Further results are presented in the preprints. The results on methane flames provide a good introduction to the work on steady flames and will be presented here. The relaxation observed for these two flames is generic for these types of flames.

Figure 1 shows results of a steady flame calculation for a one-dimensional burner-stabilized premixed flame using the Chemkin code “Premix”. This flame results from an incoming CH_4/O_2 mixture which is 9.5% CH_4 and 90.5% O_2 . To accurately model such a flame it is necessary to follow 14 species: H_2 , O_2 , H , O , OH , H_2O , HO_2 , H_2O_2 , CH_4 , CH_3 , HCO , CO , CO_2 , and CH_2O , as well as temperature. The model includes 54 reactions and their reverses and multi-component transport. The energy equation was solved to follow temperature. The mass fractions (Y) for seven of the species are presented in Fig. 1. The coordinate “ x ” is the distance above the burner.

To investigate the spatial dynamics of this flame, the problem is cast as a dynamical system,¹ which means studying the flame as a set of first order ordinary differential equations. These flames are more commonly modeled with second-order differential equations, as is done in the Premix code, which solves a flame as a boundary-value problem. The dynamical-system approach solves it as an initial-value problem.

It is well known that the system of first order differential equations describing the spatial dynamics of steady flames is unstable and that standard integration techniques cannot be employed under most conditions. An alternative algorithm for generating trajectories was developed and implemented.² This algorithm generates steady flames from the dynamical system using finite difference approximations to derivatives and a Newton-Raphson search to satisfy the differential equations. It is similar to the method used in the second-order boundary-value approach of the Premix code.

Once the flame is posed as a dynamical system it is studied in phase space. The coordinates of the phase space are mass flux fractions and either mole or mass fractions. Figure 2 highlights the advantage of studying the flame in phase space. The top panel repeats the CO_2 profile of Fig. 1 shown as a solid black line. A second solid, red line shows a CO_2 profile for another flame that has a different chemical mixture coming out of the burner, but with the same asymptotic behavior (it lies above the original curve at 5

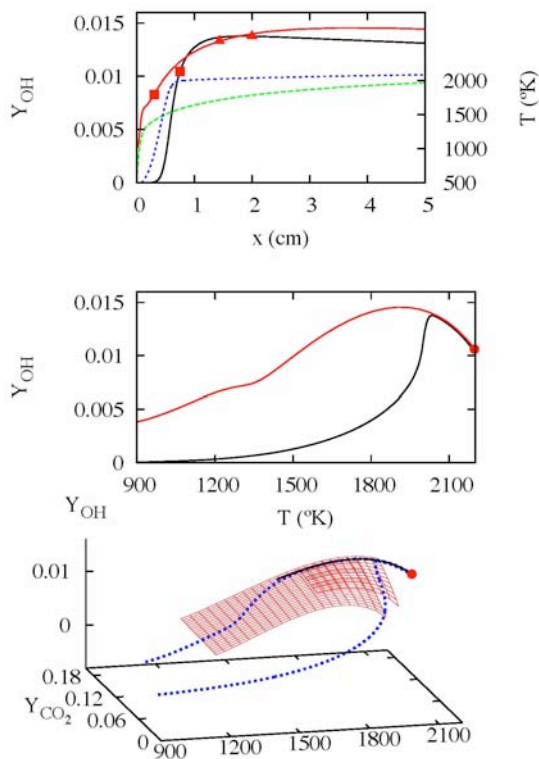


Fig. 2

cm). This trajectory was generated with the code described in the previous paragraph. The top panel of Fig. 2 also includes the temperature profile for both flames.

The top panel of Fig. 2 does not give a complete picture of the relaxation that occurs for these flames. A better way of viewing the relaxation is presented in the middle panel of Fig. 2. This plot shows a projection of the phase-space dynamics for the same two flames. The progress variable is still the spatial coordinate, x , but it is suppressed in the plot. The plot demonstrates that not only do the flames approach the same final state (solid dot), they approach it along the same one-dimensional curve, commonly called a one-dimensional manifold. The flame can be described by a one-dimensional system along the manifold.

The bottom plot of Fig. 2 presents further analysis, where three-dimensional projections of the two flames are shown (temperature and the mass fractions of CO_2 and OH). The flames are plotted as dashed, blue lines. Also included on the plot is a solid black line that shows a one-dimensional manifold and a surface drawn as a red grid, generated in two, overlapping pieces. Reference 3 describes the algorithm used to generate the one- and two-dimensional manifolds. The bottom plot demonstrates that the flames first relax to a two-dimensional manifold before relaxing to a one-dimensional manifold. Thus, the steady flames first become two-dimensional systems before they become one-dimensional. The top panel of Fig. 2 indicates where the relaxation occurs for each flame as a function of distance above the burner. The solid squares on each curve show where the flames reach the two-dimensional manifold and the solid triangles show where the flames reach the one-dimensional manifolds.

As noted above the dynamical system that describes the flame is an unstable one. This means that any randomly chosen trajectory is unphysical and will propagate to

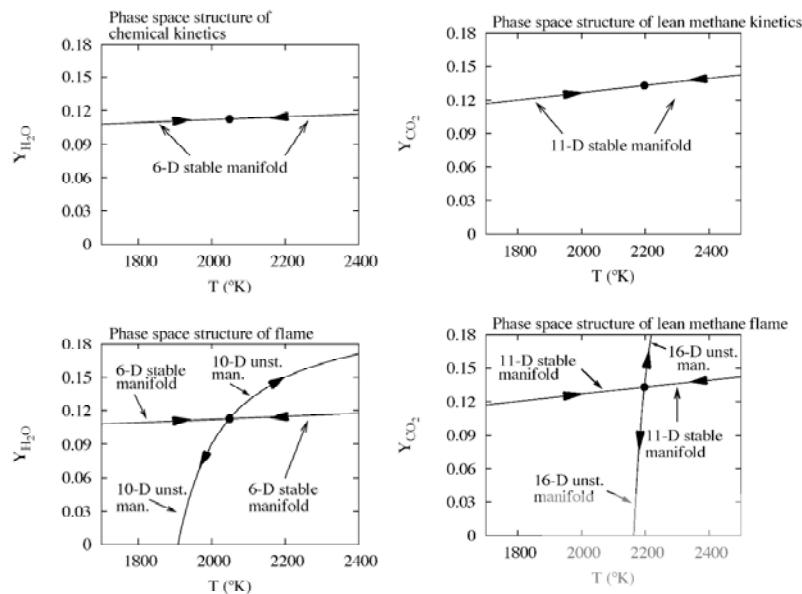


Fig. 3

infinity when integrated. It does not mean that all possible initial conditions lead to this result. The situation that occurs for the dynamical system describing the flame is similar to many problems encountered in the physical sciences and engineering. Differential

equations often have physical and unphysical solutions. For these steady flames, the physical solutions asymptotically approach a point that is an equilibrium point of an adiabatic, isobaric chemical-kinetic system, while the unphysical solutions blow-up. The equilibrium point of the kinetics system becomes a saddlepoint in the flame system due to transport, and all physical solutions lie on the stable manifold of the saddlepoint.

Figure 3 summarizes the phase space structure of the cases outlined here and in Refs. 2 and 3. The H_2/O_2 systems are on the left and the methane systems are on the right. The top row of Fig. 3 describes adiabatic, isobaric chemical kinetics and the bottom row premixed flames. The kinetic systems are stable. All initial mixtures relax to equilibrium. The stable manifolds of these systems have the same dimension as the full system. In the flame system, steady flames propagate on the stable manifold of a saddlepoint. This saddlepoint matches the equilibrium point of the system above it. Steady flames are trajectories on the stable manifold of the saddlepoints. All relaxation described above for the steady flames occurs on the stable manifold. Randomly chosen trajectories have stable and unstable components and thus propagate to infinity.

Future Plans

The project on model reduction will end with the study of the lean methane flames and an examination of strained flames, not described here. The future work will concentrate on combustion modeling. The new work will include a careful examination of important reactions that will be targeted with uncertainty quantification and related methods.

References

- ¹ For example, J. O. Hirschfelder and C. F. Curtiss, *Adv. Chem. Phys.* **3**, 59 (1961).
- ² M. J. Davis and A. S. Tomlin, “Spatial dynamics of Steady Flames 1. Phase Space Structure and the Dynamics of Individual Trajectories”, submitted to *J. Phys, Chem. A*.
- ³ M. J. Davis and A. S. Tomlin, “Spatial dynamics of Steady Flames 2. Low-dimensional Manifolds and the Role of Transport Processes”, submitted to *J. Phys, Chem. A*.

Publications

- M. J. Davis, “Low-dimensional manifolds in reaction-diffusion equations. 1. Fundamental aspects”, *J. Phys. Chem. A* **110**, 5235 (2006).
- M. J. Davis, “Low-dimensional manifolds in reaction-diffusion equations. 2. Numerical analysis and method development”, *J. Phys. Chem. A* **110**, 5257 (2006).
- M. J. Davis and A. S. Tomlin, “Spatial dynamics of Steady Flames 1. Phase Space Structure and the Dynamics of Individual Trajectories”, submitted to *J. Phys, Chem. A*.
- M. J. Davis and A. S. Tomlin, “Spatial dynamics of Steady Flames 2. Low-dimensional Manifolds and the Role of Transport Processes”, submitted to *J. Phys, Chem. A*.

COMPREHENSIVE MECHANISMS FOR COMBUSTION CHEMISTRY: EXPERIMENT, MODELING, AND SENSITIVITY ANALYSIS

Frederick L. Dryer

*Department of Mechanical and Aerospace Engineering
Princeton University, Princeton, New Jersey 08544 5263*

fldryer@princeton.edu

Grant No. DE FG02 86ER 13503

Our experimental work is conducted in a Variable Pressure Flow Reactor (VPFR) at pressures from 0.3 to 20 atm and temperatures from 500 K to 1200 K, with observed reaction times from 0.5×10^{-2} to 2 seconds, and through laminar flame speed measurements. Results are combined with literature data and numerical studies to develop and validate chemical kinetic reaction mechanisms and to improve determinations of important elementary rates. In the work summarized below, we provide some further insights on recently reported discrepancies between kinetic model predictions and experimentally measured ignition delays for hydrogen/carbon monoxide (syngas) - air as well as toluene-air mixtures. We also report additional experimental/modeling results on the oxidation properties of DME and ethanol.

Shock Tube Ignition Delay Modeling at Lower Temperature, and Higher Energy Densities

Experimental ignition delay data are viewed as an important validation resource in the development of comprehensive kinetic models. There is, however, an emerging concern about the interpretation of ignition delay observations at longer characteristic reaction times and lower temperatures, most prominently raised by recent discussions concerning the ignition behavior of syngas mixtures [1]. Similarities in ignition delay measurements from various shock tube, flow reactor, and rapid compression observations were noted to differ considerably from kinetic predictions generated using modeling assumptions typically employed in the literature. As a result, the fundamental understanding of syngas elementary chemical kinetics was brought into question. In considering these observations [2, 3], we argued the disparities were caused by the inability of the modeling assumptions to represent the experimental phenomena appropriately. In the particular case of shock tube observations, we noted the multi-dimensional nature of the ignition event in the mild ignition regime, and we hypothesized a number of potential perturbing phenomena that would not be captured by modeling that assumes uniform, constant internal energy (U) and volume (V) or constant enthalpy (H) and pressure (P) conditions in the reflected shock gases. We emphasized the high sensitivity of induction chemistry in the mild ignition regime to any type of experimental perturbation as the principal reason for similarities in observations amongst the various experimental venues.

Homogenous, constant U , V or H , P modeling assumptions have been routinely applied by the shock tube community and others modelers alike, though it has been known that non-ideal reflected shock conditions can lead to subsequent variations of temperature and pressure from the initial reflected shock end-wall values [4, 5]. With few exceptions, however, shock tube ignition delay data have been reported without pressure history information. Recently [6-8], it has come to light that shock tube ignition delay data for hydrogen or syngas at conditions in the mild ignition regime are accompanied by significant pressure rise and even OH* emission prior to ignition. Li et al. [9] have proposed CHEMSHOCK as a computational approach to embody the observed pressure rise in modeling predictions. Pang et al. [6, 7] showed promising results using CHEMSHOCK in modeling ignition delay data of H₂/O₂ mixtures, concluding that facility dependent effects and heat release prior to ignition can lead to polytropic compression of the reacting mixture, and subsequent ignition at temperatures much higher than the initial reflected shock value. We point out that SENKIN [10], part of the CHEMKIN-II [11] suite of programs, is capable of similar calculations using the VTIM (i.e. volume as a function of time) option along with a polytropic state change with time, developed from the measured pressure history. This approach has been utilized for some time in modeling rapid compression machine ignition data [12], as will be discussed further below.

Figure 1 compares predictions against the shock tube data found in [1] using assumed linear pressure gradients of 2, 5, and 10%/ms prior to ignition, within the range of those noted in experiments. Facility dependent phenomena that cause polytropic compression can be minimized by using large-diameter shock tubes, dilute fuel/oxidizer mixtures in monoatomic gases, and short test times (less than about 500 μ s) [4, 5, 13]. However, at high energy density conditions, localized, inhomogeneous ignition occurs, followed by deflagrative phenomena [14, 15]. Apparently these phenomena also cause polytropic compression of the unreacted mixture behind the reflected shock. Both phenomena can drive the remaining mixture conditions across the extended second explosion limit and into the strong ignition regime. The ignition kinetics in these cases are then dominated by those reactions that define the extended second limit. However, the most troubling result is that these observations point to significant non-

uniform phenomena in the reflected shock gases as a cause of polytropic compression (and likely OH* emission). In fact, in the case of hydrogen or syngas oxidation, no homogenous pre-ignition heat release can occur without substantial depletion of reactants, voiding the philosophical definition of “ignition.”

Noting the above and that hydrocarbon ignition delay kinetic observations at lower temperatures, high pressures, high energy densities, and longer ignition delays have also been commonly modeled as constant U , V or H , P processes, we hypothesized [2, 3] that similar misinterpretations to those described above for syngas mixtures may have occurred. A revealing test case is that for toluene [16]. Davidson et al. [16] acknowledge the presence of the pre-ignition pressure rise in reflected shock tube ignition delay studies (Fig. 2), considering this behavior to be due to homogenous chemical-kinetic phenomena. Predicting the pre-ignition pressure-time history (and associated heat release) was postulated as a chemical kinetic model validation constraint. Using constant U , V modeling assumptions, Davidson et al. showed that an available toluene model [17] considerably over-predicted ignition delays of stoichiometric toluene/air mixtures (see Fig. 3) while providing reasonable results for lean mixtures at 17 atm pressure. No pressure histories were published for the lean data, but it is noteworthy that the ignition delays exhibit a near turnover in temperature dependence as lower temperatures are approached. However, toluene does not exhibit two stage, negative temperature coefficient behavior [18]. Approximating the traces shown in Fig. 2 as having constant pressure for a finite amount of time and then increasing linearly until the moment of ignition, and applying this assumption to the five conditions shown in Fig. 2 using SENKIN/VTIM, the computed ignition delays show excellent agreement with experimental data (Fig. 4). It appears that the pre-ignition observations in these experiments are not solely the result of homogenous chemical kinetics, but are complex observations resulting from non-uniform phenomena resulting in polytropic compression. This corrected interpretation of shock tube ignition delay data may remove disparities of observations with those found in rapid compression machines [19]. Results strongly suggest that pressure history data should be reported with all shock tube kinetic observations. Concerns remain about the interpretation of long characteristic time observations as pure, uniformly occurring, kinetic phenomena.

Dimethyl Ether

We recently published an updated, comprehensive model for DME pyrolysis and oxidation which included validations against flow reactor, jet-stirred reactor, shock-tube ignition, burner-stabilized flame, and laminar premixed flame speed experimental data [20]. Predictions have also been recently compared against low pressure flame data [21, 22] and also reproduce measurements of pure DME flame speeds as well as those of DME-doped CH₄/air premixed flames at atmospheric pressure [23]. Further developments of the DME kinetic model have focused on low-temperature oxidation pathways, and on modeling ignition in a rapid compression machine [24].

DME/O₂/N₂ homogeneous mixtures were studied over an equivalence ratio range of 0.43–1.5, at compressed pressures ranging from 10 to 20 bar and at compressed temperatures from 615 to 735 K. Results show the well-known two-stage ignition characteristics of DME and the negative temperature coefficient (NTC) region is noted to become more prominent at lower pressures and for fuel rich mixtures. To interpret the experimental results, chemical kinetic simulations of the ignition process were carried out by modeling the entire compression process, corrected for heat losses, as described in [12]. The model of Zhao et al. [20] was found to provide good agreement overall; thus, extending its range of validation. However, the predicted first-stage ignition delays were consistently longer than experimental observations. The decomposition of hydroperoxymethyl formate was identified as a key reaction during the chemical induction process and should be further investigated [24].

Modeling the compression process accurately was found to be important to properly interpreting RCM ignition delay results, even though it was demonstrated that essentially no thermochemical activity occurred that might affect mixture temperature at the end of compression. However, it was conclusively shown that radicals are produced during the compression that affect induction chemistry, thus modifying the overall ignition delay observations and kinetic evolution subsequent to compression. The use of effective thermodynamic parameters when modeling RCM ignition delay cannot account for this effect on compression ignition observations. Furthermore, the specific design of the compression process in various RCMs as well as their heat loss characteristics must be taken into account in comparing directly ignition delay observations among different apparatus for the same operating parameters.

Ethanol

We are continuing to further refine an ethanol pyrolysis and oxidation model [25] that has been developed under this program in a hierarchical manner, which combines our H₂/O₂ and C₁ mechanism [26] and C₂H_X/O₂ (X = 1 – 6), CH₃CHO/O₂, and C₂H₅OH/O₂ subsets, in order of increasing complexity. The ethanol mechanism so derived predicts reasonably well the major species profiles for both pyrolysis and oxidation experiments in the VPFR, as well as shock tube ignition data, laminar burning velocities, and partially premixed and diffusive conditions in flames [25]. We have initiated investigations of the low and intermediate temperature kinetics of pure ethanol and

ethanol blended with gasoline primary reference fuel components (n-heptane and iso-octane). No low temperature activity is observed for pure ethanol oxidation at pressures of 12.5 atm and in residence times where n-heptane-iso-octane mixtures show such behavior. This is a rather surprising result, as acetaldehyde is a major intermediate produced in the oxidation of ethanol and is known to exhibit negative temperature coefficient behavior. Initial results of this work were recently reported [27], and future efforts will bring this work to completion.

Plans

Reaction systems of presently under investigation and of continuing interest over the coming year, include the pyrolyses and oxidations of acetaldehyde, methyl formate, acetone, and toluene, all over a range of pressures and temperatures similar to our previous work.

References (Items in *italics* are our present publications)

1. E.L. Petersen, D.M. Kalitan, A.B. Barrett, S.C. Reehal, J.D. Mertens, D.J. Beerer, R.L. Hack, V.G. McDonell, *Combust. Flame* 149 (2007) 244-247.
2. *F.L. Dryer, M. Chaos, "Ignition of Syngas/Air and Hydrogen/Air Mixtures at Low Temperatures and High Pressures: Experimental Data Interpretation and Kinetic Modeling Implications." Combust. Flame* 152 (2008) 293-299.
3. *M. Chaos, F.L. Dryer, "Syngas Combustion Kinetics and Applications." Combust. Sci. Technol.* 180 (2008) 1051-1084.
4. J.V. Michael, J.W. Sutherland, *Int. J. Chem. Kinet.* 18 (1986) 409-436.
5. E.L. Petersen, R.K. Hanson, *Shock Waves* 10 (2001) 405-420.
6. G.A. Pang, D.F. Davidson, R.K. Hanson, Fall Meeting of the Western States Section of the Combustion Institute, Livermore, CA, October 2007, Paper No. 07F-12.
7. G.A. Pang, D.F. Davidson, R.K. Hanson, Spring Meeting of the Western States Section of the Combustion Institute, Los Angeles, CA, March 2008, Paper No. 08S-10
8. J.D. Mertens, S.S. Musmann, D.M. Kalitan, E.L. Petersen, Spring Meeting of the Western States Section of the Combustion Institute, Los Angeles, CA, March 2008, Paper No. 08S-3.
9. H. Li, Z.C. Owens, D.F. Davidson, R.K. Hanson, *Int. J. Chem. Kinet.* 40 (2008) 89-98.
10. A.E. Lutz, R.J. Kee, J.A. Miller, Technical Report SAND87-8248, Sandia National Laboratories (1987).
11. R.J. Kee, F.M. Rupley, J.A. Miller, Technical Report SAND89-8009, Sandia National Laboratories (1989).
12. G. Mittal, C.-J. Sung, *Combust. Sci. Technol.* 179 (2007) 497-530.
13. D.F. Davidson, R.K. Hanson, *Int. J. Chem. Kinet.* 36 (2004) 510-523.
14. R. Blumenthal, K. Fieweger, K.H. Komp, G. Adomeit, *Combust. Sci. Technol.* 113 (1996) 137-166.
15. B.L. Wang, H. Olivier, H. Grönig, *Combust. Flame* 133 (2003) 93-106.
16. D.F. Davidson, B.M. Gauthier, R.K. Hanson, *Proc. Combust. Inst.* 30 (2005) 1175-1182.
17. W.J. Pitz, R. Seiser, J.W. Bozzelli, I. Da Costa, R. Fournet, F. Billaud, F. Battin-Leclerc, K. Seshadri, C.K. Westbrook, Fall Meeting of the Western States Section of the Combustion Institute, Salt Lake City, UT, October 2001, Paper No. 01F-28.
18. M. Chaos, Z. Zhao, A. Kazakov, P. Gokulakrishnan, M. Angioletti, F.L. Dryer, 5th US Combustion Meeting, San Diego, CA, March 2007, Paper No. E26.
19. G. Mittal, C.-J. Sung, *Combust. Flame* 150 (2007) 355-368.
20. *Z. Zhao, M. Chaos, A. Kazakov F.L. Dryer "Thermal Decomposition Reaction and a Comprehensive Kinetic Model of Dimethyl Ether." Int. J. Chem. Kin.* 40 (2008) 1-18.
21. *T.A. Cool, J. Wang, N. Hansen, P.R. Westmoreland, F.L. Dryer, Z. Zhao, A. Kazakov, T. Kasper, K. Kohse-Höinghaus, "Photoionization Mass Spectrometry and Modeling Studies of the Chemistry of Fuel-Rich Dimethyl Ether Flames." Proc. Combust. Inst.* 31 (2007) 285-294.
22. *T.A. Cool, Studies of Flame Chemistry with Photoionization Mass Spectrometry (2008) Abstract, this meeting.*
23. *Z. Chen, X. Qin, Y. Ju, Z. Zhao, M. Chaos, F.L. Dryer, "High Temperature Ignition and Combustion Enhancement by Dimethyl Ether Addition to Methane-Air Flames." Proc. Combust. Inst.* 31 (2007) 1215-1222.
24. *G. Mittal, M. Chaos, C.-J. Sung, F. L. Dryer, "Dimethyl Ether Autoignition in a Rapid Compression Machine: Experiments and Chemical Kinetic Modeling." Special Issue on Dimethyl Ether, A. Boehman, ed., Fuel Proc. Technol.* (2008). Accepted for Publication.
25. *J. Li, A. Kazakov, M. Chaos, F.L. Dryer, "Chemical Kinetics of Ethanol Oxidation," Paper C26, 5th US Combustion Meeting, San Diego, CA, March 25-28, 2007.*
26. *J. Li, Z. Zhao, A. Kazakov, M. Chaos, F.L. Dryer, J.J. Scire, "A Comprehensive Kinetic Mechanism for CO, CH₂O, CH₃OH Combustion." Int. J. Chem. Kinet.* 39 (2007) 109-136.
27. *F. M. Haas, M. Chaos, F.L. Dryer, "Oxidation of PRF-Ethanol Blends: Kinetic Modeling at Low and Intermediate Temperatures," ACS Spring 2008 National Meeting, New Orleans, LA April 6-10. Paper # FUEL 67.*

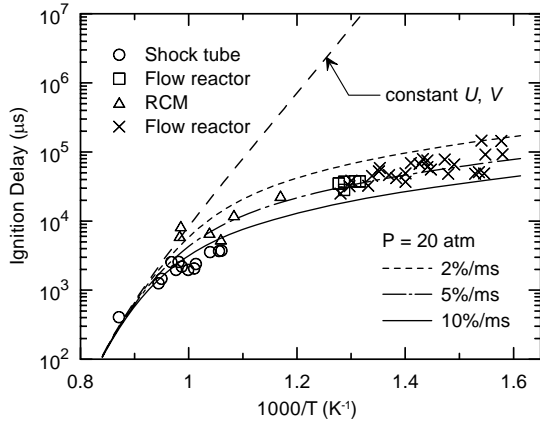


Fig. 1. Effect of pre-ignition linear pressure rise applied to the modeling of syngas/air ignition under the conditions of Petersen et al. [1]. Experimental conditions and associated references for the data shown can be found in Refs. 1-3.

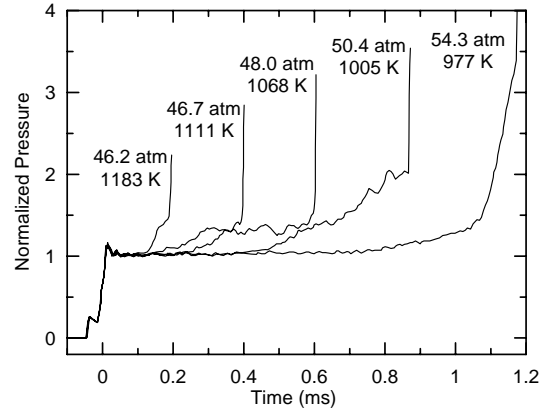


Fig. 2. Experimental pressure traces during toluene/air ignition in a shock tube (from Davidson et al. [16]).

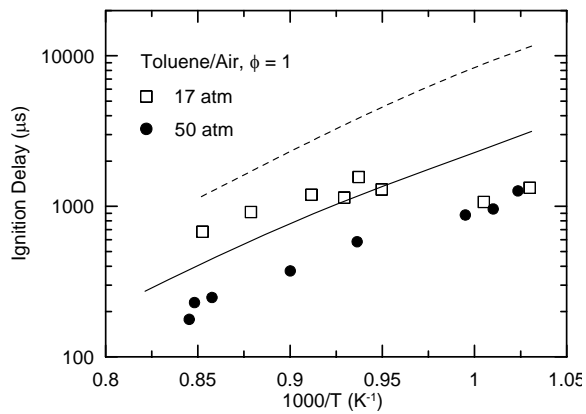


Fig. 3. Experimental [16] (symbols) and model [17] predictions (lines, employing constant U, V assumptions) for stoichiometric toluene/air mixtures. Dashed line corresponds to open symbols. Experimental data have been normalized to the pressures shown assuming proportionality to P^{-1} . Pressure traces for data represented by solid symbols can be found in Fig. 2.

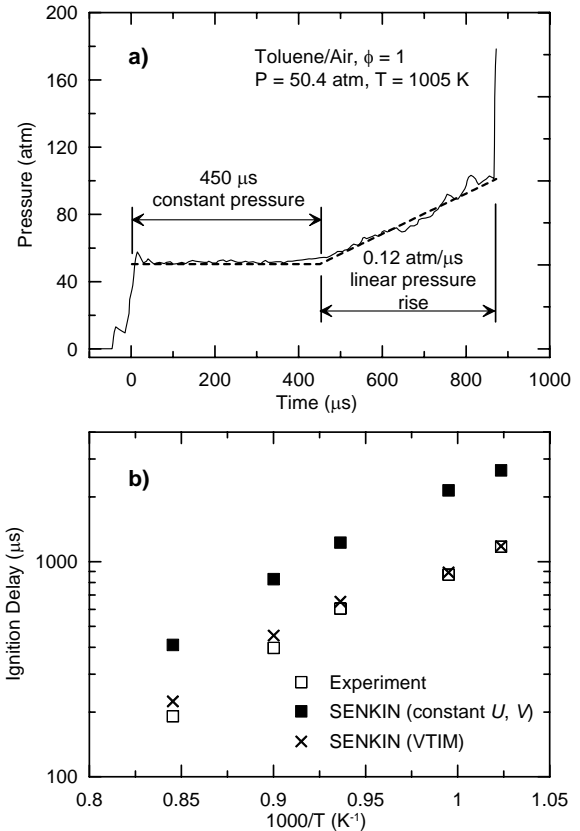


Fig. 4. Effect of pressure rise in modeling of toluene/air ignition delays; a) pressure profile approximation used as input for SENKIN/VTIM, similar profiles were used for the traces shown in Fig. 2; b) experimental data and computational results (using the model of Pitz et al. [17]) using constant U, V and including the effect of pre-ignition pressure rise.

Hydrocarbon Radical Thermochemistry: Gas-Phase Ion Chemistry Techniques

Kent M. Ervin

Department of Chemistry and Chemical Physics Program
University of Nevada, Reno
Reno, Nevada 89557-0216
ervin@unr.edu

I. Program Scope

Gas-phase ion chemistry and mass spectrometric methods are employed to determine enthalpies of formation of hydrocarbon radicals that are important in combustion processes and to investigate the dynamics of ion–molecule reactions. Guided ion beam tandem mass spectrometry is used to measure the activation of endoergic ion-molecule reactions as a function of kinetic energy. Modeling the measured reaction cross sections using statistical rate theory or empirical reaction models allows extraction of reaction threshold energies. These threshold energies yield relative gas-phase acidities, proton affinities, or hydrogen-atom affinities, which may then be used to derive neutral R–H bond dissociation enthalpies using thermochemical cycles involving established electron affinities or ionization energies. The reactive systems employed in these studies include endoergic bimolecular proton transfer reactions, hydrogen-atom transfer reactions, and collision-induced dissociation of heterodimer complex anions and cations. Electronic structure calculations are used to evaluate the possibility of potential energy barriers or dynamical constrictions along the reaction path, and as input for RRKM and phase space theory calculations.

II. Recent Progress

A. Bond Dissociation Energies of Linear H–C_{2n}[•] and H–C_{2n}[–] (n = 1, 2, 3)¹

Polyynyl radicals, C_{2n}H, are important in combustion processes^{2–4} as well as in astrophysical environments. Although these radicals have been characterized spectroscopically^{5–7} and theoretically,^{8–10} the C_{2n}H bond dissociation energies are still not well established experimentally. Accurate theoretical calculation of the energies is also problematic because of the complex electronic structures of C_{2n}H radicals, which have low-lying ²Σ and ²Π electronic states mixing acetylenic and cumulenic electronic structures.² While the electron affinities of the polyynyl radicals are accurately known^{5–7,11,12} the C–H bond dissociation energies of the anions are poorly established.

In this work, the hydrogen-atom reactions of C₂[•], C₄[•],

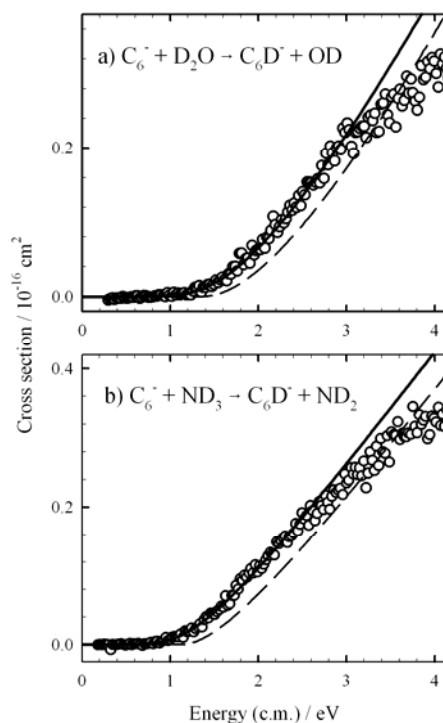


Fig.1. Deuterium atom transfer cross sections for reaction of C₆[•] with (a) D₂O and (b) ND₃. Solid lines show the fits to the data and dashed lines show the cross section model at 0 K without energy convolutions.

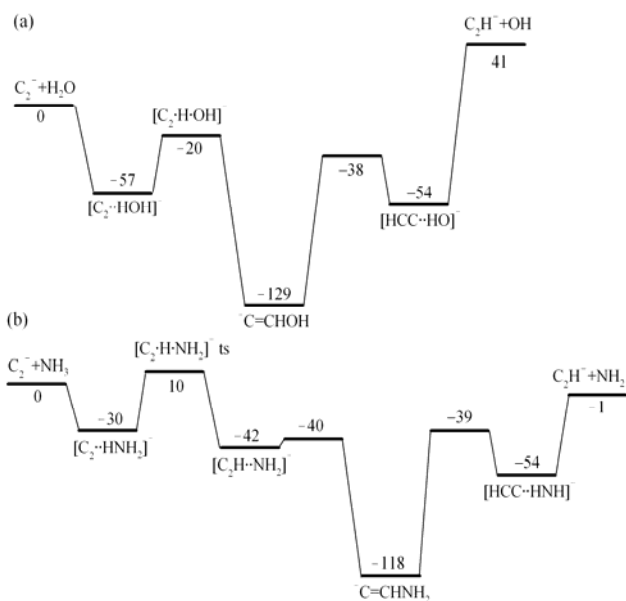


Fig. 2. Potential energy surfaces for hydrogen atom transfer to C_2^- from H_2O and NH_3 . Relative energies calculated at the B3LYP/aug-cc-pVTZ level (kJ/mol).

and C_6^- with D_2O and ND_3 and of C_4^- with CH_3OH , CH_4 , and C_2H_6 have been investigated using guided ion beam tandem mass spectrometry.¹ For example, the reaction cross sections with threshold fits for C_6^- reacting with D_2O and ND_3 are shown in Figure 1. Hydrogen (or deuterium) atom transfer is the major product channel for each of the reactions. The reaction threshold energies for collisional activation are reported. Several of the reactions exhibit threshold energies in excess of the reaction endothermicity. Potential energy calculations using density functional theory show intermediate energy barriers for some of the reactions, for example $C_2^- + H_2O$ and NH_3 in Figure 2. Dynamic restrictions related to multiple wells along the reaction path may also contribute to elevated threshold energies. The results indicate that the reactions with D_2O have the smallest excess threshold energies, which may therefore be used to derive lower limits on the C-H bond dissociation energies of the $C_{2n}H^-$ and $C_{2n}H$ ($n = 1-3$) linear species. The experimental lower limits for the bond dissociation energies of the neutral radicals to linear products are $D_0(C_2-H) \geq 460 \pm 15$ kJ/mol, $D_0(C_4-H) \geq 427 \pm 12$ kJ/mol, and $D_0(C_6-H) \geq 405 \pm 11$ kJ/mol.

B. Collision-Induced Dissociation of Hydrogen-Bonded Dimers of Carboxylic Acids¹³

Energy-resolved competitive collision-induced dissociation is used to investigate the proton-bound heterodimer anions of a series of carboxylic acids (formic, acetic and benzoic acid) and nitrous acid with their conjugate bases. In particular, the dissociation reactions of the complexes $[CH_3COO \cdot H \cdot OOC]^-$, $[CH_3COO \cdot H \cdot ONO]^-$, $[HCOO \cdot H \cdot ONO]^-$, $[C_6H_5COO \cdot H \cdot OOC]^-$ and $[C_6H_5COO \cdot H \cdot ONO]^-$ are investigated using a guided ion beam tandem mass spectrometer, reaction (1).



Cross sections of the two dissociation channels are measured as a function of the collision energy between the complex ions and xenon target gas. The reaction cross sections and production branching ratios are modeled by RRKM theory and the relative activation energies for dissociation are found.¹⁴⁻¹⁶ Using the standard treatment of a single complex dissociating into two product channels, the relative energies are ascribed to thermochemical acidity differences but these showed significant internal inconsistencies in the relative acidities of the various acids. The apparent deviations are ascribed to formation of conformational structures of the proton-bound complexes that must isomerize along the dissociation pathway to reach ground state product conformers, as illustrated in Figure 3. The complex isomerization barriers, although below the total available energy, can affect the kinetics of dissociation to ground-state products and therefore affect the branching ratios between the two proton transfer channels. The reaction dynamics of dissociation from multiple cluster ion conformations into multiple conformations of the products must be included in the statistical treatment of the dissociation process. The use of a local thermochemical network with multiple redundant and interconnected relative acidity measurements constrains the absolute acidities to values that agree with theory and previous equilibrium measurements within their uncertainties.

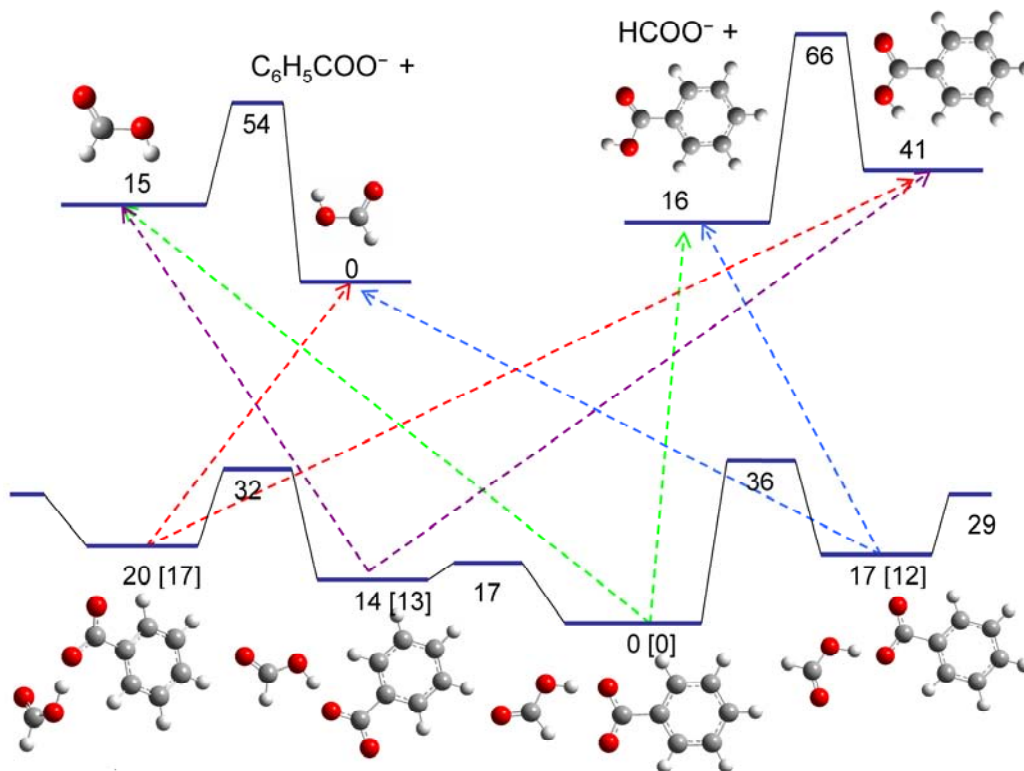


Fig. 3. Schematic energy level diagram showing the dissociation of $[\text{HCOO}\cdots\text{H}\cdots\text{OCC}_6\text{H}_5]^-$ complexes. Dashed lines show the “adiabatic” dissociations if the conformations of the acids within the complex are conserved in the product channels. The statistical dissociation model must take into account the possibility of inter-conversion among the complex conformations along the dissociation pathway. Relative energies at the B3LYP/aug-cc-pVDZ level in kJ/mol.

C. Instrumentation projects

We have completed the conversion our guided ion beam tandem mass spectrometer to allow study of positive ions as well as negative ions. This opens up the possibility of using TCID methods to measure proton affinities of hydrocarbon radicals. Diagnostic measurements of the reaction cross section for the $\text{Ar}^+ + \text{H}_2 \rightarrow \text{ArH}^+ + \text{H}$ reaction¹⁷ show that the modified instrumentation is working well.

We are also continuing development of a new Quadrupole Ion Trap (QIT)/Crossed Ion-Molecular Beam/Time-of-Flight (TOF) tandem mass spectrometer. While unrelated experiments are underway on spectroscopy of trapped ions using the QIT/TOF configuration, a graduate student and postdoctoral researcher have constructed the interaction region including the molecular beam source and related vacuum and electronic systems. This apparatus will open up the possibility of velocity-mapped imaging measurements on the products of ion–molecule reactions, with the potential of achieving our long-term goal of measuring the complete energy balance in ion–molecule reactions related to thermochemistry of hydrocarbon radicals.

III. Future Work

During the next project period, we will continue our guided ion beam tandem mass spectrometry experiments on proton bound ion clusters, expanded to include positive-ion systems in addition to the negative-ion systems studied previously. Energy-resolved collision-induced dissociation experiments provide relative gas-phase acidities (negative ion systems) or proton affinities (positive ion systems). High-level computational chemistry calculations are used for kinetics modeling and for thermochemical comparisons. We aim to measure thermochemical quantities for molecular radicals that are either too

large for accurate *ab initio* energy calculations, or else have complex electronic structures that are challenging for theory.

We will also develop ion-imaging techniques for product velocity measurements in endoergic and exoergic ion-molecule reactions. Velocity-mapped product ion imaging will allow measurement of the full energy disposal in ion-molecule reactions. The measured maximum kinetic energy of products can be used in an energy balance equation to determine the reaction enthalpies.

The reactive systems employed in these studies will include bimolecular proton transfer reactions, hydrogen-atom transfer reactions, and collision-induced dissociation of hydrogen-bonded heterodimer complexes. The targeted hydrocarbon radical species include the dehydrogenation products of oxygen-containing molecules that are increasingly important in synthetically oxygenated fuels and biofuels such as biodiesel or cellulosic feedstocks, and their intermediate combustion products. Such molecules include fatty acids and esters, ethers, peroxy compounds, and oligosaccharides. The results of this work will provide accurate thermochemical information for use in combustion kinetics databases, computer simulations of combustion, and as benchmarks for theoretical calculations on similar classes of molecules

IV. References

- ¹Y. Shi and K. M. Ervin, *J. Phys. Chem. A*, **112**, 1261-1267 (2008).
- ²J. H. Kiefer, S. S. Sidhu, R. D. Kern, K. Xie, H. Chen, and L. B. Harding, *Combust. Sci. Tech.* **82**, 101 (1992).
- ³H.-Y. Zhang and J. T. McKinnon, *Combust. Sci. Tech.* **1-7**, 261 (1995).
- ⁴T. Kruse and P. Roth, *J. Phys. Chem. A* **101**, 2138 (1997).
- ⁵K. M. Ervin and W. C. Lineberger, *J. Phys. Chem.* **95**, 1167 (1991).
- ⁶T. R. Taylor, C. Xu, and D. M. Neumark, *J. Chem. Phys.* **108**, 10018 (1998).
- ⁷T. Pino, M. Tulej, F. Güthe, M. Pachkov, and J. P. Maier, *J. Chem. Phys.* **116**, 6126 (2002).
- ⁸S. T. Brown, J. C. Rienstra-Kiracofe, and H. F. Schaefer, III, *J. Phys. Chem. A* **103**, 4065 (1999).
- ⁹S. Graf, J. Geiss, and S. Leutwyler, *J. Chem. Phys.* **114**, 4542 (2001).
- ¹⁰P. G. Szalay, A. Tajti, and J. F. Stanton, *Mol. Physics* **103**, 2159 (2005).
- ¹¹D. W. Arnold, S. E. Bradforth, T. N. Kitsopoulos, and D. M. Neumark, *J. Chem. Phys.* **95**, 8753 (1991).
- ¹²C. C. Arnold, Y. Zhao, T. N. Kitsopoulos, and D. M. Neumark, *J. Chem. Phys.* **97**, 6121 (1992).
- ¹³B. Jia, L. A. Angel, and K. M. Ervin, *J. Phys. Chem. A*, **112**, 1773-1782 (2008).
- ¹⁴V. F. DeTuri and K. M. Ervin, *J. Phys. Chem. A* **103**, 6911 (1999).
- ¹⁵M. T. Rodgers, K. M. Ervin, and P. B. Armentrout, *J. Chem. Phys.* **106**, 4499 (1997).
- ¹⁶M. T. Rodgers and P. B. Armentrout, *J. Chem. Phys.* **109**, 1787 (1998).
- ¹⁷K. M. Ervin and P. B. Armentrout, *J. Chem. Phys.* **83**, 166 (1985).

V. Publications and submitted journal articles supported by this project 2006-2008

- (a) "Hydrogen Atom Transfer Reactions of C_2^- , C_4^- , and C_6^- : Bond Dissociation Energies of Linear $H-C_{2n}^-$ and $H-C_{2n}$ ($n = 1, 2, 3$):", Yang Shi and Kent M. Ervin, *J. Phys. Chem. A*, **112**, 1261-1267 (2008).
- (b) "Threshold Collision-Induced Dissociation of Hydrogen-Bonded Dimers of Carboxylic Acids", Beike Jia, Laurence A. Angel, and Kent M. Ervin, *J. Phys. Chem. A*, **112**, 1773-1782 (2008).
- (c) "Gas-phase acidities and O-H bond dissociation enthalpies of phenol, 3-methylphenol, 2,4,6-trimethylphenol, and ethanoic acid", Laurence A. Angel and Kent M. Ervin, *J. Phys. Chem. A*, **110**, 10392-10403 (2006).
- (d) "Collision-induced dissociation of $HS^-(HCN)$: unsymmetrical hydrogen bonding in a proton-bound dimer anion", F. Ahu Akin and Kent M. Ervin, *J. Phys. Chem. A*, **110**, 1342-1349 (2006).
- (e) PESCAL, Fortran program for Franck-Condon analysis of photoelectron spectra, Kent M. Ervin, (major revisions 2008), <http://wolfweb.unr.edu/~ervin/pes>.
- (f) CRUNCH, Fortran program for analysis of reaction cross sections with RRKM and PST models, Kent M. Ervin and P. B. Armentrout, version 5.10 (2007), <http://wolfweb.unr.edu/~ervin/crunch>.

Spectroscopic and Dynamical Studies of Highly Energized Small Polyatomic Molecules

Robert W. Field

Massachusetts Institute of Technology

Cambridge, MA 02139

rwfield@mit.edu

I. Program Scope

The fundamental goal of this program is to develop the experimental techniques, diagnostics, interpretive concepts, and pattern-recognition schemes needed to reveal and understand how large-amplitude motions are encoded in the vibration-rotation energy level structure of small, gas-phase, combustion-relevant polyatomic molecules. We are focusing our efforts on unimolecular isomerization in several prototypical systems, including the $\text{HNC} \leftrightarrow \text{HCN}$ and $\text{HCCH} \leftrightarrow \text{CCH}_2$ isomerization systems. We are developing chirped-pulse millimeter wave spectroscopy as a technique that can be used in conjunction with Stimulated Emission Pumping (SEP) and the Stark effect to create and identify molecular states with high excitation in local vibrational modes, which are of key importance in understanding isomerization processes.

II. Recent Progress

A. Nuclear hyperfine structure as a diagnostic of large amplitude motion and isomerization

The S_0 HNC-HCN potential energy surface is a prototype for high-barrier, bond-breaking isomerization. One of the primary goals of this research program is to observe and identify barrier-proximal states, i.e. the states that are energetically located near the isomerization barrier and have amplitude localized along the minimum energy isomerization path. The large amplitude motion embodied in the barrier-proximal states provides the basis for their detectability. When a large amplitude motion alters the molecular geometry, the electronic structure of the molecule inevitably changes as well. Thus, electronic properties can serve as markers to distinguish the rare barrier proximal states from the vastly more numerous “ergodic” states in which excitation is divided among many modes. Hyperfine structure, which arises from the interaction of the nuclear quadrupole moment of the nitrogen nucleus with the gradient of the field due to the electronic wavefunction, is one such nuclear dynamics-sensitive electronic property. For HCN in the ground vibrational state, the quadrupole coupling constant is large and negative, $(eQq)_N = -4.7$ MHz, whereas for HNC in the ground vibrational state, it is small and positive $(eQq)_N = 0.26$ MHz. Electronic structure calculations in our group have demonstrated that the quadrupole coupling constant is strongly dependent on the bond angle and therefore on the extent of bend

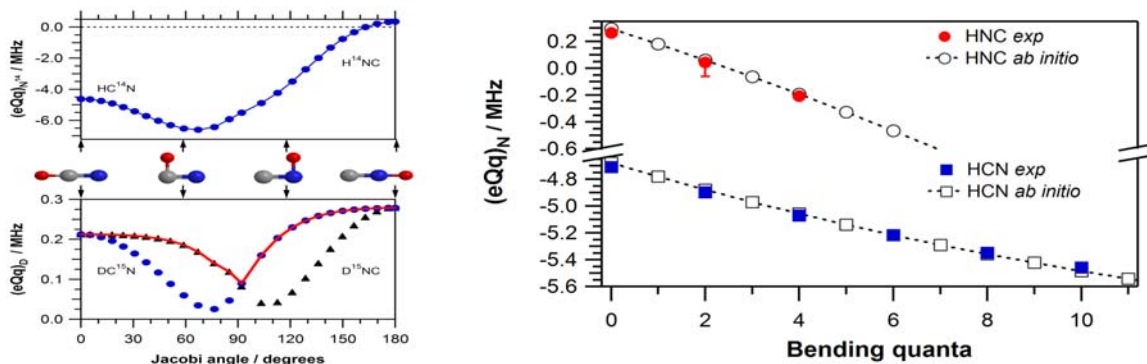


Figure 1. (a) (left, top) *Ab initio* $(eQq)_N$ values in the C-N bond axis frame as a function of Jacobi angle. (b) (left, bottom) *Ab initio* $(eQq)_D$ values in the C-D bond axis frame (black triangles) and the N-D bond axis frame (blue circles). The red line follows the $(eQq)_D$ values in the C-D bond axis frame for $\theta < 90^\circ$ and follows the $(eQq)_D$ values in the N-D bond axis frame for $\theta > 90^\circ$. (c) (right) Experimental and *ab initio* $(eQq)_N$ values for HC^{14}N and H^{14}NC in the principal inertial axis frame, which is approximately aligned with the C-N bond.

excitation. The predicted changes in quadrupole coupling constant have recently been experimentally verified in our laboratory for up to 10 quanta of bend excitation in HCN and 4 quanta in HNC by recording mm-wave pure rotational spectra of vibrationally excited HCN and HNC produced in the laser photolysis of acrylonitrile. The agreement between our simple one-dimensional theoretical model and the experimental data is remarkably good up to the highest detectable vibrational levels. We are attempting to populate higher vibrational states in both the HCN and HNC wells, in order to extend our novel use of nuclear quadrupole *hfs* as an embedded reporter of electronic structure to the isomerization process itself. At high excitation, the established pattern of the evolution of hyperfine structure with vibrational excitation will break down, first due to quantum-mechanical tunneling, and ultimately due to reorganization of the bonding electrons at the isomerization barrier. The hyperfine structure of the states exhibiting delocalization will provide a glimpse of the electronic structure at the isomerization transition state.

B. High- and low-barrier unimolecular isomerization in S_0 and S_1 HCCH

As in the HNC \leftrightarrow HCN system, the goal of our studies on the acetylene \leftrightarrow vinylidene system is to observe barrier-proximal states. Large-amplitude motion on the acetylene S_0 surface, however, is considerably more complicated than in HCN, due both to the increased number of vibrational modes and to the inversion symmetry of the molecule. Many studies have demonstrated that the vibrational eigenstates of acetylene and similar molecules undergo a normal-to-local transition in which the normal modes appropriate to describe small deviations from the equilibrium geometry evolve into local modes in which the excitation is isolated in a single C-H bond stretch or CCH bend. The evolution of vibrational character is of particular interest in the acetylene bending system because the local bending vibration bears a strong resemblance to the reaction coordinate for isomerization from acetylene to vinylidene, with one hydrogen moving a large distance off of the C-C bond axis while the other hydrogen remains relatively stationary.

1. Experimental population of lowest energy local-bender eigenstates

While the existence of local bender eigenstates in S_0 acetylene has been predicted by a variety of theoretical models, including effective Hamiltonian fits to the available experimental data, experimental verification of the character of these states has been difficult to achieve. We recently observed the first direct evidence of the S_0 local bender states. Using “local bender pluck” states on the S_1 surface as SEP intermediates, we recorded spectra that show a degenerate pair of levels with *g/u* symmetry in the energy region where the local benders are predicted to emerge. The observed degeneracy corresponds with expectations for the local bender states. We plan to record Stark effect spectra of these highly vibrationally excited levels, in order to measure their vibrationally averaged dipole moments. The barrier-proximal states we seek will have significant dipole moments due to their large amplitude motion. The ability to distinguish large amplitude motion states on the basis of the dipole moment has been demonstrated by the comparison of a one-dimensional *ab initio* model for the large amplitude vibrations with a full-dimensional calculation performed by Hua Guo (University of New Mexico). The full dimensional calculation shows that vibrational levels that are not well-described in the local mode basis have very small dipole moments and will therefore be silent in our Stark measurements.

2. Observation and theoretical treatment of vibrational levels of S_1 *cis* acetylene

Aside from its utility as an intermediate for studying highly excited vibrational states of the S_0 surface, the S_1 state also presents the possibility of low-barrier isomerization from its *trans* geometry minimum to a local energy minimum at a *cis* geometry. This process has been the focus of many theoretical studies, but it has been difficult to study experimentally because, though the *trans* minimum has been exhaustively characterized, the transition from the ground electronic state to the *cis* geometry is electronically forbidden and no transitions to this geometry have previously been observed. In the course of characterizing the S_1 surface, several levels were observed which could not be ascribed to S_1 *trans* or other electronic states. S_1 *cis* seems a likely candidate for explaining these “interloper” levels, which were, surprisingly, observed below the calculated barrier to *trans-cis* isomerization, and must therefore owe their intensity to mixing via tunneling with *trans* geometry localized states.

As part of our investigation of the *cis* well states, we undertook a discrete variable representation (DVR) calculation to try to obtain information on the delocalized wavefunctions of S_1 . Based on the input from levels of *ab initio* electronic structure calculations that reasonably reproduce the known characteristics of the *trans* isomer, our reduced dimension DVR was designed to capture the planar isomerization dynamics due to modes ν_3 and ν_6 . The initial results appear to corroborate our assignments of the interloper levels to the *cis* well, as well as revealing very intriguing and as yet uninterpreted insights into the molecular dynamics close to and above the isomerization barrier energy.

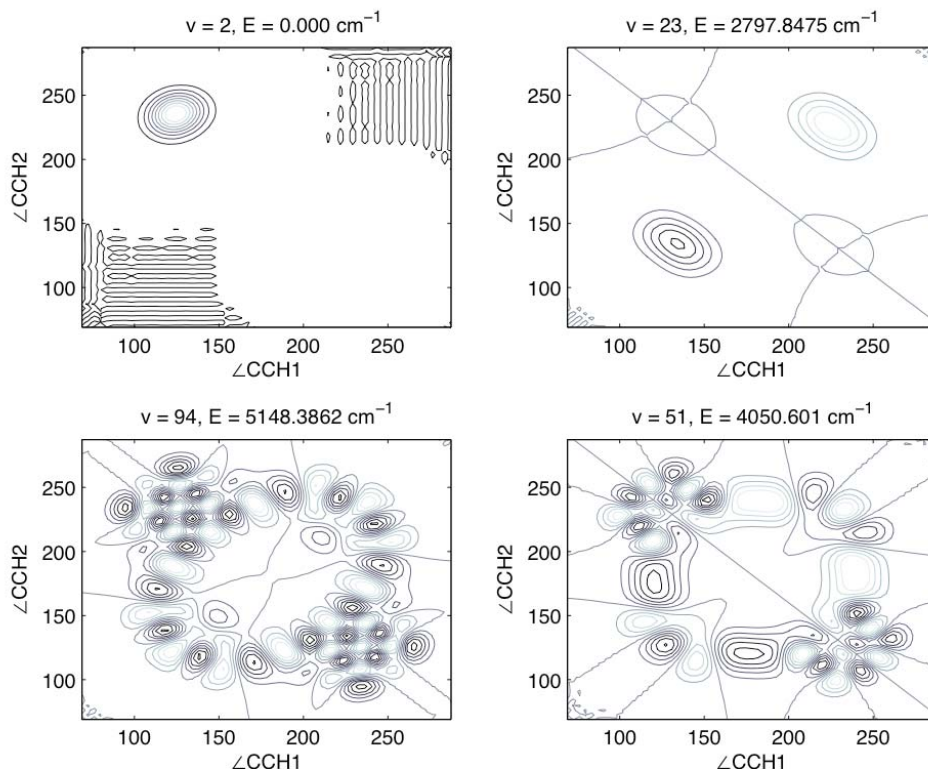


Figure 2. DVR results showing wavefunctions and energies relative to the zero point for four representative levels. (a) (top, left) The lowest *trans* well level. (b) (top, right) The lowest level localized in the *cis* well. (c) (bottom, right) A delocalized level near the isomerization barrier energy, exhibiting large probability amplitude at the transition state geometry. (d) (bottom, left) A highly excited vibrational level, representative of the qualitatively different patterns we observe above the isomerization barrier. The large elliptical orbit that connects the two *cis* wells is indicative of an out of phase *cis* bending motion.

C. Chirped pulse millimeter-wave spectroscopy

We recently began a collaboration with Brooks Pate at the University of Virginia to develop a broadband Fourier-Transform millimeter-wave spectrometer. The design is based on the chirped-pulse microwave spectrometer of Brooks Pate and coworkers (Brown, G. G.; Dian, B. C.; Douglass, K. O.; Geyer, S. M.; Pate, B. H. *J. Mol. Spec.* **238**, 200.). The Pate spectrometer takes an absorption spectrum of the 7.5-18.5 GHz region and improves acquisition time several orders of magnitude over the previous state-of-the-art Balle-Flygare microwave spectrometer, which is based on a tunable Fabry-Perot cavity. The molecules are excited by a chirped excitation pulse, which must be short relative to the molecular dephasing time, and the molecular free induction decay (FID) is downconverted and detected on a broadband 12 GHz oscilloscope. We have built a prototype spectrometer that operates in the 33-39 GHz region (Figure 3) and we are currently working to develop a spectrometer that covers the 70-100 GHz region, which contains rotational lines of interest to the C_2H_2 and HCN isomerization systems.

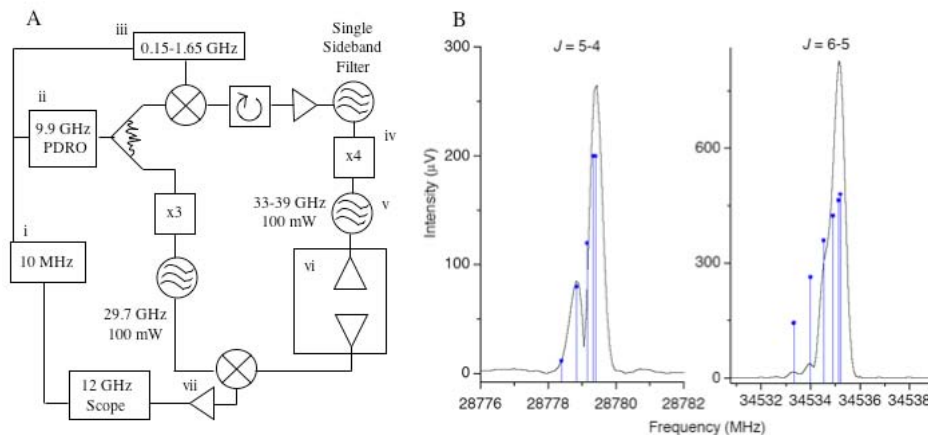


Figure 3. All components of 33-39 GHz chirped-pulse spectrometer (A) are phase-locked to the same 10 MHz Rubidium oscillator (i). A 4.2 GHz arbitrary waveform generator (iii) creates a linearly chirped pulse which is upconverted by the 9.9 GHz output of a phase-locked dielectric resonance oscillator (ii). A single sideband is selected and sent through an active frequency quadrupler (iv) and a high-pass filter (v) and into a molecular beam chamber (vi). The molecular FID is collected and downconverted by the frequency tripled output of the 9.9 GHz oscillator. The IF is sent through a low-noise amplifier (vii) and averaged on an oscilloscope. (B) A sample spectrum from trifluoropropyne was collected and the $J = 5 \leftarrow 4$ and $J = 6 \leftarrow 5$ bands are shown with expected K-structure in blue. It was possible to collect the $J = 5 \leftarrow 4$ band at 28.779 GHz because the frequency quadrupler produced some frequency tripled radiation, which extended the range of the spectrometer.

III. Future Work

We plan to use the chirped-pulse Fourier-transform millimeter-wave (CP-FTmmW) technique to locate and interrogate local bender states on the S_0 surface of acetylene. After pumping a “local bender pluck” state on the S_1 surface, the S_0 vibrational levels reached by spontaneous relaxation will be probed with CP-FTmmW. Interesting vibrational levels will be quickly identified because levels with large amplitude motion along the bending reaction coordinate will demonstrate a significant mm-wave Stark effect. Assignments of these levels can then be made using SEP.

CP-FTmmW Stark spectra will also be used to probe the electronic character of excited vibrational states in the C_2H radical. These states are of fundamental interest because the low-lying $A^2\Pi$ electronic state intersects the ground $X^2\Sigma$ state at around the energy of the ν_1 stretch (3300 cm^{-1}). The interaction is mediated by the CC stretch and the bend angle. The rovibronic spectrum of C_2H has been the subject of much investigation, but to our knowledge, no one has attempted to make direct measurements of the dipole moment. Theoretical calculations show that $A^2\Pi$ has a dipole moment that exceeds that of $X^2\Sigma$ by an order of magnitude. CP-FTmmW Stark spectroscopy will allow the dipole to be measured in C_2H vibrational states, which will yield information about the degree of electronic mixing.

IV. Publications supported by this project 2006-2008

- [1] H. A. Bechtel, A. H. Steeves, and R. W. Field, “Laboratory measurements of the hyperfine structure of $H^{14}N^{12}C$ and $D^{14}N^{12}C$,” *Astrophys. J.* **649**(1), L53–L56 (2006).
- [2] Z. Duan, R. W. Field, N. Yamakita, and S. Tsuchiya, “Differential temperature laser induced fluorescence spectroscopy,” *Chem. Phys.* **324**(2-3), 709–720 (2006).
- [3] B. M. Wong, R. L. Thom, and R. W. Field, “Accurate inertias for large-amplitude motions: Improvements on prevailing approximations,” *J. Phys. Chem. A* **110**(23), 7406–7413 (2006).
- [4] B. M. Wong, A. H. Steeves, and R. W. Field, “Electronic signatures of large amplitude motions: Dipole moments of vibrationally excited local-bend and local-stretch states of S_0 acetylene,” *J. Phys. Chem. B* **110**(38), 18,912–18,920 (2006).
- [5] B. H. Layne, L. M. Duffy, H. A. Bechtel, A. H. Steeves, and R. W. Field, “Beam action spectroscopy via inelastic scattering,” *J. Phys. Chem. A* **111**(31), 7398–7403 (2007).
- [6] W. B. Lynch, H. A. Bechtel, A. H. Steeves, J. J. Curley, and R. W. Field, “Observation of the \bar{A}^1A' state of isocyanogen,” *J. Chem. Phys.* **126**(24) (2007).
- [7] W. L. Virgo, K. L. Bittinger, A. H. Steeves, and R. W. Field, “Contrasting singlet-triplet dynamical behavior of two vibrational levels of the acetylene S_1 , $2^13^1B^2$ polyad,” *J. Phys. Chem. A* **111**, 12,534–12,537 (2007).
- [8] H. A. Bechtel, A. H. Steeves, B. M. Wong, and R. W. Field, “Evolution of Chemical Bonding during HCN/HNC Isomerization as Revealed through Nuclear Quadrupole Hyperfine Structure,” *Angew. Chemie. Int. Ed.* **47**, in press (2008).
- [9] A. J. Merer, N. Yamakita, S. Tsuchiya, A. H. Steeves, H. Bechtel, and R. W. Field, “Darling-Dennison resonance and Coriolis coupling in the bending overtone of the \bar{A}^1A_u state of acetylene, C_2H_2 ,” *J. Chem. Phys.* (submitted).

Scanning Tunneling Microscopy Studies of Chemical Reactions on Surfaces

George Flynn, Department of Chemistry, Columbia University

Mail Stop 3109, 3000 Broadway, New York, New York 10027

gwf1@columbia.edu

Introduction and Overview

Our Department of Energy sponsored work is now focused on fundamental chemical events taking place on graphite, modified graphite, graphene (single atom thick sheets of graphitic carbon), and metal surfaces with the intent of shedding light on the role of these surfaces in mediating the formation of polycyclic aromatic hydrocarbons (PAHs) and the growth of soot particles. Interest in soot is ultimately driven by the environmental and health implications arising from its formation in combustion reactions [1]. Soot growth can be divided into four consecutive stages [2-4]: formation of molecular precursors, heavy polycyclic aromatic hydrocarbons (PAHs), through homogeneous reactions of small aliphatics; nucleation of particles from these heavy PAHs followed by further coagulation; continued growth of particles through surface reactions; and finally, particle agglomeration. Polyacetylene [5] and ionic species [6] are among the proposed, key gaseous species in the formation and continuous growth of PAHs, and acetylene is thought to play a major role in the growth process via the hydrogen-abstraction-C₂H₂-addition (HACA) mechanism [7]. The application of this mechanism to the surface reaction stage of soot formation is based on the assumption that reactions occurring at the soot surface are similar to gaseous reactions taking place at the edges of PAH molecules. Experimental support for this mechanism is derived from the observation that surface growth rates for soot particle formation are proportional to the concentration of C₂H₂ in both laminar premixed [8,9] and diffusion [10] flames.

Since its invention some 25 years ago, scanning tunneling microscopy (STM) has become a powerful tool for interfacial studies mainly because of its ability to investigate surface structure and dynamics with molecular or even atomic resolution. For example, the same region of a surface can be investigated before and after exposure to reactive species using STM tip engagement techniques[11], thereby extracting information about reaction mechanisms localized at single atomic surface sites. In terms of chemical reactivity, the edges of large PAHs and the surfaces of soot particles in the third stage of growth are analogous to the edges of pits, defect sites and step edges on graphite. Studies of reaction processes on graphene (single graphite sheets) open another route for investigating the chemistry and mechanisms of reactions on carbon surfaces. These unique materials can be investigated with scanning probe methods and their reactivity compared to that of defected graphite. Exposure of well characterized, defected graphite and graphene surfaces to oxygen or hydrocarbon fuels (e.g. C₂H₂) in a controlled manner under ultra-high vacuum (UHV) conditions, thus, provides an opportunity to investigate the fundamental chemical steps involved in carbon chemistry and soot formation. Scanning Tunneling Microscopy can be used to identify surface defects and step edges, as well as to resolve and probe individual molecules on surfaces. The convenience and importance of being able to probe

single molecules and/or single sites on surfaces probably cannot be overemphasized. Graphite itself is largely inert and reactive events are likely to occur when individual molecules are at or near dangling surface bonds typically found only at defect sites or step edges. As noted below, reactions of graphene surfaces with O₂ proceed more rapidly than the analogous processes on graphite, and this may signal the presence of a different oxidation mechanism for graphite and graphene, one which is likely related to the non-planar properties of graphene.

In the present study, single- and multiple-layer graphene regions are present simultaneously in a single sample; thus, oxidation as a function of the number of carbon layers can be directly compared. Samples were heated in an O₂/Ar gas flow at various temperatures (typically for a fixed 2 hour period). Tens of samples, oxidized at different temperatures, were examined, and oxidative etching was observed to proceed faster in single layers than in multiple layers. Oxidation at 500°C causes etch pits 20 to 180 nm in diameter to appear in single-layer graphene, but not in double-layer sheets.

Results: Oxidation of Single, Double and Triple Layer Graphene

Oxidative etching was carried out at 200°C, 250°C, 300°C, 400°C, 450°C, 500°C, and 600°C. Atomic Force Microscopy (AFM) showed no etching of single-, double-, and triple-layer graphenes for oxidation at or below 400°C. Etch pits (~20 nm diameter) were found on single layers at 450°C, but not on multiple-layer samples even up to 500°C. The distributions of etch pit diameters on single graphene layers are quite broad. Higher temperatures induce faster oxidation. At 600°C most of the etch pits merged to give fewer, larger pits in single-layer samples. Etch pits also occurred in both double-layer and triple-layer graphene. Both one- and two-layer-deep etch pits were observed in double-layer graphene. In contrast, only single-layer-deep pits were observed in triple-layer (or thicker) graphene. Remarkably, the diameters of one-layer-deep pits on both double-layer and triple-layer sheets show narrow distributions with peaks around 220 nm. A similar distribution was obtained in the oxidation of many-layer thick “graphite flakes” on the same substrate. This narrow distribution of pit sizes has been previously observed in the oxidation of the top layer in highly oriented pyrolytic graphite (HOPG)[^{12, 13}]. The diameters of two-layer-deep etch pits on double-layer sheets are much greater (300 - 550 nm).

Oxidative etching of triple-layers is similar to oxidation of natural graphite[^{14, 15}] and HOPG[^{12, 13}]. Uniformly-sized one-layer-deep etch pits were observed in these studies, leading to the conclusion that oxidation was initiated at pre-existing point defects, followed by constant radial growth of the pits. This mechanism is supported by a study in which uniformly-sized pits were found on a HOPG sample after point defects were intentionally introduced by argon ion bombardment[¹⁶]. The one-layer-deep pits on our triple-layers are attributed to these same pre-existing defects since the pit diameters are nearly identical to those found on graphite flakes on the same substrate. In addition, the pit density (~4/μm²) on the triple-layer sheet is the same as that on the graphite flake and within

the same range as that reported for naturally-occurring defect densities for various graphites^[14, 15]. Thus, it appears that oxidative etching is not initiated on defect-free basal planes of triple-layers, at least at or below 600°C.

At high temperatures irreversible oxidation clearly occurs, the extent of which varies with layer-thickness: single-layers oxidize more quickly than double-layers, which oxidize more quickly than triple-layers and bulk graphite. The thickness dependence should be linked to the geometries of the oxidation transition states and intermediates. Any covalent bond formed between an oxygen atom and a carbon atom in graphene will result in one or perhaps two tetrahedral carbon atoms. This implies an abrupt and local bend in the carbon sheet. The height of the oxidation activation barrier is directly related to the energetic cost of this bend: the stiffer the carbon sheet, the higher the activation barrier. There is a strong conformal attraction between graphene sheets. Thus, although sheets can easily slip across one another, perpendicular motion is very costly. Any bending of a single sheet in a graphene stack will be opposed by the inter-sheet attraction. The graphene stack acts like a leaf spring; the larger the number of sheets, the stiffer the “spring” and, therefore, the higher the activation barrier.

Present and Future Experimental Program

Variable temperature, UHV STM will be a powerful tool with which to investigate the oxidation mechanism for graphene. For example, single graphene sheets mounted on a silicon oxide substrate show height variations across the sample that must be correlated with local tetrahedral bond formation^[17]. It should be possible to probe reaction localized at individual atomic sites with STM and to correlate this reactivity with local surface curvature. Of course, reactions occurring at defect sites in the graphene surface can also be investigated in the same way.

References

- (1) Neilson, A. H.; Editor *The Handbook of Environmental Chemistry, Volume 3: Anthropogenic Compounds, Part J: PAHs and Related Compounds: Biology*, 1997.
- (2) Harris, S. J.; Weiner, A. M. *Annual Review of Physical Chemistry* **1985**, 36, 31.
- (3) Richter, H.; Howard, J. B. *Progress in Energy and Combustion Science* **2000**, 26, 565.
- (4) Frenklach, M. *Physical Chemistry Chemical Physics* **2002**, 4, 2028.
- (5) Homann, K. H.; Wagner, H. G. *Symposium (International) on Combustion, [Proceedings]* **1967**, 11, 371.
- (6) Calcote, H. F. *Combustion and Flame* **1981**, 42, 215.
- (7) Frenklach, M.; Wang, H. *Symposium (International) on Combustion, [Proceedings]* **1991**, 23rd, 1559.
- (8) Harris, S. J.; Weiner, A. M. *Combustion Science and Technology* **1983**, 32, 267.
- (9) Xu, F.; Sunderland, P. B.; Faeth, G. M. *Combustion and Flame* **1997**, 108, 471.

- (10) Xu, F.; Faeth, G. M. *Combustion and Flame* **2001**, *125*, 804.
- (11) Rim, K. T.; Mueller, T.; Fitts, J. P.; Adib, K.; Camillone, N., III; Osgood, R. M.; Batista, E. R.; Friesner, R. A.; Joyce, S. A.; Flynn, G. W. *Journal of Physical Chemistry B* **2004**, *108*, 16753.
- (12) Chang, H.; Bard, A. J. *Journal of the American Chemical Society* **1990**, *112*, 4598-9.
- (13) Tracz, A.; Wegner, G.; Rabe, J. P. *Langmuir* **1993**, *9*, 3033-3038.
- (14) Yang, R. T.; Wong, C. *Journal of Chemical Physics* **1981**, *75*, 4471-6.
- (15) Evans, E. L.; Griffiths, R. J. M.; Thomas, J. M. *Science (Washington, DC, United States)* **1971**, *171*, 174-5.
- (16) Lee, S. M.; Lee, Y. H.; Hwang, Y. G.; Hahn, J. R.; Kang, H. *Physical Review Letters* **1999**, *82*, 217-220.
- (17) Stolyarova, E.; Rim, K. T.; Ryu, S.; Maultzsch, J.; Kim, P.; Brus, L.E.; Heinz, T. F.; Hybertsen, M. S.; Flynn, G. W.; *Proc. Nat. Acad. Sci.* **2007**, *104*, 9209-9212.

DOE Publications: (2005-2008)

1. Gina M. Florio, Tova L. Werblowsky, Thomas Mueller, Bruce J. Berne, and George W. Flynn, "The Self-Assembly of Small Polycyclic Aromatic Hydrocarbons on Graphite: A Combined STM and Theoretical Approach", *J. Phys. Chem. B*, **109**, 4520-4532 (2005)
2. Elena Stolyarova, Kwang Taeg Rim, Sunmin Ryu, Janina Maultzsch, Philip Kim, Louis E. Brus, Tony F. Heinz, Mark S. Hybertsen, and George W. Flynn, "High-Resolution Scanning Tunneling Microscopy Imaging of Mesoscopic Graphene Sheets on an Insulating Surface", *Proc. Nat. Acad. Sci.*, **104**, 9209-9212 (2007)
3. Kwang Taeg Rim, Mohamed Siaj, Shengxiong Xiao, Matthew Myers, Vincent D. Carpentier, Li Liu, Chaochin Su, Michael L. Steigerwald, Mark S. Hybertsen, Peter H. McBreen, George W. Flynn, and Colin Nuckolls, "Forming Aromatic Hemispheres on Transition Metal Surfaces", *Angew. Chem. Int. Ed.* **46**, 7891-7895 (2007)
4. Elena Stolyarova, Daniil Stolyarov, Li Liu, Kwang T. Rim, Yuanbo Zhang, Melinda Han, Mark Hybertsen, Philip Kim and George Flynn, "STM Studies of Ultrathin Graphitic (Graphene) Films on an Insulating Substrate under Ambient Conditions", *J. Phys. Chem.*, accepted.
5. Li Liu, Sunmin Ryu, Michelle R. Tomasik, Elena Stolyarova, Naeyoung Jung, Mark S. Hybertsen, Michael L. Steigerwald, Louis E. Brus, George W. Flynn, "Graphene Oxidation: Thickness Dependent Etching and Strong Chemical Doping", submitted
6. Li Liu, Kwang Taeg Rim, Daejin Eom, Tony Heinz, and George W. Flynn "Growth of Graphitic Layers at Defect Sites on Highly Ordered Pyrolytic Graphite Studied by Scanning Tunneling Microscopy," submitted
7. Daejin Eom, K. T. Rim, H. Zhou, L. Liu, M. Lefenfeld, S. Xiao, E. Stolyarova, P. Lewis, M. Hybertsen, C. Nuckolls, Tony Heinz, and George W. Flynn, "STM Probes of Edge-Localized States of Graphene Quantumdots on Co(0001)", in preparation.

Quantitative Imaging Diagnostics for Reacting Flows

Jonathan H. Frank

Combustion Research Facility
Sandia National Laboratories
P.O. Box 969, MS 9051
Livermore, CA 94551-0969
email: jhfrank@sandia.gov

Program Scope

The primary objective of this project is the development and application of laser-based imaging diagnostics for studying the interactions of fluid dynamics and chemical reactions in reacting flows. Imaging diagnostics provide temporally and spatially resolved measurements of species, temperature, and velocity distributions over a wide range of length scales. Multi-dimensional measurements are necessary to determine spatial correlations, scalar and velocity gradients, flame orientation, curvature, and connectivity. Current efforts in the Advanced Imaging Laboratory focus on planar laser-induced fluorescence (PLIF) and Rayleigh scattering techniques for probing the detailed structure of both isolated flow-flame interactions and turbulent flames. The investigation of flow-flame interactions is of fundamental importance in understanding the coupling between transport and chemistry in turbulent flames. These studies require the development of new imaging diagnostic techniques to measure key species in the hydrocarbon-chemistry mechanism as well as to image rates of reaction and dissipation.

Recent Progress

Recent research has continued to emphasize imaging diagnostics for probing the detailed structure of reaction zones during flow-flame interactions. Research activities have included: i) Studies of dissipation and localized extinction in turbulent jet flames, ii) Studies of extinction and re-ignition dynamics in isolated flow-flame interactions, iii) Interference-free two-photon H-atom PLIF imaging.

Probing Dissipation and Localized Extinction in Turbulent Flames

We have conducted detailed studies of thermal dissipation length scales and localized extinction in turbulent non-premixed jet flames. The thermal dissipation is closely correlated with the mixture fraction dissipation, which is a fundamental quantity governing the rate of molecular mixing in turbulent non-premixed combustion. Turbulent fluctuations in the mixing rates induce significant variations in the combustion reaction rates and can result in localized extinction. Intermittent extinction events affect the stability, efficiency, and pollutant emissions of practical combustion devices.

Building on our advances in high-resolution measurements of thermal dissipation, we have combined dissipation imaging with laser-induced fluorescence imaging of the OH radical. Figure 1 shows an example of simultaneous temperature and OH PLIF measurements in non-premixed $\text{CH}_4/\text{H}_2/\text{N}_2$ jet flames ($\text{Re} = 15,200$ and $22,800$) that are target flames in the TNF Workshop. Thermal dissipation is determined from the temperature images, and extinguished regions are identified by discontinuities in the OH radical distribution. The presence of the OH radical is an indicator of the intact system of high-temperature combustion reactions. We have measured the probability of localized extinction and the size distributions of the extinguished

regions throughout the near field ($x/d = 5-20$) of these turbulent jet flames. The results provide unique insight into extinction from turbulence-flame interactions. The size distributions of the extinguished regions showed very little variation throughout the near field of the flames despite the increase in turbulence length scales with downstream location. In the lower Reynolds number flame, the probability of extinction events was approximately constant from $x/d = 5-15$. In contrast, the higher Reynolds flame showed a progression from fragmented reaction zones with a high probability of local extinction near the nozzle to mostly continuous reaction zones at $x/d = 20$.

We have also used the simultaneous temperature/OH-PLIF measurements to study statistics of thermal dissipation length scales conditioned on rich and lean regions of the flame. The temperature dependence of the dissipation length scales were very different for lean and rich conditions. For rich conditions, the dissipation layer widths increased significantly with temperature. Dissipation layers on the lean side had the opposite temperature dependence due to entrainment of the coflowing air stream. This finding represents an important refinement to our earlier work, which only considered the unconditional layer width statistics. The new results on dissipation length scales and localized extinction will be compared with simulations to improve understanding of turbulence-flame interactions and to develop accurate turbulent combustion models.

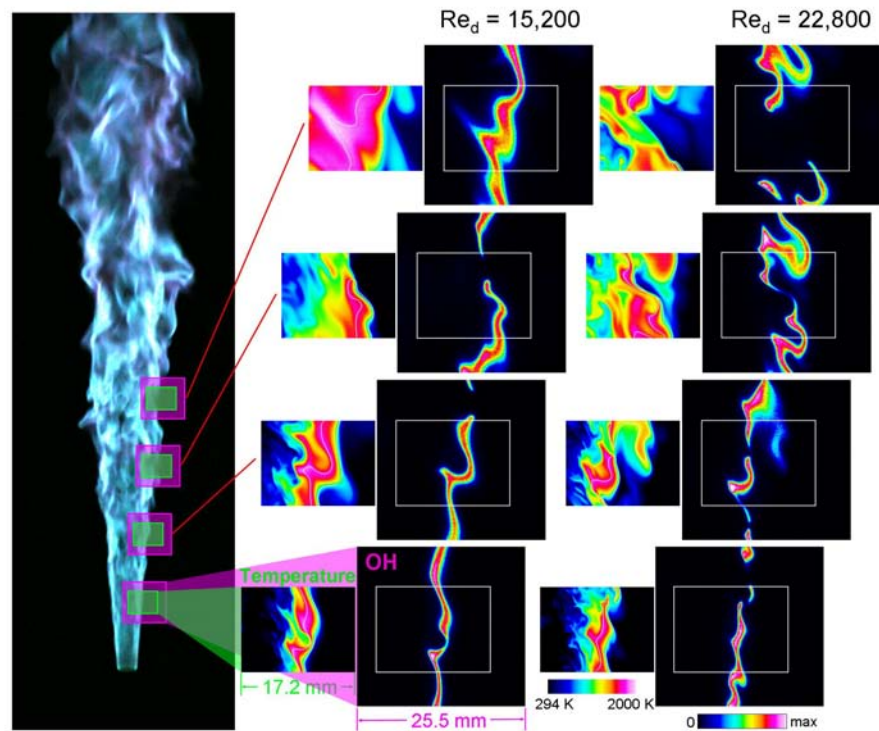


Fig. 1: Simultaneous single-shot temperature and OH PLIF measurements in turbulent jet flames with Reynolds numbers of 15,200 and 22,800. The white rectangles in the OH PLIF images indicate the location of the temperature measurements. Temperatures were measured by laser Rayleigh scattering.

Dynamics of Extinction and Ignition

We have continued an extensive series of studies on isolated well-controlled extinction and ignition events in transient counterflows. The experiments are closely coupled with direct numerical simulations by Jackie Chen (Sandia). The goal of this effort is to provide a detailed understanding of the interactions between ignition chemistry and unsteady transport, including effects of diluents and trace species. We have studied the counteracting effects of NO and water vapor addition on the dynamics of extinction and re-ignition of hydrogen flames in a transient counterflow. The catalytic effect of NO and the retardant effect of water vapor compete to determine whether the flame recovers by autoignition, edge-flame propagation, or a combination of both mechanisms. These re-ignition modes have very different flame recovery times. The results provide insight into dynamics of ignition and extinction in systems with partial mixing of combustion products and reactants.

Interference-Free Two-photon LIF Imaging of Atomic Hydrogen

Atomic hydrogen is highly diffusive and reactive and is central to combustion chemistry. Quantitative detection of atomic hydrogen in flames is challenging because it requires multi-photon diagnostic techniques that are susceptible to interferences. We have demonstrated interference-free laser-induced fluorescence imaging of atomic hydrogen in laminar premixed methane flames using two-photon excitation ($\lambda_{\text{excitation}}=205 \text{ nm}$, $3d \ ^2D \leftarrow \leftarrow 1s \ ^2S$, $\lambda_{\text{detection}}=656 \text{ nm}$ from $H(n=3) \rightarrow H(n=2)$ transitions) with 100-ps laser pulses from a distributed feedback dye laser. The use of picosecond laser pulses significantly reduces interferences from photodissociation that can be problematic for nanosecond laser excitation. This effort builds upon our demonstration of interference-free two-photon O-atom LIF imaging with a ps pulsed laser for excitation. These studies are conducted in collaboration with Tom Settersten (Sandia).

Future Plans

We plan to extend the studies of extinction and re-ignition dynamics to consider a range of hydrocarbon fuels and additives. The results will provide test cases for DNS with detailed chemical mechanisms. The interference-free H-atom LIF measurement technique will be used to study the effects of differential diffusion of atomic hydrogen in edge-flames that are formed during extinction and re-ignition. Differential diffusion of H-atoms will also be studied in fuel mixtures with different Lewis numbers.

The detailed studies of localized extinction and turbulence structures in jet flames will be coupled with large-eddy simulations (LES) by Joe Oefelein (Sandia). The turbulence length scale measurements have already helped guide the selection of the computational grid for these simulations. Comparisons of LES simulations and experiments provide a unique opportunity for advancing our understanding of the spatial structures and temporal evolution of turbulent flames.

Our studies of the spatial structure of dissipation and extinction in turbulent jet flames will be complemented by the development of a high repetition-rate imaging facility for measuring the temporal evolution of turbulent flames. It is important to understand time history effects in the interactions between turbulent flows and flames. This information is not available from ensemble statistics of instantaneous snapshot measurements because the measurements are temporally uncorrelated. The ability to measure time sequences, or movies, will allow us, and users of this facility from the combustion community, to study the temporal development of turbulent structures and to understand the events that lead up to and follow localized extinction and re-ignition.

DOE Supported Publications (2006–2008)

- B.O. Ayoola, R. Balachandran, J.H. Frank, E. Mastorakos, C.F. Kaminski, "Spatially resolved heat release rate measurements in turbulent premixed flames," *Combust. Flame* 144:1 (2006).
- A. D. Elder, S. M. Matthews, J. Swartling, K. Yunus, J. H. Frank, C. M. Brennan, A. C. Fisher, C. F. Kaminski, "The application of frequency-domain fluorescence lifetime imaging microscopy as a quantitative analytical tool for microfluidic devices," *Opt. Exp.* 14:5456 (2006).
- C.M. Vagelopoulos, J.H. Frank, "Transient Response of Premixed CH₄ Flames," *Combust. Flame* 146:572 (2006).
- G. Amantini, J. H. Frank, M. D. Smooke, A. Gomez, "Computational and experimental study of standing CH₄ edge flames in the two-dimensional axisymmetric counterflow geometry", *Combust. Flame* 147:133 (2006).
- A.D. Elder, J.H. Frank, J. Swartling, C.F. Kaminski, "Calibration of a wide-field frequency-domain fluorescence lifetime microscopy system using LEDs as light sources", *J. Microscopy* 224:166 (2006).
- G. Amantini, J. H. Frank, M. D. Smooke, A. Gomez, "Computational and experimental study of steady axisymmetric non-premixed CH₄ counterflow flames," *Combust. Theory and Modeling* 11:47 (2007).
- G. Amantini, J.H. Frank, B.A.V. Bennett, M.D. Smooke, A. Gomez, "Comprehensive study of the evolution of an annular edge flame during extinction and reignition of a counterflow diffusion flame perturbed by vortices," *Combust. Flame*, 150:292 (2007).
- J.H. Frank, A.D. Elder, J. Swartling, A.R. Venkitaraman, A.D. Jeyasekharan, C.F. Kaminski, "A white light confocal microscope for spectrally resolved multidimensional imaging," *J. Microscopy* 227:203 (2007).
- S.A. Kaiser and J.H. Frank, "Imaging of dissipative structures in the near field of a turbulent non-premixed jet flame," *Proc. Combust. Inst.* 31:1515 (2007).
- J.H. Frank and S.A. Kaiser, "High-resolution imaging of dissipative structures in a turbulent jet flame with Rayleigh scattering," *Exp. Fluids* 44:221 (2008).
- W.D. Kulatilaka, J.H. Frank, T.B. Settersten, "Interference-free two-photon LIF imaging of atomic hydrogen in flames using picosecond excitation," *Proc. Combust. Inst.*, submitted (2008).
- S.A. Kaiser and J.H. Frank, "Spatial scales of extinction and dissipation in the near field of non-premixed turbulent jet flames," *Proc. Combust. Inst.*, submitted (2008).
- U.D. Lee, C.S. Yoo, J.H. Chen, J.H. Frank, "Effects of H₂O and NO on extinction and re-ignition of vortex-perturbed hydrogen counterflow flames," *Proc. Combust. Inst.*, submitted (2008).
- E.R. Hawkes, R. Sankaran, J.H. Chen, S.A. Kaiser, J.H. Frank, "An analysis of lower-dimensional approximations to the scalar dissipation rate using direct numerical simulations of plane jet flames," *Proc. Combust. Inst.*, submitted (2008).

MECHANISM AND DETAILED MODELING OF SOOT FORMATION

Principal Investigator: Michael Frenklach

Department of Mechanical Engineering
The University of California
Berkeley, CA 94720-1740
Phone: (510) 643-1676; E-mail: myf@me.berkeley.edu

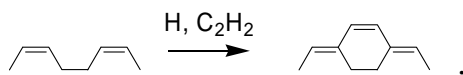
Project Scope: Soot formation is one of the key environmental problems associated with operation of practical combustion devices. Mechanistic understanding of the phenomenon has advanced significantly in recent years, shifting the focus of discussion from conceptual possibilities to specifics of reaction kinetics. However, along with the success of initial models comes the realization of their shortcomings. This project focuses on fundamental aspects of physical and chemical phenomena critical to the development of predictive models of soot formation in the combustion of hydrocarbon fuels, as well as on computational techniques for the development of predictive reaction models and their economical application to CFD simulations. The work includes theoretical and numerical studies of gas-phase chemistry of gaseous soot particle precursors, soot particle surface processes, particle aggregation into fractal objects, and development of economical numerical approaches to reaction kinetics.

Recent Progress:

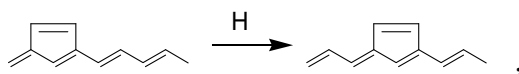
Graphene Layer Growth Chemistry: Embedded-ring Migration on Graphene Zigzag Edge (with R. Whitesides, D. Domin, R. Salomón-Ferrer, W. A. Lester, Jr.)

The mechanisms of soot formation have been studied for quite some time, and there is general consensus that polycyclic aromatic hydrocarbons (PAH) are key intermediates: their growth leads to nucleation of particles and the latter continue to add mass via surface growth. Detailed understanding of the underlying phenomena often invokes HACA, which describes the growth of both gaseous PAH molecules and graphitic edges of soot particles as a repetitive reaction sequence of substrate activation by gaseous hydrogen atoms followed by addition of carbon (usually acetylene) to the activated site thereby leading to the formation of the aromatic rings.

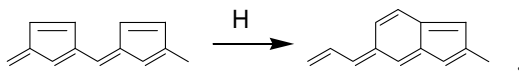
In the initial formulation, the HACA sequence was presumed to take place on the arm-chair edge of graphene sheets,



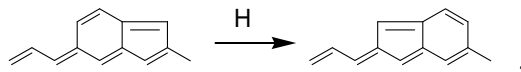
as the geometry of the arm-chair edge leads to energy-favorable ring closure. Recent studies have focused on zigzag graphene edges. On a flat zigzag edge, the HACA sequence forms a five-membered ring, which can move (or migrate) along the zigzag edge,



and transform into a six-membered ring at corners of the edge. The mobility of surface rings is of critical importance to the growth rate and evolving morphology, thus pointing to the need for understanding the ring-migration chemistry. The ring collision,

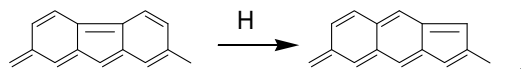


was found to be one of the important reaction steps. The collision reaction allows a new layer to be initiated at the center of a layer instead of at the corners, implying that five-member rings could also be included in the layer nucleation process in addition to being transformed into six-member rings. Most recently, the product of the ring collision has been examined and a pathway in which it isomerizes to reverse its orientation, or flips,



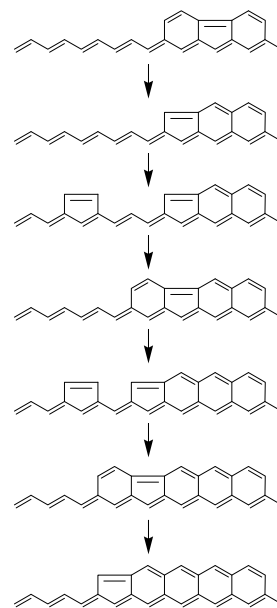
has been identified. The rate of the flip reaction was found to be of the same order of magnitude as those of collision and migration, thus further implicating five-member rings in zigzag-edge processes.

One of the intriguing questions that the flip reaction brings is whether a five-member ring will be embedded in the growing layer or whether it will be “pushed out” to the corner of the edge via reactions like



This constitutes the subject of our past-year study. We computed the minimum energy path of the above reaction on the smallest substrate, determined its rates, and compared them with previously reported zigzag-edge reactions. The elementary steps of the pathways were analyzed using density-functional theory (DFT). Rate coefficients were obtained by classical transition-state-theory utilizing the DFT energies, frequencies, and geometries.

The results indicate that this new reaction sequence is competitive with the flip reaction and other zigzag-edge reactions. The fast kinetics indicates that the embedded ring moves essentially freely within the zigzag edge. On larger substrates, the reaction thermodynamically slightly favors the configuration with the five-member ring in the interior of the edge as opposed to at the corner, causing embedded rings to be found more often away from the corner of zigzag edges. In spite of this slight thermodynamic preference, the occurrence of the embedded-ring migration reaction gives embedded rings ample access to the edge corner where they may interact with migrating rings or with gas phase species. The high mobility of embedded rings enables the layer to minimize the inclusion of five-member rings, and thus should contribute significantly to annealing and smoothing of growing surfaces, as illustrated on the right.



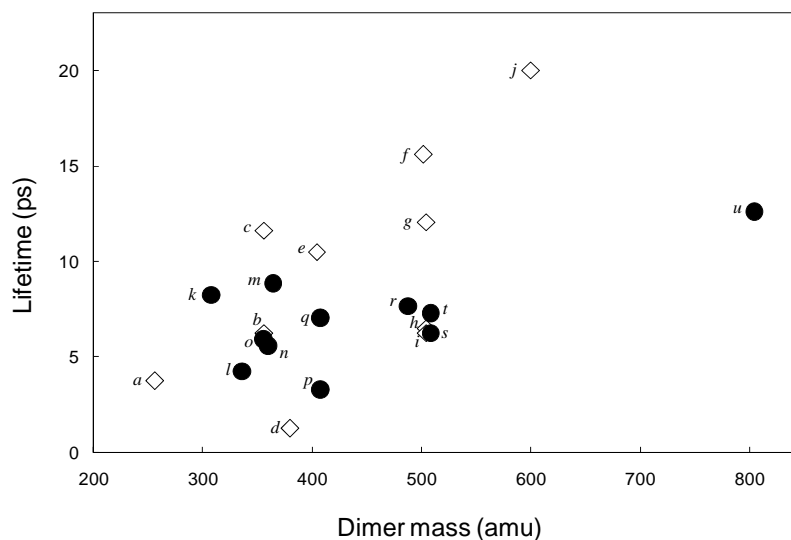
Molecular Dynamics Simulations of PAH Dimerization (with D. Wong, R. Whitesides, and A. C. Schuetz)

In pursuit of mechanistic understanding of soot nucleation, collisions between aromatic molecules were investigated using molecular dynamics (MD) simulations with on-the-fly quantum forces. Simulations were conducted at a temperature of 1600 K, with vibrationally and rotationally equilibrated colliders, investigating the formation of dimers for a series of aromatic hydrocarbons. The new results are collisions of aromatic molecules linked by aliphatic chains (AALH) and comparison of these results to those of peri-condensed aromatics (PCAH).

The following figure summarizes the present MD results, displaying the maximum lifetimes of PCAH dimers with open diamonds and those of AALH dimers with solid circles. For PCAH

dimers, we see a clear trend of increasing lifetimes with the dimer mass. For AALH this trend is less evident.

(naphthalene) ₂	<i>a</i>
(anthracene) ₂	<i>b</i>
(phenanthrene) ₂	<i>c</i>
perylene-naphthalene	<i>d</i>
(pyrene) ₂	<i>e</i>
pyrene-coronene	<i>f</i>
(perylene) ₂	<i>g</i>
(benzo[e]pyrene) ₂	<i>h</i>
(benzopyrene) ₂	<i>i</i>
(coronene) ₂	<i>j</i>
(biphenyl) ₂	<i>k</i>
(biphenylmethane) ₂	<i>l</i>
(biphenylethane) ₂	<i>m</i>
(biphenylethylene) ₂	<i>n</i>
(biphenylacetylene) ₂	<i>o</i>
(1-phenylnaphthalene) ₂	<i>p</i>
(2-phenylnaphthalene) ₂	<i>q</i>
(triphenylmethane) ₂	<i>r</i>
(1,1-binaphthyl) ₂	<i>s</i>
(1,2-binaphthyl) ₂	<i>t</i>
(1,2-bipyrene) ₂	<i>u</i>



Comparing the results for smaller masses, we observe that collisions of *two*-ring AALH (e.g., biphenyl molecules, Point *k*, and biphenylethane molecules, Point *m*) produced dimers with lifetimes comparable to those produced in collisions of larger, *four*-ring PCAH (e.g., pyrene molecules, Point *e*) and significantly larger than those from *two*-ring PCAH (naphthalene molecules, Point *a*). While this observation could be interpreted as an increased stickiness of AALH as compared to PCAH, the effect, perhaps surprisingly, is not as dramatic as one would expect. Indeed, based on the mechanism of PAH dimerization identified as being energy trapping in internal rotors, the expectation, and hence motivation for the present study, was that a substantial increase in the number of internal rotors in the colliding molecules should substantially increase the dimer lifetimes. Yet, the numerical effect is not an order-of-magnitude but a relatively small factor.

Still, it could be that even these relatively small differences in the stickiness of the smaller, incepting particles have a profound influence on the overall rate of nucleation. The two types of precursor molecules should produce different precursor particles: collisions of PCAHs resulting in graphitic-like turbostratic stacks of graphene sheets and collisions of AALHs producing kerogen-like material. The past numerical results suggested that soot particle nucleation can proceed through two regimes, via AALH at conditions of high propensity to chemical growth (e.g., low temperatures, fuel-rich composition) and via most stable intermediates, PCAH, at harsh growth condition (e.g., high temperatures, near-stoichiometric mixtures). Following the present MD results, the initial, small-ring-size AALH molecules will dimerize faster than equivalent-ring-size PCAH molecules, consistent with the high- and low-propensity to growth, and hence soot formation, regimes.

At the same time, and perhaps more importantly, the results obtained for the smaller AALH dimers seem to follow the same trend with the dimer *mass* as seen for the PCAH dimers, perhaps implying that the aliphatic linking is not really a dominating factor.

With the increase in mass there is a clear difference between the two groups: AALH dimers appear to have substantially lower lifetimes than the PCAH ones of comparable mass. This

result could be consistent with the interpretation given to recent experimental observations of D'Alessio et al. on lower stickiness of emergent carbon nanoparticles.

Future Plans

Graphene Layer Growth Chemistry: We will continue exploration of reactions on zigzag edges of a graphene sheet. This work will be performed in collaboration with William Lester's group, performing DFT analysis of the reaction systems and then QMC analysis on most critical reaction steps identified in the prior DFT studies. For every reaction system, a complete set of rate coefficients will be established in master-equation solutions.

Homogeneous Nucleation of Carbon Nanoparticles: We will continue exploration of clustering of aromatic species through molecular dynamics simulations with on-the-fly quantum forces. Our objective is to complete the comparison of the AALH and PCAH collision dynamics.

Developing Models for Representing Combustion Chemistry at Varying Levels of Complexity to Use with Models for Laminar and Turbulent Flow Fields to Describe Combustion Processes: The collaboration with the Sandia group of Habib Najm will continue on the combination of the CSP-slow-manifold projection method and PRISM to construct an adaptive reduced-order model for stiff dynamical systems.

DOE-BES Supported Publications (2006-2008)

1. "Quantum Monte Carlo Study of Small Hydrocarbon Atomization Energies," A. C. Kollias, D. Domin, G. Hill, M. Frenklach, W. A. Lester, Jr., *Mol. Phys.* **104**, 467 (2006).
2. "Graphene Layer Growth: Collision of Migrating Five-Membered Rings," R. Whitesides, A. C. Kollias, D. Domin, W. A. Lester, Jr., and M. Frenklach, *Prepr. Pap.-Am. Chem. Soc., Div. Fuel Chem.* **51**, 174 (2006).
3. "A CSP and Tabulation Based Adaptive Chemistry Model," J. C. Lee, H. N. Najm, S. Lefantzi, J. Ray, M. Frenklach, M. Valorani, and D. A. Goussis, *Combust. Theory Model.* **11**, 73 (2007).
4. "Transforming Data into Knowledge—Process Informatics for Combustion Chemistry," M. Frenklach, *Proc. Combust. Inst.* **31**, 125 (2007), Invited Topical Review.
5. "Graphene layer growth: Collision of migrating five-member rings," R. Whitesides, A. C. Kollias, D. Domin, W.A. Lester, Jr., and M. Frenklach, *Proc. Combust. Inst.* **31**, 539 (2007).
6. "Numerical Simulations of Soot Aggregation in Premixed Laminar Flames," N. Morgan, M. Kraft, D. Wong, M. Frenklach, P. Mitchell, *Proc. Combust. Inst.* **31**, 693 (2007).
7. "Efficient Slow Manifold Identification for Tabulation Based Adaptive Chemistry," *Proceedings of the 5th U.S. National Combustion Meeting*, San Diego, CA, March 25-28, 2007, Paper No. C31.
8. "Graphene Layer Growth Chemistry: Five-Six-Ring Flip Reaction," R. Whitesides, D. Domin, W. A. Lester, Jr., and M. Frenklach, *Proceedings of the 5th U.S. National Combustion Meeting*, San Diego, CA, March 25-28, 2007, Paper No. D31.
9. "Molecular Dynamics Simulations of PAH Dimerization," D. Wong, C. A. Schuetz, and M. Frenklach, *Proceedings of the 5th U.S. National Combustion Meeting*, San Diego, CA, March 25-28, 2007, Paper No. F21.
10. "Optimization of Reaction Models with Solution Mapping," M. Frenklach, A. Packard, and R. Feeley, in *Modeling of Chemical Reactions* (R. W. Carr, Ed.), Elsevier: Amsterdam 2007, (Elsevier series Comprehensive Chemical Kinetics, Vol. 42), pp. 243-291.
11. "Efficient Slow Manifold Identification for Tabulation Based Adaptive Chemistry," J. M. Ortega, H. N. Najm, M. Valorani, D. A. Goussis, and M. Y. Frenklach, 21st International Colloquium on the Dynamics of Explosions and Reactive Systems, Poitiers, France, July 22-27, 2007, Paper 231.
12. "Isomer Energy Differences for the C₄H₃ and C₄H₅ Isomers Using Diffusion Monte Carlo," D. Domin, W. A. Lester Jr., R. Whitesides, and M. Frenklach, *J. Phys. Chem.* **112**, 2065 (2008).
13. "Graphene Layer Growth Chemistry: Five- and Six-Member Ring Flip Reaction," R. Whitesides, D. Domin, R. Salomón-Ferrer, W. A. Lester Jr., and M. Frenklach, *J. Phys. Chem.* **112**, 2125 (2008).
14. "Molecular Dynamics Simulations of PAH Dimerization," D. Wong, R. Whitesides, C. A. Schuetz and M. Frenklach, *Proceedings of the International Workshop on Combustion Generated Fine Carbon Particles*, accepted for publication.

CHEMICAL DYNAMICS IN THE GAS PHASE: QUANTUM MECHANICS OF CHEMICAL REACTIONS

Stephen K. Gray

Chemical Sciences and Engineering Division
Argonne National Laboratory
Argonne, IL 60439

Email: gray@tcg.anl.gov

PROGRAM SCOPE

This program focuses on theoretical chemical reaction dynamics, with an emphasis on the development and application of rigorous quantum dynamics approaches. Time-dependent quantum methods (wave packets) and iterative time-independent quantum methods are used to study the spectroscopy and dynamics of combustion-relevant problems. The results obtained allow one to gauge the quality of potential energy surfaces, and to infer the validity of more approximate theoretical methods such as quasiclassical trajectories and statistical theories. The results also yield important mechanistic insights into the dynamics.

RECENT PROGRESS

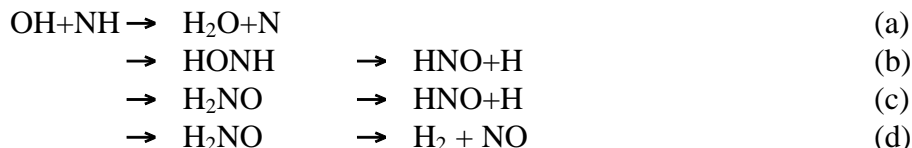
Extending our previous total angular momentum $J = 0$ work on the $\text{CH} + \text{H}_2 \rightarrow \text{CH}_2 + \text{H}$ reaction [1], a variety of $J > 0$ wave packet calculations were carried out in collaboration with Goldfield. A capture model similar in spirit to that of Lin and Guo [2] was used to allow prediction of the low and high pressure rate constants. The quantum capture probabilities were found to be highly dependent on the initial alignment of reactants. Our quantum results were contrasted with experimental results [3] and phase space theory predictions.

We completed a wave packet study of the fundamental $\text{D} + \text{H}_2 \rightarrow \text{HD} + \text{H}$ exchange reaction when confined within a carbon nanotube [4]. This work showed that reaction probabilities can be considerably enhanced owing to orientational effects and that the reaction thresholds can be lowered due to zero-point energy effects.

Work was initiated on the quantum dynamics of the unimolecular decompositions of HOOH and H_2CO . In the case of HOOH , a quantum treatment is needed owing to zero-point energy loss in classical trajectories [5]. Our quantum work will also allow us to determine the relative roles of intramolecular vibrational energy redistribution and dissociation, and will be compared with experiment [6]. In the case of H_2CO , we are focusing on dynamics near the $\text{H} + \text{HCO}$ threshold and developing a quantum analog of the roaming hydrogen mechanism [7] for dissociation to H_2 and CO .

FUTURE PLANS

We will complete the HOOH and H₂CO unimolecular dissociation studies, and extend our study of reactivity in confined environments to allow for more significant wall interactions. New quantum dynamics work will also be carried out on the reactions of OH+NH, in parallel with other theoretical and experimental efforts at Argonne. This system, with two relevant potential energy surfaces, is one of the most important NH reactions in combustion, and yet there is a dearth of direct experimental work or theoretical dynamics work on it. There are two product channels but three pathways to these products:



Reaction (a) is a direct abstraction reaction, which takes place on a quartet surface. CCSD(T) calculations by Harding shows no barrier for this reaction. Reactions (b), (c) and (d) proceed on a doublet surface and involve the intermediacy of the fairly strongly bound, HONH and H₂NO complexes. This system is sufficiently small that it will be possible to fit an accurate, analytic, global potential surface. We will then use our four-atom wave packet code to determine the quantum dynamics on both the doublet and quartet surfaces. As with the CH+H₂ system, this work will provide a benchmark against which the accuracy of approximate methods such as TST and PST can be judged. Barrierless abstractions such as reaction (a) may be important chain-terminating processes in combustion models, but are poorly understood and difficult to measure. Of particular interest, therefore, will be the development of new approximate methods for treating these reactions based on our rigorous quantum dynamics results.

REFERENCES

- [1] J. Mayneris, A. Saracibar, E. M. Goldfield, M. Gonzalez, E. Garcia, and S. K. Gray, *J. Phys. Chem. A*, **110**, 5542 (2006).
- [2] S. Y. Lin and H. Guo, *J. Chem. Phys.* **120**, 9907 (2004).
- [3] R. A. Brownsword, A. Canosa, B. R. Rowe, I. R. Sims, I. W. M. Smith, D. W. A. Stewart, A. C. Symonds and D. Travers, *J. Chem. Phys.* **106**, 7662 (1997).
- [4] T. Lu, E. M. Goldfield and S. K. Gray, *J. Phys. Chem. C*, **112**, 2674-2659 (2008).
- [5] Y. Guo and D. L. Thompson, *Chem. Phys. Lett.* **382**, 654 (2003).
- [6] B. Kuhn and T. R. Rizzo, *J. Chem. Phys.* **112**, 7461 (2000).
- [7] D. Townsend, S. A. Lahankar, S. K. Lee, S. D. Chambreau, A. G. Suits, X. Zhang, J. Rheinecker, L. B. Harding, and J. M. Bowman, *Science* **306**, 1158 (2004).

DOE COMBUSTION PROGRAM SUPPORTED PUBLICATIONS (2006-2008)

1. D. M. Medvedev, L. B. Harding, and S. K. Gray Methyl radical: ab initio global potential energy surface, vibrational levels, and partition function, *Mol. Phys.* **104**, 73-82 (2006).
2. J. Mayneris, A. Saracibar, E. M. Goldfield, M. Gonzalez, E. Garcia, and S. K. Gray, Theoretical study of the complex-forming $\text{CH} + \text{H}_2 \rightarrow \text{CH}_2 + \text{H}$ reaction, *J. Phys. Chem. A*, **110**, 5542-5548 (2006).
3. S. Zhang, D. M. Medvedev, E. M. Goldfield, and S. K. Gray, Quantum dynamics study of the dissociative photodetachment of HOCO^- , *J. Chem. Phys.* **125**, 164312 (2006) (8 pages).
4. R. Martinez, J. D. Sierra, S. K. Gray, and M. Gonzalez, Time-dependent quantum dynamics study of the $\text{O}^+ + \text{H}_2(v=0, j=0) \rightarrow \text{OH}^+ + \text{H}$ ion-molecule reaction and isotopic variants (D_2 , HD), *J. Chem. Phys.* **125**, 164305 (2006) (7 pages).
5. M. Hankel, S. C. Smith, R. J. Allan, S. K. Gray, and G. G. Balint-Kurti, State-to-state reactive differential cross sections for the $\text{H} + \text{H}_2 \rightarrow \text{H}_2 + \text{H}$ reaction on five different potential energy surfaces: DiffRealWave, *J. Chem. Phys.* **125**, 164393 (2006) (12 pages).
6. E. M. Goldfield and S. K. Gray, The quantum dynamics of chemical reactions, *Adv. Chem. Phys.* **136**, 1-38 (2007).
7. T. Lu, E. M. Goldfield and S. K. Gray, Chemical reactivity within carbon nanotubes: A quantum mechanical study of the $\text{D} + \text{H}_2 \rightarrow \text{DH} + \text{H}$ reaction, *J. Phys. Chem. C*, **112**, 2674-2659 (2008).
8. S. K. Gray, Keeping time. Review of Introduction to Quantum Mechanics by David Tannor. *Science* **319**, 161 (2008).
9. J. Mayneris, R. Martinez, J. Hernando, S. K. Gray, and M. Gonzalez, Quantum dynamics study of the $\text{K} + \text{HF}(v=0-2, j=0) \rightarrow \text{KF} + \text{H}$ reaction and comparison with quasiclassical trajectory results: *J. Chem. Phys.*, *in press* (2008).
10. M. Zhang, L. B. Harding, S. K. Gray and S. A. Rice, Quantum states of the endohedral fullerene $\text{Li}@\text{C}_{60}$, *J. Phys. Chem. A*, *in press* (2008).
11. M. Hankel, S. C. Smith, S. K. Gray, and G. G. Balint-Kurti, DIFFREALWAVE: A parallel real wavepacket code for the quantum mechanical calculation of reactive state-to-state differential cross sections in atom plus diatom collisions, *Comp. Phys. Comm.*, *submitted* (2008).

This work was supported by the Office of Basic Energy Sciences, Division of Chemical Sciences, Geosciences, and Biosciences, U.S. Department of Energy under Contract No. DE-AC02-06CH11357

Computer-Aided Construction of Chemical Kinetic Models

William H. Green, MIT Department of Chemical Engineering,
77 Massachusetts Ave., Cambridge, MA 02139. email: whgreen@mit.edu

Project Scope

The combustion chemistry of even simple fuels can be extremely complex, involving hundreds or thousands of kinetically significant species. The most reasonable way to deal with this complexity is to use a computer not only to numerically solve the kinetic model, but also to construct the kinetic model in the first place. Our research spans a wide range from quantum chemical calculations on individual molecules and elementary-step reactions, through the development of improved rate/thermo estimation procedures, the creation of algorithms and software for constructing and solving the simulations, the invention of methods for model-reduction while maintaining error control, through comparisons with experiment. We are developing methods needed to make computer-construction of accurate combustion models practical, as well as tools to make it feasible to handle and solve the resulting large kinetic models, even in multidimensional reacting flows. Many of the parameters in the models are derived from quantum chemistry, and the models are compared with experimental data measured in our lab or in collaboration with other researchers.

Recent Progress

The main focus of our research continues to be the development of methodology for constructing, reducing, and solving combustion simulations [6,9], supplemented by experimental measurements. With funding from NSF, we are currently integrating our extensible open-source mechanism-construction software RMG (<http://sourceforge.net/projects/rmg>) with the PrIME database (<http://primekinetics.org>). We also developed software for fast multi-cycle HCCI engine simulations, useful for understanding engine transients and misfires.[10] During 2007-2008 we made significant progress in automated mechanism reduction and in numerical methods for solving reacting flow simulations involving complex chemistry.[5,11,12] We also directly measured the rate coefficients of several reactions of free radicals important in combustion (e.g. vinyl, allyl) using laser flash photolysis.[7,8]

Notable recent accomplishments include:

- 1) Development of several different automated approaches to reducing large mechanisms; most of these were done in ways which facilitate control of the error associated with the model reduction. The first rigorous method for controlling the effects of this error on the solution of a CFD simulation was demonstrated in [5].
- 2) Experimental measurements and quantum chemical calculations on the reactions of the vinyl radical with several different alkenes ([8] and several submitted manuscripts), to facilitate generalizations about the reactions of any vinylic radical with any molecule containing a C=C double bond.

Future Plans

We have recently computed the thermochemistry of a large number of nitrogen-containing species, and derived group-additivity parameters for nitrogen-containing

functional groups (submitted to *J. Phys. Chem.*). This will allow the automated reaction mechanism generation software to model systems containing virtually any molecules made of C, H, N, and O atoms. With separate funding we have developed and published models for the co-oxidation of ethanol and ammonia in supercritical water and for the effect of NO_x on the partial oxidation of methane under fuel-rich cool-flame conditions. With DOE funding, we are now using the automated reaction generation software to construct a model for the effect of NO_x and organic nitrates (cetane improvers) on more typical combustion conditions; this has required significant extensions in our database of reaction types and associated rate coefficient estimates. With separate funding, we have recently developed and published predictive kinetic models for complicated gas-phase chemical systems including Fe, P, Ti, and Cl atoms. We plan to incorporate this chemistry into the open-source mechanism generation software package as well.

We are currently modeling McEnally & Pfefferle's measurements on aromatic formation in methane diffusion flames, and how this is affected by doping with different hexadienes. Interestingly, under these ordinary burner flame conditions, most hexadienes react predominantly through cyclic C5 intermediates. We expect to submit a manuscript detailing this line of research this summer.

Our new automated mechanism-reduction methods eliminate both reactions and species, and these methods make it relatively straightforward to bound the error associated with simplifying the chemistry.[11,12] There are potentially large benefits from eliminating the species which are not important in certain zones of a CFD simulation. We are currently working the tricky error-control issues that arise when kinetic models involving different chemical species are adjacent to each other in a reacting flow simulation; special error tolerances and control procedures are needed at the boundaries between the zones.

We are preparing for a new campaign of flash photolysis experiments measuring the reactions of mid-sized combustion free radicals. During our experiments on vinyl + O₂ and vinyl + isobutene, we observed several transient absorptions ~400 nm growing in as the vinyl decays. Several product channels are possible in these experiments. Our initial target is to unambiguously identify these species, through a combination of experiments and quantum chemical calculations.

Acknowledgements

Several of our recent flash photolysis experiments have been done in collaboration with Craig Taatjes, and we are also grateful to him for lending us a laser needed for our radical recombination experiments. The kinetic experiments at MIT were made possible by Bob Field lending us lasers and other equipment. The probe laser system was paid for in part by an NSF equipment grant to the Harrison Spectroscopy Laboratory. The HCCI engine research at MIT was supported in large part through funding by Ford and BP, and was done in collaboration with Wai Cheng. Our work on Ti chemistry was done in collaboration with Markus Kraft. Our work on numerical methods has benefited significantly from ongoing interactions with Paul Barton.

Publications Resulting from DOE Sponsorship (Since 2006)

1. K. Van Geem, M.F. Reyniers, G. Marin, J. Song, D.M. Matheu, and W.H. Green, "Automatic Reaction Network Generation using RMG for Steam Cracking of n-Hexane", *A.I.Ch.E. Journal* **52**(2), 718-730 (2006).
2. A.B. Singer, J.W. Taylor, P.I. Barton, and W.H. Green, "Global Dynamic Optimization for Parameter Estimation in Chemical Kinetics", *Journal of Physical Chemistry A* **110**(3), 971-976 (2006).
3. J. Yu, R. Sumathi, and W.H. Green, "Accurate and Efficient Estimation Method for Predicting the Thermochemistry of Furans and *ortho*-Arynes -- Expansion of the Bond-Centered Group Additivity Method", *J. Phys. Chem. A* **110**(21), 6971(2006).
4. O.O. Oluwole, B. Bhattacharjee, J.E. Tolsma, P.I. Barton, and W.H. Green, "Rigorous Valid Ranges for Optimally-Reduced Kinetic Models", *Combustion and Flame* **146**, 348-365 (2006).
5. O.O. Oluwole, P.I. Barton, & W.H. Green, "Obtaining Accurate Solutions using Reduced Chemical Kinetic Models: A new Model Reduction method for models rigorously validated over ranges", *Combust. Theory Model.* **11**(1), 127-146 (2007).
6. William H. Green, "Predictive Kinetics: A New Approach for the 21st Century", *Advances in Chemical Engineering* **32**, 1-50 (2007).
7. S.V. Petway, H. Ismail, W.H. Green, E.G. Estupiñán, L.E. Jusinski, and C.A. Taatjes, "Measurements and Automated Mechanism Generation Modeling of OH Production in Photolytically-Initiated Oxidation of the Neopentyl Radical", *Journal of Physical Chemistry A* **111**, 3891-3900 (2007).
8. Huzeifa Ismail, C. Franklin Goldsmith, Paul R. Abel, Pui-Teng Howe, Askar Fahr, Joshua B. Halpern, Leonard E. Jusinski, Yuri Georgievskii, Craig A. Taatjes and William H. Green, "Pressure and Temperature Dependence of Reaction of Vinyl Radical (C₂H₃) with Ethylene", *J. Phys. Chem. A* **111**, 6843-6851 (2007).
9. William H. Green, "Building and Solving Accurate Combustion Chemistry Simulations", *Journal of the Combustion Society of Japan* **50**, 19-28 (2008).
10. John P. Angelos, Marcel Puignou, Morgan M. Andreae, Wai K. Cheng, William H. Green & Michael A. Singer, "Detailed Chemical Kinetic Simulations of HCCI Engine Transients", *International Journal of Engine Research* (accepted).
11. Michael A. Singer and William H. Green, "Using adaptive proper orthogonal decomposition to solve the reaction-diffusion equation", *Applied Numerical Mathematics* (accepted).
12. Alexander Mitsos, Geoffrey M. Oxberry, Paul I. Barton, and William H. Green, "Optimal Automatic Reaction and Species Elimination in Kinetic Mechanisms", *Combustion & Flame* (accepted).

Wave packet based quantum statistical model for complex-forming reactions

Hua Guo

Department of Chemistry and Chemical Biology, University of New Mexico

ABSTRACT

Complex-forming reactions are prevalent in combustion, in atmospheres and in interstellar media. Such reactions proceed on potential energy surfaces (PESs) dominated by deep wells. Because of the large number of quantum states supported by the potential wells and their often long lifetimes, quantum mechanical characterization of such reactions is quite challenging. However, much progress has been made in the last few years, due partly to the ever increasing computer power and partly to efforts of several theoretical groups including us. Here, we summarize some recent progress in our group.

We have tackled the problem using both the exact quantum mechanical treatment of the dynamics with as few approximations as possible and approximate methods such as quasi-classical trajectory (QCT) method and statistical wave packet model. In the current funding year, we have focused on the $\text{H} + \text{O}_2 \leftrightarrow \text{HO} + \text{O}$ reaction, which serves as a prototype for complex-forming reactions. In addition, the forward reaction features prominently in combustion as “the single most important combustion reaction”.¹

Based on our earlier work on the PES of the ground electronic state HO_2 ,² we have systematically carried out quantum statistical,³ QCT,^{4,5} and exact quantum mechanical investigations⁶⁻¹⁰ of this reaction system. In addition, we have studied the vibrational dynamics of the HO_2 intermediate on the same PES using full quantum mechanical methods,^{11,12} which helps us to understand the reaction dynamics.

The forward reaction, $\text{H} + \text{O}_2 \rightarrow \text{HO} + \text{O}$, is an endothermic process, which renders it a dominant reaction bottleneck in flames. It has been shown that a quantitatively accurate characterization of the reaction using QCT methods is very difficult, if not impossible. This is because the large zero-point energy of the OH product cannot be included in the QCT treatment in a rigorous fashion.¹³ As a result, it is difficult to determine if a reactive trajectory is productive or not when its energy falls below the quantum threshold. To provide a better understanding of the reaction dynamics, we have carried out extensive quantum calculations of the reactive integral cross section (ICS) and rate constant.¹⁰ Because of the large number of quantum states involved, an exact quantum characterization of the reaction dynamics is very challenging, even for this seemingly simple system. In addition, the HO_2 system is rather floppy and requires full Coriolis coupling. The difficulties are further compounded by the fact that many partial waves are needed for this barrierless reaction. The dynamic calculations were performed using a recursive Chebyshev method.¹⁴

The calculated rate constant is compared in Fig. 1 with previous theoretical results and experimental data. Several observations are immediately in order. First, the good agreement between experiment and previous theoretical (both QCT and approximate quantum) results appear to be fictitious because the quantum mechanical rate constant on

the DMBE IV PES substantially underestimates the experiment. This underscores the importance of the exact quantum approach in characterizing the dynamics of complex-forming reactions. Second, the new ab initio PES used in our studies improves the agreement with experiment over the older DMBE IV PES, whose deficiencies have been noted by us before.^{6,11} Third, the reactant vibration is found to have a significant impact on the rate constant, as evidenced by the increase of k when thermal average of the reactant

vibrational state population is included. This observation can be rationalized by the fact that the effective barrier of the reaction is deep in the product valley and the vibration is effective in promoting the reaction. Finally, the calculated rate constant is approximately one order of magnitude smaller than the experimental consensus. Interestingly, the slope of the calculated rate constant in Fig. 1 is the same as the experimental curve, indicating the effective reaction barrier is well reproduced by our calculations. So what are the possible errors? At this point, we speculate that non-adiabatic transitions involving the Renner-Teller interaction between the lowest two electronic states of HO_2 might be responsible. To this end, we are mapping out the $\text{HO}_2(A^2A')$ PES and will carry out dynamic calculations on the two coupled PESs to resolve this issue.

We have also carried out exact quantum dynamic calculations on the reverse reaction: $\text{HO} + \text{O} \rightarrow \text{H} + \text{O}_2$.^{7,9} This is an important reaction in atmospheres and in interstellar clouds. Despite its exothermic nature, a large number of bases/grid points is required in a quantum mechanical treatment due to the deep HO_2 well. Besides, many partial waves (>100) are necessary to converge the ICS at moderate energies. In Fig. 2, the calculated rate constant is compared with

previous theoretical results and available experimental data. Unlike the forward reaction, the temperature dependence of the rate constant is complex and decidedly non-Arrhenius,

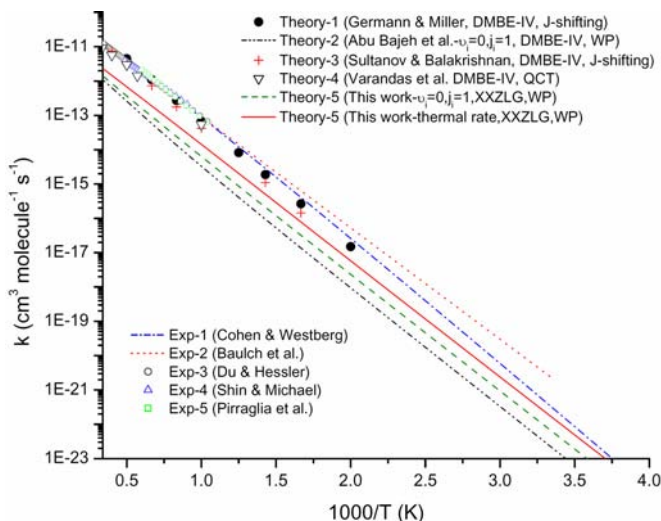


Fig. 1. Comparison of experimental and theoretical rate constants for the $\text{H} + \text{O}_2$ reaction.

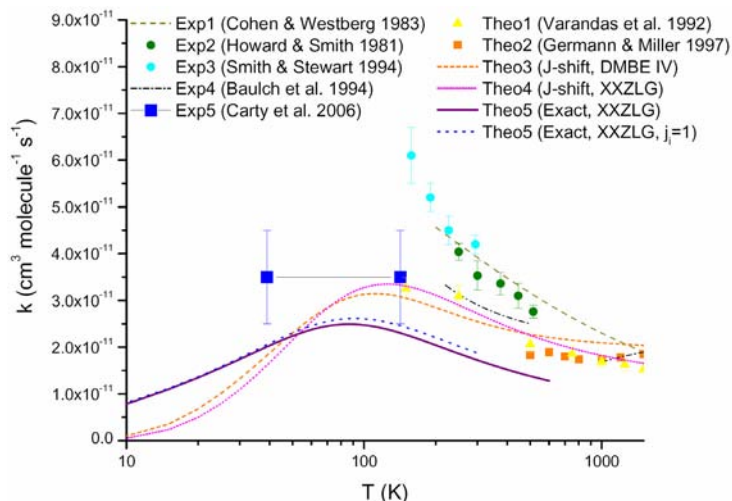


Fig. 2. Comparison of experimental and theoretical rate constants for the $\text{HO} + \text{O}$ reaction.

due to the barrierless nature of the exothermic reaction pathway. As in the forward reaction, on the other hand, the quantum mechanical rate constant underestimates the experimental data, presumably due to same reasons. One of the interesting observations of the rate constant is that its value at interstellar temperatures (10-30 K) is significantly lower than the corresponding values at higher temperatures. Recent simulations in the Herbst group have shown that this reduced rate constant might hold the key to the long-standing “interstellar oxygen problem” in astrophysics.¹⁵

Mechanistically, there is much debate on the statistical nature of the reactions. Miller has for example shown that the decay of the HO₂ intermediate does not follow statistical models.^{16,17} We have also found that the rate constant for the OH + O reaction obtained from a quantum statistical model significantly overestimates the exact result.⁹ The non-statistical nature of the reaction might be traced back to the vibrational dynamics, where significant regularity was found.^{11,12} Very recently, we have analyzed the QCT lifetimes for the H + O₂ reaction and found indeed a large non-statistical behavior.⁵ As shown in Fig. 3, the lifetime distributions of the HO₂ complex are not exponential and the intermediate decays rapidly.

In addition to the ICS and rate constant, we have also obtained state-to-state scattering attributes. The differential cross section (DCS) for the H + O₂ reaction was calculated quantum mechanically (with P. Honvault) at low collision energies⁸ and classically (with G. Lendvay) at moderate and high energies.⁵ The QCT angular distributions at various energies are displayed in Fig. 4. As shown, the DCS is dominated by forward and backward scatterings, but the asymmetry increases with energy. Even at low energies where the DCS is forward-backward symmetric, lifetime distributions

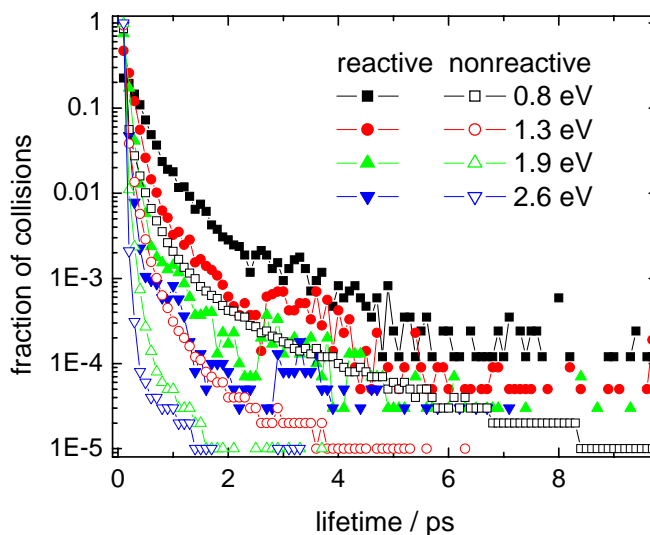


Fig. 3. Lifetime distributions for both reactive and nonreactive cross sections for the H + O₂ reaction

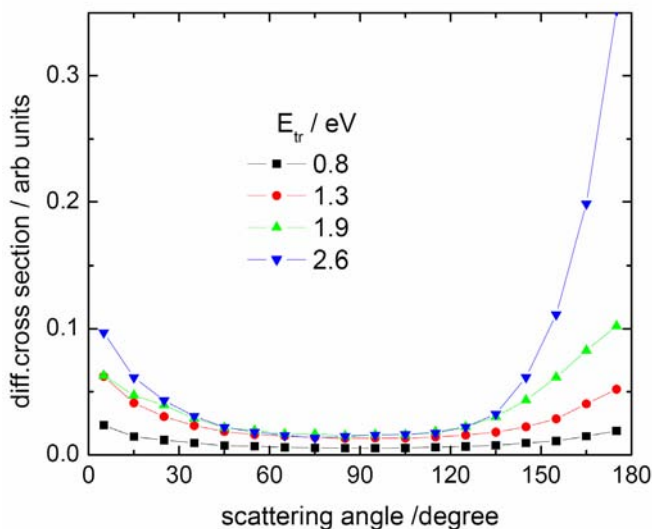


Fig. 4. Angular distributions for the H + O₂ reaction (arbitrary units)

in Fig. 3 still show significant non-statistical behaviors. It is our hope that these new theoretical results will stimulate further experimental exploration on this important system.

In addition to the HO₂ system, we have recently studied the C + OH → H + CO¹⁸ and N(²D) + H₂ → NH + H systems.¹⁹ In the former case, we showed that a quantum capture model provides an accurate description of this exothermic reaction. The latter system has served as a prototype for insertion-type reactions and we have developed a quantitatively accurate PES based on high level ab initio calculations. Exact quantum rate constant calculated on the new PES shows an unprecedented agreement with experiment. Other work funded by the DOE grant includes a new study of the emission spectra of the HNC system,²⁰ and a path integral Monte Carlo study of the CO₂ ro-vibrational spectrum in ⁴He clusters.²¹ In the future, we plan to continue our effort in providing quantum mechanical characterization of dynamics of combustion related reactions.

References:

- ¹ J. A. Miller, R. J. Kee, and C. K. Westbrook, *Annu. Rev. Phys. Chem.* **41**, 345 (1990).
- ² C. Xu, D. Xie, D. H. Zhang, S. Y. Lin, and H. Guo, *J. Chem. Phys.* **122**, 244305 (2005).
- ³ S. Y. Lin, E. J. Rackham, and H. Guo, *J. Phys. Chem. A* **110**, 1534 (2006).
- ⁴ D. Xie, C. Xu, T.-S. Ho, H. Rabitz, G. Lendvay, S. Y. Lin, and H. Guo, *J. Chem. Phys.* **126**, 074315 (2007).
- ⁵ G. Lendvay, D. Xie, and H. Guo, *Chem. Phys.* (in press).
- ⁶ S. Y. Lin, H. Guo, P. Honvault, and D. Xie, *J. Phys. Chem. B* **110**, 23641 (2006).
- ⁷ C. Xu, D. Xie, P. Honvault, S. Y. Lin, and H. Guo, *J. Chem. Phys.* **127**, 024304 (2007).
- ⁸ P. Honvault, S. Y. Lin, D. Xie, and H. Guo, *J. Phys. Chem. A* **111**, 5349 (2007).
- ⁹ S. Y. Lin, H. Guo, P. Honvault, C. Xu, and D. Xie, *J. Chem. Phys.* **128**, 014303 (2008).
- ¹⁰ S. Y. Lin, Z. Sun, H. Guo, D. H. Zhang, P. Honvault, D. Xie, and S.-Y. Lee, *J. Phys. Chem. A* **112**, 602 (2008).
- ¹¹ S. Y. Lin, D. Xie, and H. Guo, *J. Chem. Phys.* **125**, 091103 (2006).
- ¹² C. Xu, B. Jiang, D. Xie, S. C. Farantos, S. Y. Lin, and H. Guo, *J. Phys. Chem. A* **111**, 10353 (2007).
- ¹³ A. J. C. Varandas, *J. Chem. Phys.* **99**, 1076 (1993).
- ¹⁴ H. Guo, *Rev. Comput. Chem.* **25**, 285 (2007).
- ¹⁵ D. Quan, E. Herbst, T. Millar, S. Y. Lin, H. Guo, P. Honvault, and D. Xie, *Astrophys. J.* (in press).
- ¹⁶ J. A. Miller, *J. Chem. Phys.* **84**, 6170 (1986).
- ¹⁷ J. A. Miller and B. C. Garrett, *Int. J. Chem. Kinet.* **29**, 275 (1997).
- ¹⁸ S. Y. Lin, H. Guo, and P. Honvault, *Chem. Phys. Lett.* **453**, 140 (2008).
- ¹⁹ S. Zhou, D. Xie, S. Y. Lin, and H. Guo, *J. Chem. Phys.* (submitted).
- ²⁰ S. Zhou, D. Xie, D. Xu, H. Guo, and R. W. Field, *Chem. Phys. Lett.* (in press).
- ²¹ Z. Li, L. Wang, H. Ran, D. Xie, N. Blinov, P.-N. Roy, and H. Guo, *J. Chem. Phys.* (to be submitted).

Gas-Phase Molecular Dynamics: Experimental Studies of the Spectroscopy and Dynamics of Transient Species

Gregory E. Hall and Trevor J. Sears
Department of Chemistry, Brookhaven National Laboratory
Upton, NY 11973-5000
gehall@bnl.gov; sears@bnl.gov

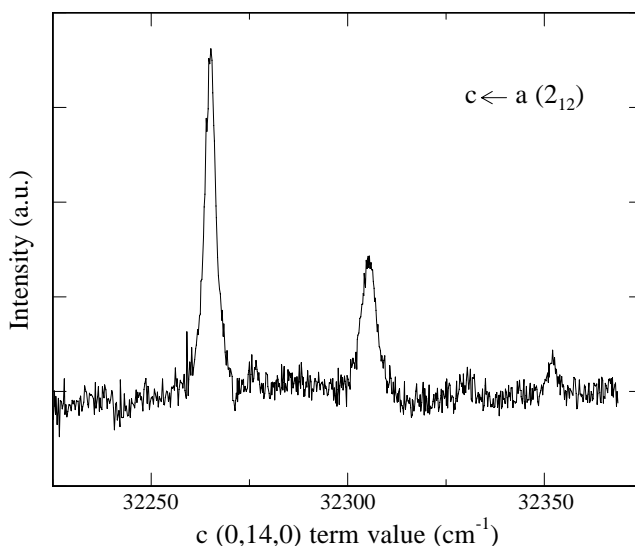
Program Scope

This research is carried out as part of the Gas-Phase Molecular Dynamics program in the Chemistry Department at Brookhaven National Laboratory. High-resolution spectroscopy, augmented by theoretical and computational methods, is used to investigate the structure and reactivity of chemical intermediates in the elementary gas-phase reactions involved in combustion chemistry and in chemical processes occurring at or near surfaces of heterogeneous catalysts. Techniques to improve the resolution and sensitivity of laser spectroscopy are developed as are models of intra- and inter-molecular interactions in molecular free radicals and other reactive species. The results lead to improved understanding and modeling of processes involving these species and are applicable to a wide variety of practical problems.

Recent Progress

A. CH₂ c-state double resonance measurements

New vibrational bands in the $\tilde{c} \leftarrow \tilde{a}$ system of CH₂ have been recorded in the region near the dissociation threshold to H + CH(X). We can explain previous puzzlement over the apparent breaking-off of the bending progression well below 31 800 cm⁻¹, the best estimate of the singlet dissociation energy. Strong fragmentation of the bright bending states (0,12,0) and (0,13,0) leads to many sharp but weaker lines, previously undetected, but not because of predissociation. A proliferation of strongly coupled vibronic levels at this energy (but not elsewhere) is evidently related to multiple state interactions in a complex region of the CH₂ potential energy surfaces. Our optical-optical double resonance spectra are measured by probing a near-IR $\tilde{b} \leftarrow \tilde{a}$ laser transient absorption while scanning a pulsed UV laser to excite transitions in the $\tilde{c} \leftarrow \tilde{a}$ band system. A depletion transient is observed when the lower rotational levels of the pump and probe transition coincide. By following the UV absorption spectrum to shorter wavelengths, we have been able to detect the onset of predissociation in CH₂ thereby placing an upper limit on the bond dissociation energy. The figure shows three observed resonances near 32 300 cm⁻¹, originating from the single rotational state 2₁₂ of the \tilde{a} state of CH₂ with lifetime-broadened widths of 3-4 cm⁻¹.



Predissociation broadened lines in the double resonance $\tilde{c} \leftarrow \tilde{a}$ spectrum of CH₂ near 32300 cm⁻¹ above the a-state minimum.

B. Reversible Intersystem Crossing in CH₂

Final analysis is underway in the interpretation of double exponential decays observed for singlet CH₂ formed from the photolysis of ketene in the presence of Ar or He. High dynamic range kinetic measurements show an initial decay, with a rate similar to those reported by numerous workers as the

collision-induced intersystem crossing rates, followed by a slower decay, with an amplitude between 0.5% and 8% of the fast decay, depending on the ketene/rare gas ratio and the nuclear spin. The dramatic nuclear spin effect is well explained by the differing vibrational states of the triplet perturbers responsible for the dominant gateway states mediating the intersystem crossing. The details of the pressure dependent rates and reversibility can be modeled with a master equation treatment of the rotational relaxation, combined with a coherent two-level treatment of the effective mixed states.

C. Double resonance studies of collision dynamics in CH₂

Rotational energy transfer within the \tilde{a} state of CH₂ is studied by saturation recovery and saturation transfer double resonance kinetic spectroscopy. The kinetics of recovery following a pulsed rotational state depletion is found to be nearly exponential, and nearly independent of rotational state. The hole in a Boltzmann rotational distribution induced by pulsed rotational state depletion broadens and spreads to all rotational states with a time-dependence that depends on details of the state-to-state matrix of energy transfer rates. Levels strongly coupled to the depleted level show larger and faster growth of depletion than weakly and indirectly coupled levels, although all will eventually be depleted by the same fraction, once the hole is thermalized. Polarization effects provide still further information on the energy transfer process: polarized light in the saturation beam creates an aligned hole, which depolarizes at a rate distinguishable from the population recovery. More challenging experimentally, but containing richer information about reorientation during state-to-state rotationally inelastic collisions, is the transfer of alignment in the saturation transfer experiments.

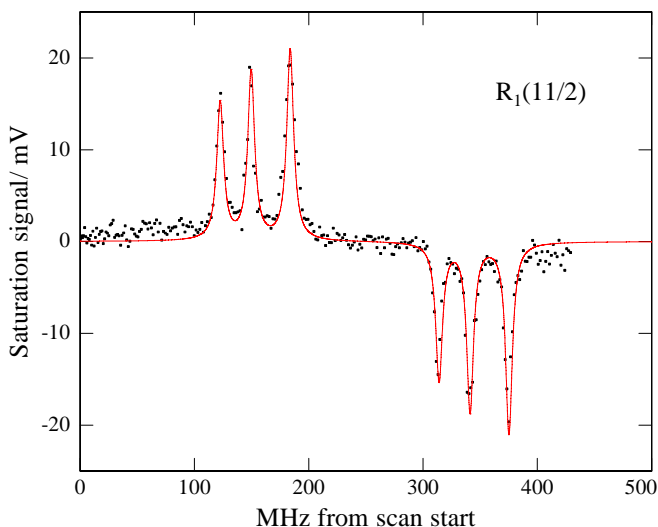
D. Biexponential decays in excited singlet states of small aromatics

In collaboration with Prof. P. Johnson (Stony Brook University) we have observed a biexponential decay from single rotational levels of phenyl acetylene in its S₁ state which is unique in the large literature on the photophysics of small aromatics. Some earlier reports of anomalously long lifetimes in beams attributed them to the decay of clusters, however the rotationally resolved S₁-S₀ excitation spectrum precludes this possibility here. No detectable IR fluorescence was found but time-dependent photoelectron spectra of the singlet and long-lived intermediate confirm the different energies of the two and also show that the states responsible for the two different decays are formed immediately upon population of the upper singlet state rotational level. That is, there is a bifurcation in the pathways for decay of a single rotational level. This is extremely unusual; normally the initially excited singlet level will undergo competitive decay via fluorescence or inter-system crossing to excited triplet levels, but population in the long-lived states will grow as the initially excited state decays.

Future Work

A. Sub-Doppler spectroscopy of radicals

We have begun a series of experiments to measure spectral lines of CN radical at sub-Doppler resolution. These measurements will provide an insight into the radical's hyperfine structure and are a necessary prelude to future ultra-precise measurements using frequency comb-stabilized lasers. The figure on the right shows an FM-detected Doppler-free scan near the center of a single rotational line of CN in the (1,0) band of the A-X transition at 10 899.118 cm⁻¹. Three strong hyperfine-resolved transitions are observed in pairs, separated by the 191.5 MHz modulation frequency. The spectrum shown is the difference of FM absorption



transients observed with a strong cw counterpropagating bleach laser blocked and unblocked. The measured data are shown as points, and the solid line is a simulation from which we can determine the *A* state hyperfine splittings of selected rotational states with an accuracy of about 1 MHz. After initial characterization of the previously unreported *A* state hyperfine structure in $v=1$, we intend to extend the measurements to time-resolved saturation spectroscopy with electro-optically switched saturation beams. Such measurements will explore the transient saturation linewidths in a regime near the uncertainty limit for time and spectral resolution.

B. Stark and Zeeman effects in radical transients

Molecular dipole moments and *g*-factors give direct information on electronic wavefunctions that is difficult to obtain otherwise. Experimental measurements of these quantities has traditionally been restricted to ground electronic states because spectroscopic experiments of resolution sufficient to measure Stark and Zeeman level shifts are mostly limited to the microwave region. Our preliminary results on the CN radical described above encourages us to pursue accurate measurements of electric and magnetic field effects on the spectra. Empirically, we have shown that any small magnetic fields substantially reduce the resolution of the spectrum shown above. For the trace shown, the absorption cell was wrapped in mu-metal shielding to eliminate the effects of the earth's magnetic field. Comparison with *ab initio* calculated dipole moments and *g*-factors will provide a very stringent test of *ab initio* wavefunctions, which are known to generally be much less reliable for excited electronic states.

C. Precise optical frequency measurement of sub-Doppler free radical spectra

Our very recent demonstration of sub-Doppler resolution electronic spectra of CN radical has opens the way to extremely precise absolute frequency measurements in such spectra. While it is easily possible to measure hyperfine and fine structure splittings in the spectra to within a few MHz, measurement of the absolute line position is limited by the precision of secondary wavelength standards, such as the iodine spectrum which is of the order of 100 MHz or larger. We propose to use a commercial frequency comb source to measure the frequency of the probe laser used in these experiments, potentially to a precision of 1 part in 10^{12} or better. In practice, we expect that our ultimate spectral line measurement precision will be limited by the lifetime of the radical's excited state, but even so 10-100 kHz should be achievable for optical transitions in the 900 nm region, i.e at 330 THz, or better than a 3×10^{-10} fractional accuracy. At this level, we will be able to investigate subtle effects resulting from the coupling of nuclear and electron spin angular momentum to rotational and vibrational motion of the molecule, well beyond the capability of current effective Hamiltonian models. With the added ability to follow the collisional decay of individual fine and hyperfine level populations, new insights into the form of radical-molecule intermolecular potentials will be possible.

D. Measuring the products of CH₂ dissociation

Following the successful detection of predissociation from CH₂ radical rovibronic levels of known energy in our laboratory, we plan two approaches towards experimental measurement of the singlet dissociation energy of this radical. Firstly, in collaborative experiments with Prof. Arthur Suits (Wayne State University) we will attempt to measure the velocity of the hydrogen atom product using resonant ionization followed by velocity map imaging. If H atom velocity rings can be associated with specific CH rotational levels, the energy balance will be complete, leading to a direct determination of the dissociation energy. Secondly, we will attempt laser-induced fluorescence of the CH product using the well known electronic spectrum of this radical around 430 nm. Observation of rotationally resolved spectra should produce lower bounds on the CH₂ bond dissociation energy based on the most highly rotationally excited CH $\tilde{X}^2\Pi$ ground state produced following predissociation at known total energies determined in our earlier work. These experiments will be conducted at BNL by modifying the existing jet expansion/LIF apparatus previously used for metal ablation studies.

E. Radicals formed in low temperature-high pressure ignition of alternative fuels

In collaboration with Prof. Philip Johnson (Stony Brook), we will construct a heated, high pressure expansion source to investigate the distribution of free radicals formed under conditions resembling those that will occur in proposed efficient and non-polluting compression ignition engines for 21st century transportation. This source will be installed in our existing free jet expansion/beam experimental chamber and we propose to investigate a number of alternative fuel prototypes such as methyl and ethyl esters for biodiesel and heavier aromatic and aliphatic hydrocarbons as surrogates for fuels derived from non-traditional hydrocarbon reserves such as tar sands. We will search for new radicals using a combination of laser absorption and fluorescence spectroscopy at BNL and ionization-based spectroscopy schemes at Stony Brook.

Publications and submitted journal articles supported by this project 2006-2008

1. Potential energy surfaces and vibrational energy levels of DCCl and HCCl in three low-lying states, H.-G. Yu, T.J. Sears and J.T. Muckerman, *Mol. Phys.* **104**, 47 (2006).
2. Rotationally resolved spectrum of the A(060)-X(000) band of HCB_r, G.E. Hall, T.J. Sears and H.-G. Yu, *J. Mol. Spectrosc.* **235**, 125 (2006).
3. Hot bands in jet-cooled and ambient temperature spectra of chloromethylene, Z. Wang, R.G. Bird, H.-G. Yu and T.J. Sears, *J. Chem. Phys.* **124**, 074314 (2006).
4. A clue to the diffuse structure in ultraviolet spectra of the GeCl₂ X-A transition, H.-G. Yu and T.J. Sears, *J. Chem. Phys.* **125**, 114316 (2006).
5. Photoinduced Rydberg ionization spectroscopy of phenylacetylene: vibrational assignments of the C state of the cation, H. Xu, P. M. Johnson and T. J. Sears, *J. Phys. Chem. A* **110**, 7822-7825 (2006).
6. The spectrum of CH₂ near 1.36 and 0.92 microns: Re-evaluation of rotational level structure and perturbations in a(010), K. Kobayashi, G. E. Hall and T. J. Sears, *J. Chem. Phys.* **124**, 184320 (2006).
7. State-resolved thermalization and singlet-triplet interconversion in CH₂, A. V. Komissarov, A. Lin, T. J. Sears and G. E. Hall, *J. Chem. Phys.* **125**, 084308 (2006).
8. AC Stark detection of optical-optical double resonance in CH₂, Y. Kim, G. E. Hall and T. J. Sears, *Phys. Chem. Chem. Phys.* **8**, 2823-2825 (2006).
9. The calculation of vibrational intensities in forbidden electronic transitions, P. M. Johnson, H. Xu and T. J. Sears, *J. Chem. Phys.* **125**, 164330 (2006).
10. Photoinduced Rydberg ionization spectroscopy of the B state of benzonitrile cation, H. Xu, P. M. Johnson and T. J. Sears, *J. Chem. Phys.* **125**, 164331 (2006).
11. Observation of the c¹A₁(0,10,0) state of CH₂ by optical-optical double resonance, Y. Kim, G. E. Hall and T. J. Sears, *J. Molec. Spectrosc.* **240** 269-271 (2006).
12. Correlated product distributions from ketene dissociation measured by DC sliced ion imaging, A. V. Komissarov, M. P. Minitti, A. G. Suits, and G. E. Hall, *J. Chem. Phys.* **124**, 014303 (2006).
13. Anisotropy of photofragment recoil as a function of dissociation lifetime, excitation frequency, rotational level and rotational constant, Hahkjoon Kim, Kristin S. Dooley, S. W. North, G. E. Hall and P. L. Houston, *J. Chem. Phys.* **125** 133316 (2006).
14. Coherent and incoherent orientation and alignment of ICN photoproducts, M. L. Costen and G. E. Hall, *Phys. Chem. Chem. Phys.* **9**, 272-287 (2007).
15. The fate of excited states in jet-cooled aromatic molecules: Bifurcating pathways and very long-lived species from the S₁ excitation of phenylacetylene and benzonitrile, J. Hofstein, H. Xu, T. J. Sears, and P. M. Johnson, *J. Phys. Chem. A* DOI: **10.102/jp077367b** (2008).
16. Predissociation in the $\tilde{c} \leftarrow \tilde{a}$ band system of singlet methylene studied by optical-optical double resonance. Z. Wang, Y. Kim, G.E. Hall and T. J. Sears, submitted (2008).

Flame Chemistry and Diagnostics

Nils Hansen

Combustion Research Facility, Sandia National Laboratories, Livermore, CA 94551-0969

Email: nhansen@sandia.gov

SCOPE OF THE PROGRAM

The goal of this program is to provide a rigorous basis for the elucidation of chemical mechanisms of combustion, combining experimental measurements employing state of the art combustion diagnostics with detailed kinetic modeling. The experimental program concentrates on the development and application of combustion diagnostics for measurements of key chemical species concentrations. These measurements are carried out in low-pressure, one-dimensional laminar flames and are designed to serve as benchmarks for the validation of combustion chemistry models. Comparison of experimental data to models employing detailed chemical kinetics is critical to determining important chemical pathways in combustion and in pollutant formation in combustion systems. As turbulent combustion models become increasingly sophisticated, accurate chemical mechanisms will play a larger role in computations of realistic combustion systems. Verification of detailed chemistry models against a range of precise measurements under thoroughly characterized steady conditions is necessary before such flame models can be applied with confidence in turbulent combustion calculations.

PROGRESS REPORT

Molecular Beam Mass Spectrometry at the Advanced Light Source

In collaboration with T. A. Cool of Cornell University and P. R. Westmoreland of the University of Massachusetts, great progress has been made measuring low-pressure flames using molecular-beam mass spectrometry (MBMS) with synchrotron photoionization at the Advanced Light Source (ALS) of the Lawrence Berkeley National Laboratory. In the past year, different flames fueled by larger hydrocarbons and oxygenated species have been characterized over a wide range of stoichiometries. The data is currently being processed for comparison to detailed kinetic flame models.

Combustion Chemistry in Flames fueled by Oxygenates and Hydrocarbon

Fuel-consumption and initial steps of aromatic ring formation were studied in fuel-rich flames of cyclohexane, 1-hexene, 1,3-butadiene, and tetrahydrofuran. These experimental studies provide a broad database for flame modeling.

Tetrahydrofuran Flame: In recent years, tightened regulations for emissions from internal combustion engines have stimulated a pronounced interest in non-conventional oxygenated fuels. Five-

and six-membered cyclic ethers, like tetrahydrofuran (THF) and its derivatives, are contained in fuels derived from biomass and furthermore, they are formed during the autoignition of alkanes and alkenes. To learn more about the oxidation chemistry of ethers in combustion processes, a fuel-rich tetrahydrofuran (THF) flame ($\phi = 1.75$) has been studied.

In fuel-rich laminar flames the first step in the decomposition of the fuel is usually hydrogen abstraction. For THF, the H-abstraction can proceed at the α - or β -carbon atom, so that initially two different C_4H_7O radicals may be formed. The first stable intermediates at $m/z = 70$ (C_4H_6O) have been identified by their ionization energies and photoionization efficiency (PIE) spectra as 2,3-dihydrofuran and 3-butenal. Contributions from 2,5-dihydrofuran are clearly missing. Furan (C_4H_4O) is identified at $m/z = 68$. The identification of the 2,3-dihydrofuran and the absence of the 2,5-dihydrofuran imply that the first hydrogen is abstracted from the α -carbon. It is conceivable that 3-butenal can be formed directly by ring-opening of the 2,3-dihydrofuran. Further interpretation of the data necessitates detailed modeling studies.

1-Hexene and Cyclohexane: Mole fractions profiles were determined for benzene and known precursors in flames fueled by cyclohexane and 1-hexene. A qualitative difference in the prominence of lower-mass fragments was immediately apparent between the two fuels. The 1-hexene flame displayed more pronounced sets of peaks arising from C_2 - C_5 molecules than does the cyclohexane flame. 1-Hexene can dissociate relatively readily into allyl and n-propyl and fragments more extensively in the preheat zone than does cyclohexane. The resultant lower-mass fragments form aromatic species by more conventional mechanisms, i.e. propargyl recombination. Additionally, greater formation of polyynes, i.e. diacetylene and triacetylene, was observed in the 1-hexene flame, as the small linear unsaturated species formed from the breakup of the 1-hexene recombined and dehydrogenated.

Species-Identification: Polyynes

Polyynes and their substituted derivatives are characterized by *sp*-hybridized carbon atom chains with alternating carbon-carbon triple and single bonds. These molecules are known to play key roles in many chemical processes. For example, polyynes have been linked to the formation of polycyclic aromatic hydrocarbon (PAH's) and soot in fuel-rich flames.

In collaboration with S. J. Klippenstein (Argonne National Laboratory), polyynic structures in fuel-rich low-pressure flames were observed using VUV photoionization molecular-beam mass spectrometry. High level *ab-initio* calculations of ionization energies for $C_{2n}H_2$ ($n = 1-5$) and partially hydrogenated C_nH_4 ($n = 7-8$) polyynes were compared with photoionization efficiency measurements in flames fueled by allene, propyne, and cyclopentene. $C_{2n}H_2$ ($n = 1-5$) intermediates were unambiguously identified, while $HC\equiv C-C\equiv C-CH=C=CH_2$, $HC\equiv C-C\equiv C-C\equiv C-CH=CH_2$ (vinyltriacetylene) and

$\text{HC}\equiv\text{C}-\text{C}\equiv\text{C}-\text{CH}=\text{CH}-\text{C}\equiv\text{CH}$ were likely to contribute to the C_7H_4 and C_8H_4 signals. Mole fraction profiles as a function of distance from the burner were presented to assist in kinetic flame modeling. C_7H_4 and C_8H_4 isomers are likely to be formed by reactions of C_2H and C_4H (with allene, propyne, or vinylacetylene) but other plausible formation pathways were also discussed. Heats of formation and ionization energies of several polyynes have been determined for the first time.

FUTURE DIRECTIONS

One key immediate task is the analysis of the large body of ALS data accumulated in the past year, which may compel further or confirmatory measurements during subsequent beam cycles. We will continue to explore isomer specific pathways of fuel-consumption and aromatic ring formation in flames fueled by C_6H_{12} isomers. Future work on the cyclopentene flame will be concerned with a more detailed modeling and with characterizing the growth of aromatic species beyond the first ring, that is the formation, for example, of indene and naphthalene.

In collaboration with J. A. Miller (Sandia National Laboratories), combined experimental and modeling studies are under way to elucidate the combustion chemistry of premixed laminar low-pressure stoichiometric allene and propyne flames and a fuel-rich 1,3-butadiene flame. The emphasis will be on main reaction pathways of fuel consumption, of allene and propyne isomerization, and of isomer-specific formation of C_6 aromatic species. Preliminary modeling results indicate that all of the benzene in the propyne flame is formed by the propargyl recombination reaction, a small contribution from the allyl + propargyl reaction is observed in the allene flame. For the 1,3-butadiene flame, the preliminary results show that C_6H_6 in the 1,3-butadiene flame is formed mainly by the $\text{C}_3\text{H}_3 + \text{C}_3\text{H}_3$ and $i\text{-C}_4\text{H}_5 + \text{C}_2\text{H}_2$ reactions, which are roughly of equal importance. Smaller contributions arise from $\text{C}_3\text{H}_3 + \text{C}_3\text{H}_5$. However, given the experimental and modeling uncertainties, other pathways cannot be ruled out.

Studies of formation of aromatic species employing synchrotron generated VUV photoionization will be complemented by resonance-enhanced multiphoton ionization (REMPI) experiments in the laser laboratory. REMPI is an ionization technique, where the ionization energy is transferred to the molecule with two or more photons. It can be used for flame studies for the detection of aromatic species like benzene, substituted benzenes, and polycyclic aromatic hydrocarbons (PAH's).

Studies of oxygenated fuel chemistry will continue with experimental and modeling investigations of flames fueled by cyclic ethers which, as contents in biomass derived fuels, are of considerable interest.

The validation of kinetic modeling, especially the submodels for pollutants formation, requires temperature measurements in well-defined laminar laboratory flames. For those temperature measurements, thermocouples are commonly used because of their robustness and low cost. Especially

for the flames measured at the ALS in Berkeley, a chemical vapor deposition experiment using AlCl_3 as a precursor will be set up to deposit alumina thin films to suppress the catalytic effect on the surface of platinum-based thermocouples.

PUBLICATIONS ACKNOWLEDGING BES SUPPORT 2006-PRESENT

1. P. C. Samartzis, N. Hansen, A. M. Wodtke, „Imaging CIN_3 Photodissociation from 234 to 280 nm“, *Phys. Chem. Chem. Phys.*, **8**, 2958-2963 (2006).
2. C. A. Taatjes, N. Hansen, J. A. Miller, T. A. Cool, J. Wang, P. R. Westmoreland, M. E. Law, T. Kasper, K. Kohse-Höinghaus, “Combustion Chemistry of Enols: Possible Ethenol Precursors in Flames”, *J. Phys. Chem. A*, **110**, 3254-3260 (2006).
3. N. Hansen, S. J. Klippenstein, C. A. Taatjes, J. A. Miller, J. Wang, T. A. Cool, B. Yang, R. Yang, L. Wei, C. Huang, J. Wang, F. Qi, M. E. Law, P. R. Westmoreland, “Identification and Chemistry of C_4H_3 and C_4H_5 Isomers in Fuel-Rich Flames”, *J. Phys. Chem. A*, **110**, 3670-3678 (2006).
4. N. Hansen, S. J. Klippenstein, J. A. Miller, J. Wang, T. A. Cool, M. E. Law, P. R. Westmoreland, T. Kasper, K. Kohse-Höinghaus, “Identification of C_5H_x Isomers in Fuel-Rich Flames by Photoionization Mass Spectrometry and Electronic Structure Calculations”, *J. Phys. Chem. A*, **110**, 4376-4388 (2006).
5. P. R. Westmoreland, M. E. Law, T. A. Cool, J. Wang, A. McIlroy, C. A. Taatjes, N. Hansen, “Analysis of Flame Structure by Molecular-Beam Mass Spectrometry Using Electron Impact and Synchrotron-Photon Ionization”, *Combust. Expl. Shock Waves*, **42**, 672-677 (2006).
6. T. A. Cool, J. Wang, N. Hansen, P. R. Westmoreland, F. L. Dryer, Z. Zhao, A. Kazakov, T. Kasper, K. Kohse-Höinghaus, „Photoionization Mass Spectrometry and Modeling Studies of the Chemistry of fuel-rich Dimethyl Ether Flames”, *Proc. Combust. Inst.*, **31**, 285-293 (2007).
7. M. E. Law, P. R. Westmoreland, T. A. Cool, J. Wang, N. Hansen, C. A. Taatjes, T. Kasper, “Benzene Precursors and Formation Routes in a Stoichiometric Cyclohexane Flame”, *Proc. Combust. Inst.*, **31**, 565-573 (2007).
8. K. Kohse-Höinghaus, P. Oßwald, U. Struckmeier, T. Kasper, N. Hansen, C. A. Taatjes, J. Wang, T. A. Cool, S. Gon, P. R. Westmoreland, „The Influence of Ethanol Addition on a premixed fuel-rich Propene-Oxygen-Argon Flame”, *Proc. Combust. Inst.*, **31**, 1119-1127 (2007).
9. N. Hansen, J. A. Miller, C. A. Taatjes, J. Wang, T. A. Cool, M. E. Law, P. R. Westmoreland, “Photoionization Mass Spectrometric Studies and Modeling of Fuel-Rich Allene and Propyne Flames”, *Proc. Combust. Inst.*, **31**, 1157-1164 (2007).
10. N. Hansen, T. Kasper, S. J. Klippenstein, P. R. Westmoreland, M. E. Law, C. A. Taatjes, K. Kohse-Höinghaus, J. Wang, T. A. Cool, „Initial Steps of Aromatic Ring Formation in a Laminar Premixed Fuel-Rich Cyclopentene Flame“, *J. Phys. Chem. A*, **111**, 4081-4092 (2007).
11. P. Oßwald, U. Struckmeier, T. Kasper, K. Kohse-Höinghaus, J. Wang, T. A. Cool, N. Hansen, P. R. Westmoreland, „Isomer-Specific Fuel Destruction Pathways in Rich Flames of Methyl Acetate and Ethyl Formate and Consequences for the Combustion Chemistry of Esters“, *J. Phys. Chem. A*, **111**, 4093-4101 (2007).
12. C. A. Taatjes, N. Hansen, D. L. Osborn, K. Kohse-Höinghaus, T. A. Cool, P. R. Westmoreland, “‘Imaging’ Combustion Chemistry via Multiplexed Synchrotron-Photoionization Mass Spectrometry”, *Phys. Chem. Chem. Phys.*, **10**, 20-34 (2008).
13. N. Hansen, S. J. Klippenstein, P. R. Westmoreland, T. Kasper, K. Kohse-Höinghaus, J. Wang, T. A. Cool, “A Combined *ab-initio* and Photoionization Mass Spectrometric Study of Polyynes in Fuel-Rich Flames”, *Phys. Chem. Chem. Phys.*, **10**, 366-374 (2008).
14. J. Wang, B. Yang, T. A. Cool, N. Hansen, T. Kasper, “Near-threshold Absolute Photoionization Cross Sections of some Reaction Intermediates in Combustion”, *Int. J. Mass Spectrom.*, **269**, 210-220 (2008).
15. J. Wang, U. Struckmeier, B. Yang, T. A. Cool, P. Oßwald, K. Kohse-Höinghaus, T. Kasper, N. Hansen, P. R. Westmoreland, “Isomer-Specific Influences on the Composition of Reaction Intermediates in Dimethyl Ether/Propene and Ethanol/Propene Flames”, *J. Phys. Chem. A*, in press.

SPECTROSCOPY AND KINETICS OF COMBUSTION GASES AT HIGH TEMPERATURES

Ronald K. Hanson and Craig T. Bowman
Department of Mechanical Engineering
Stanford University, Stanford, CA 94305-3032
rkhanon@stanford.edu, ctbowman@stanford.edu

Program Scope

This program involves two complementary activities: (1) development and application of cw laser absorption methods for the measurement of concentration time-histories and fundamental spectroscopic parameters for species of interest in combustion; and (2) shock tube studies of reaction kinetics relevant to combustion. Species investigated in the spectroscopic portion of the research include OH, CH, and NCN using narrow-linewidth ring dye laser absorption. Reactions of interest in the shock tube kinetics portion of the research include: $\text{CH}_3 + \text{M} \rightarrow \text{products}$; $\text{CH} + \text{N}_2 \rightarrow \text{products}$, including $\text{NCN} + \text{H}$; and $\text{H} + \text{O}_2 + \text{Ar} \rightarrow \text{HO}_2 + \text{Ar}$.

Recent work has also investigated reasons for the discrepancy between the predictions of current hydrogen and propane mechanisms and shock tube ignition delay time measurements of these fuels at low temperatures. We have also begun to implement new methods for reducing non-ideal facility effects in shock tubes, and improved gasdynamic modeling of reaction kinetic behind reflected shock waves in shock tubes. Lastly, we have begun study of a new class of fuels, oxygenated hydrocarbons, beginning with the reactions of methyl esters.

Recent Progress: Shock Tube Chemical Kinetics

Prompt-NO Initiation: We have completed study of the reaction between CH and N_2 , (1) $\text{CH} + \text{N}_2 \rightarrow \text{Products}$, in shock tube experiments using CH and NCN laser absorption. CH was monitored by continuous-wave, narrow-linewidth laser absorption at 431.1 nm. The overall rate coefficient of the $\text{CH} + \text{N}_2$ reaction was measured between 1943 K and 3543 K, in the 0.9-1.4 atm pressure range, using a CH perturbation approach. CH profiles recorded upon shock-heating dilute mixtures of ethane in argon and acetic anhydride in argon were perturbed by the addition of nitrogen. The perturbation in the CH concentration is principally due to the reaction between CH and N_2 . Rate coefficients for the overall reaction were inferred by kinetically modeling the perturbed CH profiles. A least-squares, two-parameter fit of the current overall rate coefficient measurements is $k_1 = 6.03 \times 10^{12} \exp(-11150 / T [\text{K}])$, $\text{cm}^3 \text{mol}^{-1} \text{s}^{-1}$. The uncertainty in k_1 was estimated to be $\sim \pm 25\%$ and $\sim \pm 35\%$ at ~ 3350 K and ~ 2100 K, respectively.

At high temperatures, there are two possible product channels for the reaction between CH and N_2 , (1a) $\text{CH} + \text{N}_2 \rightarrow \text{HCN} + \text{N}$, and (1b) $\text{CH} + \text{N}_2 \rightarrow \text{H} + \text{NCN}$. The large difference in the rates of the reverse reactions (-1a) and (-1b) enabled inference of the branching ratio of reaction (1), $k_{1b}/(k_{1b}+k_{1a})$, in the 2228-2905 K temperature range from CH laser absorption in experiments in a nitrogen bath. The current CH measurements are consistent with a branching ratio of 1, and establish NCN and H as the primary products of the $\text{CH} + \text{N}_2$ reaction. A detailed and systematic uncertainty analysis, taking into

account experimental and mechanism-induced contributions, yields a conservative lower bound of 0.70 for the branching ratio. NCN was also detected by continuous-wave, narrow-linewidth laser absorption at 329.13 nm. The measured NCN time-histories were used to infer the rate coefficient of the reaction between H and NCN, $\text{H} + \text{NCN} \rightarrow \text{HCN} + \text{N}$, and to estimate an absorption coefficient for the NCN radical. A sample perturbation experiment is shown in Figure 1 and a sample NCN absorption time-history is shown in Figure 2.

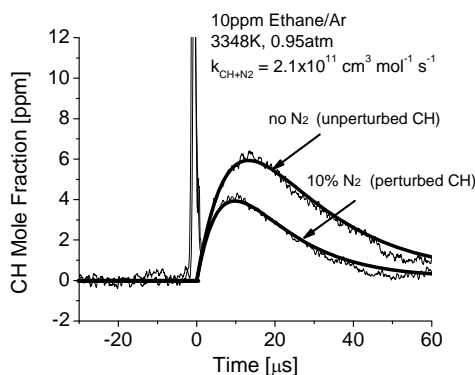


Figure 1 Example high-temperature CH perturbation experiment.

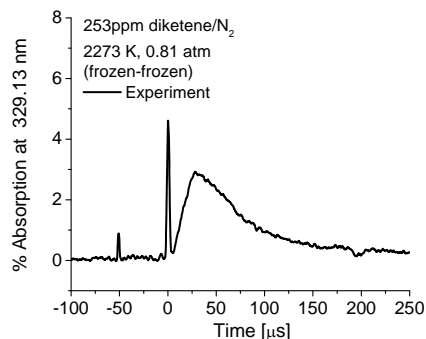


Figure 2 First laser absorption measurement of NCN.

CH₃ Thermal Decomposition: The methyl radical plays an important role in hydrocarbon combustion and pyrolysis and is directly relevant to high-temperature studies of the $\text{CH} + \text{N}_2$ reaction system that are currently underway in our laboratory. We have studied the overall decomposition rate and branching ratio of the two-channel thermal decomposition of the methyl radical, $\text{CH}_3 + \text{M} \rightarrow \text{CH} + \text{H}_2 + \text{M}$ (a) and $\rightarrow \text{CH}_2 + \text{H} + \text{M}$ (b), in shock tube experiments at temperatures of 2400 to 3500 K and pressures between 0.1 and 4 atm. Continuous-wave laser absorption diagnostics for CH and OH radicals were employed to infer rate coefficient data for reactions (a) and (b), respectively. Reaction (b) was studied by measuring OH in shock-heated mixtures of C_2H_6 or CH_3I and O_2 dilute in argon. H-atoms that were generated via reaction (b) rapidly reacted with O_2 , which was present in excess, to form OH.

Hydrogen/Oxygen and Propane/Oxygen Ignition: Validation of detailed reaction mechanisms to describe combustion processes relies on a direct comparison of mechanism simulations with reliable experimental measurements. However, even for two of the simplest hydrocarbon-related combustion systems, hydrogen and propane oxidation, large uncertainties still exist in the abilities of current detailed mechanisms and gas dynamic models to accurately simulate ignition time and species time-histories in shock tube experiments conducted at lower temperatures. These uncertainties are linked to uncertainties in the detailed reaction mechanism at low temperatures (below 1000 K) where hydroperoxyl reactions are believed to be important, and to uncertainties introduced by, or associated with, facility-related non-ideal effects. These facility effects become important only at long test times (typically greater than 1 ms). At shorter test times, large diameter shock tubes are very nearly ideal and relatively immune to non-ideal problems, especially when relatively dilute fuel-oxidizer mixtures are employed.

The effects of shock tube facility-dependent gasdynamics and localized pre-ignition energy release were explored by measuring and simulating hydrogen-oxygen ignition delay times. Shock tube hydrogen-oxygen ignition delay time data were taken behind reflected shock waves for two test mixtures: 4% H₂, 2% O₂, balance Ar, and 15% H₂, 18% O₂, balance Ar. The experimental ignition delay times at temperatures below 960 K are found to be shorter than those predicted by current mechanisms when the normal idealized constant volume (V) and constant internal energy (E) assumptions are employed. However, if non-ideal effects associated with facility performance and energy release are included in the modeling (using a new model which couples the experimental pressure trace with the constant V, E assumptions), the predicted ignition times more closely follow the experimental data. Applying the new model to current experimental data allows refinement of the reaction rate for $\text{H} + \text{O}_2 + \text{Ar} \leftrightarrow \text{HO}_2 + \text{Ar}$, a key reaction in determining the hydrogen-oxygen ignition delay time in the low-temperature region. Similar experiments are in progress with propane/oxygen/argon mixtures.

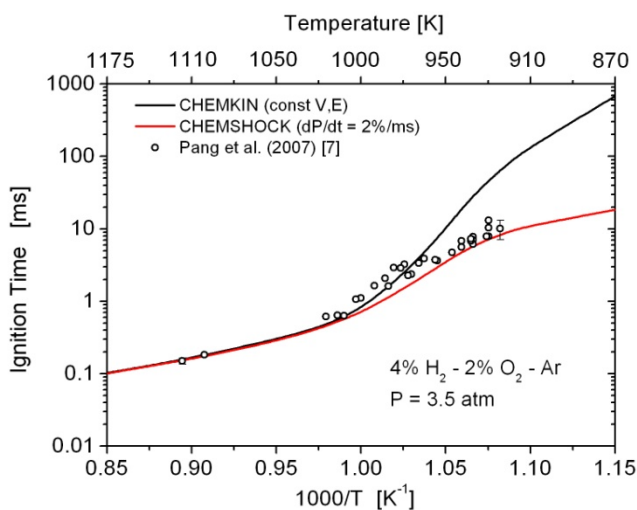


Figure 3. Experimental ignition time data and CHEMSHOCK modeling using different chemical mechanisms. The pressure variation imposed in the model, 2%/ms, matches that of the experiments.

Advances in Shock Tube/Laser Diagnostic: We are developing several methods to improve shock tube chemical kinetics measurements. 1) We have developed and are applying an improved chemical kinetic/gas dynamic model, CHEMSHOCK, that accounts for changes in the test gas volume that occurs during shock tube experiments, including relevant facility effects. 2) We are improving shock tube performance by reducing (and in some cases effectively eliminating) facility effects by the addition of driver-section inserts and the use of driven section buffer gas volumes. 3) We have extended shock tube test times to greater than 35 ms by using driver-section extensions and tailored gas mixtures. 4) We are developing an aerosol shock tube that enables the study of low-vapor-pressure fuels without fuel cracking by pre-heating. 5) We are developing new mid-IR laser absorption strategies for the detection of fuels (e.g., alkanes) and product species (e.g., CO₂, CO and H₂O).

Recent Progress: Spectroscopy

CH Spectroscopy: The collision-broadening coefficient for CH in argon, $2\gamma_{\text{CH-Ar}}$, was measured via repeated single-frequency experiments in the ethane pyrolysis system

behind reflected shock waves. The initial mixture was 20 ppm ethane in argon. The experimental line shape was simulated using LIFBASE with the broadening coefficient as the only free parameter. The measured $2\gamma_{\text{CH-Ar}}$ value and updated spectroscopic and molecular parameters were used to calculate the CH absorption coefficient at 431.1311 nm, which was then used to convert raw traces of fractional transmission to quantitative CH concentration time-histories in the methyl decomposition and CH + N₂ experiments.

NCN Spectroscopy: We have developed a cw laser absorption system for the NCN radical using the $X^3\Sigma - A^3\Pi$ transition near 329 nm. Light at 329 nm is generated by doubling 658 nm radiation generated in a ring dye laser cavity with an external-cavity frequency doubler with a BBO crystal. A quantitative absorption analysis of this transition based on comparison with existing reaction mechanism predictions was carried out.

Future Plans

In the next year, we plan to further investigate facility-related and mechanistic reasons for the discrepancies between the predictions of detailed mechanisms and shock tube measurements for the hydrogen and propane oxidative systems. We also plan to investigate reaction kinetics of selected oxygenate fuels, such as the methyl esters, e.g., methyl butanoate. Lastly, we plan to advance development of our deep-UV frequency-doubled laser capabilities and use this to measure several important radical species including: methyl (CH₃) propargyl (C₃H₃), alkyl radicals (C₂H₅, C₃H₇), peroxy radical and hydrogen peroxide (HO₂ and H₂O₂).

List of Recent Publications

V. Vasudevan, R. K. Hanson, C. T. Bowman, D. M. Golden, D. F. Davidson, "Shock Tube Study of the Reaction of CH with N₂: Overall Rate and Branching Ratio," *Journal of Physical Chemistry A* 111 (2007) 11818-11830.

M. A. Oehlschlaeger, D. F. Davidson, R. K. Hanson, "Thermal Decomposition of Toluene: Overall Rate and Branching Ratio," *Proceedings of the Combustion Institute* 31 (2007) 211-219.

V. Vasudevan, R. K. Hanson, D. M. Golden, C. T. Bowman, D. F. Davidson, "High-Temperature Shock Tube Measurements of Methyl Radical Decomposition," *Journal of Physical Chemistry A* 111 (2007) 4062-4072 .

V. Vasudevan, "Shock Tube Measurements of Elementary Oxidation and Decomposition Reactions Important in Combustion Using OH, CH and NCN Laser Absorption," Ph. D. thesis (also as Report TSD-173), Mechanical Engineering Department, Stanford University, September 2007.

G. A. Pang, D. F. Davidson, R. K. Hanson, "Experimental Study and Modeling of Shock Tube Ignition Delay Times for Hydrogen-Oxygen-Argon Mixtures at Low Temperatures," submitted for publication to the *Proceedings of the Combustion Institute* Volume 32, December 2007; also Paper 08F-12, Western States Section/Combustion Institute Fall Meeting, Livermore CA, March 2007; also Paper 08S-10, Western States Section/Combustion Institute Spring Meeting, Los Angeles, March 2008.

D. F. Davidson, R. K. Hanson, "Recent Advances in Shock Tube/Laser Diagnostic Methods for Improved Chemical Kinetics Measurements," Paper 08S-01, Western States Section/Combustion Institute Spring Meeting, Los Angeles, March 2008.

Theoretical Studies of Potential Energy Surfaces*

Lawrence B. Harding
Chemistry Division
Argonne National Laboratory
Argonne, IL 60439
harding@anl.gov

Program Scope

The goal of this program is to calculate accurate potential energy surfaces for both reactive and non-reactive systems. Our approach is to use state-of-the-art electronic structure methods (CASPT2, MR-CI, CCSD(T), etc.) to characterize multi-dimensional potential energy surfaces. Depending on the nature of the problem, the calculations may focus on local regions of a potential surface (for example, the vicinity of a minimum or transition state), or may cover the surface globally. A second aspect of this program is the development of techniques to fit multi-dimensional potential surfaces to convenient, global, analytic functions that can then be used in dynamics calculations. Finally a third part of this program involves the use of direct dynamics for high dimensional problems to by-pass the need for surface fitting.

Recent Progress

CH+N₂: The reaction of CH with N₂ is thought to be the first step in the mechanism of formation of “prompt NO”. We (with Stephen Klippenstein and Jim Miller) have completed a new study of this reaction using high level, multi-reference, ab initio, electronic structure calculations. These calculations have demonstrated that two key rate-controlling parts of the potential surface are poorly described with the single reference, electronic structure methods used in previous calculations. Transition state theory rate coefficients, based on the new, ab initio calculations are in excellent agreement with new measurements reported by Hanson and coworkers¹.

OH+NH: The reactions of OH with NH have been cited as the most important reactions of NH in flames, yet there have been no direct measurements of the rates of these reactions. We have begun a detailed theoretical study of these reactions. To date we have located the relevant stationary points using the CCSD(T)/aug-cc-pvqz // CCSD(T)/aug-cc-pvtz level of theory. Schematic diagrams of the doublet and quartet potential surfaces are shown in Figures 1a and 1b

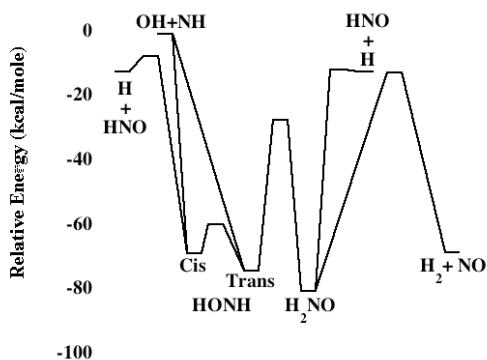


Figure 1a.

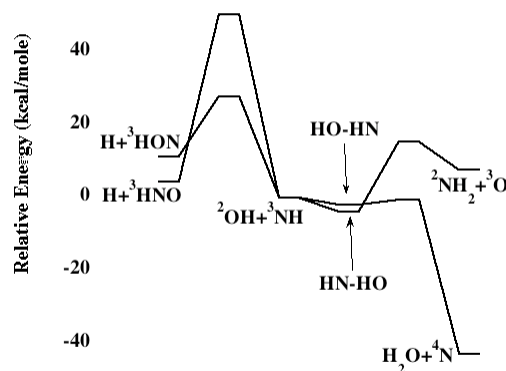


Figure 1b.

respectively. On the doublet surface the reaction proceeds by a barrier-less addition to form HONH which can isomerize to H₂NO and eliminate either an H atom or molecular hydrogen. On the quartet surface, the dominant process is abstraction to form H₂O+N. The barrier for this lies

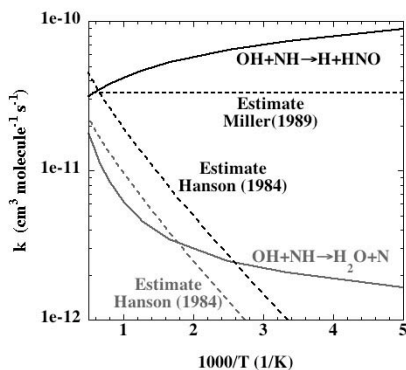


Figure 2.

slightly below the energy of the reactants. In collaboration with Stephen Klippenstein we have calculated transition state theory rate coefficients for these processes using the CCSD(T) stationary point properties and a CASPT2, VRC-TST treatment of the addition on the doublet surface. The results of these calculations are shown in Figure 2 (solid lines) along with previous estimates of Hanson² and Miller³ (dashed lines). In this plot the addition/elimination channel is shown in black while the abstraction is shown in gray. Elimination of molecular hydrogen (not shown on the plot) is calculated to occur with a rate approximately a factor of three slower than abstraction at 1000 K.

Cyclohexane Decomposition: Preliminary CASPT2 results for decomposition of cyclohexane show two distinct mechanisms: (1) the generally accepted biradical mechanism in which cyclohexane ring opens to a 1,6 biradical which then undergoes a 1,5 intramolecular hydrogen abstraction to form 1-hexene and (2) a direct path to 1-hexene which does not go through the biradical intermediate. The energetics of the two paths are predicted to be very close, close enough that both should contribute.

Roaming Radical Mechanisms: CASPT2 searches have located saddle points for roaming radical reactions in the decomposition of formaldehyde, acetaldehyde, propane and propene. In formaldehyde and acetaldehyde the geometry of the roaming saddle points place the roaming radical (H or CH₃) roughly perpendicular to the plane of the HCO fragment. For propane and propene the roaming methyl stays in the symmetry plane of the remaining fragment but, interestingly, the methyl is predicted to invert during these two processes.

Future Plans

We plan to fit global analytic surfaces for the OH+NH reactive system (both doublet and quartet) using Bowman's approach (direct product, multinomial in Morse variables). A preliminary fit to the quartet surface involving ~100,000 CCSD(T)/aug-cc-pvtz calculations has already been completed and is in the process of being tested and refined. It is intended that these surfaces will be used (in collaboration with Stephen Gray) in full-dimensional quantum dynamics studies of the OH+NH reactions.

Acknowledgement: This work was performed under the auspices of the Office of Basic Energy Sciences, Division of Chemical Sciences, Geosciences and Biosciences, U.S. Department of Energy, under Contract DE-AC02-06CH11357.

References:

- (1) V. Vasudevan, R. K. Hanson, C. T. Bowman, D. M. Golden, D. F. Davidson, *J. Phys. Chem. A*, **111**, 11818 (2007)
- (2) R. K. Hanson and S. Salimian, in *Combustion Chemistry* (W. C. Gardiner Jr., Ed.) Springer-Verlag, New York, P.361, (1984).
- (3) J. A. Miller and C. T. Bowman, *Prog. Energy Combust. Sci.* **15**, 287 (1989).

PUBLICATIONS (2006 - Present):

The Determination of molecular properties from MULTIMODE with an application to the calculation of Franck-Condon factors for photoionization of CF_3 to CF_3^+

J. M. Bowman, X. Huang, L.B. Harding and S. Carter, *Mol. Phys.* **104**, 33-45 (2006)

Methyl Radical: Ab Initio Global Potential Surface, Vibrational Levels, and Partition Function

D. M. Medvedev, L.B. Harding and S. K. Gray, *Mol. Phys.* **104**, 73-81 (2006)

Predictive Theory for the Association Kinetics of Two Alkyl Radicals

S.J. Klippenstein, Y. Georgievskii, L.B. Harding, *Phys. Chem. Chem. Phys.* **8**, 1133-1147 (2006)

Pyrolysis of Acetaldehyde, Rates for Dissociation and Following Chain Decomposition

K.S. Gupte, J.H. Kiefer, R.S. Tranter, S.J. Klippenstein and L.B. Harding
Proc. Combust. Inst. **31**, 167-174 (2007)

On the Formation and Decomposition of C_7H_8

S.J. Klippenstein, L.B. Harding and Y. Georgievskii, *Proc. Combust. Inst.* **31**, 221-229 (2007)

Direct Measurement and Theoretical Calculation of the Rate Coefficient for $\text{Cl} + \text{CH}_3$ from $T=202\text{-}298\text{ K}$

J. K. Parker, W. A. Payne, R. J. Cody, F.L. Nesbitt, L.J. Stief, S.J. Klippenstein, and L.B. Harding *J. Phys. Chem. A* **111**, 1015-1023 (2007)

Experimental and Theoretical Rate Constants for $\text{CH}_4 + \text{O}_2 \rightarrow \text{CH}_3 + \text{HO}_2$

N. K. Srinivasan, J. V. Michael, L. B. Harding and S. J. Klippenstein
Combustion and Flame **149**, 104-111 (2007)

Interpolated Moving Least-Squares Methods for Fitting Potential Energy Surfaces: Application to the H_2CN Unimolecular Reaction

Y. Gao, L. B. Harding, A. F. Wagner, M. Minkoff and D. L. Thompson
J. Chem. Phys. **126**, 104105 (2007)

On the Combination Reactions of Hydrogen Atoms with Resonance Stabilized Hydrocarbon Radicals

L.B. Harding, S.J. Klippenstein and Y. Georgievskii, *J. Phys. Chem. A* **111**, 3789-3801 (2007)

Kinetics of Methyl Radical-Hydroxyl Radical collisions and Methanol Decomposition

A. W. Jasper, S. J. Klippenstein, L. B. Harding, and B. Ruscic
J. Phys. Chem. A **111**, 3932-3950 (2007)

Reflected Shock Tube and Theoretical Studies of High-Temperature Rate Constants for $\text{OH}+\text{CF}_3\text{H}\leftrightarrow\text{CF}_3+\text{H}_2\text{O}$ and $\text{CF}_3+\text{OH}\rightarrow\text{Products}$

N. K. Srinivasan, M.-C. Su, J. V. Michael, S. J. Klippenstein and L. B. Harding
J. Phys. Chem. A **111**, 6822-6831 (2007)

Ab Initio Methods for Reactive Potential Surfaces

L. B. Harding, S. J. Klippenstein, and A. W. Jasper
Phys. Chem. Chem. Phys. **9**, 4055-4070 (2007)

Dissociative Ionization of Hot C_3H_5 Radicals

H. Fan, L. B. Harding, and S. T. Pratt, Mol. Phys. **105**, 1517-1534 (2007)

Secondary Kinetics of Methanol Decomposition: Theoretical Rate Coefficients for $^3\text{CH}_2+\text{OH}$, $^3\text{CH}_2+^3\text{CH}_2$ and $^3\text{CH}_2+\text{CH}_3$

A. W. Jasper, S. J. Klippenstein, L. B. Harding, J. Phys. Chem. A **111**, 8699-8707 (2007)

Performance of the Spin-Flip and Multi-reference methods for Bond-Breaking in Hydrocarbons: A Benchmark Study

A. A. Golubeva, A. V. Nemukhin, S. J. Klippenstein, L. B. Harding and A. Krylov
J. Phys. Chem. A **111**, 13264-13271 (2007)

The Thermal Decomposition of CF_3 and the Reaction of $\text{CF}_2+\text{OH}\rightarrow\text{CF}_2\text{O}+\text{H}$

N. K. Srinivasan, M.-C. Su, J. V. Michael, A. W. Jasper, S. J. Klippenstein and L. B. Harding, J. Phys. Chem. A **112**, 31-37 (2008)

The Kinetics of $\text{CH} + \text{N}_2$ Revisited with Multi-Reference Methods

L. B. Harding, S. J. Klippenstein and J. A. Miller, J. Phys. Chem. A **112**, 522-532 (2008)

Quantum States of the Endohedral Fullerene $\text{Li}@\text{C}_{60}$

M. Zhang, L. B. Harding, S. K. Gray, S. A. Rice, J. Phys. Chem. A (in press)

Kinetics of the $\text{H} + \text{NCO}$ Reaction

S. J. Klippenstein and L. B. Harding, 32nd Symposium (International) on Combustion (submitted)

Theoretical rate coefficients for the reaction of methyl radical with hydroperoxyl radical and for methylhydroperoxide decomposition

A. W. Jasper, S. J. Klippenstein and L. B. Harding
32nd Symposium (International) on Combustion (submitted)

CHEMICAL ACCURACY FROM AB INITIO MOLECULAR ORBITAL CALCULATIONS

Martin Head-Gordon

Department of Chemistry, University of California, Berkeley, and,
Chemical Sciences Division, Lawrence Berkeley National Laboratory,
Berkeley, CA 94720.
mhg@cchem.berkeley.edu

1. Scope of Project.

Short-lived reactive radicals and intermediate reaction complexes are believed to play central roles in combustion, interstellar and atmospheric chemistry. Due to their transient nature, such molecules are challenging to study experimentally, and our knowledge of their structure, properties and reactivity is consequently quite limited. To expand this knowledge, we develop new theoretical methods for reliable computer-based prediction of the properties of such species. We apply our methods, as well as existing theoretical approaches, to study prototype radical reactions, often in collaboration with experimental efforts. These studies help to deepen understanding of the role of reactive intermediates in diverse areas of chemistry. They also sometimes reveal frontiers where new theoretical developments are needed in order to permit better calculations in the future.

2. Summary of Recent Major Accomplishments.

2.1 *Density functional theory methods for ground and excited states.*

One of the principal problems with present-day density functional theory (DFT) methods is self-interaction error [5], which causes problems ranging from reaction energy barriers being too low, to radical electrons being overly delocalized to the gross failure of charge-transfer excited states [9]. We have recently completed the systematic optimization of a new density functional that includes 100% exact exchange at long range. This means that long-range self-interaction error is entirely eliminated [25]. This functional, called ω B97, takes the existing 1997 Becke generalized gradient approximation form, and entirely reoptimizes it to be appropriate for the inclusion of 100% long-range exchange. The results show that this functional, and an additional functional, ω B97X, which includes a fraction of short-range exact exchange also, out-perform widely used density functionals such as B3LYP and B97 for thermochemical properties, reaction barriers, and intermolecular interactions, while eliminating the worst pathologies for charge transfer excited states and the treatment of radical electrons [25]. Work is currently underway to also include non-local correlation effects, as we have recently experimented with [29].

2.2 *Excited states of large molecules without self-interaction errors.*

The density functionals described above are one way to overcome some of the difficulties of present-day DFT. Another approach is to use wavefunction-based methods, and modify relatively simple treatments of electron correlation effects to improve accuracy and at the same time enable applications to large molecules. For excited states, we recently proposed the scaled opposite spin (SOS) doubles correction to single excitation

CI for this purpose. SOS-CIS(D) [18] has a number of desirable properties. The cost scales only 4th order with molecular size, versus 5th order for conventional perturbation methods such as CIS(D). And, because the method is wavefunction-based, there is no self-interaction error, and charge-transfer excited states are correctly described. Since there is a single empirical parameter describing excited state correlations and one describing ground state correlations, it is possible to also achieve accuracy for excitation energies that exceeds the conventional CIS(D) method by nearly a factor of two. This approach appears promising for valence excited states of large organic molecules.

2.3 *Spin contamination and low-order perturbation theory.*

One of the reasons that the SOS-CIS(D) method described above cannot be recommended for excited states of radicals is that it is the excited state counterpart of the ground state second order Moller-Plesset (MP2) method, which can perform very poorly for radicals because of spin-contamination in the Hartree-Fock (HF) reference. For instance, if one takes a large conjugated radical such as phenalenyl (C₁₃H₉), the HF determinant exhibits $\langle S^2 \rangle > 2.0$ rather than 0.75 as desired. We have explored a modification of MP2 that is designed to overcome this problem by optimizing the orbitals in the presence of electron correlation [17]. We include only opposite spin correlations (as above) and scale them by a single empirical factor (chosen as 1.2). The resulting optimized second order method (termed the O2 method) dramatically reduces spin contamination in calculations on large radicals, and therefore is a promising inexpensive approach to studying such systems. Returning to the C₁₃H₉ example, the O2 reference determinant has $\langle S^2 \rangle = 0.76$, which is virtually free of spin-contamination.

2.4 *Pairing methods for strong electron correlations.*

To treat large molecules that have strong electron correlations (e.g. singlet biradicaloids), we have been developing generalized valence bond coupled cluster methods [2,3]. They take perfect pairing as a starting point, and then systematically include the main classes of additional excitations that we have established as important through pilot studies [4]. The resulting methods are already useful for chemical applications, and some application examples can be seen below. However, they suffer from symmetry-breaking problems for molecules with multiple resonance structures – benzene for example prefers a D_{3h} symmetry structure to D_{6h}. We have recently explored methods that can greatly reduce this symmetry-breaking by including weaker valence space correlations by perturbation theory. These additional correlations are required to yield a balanced treatment of symmetric versus symmetry-broken geometries in aromatic species, and reduce symmetry-breaking effects by more than an order of magnitude [22].

2.5 *Fundamental studies of chemical bonding.*

We have used the ground and excited state methods discussed above in a variety of chemical applications for which they are appropriate. The coupling of the cation of a polycyclic aromatic hydrocarbon (PAH) radical and a neutral PAH molecule is one interesting example that may have relevance to the mechanism of condensation of charged PAH clusters [13]. This work developed from earlier studies on the nature of intermolecular interactions between PAH radicals [1], and a radical with a closed shell anion [6]. Separately we have recently examined the changes in chemical bonding as a

function of oxidation state in 4-membered CuPCuP heterocycles [28], and the coordination of alkanes to transition metal centers [16].

3. Summary of Research Plans.

- Testing the new density functionals for excited states (including charge-transfer)
- Development and testing of simplified pairing methods for radicals
- New studies of the properties of reactive radicals and radical reactions.

4. Publications from DOE Sponsored Work, 2006-present.

- [1] “Steric modulations in the reversible dimerizations of phenalenyl radicals via unusually weak π - and σ - carbon-centered bonds”, V. Zaitsev, S.V. Rosokha, M. Head-Gordon, and J.K. Kochi, *J. Org. Chem.* 71, 520-526 (2006).
- [2] “A fast implementation of perfect pairing and imperfect pairing using the resolution of the identity approximation”, A. Sodt, G.J.O. Beran, Y. Jung, B. Austin, and M. Head-Gordon, *J. Chem. Theor. Comput.* 2, 300-305 (2006).
- [3] “Computational studies of molecular hydrogen binding affinities: The role of dispersion forces, electrostatics and orbital interactions”, R.C. Lochan and M. Head-Gordon, *Phys. Chem. Chem. Phys.* 8, 1357-1370 (2006).
- [3] “Second order correction to perfect pairing: an inexpensive electronic structure method for the treatment of strong electron-electron correlations”, G.J.O. Beran, M. Head-Gordon, and S.R. Gwaltney, *J. Chem. Phys.* 124, 114107 (2006) (15 pages).
- [4] “The localizability of valence space electron-electron correlations in pair-based coupled cluster models”, G.J.O. Beran and M. Head-Gordon, *Mol. Phys.* 104, 1191-1206 (2006).
- [5] “Self-interaction error of local density functionals for alkali halide dissociation”, A.D. Dutoi, and M. Head-Gordon, *Chem. Phys. Lett.* 422, 230-233 (2006).
- [6] “Mulliken–Hush elucidation of the encounter (precursor) complex in intermolecular electron transfer via self–exchange of tetracyanoethylene anion-radical”, S.V. Rosokha, M.D. Newton, M. Head-Gordon and J.K. Kochi, *Chem. Phys.* 324, 117-128 (2006)
- [7] “Ab initio quantum chemistry calculations on the electronic structure of the heavier alkyne congeners: diradical character and reactivity”, Y. Jung, M. Brynda, P.P. Power and M. Head-Gordon, *J. Am. Chem. Soc.* 128, 7185-7192 (2006)
- [8] “Advances in methods and algorithms in a modern quantum chemistry program package”, Y. Shao, L. Fusti Molnar, Y. Jung, J. Kussmann, C. Ochsenfeld, S.T. Brown, A.T.B. Gilbert, L.V. Slipchenko, S.V. Levchenko, D.P. O'Neill, R.A. DiStasio Jr, R.C. Lochan, T. Wang, G.J.O. Beran, N.A. Besley, J.M. Herbert, C.Y. Lin, T. Van Voorhis, S.H. Chien, A. Sodt, R.P. Steele, V.A. Rassolov, P.E. Maslen, P.P. Korambath, R.D. Adamson, B. Austin, J. Baker, E.F.C. Byrd, H. Dachsel, R.J. Doerksen, A. Dreuw, B.D. Dunietz, A.D. Dutoi, T.R. Furlani, S.R. Gwaltney, A. Heyden, S. Hirata, C.-P. Hsu, G. Kedziora, R.Z. Khalliulin, P. Klunzinger, A.M. Lee, M.S. Lee, W.Z. Liang, I. Lotan, N. Nair, B. Peters, E.I. Proynov, P.A. Pieniazek, Y.M. Rhee, J. Ritchie, E. Rosta, C.D. Sherrill, A.C. Simmonett, J.E. Subotnik, H.L. Woodcock III, W. Zhang, A.T. Bell, A.K. Chakraborty, D.M. Chipman, F.J. Keil, A. Warshel, W.J. Hehre, H.F. Schaefer III, J. Kong, A.I. Krylov, P.M.W. Gill and M. Head-Gordon, *Phys. Chem. Chem. Phys.* 8, 3172-3191 (2006)
- [9] “Comment on: “failure of time-dependent density functional methods for excitations in spatially separated systems” by W. Hieringer and A. Görling”, A. Dreuw and M. Head-Gordon, *Chem. Phys. Lett.* 426, 231-233 (2006).
- [10] “On the nature of unrestricted orbitals in variational active space wavefunctions”, G.J.O. Beran and M. Head-Gordon, *J. Phys. Chem. A* 110, 9915-9920 (2006)

- [11] “A near linear-scaling smooth local coupled cluster algorithm for electronic structure”, J.E. Subotnik, A. Sodt, and M. Head-Gordon, *J. Chem. Phys.* 125, 074116 (2006)
- [12] “Linear scaling density fitting”, A.Sodt, J.E. Subotnik, and M. Head-Gordon, *J. Chem. Phys.* 125, 194109 (2006) (9 pages).
- [13] “Charged polycyclic aromatic hydrocarbon clusters and the galactic extended red emission”, Y.M. Rhee, T.J. Lee, M.S. Gudipati, L.J. Allamandola, and M. Head-Gordon, *Proc. Nat. Acad. USA* 104, 5274-5278 (2007).
- [14] “Quartic scaling analytical gradient of scaled opposite spin second order Møller-Plesset Perturbation theory”, R.C. Lochan, Y. Shao, and M. Head-Gordon, *J. Chem. Theory Comput.* 3, 988-1003 (2007).
- [15] “Fast evaluation of scaled opposite spin second order Møller-Plesset correlation energies using auxiliary basis expansions and exploiting sparsity”, Y. Jung, Y. Shao, and M. Head-Gordon, *J. Comput. Chem.* 28, 1953-1964 (2007).
- [16] “Theoretical study of the rhenium-alkane interaction in transition metal-alkane sigma-complexes”, Erika A. Cobar, Rustam Z. Khaliulin, Robert G. Bergman, and Martin Head-Gordon, *Proc. Nat. Acad. USA* 104, 6963-6968 (2007).
- [17] “Orbital-optimized opposite-spin second order correlation: an economical method to improve the description of open-shell molecules”, R.C. Lochan and M. Head-Gordon, *J. Chem. Phys.* 126, 164101 (2007)
- [18] “Scaled second order perturbation corrections to configuration interaction singles: efficient and reliable excitation energy methods”, Y.M. Rhee and M. Head-Gordon, *J. Phys. Chem. A* 111, 5314-5326 (2007).
- [19] “A correction to constrained CCSD models based on the 2nd order coupled cluster moment”, D.W. Small, and M. Head-Gordon, *J. Chem. Phys.* 127, 064102 (2007).
- [20] “Theoretical study of solvent effects on the thermodynamics of Iron(III) [Tetrakis(pentafluorophenyl)]porphyrin Chloride Dissociation”, R.Z. Khaliullin, M. Head-Gordon, and A.T. Bell, *J. Phys. Chem. B.* 111, 10992-10998 (2007)
- [21] “Localized orbital theory and ammonia triborane”, J.E. Subotnik, A. Sodt and M. Head-Gordon, *Phys. Chem. Chem. Phys.* 9, 5522-5530 (2007).
- [22] “Symmetry-breaking in benzene and larger aromatic molecules within generalized valence bond coupled cluster methods”, K.V. Lawler, G.J.O. Beran, and M. Head-Gordon, *J. Chem. Phys.* 128, 024107 (2008) (13 pages).
- [23] “The limits of local correlation theory: electronic delocalization and chemically smooth potential energy surfaces”, J.E. Subotnik, A. Sodt and M. Head-Gordon, *J. Chem. Phys.* 128, 034103 (2008) (12 pages).
- [24] “Central moments in quantum chemistry”, D.W. Small and M. Head-Gordon, *Int. J. Quantum Chem.* 108, 1220-1231 (2008)
- [25] “Systematic optimization of long-range corrected hybrid density functionals”, Jeng-Da Chai and M. Head-Gordon, *J. Chem. Phys.* 128, 084106 (2008).
- [26] “A two-parameter Coulomb attenuator with a cutoff radius for two-electron repulsion integrals: the effect of attenuation on correlation energies”, A.D. Dutoi and M. Head-Gordon, *J. Phys. Chem A* 112, 2110-2119 (2008).
- [27] “Hartree-Fock exchange computed using the atomic resolution of the identity approximation”, A. Sodt and M. Head-Gordon. *J. Chem. Phys.* 128, 104106 (2008).
- [28] “A Delicate Electronic Balance between Metal and Ligand in [Cu-P-Cu-P] Diamondoids: Oxidation State Dependent Plasticity and the Formation of a Singlet Diradical”, Y.M. Rhee and M. Head-Gordon, *J. Am. Chem. Soc.* 130, 3878-3887 (2008)
- [29] “Semiempirical double-hybrid density functional with improved description of long-range correlation”, T. Benighaus, R.A. Distasio Jr., R.C. Lochan, J.D. Chai and M. Head-Gordon, *J. Phys. Chem. A*, 112, 2702-2712 (2008).

Laser Studies of Combustion Chemistry

John F. Hershberger

Department of Chemistry
North Dakota State University
Fargo, ND 58105
john.hershberger@ndsu.edu

Time-resolved infrared absorption and laser-induced fluorescence spectroscopy are used in our laboratory to study the kinetics and product channel dynamics of chemical reactions of importance in the gas-phase combustion chemistry of nitrogen-containing radicals. This program is aimed at improving the kinetic database of reactions crucial to the modeling of NO_x control strategies such as Thermal de-NO_x, RAPRENO_x, and NO-reburning. The data obtained is also useful in the modeling of propellant chemistry. The emphasis in our study is the quantitative measurement of both total rate constants and product branching ratios.

HCNO Kinetics

Previous to recent studies in our laboratory, there have been no literature data available on the kinetics of HCNO, the fulminic acid molecule. Recent modeling studies have suggested the importance of this molecule in NO-reburning mechanisms.¹ In combustion, HCNO is primarily formed via acetylene oxidation:



Recent experimental and computational work in several laboratories, including ours, has identified (2a) as a major product channel.²⁻⁵

One reason for the paucity of experimental data on HCNO kinetics is the difficulty of synthesizing this reagent, and its limited stability. After recent work in our laboratory to reliably synthesize pure HCNO to calibrate IR absorption signals in our HCCO+NO studies,² we are in a position to examine the kinetics of this species. The HCNO synthesis is slow and inefficient, but our reaction cell geometry is ideally suited to dealing with reagents that are only available in small quantities.

A. OH+HCNO Reaction.

Results on this reaction have been reported previously. See the 2007 DOE Abstract or publication #1 for details. We summarize the results:

$$k(T) = (2.69 \pm 0.41) \times 10^{-12} \exp[(750.2 \pm 49.8)/T] \text{ cm}^3 \text{ molecule}^{-1} \text{ s}^{-1}$$

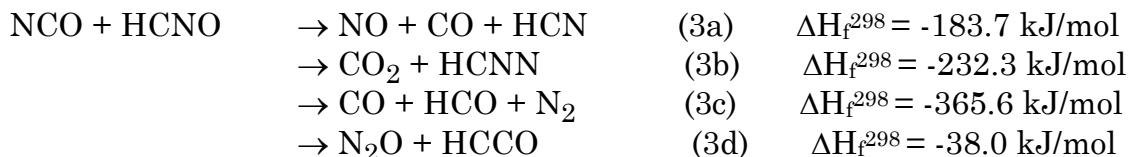
over the temperature range 298-386 K. At 296 K, the rate constant is $k = (3.39 \pm 0.3) \times 10^{-11} \text{ cm}^3 \text{ molecule}^{-1} \text{ s}^{-1}$. Major product channels include CO + H₂NO and HNO + HCO.

B. CN + HCNO Reaction.

We summarize the results; see publication #3 for details:

$k = (3.95 \pm 0.53) \times 10^{-11} \exp[(287 \pm 45)/T] \text{ cm}^3 \text{ molecule}^{-1} \text{ s}^{-1}$ (T=298-388 K). At 296 K, $k = (1.03 \pm 0.04) \times 10^{-10} \text{ cm}^3 \text{ molecule}^{-1} \text{ s}^{-1}$. The major product channel is NO + HCCN.

C. NCO+HCNO Reaction.

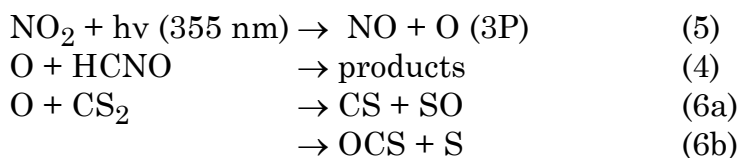


NCO is produced by ICN photolysis followed by the CN+O₂ reaction, and detected by infrared absorption spectroscopy. The total rate constant is $(1.58 \pm 0.2) \times 10^{-11} \text{ cm}^3 \text{ molecule}^{-1} \text{ s}^{-1}$ at 298 K, somewhat slower than the OH and CN reactions. Unfortunately, signal/noise limitations prevented measurements at elevated temperatures. After detection of products, and consideration of secondary chemistry, we conclude that NO + CO + HCN is the dominant product channel, with a minor contribution from CO₂ + HCNN.

D. O + HCNO Reaction.



Because we do not have oxygen atom detection capabilities in our laboratory, we measured the total rate constant of this reaction using a relative rate technique, according to the following scheme:



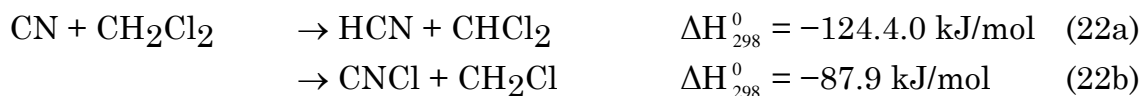
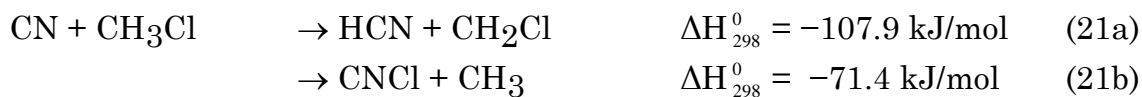
Among the various product in the above reactions, we chose to measure [OCS] as a function of HCNO concentration, because reaction (6) is the only source of OCS, and this molecule is easily detected by infrared absorption spectroscopy, even though (6b) is a minor channel ($\phi_{6b} \sim 0.09$).

Analysis of our data gives $k_4 = (9.84 \pm 3.52) \times 10^{-12} \exp[(-195 \pm 120)/T]$ ($\text{cm}^3 \text{ molecule}^{-1} \text{ s}^{-1}$) over the temperature range 298 - 375 K, with a value of $k_4 = (5.32 \pm 0.40) \times 10^{-12} \text{ cm}^3 \text{ molec}^{-1} \text{ s}^{-1}$ at 298 K. Detection and quantification of products indicates that CO forming channels dominate the reaction, with $\phi_{4f} (\text{CO} + \text{NO} + \text{H}) > 0.74$. CO + HNO and/or HCO + NO may be minor channels ($\phi_{4c} + \phi_{4d} < 0.22$), but channels (4b) and (4e) are insignificant ($\phi < 0.02$). We cannot probe channel (4a) by diode infrared laser spectroscopy, but static FTIR analysis indicates that this channel is also insignificant.

We have also performed ab initio calculations on this system. Using B3LYP/6-311++G(d,p) optimizations followed by single point energy CCSD(T)/6-311++G(d,p) calculations, we find that O+HCNO readily forms an HC(O)NO intermediate, which may then dissociate to HCO+NO and again to H+CO+NO. Initial calculations indicated that the initial intermediate is formed without any barrier, a rather surprising result in comparison with the quite low rate constant measured experimentally. Further calculations, however, using optimizations at the CCSD(T)/6-31G(d,p) level have revealed a small barrier of ~ 3.6 kcal/mole to HC(O)NO formation.

CN + Chlorinated Species

We have recently initiated a study of the kinetics of CN and NCO radicals with chlorinated species, with initial studies on CN reactions with chlorinated methanes. At present, no literature data exists for these reactions. For example,



Part of our goal is to examine whether these reactions occur via hydrogen abstraction to form HCN, or whether CNCl formation plays a significant role.

Using ICN photolysis to form CN radicals, and detecting CN by LIF spectroscopy, we obtain rate constants (298 K) of 9.0×10^{-13} , 8.8×10^{-13} , 9.0×10^{-13} , and 4.3×10^{-13} $\text{cm}^3 \text{ molecule}^{-1} \text{ s}^{-1}$ for $\text{CN} + \text{CH}_3\text{Cl}$, CH_2Cl_2 , CHCl_3 , and CCl_4 , respectively. The rate constants of the partially chlorinated species are all nearly identical to each other, and only slightly greater than literature values for $\text{CN} + \text{CH}_4$ ($k \sim 7.5 \times 10^{-13}$). The $\text{CN} + \text{CH}_3\text{Cl}$ and $\text{CN} + \text{CH}_2\text{Cl}$ reactions were found to have positive activation energies (10.1 and 10.8 kJ/mol, respectively), and $k_{\text{H}}/k_{\text{D}}$ kinetic isotope ratios of around 2.2, consistent with hydrogen abstraction. Furthermore, attempts at infrared detection of CNCl (near 2200 cm^{-1}) were unsuccessful for CN reactions with CH_3Cl , CH_2Cl , and CHCl_3 , although small amounts of CNCl were detected from the slower $\text{CN} + \text{CCl}_4$ reaction. We therefore conclude that hydrogen abstraction dominates the reaction of CN with the partially chlorinated methanes.

References

1. J.A. Miller, S.J. Kilppenstein, and P. Glarborg, *Comb. Flame* **135**, 357 (2003).
2. J.P. Meyer and J.F. Hershberger, *J. Phys. Chem B* **109**, 8363 (2005).
3. I.V. Tokmakov, L.V. Moskaleva, D.V. Paschenko, and M.C. Lin, *J. Phys. Chem. A* **107**, 1066 (2003).
4. L. Vereecken, R. Sumathy, S.A. Carl, and J. Peeters, *Chem. Phys. Lett.* **344**, 400 (2001).
5. U. Eickhoff and T. Temps, *Phys. Chem. Chem. Phys.* **1**, 243 (1999).

Publications acknowledging DOE support (2006-present)

1. "Ab Initio Study of the $\text{HCCO} + \text{NO}_2$ Reaction", J.P. Meyer and J.F. Hershberger, *Chem. Phys.* **325**, 545 (2006).
2. "Kinetics of the $\text{OH} + \text{HCNO}$ Reaction", W. Feng, J.P. Meyer, and J.F. Hershberger, *J. Phys. Chem. A* **110**, 4458 (2006).
3. "Kinetics of the $\text{CN} + \text{HCNO}$ Reaction", W. Feng and J.F. Hershberger, *J. Phys. Chem. A* **110**, 12184 (2006).
4. "Kinetics of the $\text{NCO} + \text{HCNO}$ Reaction", W. Feng and J.F. Hershberger, *J. Phys. Chem. A* **111**, 3831 (2007).
5. "Kinetics of the $\text{O} + \text{HCNO}$ Reaction", W. Feng and J.F. Hershberger, *J. Phys. Chem. A* **111**, 10654 (2007).
6. "Theoretical Study of the Reaction of $\text{O}(^3\text{P})$ with HCNO ", W. Feng and J.F. Hershberger, *Chem. Phys. Lett.*, submitted.

Non-Born–Oppenheimer Molecular Dynamics and Theoretical Chemical Kinetics

Ahren W. Jasper
Combustion Research Facility, Sandia National Laboratories
Livermore, CA 94551-0969
ajasper@sandia.gov

I. Program Scope

Excited electronic states play an important role in a wide variety of chemical processes, including intersystem crossing, photodissociation, internal conversion, charge transfer, etc. The term “non-Born–Oppenheimer” (NBO) may be generally applied to these systems to emphasize the idea that the Born–Oppenheimer separation of the nuclear and electronic time scales breaks down and that electronic surfaces other than the ground adiabatic surface play a key role in the dynamics. The focus of this program is the development and validation of theoretical methods for making quantitative predictions of the dynamics of NBO processes using molecular dynamics (MD) simulations, transition state theory (TST), and quantum chemical calculations.

MD methods are useful for elucidating reaction mechanisms, identifying important product species, modeling energy transfer, and simulating ensembles, and we are particularly interested in continuing the development of generalized MD methods capable of treating NBO systems. In NBO MD simulations, classical mechanics is used to describe the nuclear motion, and electronic transitions between the various electronic states are modeled via potential energy surface switches. Surface hopping (SH) methods model these electronic transitions as instantaneous hops, whereas in decay of mixing (DM) methods the surface switches occur over some finite time. Several variants of the SH and DM methods have been proposed, and these methods differ from one another in the details of how they treat electronic state coherence, electronic-nuclear energy transfer, and electronic state tunneling. We have recently summarized our previous systematic tests of several NBO MD methods against accurate quantum mechanical calculations for a series of triatomic two-state systems.ⁱ The best NBO MD methods predict branching ratios and product rovibrational energy distributions for these model systems with errors of only ~25%. The computational cost of the NBO MD methods is similar to that of single surface MD, and these validated methods may be readily applied to polyatomic systems.

NBO MD simulations require efficient methods for generating a potential energy surface and its gradient for each electronic state over a wide range of nuclear configurations. One strategy is to generate these surfaces “on-the-fly” by making direct calls to electronic structure programs. This strategy may be used to perform NBO MD calculations, but the large number of potential energy surface evaluations required often limits the accuracy of the electronic structure method that may be used. Another strategy is to use a semiautomated surface fitting algorithm. Several such methods have been proposed.ⁱⁱ In general, these methods use the results of previous nearby electronic structure calculations to make interpolated surface fits and require significantly fewer electronic structure calculations than full direct dynamics. These methods have not been widely applied to NBO systems.

We are also interested in characterizing the kinetics of elementary reactions relevant to combustion systems. In these studies, accurate rate coefficients are obtained using a combination of variable reaction coordinate TST for barrierless reactions, variational rigid rotor–harmonic oscillator TST for finite barrier reactions, master equation simulations, and high level ab initio calculations.

II. Recent Progress

A. Non-Born–Oppenheimer Molecular Dynamics Simulations

Several improvements to the SH and DM methods have been made via systematic comparisons with accurate quantum mechanical results. In one such study, the accuracy of NBO MD methods for simulating deep quantum systems (i.e., systems with large electronic state energy gaps) was reevaluated recently in light of new quantum mechanical calculationsⁱⁱⁱ of the photodissociation of the Na⁺FH van der Waals complex. Previously, it was suggested that the accuracy of the NBO MD methods would degrade for systems with large energy gaps. In our work and contrast to the conclusion arrived at in an earlier study,^{iv} the semiclassical trajectory methods were shown to be qualitatively accurate for the Na⁺FH system, thus validating their use for deep quantum systems.

In the course of this study, product branching in the NBO MD simulations was found to be affected by a region of coupling where the excited state was (classically) energetically forbidden. In the SH simulations, energetically frustrated surface hops in this region were attributed to a failure of the treatment of electronic decoherence, and a stochastic decoherence (SD) model was introduced into the SH method. Results obtained using the improved SH method were shown to be in quantitative agreement with the quantum mechanical results. An analogous modification of the DM method resulting in faster decoherence in this critical region was shown to give similarly improved results. This study highlights the importance of accurate treatments of electronic decoherence in trajectory-based simulations of systems with coupled electronic states.

In other work and in collaboration with D. G. Truhlar and R. Valero, the nonadiabatic photodissociation of HBr was modeled using several semiclassical trajectory methods. The calculated branching fractions for the H + Br(²P_{3/2}) and H + Br(²P_{1/2}) products were found to be in good agreement with experimental measurements and with the results of more complete theoretical treatments over a wide range of photon energies. The results were found to be very sensitive to surface couplings in the long-range region of the potential energy surfaces.

B. Theoretical Chemical Kinetics

In collaboration with S. J. Klippenstein and L. B. Harding, several detailed kinetics studies of elementary reactions have been made. Rate coefficients for the CH₃ + OH bimolecular reaction and for the decomposition of methanol were obtained over a wide range of temperatures and pressures. Of particular importance in this study was the use of variable reaction coordinate TST to describe the kinetics of the barrierless bimolecular channels, the use of a two transition state model for the important product channel ¹CH₂ + H₂O, and the use of accurate experimental thermochemistry obtained from the Active Thermochemical Tables of B. Ruscic and co-workers. Comparisons were made with available experimental and previous theoretical results, including a companion set of shock tube studies carried out by N. K. Srinivasan and J. V. Michael.^v The predicted results were found to be in excellent agreement with the experimental results. The major products of the bimolecular reaction at 1 atm are CH₃OH (for T < 1200 K) and CH₂ + H₂O (for T > 1200 K). The H + CH₂OH product channel is also important at high temperatures. The major product channels for CH₃OH decomposition are CH₃ + OH and CH₂ + H₂O, formed in a ratio of 4:1.

In the course of the methanol study, we computed several rate coefficients useful for describing the secondary chemistry of methanol decomposition. Specifically, rates for the ³CH₂ + OH, ³CH₂ + ³CH₂, and ³CH₂ + CH₃ barrierless association reactions were obtained; these reactions were previously not well characterized. The use of the theoretical rate coefficients for these reactions qualitatively

improved the accuracy of the reaction mechanism used to model the long-time behavior of the OH absorption profiles measured in the shock tube experiments of N. K. Srinivasan and J. V. Michael.^v

We also tested the “geometric mean rule” approximation for the CH₃, ³CH₂, and OH fragments. This rule was found to be very accurate for predicting rate coefficients for the ³CH₂ + OH and ³CH₂ + CH₃ cross reactions, with errors of only 20%. The geometric mean rule was found to perform less well for the CH₃ + OH reaction, with errors as large as a factor of 2, due to an improper treatment of steric effects by the geometric mean rule.

A theoretical study of the kinetics of the CH₃ + HO₂ bimolecular reaction was performed at temperatures and pressures relevant to combustion. The predicted product branching ratio of 4:1 for the CH₃O + OH and CH₄ + O₂ products was found to be in close agreement with revised values recently obtained in two modeling studies. Earlier theoretical and modeling studies predicted significantly more formation of CH₃O + OH. This result has important consequences for understanding ignition in hydrocarbon combustion at high pressures. Rate coefficients for the CH₃O + OH reaction and for CH₃OOH decomposition were also presented.

III. Future Work

A. Non-Born–Oppenheimer Molecular Dynamics Simulations

A major component of future work will involve the application of the improved NBO MD methods discussed above to polyatomic systems. Trajectory studies of the photodissociation of the series of vinyl halides will be used to interpret the experimental results of D. L. Osborn and co-workers^{vi} and others. The doublet-quartet crossing of C_{2v} HCN₂ has been implicated as an important dynamical bottleneck in the CH + N₂ reaction, and, while this process has been studied previously using quantum chemistry and TST calculations,^{vii} future NBO MD trajectory studies will further characterize the dynamics at this crossing. We will also study intersystem crossing in the spin-orbit coupled systems formed from the addition of oxygen atoms to hydrocarbons.

An important practical bottleneck for performing NBO MD simulations is the need for inexpensive and accurate potential energy surfaces and their couplings. Two strategies will be pursued for obtaining potential energy surfaces in the NBO MD simulations. Direct dynamics methods will be developed based on single reference methods (DFT, MP2, etc) for spin-orbit coupled systems and multireference methods (CASPT2, etc) for valence coupled systems. Semiautomated surface fitting strategies will also be implemented. Schemes for modeling the coupling between the electronic surfaces will also be developed.

B. Theoretical Chemical Kinetics

We will continue to use established theoretical kinetics techniques to make quantitative predictions for important elementary combustion reactions. We will also study and extend the applicability of TST to systems that are currently not well described by statistical theories. One such class of systems features spin-orbit split electronic states. We will study the effect of spin-orbit splitting on the kinetics of barrierless reactions by considering the reactions of halogen atoms with several hydrocarbon radicals. Barrierless abstraction reactions are also challenging to treat using TST. For these reactions, variable reaction coordinate TST is appropriate for characterizing the kinetics at low temperatures, but the assumptions involved in this approach are not suitable at higher temperatures where the reacting fragments are significantly distorted from their isolated geometries at the important dynamical bottlenecks. A two transition state approach will be applied to study these systems.

IV. References

- i. A. W. Jasper, S. Nangia, C. Zhu, and D. G. Truhlar, *Acc. Chem. Res.* **39**, 101–108 (2006).
- ii. See, e.g., O. Godsi, C. R. Evenhuis, and M. A. Collins, *J. Chem. Phys.* **125**, 104105 (2006). O. Tishchenko and D. G. Truhlar, *J. Chem. Theory Comput.* **3**, 938–948 (2007). R. Dawes, D. L. Thompson, Y. Guo, A. F. Wagner, and M. Minkoff, *J. Chem. Phys.* **126**, 184108 (2007).
- iii. S. Garashchuk and V. A. Rassolov, *Chem. Phys. Lett.* **446**, 395 (2007).
- iv. Y. Zeiri, G. Katz, R. Kosloff, M. S. Topaler, D. G. Truhlar, and J. C. Polanyi, *Chem. Phys. Lett.* **300**, 523 (1999).
- v. N. K. Srinivasan, M.-C. Su, and J. V. Michael, *J. Phys. Chem. A* **111**, 3951 (2007).
- vi. P. Zou, K. E. Strecker, J. Ramirez-Serrano, L. E. Jusinski, C. A. Taatjes, and D. L. Osborn, *Phys. Chem. Chem. Phys.* **10**, 713–728 (2008).
- vii. Q. Cui, K. Morokuma, J. M. Bowman, and S. J. Klippenstein, *J. Chem. Phys.* **110**, 9469–9482 (1999).

V. Publications and submitted journal articles supported by this project 2006-2008

1. A. W. Jasper, S. J. Klippenstein, L. B. Harding, and B. Ruscic, "Kinetics of the reaction of methyl radical with hydroxyl radical and methanol decomposition," *J. Phys. Chem. A* **111**, 3932–3950 (2007). (James A. Miller Festschrift)
2. L. B. Harding, S. J. Klippenstein, and A. W. Jasper "Ab initio methods for reactive potential energy surfaces," *Phys. Chem. Chem. Phys.* **9**, 4055–4070 (2007).
3. A. W. Jasper and D. G. Truhlar, "Non-Born–Oppenheimer molecular dynamics study of the photodissociation of Na⁺FH," *J. Chem. Phys.* **127**, 194306 (2007).
4. N. K. Srinivasan, M.-C. Su, J. V. Michael, A. W. Jasper, S. J. Klippenstein, and L. B. Harding, "The thermal decomposition of CF₃ and the reaction of CF₂ + OH → CF₂O + H," *J. Chem. Phys. A*, accepted.
5. A. W. Jasper, S. J. Klippenstein, and L. B. Harding, "Theoretical rate coefficients for the reaction of methyl radical with hydroperoxyl radical and for methylhydroperoxide decomposition," *Proc. Combust. Inst.*, submitted.
6. R. Valero, D. G. Truhlar, and A. W. Jasper, "Photodissociation of HBr: Semiclassical trajectory study using adiabatic states derived from a spin-coupled diabatic transformation," *J. Phys. Chem. A*, submitted.

IONIZATION PROBES OF MOLECULAR STRUCTURE AND CHEMISTRY

Philip M. Johnson
Department of Chemistry
Stony Brook University, Stony Brook, NY 11794-3400
Philip.Johnson@sunysb.edu

I. Program Scope

Photoionization processes provide very sensitive probes for the detection and understanding of molecules and chemical pathways relevant to combustion processes. Laser based ionization processes can be species-selective by using resonances in the excitation of the neutral molecule under study or by exploiting different sets of ionization potentials of different molecules. Therefore the structure and dynamics of individual molecules can be studied, or species monitored, even in a mixed sample. We are continuing to develop methods for the selective spectroscopic detection of molecules by ionization, to use these spectra for the greater understanding of molecular structure, and to use these methods for the study of some molecules of interest to combustion science.

II. Recent Progress

The introduction of a high resolution CW pulse-amplified dye laser into our laboratory has given us the capability of studying the spectroscopy and photophysics of larger, less symmetric molecules with rotational resolution. Exploiting this capability, we recently have been looking at various interesting properties of the molecules benzonitrile and phenylacetylene. Phenylacetylene, in particular, plays an important role in soot formation in combustion, and in the chemistry of the atmosphere of Saturn's moon Titan. Our recent discovery that phenylacetylene can store electronic energy practically indefinitely (on a molecular time scale) could have some implications in its reactivity in those situations.

The evolution of energy in an isolated large molecule excited to its lowest singlet state is usually thought of in terms of a kinetic competition between pathways leading out of the non-stationary state carrying the oscillator strength of the transition. Thus the various pathways leading to fluorescence, a vibrationally excited ground state surface, or a vibrationally excited triplet state surface all lead from, and are fed by, the initially pumped singlet state. In the case of phenylacetylene this simple picture appears to break down.

In radiationless transition theory, it is assumed that the wavefunction of an isolated excited state of a molecule can mix with the high density of isoenergetic states having the same (Internal Conversion) or different (Intersystem Crossing) multiplicity. Following the absorption of light, most aromatic molecules have been found to have emission quantum yield less than unity, indicating radiationless transitions play an important role in the decay of excited states. Numerous experiments of various types have been performed to illuminate the nature of state interactions in a variety of aromatic molecules.

Over the past few decades, two-color pump-probe photoionization techniques have been used to investigate the time evolution of excited states of large molecules under collision-free conditions in the environment of a supersonic beam. In these experiments, the first laser is used to excite the molecules to a singlet vibronic level which evolves in time, crossing over to an

isoenergetic point in the triplet manifold. By using another laser with sufficient photon energy to overcome Franck-Condon factor differences, both singlet and triplet molecules can be ionized with about the same efficiency, but molecules that go into the electronic ground state cannot be ionized because the Franck-Condon favorable region of the ionization continuum is above the photon energy. The time evolution of excited state populations can be measured by varying the delay time between the ionizing laser and the pump laser. Unlike fluorescence spectroscopy, which is only sensitive to the singlet component of the mixed state, photoionization is not constrained by spin selection rules. Therefore, the time evolution of both the singlet and triplet state can both be monitored by detection of either ions or photoelectrons produced from the ionization.

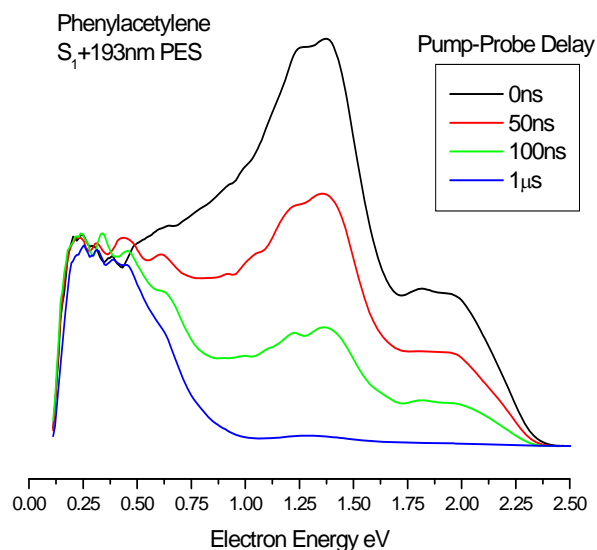
Recently we have been investigating the pump-probe photoionization studies of isolated benzonitrile (BN) and phenylacetylene (PA) in which both molecules evolve into very long-lived species (living hundreds of microseconds or more), with low ionization potentials, in an energy region for which short lifetimes would be expected if simple intersystem crossing were taking place. Furthermore, excited state photoelectron spectroscopy shows that the excited S_1 states do not continue to evolve into this long-lived product after the light pulse has ended, a result not expected from the standard kinetic model. To ensure that the properties measured belong strictly to the monomers of these molecules, the present study used a high resolution pulse amplified cw laser to excite the molecules to their S_1 states, allowing a comparison between the rotational structure of the action spectra for various ionization processes and the known rotational structure of the monomer. Thus an absolute determination can be made that the signals described here arise from monomers.

Mechanisms that can produce such a stable and easily ionizable species in a collisionless environment are few. These include:

1. Intersystem crossing into an isoenergetic set of states in the triplet manifold.
2. Internal conversion into highly excited vibrational levels of the molecular ground state.
3. Intersystem crossing followed by near-IR emission to low vibrational levels of the lowest triplet state.
4. Isomerization.

Various experimental tests have been performed to exclude as many of these mechanisms as possible. A search for near-IR emission was negative to a good degree of certainty, so mechanism 3 can be discounted, while excited triplet states with $10,000\text{ cm}^{-1}$ of vibrational energy would not have such a long lifetime. The preponderance of evidence currently points to isomerization as the primary mechanism, but the identity of the isomer has yet to be determined.

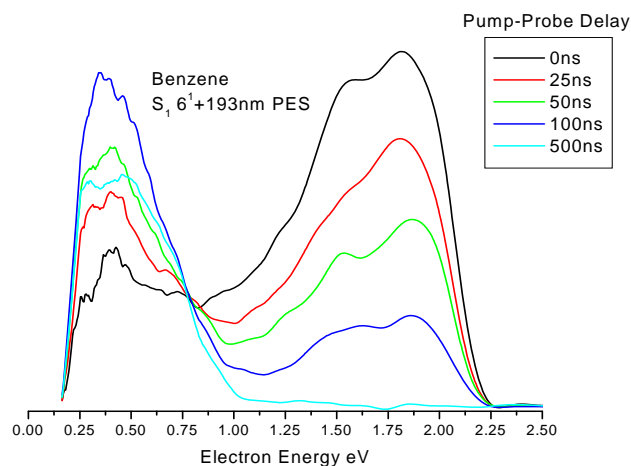
The pump-probe PES of the vibrationless S_1 state using 193nm ionization photons is shown at right for various time delays between the lasers and can be compared with similar measurements on benzene shown below.



For PA, three distinct features are present in the spectra at about 2.0, 1.4 and 0.65 eV, with the first two of them dependent upon the laser delay, going away with the fluorescence lifetime. The decaying peaks can easily be assigned as the transitions from singlet S_1 to the ground state (\tilde{X}^2B_1) and first excited state of the ion (\tilde{A}^2A_2). The lower energy electrons are not dependent on the delay and come from the long-lived state, persisting to delays of over 150 μ s. The high energy onset of the 1 μ s curve is consistent with the threshold scan described above, and the fall-off of all the curves at low energy is due to the loss of low-energy electrons in the flight tube. Spectra using negative repeller voltages show a continuing increase of intensity down to 0.1 eV.

The remarkable feature of the phenylacetylene PES is that the low energy feature does not change at all with the laser delay, while the singlet is decaying. This means that whatever entity is being ionized is produced independently of the singlet during the laser pulse, and is not a daughter product of the singlet. This contradicts the usual concept of an excited state being formed, and then decaying along a variety of paths that depend upon a competition between their kinetic rates. The normal kinetic picture is seen in benzene (below), where the triplet signal initially increases as the singlet decreases, and then decays with its characteristic triplet lifetime.

These spectra, in conjunction with the rotationally resolved action spectra, indicate that each different rotational level excited in PA can follow at least two independent routes, leading to either fluorescence or the long-lived species (or other products we cannot detect), and the selection between these routes takes place during the laser pulse or shortly thereafter. A certain population of molecules stays in the singlet state and eventually fluoresces, while another population enters a stabilizing pathway. If these rotational levels were truly homogeneous singlet eigenstates, the selection could take place at any time during the singlet lifetime. The fact that it does not, implies the existence of a set of uncoupled states with the same action spectrum. This behavior does not change when the S_1 excitation is done with a normal dye laser with a bandwidth of fractions of a cm^{-1} , so it is not a feature of high resolution excitation.



Since a pure quantum state cannot evolve in two different ways, one must assume that the pumped state is not pure, even though a single rotational level is selected. Substructure in rotational levels can be created by nuclear spin states, and PA has two sets of identical protons. It is conceivable that isomerization of some of its nuclear spin states into a particular isomer could be impossible because of symmetry and parity restrictions, explaining the bifurcation.

There are a large number of isomers of phenylacetylene, some of which require minimal bond rearrangement, and we have considered whether the long-lived state is one of them. The most facile isomerization, one where there do not even have to be any hydrogen shifts, is to go to cyclooctyne (1,2-dehydrocyclooctatetraene). The anion photoelectron spectroscopy of this molecule is known, and it is found that the ground state moves up to only 0.7 eV below the triplet because of loss of aromaticity. One could therefore envision that the density of cyclooctyne S_0 states at the level of T_1 is low enough that intersystem crossing is suppressed

between those states Preliminary calculations at the DFT-B3LYP 6-31G(2d,p) level indicate that the T_1 state of cyclooctyne will be about 0.3 eV below that of PA, allowing for easy conversion in a hot molecule. The ionization potential of cyclooctyne triplet is calculated to be 6.7eV, which is just above the 193nm photon energy of 6.42 eV. The IP could shift with better calculations, and excited vibrations could make up the extra energy, so stabilization by isomerization remains a possibility for explaining the very long lifetime.

III. Future Work

To proceed with the understanding of PA photophysics, it is vital to uncover the identity of the long-lived species. The best method to accomplish this is photoelectron spectroscopy, but the time-of-flight method we have been using has had enough resolution to provide a definitive answer. A new apparatus using velocity map imaging PES is just being completed, which should give us much more accurate results. These will be compared to higher level calculations of all of the possible isomers, followed by the analysis of spin statistics using molecular symmetry groups. A new F_2 laser will also enable the measurement of any low-lying ionic states of the long-lived species, giving new clues to its identity.

Using these new capabilities, along with fluorescence excitation and ionization techniques we have previously developed, we are planning to determine and investigate the species formed from the thermal reaction of oxygen with various molecules representing species present in combustion fuels. These measurements will provide information about the initial reactions that take place in low temperature compression ignition engines being considered as new, more efficient power sources.

IV. Publications and submitted journal articles supported by this project 2006-2008

Haifeng Xu, Trevor Sears, and Philip Johnson, "Photoinduced Rydberg Ionization spectroscopy of Phenylacetylene: Vibrational assignments of the \tilde{C} state of the cation," *J. Phys. Chem. A*, **110**, 7822-7825 (2006).

Philip Johnson, Haifeng Xu, and Trevor Sears, "The calculation of vibrational intensities in forbidden electronic transitions," *J. Chem. Phys.* **125**, 164330 (2006).

Haifeng Xu, Philip Johnson, and Trevor Sears, "Photoinduced Rydberg ionization spectroscopy of the \tilde{B} state of benzonitrile cation," *J. Chem. Phys.* **125**, 164331 (2006).

Jason Hofstein, Haifeng Xu, Trevor Sears, and Philip Johnson, "The fate of excited states in jet-cooled aromatic molecules: Bifurcating pathways and very long-lived species from the S_1 excitation of phenylacetylene and benzonitrile," *J. Phys. Chem. A* **112**, 077367 (2008).

Probing the Reaction Dynamics of Hydrogen-Deficient Hydrocarbon Molecules and Radical Intermediates via Crossed Molecular Beams

Ralf I. Kaiser
Department of Chemistry
University of Hawai'i at Manoa
Honolulu, HI 96822
ralfk@hawaii.edu

1. Program Scope

The major goals of this project are to explore experimentally in crossed molecular beams experiments the reaction dynamics and potential energy surfaces (PESs) of hydrocarbon molecules and their corresponding radical species which are relevant to combustion processes. The reactions are initiated under single collision conditions by crossing two supersonic reactant beams containing radicals and/or closed shell species under a well-defined collision energy and intersection angle. By recording angular resolved time of flight (TOF) spectra, we obtain information on the reaction products, intermediates involved, on branching ratios for competing reaction channels, on the energetics of the reaction(s), and on the underlying reaction mechanisms. These data are of crucial importance to understand the formation of carbonaceous nanostructures ('soot') as well as of polycyclic aromatic hydrocarbons and their hydrogen deficient precursors in combustion flames. Chemical networks concur that reactions of the phenyl radical with unsaturated hydrocarbons initiate the PAH synthesis. Due to the central role of the phenyl – unsaturated hydrocarbon reactions, the kinetics of these systems have been well-established up to temperatures of a couple of thousand Kelvin. However, the nature of the true reaction products formed under single collision conditions and the intermediates involved have remained elusive so far. Therefore, we initiated a systematic research program to untangle the reaction dynamics of phenyl radicals with unsaturated hydrocarbons.

Here, we have utilized a newly commissioned phenyl radical source and investigated the chemical dynamics of bimolecular reactions involving phenyl radicals with unsaturated hydrocarbon molecules. These are acetylene (C_2H_2), ethylene (C_2H_4), methylacetylene (CH_3CCH)*, allene (H_2CCCH_2)*, benzene (C_6H_6)*, propylene (C_3H_6)*, and molecular oxygen (O_2)*; systems denoted with '*' present investigations conducted in the current year of funding (Fig. 1). Reactions with (partially) deuterated counterparts were conducted to identify the position of the atomic hydrogen loss pathway(s) and to derive the branching ratios if multiple exit channels are involved. Acetylene, ethylene, and benzene serve as prototype reaction partners and simplest representatives of reactant molecules with acetylenic, olefinic, and 'aromatic' bonds. Methylacetylene and allene were selected to investigate how the reaction dynamics change from one structural isomer to the other.

2. Recent Progress

2.1. Phenyl – Benzene Reaction

The chemical dynamics to form the D5-diphenyl molecule, $C_6H_5C_6D_5$, via the neutral-neutral reaction of phenyl radicals (C_6H_5) with D6-benzene (C_6D_6) was investigated in a crossed molecular beams experiment at a collision energy of 185 kJmol^{-1} . The laboratory angular distribution and time-of-flight spectra of the $C_6H_5C_6D_5$ product were recorded at mass-to-charge, m/z , of 159. Forward-convolution fitting of our data reveals that the reaction dynamics are governed by an initial addition of the phenyl radical to the π electron density of the D6-benzene molecule yielding a short-lived $C_6H_5C_6D_6$ collision complex. The latter undergoes atomic deuterium elimination via a tight exit transition state located about 30 kJmol^{-1} above the separated reactants; the overall reaction to form D5-diphenyl from phenyl and D6-benzene was found to be weakly exoergic. The explicit identification of the D5-biphenyl

molecules suggests that in high temperature combustion flames, a diphenyl molecule can be formed via a single collision event between a phenyl radical and a benzene molecule.

2.2. Phenyl – Methylacetylene/Allene Reactions

Crossed molecular beam experiments were utilized to untangle the reaction dynamics to form 1-phenylmethylacetylene [$\text{CH}_3\text{CCC}_6\text{H}_5$] and 1-phenylallene [$\text{C}_6\text{H}_5\text{HCCCH}_2$] in the reactions of phenyl radicals with methylacetylene and allene, respectively, over a range of collision energies from 91.4 to 161.1 kJmol^{-1} . Both reactions proceed via indirect scattering dynamics and are initiated by an addition of the phenyl radical to the terminal carbon atom of the methylacetylene and allene reactants to form short-lived doublet C_9H_9 collision complexes $\text{CH}_3\text{CCHC}_6\text{H}_5$ and $\text{C}_6\text{H}_5\text{H}_2\text{CCCH}_2$. Studies with isotopically labeled reactants and the information on the energetics of the reactions depict that the energy randomization in the decomposing intermediates is incomplete. The collision complexes undergo atomic hydrogen losses via tight exit transition states leading to 1-phenylmethylacetylene [$\text{CH}_3\text{CCC}_6\text{H}_5$] and 1-phenylallene [$\text{C}_6\text{H}_5\text{HCCCH}_2$].

2.3. Phenyl - Propylene

The reactions between phenyl radicals (C_6H_5) and propylene (CH_3CHCH_2) together with its D6- and two D3-isotopologues were studied under single collision conditions using the crossed molecular beams technique. The chemical dynamics inferred from the center-of-mass translational and angular distributions suggest that the reactions are indirect and initiated by an addition of the phenyl radical to the α -carbon atom (C1 carbon atom) of the propylene molecule at the $=\text{CH}_2$ unit to form a radical intermediate [$\text{CH}_3\text{CHCH}_2\text{C}_6\text{H}_5$] on the doublet surface. Investigations with D6-propylene specified that only a deuterium atom was emitted; the phenyl group was found to stay intact. Studies with 1,1,2-D3 and 3,3,3-D3 propylene indicated that the initial collision complexes $\text{CH}_3\text{CD}_2\text{C}_6\text{H}_5$ (from 1,1,2-D3 propylene) and $\text{CD}_3\text{CHCH}_2\text{C}_6\text{H}_5$ (from 3,3,3-D3 propylene) eject both a hydrogen atom via rather loose exit transition states to form the D3-isotopomers of cis/trans 1-phenylpropene [$\text{CH}_3\text{CHCHC}_6\text{H}_5$] (80 – 90 %) and 3-phenylpropene [$\text{H}_2\text{CCHCH}_2\text{C}_6\text{H}_5$] (10 – 20 %), respectively.

2.4. Phenyl – Oxygen Reaction

The chemical dynamics of the combustion-relevant reaction of phenyl radicals with molecular oxygen were investigated in a crossed beam reaction at a collision energy of 107 kJmol^{-1} . Under these conditions, the formation of the phenoxy radical ($\text{C}_6\text{H}_5\text{O}$) plus ground state atomic oxygen was observed; no atomic hydrogen exchange pathway was opened. The reaction dynamics of the phenoxy radical channel were found to be direct, involved a stripping-like reaction mechanism, and were initiated by a radical-radical recombination of phenyl plus molecular oxygen forming a short lived phenylperoxy radical ($\text{C}_6\text{H}_5\text{O}_2$). The latter decomposed to the phenoxy radical plus atomic oxygen; the overall reaction was exoergic by about $38 \pm 15 \text{ kJmol}^{-1}$.

3. Future Plans

Within the ongoing project, we aim to propel this research to the next level and investigate the reaction dynamics of phenyl radicals with various C_4H_6 isomers (1,3-butadiene, 1,2-butadiene, 1-butyne, 2-butyne) as present in combustion flames and with their (partially) deuterated counterparts. Here, 1,3-butadiene was detected in cyclohexane, isobutene, heptane, ethane, and methane flames utilizing, for instance, the Advanced Light Source in Berkeley. These isomers can be interconverted via hydrogen atom addition – hydrogen atom elimination pathways. The crossed beam reactions of phenyl radicals with these C_4H_6 isomers will access the important $\text{C}_{10}\text{H}_{11}$ and $\text{C}_{10}\text{H}_{10}$ potential energy surfaces including dihydronaphthalene and its isomers.

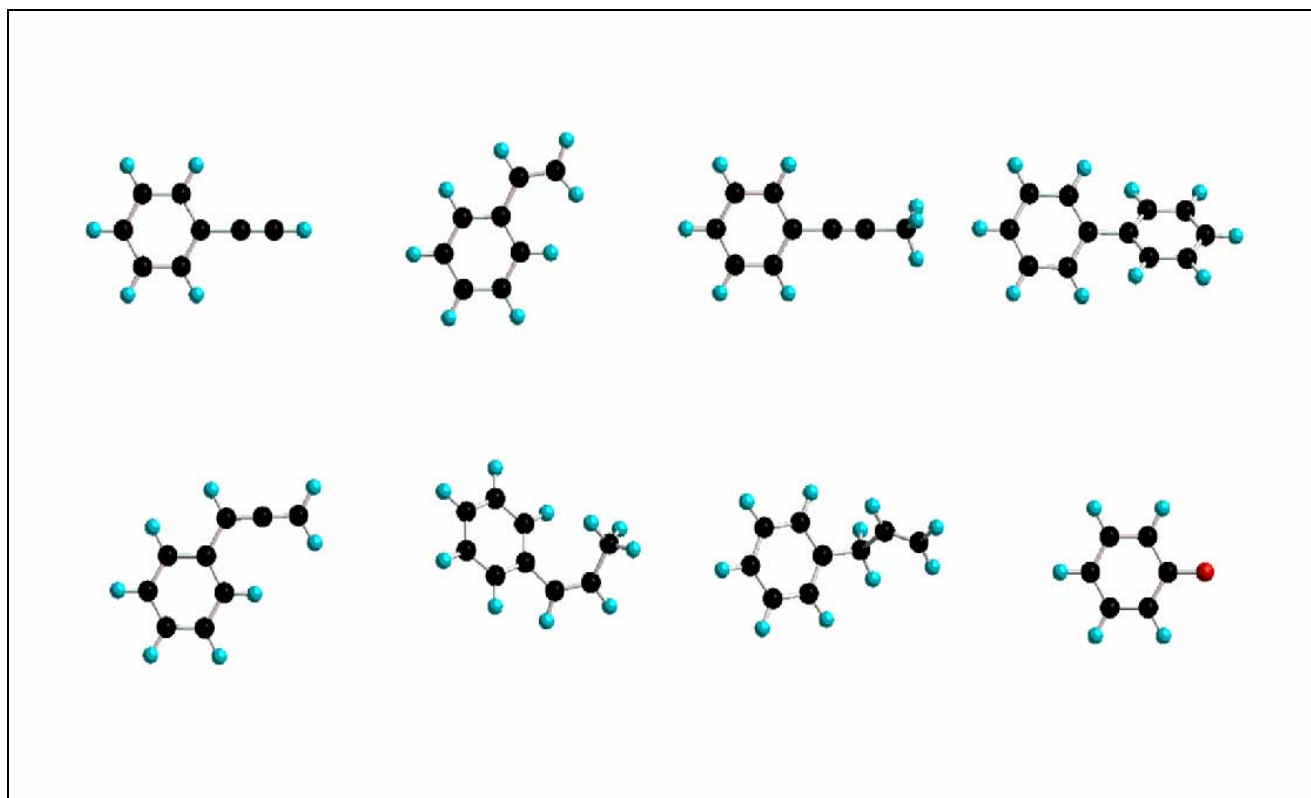


Fig. 1: Upper row from left to right: reaction products in the reactions of phenyl radicals with acetylene, ethylene, methylacetylene, and benzene. Lower row from left to right: reaction products in the reactions of phenyl radicals with allene, propylene (two isomers), and oxygen.

4. Publications Acknowledging DE-FG02-03ER15411 (2006-2008)

A. M. Mebel, V. V. Kislov, R. I. Kaiser, *Potential Energy Surface and Product Branching Ratios for the Reaction of Dicarbon, $C_2(X^1\Sigma_g^+)$, with Methylacetylene, $CH_3CCH(X^1A_1)$: An Ab Initio/RRKM Study*, JPCA 110, 2421-2433 (2006).

Y. Guo, X. Gu, N. Balucani, R.I. Kaiser, *Formation of the 2,4-pentadiynyl-1 radical ($H_2CCCCCH$, X^2B_1) in the Crossed Beams Reaction of Dicarbon Molecules with Methylacetylene*. JPCA 110, 6245-6249 (2006).

X. Gu, Y. Guo, A.M. Mebel, R.I. Kaiser, *Chemical Dynamics of the Formation of the 1,3-Butadiynyl Radical ($C_4H(X^2\Sigma^+)$) and its Isotopomers*. JPCA, 110, 11265-11278 (2006).

Y. Guo, X. Gu, F. Zhang, A.M. Mebel, R.I. Kaiser, *Unimolecular Decomposition of Chemically Activated Pentatetraene ($H_2CCCCCH_2$) Intermediates – A Crossed Beams Study of Dicarbon Molecule Reactions with Allene*. JPCA 110, 10699-10707 (2006).

A. M. Mebel, V. V. Kislov, R. I. Kaiser, *Ab Initio/RRKM Study of the Singlet C_4H_4 Potential Energy Surface and of the Reactions of $C_2(X^1\Sigma_g^+)$ with $C_2H_4(X^1A_{1g})$ and $C(^1D)$ with C_3H_4 (Allene and Methylacetylene)*, J. Chem. Phys. 125, 133113-1/15(2006).

X. Gu, Y. Guo, F. Zhang, A. M. Mebel, R.I. Kaiser, *A Crossed Molecular Beams Study of the Reaction of Dicarbon Molecules with Benzene*, Chem. Phys. Lett 436, 7-14 (2007).

- Y. Guo, X. Gu, F. Zhang, A.M. Mebel, R.I. Kaiser, *A Crossed Molecular Beams Study on the Formation of Hexenediynyl Radicals ($H_2CCCCCCH$; C_6H_3 (X^2A')) via Reactions of Tricarbon Molecules, $C_3(X^1\Sigma_g^+)$, with Allene (H_2CCCH_2 ; X^1A_1) and Methylacetylene (CH_3CCH ; X^1A_1). PCCP 9, 1972 – 1979 (2007).*
- X. Gu, Y. Guo, F. Zhang, A.M. Mebel, R.I. Kaiser, *A Crossed Molecular Beams Study on the Formation and Energetics of the Resonantly Stabilized i - C_4H_3 radical, $H_2CCCH(X^2A')$, together with its Isotopomers. Chemical Physics 335, 95-108 (2007).*
- A.M. Mebel, G.S. Kim, V.V. Kislov, R.I. Kaiser, *The Reaction of Tricarbon with Acetylene: An Ab Initio/RRKM Study of the Potential Energy Surface and Product Branching Ratios. JPCA 111, 6704-6712 (2007).*
- X. Gu, Y. Guo, F. Zhang, A.M. Mebel, R.I. Kaiser, *Unimolecular Decomposition of Chemically Activated Singlet and Triplet D3-Methylacetylene. Chem. Phys. Lett. 444, 220-225 (2007).*
- X. Gu, F. Zhang, Y. Guo, R.I. Kaiser, *A Crossed Molecular Beam Study on the Formation of Phenylacetylene from Phenyl Radicals and Acetylene. Angew. Chemie Int. Edition 46, 6866-6869 (2007).*
- F. Zhang, X. Gu, Y. Guo, R. I. Kaiser, *Reaction Dynamics on the Formation of Styrene ($C_6H_5C_2H_3$) - A Crossed Molecular Beam Study of the Reaction of Phenyl Radicals (C_6H_5) with Ethylene (C_2H_4), J. Organic Chem. 72, 7597-7604 (2007).*
- X. Gu, F. Zhang, R.I. Kaiser, *A Crossed Beam Reaction of the Phenyl Radical, (C_6H_5 , X^2A_1) with Molecular Oxygen (O_2 , $X^3\Sigma_g^-$): Observation of the Phenoxy Radical, (C_6H_5O , X^2A'). Chem. Phys. Lett. 448, 7-10 (2007).*
- X. Gu, F. Zhang, Y. Guo, R. I. Kaiser, *Reaction Dynamics of Phenyl Radicals (C_6H_5 , X^2A_1) with Methylacetylene ($CH_3CCH(X^1A_1)$), Allene ($H_2CCCH_2(X^1A_1)$), and Their D4-Isotopomers. J. Phys. Chem. A 111, 11450-11459 (2007).*
- A. M. Mebel, V. V. Kislov, R. I. Kaiser, *Theoretical Studies of Potential Energy Surfaces and Product Branching Ratios for the Reactions of C_2 with Small Unsaturated Hydrocarbons (Acetylene, Ethylene, Methylacetylene, and Allene). in: Gas Phase Molecular Reaction and Photodissociation Dynamics, Editors: K.C. Lin and P.D. Kleiber, Transworld Research Network 2007, pp. 113-159*
- X. Gu, Y. Guo, A.M. Mebel, R.I. Kaiser, *A Crossed Beams Investigation of the Reactions of Tricarbon Molecules, $C_3(X^1\Sigma_g^+)$, with Acetylene, $C_2H_2(X^1\Sigma_g^+)$, Ethylene, $C_2H_4(X^1A_g)$, and Benzene $C_6H_6(X^1A_{1g})$. Chem. Phys. Lett. 449, 44-52 (2007).*
- X. Gu, R.I. Kaiser, A.M. Mebel, *Chemistry of Energetically Activated Cumulenes - From Allene (H_2CCCH_2) to Hexapentaene ($H_2CCCCCCH_2$). Invited Review. Chem. Phys. Chem. 9, 350-369 (2008).*
- F. Zhang, X. Gu, R.I. Kaiser, *Formation of the Diphenyl Molecule in the Crossed Beam Reaction of Phenyl Radicals with Benzene. J. Chem. Phys. 128, 084315/1-5(2008).*
- F. Zhang, X. Gu, Y. Guo, R.I. Kaiser, *Reaction Dynamics of Phenyl Radicals (C_6H_5) with Propylene (CH_3CHCH_2) and Its Deuterated Isotopologues. JPCA (in press 2008).*
- X. Gu, R.I. Kaiser, *From Phenyl Radicals to Soot. Invited Review. Acc. Chem. Res. (to be submitted June 2008).*

DYNAMICAL ANALYSIS OF HIGHLY EXCITED MOLECULAR SPECTRA

Michael E. Kellman

Department of Chemistry, University of Oregon, Eugene, OR 97403

kellman@uoregon.edu

PROGRAM SCOPE:

Highly excited internal dynamics of small molecular species are crucial to understanding fundamental processes important for combustion systems. The goal of our program is to develop theoretical tools to understand spectra and dynamics of these highly excited species. It is clear that anharmonic effects lead to profound changes in the vibrational dynamics of molecules when nonlinearities can no longer be treated as perturbative effects, and the standard picture of anharmonic normal modes breaks down. We emphasize particularly the role of bifurcations and the “birth of new modes in bifurcations from the low energy normal modes”. References to numerous examples can be found in a recent detailed study of acetylene bends spectra [2] and a recent review [3]. For this we use bifurcation analysis of semiclassical versions of the effective Hamiltonians used by spectroscopists to fit complex experimental spectra. Observable phenomena associated with bifurcations such as changes in spectral patterns have been predicted and observed. A future long-range desired focus is chemical reactivity, including above-barrier intramolecular (isomerization) reactions.

RECENT PROGRESS: The progress described here is in collaboration with postdoctoral associate Vivian Tyng.

Bifurcation analysis: Branchings of the normal modes into new anharmonic modes.

Much of our work builds on earlier work [2] on the acetylene bends system in which we found four new modes born in bifurcations of the low-energy normal mode states with vibrational angular momentum $\ell = 0$. The acetylene/vinylidene system is of great importance in combustion, acetylene as an intermediate, and the vinylidene isomer as precursor of the radical pool formed by reaction with O_2 . Ref. [2] was an effort to gain a systematic understanding of the bending dynamics.

Higher ℓ -vibrational angular momentum states of acetylene. The bifurcation analysis of the pure bends system in Ref. [2] is for spectra with vibrational angular momentum $\ell = 0$. We are in the final stages of a study that extends this analysis to systems with $\ell > 0$. We have performed the bifurcation analysis for ℓ up to 20 in work to be submitted. We find that there are four new modes born in bifurcations, as for the $\ell = 0$ case. However, these new modes are precessing orbits, due to the ℓ excitation. The figure (below left) shows one of these, the precessing Orthogonal mode.

Catastrophe map analysis of acetylene bends system. The acetylene bends system is a four-mode system with several resonances, nonintegrability and chaotic dynamics. There are two principal resonances of Darling-Dennison type called “Darling-Dennison I” and “ ℓ -resonance” and a third weaker resonance called “Darling-Dennison II”. The system is not separable in any sense. However, the bifurcation behavior observed in Ref. [2] has certain key resemblances to that obtained with an earlier simplified integrable model of two bend modes coupled by a single resonance. It seems that there is something about the structure of the bifurcation problem in Ref. [2] that remains to be fully understood. Our goal has been to understand the evident regularities observed in Ref. [2], while keeping sight of the full complexity of the system.

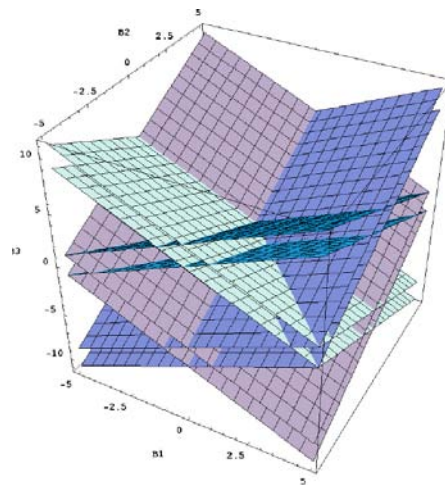
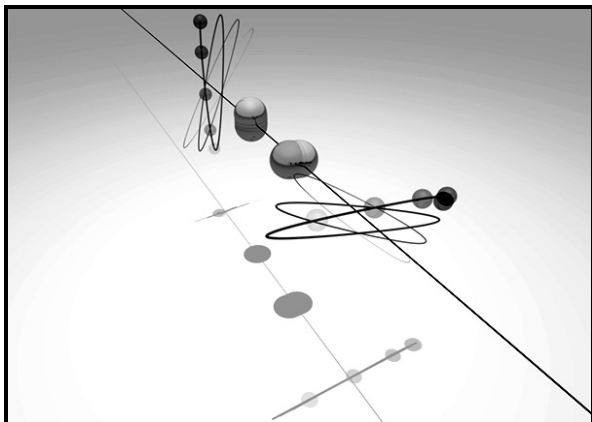
We approach this problem using a catastrophe map analysis. The catastrophe map is a kind of “phase diagram” of the dynamics of the effective fitting Hamiltonian. This gives a systematic, exhaustive classification of all the bifurcation behavior possible for the spectral fit of any molecule, given the form of the Hamiltonian. Now we have developed the method for the first time for a multiresonance system. In this way, regularities in the observed bifurcation behavior of a particular molecule are explained as part of an overarching general structure.

We find that the multiresonance problem splits into a direct sum $\mathbf{M} = \mathbf{M}_{\text{DDI}} + \mathbf{M}_{\ell}$ of two independent submaps, each submap associated with the frequency condition of one of the resonances. (The submap \mathbf{M}_{DDI} is shown in the figure, below left.) Each submap contains the effects of both resonance couplings in a completely symmetrical way, reflecting the nonseparability of the Hamiltonian. This combination of direct sum structure with nonseparability cannot be overemphasized. It accounts for the way that useful information is obtained from independent single resonance catastrophe maps, but also for the greater complexity of the true bifurcation behavior of the multiresonance system.

The catastrophe map analysis is part of a general inquiry “What is the role of individual resonances in the bifurcation behavior of molecular systems with complex dynamics?” In the present study of bending dynamics of acetylene, we have been able to delineate an intelligible role for individual resonances. The key is recognition of the distinction between *resonant degrees of freedom* and *resonance couplings*, with the phase space splitting into a direct sum of resonant degrees of freedom, each acted upon by both resonance couplings. The critical lesson that carries forward to general systems such as the full stretch-bend acetylene problem is that one will still have the direct sum structure.

These seemingly abstract methods and results in fact constitute a generalization of the notion of anharmonic or Fermi resonances that should have practical applications. Our work suggests that for the general problem with multiple independent resonances a reduction to a problem similar to a set of individual resonances. This could be an important key to going to higher dimensions. However there surely must be an important interplay of resonances. How this will work is a question that can only be answered by investigation of specific cases. The full acetylene acetylene stretch-bend

system, with a well-developed spectroscopic fitting Hamiltonian, will be a very good case.



Spectral anomalies, experimental signature of bifurcation, moment of inertia backbending. The interplay of bifurcations and angular momentum remains mostly a mystery. In a recent paper [4], we focused on one of the most elementary possible systems, pure vibrational angular momentum $J = \ell$ excitations of acetylene. From the effective fitting Hamiltonian we predict clearly anomalous spectral behavior. In order to understand this, we invoke a moment of inertia “backbending” effect as the molecule undergoes a sequence of bifurcations. Essentially, the molecule undergoes a change in vibrational “shape” due to the bifurcations, while retaining its linear equilibrium symmetry. This spectral pattern represents both a departure from and extension of the standard rotational dynamics paradigm of a linear symmetric top molecule, as treated, for example, by Herzberg.

FUTURE PLANS:

In the future, our goals are (1) completion of a major effort to understand the full range of bending dynamics for high values both of the total bend quantum number N_b and vibrational angular momentum $\ell > 0$; (2) extension of bifurcation analysis to full stretch-bend dynamics, including rotation-vibration dynamics; (3) spectroscopic Hamiltonians for spectra in which the total or polyad number is broken on the route to isomerization; (4) and further along these lines, incorporation of multiple potentials and above-barrier dynamics, with the goal of extending our methods to encompass isomerization phenomena. Space constraints allow detailed explication only of topic (3) which is currently being pursued intensely with postdoctoral associate Aniruddha Chakraborty.

Spectroscopic Hamiltonians for polyad breaking spectra. All spectroscopic fitting Hamiltonians to date invoke the “polyad approximation” of a conserved total vibrational quantum number. At high enough energy, the polyad approximation must fail. We are investigating the polyad breakdown in highly excited model systems, in order to begin to construct an effective spectroscopic Hamiltonian to encompass this. While effective quantum matrix Hamiltonians with conserved action are routinely used to fit experimental data, spectra of systems that break the polyad action, time-dependent transport in these systems, and the representation of these phenomena with a generalized effective fitting Hamiltonian are mostly unexplored areas.

In work in progress, we are testing a simple generalized effective Hamiltonians capable of encompassing the major dynamical and spectral effects of the polyad breakdown. We demonstrate that a generalized effective Hamiltonian successfully describes the polyad breaking by successively adding a very small number of additional resonance couplings. Each additional resonance coupling induces bifurcations to give new low-order periodic orbits, incompatible with the original polyad number, that reorganize the surrounding phase space structure into large-scale resonance zones. In a quantum system, the spectrum shows clear signatures of these new structures that should be observable in experiments.

This work is concerned with fitting Hamiltonians for breaking of the polyad action in model two degree of freedom systems. Polyad breaking is of great interest in systems of higher degrees of freedom. The polyad number acts as an exact barrier to transport. The nature of the phase space transformation when the polyad number is broken is therefore of great interest. The signatures of polyad breaking in multidimensional systems are almost completely unexplored either experimentally or in dynamical studies. Our work on two degree of freedom systems, and also earlier work of M.J. Davis, demonstrates that the polyad breaking results in new periodic orbits that organize the phase space into resonance zones on a large scale. The periodic orbits are characterized by their incompatibility with the polyad number and their correspondence with the new resonance couplings that are added to the effective Hamiltonian. This strongly suggests that analogous effects will be present in many degree of freedom systems, in particular, new periodic orbits incompatible with the polyad number as the signature of polyad-breaking resonance interactions. The generalized spectroscopic fitting Hamiltonian should be a useful tool for investigating these systems.

Recent publications (in print, in press 2006-2008) related to DOE supported research:

1. S. Yang and M.E. Kellman, “Semiclassical Wave Function From a Quantizing Cantorus”, *Chem. Phys.*, 322, 30-40 (2006).
2. V. Tyng and M.E. Kellman, “Bending Dynamics of Acetylene: New Modes Born in Bifurcations of Normal Modes”, *J. Phys. Chem. B*, 110, 18859-18871 (2006)
3. M.E. Kellman and V. Tyng, “The Dance of Molecules: New Dynamical Perspectives on Highly Excited Molecular Vibrations”, *Accounts of Chemical Research* 40, 243-250 (2007).
4. V. Tyng and M.E. Kellman, “Spectral Anomaly, Moment of Inertia Backbending, and Bifurcations”, *J. Chem. Phys.* 041101, 1-4 (2007).

Theory and Modeling of Small Scale Processes in Turbulent Flow

Alan R. Kerstein
Combustion Research Facility
Sandia National Laboratories
Livermore, CA 94551-0969
Email: arkerst@sandia.gov

PROJECT SCOPE

Combustion and numerous other applications involving engineered or naturally occurring turbulent flow require simplified representations of turbulence interactions with other system processes, such as chemical reaction and species molecular transport, in order to perform affordable numerical simulations of the flow. The conventional simplification strategy is coarse-grained flow simulation supplemented by parameterization of processes at unresolved small scales. This project focuses on the development of alternative simplification strategies.

Parameterization typically involves the advancement, within each mesh cell of the resolved flow, of algebraic or ordinary differential equations intended to model the spatiotemporal evolution of processes at unresolved scales. This strategy has met with some success, but leads to increasing formal complexity and a tendency to perform as an interpolation rather than a predictive tool as it is applied to the increasingly challenging problems posed by current energy and environmental concerns. This suggests that the spatially distributed dynamical systems associated with the time evolution of small scale processes coupled to turbulent motions are not adequately represented by lumped models and instead require modeling involving a simplified yet spatially and temporally resolved subgrid formulation.

Such a formulation has been developed during this project based on the strategy of reduced-dimensional representation. The sheet-like topology of flame surfaces motivates the familiar flame-structure representation in terms of property profiles along lines normal to the flame surface. This suggests a subgrid approach formulated on a 1D domain that captures local flame structure but additionally, captures flame advection and distortion by turbulence through the introduction of a 1D advection process that is a mathematical abstraction of 3D turbulent eddy motion. The mathematical abstraction involves instantaneous maps (rearrangements) of property profiles on the 1D domain in a manner that obeys applicable conservation laws while emulating the scale-reduction and consequent gradient-amplification effects of turbulent eddy motion.

Pursuit of this strategy to date has led to a model, called One-Dimensional Turbulence (ODT), that is a predictive model of turbulence and turbulent combustion in its own right as well as a promising candidate for subgrid closure of under-resolved 3D turbulent flow simulations such as large eddy simulation (LES). An early version of ODT called the Linear-Eddy Model (LEM), which predicts mixing under prescribed flow conditions but does not predict the flow *per se*, has been used as a mixing-reaction closure for LES [A], demonstrating the advantages of a spatially and temporally resolved subgrid treatment.

ODT offers the possibility of a promising path to economical 3D turbulent flow simulation that is fundamentally different from LES and other existing approaches. Namely, arrays of ODT domains can be coupled in a way that simulates 3D turbulent flow at all scales without the need for distinct coarse-grained advancement operations, an approach termed Autonomous Microstructure Evolution (AME) [5].

Development, demonstration, and scientific application of this new approach are major goals of planned future activities of the present project. By avoiding the coupling of resolved small scale advancement to coarse-grained advancement, and the consequent information loss, AME offers the prospect of achieving needed predictive capabilities that are presently attainable only by using direct numerical simulation (DNS), which is affordably only for the most idealized flow configurations. AME will have the same spatial and temporal resolution but orders of magnitude fewer control volumes than DNS due to reduced dimensionality at small scales. (Scales larger than the separation of domains in the ODT array are effectively 3D-resolved.) AME will affordably simulate technologically relevant processes with substantially higher fidelity than LES at much lower computational cost than DNS.

RECENT PROGRESS

The 1D map that advects fluid during LEM and ODT simulations has two distinct mathematical representations. On a fixed uniform mesh, it is a permutation of fluid cells, a representation that manifestly obeys the 1D analogs of the applicable conservation laws of fluid motion. On an adaptive mesh whose cell boundaries are advected by the flow, the 1D map compresses fluid parcels but also generates multiple copies of them such that the conservation laws are again obeyed, albeit less transparently.

The uniform mesh is simpler to implement computationally, but the adaptive mesh enables more efficient simulation with better numerical properties in some situations. Therefore an adaptive-mesh implementation of ODT has been developed to replace the existing uniform-mesh algorithm in applications for which the adaptive mesh is preferable. Agreement of the two methods has recently been demonstrated for turbulent channel flow. The adaptive mesh will enable several extensions and new applications of ODT, as explained in Planned Work.

As noted in Project Scope, LEM has been used as a mixing-reaction closure for LES. In addition, ODT has been used as a near-wall momentum closure for LES of wall-bounded flow [B]. A demonstration of ODTLES, which is a 3D ODT-based flow simulation with some AME-like features (but with coarse-grained pressure projection to enforce continuity) was recently completed [7]. ODTLES is fundamentally the same physical flow representation that is envisioned for the planned AME formulation, so the demonstrated capability of ODTLES to reproduce the measured energy-spectrum evolution of homogeneous decaying turbulence serves as a proof of principle that the AME strategy is viable.

The LEM closure that has been used in LES involves an LEM domain (line segment) of indeterminate orientation with each LES control volume. An alternate geometry for LEM subgrid implementation has been formulated that consists of an array of parallel LEM domains traversing the entire flow in each of the three coordinate directions. Three orthogonal LEM domains intersect each LES control volume. Where they intersect, they are coupled in a way that advects fluid parcels in conformance with LES-resolved fluid motions.

This new formulation has a complete enough representation of unsteady turbulent mixing so that it is potentially suitable as a mixing-reaction closure for steady-state Reynolds averaged Navier Stokes (RANS) simulation of turbulent combustion. To test this, a measured turbulent jet mean flow field is being used as a surrogate RANS solution to drive the LEM mixing. Preliminary comparisons to measurements [C] of mixing of scalars issuing from ring-shaped sources in the interior of a turbulent jet indicate good model performance. This challenging configuration has not previously been modeled successfully.

A 2D DNS of hydrogen-air combustion under homogeneous-charge compression-ignition (HCCI) conditions that was performed at the Combustion Research Facility identified distinct auto-ignition and deflagration-wave burning modes that arise depending on initial temperature fluctuations [D]. Using a parametric representation of the DNS turbulence and an initial temperature field analogous to a line of sight through the DNS initial field, an LEM simulation of the DNS cases was performed [8] that reproduced the key features revealed by the DNS. This result suggests that LEM will be a useful tool for future HCCI study, as described in Future Work. Another recent LEM study showed that an economical turbulent premixed combustion simulation using the LEM representation of turbulent advection and a chemistry tabulation provides predictivity of the turbulent burning velocity that previously could be attained only by using much more costly multidimensional simulation methods [9].

Motivated by a mathematical demonstration that the 1D map used in LEM and ODT reproduces a mechanism that induces clustering of inertial particles in turbulent flow [1], a 3D map-based computational model that simulates inertial particle motion in turbulence has been developed. Preliminary comparisons to DNS results indicate that this formulation captures the parameter dependences of collision rates of small particles that are subject to inertial drag and gravity in much greater detail than the comparably efficient Gillespie algorithm [E], a commonly used stochastic method with no representation of particle spatial distributions. The new method will be superior to the Gillespie algorithm for simulating cloud droplet coalescence leading to rain formation, among other applications.

An LEM simulation has been developed to study scenarios for deflagration-to-detonation transition (DDT) in supernova progenitors. The model has been benchmarked to DNS and is now being used for parameter studies.

FUTURE WORK

The key step in converting ODTLES into a true AME formulation will be the replacement of the pressure-projection method of continuity enforcement by a pseudo-compressible (relaxation-type) method that will not rely on advancement of coarse-grained fields. An important step for achieving needed efficiency and numerical properties (and also for eventual extension from low-Mach-number to fully compressible simulations) will be the replacement of uniform-mesh ODT by adaptive-mesh ODT in ODTLES and subsequently in AME. The initial proof-of-principle application of AME will be turbulent channel flow.

One advantage of the adaptive mesh is that it facilitates the formulation of ODT in curvilinear coordinates. This will broaden the future scope of AME application, and also the scope of application of simulations on a single ODT domain. In particular, development of a cylindrical formulation will be completed for application to turbulent round jets. This will enable simulation of turbulent jet diffusion flames that have been studied experimentally at the Combustion Research Facility. In conjunction with a planned extension of ODT to represent the flow of multiple immiscible fluid phases, it will enable simulation of the breakup of turbulent liquid jets, a key process in fuel-injected engines.

In other planned efforts, the LEM studies described in Recent Progress will be continued. The new LEM subgrid construction for RANS will be generalized to incorporate thermal expansion, implying a back-coupling to the RANS that requires iteration between RANS and LEM computations in order to converge to a consistent solution. This LEM methodology, which is currently implemented on a uniform mesh, will then be re-implemented on an adaptive mesh for

use as the scalar advancement process in the planned AME formulation for turbulent combustion simulation. In that context, ODT rather than LEM will govern the occurrence of the 1D maps, reflecting the self-contained, predictive nature of the flow simulation in the AME framework.

The recent LEM study of hydrogen-air combustion under HCCI conditions will be extended by incorporating n-heptane and iso-octane chemistry and comparing results to planned DNS using n-heptane as well as to measurements. The LEM turbulent premixed combustion study will be extended by developing and testing a correction method for improving the tabulated chemistry. This will involve modifying chemical source terms by evaluating temperature based on the temperature field computed on the fly during the LEM simulation rather than using temperature values corresponding to the steady-state flame conditions used to construct the tables. This will introduce a coupling between the chemical evolution and the unsteady mixing captured by LEM. The LEM parameter studies of DDT leading to supernova explosion will continue with the goal of assessing whether this path to explosion is plausible and consistent with measured explosion behaviors.

REFERENCES

- A. V. K. Chakravarthy and S. Menon, *Flow Turb. Combust.* **65**, 133 (2000).
- B. R. C. Schmidt, A. R. Kerstein, *et al.*, *J. Comput. Phys.* **186**, 317 (2003).
- C. C. Tong and Z. Warhaft, *J. Fluid Mech.* **292**, 1 (1995).
- D. J. H. Chen, E. R. Hawkes, *et al.*, *Combust. Flame* **145**, 128 (2006).
- E. D. T. Gillespie, *J. Atmos. Sci.* **32**, 1977 (1975).

PUBLICATIONS SINCE 2006

1. A. R. Kerstein and S. K. Krueger, "Clustering of Randomly Advected Low-Inertia Particles: A Solvable Model," *Phys. Rev. E* **73**, 025302 (2006).
2. J. Cuxart, A. A. M. Holtslag, A. R. Kerstein, S. Wunsch, *et al.*, "Single-Column Model Intercomparison for a Stably Stratified Atmospheric Boundary Layer," *Bound. Layer Meteorol.* **118**, 273 (2006).
3. A. R. Kerstein and S. Wunsch, "Simulation of a Stably Stratified Atmospheric Boundary Layer Using One-Dimensional Turbulence," *Bound. Layer Meteorol.* **118**, 325 (2006).
4. J. R. Mayo and A. R. Kerstein, "Scaling of Huygens-Front Speedup in Weakly Random Media," *Phys. Lett. A* **372**, 5 (2007).
5. A. R. Kerstein, "ODT: Stochastic Simulation of Multi-Scale Dynamics," in *Interdisciplinary Aspects of Turbulence*, Springer Lecture Notes in Physics, eds. W. Hillebrandt and F. Kupka (Springer-Verlag, New York, 2008).
6. J. R. Mayo and A. R. Kerstein, "Fronts in Randomly Advected and Heterogeneous Media and Nonuniversality of Burgers Turbulence: Theory and Numerics," *Phys. Rev. E* (submitted).
7. R. C. Schmidt, A. R. Kerstein, and R. J. McDermott, "ODTLES: A Multi-Scale Model for 3D Turbulent Flow Based on One-dimensional Turbulence Modeling," *Comput. Methods Appl. Mech. Eng.* (submitted).
8. M. Oevermann, H. Schmidt, A. R. Kerstein, "Linear-Eddy Modeling of Autoignition under Thermal Stratification," *Combust. Flame* (submitted).
9. H. Schmidt, M. Oevermann, R. J. M. Bastiaans, and A. R. Kerstein, "A priori Tabulation of Turbulent Flame Speeds via a Combination of a Stochastic Mixing Model and Flamelet Generated Manifolds," *Flow Turb. Combust.* (submitted).

KINETICS OF COMBUSTION-RELATED PROCESSES AT HIGH TEMPERATURES

J. H. Kiefer

Department of Chemical Engineering

University of Illinois at Chicago
Chicago, IL 60607
(kiefer@uic.edu)

Program Scope

As always, this program again involves the use of the shock tube with laser-schlieren (LS) and time-of-flight mass spectrometry (TOF) diagnostics for the exploration of reaction rates and energy relaxation processes over a range of temperatures and pressures of particular interest in combustion. We are particularly interested in energy transfer and falloff in unimolecular reactions. The work includes a significant amount of collaboration with R. S. Tranter, L.B. Harding and S J. Klippenstein at Argonne Nat'l Lab.

Decomposition of fluoroethane

This project is essentially complete, and is undergoing final polishing by R. S. Tranter. The project involves a joint laser-schlieren/time-of-flight mass spec. (LS/TOF) study of the dissociation, here a simple HF elimination to ethylene which would normally be straightforward. However, the situation is rendered difficult because the small heat of this reaction (most recently 13.9 kcal/mol [1]) produces extremely small density gradients. See the abstract of R. S. Tranter for details

Vibrational relaxation of HCN

This project is complete and a paper has been submitted to J. Chem. Phys. The abstract of this paper is as follows.

Thermal vibrational relaxation in HCN mixtures with Kr has been observed with the laser-schlieren technique. These experiments cover the temperatures 750-2900 K and a large pressure range of 13-420 Torr in 5 and 20% HCN/Kr. Relaxation is fast but appears to occur in two well-separated stages that are assigned to the processes (000) → (010) and (000) → (100) with perhaps some contribution from (000) → (001). This interpretation is strongly supported by a comparison of integrated density changes. The first and faster process shows near constant relaxation times whereas the latter, slower stage has a slight decrease with T. Relaxation times in pure HCN obtained by extrapolation are:

$$P\tau_{\text{HCN-HCN}} = 53.49 \exp(-1.97/T^{1/3}) \text{ (000) } \rightarrow \text{ (010)}$$

$$P\tau_{\text{HCN-HCN}} = 14.71 \exp(32.6/T^{1/3}) \text{ (000) } \rightarrow \text{ (100)}$$

Probabilities suggested by these results are 0.055 for the fast and 0.0035 to 0.005 for the slow step. These are close to those found by laser fluorescence measurements for deactivation of levels involving excitation of the C-H stretch at 3312 cm⁻¹. These results are also consistent with the notion of dominance of VV transfer in a weakly bound

complex. It is also suggested that the slow step occurs through $(03^10) \rightarrow (100)$, $\Delta E = 27.7 \text{ cm}^{-1}$. These are the first fully thermal measurements of relaxation in HCN, and the first to see energy transfer to the low-frequency modes.

Dissociation of Acetone

This work is complete and has been submitted to the 32nd Combustion Symposium. The abstract of this submission is:

The dissociation of acetone: $\text{CH}_3\text{C}=\text{OCH}_3 \rightarrow \text{CH}_3\text{C}=\text{O} + \text{CH}_3$, quickly followed by $\text{CH}_3\text{CO} \rightarrow \text{CH}_3 + \text{CO}$, has been examined with laser-schlieren measurements in incident shock waves over 32-717 Torr and 1429-1936 K using 5% acetone dilute in krypton. A few very low pressure experiments (~ 10 Torr) were used in a marginal effort to resolve the extremely fast relaxation of this molecule. A primary motivation was the use of this decomposition for the production of methyl radicals to test the application of a recent high-temperature mechanism for ethane decomposition [2] on the reverse methyl combination. Rates obtained for the dissociation show strong falloff well fit by variable reaction coordinate transition state theory when combined with a master equation. The calculated barrier is 82.8 kcal/mol, the fitted $\langle \Delta E \rangle_{\text{down}} = 400(T/298) \text{ cm}^{-1}$, similar to what was found in a recent study of C-C fission in acetaldehyde [3], and the calculated $k_{\infty} = 10^{25.86} T^{-2.72} \exp(-87.7(\text{kcal/mol})/RT)$. This high-pressure rate is also in full agreement with the literature on the reverse rate of $\text{CH}_3 + \text{CH}_3\text{CO}$. Large negative (exothermic) gradients appearing after initial endothermic dissociation in high T,P experiments, mainly arising from methyl combination, are accurately fit in both time of onset and magnitude by the earlier ethane dissociation mechanism, confirming its accuracy in the reverse direction. The measured dissociation rates are in close accord with one earlier shock-tube study [4] but show much less severe falloff than the high-pressure experiments of Ernst et al.[5].

Dissociation of s-triazine

The three-body dissociation of 1,3,5-triazine ($s\text{-C}_3\text{H}_3\text{N}_3 \rightarrow 3\text{HCN}$) has been observed in incident shock waves with the laser-schlieren technique. The experiments use 5% triazine/Kr and cover 1630-2350K, and 100-600 torr. This dissociation is without secondary reaction save for a possible contribution from the isomerization $\text{HCN} \rightarrow \text{HNC}$. A rough estimate for the rate of this process does result in a slightly better fit to the experiments, but this conclusion is very uncertain. The dissociation shows rates with strong falloff from k_{∞} and a small but consistent pressure dependence. Electronic structure calculations of the transition-state properties (G3B3, HL1, $E_o = 84.6 \text{ kcal/mol}$) are used to construct an RRKM model fit that suggests a $\langle \Delta E \rangle_{\text{down}}$ of 1200 cm^{-1} . However, a slightly better fit is achieved using the barrier of 81 kcal/mol proposed by Dyakov, et al. [6]. For this barrier $k_{\infty} (\text{s}^{-1}) = 5.3 \times 10^{16} \exp(-86.6(\text{kcal/mol})/RT)$, and the fit now is able to use the more routine $\langle \Delta E \rangle_{\text{down}} = 126(T/298)^{0.9}$. Vibrational relaxation of the triazine was also examined in 5 and 20% mixtures with Kr and over 770-1500K for pressures between 6 and 14 torr. Relaxation is very fast, with $P\tau$ rising from 100 to 200 nsec-atm over the full temperature range. Integrated gradients are in good accord with calculated total changes in density indicating an accurately single exponential relaxation. A separate investigation of relaxation in the related molecule pyrazine (500-1300 K, in 1

and 5% in Kr, between 13 and 66 torr) is included. Again relaxation is rapid, but here the temperature dependence seems normal, the relaxation times decreasing with temperature.

Decomposition of cyclohexane and 1-hexene

This is our primary current effort. The project attacks an essential part of the mechanism of decomposition of cyclohexane, an important surrogate for naphthene-containing fuels. The purpose here is to fully explore these reactions over the high temperatures used in combustion. We have now completed some 100 LS experiments on cyclohexane covering 1550-2100 K, for 2, 4 and 10 % in Kr for 50, 150, and 200 Torr. Also 27 experiments on 1-hexene, over 1218-1714 K, 50 and 200 Torr, in 2 and 3% 1-1-C₆H₁₂ in Kr have been analyzed. Reactions making a significant contribution are:



(where C₃H₅ is allyl radical) together with the chain reactions initiated by the radical dissociations. A chemically activated ‘direct’ path $c\text{-C}_6\text{H}_{12} \rightarrow \ell\text{-C}_3\text{H}_7 + \text{C}_3\text{H}_5$ (91 kcal/mol) may also occur at high temperatures and/or low pressures through an intermediate but unstabilized 1-hexene, but this route does not appear to be significant. Modeling of the 1-hexene experiments was successful using a chain mechanism based on literature rates. Subsequent modeling of the cyclohexane decomposition (see below) including this mechanism without modification also works well. Our model also works extremely well on the ARAS experiments of Braun-Unkhoff, et al.[7].

Future projects.

There are but two new studies anticipated: The dissociation of biacetyl and a summary review of shock-tube studies of relaxation in large molecules. Biacetyl (CH₃C=OC=OCH₃) dissociates readily to 2CH₃ + 2CO. As such it should be an excellent precursor for the pyrolytic generation of methyl radical which can then be used for an improved and wide-ranging examination of the methyl recombination, extending and improving on our efforts using acetaldehyde and acetone.

References

- 1) B. L. Kormos, J. F. Liebman, C. J. Cramer, *J. Phys. Org. Chem.* 17 (2004) 656.
- 2) J. H. Kiefer, S. Santhanam, N. K. Srinivasan, R. S. Tranter, S. J. Klippenstein, M. A. Oehlschlager, *Proc. Combust. Inst.*, 30 (2005) 1129.
- 3) K. S. Gupte, J. H. Kiefer, R. S. Tranter, S. J. Klippenstein, L. B. Harding, *Proc. Comb. Inst.* 31 (2007) 167.
- 4) K. Sato, Y. Hidaka, *Combust. Flame*, 122 (2000) 291-311.
- 5) J. Ernst, K. Spindler, H. Gg. Wagner, *Ber. Bunsenges. Phys. Chem.*, 80 (1976) 645.
- 6) Y. A. Dyakov, A. M. Mebel, S. H. Lin, Y. T. Lee, C.-K. Ni, *J. Phys. Chem. A* 111 (2007) 9591.
- 7) M. Braun-Unkhoff, C. Nauman, P. Frank, *Abstr. Pap. Am. Chem. Soc.* (2204), 227 U1096.

Publications

- 1) “Decomposition of Acetaldehyde: Experiment and Theory”, K. S. Gupte, J. H. Kiefer, R.S. Tranter, S. J. Klippenstein, and L.B. Harding, *Proc. Combust. Inst.* 31, 167 (2007)

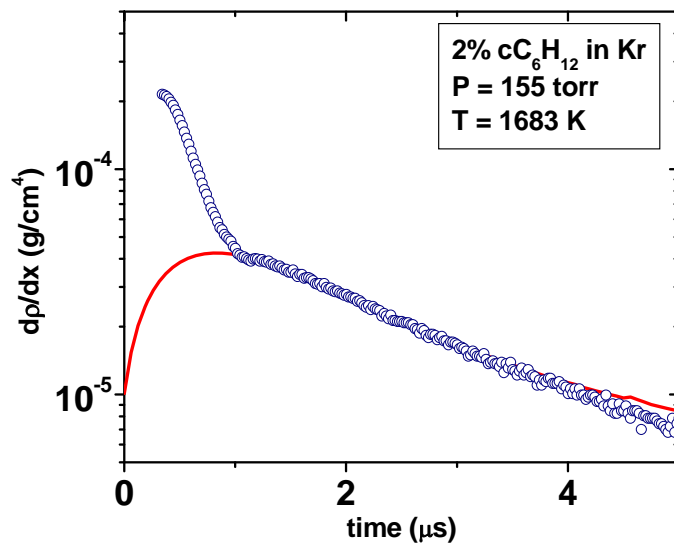
2) “Relaxation, Incubation, and Dissociation in CO₂”, S. Saxena, J. H. Kiefer, and R. S. Tranter, *J. Phys. Chem. A*, **111**,3884-3890 (2007).

3) “Shock tube Study of Dissociation and Relaxation in 1,1-difluoroethane and Vinyl fluoride”, Hui Xu, John H. Kiefer, Raghu Sivaramakrishnan, Binod R. Giri and Robert S. Tranter, *Phys. Chem. Chem. Phys.* **9**, 4164-4176 (2007).

4) “A Shock tube and Theory Study of the Dissociation of Acetone and Subsequent Recombination of Methyl Radicals”, S. C. Saxena, J. H. Kiefer and S. J. Klippenstein, Submitted for the 32nd Combustion Symposium.

5) “Shock tube Study of Relaxation in HCN” N. K. Srinivasan, K. S. Gupte and J. H. Kiefer” *J. Chem. Phys.*, submitted.

Figure: This shows an LS experiment for the cited conditions together with a modeling using reactions (1) and (2) above. The fit for such experiments is of such uniformly excellent quality and this seems impossible with any other mechanism.



THEORETICAL CHEMICAL KINETICS

Stephen J. Klippenstein
Chemical Sciences and Engineering Division
Argonne National Laboratory
Argonne, IL, 60439
sjk@anl.gov

Program Scope

The focus of this program is the theoretical estimation of the kinetics of elementary reactions of importance in combustion chemistry. The research involves a combination of *ab initio* quantum chemistry, variational transition state theory, direct dynamics, and master equation simulations. The emphasis of our current applications is on (i) reactions of importance in soot formation, (ii) radical oxidation reactions, and (iii) NO_x chemistry. We are also interested in a detailed understanding of the limits of validity of and, where feasible, improvements in the accuracy of specific implementations of transition state theory. Detailed comparisons with experiment and with other theoretical methods are used to explore and improve the predictive properties of the transition state theory models. Direct dynamics simulations are performed as a means for testing the statistical assumptions, for exploring reaction mechanisms, and for generating theoretical estimates where statistical predictions are clearly inadequate. Master equation simulations are used to study the pressure dependence of the kinetics and to obtain phenomenological rate coefficients for use in kinetic modeling.

Recent Progress

NO_x Chemistry

We have completed a detailed analysis of the CH + N₂ reaction in collaboration with Larry Harding and Jim Miller. This analysis was based on a coupling of high level multi-reference electronic structure evaluations with sophisticated transition state theory analyses. This reaction has long been thought to provide an explanation for the observation of prompt NO. Recent theoretical work by Lin and coworkers, suggesting that this reaction proceeds via the formation of NCN + H rather than via HCN + N, resolved some discrepancies in the expected and calculated rate coefficients. However, very recent experimental and modeling studies suggest that the rate coefficients predicted by Lin and coworkers are still about an order of magnitude lower than required. Our reanalysis of the reaction yields predicted rate coefficients that are an order of magnitude larger than Lin's, putting them in quantitative agreement with the experiments of Hanson and coworkers and qualitative agreement with the modeling study of Pauwels and coworkers.

Ab initio transition state theory based master equation simulations were also used to predict the H + NCO reaction rate and product branching (with Larry Harding). The kinetics of this reaction, which is of central importance to NO_x formation and removal in rich flames, is rather poorly understood due to the difficulties of producing and monitoring two separate radical species. The implementation of a simple model for the intersystem crossing involved in the formation of ³NH

+ CO yields a consistent description of this reaction as well as the branching observed in HNCO photodissociation studies.

Hydrocarbon Oxidation

The reaction of CH₃ with HO₂ has been identified as a key reaction in a number of modeling studies of Dryer and coworkers. We have recently completed a theoretical analysis of this reaction implementing direct variable reaction coordinate transition state theory for the entrance and CH₃O + OH exit channel (with Ahren Jasper and Larry Harding). The resulting predictions, which differ substantially from the prior theoretical study of Lin and coworkers, are in good agreement with the expectations from the modeling studies of Dryer and coworkers and Curran and coworkers.

We have also performed master equation based simulations of the dissociation kinetics for acetone. With an appropriate energy transfer model the predicted rate coefficients are in good agreement with the results of laser schlieren shock tube experiments of Kiefer. In contrast, the modeling of earlier experiments of Wagner and coworkers requires inordinately small energy transfer rates.

In collaboration with Ian Smith and Ian Sims we have studied the low temperature kinetics of a series of O(³P) + alkene reactions. The CRESU measurements provided an interesting illustration of the variation of the temperature dependence of the rate coefficients with the height of the submerged saddle point for the addition reaction. An *a priori* implementation of a two transition state model yielded remarkably good agreement with the experimental observations. A review describing our theoretical methods for treating low temperature kinetics was also written.

Species Identification in Flames (in collaboration with ALS Flame Team)

Our efforts at identifying key combustion intermediates focused on a variety of polyynes in fuel-rich allene, propyne, and cyclopentene flames. The C_{2n}H₂ (n=1-5) polyynes were clearly identified, while CHCCCCCHCCH₂, CHCCCCCCHCH₂, and CHCCCCCHCHCCH appeared to contribute to the C₇H₄ and C₈H₄ signals. Possible formation pathways were also discussed.

Future Directions

We will continue our studies of hydrocarbon oxidation, aromatic ring formation, and NO_x chemistry. Our oxidation studies will consider the decompositions of ethanol and 1-butanol, as model alcohols. We are also considering the kinetics of O₂ reacting with C₃H₆OOH species. This reaction serves as a prototype for the second oxygen addition, which is a key step in low temperature combustion. We will consider the reaction of CH₂ with various alkenes, which may be of importance to hydrocarbon growth processes. We are studying the branching between different bond fission channels in the decomposition of n-heptane, since this branching affects the ignition properties in this simple fuel surrogate. Finally, we are interested in studying the kinetics of roaming fragment mechanisms with transition state theory. The branching between the roaming fragment and radical-radical channels may have an impact on the combustion properties of essentially all fuels.

DOE Supported Publications, 2006-Present

1. **Predictive Theory for the Association Kinetics of Two Alkyl Radicals**, Stephen J. Klippenstein, Yuri Georgievskii, and Larry B. Harding, *Phys. Chem. Chem. Phys.*, invited article, **8**, 1133-1147 (2006).
2. **Identification and Chemistry of C₄H₃ and C₄H₅ Isomers in Fuel Rich Flames**, Nils Hansen, Stephen J. Klippenstein, Craig A. Taatjes, James A. Miller, Juan Wang, Terrill A. Cool, Bin Yang, Rui Yang, Lixia Wei, Chaoqun Huang, Jing Wang, Fei Qi, Matthew E. Law, and Phillip R. Westmoreland, *J. Phys. Chem. A*, **110**, 3670-3678, (2006).
3. **Identification of C₅H_x Isomers in Fuel-Rich Flames by Photoionization Mass Spectrometry and Electronic Structure Calculations**, Nils Hansen, Stephen J. Klippenstein, James A. Miller, Juan Wang, Terrill A. Cool, Matthew E. Law, Phillip R. Westmoreland, Tina Kasper, and Katharina Kohse-Hoinghaus., *J. Phys. Chem. A*, **110**, 4376-4388 (2006).
4. **Pathways and Rate Coefficients for the Decomposition of Vinyloxy and Acetyl Radicals**, Juan P. Senosiain, Stephen J. Klippenstein, and James A. Miller, *J. Phys. Chem. A*, **110**, 5772-5781 (2006).
5. **Reaction of Ethylene with Hydroxyl Radicals: A Theoretical Study**, Juan P. Senosiain, Stephen J. Klippenstein, and James A. Miller, *J. Phys. Chem. A*, **110**, 6960-6970 (2006).
6. **Master Equation Methods in Gas Phase Chemical Kinetics**, James A. Miller and Stephen J. Klippenstein, *J. Phys. Chem. A*, feature article, **110**, 10528-10544 (2006).
7. **Energy-Resolved Photoionization of Alkyl Peroxy Radicals and the Stability of their Cations**, Giovanni Meloni, Peng Zou, Stephen J. Klippenstein, Musahid Ahmed, Stephen R. Leone, Craig A. Taatjes, and David L. Osborn, *J. Am. Chem. Soc.*, **128**, 13559-13567 (2006).
8. **Bimolecular Reactions**, Antonio Fernandez Ramos, James A. Miller, Stephen J. Klippenstein, and Donald G. Truhlar, *Chem. Rev.*, **106**, 4518-4584 (2006).
9. **Decomposition of Acetaldehyde: Experiment and Detailed Theory**, K. S. Gupte, J. H. Kiefer, R. S. Tranter, S. J. Klippenstein, and L. B. Harding, *Proc. Comb. Inst.*, **31**, 167-174 (2007).
10. **Oxidation Pathways in the Reaction of Diacetylene with OH Radicals**, Juan P. Senosiain, Stephen J. Klippenstein, and James A. Miller, *Proc. Comb. Inst.*, **31**, 185-192 (2007).
11. **On the Formation and Decomposition of C₇H₈**, Stephen J. Klippenstein, Lawrence B. Harding, and Yuri Georgievskii, *Proc. Comb. Inst.*, **31**, 221-229 (2007).
12. **Experimental and Theoretical Rate Constants for CH₄ + O₂ → CH₃ + HO₂**, N. K. Srinivasan, J. V. Michael, L. B. Harding, and S. J. Klippenstein, *Comb. Flame*, **149**, 104-111 (2007).
13. **Direct Measurement and Theoretical Calculation of the Rate Coefficient for Cl + CH₃ from T = 202 – 298 K**, James K. Parker, Walter A. Payne, Regina J. Cody, Fred L. Nesbitt, Louis J. Stief, Stephen J. Klippenstein, and Lawrence B. Harding, *J. Phys. Chem. A*, **111**, 1015-1023 (2007).
14. **On the Combination Reactions of Hydrogen Atoms with Resonance Stabilized Hydrocarbon Radicals**, Lawrence B. Harding, Stephen J. Klippenstein, and Yuri Georgievskii, *J. Phys. Chem. A*, **111**, 3789-3801 (2007). [Miller Festschrift issue]
15. **Strange Kinetics of the CN + C₂H₆ Reaction Explained**, Yuri Georgievskii and Stephen J. Klippenstein, *J. Phys. Chem. A*, **111**, 3802-3811 (2007). [Miller Festschrift issue]
16. **Kinetics of the Reaction of Methyl Radical with Hydroxyl Radical and Methanol Decomposition**, Ahren W. Jasper, Stephen J. Klippenstein, Lawrence B. Harding, and Branko Ruscic, *J. Phys. Chem. A*, **111**, 3932-3950 (2007). [Miller Festschrift issue]
17. **Measurements and Modeling of DO₂ Formation in the Reactions of C₂D₅ and C₃D₇ Radicals with O₂**, Edgar G. Estupinan, Jared D. Smith, Atsumu Tezaki, Stephen J. Klippenstein, and Craig A. Taatjes, *J. Phys. Chem. A*, **111**, 4015-4030 (2007). [Miller Festschrift issue]
18. **Reaction Kinetics of CO + HO₂ → Products: Ab Initio Transition State Theory Study with Master Equation Modeling**, Xiaoqing You, Hai Wang, Elke Goos, C.-J. Sung, Stephen J. Klippenstein, *J. Phys. Chem. A*, **111**, 4031-4042 (2007). [Miller Festschrift issue]
19. **Initial Steps of Aromatic Formation in a Laminar Premixed Fuel-Rich Cyclopentene Flame**, N. Hansen, T. Kasper, S. J. Klippenstein, P. R. Westmoreland, M. E. Law, C. A. Taatjes, K. Kohse-

- Hoinghaus, J. Wang, and T. A. Cool, *J. Phys. Chem. A*, **111**, 4081-4092 (2007). [Miller Festschrift issue]
20. **A Two Transition State Model for Radical-Molecule Reactions: Applications to Isomeric Branching in the OH-Isoprene Reaction**, Erin E. Greenwald, Simon W. North, Yuri Georgievskii, and Stephen J. Klippenstein, *J. Phys. Chem. A*, **111**, 5582-5592 (2007).
 21. **Reflected Shock Tube and Theoretical Studies of High-Temperature Rate Constants for OH + CF₃H ⇌ CF₃ + H₂O and CF₃ + OH → Products**, N. K. Srinivasan, M.-C. Su, J. V. Michael, S. J. Klippenstein, and L. B. Harding, *J. Phys. Chem. A*, **111**, 6822-6831 (2007). [Lin Festschrift issue]
 22. **Ab Initio Methods for Reactive Potential Energy Surfaces**, Lawrence B. Harding, Stephen J. Klippenstein, and Ahren W. Jasper, *Phys. Chem. Chem. Phys.*, **9**, 4055-4070 (2007). [Invited; Theory/Experiment Synergy Special Issue]
 23. **Association Rate Constants for Reactions between Resonance Stabilized Radicals: C₃H₃ + C₃H₃, C₃H₃ + C₃H₅, and C₃H₅ + C₃H₅**, Yuri Georgievskii, Stephen J. Klippenstein, and James A. Miller, *Phys. Chem. Chem. Phys.*, **9**, 4259-4268 (2007). [Theory/Experiment Synergy Special Issue]
 24. **Theory, Measurements, and Modeling of OH and HO₂ Formation in the Reaction of Cyclohexyl Radicals with O₂**, Adam M. Knepp, Giovanni Meloni, Leonard E. Jusinski, Craig A. Taatjes, Carlo Cavallotti, and Stephen J. Klippenstein, *Phys. Chem. Chem. Phys.*, **9**, 4315-4331 (2007). [Theory/Experiment Synergy Special Issue; hot article]
 25. **Understanding Reactivity at Very Low Temperatures: The Reactions of Oxygen Atoms with Alkenes**, Hassan Sabbah, Ludovic Biennier, Ian R. Sims, Yuri Georgievskii, Stephen J. Klippenstein, and Ian W. M. Smith, *Science*, **317**, 102-105 (2007).
 26. **Secondary Kinetics of Methanol Decomposition: Theoretical Rate Coefficients for ³CH₂ + OH, ³CH₂ + ³CH₂, and ³CH₂ + CH₃**, Ahren W. Jasper, Stephen J. Klippenstein, and Lawrence B. Harding, *J. Phys. Chem. A*, **111**, 8699-8707 (2007).
 27. **Performance of the Spin-Flip and Multi-Reference Methods for Bond-Breaking in Hydrocarbons: A Benchmark Study**, Anna A. Golubeva, Alexandr V. Nemukhin, Stephen J. Klippenstein, Lawrence B. Harding, and Anna I. Krylov, *J. Phys. Chem. A*, **111**, 13264-13271 (2007).
 28. **Thermal Decomposition of CF₃ and the Reaction of CF₂ + OH → CF₂O + H**, N. K. Srinivasan, M.-C. Su, J. V. Michael, A. W. Jasper, S. J. Klippenstein, and L. B. Harding, *J. Phys. Chem. A*, **112**, 31-37 (2008).
 29. **A Combined Ab Initio and Photoionization Mass Spectrometric Study of Polyynes in Fuel-Rich Flames**, N. Hansen, S. J. Klippenstein, P. R. Westmoreland, T. Kasper, K. Kohse-Hoinghaus, J. Wang, and T. A. Cool, *Phys. Chem. Chem. Phys.*, **10**, 366-374 (2008).
 30. **Kinetics of CH + N₂ Revisited with Multireference Methods**, Lawrence B. Harding, Stephen J. Klippenstein, and James A. Miller, *J. Phys. Chem. A*, **112**, 522-532 (2008).
 31. **Theory of Low Temperature Gas-Phase Reactions**, Stephen J. Klippenstein and Yuri Georgievskii, in "Low Temperatures and Cold Molecules", edited by I. W. M. Smith, World Scientific, *in press* (2008).
 32. **Theoretical Rate Coefficients for the Reaction of Methyl Radical with Hydroperoxyl Radical and for Methylhydroperoxide Decomposition**, Ahren W. Jasper, Stephen J. Klippenstein, and Lawrence B. Harding, *Proc. Comb. Inst.* **32**, *submitted* (2008).
 33. **Kinetics of the H + NCO Reaction**, Stephen J. Klippenstein and Lawrence B. Harding, *Proc. Comb. Inst.* **32**, *submitted* (2008).
 34. **A Shock Tube and Theory Study of the Dissociation of Acetone and Subsequent Recombination of Methyl Radicals**, Saumitra Saxena, John H. Kiefer, and Stephen J. Klippenstein, *Proc. Comb. Inst.* **32**, *submitted* (2008).

Theoretical modeling of spin-forbidden channels in combustion reactions

Anna I. Krylov

Department of Chemistry, University of Southern California,
Los Angeles, CA 90089-0482

krylov@usc.edu

1 Scope of the project

The goal of our research is to develop predictive theoretical methods, which can provide crucial quantitative data (e.g., rate constants, branching ratios, heats of formation), identify new channels and refine reaction mechanisms. Specifically, we are developing tools for computational studies of spin-forbidden and non-adiabatic pathways of reactions relevant to combustion, and applying these tools to study electronic structure and reactions of open-shell and electronically excited species involved in these processes.

2 Summary of recent major accomplishments

During the past year, we conducted several computational studies of open-shell and electronically excited species. The common theme in these studies is interactions between states of different character and intersections between the corresponding potential energy surfaces (PESs). Continuing our research on electronic structure of open-shell and electronically excited species[1, 2, 3, 4, 5], we characterized vibrational spectra of the Rydberg and valence states of diazomethane[6]. We have been also developing methodology for modeling spin-forbidden and non-adiabatic reaction pathways, e.g., we implemented an algorithm for characterizing intersections between PESs of the same and different multiplicity within the equation-of-motion family of methods[7]. We also conducted extensive benchmarking of different energy additivity schemes within the spin-flip family of methods for bond-breaking[8]. The DOE support is also acknowledged in our recent review on equation-of-motion coupled-cluster (EOM-CC) methodology[9]. Some of the recent results are highlighted below.

2.1 Minimum energy crossing points between PES's for the EOM family of methods: Implementation and initial applications

Although a full description of a non-adiabatic or spin-forbidden process requires a calculation of nuclear dynamics that brings the system from the Franck-Condon region towards the point where the two states are nearly degenerate and the probability of the transition

is larger, one can gain considerable mechanistic insight and even quantitative information about the likelihood of the transitions from the geometry and energy of the minimum energy point on the intersection seam (minimum energy crossing point, MECP). The MECP can be thought of as a characteristic point of the process, just like the transition state in a thermal chemical reaction. The energy of the MECP can help assess the likelihood of the process, and with the use of the non-adiabatic transition state theory, the rate of the non-adiabatic (or spin-forbidden) process can be estimated. The geometry of the MECP suggests which modes are most efficient in facilitating the transition.

We implemented[7] the projected gradient method of finding MECP within the EOM-CC family of methods in the *Q-CHEM* quantum chemistry package. The method was applied to characterize intersections between electronic states in N_3^+ , NO_2 , and *para*-benzyne using the excitation energies (EE), ionization potential (IP), and SF variants of EOM-CC. This first implementation of an MECP algorithm within the EOM-CC family opens up several exciting possibilities, and we are currently investigating singlet-triplet crossings in prototypical diradicals.

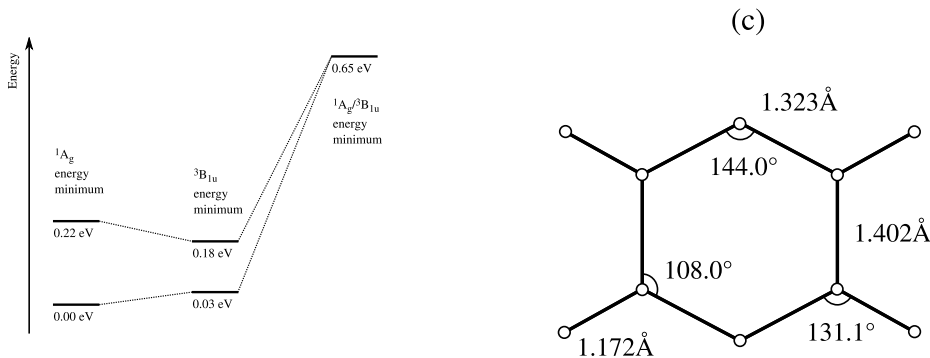


Figure 1: Relative energies of the 1A_g and $^3B_{1u}$ states of *para*-benzyne diradical at their equilibrium structures and the geometry of the MECP (right panel). At the singlet and triplet equilibrium geometry, the singlet lies below the triplet. The two states intersect 0.65 eV above the ground state minimum. Quite surprisingly, the structure of the MECP (shown in the left) corresponds to the distortion that brings the two radical centers closer together.

Although different aspects of the electronic structure of benzynes (including ST gaps) have been investigated experimentally and theoretically, their singlet-triplet MECPs have not been characterized. Fig. 1 shows our preliminary results for *para*-benzyne, one of the three benzyne isomers. Note that despite relatively small ST gaps, both vertical and adiabatic, significant distortion is necessary for the surfaces to cross. The MECP is located 0.65 eV above the singlet minimum. The structure at the MECP is rather interesting: the two radical centers are closer together than in the equilibrium structures, which *increases* the through-space interaction and, consequently, the splitting between the frontier MOs. This increase is offset by the *stabilization* of the higher frontier MO, a_g , by the favorable through-bond interactions.

Preliminary calculations of geometries and energies of the MECPs in methylene and hydroxycarbene are summarized in Table 1, and are in the stark contrast to the *para*-benzyne example. The singlet-triplet MECP in these diradicals is much closer to the equilibrium

geometries of the excited state, i.e., singlet and triplet, respectively. In methylene, it is just 0.01 eV above the singlet minimum, whereas in HCOH it is 0.25 eV above the triplet minimum. Thus, no significant geometric distortions are necessary to reach the MECP. Would this feature manifest itself experimentally and how?

Table 1: Methylene and hydroxycarbene. Equilibrium geometries for the lowest singlet and triplet states and their MECP. Energy differences are in eV, distances are in Angstroms, and angles are in degrees. ΔE is computed relative to the ground state minimum. Negative ΔE_{ST} correspond to the triplet being below the singlet. EOM-SF-CCSD/cc-pVTZ.

	R_{CH}	R_{OH}	α_C	Vertical ΔE_{ST} , eV	ΔE , eV
Methylene					
Singlet min	1.11		102	-0.01	0.45
Triplet min	1.08		133	-0.93	0.00
ST MECP	1.11		102	0.00	0.46
Hydroxycarbene					
Singlet min	1.11	1.31	107	1.48	0.00
Triplet min	1.08	1.33	124	0.56	1.43
ST MECP	1.09	1.34	122	0.00	1.68

2.2 Performance of the spin-flip and multi-reference methods for bond-breaking in hydrocarbons: A benchmark study

In collaboration with Stephen Klippenstein and Larry Harding, we conducted a benchmark study assessing the accuracy of multi-reference and spin-flip methods for bond-breaking[8]. We considered two examples: C-H bond breaking in methane and C-C bond-breaking in ethylene. The methods were calibrated against FCI (methane, 6-31G* basis) and MR-CISD+Q/aug-cc-pVTZ data. We considered non-parallelety errors (NPEs) for the entire range of nuclear distortions from equilibrium to the dissociation limit, as well as in the intermediate range (2.5-4.5 Å), which is the most relevant for kinetics modeling. In the case of methane, for the entire potential energy curves, the NPEs for the SF model with single and double substitutions (SF-CCSD) are slightly less than 3 kcal/mol. Inclusion of triple excitations reduces the NPEs to 0.32 kcal/mol. The corresponding NPEs for the MR-CI are less than 1 kcal/mol, while those of multi-reference perturbation theory are slightly larger (1.2 kcal/mol). The NPEs in the intermediate range are smaller for all the methods: MR-CI, CASPT2, and SF-CCSD curves are very close to each other and are within 0.1-0.2 kcal/mol from FCI. For a larger basis set, the difference between MR-CI and CASPT2 is about 0.2 kcal/mol, while SF-CCSD is within 0.4 kcal/mol from MR-CI. For the C-C bond breaking in ethane the results of the SF-CCSD are within 1 kcal/mol from MR-CI for the entire curve, and within 0.4 kcal/mol in the intermediate region. The corresponding NPEs for CASPT2 are 1.8 and 0.4 kcal/mol, respectively. Overall, our results indicate that the SF-CCSD method provides reliable and economical alternative to MR treatment for single-bond breaking.

3 Current developments and future plans

Currently, we are pursuing modeling IR and photoelectron spectra of two elusive isomers of formaldehyde, cis- and trans- hydroxycarbenes (in collaboration with Prof. Joel Bowman). We are also finalizing for publication the results of the collaborative study with Prof. Hanna Reisler in which we investigate the origin of the dramatic difference (about 1 eV) between the ionization energies of CH₂OH and CH₃CHOH. We are currently employing our code for EOM-CC MECP calculations for characterization of singlet-triplet crossings in formaldehyde and hydroxycarbenes (in collaboration with Prof. Joel Bowman), the oxygen-benzene diradical (in collaboration with Prof. Hai Wang and Prof. John Stanton), and prototypical hydrocarbon diradicals.

References

- [1] L. Koziol, S.V. Levchenko, and A.I. Krylov, Beyond vinyl: Electronic structure of unsaturated propen-1-yl, propen-2-yl, 1-buten-2-yl, and trans-2-buten-2-yl hydrocarbon radicals, *J. Phys. Chem. A* **110**, 2746 (2006).
- [2] V.A. Mozhayskiy, D. Babikov, and A.I. Krylov, Conical and glancing Jahn-Teller intersections in the cyclic trinitrogen cation, *J. Chem. Phys.* **124**, 224309 (2006).
- [3] D. Babikov, V.A. Mozhayskiy, and A.I. Krylov, Photoelectron spectrum of elusive cyclic-N₃ and characterization of potential energy surface and vibrational states of the ion, *J. Chem. Phys.* **125**, 084306 (2006).
- [4] L. Koziol, M. Winkler, K.N. Houk, S. Venkataramani, W. Sander, and A.I. Krylov, The 1,2,3-tridehydrobenzene triradical: ²B or not ²B? The answer is ²A!, *J. Phys. Chem. A* **111**, 5071 (2007).
- [5] I. Fedorov, L. Koziol, G. Li, J.A. Parr, A.I. Krylov, and H. Reisler, Theoretical and experimental investigations of electronic Rydberg states of diazomethane: Assignments and state interactions, *J. Phys. Chem. A* **111**, 4557 (2007).
- [6] L. Koziol, I. Fedorov, G. Li, J.A. Parr, H. Reisler, and A.I. Krylov, Vibronic structure and ion core interactions in Rydberg states of diazomethane: An experimental and theoretical investigation, *J. Phys. Chem. A* **111**, 13347 (2007).
- [7] E. Epifanovsky and A.I. Krylov, Direct location of the minimum point on intersection seams of potential energy surfaces with equation-of-motion coupled-cluster methods, *Mol. Phys.* **105**, 2515 (2007).
- [8] A. Golubeva, A.V. Nemukhin, L. Harding, S.J. Klippenstein, and A.I. Krylov, Performance of the spin-flip and multi-reference methods for bond-breaking in hydrocarbons: A benchmark study, *J. Phys. Chem. A* **111**, 13264 (2007).
- [9] A.I. Krylov, Equation-of-motion coupled-cluster methods for open-shell and electronically excited species: The hitchhiker's guide to Fock space, *Annu. Rev. Phys. Chem.* **59**, 433 (2008).

SYNCHROTRON STUDIES OF PHOTOFRAGMENTATION, RADICAL REACTIONS, AND AEROSOL CHEMISTRY RELATED TO COMBUSTION

*Stephen R. Leone, Christopher Howle, Fabien Goulay, Leonid Belau,
Jared Smith, Kevin Wilson, Daphne Che, Andrea De Filippo,
Adam Trevitt, and Musahid Ahmed*

*Departments of Chemistry and Physics and Lawrence Berkeley National Laboratory
University of California
Berkeley, California 94720
(510) 643-5467 srl@berkeley.edu*

Scope of the Project

Combustion is a complex process involving short-lived radical species, highly excited states, kinetics, transport processes, heterogeneous chemistry on aerosols such as organic liquid nanoparticles and soot, fluid dynamics, and energy transfer. Detailed measurements of microscopic reaction pathways, rate coefficients, product state distributions, and thermochemistry result in considerable information to aid in the understanding of combustion processes. VUV light from the Chemical Dynamics Beamline of the Advanced Light Source (ALS) provides a powerful tool to study photoionization properties of small molecules and radicals and to selectively detect reaction products of carbon-based species (e.g. C₂H, CH) with unsaturated hydrocarbons and to measure the energetics and photoionization spectroscopy of important combustion species. For example, the photoionization of 1- alkenylperoxy and alkylperoxy radicals (work performed by Craig Taatjes and David Osborn, Combustion Research Facility, Sandia) reveals a general rule for the photoionization of these radical species, namely. Furthermore, products from key combustion reactions are detected and branching ratios estimated by members of the Leone group in collaboration with Craig Taatjes and David Osborn. A new theme has been initiated to study aerosol formation, light scattering, and heterogeneous chemistry. This endeavor is exploring aerosol species, their reactivity from fuel sprays and their production in combustion, and the resulting particulate species.

Photodissociation of CH₃CN

Nitrile species, such as CH₃CN (acetonitrile), are involved in chemical mechanisms of relevance to combustion processes as reaction byproducts and flame additives. Indeed, CH₃CN has recently been detected as a constituent of vehicle exhaust fumes. To investigate the photodissociation dynamics and pathways of CH₃CN, Fourier transform visible (FTVIS) emission spectroscopy, in conjunction with VUV photons produced at the ALS, is employed. Rotationally-resolved emission is observed from both the CN(B²Σ⁺ – X²Σ⁺) and CH(A²Δ – X²Π) transitions; only the former is observed in spectra recorded at 10.2 and 11.5 eV photon energies, whereas both are observed in the 16 eV dissociation. Surprisal analyses indicate clear bimodal rotational distributions for CN(B²Σ⁺), suggesting this excited fragment is formed via both linear and bent transition states, depending on the extent of rotational excitation. From thermodynamic calculations, it is evident that CH(A²Δ) is produced along with ground state CN(X²Σ⁺) + H₂. These products can be formed by a two step mechanism (via excited CH₃* and CN(X²Σ⁺)) or a process similar to the "roaming" atom mechanism; the data obtained here are insufficient to definitively conclude whether either pathway occurs. A comparison of the CH(A²Δ) and CN(B²Σ⁺) rovibrational distributions from the 16 eV dissociation, obtained from spectral simulations, allows the branching ratio between the two fragments at this energy to be determined. The derived CH(A²Δ):CN(B²Σ⁺) ratio is (1.2 ± 0.1):1.

CH with C₂H₂, C₂H₄, linear or cyclic C₃H₂

Ongoing projects using the new kinetics machine at the Advanced Light Source in collaboration with the David Osborn and Craig Taatjes at the Sandia Combustion Research Facility aim to probe the products of simple radical reactions such as CH radicals with unsaturated hydrocarbons. Allene has been detected as the main product of the CH reaction with ethylene, with propyne being produced in a lower amount (60%/40%, respectively). The cyclic isomer, cyclopropene, is a minor product. Very recently propargylene and evidence for cyclic-C₃H₂ have been observed in our studies of the CH radical reaction

with acetylene. Work is in progress to elucidate the nature of the cyclic intermediate by studies with selective deuteration.

C₂H and CH with C₃H₄ (allene and propyne)

Although polyacetylenes are identified in carbon rich flames, the reactions leading to their formation are still unknown. In a recent work, we used the kinetics apparatus developed at the ALS to measure the product branching ratio for the reaction of the ethynyl radical with propyne and allene at room temperature. The tunability of the synchrotron radiation allows selective ionization of the reaction products at their specific threshold wavelengths for ionization, with subsequent detection by mass spectrometry. Each product can be identified by its mass and ionization energy. Polyacetylenes and other C₅ species produced by these two reactions are identified in the experiments. By using estimated photoionization cross sections for the different species, we determine the reaction product branching ratios. The reaction of ethynyl with propyne gives diacetylene, C₄H₂ 50-70% of the time and C₅H₄ 50-30% of the time. Of the C₅H₄ isomers, methyldiacetylene is 80-85% and ethynylallene is 20-15%. The reaction of ethynyl with allene produced no detectable diacetylene, and the branching ratio of C₅H₄ isomers is 35-45% ethynylallene, 20-25% methyldiacetylene and 45-30% 1,4-pentadiyne. These results are in agreement with theoretical calculations and unravel an addition-elimination mechanism for both reactions.

Reactions of CH with allene and propyne reveal cyclic isomers of C₄H₄ for the reaction with propyne, but no cyclic isomers for the reaction of CH with allene. The C₄H₄ product branches for CH with allene are 20-30% 1,2,3-butatriene and 80-70% vinyl acetylene. Reaction of CH with propyne produces 1,2,3-butatriene 15-25% of the time and vinyl acetylene 60-30% of the time, with cyclic isomers occurring 25-45% of the time. The complete C₄H₅ intermediate potential surface is not well known, however insertion reactions, and the fact that the two reactions differ in the cyclic product isomer, suggest that there are two different entrance channels leading to different products on the potential surface. For example, direct cyclo-addition of CH to the triple bond in propyne could lead to some cyclic product species.

Physical properties of aerosols

Angle-resolved photoelectron images of nanoparticle ionization are acquired with a new aerosol apparatus. Nanoparticles of combustion-related organic molecules are formed and size-selected using a scanning mobility particle sizer (SMPS). In a first study, NaCl (insulator) particles are studied, and the photoelectron angular distribution shows a distinct asymmetry, which becomes stronger with larger size particles. The vacuum ultraviolet light is absorbed in a thin layer of the surface of the nanoparticle and photoelectrons emanate from this thin layer. As the particle size decreases, the vacuum ultraviolet light penetrates deeper into the particle, creating a more symmetric photoelectron angular distribution. A detailed model obtains good agreement and elucidates the competition between the photon penetration depth and the electron escape length. Different results are obtained for conductor particles, in which the electron angular distributions are isotropic over a wide range of particle sizes.

Aerosol Chemistry – dynamics of aerosol droplet reactions and OH and O₃ initiated aerosol chemistry

New experiments are being developed to investigate the oxidation of fuel droplet sprays, such as biodiesel nanodroplet surfaces, using the aerosol apparatus. Studies will address the reactions from the fuel perspective as well as subsequent chemistry relating to the atmosphere. Ambient aerosols are known to play a significant role in a variety of atmospheric processes such as direct and indirect effects on radiative forcing. Chemical composition can be an important factor in determining the magnitude of these effects (optical density, hygroscopicity, etc.). However, a major fraction (80 – 90%) of organic aerosols cannot be resolved on a molecular level. Recent identification of high mass oligomeric species as a major component in laboratory and ambient organic aerosols has received much attention due to the possibility that these species may account for much of the unknown organic mass in ambient aerosols. Although, a few mechanisms have been proposed, the origin and formation processes of these compounds remain largely unknown. Using VUV photoionization aerosol mass spectrometry we find strong evidence for a

sequential oxidation mechanism of organic aerosols. We also observe the rapid condensed phase formation of high molecular weight species (oligomers), via OH radical initiated oxidation of organic aerosols. Rapid volatilization, followed by oligomerization, is also important for specific reaction systems (i.e. n-alkane particles) and can lead to the loss of a large fraction (> 60%) of a particle. Such rapid processing (oxidation, oligomerization and volatilization) could be driven by radical chain reactions that propagate throughout the particle when initiated by the surface OH reaction.

In other experiments, we have investigated the chemistry of particle surfaces coated by PAHs. The reaction between gas phase ozone and solid anthracene deposited at the surface of sodium chloride particles is studied by measuring both the particle size and chemical composition using a SMPS and the VUV aerosol mass spectrometer. Experiments varying ozone concentration and anthracene coating thickness have been recorded to better understand the surface chemistry of semi-volatile PAHs.

Future Plans

New studies will explore radical-molecule and radical-radical reactions using VUV-ionization. Using the kinetics machine developed in conjunction with Sandia National Laboratory, we will investigate coupled carbon-nitrogen chemistry by studying the products of CN radical reactions with unsaturated hydrocarbons, especially aromatic molecules. Important experiments will be performed concerning the reaction of hydrocarbon radicals on biodiesel and oil shale related chemical species in nanodroplets using VUV ionization to probe volatile and nonvolatile components of the heterogeneous reactions. Major studies will exploit the aerosol generation and detection instrumentation discussed above.

Recent Publications Citing DOE Support (2006-2008):

G. Meloni, T. M. Selby, F. Goulay, S. R. Leone, D. L. Osborn, and C. A. Taatjes, "Photoionization of 1-alkenylperoxy and alkylperoxy radicals and a general rule for the stability of their cations," *J. Am. Chem. Soc.* **129**, 14019, (2007).

L. Belau, S. E. Wheeler, B. W. Ticknor, M. Ahmed, S. R. Leone, W. D. Allen, H. F. Schaefer III, and M. A. Duncan, "Ionization thresholds of small carbon clusters: tunable VUV experiments and theory," *J. Am. Chem. Soc.* **129**, 10229 (2007).

L. Belau, K. R. Wilson, S. R. Leone, and M. Ahmed, "Vacuum Ultraviolet (VUV) photoionization of small water clusters," *J. Phys. Chem. A* **111**, 10075 (2007).

K. R. Wilson, S. Zou, J. Shu, E. Rühl, S. R. Leone, G. C. Schatz, and M. Ahmed, "Size-dependent angular distributions of low energy photoelectrons emitted from NaCl nanoparticles," *Nano Lett.* **7**, 2014 (2007).

R. I. Kaiser, L. Belau, S. R. Leone, M. Ahmed, Y. Wang, B. J. Braams, and J. M. Bowman, "A combined experimental and computational study on the ionization energies of the cyclic and linear C₃H isomers," *Chem. Phys. Chem.* **8**, 1236 (2007).

C. Howle, A. N. Arrowsmith, V. Chikan, and S. R. Leone, "State-resolved dynamics of the CN(B₂Σ⁺) and CH(A²Δ) excited products resulting from the VUV photodissociation of CH₃CN," *J. Phys. Chem. A* **111**, 6637 (2007).

L. Belau, K. R. Wilson, S. R. Leone, and M. Ahmed, "Vacuum-ultraviolet photoionization studies of the microhydration of DNA bases (Guanine, Cytosine, Adenine, and Thymine)," *J. Phys. Chem. A* **111**, 7562 (2007).

F. Goulay, D. L. Osborn, C. A. Taatjes, P. Zou, G. Meloni, and S. R. Leone, "Direct detection of polyynes formation from the reaction of ethynyl radical (C₂H) with propyne (CH₃CCH) and allene (CH₂=C=CH₂)," *Phys. Chem. Chem. Phys.* **9**, 4291 (2007).

C. Nicolas, J. Shu, D. S. Peterka, M. Hochlaf, L. Poisson, S. R. Leone, and M. Ahmed, "Vacuum ultraviolet photoionization of C₃," *J. Am. Chem. Soc.* **128**, 220 (2006).

F. Goulay and S. R. Leone "Low temperature rate coefficients for the reaction of ethynyl radical (C₂H) with benzene," *J. Phys. Chem. A*, **110**, 1875 (2006).

A. N. Arrowsmith, V. Chikan, and S. R. Leone, "Dynamics of the CH(A²Δ) product from the reaction of C₂H with O₂ studied by Fourier transform visible spectroscopy," *J. Phys. Chem. A*, **110**, 7521 (2006).

E. Gloaguen, E. R. Mysak, S. R. Leone, M. Ahmed, and K. R. Wilson "Investigating the chemical composition of

mixed organic-inorganic particles by 'soft' VUV photoionization: the reaction of ozone with anthracene on sodium chloride particles," *Int. J. Mass Spectrom.* **258**, 74 (2006).

G. Meloni, P. Zou, S.J. Klippenstein, M. Ahmed, S. R. Leone, C. A. Taatjes, and D. L. Osborn, "Energy-resolved photoionization of alkyl peroxy radicals and the stability of their cations," *J. Am. Chem. Soc.* **128**, 13559 (2006).

J. Shu, K. R. Wilson, M. Ahmed, and S. R. Leone, "Coupling a versatile aerosol apparatus to a synchrotron: vacuum ultraviolet light scattering, photoelectron imaging, and fragment free mass spectrometry," *Rev. Sci. Instrum.* **77**, 043106 (2006).

J. Shu, K. R. Wilson, M. Ahmed, S. R. Leone, C. E. Graf, and E. Rühl, "Elastic light scattering from nanoparticles by monochromatic vacuum-ultraviolet radiation," *J. Chem. Phys.* **124**, 034707 (2006).

J. Plenge, C. Nicolas, A. G. Caster, M. Ahmed, and S. R. Leone, "Two-color visible/vacuum ultraviolet photoelectron imaging dynamics of Br₂," *J. Chem. Phys.* **125**, 133315 (2006).

K. R. Wilson, M. Jimenez-Cruz, C. Nicolas, L. Belau, S. R. Leone, and M. Ahmed, "Thermal vaporization of biological nanoparticles: Fragment-free VUV photoionization mass spectra of tryptophan, phenylalanine-glycine-glycine and β -carotene," *J. Phys. Chem. A* **110**, 2106 (2006).

K. R. Wilson, D. S. Peterka, M. Jimenez-Cruz, S.R. Leone, and M. Ahmed. "VUV Photoelectron Imaging of Biological Nanoparticles – Ionization energy determination of nano-phase glycine and phenylalanine-glycine-glycine". *Phys. Chem. Chem. Phys.* **8**, 1884 (2006).

K. R. Wilson, L. Belau, C. Nicolas, M. Jimenez-Cruz, S. R. Leone, and M. Ahmed, "Direct determination of the ionization energy of histidine with VUV synchrotron radiation" *Int. J. Mass Spectrom.* **249-250**, 155, (2006).

V. Chikan, B. Nizamov, and S. R. Leone, "State-resolved dynamics of the CH(A² Δ) channels from single and multiple photon dissociation of bromoform in the 10–20 eV energy range," *J. Phys. Chem. A* **110**, 2850 (2006).

Theoretical Studies of Molecular Systems

William A. Lester, Jr.
Chemical Sciences Division,
Ernest Orlando Lawrence Berkeley National Laboratory and
Kenneth S. Pitzer Center for Theoretical Chemistry
Department of Chemistry, University of California, Berkeley
Berkeley, California 94720-1460
walester@lbl.gov

Program Scope

This research program is directed at extending fundamental knowledge of atoms and molecules. The approach combines the use of ab initio basis set methods and the quantum Monte Carlo (QMC) method to describe the electronic structure and energetics of systems of primarily combustion interest.

Recent Progress

Breathing Orbital Valence Bond (BOVB) Trial Functions (with D. Domin)

The quest for improved diffusion MC (DMC) trial functions has prompted our study of valence bond methods. There has been a resurgence of interest in this direction, in particular, in the variant labeled breathing orbital valence bond (BOVB). This approach generates wave functions that can be used in DMC especially to assist a balanced treatment of fragments and precursor in the calculation of a dissociation energy. The BOVB method has been tested in the calculation of the C-H bond dissociation from acetylene. The resultant energy is in excellent accord with experiment and a modest improvement over BDEs obtained using Hartree-Fock and post Hartree-Fock trial wave functions, which are already quite good.

Electron Transfer and Excitation Energy Transfer (with R. Salomon-Ferrer and B. Austin)

Studies directed at triplet-triplet (TT) energy transfer have been pursued in the past year. Such processes play an important role in many photophysical processes in chemistry and biology. These studies have been carried out to date at the DFT level of theory in preparation for higher accuracy DMC computations. TT energy transfer can be viewed as a process of two simultaneous electron transfers with different spins and is similar to singlet-singlet energy exchange coupling mechanism for electrons of the same spin, but different energy. A stimulus for this research, besides the fundamental importance of the problem, is our excellent DMC results for the singlet-triplet energy gap in free-base porphyrin.

DMC-MM Approach (with H.-M. Cho)

The QM-MM (quantum mechanics-molecular mechanics) formulations developed to treat a reactive center or other process requiring quantum mechanics (QM), and the surrounding media by molecular mechanics (MM) is now a standard approach when the QM treatment is one of a number of semiempirical or density functional theory approaches. Owing to the high accuracy that can be achieved with DMC, a DMC-MM approach has been developed. Because of the local character of DMC, special steps must be taken to make possible this approach. A major benefit of success in this direction will be the treatment of larger reactive centers than those accessible using alternative ab initio methods owing to the advantageous scaling with system size that has been recently demonstrated with DMC.

Future Plans

QMC studies of trial function construction will continue. This is an area of critical importance for the development of the DMC method where the emphasis remains on achieving compact descriptions. As mentioned, valence bond functions are being investigated along with molecular-orbital based approaches. Small combustion molecules and radicals remain the test bed for the various approaches.

The collaborative effort with M. Frenklach on the graphene layer chemistry will continue. DFT methods will be used for the reaction systems and QMC studies performed on the most critical steps identified in the DFT studies. With this data, reaction rates will be determined from the solution of master equations.

Efforts will continue in the pursuit of approaches for the accurate calculation of forces in DMC in collaboration with Roland Assaraf, CNRS (Paris). Although methods for the evaluation of forces have been pursued in this and other laboratories for a number of years, there is still no approach that can be routinely applied that yields accuracy of predictive merit.

DoE Supported Publications (2006-2008)

1. R. Whitesides, A. Kollias, D. Domin, W. A. Lester, Jr., and M. Frenklach, "Graphene layer growth: Collision of migrating five-membered rings," Symposium on *Nanoparticles in Energy Processes: Friend and Foe: Combustion Synthesis: From Pollutants to Advanced Materials*, 231st National Meeting of the American Chemical Society, Atlanta, GA, March 26-30, 2006.
2. R. Whitesides, A. Kollias, D. Domin, W. A. Lester, Jr., and M. Frenklach, "Graphene Layer Growth: Collision of Migrating Five-Membered Rings", *Prepr. Pap.-Am. Chem. Soc., Div. Fuel Chem.* **51**(1), 2006, pp. 174-175.
3. A. C. Kollias, D. Domin, G. Hill, M. Frenklach, and W. A. Lester, Jr., "Quantum Monte Carlo Study of Small Hydrocarbon Atomization Energies," *Mol. Phys.* **104**, 467 (2006).
4. W. A. Lester, Jr. and R. Salomon-Ferrer, "Some Developments in Quantum Monte Carlo for Electronic Structure: Methods and Application to a Bio System," *THEOCHEM* 771, 51 (2006).
5. P. T. A. Galek, N. C. Handy, and W. A. Lester, Jr. "Quantum Monte Carlo Studies on Small Molecules," *Mol. Phys.* **104**, 3069 (2006).

7. R. Whitesides, A. C. Kollias, D. Domin, W. A. Lester, Jr., and M. Frenklach, "Graphene Layer Growth: Collision of Migrating Five-Member Rings," *Proc. Comb. Inst.* **31**, 539 (2007).
8. R. Whitesides, A. C. Kollias, D. Domin, W. A. Lester, Jr., and M. Frenklach, "Graphene Layer Growth: Five-Six-Ring Flip Reaction," Proceedings of the 5th U.S. National Combustion Meeting, San Diego, CA, March 25-28, 2007, Paper No. D31,
9. B. Austin, A. Aspuru-Guzik, R. Salomon-Ferrer, and W. A. Lester, Jr., "Linear –Scaling Evaluation of the Local Energy in Quantum Monte Carlo," in Proceedings of the Pacificchem Symposium on Advances in Quantum Monte Carlo, J. B. Anderson and S. M. Rothstein, eds., ACS Symposium Series **953**, 55 (2007).
10. R. Prasad, N. Umezawa, D. Domin, R. Salomon-Ferrer, and W. A. Lester, Jr., "Quantum Monte Carlo Study of First-Row Atoms using Transcorrelated Variational Monte Carlo Trial Functions," *J. Chem. Phys.* **126**, 164109 (2007).
11. C. Amador-Bedolla, R. Salomon-Ferrer, J. A. Vazquez-Martinez, and W. A. Lester, Jr., "Reagents for Electrophilic Amination: A Quantum Monte Carlo Study," *J. Chem. Phys.* **126**, 204308 (2007).
12. A. Aspuru-Guzik, B. Austin, D. Domin, P. T. A. Galek, N. Handy, R. Prasad, R. Salomon-Ferrer, N. Umezawa, and W. A. Lester, Jr., "Recent Developments in Quantum Monte Carlo: Methods and Applications," in *Computation in Modern Science and Engineering*, **2**, Part A, T. E. Simos and G. Maroulis, eds., AIP Conference Proceedings, 963 (2007), p. 210.
13. D. Domin, W. A. Lester, Jr., R. Whitesides, and M. Frenklach, "Isomer Energy Differences for the C₄H₃ and C₄H₅ Isomers Using Diffusion Monte Carlo," *J. Phys. Chem. A*, **112**, 2065 (2008).
14. M. T. Nguyen, M. H. Matus, W. A. Lester, Jr., and D. A. Dixon, "Heats of Formation of Triplet Ethylene, Ethylidene, and Acetylene," *J. Phys. Chem. A*, **112**, 2082 (2008).
15. R. Whitesides, D. Domin, R. Salomon-Ferrer, W. A. Lester, Jr., and M. Frenklach, "Graphene Layer Growth Chemistry: Five-Six-Ring Flip Reaction," *J. Phys. Chem. A*, **112**, 2125 (2008).

Intermolecular Interactions of Hydroxyl Radicals on Reactive Potential Energy Surfaces

Marsha I. Lester

Department of Chemistry, University of Pennsylvania
Philadelphia, PA 19103-6323
milester@sas.upenn.edu

I. Program Scope

The hydroxyl radical plays a major role in combustion and atmospheric environments, where it is often detected by laser-induced fluorescence (LIF) using the $A\ ^2\Sigma^+ - X\ ^2\Pi$ band system. Collision partners that efficiently quench electronically excited $\text{OH } A\ ^2\Sigma^+$ radicals are ubiquitous in these environments. Thus, great effort has been made to quantify the rates for collisional quenching, so that its effects on LIF signals may be taken into account, thereby allowing for an accurate determination of OH concentrations.^{1,2} Despite the experimental determination of the magnitude of overall quenching rates, the mechanism by which $\text{OH } A\ ^2\Sigma^+$ is quenched by H_2 or other molecular partners has remained elusive. The experimental work carried out under DOE funding in this laboratory is aimed at understanding the fundamental chemical dynamics governing quenching of $\text{OH } A\ ^2\Sigma^+$ by H_2 and other partners of significance in combustion environments.

II. Recent Progress

Collisions with H_2 can remove population from the electronically excited $\text{OH } A\ ^2\Sigma^+$ state by two competing channels. The first is nonreactive quenching, which returns OH to its ground electronic state



while the second is reactive, and leads to the formation of water and hydrogen atoms³⁻⁵



Quenching of $\text{OH } A\ ^2\Sigma^+$ by H_2 is rapid at room temperature ($10\ \text{\AA}^2$),⁶⁻⁸ and displays the typical negative temperature and initial rotational dependencies. *Ab initio* calculations of the interaction energy between H_2 and OH in its ground $X\ ^2\Pi$ and excited $A\ ^2\Sigma^+$ electronic states have identified specific orientations that lead to seams of *conical intersection* between the ground and excited state surfaces.^{2,9,10}

In this grant period, we examined the outcome of $\text{OH } A\ ^2\Sigma^+$ ($v'=0, N'=0$) + H_2 quenching events that lead to $\text{OH } X\ ^2\Pi$ + H_2 products (nonreactive quenching) as well as the branching between reactive and nonreactive quenching. Initially, we measured the $\text{OH } X\ ^2\Pi$ product state distribution in $v''=1$ (and in the lowest rotational levels of $v''=2$).¹¹ We found that the OH products were generated with significant rotational excitation. We attribute this signature to the forces at play as the $\text{OH}-\text{H}_2$ system passes through the conical intersection region that couple the ground and excited state potential energy surfaces.

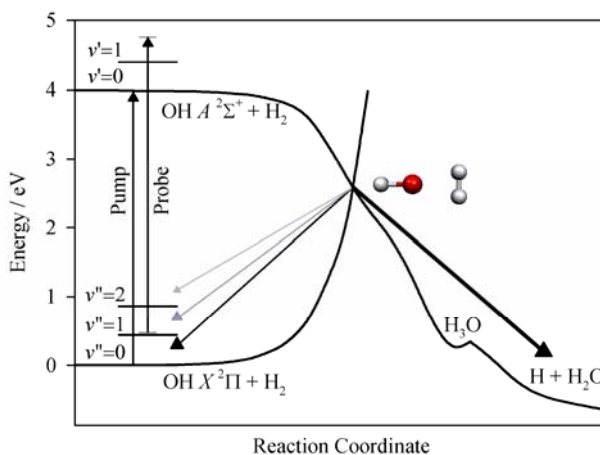


Fig. 1 Schematic potentials for quenching of OH in its excited $A\ ^2\Sigma^+$ electronic state by H_2 , illustrating a conical intersection (CI) that couples the potentials in the T-shaped $\text{HO}-\text{H}_2$ configuration. Two pathways emerge from the CI, leading to nonreactive (R1) and reactive (R2) quenching products; arrows indicate qualitative distribution of products. The pump-probe laser scheme for characterizing the $\text{OH } X\ ^2\Pi$ product state distribution is also shown.

The time delay between the quenching event and probe laser detection of the OH $X^2\Pi$ products, however, allowed for the possibility of relaxation of the nascent OH $X^2\Pi$ product state distribution by secondary collisions.

More recently, we characterized the OH $X^2\Pi$ products from nonreactive quenching of OH $A^2\Sigma^+$ by H_2 under *single-collision conditions*.¹² These studies also encompass a broader range of quantum states than had been reported previously, including OH $X^2\Pi$ ($v''=0, N''$), which was extremely challenging because of the similar pump, probe, and detection wavelengths. The OH $X^2\Pi$ products were detected in $v''=0, 1$ and 2 ; the distribution peaks in $v''=0$ and decreases monotonically with increasing vibrational excitation as shown in Fig. 2. In all vibrational levels probed, the OH $X^2\Pi$ products are found to be highly rotationally excited, with the distribution peaking at $N''=15$ when H_2 was used as the collision partner and $N''=17$ for D_2 . A marked propensity for production of $\Pi(A')$ Λ -doublet levels was observed. By contrast, both OH $X^2\Pi$ spin-orbit manifolds were equally populated. The main difference in the observed OH $X^2\Pi$ product state distributions when H_2 or D_2 was used as the collision is the peak in the rotational distribution, which can be rationalized on kinematic grounds.

To better understand these results, the measurements have been complemented by an extensive theoretical study of the OH- H_2 interaction potential in the conical intersection region by Kłos and Alexander.¹¹ Calculations exploring the potential energy surface (PES) show a steep angular gradient into and away from the conical intersection whenever the O-end of the OH radical approaches the H_2 molecule. This causes a substantial torque to be placed on the OH radical as it passes through the conical intersection, resulting in the pronounced rotational excitation observed experimentally. The recent calculations did not examine the OH vibrational dependence. The earlier theoretical work of Hoffman and Yarkony¹⁰ indicated little change in OH bond length as the system evolves through the conical intersection region, suggesting minimal vibrational excitation of OH products as now observed experimentally.

The observed propensity for production of the $\Pi(A')$ Λ -doublet is a consequence of the symmetries of the electronic states that form the conical intersection, and which correlate with A' surfaces in planar geometries. For low rotational levels, the approximation of H_2 or D_2 as a spherical partner is fairly reasonable and the system can be considered as pseudo-triatomic. The OH $X^2\Pi$ products emerge on the lower $1^2A'$ surface, with the unpaired electron primarily in the plane of the collision, which is also the plane of OH rotation. These theoretical studies indicate that state-resolved measurements of the product quantum state distribution as well as the branching between the reactive and nonreactive pathways should provide sensitive probes of the dynamics of passage through a conical intersection region.

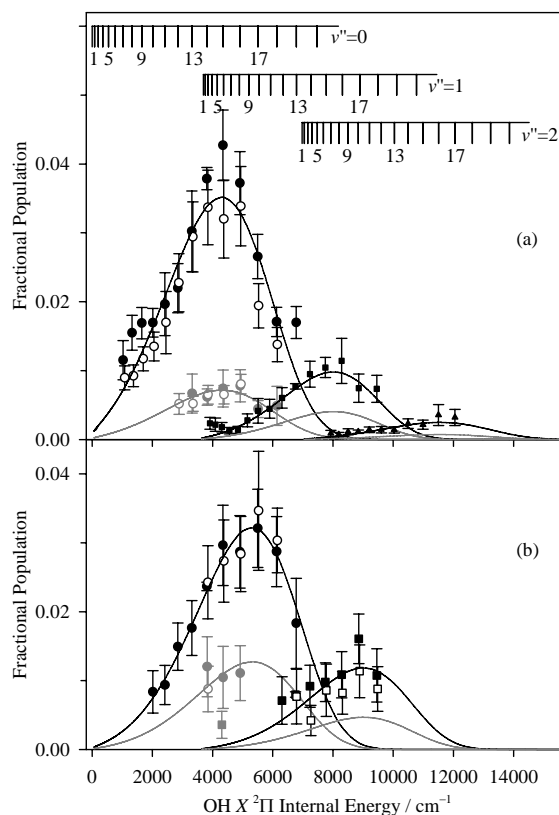


Fig. 2 Nascent OH $X^2\Pi$ (v'', N'') state distribution following collisional quenching of OH $A^2\Sigma^+$ by (a) H_2 and (b) D_2 . Symbols indicate the populations in $v''=0$ (circles), $v''=1$ (squares) and $v''=2$ (triangles); filled and open symbols show the F_1 and F_2 spin-orbit manifolds; the $\Pi(A')$ Λ -doublets are indicated in black and $\Pi(A'')$ levels in gray. The lines are best-fit functions.

We have also made the first experimental determination of the branching between the nonreactive and reactive quenching pathways.¹³ The branching fraction is measured by comparing the total population in OH $X^2\Pi$ product states arising from nonreactive quenching with the initial population excited to the OH $A^2\Sigma^+$ ($v'=0, N'=0$) state. Our detailed measurements indicate that collisional quenching of OH $A^2\Sigma^+$ by H_2 yields only $\sim 12(5)\%$ of the products through the nonreactive pathway with the majority of products generated via the reactive pathway ($\sim 88\%$). Analogous measurements have been performed for the collisional quenching of OH $A^2\Sigma^+$ by D_2 , yielding a branching fraction of 0.15(8), which is consistent with the value determined for H_2 . It is, however, *counter to theoretical predictions*, which suggest that the steeper paths leading to OH $X^2\Pi + H_2$ should be dynamically more facile than the much shallower paths leading to $H_2O + H$.¹⁰ Note that no collision-induced OD $X^2\Pi$ products were detected from an exchange reaction.

These results for the prototypical OH + H_2/D_2 systems are an important step towards understanding nonadiabatic passage via conical intersections. However, there is still a need for more work on this and other systems of significance in combustion environments to fully understand the dynamical processes by which quenching occurs.

III. Future Work

We have also predicted,¹⁴ and recently observed, the rotational band structure associated with infrared transitions of the OH-water complex as an initial step to our infrared spectroscopic studies of this complex and OH embedded in small water clusters. The OH monomer orbital angular momentum is predicted to be partially quenched in the OH-water complex, resulting from a significant splitting of the OH monomer orbital degeneracy into $^2A'$ and $^2A''$ electronic states. This orbital angular momentum quenching and associated decoupling of the electron spin from the a inertial axis has since been shown to have a dramatic effect on the rotational structure of microwave transitions observed for the OH-water complex.^{15,16} At the *ab initio* values for the splitting between the $^2A'$ and $^2A''$ surfaces, simulated spectra of a - and b -type bands, such as those expected for the OH radical stretch and water asymmetric stretch, are predicted to have a noticeably different appearance than the well established limiting cases associated with fully quenched or completely unquenched orbital angular momentum.

IV. References

- ¹ D. R. Crosley, J. Phys. Chem. **93**, 6273 (1989).
- ² M. I. Lester, R. A. Loomis, R. L. Schwartz, and S. P. Walch, J. Phys. Chem. A **101**, 9195 (1997).
- ³ D. T. Anderson, M. W. Todd, and M. I. Lester, J. Chem. Phys. **110**, 11117 (1999).
- ⁴ M. W. Todd, D. T. Anderson, and M. I. Lester, J. Phys. Chem. A **105**, 10031 (2001).
- ⁵ M. Ortiz-Suárez, M. F. Witinski, and H. F. Davis, J. Chem. Phys. **124**, 201106 (2006).
- ⁶ D. E. Heard and D. A. Henderson, Phys. Chem. Chem. Phys. **2**, 67 (2000).
- ⁷ B. L. Hemming, D. R. Crosley, J. E. Harrington, and V. Sick, J. Chem. Phys. **115**, 3099 (2001).
- ⁸ B. L. Hemming and D. R. Crosley, J. Phys. Chem. A **106**, 8992 (2002).
- ⁹ D. R. Yarkony, J. Chem. Phys. **111**, 6661 (1999).
- ¹⁰ B. C. Hoffman and D. R. Yarkony, J. Chem. Phys. **113**, 10091 (2000).
- ¹¹ P. A. Cleary, L. P. Dempsey, C. Murray, M. I. Lester, J. Kłos, and M. H. Alexander, J. Chem. Phys. **126**, 204316 (2007).
- ¹² L. P. Dempsey, C. Murray, P. A. Cleary, and M. I. Lester, Phys. Chem. Chem. Phys. **10**, 1424 (2008).
- ¹³ L. P. Dempsey, C. Murray, and M. I. Lester, J. Chem. Phys. **127**, 151101 (2007).
- ¹⁴ M. D. Marshall and M. I. Lester, J. Phys. Chem. B **109**, 8400 (2005).
- ¹⁵ Y. Ohshima, K. Sato, Y. Sumiyoshi, and Y. Endo, J. Am. Chem. Soc. **127**, 1108 (2005).
- ¹⁶ C. S. Brauer, G. Sedo, E. M. Grumstrup, K. R. Leopold, M. D. Marshall, and H. O. Leung, Chem. Phys. Lett. **401**, 420 (2005).

V. Publications supported by this project 2006-2008

1. I. B. Pollack, Y. Lei, T. A. Stephenson, and M. I. Lester, "Electronic Quenching of OH A $^2\Sigma^+$ Radicals in Collisions with Molecular Hydrogen", *Chem. Phys. Lett.* **421**, 324-328 (2006).
2. P. A. Cleary, L. P. Dempsey, C. Murray, M. I. Lester, J. Klos and M. H. Alexander, "Electronic Quenching of OH A $^2\Sigma^+$ Radicals in Single Collision Events with Molecular Hydrogen: Quantum State Distribution of the OH X $^2\Pi$ Products", *J. Chem. Phys.* **126**, 204316 (2007).
3. L. P. Dempsey, C. Murray, and M. I. Lester, "Product Branching between Reactive and Nonreactive Pathways in the Collisional Quenching of OH A $^2\Sigma^+$ Radicals by H₂", *J. Chem. Phys.* [Communication] **127**, 151101 (2007).
4. L. P. Dempsey, C. Murray, P. A. Cleary, and M. I. Lester, "Electronic Quenching of OH A $^2\Sigma^+$ Radicals in Single Collision Events with H₂ and D₂: A Comprehensive Quantum State Distribution of the OH X $^2\Pi$ Products", *Phys. Chem. Chem. Phys.* **10**, 1424-1432 (2008).

Kinetics of Elementary Processes Relevant to Incipient Soot Formation

PI : M. C. Lin

Co-PI : M. C. Heaven

Department of Chemistry

Emory University, Atlanta, GA 30322

chemmcl@emory.edu, heaven@euch4e.chem.emory.edu

I. Program Scope

Soot formation and abatement processes are some of the most important and challenging problems in hydrocarbon combustion. The key reactions involved in the formation of polycyclic aromatic hydrocarbons (PAH's), the precursors to soot, remain elusive. Small aromatic species such as C₅H₅, C₆H₆ and their derivatives are believed to play a pivotal role in incipient soot formation.

The goal of this project is to establish a kinetic database for elementary reactions relevant to soot formation in its incipient stages. In the past year, we have completed by CRDS the kinetics for the formation and decomposition of C₆H₅C₂H₂O₂ in the C₆H₅C₂H₂ + O₂ reaction and the formation of C₁₀H₇O₂ in the C₁₀H₇ + O₂ reaction by directly monitoring C₆H₅C₂H₂O₂ and C₁₀H₇O₂ radicals in the visible region; their mechanisms have been elucidated computationally by quantum-chemical calculations. The O + C₂H₅OH reaction has been studied experimentally and computationally and the OH + HNCN reaction has been investigated by *ab initio* molecular orbital calculation. In addition, a new pulsed slit molecular beam system has been constructed and tested for spectroscopic studies of aromatic radicals and their derivatives by the cavity ringdown technique (CRDS).

II. Recent Progress

1. C₆H₅C₂H₂ + O₂ → C₆H₅C₂H₂O₂ → C₆H₅CHO + CHO (ref. # 1)

The C₆H₅C₂H₂ radical is the key intermediate of the C₆H₅ + C₂H₂ reaction which plays a pivotal role in the formation of the second aromatic ring.^{2,3} The effects of temperature and pressure on the formation and decomposition of C₆H₅C₂H₂O₂ in the C₆H₅C₂H₂ + O₂ reaction (which competes with the formation of PAHs) have been investigated at temperatures from 298 - 378 K by directly monitoring the C₆H₅C₂H₂O₂ radical in the visible region with CRDS. The rate constant for the C₆H₅C₂H₂ + O₂ association and that for fragmentation of C₆H₅C₂H₂O₂ were found to be respectively

$$k_1 (\text{C}_6\text{H}_5\text{C}_2\text{H}_2 + \text{O}_2 \rightarrow \text{C}_6\text{H}_5\text{C}_2\text{H}_2\text{O}_2) = (3.20 \pm 1.19) \times 10^{11} \exp(+760/T) \text{ cm}^3 \text{ mol}^{-1} \text{ s}^{-1}$$
$$k_2 (\text{C}_6\text{H}_5\text{C}_2\text{H}_2\text{O}_2 \rightarrow \text{C}_6\text{H}_5\text{CHO} + \text{HCO}) = (1.68 \pm 0.13) \times 10^4 \text{ s}^{-1}$$

Both reactions rates, k_1 and k_2 , were found to be independent of pressure in the range of 40 – 80 Torr Ar. The mechanism for this very fast reaction has been elucidated quantum-chemically by B3LYP/6-31G(d,p) calculations. The result of the calculations indicate that the reaction effectively occur by two competitive association paths giving 3- and 4-member-ring peroxide intermediates which fragment rapidly to C₆H₅CHO + CHO with a predicted 382 kJ/mol exothermicity.

Additional kinetic measurements by PLP/MS and a more detailed computational study of the mechanism and associated kinetics have been done for interpretation of measured temperature dependent data. The result of our preliminary calculation for its removal of C₆H₅C₂H₂ by O₂ measured by the CRDS and PLP/MS techniques suggests that C₆H₅CHO could be formed exothermically. Our mass-spectrometric measurements indeed show that C₆H₅CHO was produced in the C₆H₅C₂H₂ + O₂ reaction as predicted by the mechanism as mentioned above. The mass-spectrometric result also indicates that the formation of C₆H₅CHO from the decomposition of C₆H₅C₂H₂O₂ is temperature-independent, consistent with the CRDS experimental data.

2. Kinetics of 1- and 2-naphthyl (C₁₀H₇) radical reactions (ref. #4)

Naphthyl radicals play a very significant role in the formation of larger PAHs during incipient soot formation stages.^{2,3} In a kinetic modeling of soot-formation, Green, Howard and coworkers³ computed the rate constant for 1-naphthyl reaction with C₂H₂ with TST and QRRK based on the transition-state parameters obtained by B3LYP/cc-pVDZ calculations. Marinov et al.⁵ proposed the reaction rate of 1-C₁₀H₇ + O₂ producing C₁₀H₇O + O in the kinetic modeling of a laminar premixed n-butane flame as 1×10^{13} cm³/mol-s. In 2002, Kunioshi⁶ and his coworkers calculated the reaction rate of 1-C₁₀H₇ + O₂ → C₁₀H₇O + O with hybrid DFT molecular orbital method at the B3LYP/6-31G(d) level. The C₁₀H₇ + O₂ reaction at T ≥ 1000 K is believed to occur primarily via the metathetical process, C₁₀H₇ + O₂ → C₁₀H₇O + O leading to the formation of a naphthyloxy radical which then can fragment yielding the C₉H₇ + CO products. Similarly to the reactions of C₆H₅ + O₂ and C₆H₅C₂H₂ + O₂, the C₁₀H₇ + O₂ reaction at low temperature has been shown to proceed by the addition-stabilization process giving rise to the naphthylperoxy radical, C₁₀H₇ + O₂ → C₁₀H₇OO. To our knowledge, however, there are no experimental kinetic data on the reactions despite of several theoretical studies by Green, Howard and coworkers² and Kunioshi.⁶ In this study we investigated the effects of temperature on the formation of C₁₀H₇O₂ in the 2-C₁₀H₇ + O₂ reaction at temperatures from 299 - 444 K by directly monitoring the C₁₀H₇O₂ radical in the visible region with CRDS, as have been demonstrated successfully in the kinetic measurements of the C₆H₅ + O₂ and C₆H₅C₂H₂ + O₂ reactions, using the 2-C₁₀H₇Br as a radical source by photolysis at 193 nm.

A least-squares analysis of the measured data gives the *first experimentally measured rate constant* for 2-C₁₀H₇ + O₂, $k_1 = (1.53 \pm 0.10) \times 10^{12} \exp[(900 \pm 45)/RT]$ cm³ mol⁻¹ s⁻¹, in the temperature range of 299 - 444 K at a total pressure of 40 Torr.

3. O + C₂H₅OH (ref. #7)

In collaboration with Y-P Lee's group at National Chiao Tung University in Taiwan, we have investigated the kinetics of the O + C₂H₅OH reaction in a diaphragmless shock tube; this is a continuing study following the O + CH₃OH reaction.⁸ Ethanol (C₂H₅OH) is an important and versatile renewable energy source; it may be used as a neat fuel, as an oxygenate additive, or a fuel extender in an internal combustion.⁹ Experimentally O atoms were generated by photolysis of SO₂ at 193 nm with an ArF excimer laser; their concentrations were monitored via atomic resonance absorption. Combining our new data in the range 886 - 1410 K with previous measurements at low temperature represents the rate coefficients determined for the temperature range 298 - 1410 K by the equation: $k(T) = (2.89 \pm 0.09) \times 10^{-16} T^{1.62} \exp[-(1210 \pm 90)/T]$ cm³ molecule⁻¹ s⁻¹. The errors represent one standard deviation in fitting. Theoretical calculations at the CCSD(T)/6-311+G(3df, 2p)//B3LYP/6-311+G(3df) level predict potential energies of various reaction paths forming CH₃CHOH + OH (1a), CH₂CH₂OH + OH (1b) and CH₃CH₂O + OH (1c). Rate coefficients are predicted with the canonical variational transition state (CVT) theory with the small curvature tunneling correction (SCT) method. Reaction paths associated with trans and gauche conformations are both identified; the latter accounts for 59 ± 17 % of the total product yield in the temperature range 300-3000 K. Predicted total rate coefficients, $1.60 \times 10^{-22} T^{3.50} \exp(16/T)$ cm³ molecule⁻¹ s⁻¹ for the range 300-3000 K, agree satisfactorily with experimental observations. The branching ratios of three accessible reaction channels forming CH₃CHOH + OH (1a), CH₂CH₂OH + OH (1b) and CH₃CH₂O + OH (1c) are predicted to vary distinctively with temperature. Below 500 K, reaction (1a) is the predominant path; the branching ratios of reactions (1b) and (1c) become ~40 % and ~12 %, respectively, at 2000 K.

4. OH + HNCN (ref. # 10)

The cyanomidyl radical (HNCN) is a reactive transient species which plays an important role in a variety of chemical environments including prompt NO formation in hydrocarbon combustion, interstellar chemistry, and primordial reactions leading to the synthesis of amino acids from simple inorganic compounds. In this study the kinetics and mechanism of the reaction of HNCN with hydroxyl radical (OH) have been investigated by ab initio calculations with rate constants prediction. The single and triplet potential energy surfaces of this reaction have been calculated by single-point calculations at the CCSD(T)/6-

311+G(3df,2p) level based on geometries optimized at the B3LYP/6-311+G(3df,2p) and CCSD/6-311++G(d,p) levels. The rate constants for various product channels in the temperature range of 300 - 3000 K are predicted by variational transition state and RRKM theories. The predicted total rate constants can be represented by the expressions $k(\text{total}) = 2.66 \times 10^2 T^{4.50} \exp(239/T)$ in T = 300-1000 K; $1.38 \times 10^{20} T^{2.78} \exp(1578/T) \text{ cm}^3 \text{ molecule}^{-1} \text{ s}^{-1}$ at T = 1000 - 3000 K. The branching ratios of primary channels are predicted: k_1 for forming singlet HON(H)CN accounts for 0.32 - 0.28 and k_4 for forming singlet HONCNH accounts for 0.68 - 0.17 in the temperature range of 300 - 800 K. $k_2 + k_7$ for producing H₂O + NCN accounts for 0.55 - 0.99 in the high temperature range of 800 - 3000 K. The branching ratios of k_3 for producing HCN + HNO, k_6 for producing H₂N + NCO, k_8 for forming 3HN(OH)CN, k_9 for producing CNOH + 3NH, and $k_5 + k_{10}$ for producing NH₂ + NCO are negligible. The rate constants for key individual product channels are provided in a table for different T,P-conditions.

5. Development of the cavity ring-down spectrometer

A cavity ring-down spectrometer (CRDS) for studies of aromatic radicals has been constructed. A slit-jet supersonic expansion is used to cool the radicals, and thereby simplify their electronic spectra. The radicals are generated from stable precursor molecules using a pulsed discharge.

The first attempts to record the phenyl radical ${}^2B_1 - \tilde{X} {}^2A_1$ band system (near 505 nm) under jet-cooled conditions were carried out using a pulsed discharge in C₆H₆/He mixtures to generate radical species. At low discharge power, intense lines of metastable He were observed. The Swann bands of C₂ appeared when the discharge voltage was increased, but the phenyl bands were not detected. Fitting to the rotational line intensity distribution of the C₂ spectrum yielded a temperature of about 100 K, indicating that cold radical species could be generated using our discharge slit nozzle assembly. In the attempts to observe the spectrum of phenyl we carried out systematic variations of the nozzle source pressure, mole fraction of benzene, and discharge voltage. In a few experiments the He carrier gas was replaced by Ar or N₂. We also explored alternative precursor molecules including bromobenzene and nitrosobenzene. In all instances the only molecular species observed was C₂. Low energy discharges produced C₂ with rotational temperatures as low as 40K.

As a further test of the capabilities of the new apparatus, we repeated the measurements of Motylewski and Linnartz¹¹ on the ${}^2\Pi - X {}^2\Pi$ bands of linear C₆H. This radical was generated using a pulsed discharge in C₂H₂. These experiments were successful, and the rotational contours of the absorption bands were consistent with a rotational temperature of 30K.

Attempts were also made to observe the ${}^2B_1 - \tilde{X} {}^2B_1$ transition of the phenoxy radical near 390 nm. Compared to the phenyl ${}^2B_1 - \tilde{X} {}^2A_1$ transition, phenoxy has a much larger absorption cross-section ($7.7 \times 10^{-18} \text{ cm}^2$ vs. $<5 \times 10^{-19} \text{ cm}^2$). Again it was found that the discharge source was overly destructive. The N₂⁺ B-X bands were observed in absorption due to He* Penning ionization of background N₂.

III. Future work

We shall devote our effort to kinetic studies of phenylvinyl and naphthyl radical reactions with combustion species by CRDS and PLP/MS techniques. We will also attempt to theoretically interpret all experimentally measured data with particular emphasis on the elucidation of the mechanisms involved in the reactions studied. Quantum-chemical calculations will be performed with the G2M method¹² for systems containing 9 heavy atoms or less and with the hybrid density functional theory for systems larger than 10 heavy atoms. Rate constants for reactions occurring via long-lived intermediates will be predicted by RRKM theory, whereas those that take place by the direct metathetical mechanism will be calculated by TST, with tunneling corrections if necessary. Spectroscopic studies of these and other small aromatic radicals by CRDS in a molecular beam will be continued. Work is currently in progress to develop a less destructive radical source for work with aromatic radicals. Pulsed photolysis is known to be an effective way of generating these species, but the short duration radical pulses generated by excimer laser photolysis are not compatible with >10 μs ring-down times. Pulsed light sources with ms duration and flash pyrolysis nozzles are being evaluated. The results of the spectroscopic studies are expected to improve the diagnostics of the radicals such as the naphthyls. Once the instrument testing and development work has been completed, the first

objective will be studies of the phenyl radical. All experimental studies will be complemented by quantum chemical calculations to help elucidate the reaction mechanisms and spectroscopic data obtained.

IV. References (DOE publications denoted by *)

1. "Temperature and Pressure Effect on Formation and Decomposition of Phenylvinylperoxy Radicals in the $C_6H_5C_2H_2 + O_2$ Reaction," J. Park and M. C. Lin, *Proceedings of the Combustion Institute* 32 (2008) accepted.*
2. H. Richter, T. G. Benish, O. A. Mazyar, W. H. Green, and J. B. Howard, *Proceedings of the Combustion Institute*, 28:2609 (2002).
3. H. Richter, O. A. Mazyar, R. Sumathi, W. H. Green, J. B. Howard and J. W. Bozzelli, *J. Phys. Chem. A*, **105**:1561 (2001).
4. "Kinetics and Mechanism of the $C_{10}H_7 + O_2$ Reaction", J. Park and M. C. Lin, in preparation.*
5. N. M. Marinov, W. J. Pitz, C. K. Westbrook, A. M. Vincitore, M. J. Castaldi, S. M. Senkan, *Combustion and Flame* 114 192-213 (1998).
6. N. Kuniyoshi, M. Touda, S. Fukutani, *Combustion and Flame* 128:292-3000 (2002)
7. Chih-Wei Wu, Yuan-Pern Lee, Shucheng Xu and M. C. Lin, *J. Phys. Chem. A*, 111, 6693-6703 (2007).*
8. C.-W. Lu, S.-L. Chou, Y.-P. Lee, S.C. Xu, Z.F. Xu, M.C. Lin, *J. Chem. Phys.* 122:244314 (2005).*
9. A. C. Hansen, Q. Zhang, and P. W. L. Lyne, *Bioresource Tech.* **96**, 277 (2005)
10. S. C. Xu and M. C. Lin, *J. Phys. Chem. A*, 111, 6730-40 (2007).*
11. T. Motylewski and H. Linnartz, *Review of Scientific Instruments* 70, 1305, (1999).
12. A. M. Mebel, K. Morokuma and M. C. Lin, *J. Chem. Phys.*103:7414 (1995).

Other DOE Publications (2005-current) not mentioned in the text

1. "Ab initio kinetic prediction of branching rate constants for reactions of H atoms with CH_3O and CH_2OH " Kun Xu, Z. F. Xu, M. C. Lin, *Molecular Physics*, accepted.
2. Chien-Ming Tseng, Yuan T. Lee Ming-Fu Lin, Chi-Kung Ni, Suet-Yi Liu, Yuan-Pern Lee, Z. F. Xu and M. C. Lin, *J. Phys. Chem. A*, 111, 9463-70 (2007).
3. Binh Bui, Ti Jo Tsay, M. C. Lin and C. F. Melius, *Int. J. Chem. Kinet.*, 39, 580-90 (2007).
4. J. Park, I. V. Tokmakov, and M. C. Lin, *J. Phys. Chem. A*, 111, 6881-89 (2007).
5. Jee-Gong Chang, Hsin-Tsung Chen, Shucheng Xu and M.C. Lin, *J. Phys. Chem., A*, 111, 6789-97 (2007).
6. Ming-Fu Lin, Yuan T. Lee, Chi-Kung Ni, Shucheng Xu and M.C. Lin, *J. Chem. Phys.*, 126, 064310 (2007).
7. S. C. Chen, S. C. Xu, E. Diau, and M. C. Lin, *J. Phys. Chem. A*, 110 (33), 10130 -10134, 2006.
8. J. Park, G. J. Nam, I. V. Tokmakov, and M. C. Lin, *J. Chem. Phys. A* (2006), 110(28), 8729-8735.
9. G. Nam, I. V. Tokmakov, J. Park and M. C. Lin, *Proceedings of the Combustion Institute* 31 (2007) 249-256.
10. Shucheng Xu and M.C. Lin, *Proceedings of the Combustion Institute* 31 (2007) 159-166.
11. Shucheng Xu, R. S. Zhu and M. C. Lin, *Int. J. Chem. Kinet. Volume 38, Issue 5* (2006) 322-326.
12. Z. F. Xu and M. C. Lin, *J. Phys. Chem., A*, (2006), 110(4), 1672-1677.
13. Igor V. Tokmakov, Joonbum Park, Ming Chang Lin, *ChemPhysChem Volume 6, Issue 10*, 2075 - 2085, 2005.
14. Igor V. Tokmakov, Gap-Sue Kim, Vadim V. Kislov, Alexander M. Mebel and Ming C. Lin, *J. Phys. Chem. A*, 109 (27), 6114 - 6127, 2005.
15. Z. F. Xu and M. C. Lin, *Journal of Physical Chemistry A* (2005), 109(40), 9054-9060.
16. R. S. Zhu, J. Park, M. C. Lin, *Chem. Phys. Letter*, (2005), 408(1-3), 25-30.
17. Chih-Wei Lu, Shen-Long Chou, Yuan-Pern Lee, Shucheng Xu, Z. F. Xu and M. C. Lin, *J. Chem. Phys.*, (2005), 122(24), 244314/1-244314/11.
18. Shucheng Xu and M.C. Lin, *J. Phys. Chem. B* (2005), 109(17), 8367-8373.
19. Y. M. Choi and M. C. Lin, *Int. J. Chem. Kinet.* **39**, 261-74 (2005).

ADVANCED NONLINEAR OPTICAL METHODS FOR QUANTITATIVE MEASUREMENTS IN FLAMES

Principal Investigator: Robert P. Lucht
School of Mechanical Engineering, Purdue University, West Lafayette, IN 47907-2088
(Lucht@purdue.edu)

I. PROGRAM SCOPE

Nonlinear optical techniques such as laser-induced polarization spectroscopy (PS) and resonant wave mixing (RWM) are techniques that show great promise for sensitive measurements of transient gas-phase species, and diagnostic applications of these techniques are being pursued actively at laboratories throughout the world. Over the last few years we have also begun to explore the use of three-laser electronic-resonance-enhanced (ERE) coherent anti-Stokes Raman scattering (CARS) as a minor species detection method with enhanced selectivity. We have also initiated both theoretical and experimental efforts to investigate the potential of femtosecond (fs) laser systems for sensitive and accurate measurements in gas-phase media. Our initial efforts have focused on fs CARS.

The objective of this research program is to develop and test strategies for quantitative concentration measurements using nonlinear optical techniques in flames and plasmas. We are investigating the physics of these processes by direct numerical integration (DNI) of the time-dependent density matrix equations for the resonant interaction. Significantly fewer restrictive assumptions are required using this DNI approach compared with the assumptions required to obtain analytical solutions. Inclusion of the Zeeman state structure of degenerate levels has enabled us to investigate the physics of PS and of polarization effects in DFWM and ERE CARS. We have incorporated the effects of hyperfine structure in our numerical calculations of H-atom PS and resonant six-wave mixing (6WM). We are concentrating on the accurate simulation of two-photon processes, including Raman transitions, where numerous intermediate electronic levels contribute to the two-photon transition strength. The DNI numerical methods can be extended to the calculation of the interaction of laser pulses as short as 50 fs simply by decreasing the integration time step (for pulses shorter than this the rotating wave approximation will no longer be valid and the density matrix equations will need to include terms that are negligible for longer pulses).

During the last year we continued our numerical simulations of our high-resolution two-photon-induced laser-induced fluorescence (LIF) measurements of nitric oxide (NO). We have incorporated an effective intermediate electronic level in our calculations to account for the effects of the numerous intermediate electronic levels for the $A^2\Sigma^+-X^2\Pi$ two-photon resonances. We have also developed and demonstrated an optical parametric generator (OPG) system with pulsed dye amplification (PDA) for the generation of pulsed, tunable, single-axial-mode laser radiation. We demonstrated the OPG/PDA system by performing two-photon-absorption LIF measurements of atomic oxygen in $H_2/O_2/N_2$ counterflow nonpremixed flames. We also continued a detailed investigation of ERE CARS spectroscopy of nitric oxide, concentrating on a DNI analysis of saturation effects in the ERE CARS process. Finally, we have continued a detailed DNI analysis of the fs CARS process for gas-phase N_2 . The fs CARS signal for N_2 is very strong because of the efficient pumping of the Raman coherences by Fourier-transform-limited pump and Stokes pulses, and temperatures can be extracted from the fs CARS signal without any effect of collisions. In the last year we have demonstrated the acquisition of single-shot fs CARS signals from flames using a chirped pulse probe pulse following excitation of the Raman coherence using nearly Fourier-transform-limited pump and Stokes pulses. We are presently concentrating on the development

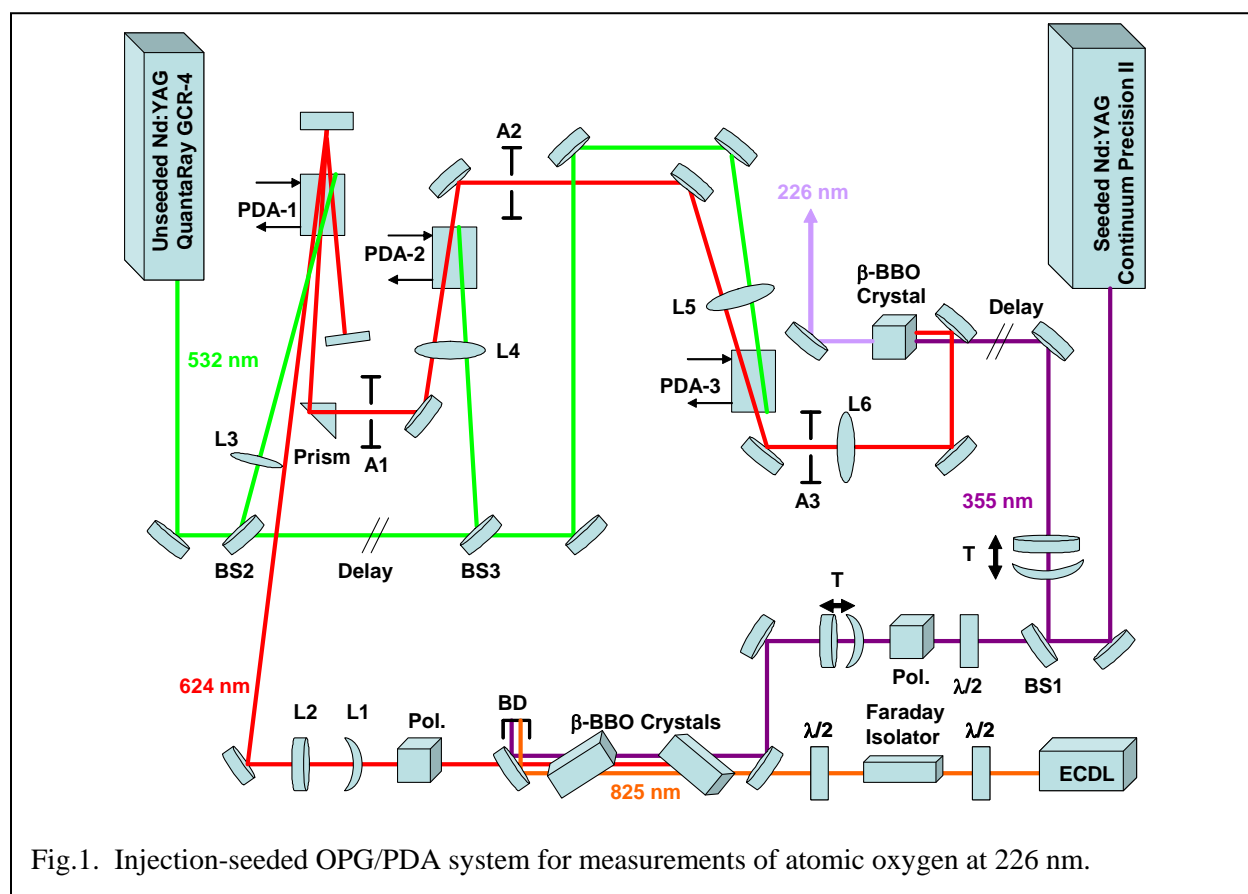
of analytical techniques for the accurate determination of temperature and species concentration from the chirped-pulse probe fs CARS signals.

II. RECENT PROGRESS

A. Development and Application of a High-Spectral-Resolution OPG/PDA System

We have worked extensively in the past few years on the development and application of tunable, high-resolution optical parametric systems. For example, we developed an optical parametric generator (OPG)/optical parametric amplifier (OPA) system and applied this system for two-photon-excited fluorescence of the NO molecule for both a single-beam configuration and a two-beam counterpropagating configuration. While this system worked well, it was difficult to align the four-crystal OPA and obtain both high output power and good beam quality. Over the past year we have developed pulsed dye amplifiers to amplify the output from either an injection-seeded OPG (no resonant cavity) or an injection-seeded optical parametric oscillator (OPO) with a resonant cavity at the signal wavelength. The OPG/PDA system is more complicated because several PDA stages are required for amplification of the low-power OPG output, as shown in Fig. 1. We are using diode lasers in the wavelength range from 760 nm to 1000 nm as injection seeding lasers for our OPG/PDA and OPO/PDA systems. The signal radiation from the OPG/OPOs can then be amplified using pulsed dye amplifiers with Rhodamine or DCM dyes. The use of PDAs has greatly simplified the alignment of the system and allowed us to optimize the beam quality of the amplified beams. A system of lenses and apertures was needed to reduce amplified spontaneous emission from the PDAs, however.

We have used the OPG/PDA system shown in Fig. 1 for measurements of atomic oxygen profiles in counterflow $H_2/O_2/N_2$ flames. This OP/PDA source technology will enhance greatly the potential for



quantitative application of nonlinear techniques such as PS, 6WM, dual-pump CARS, and ERE CARS spectroscopy. We plan to use these systems for PS and 6WM measurements of atomic oxygen and atomic hydrogen; this will require simultaneous operation of OPO/PDA and OPG/PDA systems at pump and probe wavelengths.

B. High-Resolution Two-Photon-Induced Fluorescence Spectroscopy of Nitric Oxide

Over the last couple of years we developed a DNI computer code for numerical simulation of this process and have investigated the saturation and Stark shifting of the two-photon line shape in detail. We have included Doppler broadening in our calculations, and these calculations can be completed in a reasonable amount of time on the Densitymatrix cluster. A single effective excited intermediate electronic level is used to account for the numerous intermediate electronic levels that can contribute to the two-photon absorption cross section. Last year we concentrated on refining our effective intermediate level model and now have obtained agreement to within an order of magnitude in terms of calculated and measured two-photon-absorption cross sections reported in the literature. Line strengths for our effective intermediate level are determined by comparing the experimental and theoretical laser intensities at which saturation and Stark shifting of the two-photon resonance transitions begin to occur.

C. Electronic-Resonance-Enhanced CARS Spectroscopy of Nitric Oxide

We have investigated the physics and explored the diagnostic potential of ERE CARS for measurements of NO [P1,P2,P4,P5,P6,P9]. The motivation for the work is to determine whether ERE CARS can be used to measure NO in high-pressure environments, where LIF measurements are very difficult because of interfering LIF signals from species such as O₂, H₂O, and CO₂. ERE CARS is inherently more selective because of the requirement for both electronic and Raman resonance for signal generation. During the last year we have developed a method of performing single-shot NO ERE CARS measurements using a broadband Stokes laser. We have obtained excellent agreement between experimental single-shot ERE CARS spectra and spectra calculated using the DNI numerical methods. As was discussed above in terms of two-photon NO LIF, an effective intermediate level is used in the DNI calculations to allow us to account for the numerous intermediate levels that contribute to the two-photon Raman cross section.

D. Femtosecond CARS Calculations

We used our DNI computational methods to perform a detailed investigation of the physics of fs CARS for gas-phase transitions [P7]. For Fourier-transform-limited pump and Stokes pulses, our calculations indicate that the Raman coherence can be excited to close its maximum value for pump and Stokes irradiances above 10¹⁷ W/m²; these irradiance levels can be achieved easily with current commercial fs laser systems. For Fourier-transform-limited laser pulses, the phase of the Raman coherence is the same for Q(J) transitions, regardless of J, right after the impulsive pump-Stokes excitation. Consequently, they all contribute to the creation of a giant Raman coherence that decays with time because the Q(J) transitions oscillate with different frequencies.

During the past year we have demonstrated the acquisition of single-shot fs CARS signals from nitrogen at atmospheric pressure in a gas cells at temperatures up to 900 K and from atmospheric pressure flames. The fs CARS signals are acquired using a 3-ps chirped-pulse probe beam to scatter from the Raman coherence induced by the 85-fs pump and Stokes beams. The resulting CARS signal is then spectrally resolved. Because of the probe chirp, the temporal dependence of the decay of the Raman coherence is mapped onto the spectrum of the fs CARS signal. The decay of the Raman coherence and hence the spectrum of the chirped-probe fs CARS signal is very sensitive to temperature. We are currently working on theoretical models of the chirped-probed fs CARS process so that we can extract

temperature from the experimental spectra by least-squares fitting of theoretical spectra, similar to the manner in which temperature is determined from ns CARS spectra.

III. FUTURE WORK

We plan to develop the capability for simultaneous operation of injection-seeded OPG/PDA and OPO/PDA systems. We will use the systems for two-color PS and 6WM measurements of atomic hydrogen and atomic oxygen. We plan to pursue further theoretical and experimental investigations of the ERE CARS process for NO, CH, and C₂H₂, especially at higher pressures where collisional narrowing may result in significant improvement in the detection limits. The DNI code for ERE CARS has been developed and will be used to explore the physics of the ERE CARS process. The different effects of saturation of the Raman transition and saturation of the ultraviolet probe transition will be investigated. Further theoretical investigations of the interaction of fs laser radiation with gas-phase resonances will be performed, and a computer code to extract temperature from single-shot, chirped-probe fs CARS signals will be developed. Our investigation of the physics of two-photon, two-color PS and 6WM for H-atom measurements will continue in collaboration with Tom Settersten at Sandia. We will continue to explore the physics of these processes using our DNI code.

IV. BES-SUPPORTED PUBLICATIONS 2006-2008

1. S. Roy, W. D. Kulatilaka, N. Chai, S. V. Naik, N. M. Laurendeau, R. P. Lucht, J. P. Kuehner, and J. R. Gord, "Effect of Quenching on Electronic-Resonance-Enhanced CARS of Nitric Oxide," *Appl. Phys. Lett.* **89**, 104105 (2006).
2. W. D. Kulatilaka, N. Chai, S. V. Naik, N. M. Laurendeau, R. P. Lucht, J. P. Kuehner, S. Roy, and J. R. Gord, "Measurement of Nitric Oxide Concentrations in Flames Using Electronic-Resonance-Enhanced Coherent Anti-Stokes Raman Scattering," *Opt. Lett.* **31**, 3357-3359 (2006).
3. W. D. Kulatilaka, R. P. Lucht, S. Roy, J. R. Gord, and T. B. Settersten, "Detection of Atomic Hydrogen in Flames Using Two-Color Two-Photon-Resonant Six-Wave-Mixing Spectroscopy," *Applied Optics* **46**, 3921-3927 (2007).
4. N. Chai, W. D. Kulatilaka, S. V. Naik, N. M. Laurendeau, R. P. Lucht, J. P. Kuehner, S. Roy, and J. R. Gord, "Nitric Oxide Concentration Measurements in Atmospheric Pressure Flames using Electronic-Resonance-Enhanced Coherent Anti-Stokes Raman Scattering" *Applied Physics B* **88**, 141-150 (2007).
5. W. D. Kulatilaka, N. Chai, S. V. Naik, S. Roy, N. M. Laurendeau, R. P. Lucht, J. P. Kuehner, and J. R. Gord, "Effects of Pressure Variations on Electronic-Resonance-Enhanced Coherent Anti-Stokes Raman Scattering of Nitric Oxide," *Optics Communications* **274**, 441-446 (2007).
6. N. Chai, W. D. Kulatilaka, S. V. Naik, N. M. Laurendeau, R. P. Lucht, S. Roy, and J. R. Gord, "Detection of Acetylene by Electronic-Resonance-Enhanced Coherent Anti-Stokes Raman Scattering" *Applied Physics B* **87**, 731-737 (2007).
7. R. P. Lucht, P. J. Kinnius, S. Roy, and J. R. Gord, "Theory of Femtosecond Coherent Anti-Stokes Raman Scattering for Gas-Phase Transitions," *Journal of Chemical Physics* **127**, 044316 (2007).
8. S. V. Naik, J. Hwang, R. P. Lucht, and N. M. Laurendeau, "Measurement and Calculation of the Q-Branch Spectrum of Nitrogen Using Inverse Raman Spectroscopy and cw Raman-Induced Polarization Spectroscopy," *Journal of Raman Spectroscopy* **39**, 68-78 (2008).
9. J. P. Kuehner, W. D. Kulatilaka, N. Chai, S. V. Naik, N. M. Laurendeau, R. P. Lucht, A. Patnaik, M. O. Scully, S. Roy, and J. R. Gord, "Perturbative Theory and Modeling of Electronic-Resonance-Enhanced Coherent Anti-Stokes Raman Scattering Spectroscopy of Nitric Oxide," *Journal of Chemical Physics*, accepted for publication (2008).

Time-Resolved Infrared Absorption Studies of Radical Reactions

R. G. Macdonald
Chemistry Division
Argonne National Laboratory
Argonne, IL 60439
Email: rgmacdonald@anl.gov

Background

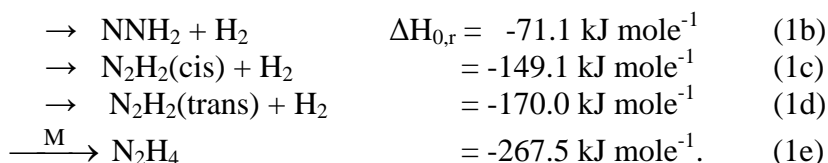
Information about the dynamics of radical-radical reactions is sparse. However, these processes are important in combustion being either chain propagating or terminating steps as well as potentially producing new molecular species. For almost all radical-radical reactions, multiple product channels are possible, and the determination of product channels will be a central focus of this experimental effort. Two approaches will be taken to study radical-radical reactions. In the first, one of the species of interest will be produced in a microwave discharge flow system with a constant known concentration and the second by pulsed-laser photolysis of a suitable photolyte. The rate constant will be determined under pseudo-first order conditions. In the second approach, both transient species will be produced by the same photolysis laser pulse, and both followed simultaneously using two different continuous-wave laser sources. This approach allows for the direct determination of the second-order rate constant under any concentration conditions if the appropriate absorption cross sections have been measured. In both approaches, the time dependence of individual ro-vibrational states of the reactants and/or products will be followed by frequency- and time-resolved absorption spectroscopy. In order to determine branching ratios and second-order rate constants, it is necessary to measure state-specific absorption coefficients and transition moments of radicals. These measurements will play an important role in this experimental study.

Recent Results

$\text{NH}_2(\text{X}^2\text{B}_1) + \text{NH}_2(\text{X}^2\text{B}_1)$. The NH_2 radical is an important intermediate in the production of NO_x in combustion and the removal of NO_x from combustion exhaust gases. The removal processes are based on the addition of NH_3 , $(\text{HOCN})_3$ or $(\text{NH}_2)_2\text{CO}$ to the gas stream, resulting in the ThermalDe NO_x , RAPRE NO_x and NO_xOUT treatment processes, respectively. A key reaction in these processes is the $\text{NH}_2 + \text{NO}$ reaction. The NH_2 radical also plays a key role in the pyrolysis of NH_3 . However, in spite of its importance, the chemistry of the NH_2 radical, especially in reactions with other radicals, has not been widely studied. As the first step in investigating the chemistry of NH_2 with other radicals, a study of the self-reaction of NH_2 at low pressure and a temperature of 293K was undertaken.

Although NH_2 is isoelectronic with $\text{OH}(\text{X}^2\Pi)$, it does not possess electronic angular momentum and this greatly reduces the number of participating potential energy surfaces. There is only a triplet and singlet spin manifold correlating to the $\text{NH}_2 + \text{NH}_2$ asymptote. Still, there are a number possible product channels:





At 293 K, only the exothermic channels will contribute significantly to the reaction products, and the first reaction channel is neglected. Only channel 1a correlates to the triplet spin manifold and for many years was assumed the main disproportionation product channel. However, recent theoretical calculations indicate that the rate constant for this channel is less than $5.0 \times 10^{-15} \text{ cm}^3 \text{ molecules}^{-1} \text{ s}^{-1}$ at 293 K (Z.-F. Xu, D.-C. Fang and X.-Y. Fu, *Int. J. Quantum Chem.* **70**, 321 (1998)). The other disproportionation channels, 1b to 1d, involve the production of an isomer of N_2H_2 and H_2 as products. The N_2H_2 product was identified in a low pressure flow tube experiment using mass spectrometric detection (N. Stothard, R. Humpfer, and H.-H. Grotheer, *Chem. Phys. Lett.* **240**, 474 (1995)). The rate constant for this two body process was reported to be $(1.3 \pm 0.5) \times 10^{-12} \text{ cm}^3 \text{ molecules}^{-1} \text{ s}^{-1}$, in good agreement with earlier studies on reaction 1.

In the present investigation, the NH_2 radical was created by the 193 nm photolysis of NH_3 dilute in CF_4 . Temporal concentration profiles of both NH_3 and NH_2 were recorded simultaneously using time- and frequency-resolved absorption spectroscopy following the photolysis laser pulse. The NH_2 radical was monitored using rotational lines of the vibrational band of the $\text{NH}_2(\text{A}^2\text{A}_1) \leftarrow (\text{X}^2\text{B}_1) (070) \leftarrow (000)$ electronic transition near 675 nm. The NH_3 molecule was monitored using a rotational transition of the $\nu_1 + \nu_3$ combination band at 1494.358 nm, identified as ${}^1\text{R}(6)_{6s/a}$ (L. Lundsberg-Nielsen, F. Hegelund and F. M. Nicolaisen, *J. Mol. Spect.* **162**, 230 (1993)). The absorption coefficient of this NH_3 feature was determined in separate experiments using following mixtures of Ar and NH_3 or under static conditions from premixed gas fills. The peak absorption coefficient for the NH_2 transition was determined from the initial depletion of NH_3 assuming the quantum yield for NH_2 production was one.

Reaction 1 was studied in dilute NH_3/CF_4 mixtures from 2 to 10 Torr and in $\text{NH}_3/\text{CF}_4/\text{Ar}$ and $\text{NH}_3/\text{CF}_4/\text{N}_2$ mixtures from 3 to 10 Torr. At these low pressures, reaction 1e is in the pure three-body regime, and the influence of different third bodies on k_{1e} was determined. At a given pressure, the total production rate for products, k_T , is given by $k_T = k_0 + k_{1e}[\text{M}][\text{NH}_2]^2$. The sum of the disproportionation rate constants, k_0 , is the intercept of a plot of k_T vs third body pressure. For every experimental condition, the photolysis laser fluence was varied by at least a factor of five and generally covered the range 3 - 15 mJ/cm^2 . The total rate constant was determined by minimizing the sum of squares of the residuals between the experimental and model predicted NH_2 concentration profiles. The first-order loss of NH_2 by diffusion from the photolysis region was an important removal process. The recovery of the NH_3 concentration following the photolysis laser pulse was dominated by diffusion of NH_3 into the photolysis region, and was used as an initial estimate in the determination of $k_{\text{diff}}^{\text{NH}_2}$.

It is known that the production of NH_2 from the 193 nm photolysis of NH_3 produces NH_2 radicals with a highly excited internal state distribution. The use of CF_4 as a collision partner provided rapid rotational and vibrational relaxation of both NH_2 and NH_3 . This is illustrated in figure 1 where the influence of the variation in the partial

pressure of CF₄ from 0 to 0.44 Torr is shown. As shown in panels a and b, without CF₄ the internal state distributions for both NH₂ and NH₃ are highly perturbed and require 100's of microseconds to recover. Panels c and d only show the concentration profiles for NH₂ with increasing P_{CF₄}. With just 0.1 Torr of CF₄, the transient on the NH₃ profile was quenched. The solid curves are the model generated concentration profiles for the best-fit values of k_T given in the text boxes. Within the scatter of the data, the determination of k_T was independent of P_{CF₄} in experiments with Ar and N₂, except the contribution by recombination with CF₄. There was little contribution to the production or removal of NH₃ by reactions, and the temporal dependence of the NH₃ was almost entirely due to replenishment by diffusion. The NH₃ profile was fit to a single exponential.

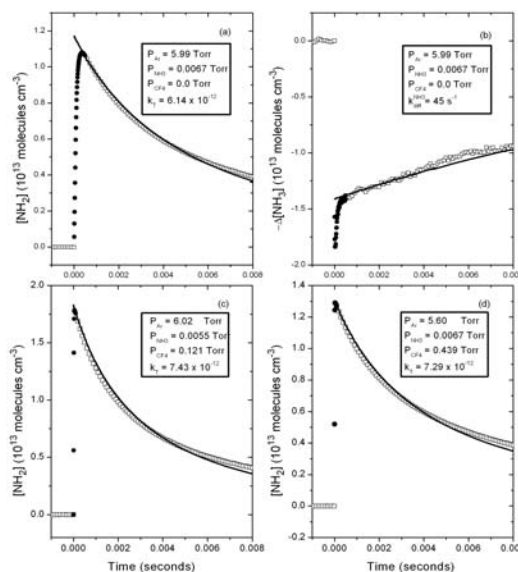


Figure 1. The relaxation of NH₂ and NH₃ internal energy as a function of P_{CF₄}. The conditions were similar for each panel. The filled circles, •, show every data point and the open squares, ◻, every tenth point. Panels a and b were recorded simultaneously. Note the relaxation time for NH₂ and NH₃ are similar.

The results of this work are summarized in the Table.

Collision Partner	k ₀ x 10 ⁻¹³ a	k _{1e} x 10 ⁻²⁹ b
CF ₄	(6.2 ± 8.8) ^c	(8.04 ± 0.46)
Ar	(0 ± 7.5)	(3.94 ± 0.37)
N ₂	(3.9 ± 1.63)	(5.69 ± 0.73)

a) units: cm³ molecules⁻¹ s⁻¹

b) units: cm⁶ molecules⁻² s⁻¹

c) uncertainties: ± 2σ

Although previous studies of reaction 1 have found a k₀ to be around 1.5 x 10⁻¹² cm³ molecules⁻¹ s⁻¹, the results of this work indicate a smaller value. However, within the scatter of the data the present experiments agree with the previous measurements, and do not provide a more definitive determination of k₀. Preliminary explorations of the NH₂ + NH₂ potential energy surface at the G3B3 level of theory by Larry Harding suggest that the bimolecular product channels, 1b to 1d, are separated from the reactants by substantial energy barriers. Thus, near room temperature k₀ should be small in agreement with the estimates determined in this work.

Future Work

Work is planned to extend the study of the self-reactions of OH and NH₂ radicals to higher pressures. The direct detection of recombination products, H₂O₂ and N₂H₄, may provide information on the magnitude of the two-body collision processes. Also, studies of the NH₂ radical with NO and OH are planned.

Publications 2006-present.

Determination of the rate constant for the $\text{NCO}(X^2\Pi) + \text{CH}_3(X^2A_2'')$ reaction at 293 K and an estimate of possible product channels.

-Y. Gao and R. G. Macdonald

J. Phys. Chem. **110A**, 977-989 (2006).

Determination of the rate constant for the $\text{OH}(X^2\Pi) + \text{OH}(X^2\Pi) \rightarrow \text{O}(^3P) + \text{H}_2\text{O}$ reaction over the temperature range 293-373 K.

-Mi-Kyung Bahng and R. G. Macdonald

J. Phys. Chem. **111A**, 3850-3861 (2007).

Determination of the rate constant and product channels for the radical-radical reaction $\text{NCO}(X^2\Pi) + \text{C}_2\text{H}_5(X^2A_2'')$ at 293 K.

-R. G. Macdonald

Phys. Chem. Chem. Phys. **9**, 4301-4314 (2007).

Theoretical studies of chemical reactions related to the formation and growth of polycyclic aromatic hydrocarbons and molecular properties of their key intermediates

Alexander M. Mebel

Department of Chemistry and Biochemistry, Florida International University
Miami, Florida 33199. E-mail: mebel@fiu.edu

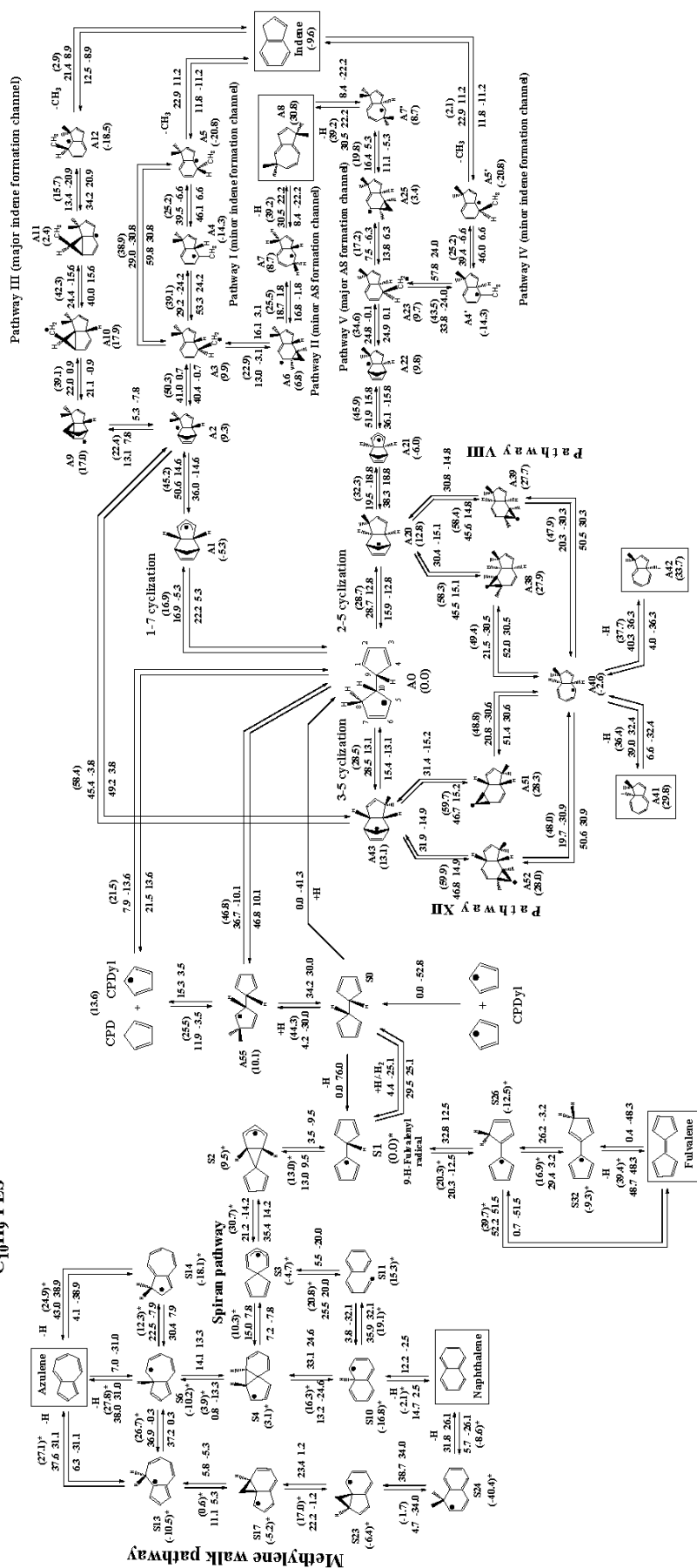
Program Scope. We perform theoretical studies of the reactions of PAH formation and growth using ab initio molecular orbital and density functional calculations of potential energy surfaces and statistical (RRKM and TST) computations of absolute rate constants and relative product yields. In particular, we address the reactions of cyclopentadienyl radicals and cyclopentadiene involving the C₁₀H₁₁, C₁₀H₁₀, and C₁₀H₉ PES and producing naphthalene, azulene, fulvalene, and indene and also investigate the formation mechanisms of naphthalene and indene from smaller hydrocarbons, alternative to the HACA sequences. Our studies additionally include related chemical reactions under single-collision conditions, such as crossed molecular beam reactions of singlet and triplet C₂ with C₄H₆ isomers and C₆H₆ accessing previously unexplored regions of the C₆H₆ (benzene) and C₈H₆ (phenylacetylene) surfaces and the reactions of phenyl radical with C₃H₄, C₃H₆, and C₄H₆ occurring on the C₉H₉, C₉H₁₁, and C₁₀H₁₁ PES and directly linked to the indene, naphthalene, and azulene formation routes. The objective of these studies is to untangle elementary reaction mechanisms for these complex reactions and to predict their rate constants and product yields in a broad range of reaction conditions.

Recent Progress

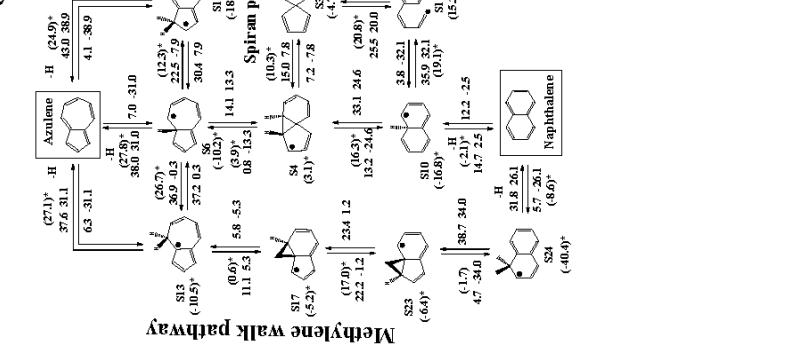
Prediction of product branching ratios in the C(³P) + C₂H₂ → l-C₃H + H / c-C₃H + H / C₃ + H₂ reaction using ab initio coupled clusters calculations extrapolated to the complete basis set combined with RRKM and radiationless transition theories. CCSD(T) calculations of intermediates and transition states on the singlet and triplet C₃H₂ potential energy surfaces extrapolated to the CBS limit were combined with statistical computations of energy-dependent rate constants of the C(³P) + C₂H₂ reaction under crossed molecular beam conditions. RRKM theory was applied for isomerization and dissociation steps within the same multiplicity and radiationless transition and non-adiabatic transition state theories were used for singlet-triplet intersystem crossing rates. The calculated rate constants are utilized to predict product branching ratios. The results demonstrated that, in agreement with experiment, c-C₃H + H and C₃ + H₂ are the most probable products at low collision energies and l-C₃H + H dominate at higher E_c.

Ab initio and RRKM study of photodissociation of 1,3,5-triazine. Reaction pathways leading to various decomposition products in photodissociation of 1,3,5-triazine have been mapped out at the G3//B3LYP level and then the RRKM and microcanonical variational transition state theories have been applied to compute rate constants for individual reaction steps. The results show that after being excited by 275, 248, or 193 nm photons, triazine isomerizes to an opened-ring structure on the first singlet excited state PES, which is followed by relaxation into the ground electronic state via internal conversion. On the contrary, excitation by the 285 and 295 nm photons cannot initiate the ring opening reaction on the excited state PES, and the molecule relaxes into the energized ring isomer in the ground state. The dissociation reaction starting from the ring isomer is calculated to have product branching ratios rather different from those for the reaction initiating from the opened-ring structure. The existence of two distinct mechanisms of 1,3,5-triazine photodissociation can explain the inconsistency in the translational energy distributions of HCN moieties at different wavelengths observed experimentally.

C₁₀H₁₁ PES



C₁₀H₉ PES



An *ab initio* G3-type / statistical theory study of the formation of indene in combustion flames.

The pathways originated from reactions of cyclic C₅ species – cyclopentadiene and cyclopentadienyl radical.

Chemically accurate *ab initio* Gaussian-3-type calculations of various rearrangements on the C₁₀H₁₁ potential energy surface have been performed to investigate the indene formation mechanism originated from the reactions of two abundant cyclic C₅ species, cyclopentadiene and cyclopentadienyl radical. Using the accurate *ab initio* data statistical theory calculations have been applied to obtain high-pressure limit thermal rate constants within the 300-3000 K temperature range, followed by calculations of relative product yields. Totally twelve reaction pathways leading to indene and several azulene precursors, 1,5-, 1,7-, 1,8a-, and 1,3a-dihydroazulene, have been mapped out and the relative contributions of each pathway to the formation of reaction products have been estimated. At temperatures relevant to combustion, the indene has been found as the major reaction product (>50%) followed by 1,5-dihydroazulene (25-35%), whereas all other products demonstrate either minor or negligible yields. The results of the present study have been combined with our previous data for rearrangements of 9-H-fulvalenyl radical on the C₁₀H₉ potential energy surface to draw

the detailed picture of radical-promoted reaction mechanisms leading from c-C₅ species to the production of indene, naphthalene, azulene, and fulvalene in combustion. The suggested mechanism and computed product yields are consistent with the experimental data obtained in low-temperature pyrolysis of cyclopentadiene, where indene and naphthalene have been found as the major reaction products.

Future Plans

We will continue theoretical studies of the reactions of cyclopentadienyl radicals and cyclopentadiene involving the C₁₀H₁₁ and C₁₀H₁₀ PES and synthesizing naphthalene, azulene, fulvalene, or indene. The emphasis will be on yet unexplored pathways on the C₁₀H₁₁ surface and detailed investigation of C₁₀H₁₀. In particular, if 9,10-dihydrofulvalene formed by the recombination of two C₅H₅ radicals does not lose an H atom immediately, it may eventually rearrange to 9,10-dihydronaphthalene, whereas the latter may produce naphthalene either by four-center 9,10-H₂ loss or via two consecutive H eliminations. The mechanism of the 9,10-dihydrofulvalene – 9,10-dihydronaphthalene isomerization may involve the formation of a tricyclic intermediate, which then ring-opens to a ten-member cyclic structure rearranging in turn to 9,10-dihydronaphthalene. Other possibilities will be also considered including alternative H₂ elimination pathways. The competitiveness of the H₂ loss as compared to two sequential H elimination or abstraction reactions needs further careful investigation.

A systematic survey of chemical reactions potentially leading to the formation of indene in combustion flames, such as C₇/C₂ (toluene + C₂H₂), C₆/C₃ (benzene, fulvene, or phenyl + C₃H₃, and phenyl + allene C₃H₄), C₅/C₂ (cyclopentadienyl + 2C₂H₂), C₅/C₄ (cyclopentadienyl + vinylacetylene), C₆/C₄ (phenyl + C₄H₆ isomers, benzene + C₄H₅), and naphthalene + O₂, will also be pursued.

DOE/BES sponsored publications (2006-2008)

1. A. M. Mebel, V. V. Kislov, R. I. Kaiser, “Potential energy surface and product branching ratios for the reactions of dicarbon C₂(X¹Σ_g⁺) with methylacetylene, CH₃CCH(X¹A₁): An ab initio/RRKM study”, *J. Phys. Chem. A* 110, 2421 (2006).
2. Y. A. Dyakov, A. M. Mebel, S. H. Lin, Y. T. Lee, C. K. Ni, “Acetylene elimination in photodissociation of neutral azulene and its cation: An ab initio and RRKM study”, *J. Chin. Chem. Soc.* 53, 161 (2006).
3. Y. A. Dyakov, C. K. Ni, S. H. Lin, Y. T. Lee, A. M. Mebel, “Ab initio and RRKM study of photodissociation of azulene cation”, *Phys. Chem. Chem. Phys.* 12, 1404 (2006).
4. Y. Guo, X. Gu, F. Zhang, A. M. Mebel, R. I. Kaiser, “Unimolecular decomposition of chemically activated pentatetraene (H₂CCCCCH₂) intermediates – a crossed beams study of dicarbon molecule reactions with allene”, *J. Chem. Phys.*, 110, 10699 (2006).
5. X. Gu, Y. Guo, A. M. Mebel, R. I. Kaiser, Chemical dynamics of the formation of the 1,3-butadiynyl radical (C₄H(X²Σ⁺)) and its isotopomers, *J. Phys. Chem. A*, 110, 11265 (2006).
6. A. M. Mebel, V. V. Kislov, R. I. Kaiser, “Ab initio/RRKM study of the singlet C₄H₄ potential energy surface and of the reactions of C₂(X¹Σ_g⁺) with C₂H₄(X¹A_{1g}⁺) and C(¹D) with C₃H₄ (allene and methylacetylene)”, *J. Chem. Phys.*, 125, 133113 (2006).
7. Y. Guo, X. Gu, F. Zhang, A. M. Mebel, R. I. Kaiser, “Reaction dynamics of carbon bearing radicals in circumstellar envelopes of carbon stars”, *Faraday Discuss.*, 133, 245 (2006).
8. X. Gu, Y. Guo, F. Zhang, A. M. Mebel, R. I. Kaiser, “A crossed molecular beam study of the reaction of dicarbon molecules with benzene – identification of the phenylethynyl radical (C₆H₅CC; X²A’)”, *Chem. Phys. Lett.*, 436, 7 (2007).

9. V. V. Kislov, A. M. Mebel, "An ab initio G3-type / statistical theory study of the formation of indene in combustion flames. I. The pathways involving benzene and phenyl radical", *J. Phys. Chem. A*, 111, 3922-3931 (2007).
10. Y. Guo, X. Gu, F. Zhang, A. M. Mebel, R. I. Kaiser, "A crossed molecular beam study on the formation of hexenediynyl radical ($\text{H}_2\text{CCCCCCH}$; C_6H_3 (X^2A')) via reactions of tricarbon molecules, $\text{C}_3(X^1\Sigma_g^+)$ with allene (H_2CCCH_2 ; X^1A_1) and methylacetylene (CH_3CCH ; X^1A_1)", *Phys. Chem. Chem. Phys.*, 16, 1972-1979 (2007).
11. A. M. Mebel, G.-S. Kim, V. V. Kislov, R.I. Kaiser, "The reaction of tricarbon with acetylene: An ab initio/RRKM study of the potential energy surface and product branching ratios", *J. Phys. Chem. A*, 111, 6704-6712 (2007).
12. A. M. Mebel, V. V. Kislov, R. I. Kaiser, "Theoretical studies of potential energy surfaces and product branching ratios for the reactions of C_2 with small unsaturated hydrocarbons (acetylene, ethylene, methylacetylene, and allene)", in *Modern Gas Phase Molecular Dynamics*, K. C. Lin, P. D. Kleiber, Eds., Transworld Research Network, Kerala, India, 113-159 (2007).
13. X. Gu, Y. Guo, F. Zhang, A. M. Mebel, R. I. Kaiser, "A crossed molecular beams study on the formation and energetics of the resonantly stabilized free $i\text{-C}_4\text{H}_3(X^2A')$ radical and its isotopomers", *Chem. Phys.*, 335, 95-108 (2007).
14. L. Yao, A. M. Mebel, H. F. Lu, H. J. Nausser, S. H. Lin, "Anharmonic effect on unimolecular reactions with application to the photodissociation of ethylene", *J. Phys. Chem. A*, 111, 6722-6729 (2007).
15. Y. Guo, A. M. Mebel, F. Zhang, X. Gu, R. I. Kaiser, "Crossed molecular beam studies of the reactions of allyl radicals, $\text{C}_3\text{H}_5(X^2A_1)$, with methylacetylene ($\text{CH}_3\text{CCH}(X^1A_1)$), allene ($\text{H}_2\text{CCCH}_2(X^1A_1)$), and their isotopomers", *J. Phys. Chem. A*, 111, 4914-4921 (2007).
16. A. M. Mebel, V. V. Kislov, M. Hayashi, "Prediction of product branching ratios in the $\text{C}(^3P) + \text{C}_2\text{H}_2 \rightarrow i\text{-C}_3\text{H} + \text{H}/c\text{-C}_3\text{H} + \text{H}/\text{C}_3 + \text{H}_2$ reaction using ab initio coupled clusters/complete basis set calculations combined with RRKM and radiationless transition theories", *J. Chem. Phys.*, 126, 204310, 11 pp. (2007).
17. X. Gu, Y. Guo, F. Zhang, A. M. Mebel, R. I. Kaiser, "Unimolecular decomposition of chemically activated singlet and triplet D3-methyldiacetylene molecules", *Chem. Phys. Lett.*, 444, 220-225 (2007).
18. V. V. Kislov, Mebel A.M., "The formation of naphthalene, azulene, and fulvalene from the recombination product of two cyclopentadienyl radicals: An ab initio/RRKM study of rearrangements of the $\text{C}_5\text{H}_5\text{-C}_5\text{H}_4$ (9-H-fulvalenyl) radical", *J. Phys. Chem. A*, 111, 9532-9543 (2007).
19. Y. A. Dyakov, A. M. Mebel, S. H. Lin, Y. T. Lee, C.-K. Ni, "Photodissociation of 1,3,5-triazine: An ab initio and RRKM study", *J. Phys. Chem. A*, 111, 9591-9599 (2007).
20. X. Gu, Y. Guo, A. M. Mebel, R. I. Kaiser, "A crossed beam investigation of the reactions of tricarbon molecules, $\text{C}_3(X^1\Sigma_g^+)$, with acetylene, $\text{C}_2\text{H}_2(X^1\Sigma_g^+)$, ethylene, $\text{C}_2\text{H}_4(X^1A_g)$, and benzene, $\text{C}_6\text{H}_6(X^1A_{1g})$ ", *Chem. Phys. Lett.*, 449, 44-52 (2007).
21. Kislov V.V., Mebel A.M., "An ab initio G3-type / statistical theory study of the formation of indene in combustion flames. II. The pathways originated from reactions of cyclic C_5 species - cyclopentadiene and cyclopentadienyl Radical", *J. Phys. Chem. A*, 112, 700-716 (2008).
22. Gu X., Kaiser R.I., Mebel A.M., "Chemistry of energetically activated cumulenes – from allene (H_2CCCH_2) to hexapentaene ($\text{H}_2\text{CCCCCCH}_2$)", *ChemPhysChem*, 9, 350-369 (2008).

FLASH PHOTOLYSIS-SHOCK TUBE STUDIES

Joe V. Michael

Gas Phase Chemical Dynamics Group, Chemistry Division
Argonne National Laboratory, Argonne, IL 60439
E-mail: jmichael@anl.gov

The scope of the program is to measure high-temperature thermal rate constants for use in high-temperature combustion with the reflected shock tube technique. As described earlier, we have used a multi-pass optical system for detecting OH-radicals.¹ The new configuration is similar to that described previously.²⁻⁴

During the past year, the reflected shock tube technique using OH-radical absorption at 308 nm has been used to study two thermal decompositions and thirteen bimolecular reactions at path lengths ranging from 1.75 to 7.00 m with $[\text{OH}]_t$ being determined from measured absorbance through an earlier determination¹ of the absorption cross-section at 308 nm ($\sigma_{\text{OH}} = (4.516 - 1.18 \times 10^{-3} T) \times 10^{-17} \text{ cm}^2 \text{ molecule}^{-1}$). The present optical configuration gives an S/N ratio of one at $\sim 1.0 \times 10^{12} \text{ radicals cm}^{-3}$.

The reflected shock tube technique with multi-pass absorption spectrometric detection (at a total path length of 1.75 m) of OH-radicals at 308 nm has been used to study the dissociation of CF_3 -radicals [$\text{CF}_3 + \text{Kr} \rightarrow \text{CF}_2 + \text{F} + \text{Kr}$ (a)] between 1803 and 2204 K at three pressures between ~ 230 to 680 Torr.⁵ The OH-radical concentration buildup resulted from the fast reaction, $\text{F} + \text{H}_2\text{O} \rightarrow \text{OH} + \text{HF}$ (b). Hence, OH is a marker for F-atoms. To extract rate constants for (a), the [OH] profiles were modeled with a chemical mechanism. The initial rise in [OH] was mostly sensitive to reactions (a) and (b), but the long time values were additionally affected by $\text{CF}_2 + \text{OH} \rightarrow \text{CF}_2\text{O} + \text{H}$ (c). Over the temperature range, rate constants for (a) and (c) were determined from the mechanistic fits to be $k_{\text{CF}_3+\text{Kr}} = 4.61 \times 10^{-9} \exp(-30020 \text{ K}/T)$ and $k_{\text{CF}_2+\text{OH}} = (1.6 \pm 0.6) \times 10^{-11}$, both in units of $\text{cm}^3 \text{ molecule}^{-1} \text{ s}^{-1}$. Reaction (a), its reverse recombination reaction (-a), and reaction (c) have also been studied theoretically. Reactions (c) and (-a) were studied with direct CASPT2 variable reaction coordinate transition state theory. A master equation analysis for reaction (a) incorporating the ab-initio determined reactive flux for reaction (-a) suggests that this reaction is close to but not quite at the low-pressure limit for the experimentally studied pressures. In contrast, reaction (c) is predicted to be in the high-pressure limit due to the high exothermicity of the products. A comparison with past and present experimental results demonstrates good agreement between the theoretical predictions and the present data for both (a) and (c).

Rate constants for H-atom abstractions by OH radicals from a series of alkanes (propane, n-butane, iso-butane and neo-pentane) have been measured at high temperatures using first-order analysis of the decaying [OH].⁶ The experiments represent the first direct measurements of these rate constants at $T > 1000 \text{ K}$ and span a wide T-range, 797-1259 K.

This work utilized 80 optical passes corresponding to a total path length of $\sim 7\text{m}$. As a result of this increased path length, the high [OH] detection sensitivity permitted pseudo-first-order analysis for unambiguously measuring the total rate constants. An [OH] profile, sensitivity analysis, and corresponding first-order plot are shown in Figs. 1-3 for a typical experiment with neo-pentane at 1094 K. The experimental rate constants for the

four alkanes can be represented in Arrhenius form as,

$$k_{\text{C}_3\text{H}_8+\text{OH}} = 6.671 \times 10^{-11} \exp(-1543 \text{ K/T}) \text{ cm}^3 \text{ molecule}^{-1} \text{ s}^{-1} \text{ (797-1248 K)} \quad (1)$$

$$k_{\text{n-C}_4\text{H}_{10}+\text{OH}} = 9.674 \times 10^{-11} \exp(-1569 \text{ K/T}) \text{ cm}^3 \text{ molecule}^{-1} \text{ s}^{-1} \text{ (800-1236 K)} \quad (2)$$

$$k_{\text{i-C}_4\text{H}_{10}+\text{OH}} = 9.114 \times 10^{-11} \exp(-1654 \text{ K/T}) \text{ cm}^3 \text{ molecule}^{-1} \text{ s}^{-1} \text{ (846-1221 K)} \quad (3)$$

$$k_{\text{neo-C}_5\text{H}_{12}+\text{OH}} = 1.060 \times 10^{-10} \exp(-1947 \text{ K/T}) \text{ cm}^3 \text{ molecule}^{-1} \text{ s}^{-1} \text{ (841-1259 K)} \quad (4)$$

The present results have been combined with prior lower-T measurements to generate three parameter rate expressions that adequately represent the available direct measurements (within 25%) over a wide temperature regime (250-1250 K). High level ab-initio electronic structure theory computations of the molecular properties of reactants, products, and transition states have then been used to estimate theoretical rate constants with conventional transition state theory (CTST), giving,

$$k_{\text{C}_3\text{H}_8+\text{OH}, \text{Theory}} = 6.678 \times 10^{-20} T^{2.74} \exp(309 \text{ K/T}) \text{ cm}^3 \text{ molecule}^{-1} \text{ s}^{-1} \text{ (250-2000 K)} \quad (5)$$

$$k_{\text{n-C}_4\text{H}_{10}+\text{OH}, \text{Theory}} = 2.594 \times 10^{-19} T^{2.575} \exp(428 \text{ K/T}) \text{ cm}^3 \text{ molecule}^{-1} \text{ s}^{-1} \text{ (250-2000 K)} \quad (6)$$

$$k_{\text{i-C}_4\text{H}_{10}+\text{OH}, \text{Theory}} = 1.605 \times 10^{-20} T^{2.912} \exp(617 \text{ K/T}) \text{ cm}^3 \text{ molecule}^{-1} \text{ s}^{-1} \text{ (250-2000 K)} \quad (7)$$

$$k_{\text{neo-C}_5\text{H}_{12}+\text{OH}, \text{Theory}} = 2.473 \times 10^{-19} T^{2.560} \exp(162 \text{ K/T}) \text{ cm}^3 \text{ molecule}^{-1} \text{ s}^{-1} \text{ (250-2000 K)} \quad (8)$$

The theoretical rate constants are excellent representations of the available experimental data (deviations less than 25%) and thereby offer a reliable method for extrapolation to higher-T as well as for extracting branching ratios for primary, secondary and tertiary abstractions.

Cycloalkanes represent an important class of saturated hydrocarbons that are present in significant amounts in diesel and jet fuels. Fuels derived from emerging sources of synthetic crude such as oil-shale/tar-sands are expected to yield increasingly higher amounts of these cycloalkanes than sweet crude sources. Despite their prevalence in existing and future commercial fuels, very limited information exists on the high-T combustion of cycloalkanes. Consequently, we have performed direct measurements of bimolecular rate constants for the reactions of OH with a series of model cycloalkanes (cyclopentane, cyclohexane, methylcyclopentane and methylcyclohexane) in order to assess one of the dominant consumption channels for cycloalkanes under practical combustion conditions.

High temperature experiments were performed with the reflected shock tube technique described above. However, in this work, 48 optical passes corresponding to a total path length ~ 4.2 m was used. The experimental rate constants can be expressed in Arrhenius form as

$$k_{\text{cyclopentane}+\text{OH}} = 1.897 \times 10^{-10} \exp(-1705/T) \text{ cm}^3 \text{ molecule}^{-1} \text{ s}^{-1} \text{ (813-1341 K)} \quad (9)$$

$$k_{\text{cyclohexane}+\text{OH}} = 1.862 \times 10^{-10} \exp(-1513/T) \text{ cm}^3 \text{ molecule}^{-1} \text{ s}^{-1} \text{ (801-1347 K)} \quad (10)$$

$$k_{\text{methylcyclopentane}+\text{OH}} = 2.017 \times 10^{-10} \exp(-1799/T) \text{ cm}^3 \text{ molecule}^{-1} \text{ s}^{-1} \text{ (859-1344 K)} \quad (11)$$

$$k_{\text{methylcyclohexane+OH}} = 2.553 \times 10^{-10} \exp(-1824/T) \text{ cm}^3 \text{ molecule}^{-1} \text{ s}^{-1} \text{ (836-1273 K)} \quad (12)$$

High level electronic structure methods are being used to characterize reactions (9) to (12) in order to provide reliable extrapolations of the rate constants over a wide temperature range. The present rate expressions for OH with cyclohexane, eqn. (10), and methylcyclohexane, eqn. (12), give rate constants that are 15-25% higher (over the T-range 800-1300 K) than the rate constants used in recent modeling efforts on the oxidation of cyclohexane⁷ and methylcyclohexane.⁸ The present measurements reduce the uncertainties in rate constants for the primary cycloalkane consumption process in high temperature oxidation.

We also have completed work on the bimolecular reactions of OH with n-pentane, n-hexane, n-heptane, 2,3-dimethyl butane, and neo-octane, and on the thermal decompositions of NH₂OH and C₂H₅OH. Additional atom and radical with molecule reaction studies (e. g. Cl + hydrocarbons) are in the planning stage. We are also planning thermal decomposition studies using H-atom ARAS on C₂H₄ and C₂H₅OH.

This work was supported by the U. S. Department of Energy, Office of Basic Energy Sciences, Division of Chemical Sciences, Geosciences, and Biosciences, under Contract No. DE-AC02-06CH11357.

References

1. Srinivasan, N. K.; Su, M.-C.; Sutherland, J. W.; Michael, J. V. *J. Phys. Chem. A* **2005**, *109*, 1857.
2. Su, M.-C.; Kumaran, S. S.; Lim, K. P.; Michael, J. V. *Rev. Sci. Inst.* **1995**, *66*, 4649.
3. Su, M.-C.; Kumaran, S. S.; Lim, K. P.; Michael, J. V.; Wagner, A. F.; Dixon, D. A.; Kiefer, J. H.; DiFelice, J. *J. Phys. Chem.* **1996**, *100*, 15827.
4. Su, M.-C.; Kumaran, S. S.; Lim, K. P.; Michael, J. V.; Wagner, A. F.; Harding, L. B.; Fang, D.-C. *J. Phys. Chem. A* **2002**, *106*, 8261.
5. Srinivasan, N. K.; Su, M.-C.; Michael, J. V.; Jasper, A. W.; Klippenstein, S. J.; Harding, L. B. *J. Phys. Chem. A* **2008**, *112*, 31.
6. Sivaramakrishnan, R.; Srinivasan, N. K.; Su, M.-C.; Michael, J. V. *Proc. Combust. Inst.* **2009**, *32* submitted.
7. Silke, E. J.; Pitz, W. J.; Westbrook, C. K.; Ribaucour, M. *J. Phys. Chem. A* **2007**, *111*, 3761.
8. Pitz, W. J.; Naik, C. V.; Ni Mhaolduin, T.; Westbrook, C. K.; Curran, H. J.; Orme, J. P.; Simmie, J. M. *Proc. Combust. Inst.* **2007**, *31*, 267.

PUBLICATIONS FROM DOE SPONSORED WORK FROM 2006-2008

- *The Thermal Decomposition of Water*, N. K. Srinivasan and J. V. Michael, *Int. J. Chem. Kinet.* **38**, 211 (2006).
- *Active Thermochemical Tables: Accurate Enthalpy of Formation of Hydroperoxyl Radical, HO₂*, B. Ruscic, R. E. Pinzon, M. L. Morton, N. K. Srinivasan, M.-C. Su, J. W. Sutherland, and J. V. Michael, *J. Phys. Chem. A* **110**, 6592 (2006).
- *Reflected Shock Tube Studies of High-Temperature Rate Constants for OH + NO₂ → HO₂ + O₂ and OH + HO₂ → H₂O + O₂*, N. K. Srinivasan, M.-C. Su, J. W. Sutherland, J. V. Michael, and B. Ruscic, *J. Phys. Chem. A* **110**, 6602 (2006).
- *Experimental and Theoretical Rate Constants for CH₄ + O₂ → CH₃ + HO₂*, N. K. Srinivasan, J. V. Michael, L. B. Harding, and S. J. Klippenstein, *Combust. Flame*, **149**, 104-111 (2007).
- *High-Temperature Rate Constants for CH₃OH + Kr → Products, OH + CH₃OH → Products, OH + (CH₃)₂CO → CH₂COCH₃ + H₂O, and OH + CH₃ → CH₂ + H₂O*,

- N. K. Srinivasan, M.-C. Su, and J. V. Michael, *J. Phys. Chem. A* **111**, 3951 (2007).
- *Experimental and Theoretical Studies of High-Temperature Rate Constants for $\text{OH} + \text{CF}_3\text{H} \rightleftharpoons \text{CF}_3 + \text{H}_2\text{O}$ and $\text{CF}_3 + \text{OH} \rightarrow \text{Products}$* , N. K. Srinivasan, M.-C. Su, J. V. Michael, S. J. Klippenstein, and L. B. Harding, *J. Phys. Chem. A* **111**, 6822 (2007).
 - *$\text{CH}_3 + \text{O}_2 \rightarrow \text{H}_2\text{CO} + \text{OH}$ Revisited*, N. K. Srinivasan, M.-C. Su, J. V. Michael, *J. Phys. Chem. A* **111**, 11589 (2007).
 - *Reflected Shock Tube Studies of High-Temperature Rate Constants for $\text{OH} + \text{C}_2\text{H}_2$ and $\text{OH} + \text{C}_2\text{H}_4$* , N. K. Srinivasan, M.-C. Su, and J. V. Michael, *Phys. Chem. Chem. Phys.* **9**, 4155 (2007).
 - *Thermal Decomposition of CF_3 and the Reaction of $\text{CF}_2 + \text{OH} \rightarrow \text{CF}_2 + \text{H}$* , N. K. Srinivasan, M.-C. Su, J. V. Michael, S. J. Klippenstein, and L. B. Harding, *J. Phys. Chem. A* **112**, 31 (2008).
 - *High Temperature Rate Constants for $\text{OH} + \text{Alkanes}$* , R. Sivaramakrishnan, N. K. Srinivasan, M.-C. Su, and J. V. Michael, *Proc. Combust. Inst.* **32**, submitted.

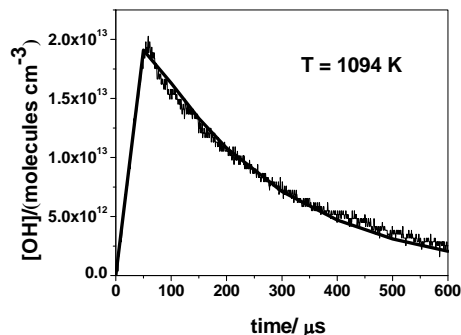


Figure 1

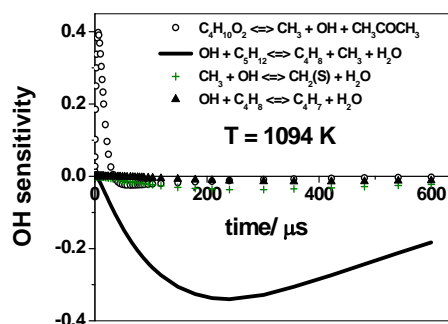


Figure 2

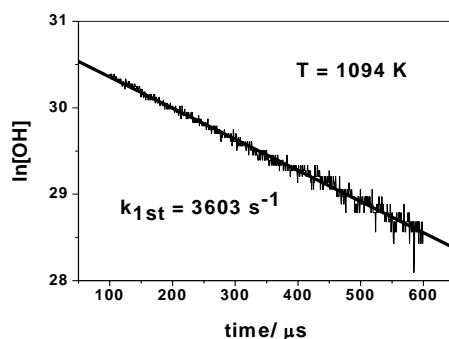


Figure 3

Fig. 1. Typical $[\text{OH}]$ temporal profile. Solid line – fit with a full reaction mechanism using $k_{\text{OH}+\text{neo-C}_5\text{H}_{12}} = 1.94 \times 10^{-11} \text{ cm}^3 \text{ molecule}^{-1} \text{ s}^{-1}$. The conditions are $P_1 = 15.84 \text{ Torr}$ and $M_S = 2.045$ giving $T_5 = 1094 \text{ K}$ with $\rho_5 = 2.435 \times 10^{18}$, $[\text{C}_5\text{H}_{12}]_0 = 1.861 \times 10^{14}$, $[(\text{CH}_3)_3\text{COOH}]_0 = 2.188 \times 10^{13}$, and $[\text{H}_2\text{O}] = 4.095 \times 10^{13}$, all in molecules cm^{-3} .

Fig. 2. OH-radical sensitivity analysis for the profile shown in Fig. 1. The four most sensitive reactions are shown as the inset.

Fig. 3. The first-order plot, $\ln[\text{OH}]$ against time, for the experiment shown in Fig. 1 for $t > 100 \mu\text{s}$. The first-order decay constant is 3603 s^{-1} giving $k_{\text{OH}+\text{neo-C}_5\text{H}_{12}} = 1.94 \times 10^{-11} \text{ cm}^3 \text{ molecule}^{-1} \text{ s}^{-1}$.

Multiphase Combustion Diagnostics Development

H. A. Michelsen

Sandia National Labs, MS 9055, P. O. Box 969, Livermore, CA 94551

hamiche@sandia.gov

1. Program Scope

Combustion in practical combustors, such as internal combustion engines, frequently evolves through multiple phases. Liquid fuels injected into such combustors are generally vaporized and mixed with a gas-phase oxidizer. Combustion processes often produce solid carbon particles, i.e., soot. These particles may be oxidized to form gas-phase species or released into the exhaust stream, where they can be coated with liquid coatings. These coatings can be comprised of any of a number of components, including unburned fuel, lube oil, sulfuric acid, water, and other combustion by-products.^{1,2} The research program described here focuses on the development of optical diagnostics for soot particles in combustion environments and combustion exhaust plumes. The goal of this work is *in situ* measurements of volume fraction, size, composition, and morphology of combustion-generated particles with fast time response and high sensitivity. Future work will expand the scope of this program to include optical diagnostics development for studies of the structure and evolution of liquid-jet sprays.

2. Recent Progress

Our work has focused on developing a detailed understanding of the chemical and physical mechanisms that influence the applicability of laser-induced incandescence (LII) for soot detection under a wide range of conditions. In our recent work we have studied the effects of photochemical interferences on the application of LII of flame-generated soot. We have spectrally and temporally resolved the emission from laser-heated soot irradiated at 532 nm over a wide fluence range. Our spectra demonstrate discrete features from electronically excited carbon clusters C_2 and C_3 . Additional, unidentified features are also observed.

We have also investigated the influence on time-resolved measurements of the pulse characteristics of a Q-switched flashlamp-pumped Nd:YAG laser with an unstable resonator configuration. The beam profile from such a laser changes over the duration of the laser pulse, such that the center of the beam precedes the outer edges by nanoseconds. This phenomenon can have significant effects on signals collected on a nanosecond timescale.

2.1. Photochemical interferences in laser-induced incandescence of flame-generated soot.

Soot is composed of branched-chain aggregates of small (15-50 nm diameter) carbon spheroids called primary particles. LII is used extensively as a sensitive optical technique for measurements of soot volume fraction and primary particle size.^{3,4} This technique involves heating the soot particles with a high-power pulsed laser to temperatures of 2500-4000 K and measuring the radiative emission from the hot particles. The magnitude of the signal is correlated with the soot volume fraction. The signal decay rate depends on particle size, and more recent efforts have focused on developing LII for particle size measurements. Broadband emission is observed for excitation wavelengths from 213 to 1064 nm,⁵⁻⁷ and LII is typically measured at wavelengths between 400 and 800 nm. For primary particle sizing measurements, time-resolved LII signals are often recorded at wavelengths in the range of 400-450 nm and/or 600-700 nm.⁷ At fluences greater than 0.2 J/cm², however, discrete features have been observed on top of the continuum emission with 532-nm and 1064-nm excitation and have been predominantly attributed to fluorescence from excited C_2 formed by carbon vaporization in response to laser irradiation.^{6,7} An example of such features is shown in Figure 1, which presents spectrally resolved emission recorded 5 ns after the peak of the laser pulse at several fluences.

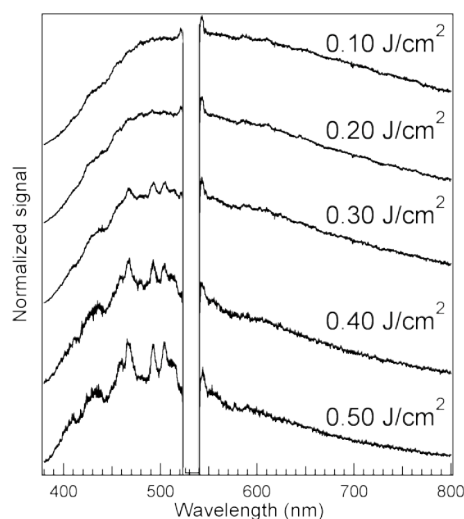


Fig. 1. Spectrally resolved emission from laser-heated soot. Spectra were recorded 5 ns after the peak of the laser pulse during laser irradiation at 532 nm at selected fluences.

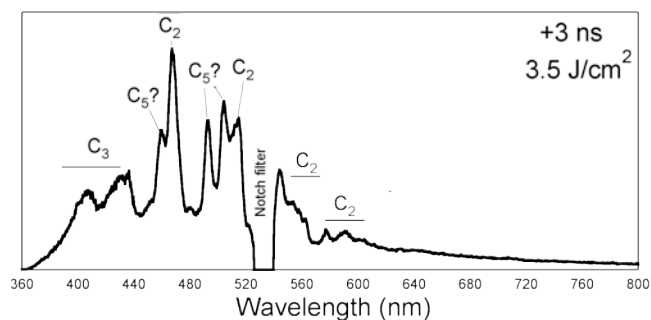


Fig. 2. Spectrally resolved emission from laser-heated soot. The spectrum was recorded 3 ns after the peak of the laser pulse during laser irradiation at 532 nm and a fluence of 3.5 J/cm².

We have used the second harmonic from a Nd:YAG laser to heat soot generated in an atmospheric laminar diffusion flame and a gated spectrograph (~2-ns gate) to spectrally and temporally resolve the emission. Spectra were recorded over a wide range of fluences to determine the extent of perturbation to the signals from interfering species; spectra were recorded at high fluences for better identification of the emitting species. At times corresponding to the peak of the LII signal, broadband emission was observed. At later times and fluences greater than 0.2 J/cm², features from C₂, C₃, and presumably larger carbon clusters appeared in the spectra, as shown in Fig. 1 at a selection of fluences and in Fig. 2 for a fluence of 3.5 J/cm². Emission from C₃ and other species was shown to perturb LII temporal profiles recorded at 448 nm at laser fluences greater than 0.2 J/cm², strongly suggesting that wavelengths between 380 and 680 nm should be avoided when performing LII measurements near or above the sublimation threshold. The breadth of the wavelength region to be avoided is more extensive than indicated by previous studies.

2.2. Complications to optical measurements introduced by a laser with an unstable resonator.

Flash-lamp pumped, Q-switched Nd:YAG lasers typically employ geometrically unstable resonator cavity configurations to achieve high-power pulsed output. An unstable cavity allows the beam to expand to fill large laser rods to make use of the entire volume of the gain medium.⁸ This configuration can be used more easily than the stable resonator geometry to produce high-power pulses in a single dominant transverse mode. Coupling the unstable resonator configuration with variable-reflectivity mirrors enables the production of beams with high quality near-field Gaussian⁸ or top-hat⁸⁻¹⁰ spatial profiles when averaged over the entire laser pulse. When time resolved, however, the spatial profile of the beam from an unstable resonator with variable-reflectivity mirrors varies throughout the pulse.^{9,10} Previous studies have shown that an unstable cavity produces pulses that first arrive along the central axis of propagation and are increasingly delayed with radial distance. The pulse first develops, and the gain is hence more quickly depleted, along the axis of the gain medium where the reflectivity of the mirrors is the highest. Later in the pulse after many cavity round-trips, gain is preferentially extracted from the less depleted regions closer to the outer edge of the gain medium.¹⁰ The result is typically a spatio-temporal profile with a nearly Gaussian leading edge and a hollow-cone shaped trailing edge.^{9,10} The shape can vary depending on the output coupler's reflectivity function. The timing variation along the beam radius can be on the order of nanoseconds. For our laser the time delay of the pulse between the center of the beam and the edge of the beam is as much as 10 ns. Our laser provides pulses with position-dependent durations

spanning 8-11.5 ns at 1064 nm and 7-10 ns at 532 nm. Pulses emerge first and have the longest duration at the center of the beam; they are shorter (by up to 4 ns) and increasingly delayed (by up to 10 ns) with increasing radial distance from the center. Figure 3 gives an example of this behavior at 532 nm and shows temporal profiles recorded at different radial positions in the beam.

The temporal spread in the pulsed beam of a laser with an unstable resonator can cause significant problems for experiments in which the signal is temporally resolved (e.g., fluorescence lifetime measurements) and for applications in which the timing of the pulse is coordinated with other events (e.g., phase-matching separate beams in nonlinear crystals). Time-resolved LII of soot is a technique that can be very sensitive to the spatio-temporal profile of the pulsed excitation beam. Either volume-fraction or primary-particle size measurements require precise timing of the signal detection relative to that of the laser pulse. To further exacerbate this problem, LII measurements are often made with an expanded beam to measure soot distributions over a wide range of positions. In this experimental configuration, the outer edges of the detection region are delayed possibly by nanoseconds relative to the central portion. Significant systematic biases in the signal with position could be caused by the variation in the timing of the laser relative to the camera gate over the detection region. The variability in the timing of the laser pulse over the beam can also cause problems with time-resolved point measurements. The depth of field of the LII collection optics allows signal to be averaged over a range of beam positions and hence pulse times, which could significantly perturb the measured signal decay rate and add substantial uncertainty to the inferred particle size.

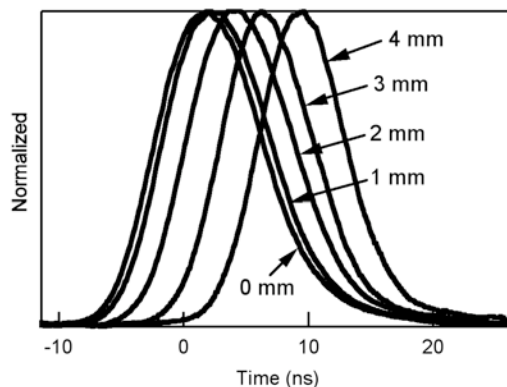


Fig. 3. Dependence of pulse timing on radial position. Temporal profiles are shown for positions along the horizontal centerline of the 532-nm beam. The peak of each curve is scaled to the top of the graph.

3. Future plans

Current work builds on these results and extends it to combustion-generated particles with inorganic and organic coatings representative of particles found in exhaust plumes. In order to simulate exhaust-plume particulates, we have modified our flow-tube system to allow controlled deposition of a coating with low volatility on flame-generated soot. The thickness of the coating can be varied and the particles collected for analysis by TEM and NEXAFS. Coatings investigated to date have been selected for diagnostic development for diesel exhaust and include sulfuric acid, heptamethylnonane, and oleic acid. These experiments are currently limited by our inability to determine the mass loading of particle coatings. Developing an understanding of the cause and magnitude of the effects of coatings will require characterization of the particle coatings. Coating the particles increases the mean aggregate size as measured by the SMPS, but measurements of electric mobility diameter provided by the SMPS do not provide a quantitative measure of the volatile coating fraction either by volume or by mass. In order to measure the volatile fraction, we will build a chamber that includes a temperature-controlled oscillating crystal microbalance for differential mass measurements on coated and evaporatively dried particles.

4. References

- (1) Kittelson, D. B. *J. Aerosol Sci.* **1998**, *29*, 575.
- (2) Lighty, J. S.; Veranth, J. M.; Sarofim, A. F. *J. Air Waste Manage. Assoc.* **2000**, *50*, 1565.
- (3) Santoro, R. J.; Shaddix, C. R. Laser-Induced Incandescence. In *Applied Combustion Diagnostics*; Kohse-Höinghaus, K., Jeffries, J. B., Eds.; Taylor & Francis: New York, NY, 2002.
- (4) Schulz, C.; Kock, B. F.; Hofmann, M.; Michelsen, H. A.; Will, S.; Bougie, B.; Suntz, R.; Smallwood, G. J. *Appl. Phys. B* **2006**, *83*, 333.
- (5) Rohlffing, E. A. *J. Chem. Phys.* **1988**, *89*, 6103.
- (6) Vander Wal, R. L.; Weiland, K. J. *Appl. Phys. B* **1994**, *59*, 445.
- (7) Schraml, S.; Dankers, S.; Bader, K.; Will, S.; Leipertz, A. *Combust. Flame* **2000**, *120*, 439.
- (8) Siegman, A. E. *Lasers*, First ed.; University Science Books: Mill Valley, CA, 1986.
- (9) Anstett, G.; Nittmann, M.; Borsutzky, A.; Wallenstein, R. *Appl. Phys. B* **2003**, *76*, 833.
- (10) Caprara, A.; Reali, G. C. *Opt. Quantum Elect.* **1992**, *24*, S1001.

5. BES-supported, peer-reviewed publications

M. A. Dansson, M. Boisselle, M. A. Linne, and H. A. Michelsen, "Complications to optical measurements using a laser with an unstable resonator: A case study on laser-induced incandescence of soot", *Appl. Opt.* **46**, 8095-8103 (2007).

H. A. Michelsen et al., "Modeling laser-induced incandescence of soot: A summary and comparison of LII models", *Appl. Phys. B* **87**, 503-521 (2007).

L. Nemes, A. M. Keszler, C. G. Parigger, J. O. Hornkohl, H. A. Michelsen, and V. Stakhursky, "On spontaneous emission from the C₃ radical in carbon plasma", *Appl. Opt.* **46**, 4032-4040 (2007).

H. A. Michelsen, A. V. Tivanski, M. K. Gilles, L. H. van Poppel, M. A. Dansson, and P. R. Buseck, "Particle formation from pulsed laser irradiation of soot aggregates studied with a scanning mobility particle sizer, a transmission electron microscope, and a scanning transmission x-ray microscope", *Appl. Opt.* **46**, 959-977 (2007).

C. Schulz et al., "Laser-induced incandescence: Recent trends and current questions", *Appl. Phys. B* **83**, 333-354 (2006).

H. A. Michelsen, "Laser-induced incandescence of flame-generated soot on a picosecond timescale", *Appl. Phys. B* **83**, 443-448 (2006).

L. Nemes, A. M. Keszler, C. G. Parigger, J. O. Hornkohl, H. A. Michelsen, and V. Stakhursky, "The C₃ puzzle: Formation of and spontaneous emission from the C₃ radical in carbon plasmas", *Int. Elect. J. Mol. Design* **5**, 150-167 (2006).

Chemical Kinetics and Combustion Modeling

James A. Miller

Combustion Research Facility, Sandia National Laboratories

MS 9055, Livermore, CA, 94551-0969

email: jamille@sandia.gov

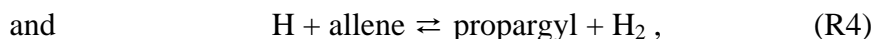
Program Scope

The goal of this project is to gain qualitative insight into how pollutants are formed in combustion systems and to develop quantitative mathematical models to predict their formation and destruction rates. The approach is an integrated one, combining theory, modeling, and collaboration with experimentalists to gain as clear a picture as possible of the processes in question. My efforts and those of my collaborators are focused on problems involved with the nitrogen chemistry of combustion systems and the formation of soot and PAH in flames, as well as on general problems in hydrocarbon combustion. Current emphasis is on determining phenomenological rate coefficients from the time-dependent, multiple-well master equation for reactions involved in the pre-cyclization and cyclization chemistry of flames burning aliphatic fuels.

Recent Results

Unimolecular and Bimolecular Reactions on a C₃H₅ Potential (with Stephen Klippenstein, Yuri Georgievskii, and Juan Senosiain)

Our original intent in pursuing this investigation was simply to obtain a good rate coefficient for allyl dissociation. However, the potential contains a wealth of kinetic information, perhaps most notably for the reactions,



in addition to allyl dissociation. Consequently, we attempted to extract all the information available. Electronic structure calculations were performed using our usual methodology. Stationary-point searches, normal mode analyses, and hindered-rotor scans were carried out using density functional theory, B3LYP in its spin-unrestricted form, with the 6-311 ++ G(d,p) basis set. To obtain accurate energies for the rate-coefficient calculations, we computed single-point energies at and near the stationary points using RQCISD(T) with Dunning's correlation-consistent basis sets. These energies were extrapolated to the infinite-basis-set limit using the triple- and quadruple- zeta calculations. Microcanonical (J-resolved) rate coefficients were computed using variational transition-state theory for the association-dissociation reactions and conventional transition-state theory for the isomerizations and abstractions. Thermal rate coefficients, $k(T,p)$, were determined using our master-equation methodology. With very modest adjustments to some of the barrier heights, typically less than 1.5 kcal/mole, we were able to obtain good agreement with all the experimental data available, most notably for both the forward and reverse rate coefficients of reaction (R2).

The C₃H₃ + OH Reaction (with Stephen Klippenstein and Yuri Georgievskii)

Because propargyl is resonance stabilized, it does not react readily with molecular oxygen. Consequently, in rich flames propargyl is oxidized primarily by reacting with hydroxyl. Because there is no information available, either experimental or theoretical, on the rate coefficient or product distribution of this reaction, we initiated a detailed theoretical investigation to provide this information for use in modeling. Electronic structure calculations of the relevant parts of the singlet PES are now complete (same methodology as described above). Even though the rate-coefficient calculations are not yet finished it is clear that there are only 2 significant product channels: C₂H₃ + HCO and C₂H₄ + CO. Both of these sets of products are formed as a result of OH adding to the CH end of propargyl followed by a 1,3 hydrogen transfer. To our surprise the C₂H₂ + CH₂O products, which can appear as a consequence of OH addition to the CH₂ end of propargyl, are not competitive. Neither are any of the channels forming water and a C₃H₂ isomer.

The Reaction Between Allyl and Propargyl (with Yuri Georgievskii, Stephen Klippenstein, and Wesley Allen)

The second most important cyclization reaction in rich flames is generally thought to be the reaction between allyl and propargyl. However, the rate coefficient commonly used in modeling for this reaction is based solely on an estimate. This estimate was obtained by assuming that the formation of a five-membered ring is controlled by the rate of association of the 2 radicals and that the association rate coefficient is the same as that for C₃H₅ + C₃H₅ in its high-pressure limit. We initiated a theoretical investigation of this reaction to obtain a better rate coefficient. We used the association rate coefficients calculated by Georgievskii, et al (*Phys. Chem. Chem. Phys.* **9**, 4259-4268 (2007)) and information on the intermediate stationary points obtained from an analysis similar to that described above. The crucial step in the reaction is closing the initial CH₂CHCH₂CHCCH₂ adduct into a five-membered ring. Our calculations indicate that this transition state is \approx 24 kcal/mole below the reactants. This leads to an upper limit on the rate coefficient for forming fulvene that is about a factor 5 smaller at T = 1500 K than that used in modeling (the rate coefficient is only weakly pressure dependent at this temperature). This result severely limits the importance of the C₃H₃ + C₃H₅ reaction as a cyclization step in flame modeling.

Detailed Balance in Multiple-Well Chemical Reactions (with Stephen Klippenstein, Struan Robertson, Mike Pilling, and Nick Green)

In this project we addressed the issue of whether or not (and to what extent) detailed balance is satisfied by phenomenological rate constants derived from solutions to master equations describing chemical reactions that take place over multiple, inter-connected potential wells. In addressing this issue we were forced to examine a number of related topics, including necessary and sufficient conditions for a system of first-order rate equations to evolve to chemical equilibrium and the relationship between detailed balance and Wegscheider conditions. The assumption of a “near-Boltzmann” distribution in the wells sheds considerable light on the issue at hand. We developed this approximation in some detail and proposed a quantitative measure of “near-Boltzmann”. Most likely the rate constants of interest do not satisfy detailed balance exactly. However, the discrepancies are expected to be vanishingly small.

Future Directions

We shall continue our work on the chemical kinetics of rich flames of aliphatic fuels, particularly that concerned with the formation of the first aromatics containing one or two rings. In the next year we expect to finish our work on the reactions of allyl and OH with propargyl. The work on allyl + propargyl is being pursued in collaboration with Wesley Allen and co-workers at the University of Georgia. We shall continue to develop our chemical kinetic model, particularly in conjunction with the flame experiments at the Advanced Light Source. We expect in the next year to begin to investigate the possibility of using the rate-controlled, constrained-equilibrium formalism to predict the concentrations of aromatic compounds with more than 2 rings. We shall also continue to maintain our interest in the nitrogen chemistry of combustion, particularly that concerned with NO_x control technologies such as reburning, Thermal De-NO_x, and RAPRENO_x.

Publications of James A. Miller 2006-2008

- J. A. Miller, S.J. Klippenstein, S. H. Robertson, N. J. B. Green, and M. J. Pilling, "Detailed Balance in Multiple-Well Chemical Reactions," *J. Phys. Chem. A*, submitted (2008)
- J. A. Miller, J. P. Senosiain, Y. Georgievskii, and S. J. Klippenstein, "Reactions Over Multiple, Interconnected Potential Wells: Unimolecular and Bimolecular Reactions on a C₃H₅ Potential", *J. Phys. Chem. A*, submitted (2008)
- N. Hansen, J. A. Miller, T. Kasper, K. Kohse-Höinghaus, P. R. Westmoreland, J. Wang, and T. A. Cool, "Benzene Formation in Premixed Fuel-Rich 1,3 Butadiene Flames," *Proc. Combust. Inst.* 32, submitted (2008)
- S. R. Sellevåg, Y. Georgievskii, and J. A. Miller, "The Temperature and Pressure Dependence of the Reactions H+O₂(+M)⇌HO₂(+M) and H+OH(+M)⇌H₂O(+M)," *J. Phys. Chem. A*, in press (2008)
- J. Zador, R. X. Fernandes, Y. Georgievskii, G. Meloni, C. A. Taatjes, and J. A. Miller, "The Reaction of Hydroxyethyl Radicals with O₂: A Theoretical Analysis and Experimental Product Study," *Proc. Combust. Inst.* 32, submitted (2008)
- L. B. Harding, S. J. Klippenstein, and J. A. Miller, "The Kinetics of CH+N₂ Revisited with Multi-Reference Methods," *J. Phys. Chem. A* 112, 522-532(2008)
- Y. Georgievskii, S. J. Klippenstein, and J. A. Miller, "Association Rate Constants for Reactions between Resonance Stabilized Radicals: C₃H₃+C₃H₃, C₃H₃+C₃H₅, and C₃H₅+C₃H₅," *Phys. Chem. Chem. Phys.* 9, 4259-4268 (2007)
- H. Fan, S. T. Pratt, and J. A. Miller, "Secondary Decomposition of C₃H₅ Radicals Formed by the Photodissociation of 2-Bromopropene," *J. Chem. Phys.* 127, 144301 (2007)
- J.A. Miller and S.J. Klippenstein, "Master Equation Methods in Gas Phase Chemical Kinetics", feature article for *J. Phys. Chem. A* 110, 10528-10544 (2006)

- A.Fernandez-Ramos, J.A. Miller, S.J. Klippenstein, and D.G. Truhlar, "Modeling the Kinetics of Bimolecular Reactions," *Chemical Reviews* **106**, 4518-4584 (2006)
- J.P. Senosiain and J.A. Miller, "The Reaction of n- and i-C₄H₅ Radicals with Acetylene," *J. Phys. Chem. A* **111**, 3740-3747(2007)
- J.P. Senosiain, S.J. Klippenstein, and J.A. Miller, "Oxidation Pathways in the Reaction of Diacetylene with OH Radicals", *Proc. Combust. Inst.* **31**, 185-192 (2007)
- J.P. Senosiain, S.J. Klippenstein, and J.A. Miller, "The Reaction of Ethylene with Hydroxyl Radicals: A Theoretical Study", *J. Phys. Chem. A* **110**, 6960-6970 (2006)
- N. Hansen, J. A. Miller, J. Wang, T. A. Cool, M.E. Law, P. R. Westmoreland, T. Kasper, and K. Kohse-Höinghaus, " Photoionization Mass Spectrometric Studies and Modeling of Fuel-Rich Allene and Propyne Flames," *Proc. Combust. Inst.* **31**, 1157-1164 (2007)
- N. Hansen, S. J. Klippenstein, J. A. Miller, J. Wang, T. A. Cool, M.E. Law, P. R. Westmoreland, T. Kasper, and K. Kohse-Höinghaus, "Identification of C₅H_x (x=3-6,8) Isomers in Fuel-Rich Flames by Photoionization Mass Spectrometry and Electronic Structure Calculations", *J. Phys. Chem. A* **110**, 4376-4388 (2006)
- J.P. Senosiain, S.J. Klippenstein, and J.A. Miller, "Pathways and Rate Coefficients for the Decomposition of Vinyloxy and Acetyl Radicals", *J. Phys. Chem. A* **110**, 5772-5781 (2006)
- C.A. Taatjes, N. Hansen, J.A. Miller, T.A. Cool, J. Wang, P.R. Westmoreland, M.E. Law, T. Kasper, and K. Kohse-Höinghaus, "Combustion Chemistry of Enols: Possible Ethanol Precursors in Flames", *J. Phys. Chem. A* **110**, 3254-3260 (2006)
- N. Hansen, S. J. Klippenstein, C. A. Taatjes, J. A. Miller, J. Wang, T. A. Cool, F. Qi, M.E. Law, and P. R. Westmoreland, "The Identification and Chemistry of C₄H₃ and C₄H₅ Isomers in Fuel-Rich Flames", *J. Phys. Chem. A* **110**, 3670-3678 (2006)

Detection and Characterization of Free Radicals Relevant to Combustion Processes

Terry A. Miller

Laser Spectroscopy Facility, Department of Chemistry
The Ohio State University, Columbus OH 43210, email: tamiller+@osu.edu

1 Program Scope

Combustion processes have been studied for many years, but under a variety of conditions the chemistry is so complex that it is yet to be fully understood. Modern computer codes for its modelling typically employ hundreds of reaction steps with a comparable number of chemical intermediates. Nonetheless the predictions of such models can be no better than the fundamental dynamical and mechanistic data that are their inputs. Spectroscopic identifications and diagnostics for the chemical intermediates in the reaction mechanisms constitute an important experimental verification of the models, as well as provide molecular parameters that are experimental “gold standards” against which quantum chemistry computations of molecular properties may be judged. Our spectroscopic work has primarily focussed recently upon the organic peroxy radical family of reactive intermediates (RO_2), which are known to be of key importance in combustion processes.

2 Recent Progress

Experimentally we have used near IR (NIR) cavity ringdown spectroscopy (CRDS) to observe the $\tilde{A} - \tilde{X}$ electronic spectra of all the isomers and many of the conformers of the alkyl peroxy radicals, $\text{C}_n\text{H}_{2n+1}\text{O}_2$, for $n = 1-5$. Specific species observed (number of distinct conformer bands in parenthesis) include methyl peroxy (1); ethyl peroxy (2); 1-propyl (3) and 2-propyl (2) peroxy; 1-butyl (3), 2-butyl (2), isobutyl (3), and t-butyl (1) peroxy; 1-pentyl (3), 2-pentyl (2), 3-pentyl (2), 2-methylbutyl (3), 3-methylbutyl (3), 3-methyl-2-butyl (2), 2-methyl-2-butyl (3), and neopentyl (2) peroxy.

Table 1 summarizes the origin band frequencies for the subset of these species for which a series of quantum chemistry calculations has been performed. It illustrates clearly the wide discrepancy among the predictions of various levels of computation for the $\tilde{A} - \tilde{X}$ origin band frequencies and their comparison to the experimental values. For the simplest species, methyl peroxy, the predicted values range from 4321 cm^{-1} (ROHF) to 9655 cm^{-1} (TDDFT) and can be compared to the experimental value of 7383 cm^{-1} . By comparison, the G2 method predicts the origin at 7375 cm^{-1} , an error of only 8 cm^{-1} ! Looking over the other molecular species in the table, it is clear that G2 is the most accurate method, although its quality does degrade a bit for the larger radicals. Table 1 also indicates that the computationally inexpensive density functional (B3LYP) method gives results of generally acceptable quality, particularly when a modest, empirical correction factor (0.97) is applied.

Clearly the results given in Table 1 provide the quantitative “gold standards” discussed above for benchmarking precisely theoretical calculations. Additionally, experiments and calculations can be used synergis-

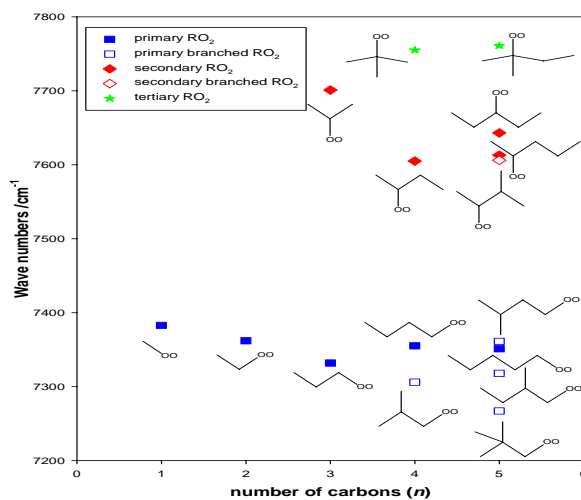


Figure 1: (Color on CD) Experimental $\tilde{A} - \tilde{X}$ origin frequencies of primary (blue squares), secondary (red diamonds), and tertiary (green stars) alkyl peroxy radicals ($T_1 \dots$ conformers). The open symbols correspond to the branched peroxy isomers, while the filled ones correspond to the straight chain peroxy isomers.

Table 2: Comparison of experimental $\tilde{A}-\tilde{X}$ transition frequencies with theoretical predictions (in cm^{-1}) for the alkyl peroxy radicals. The experimental values are all derived from NIR CRDS experiments by our group while calculated values without references were reported in our publication 6

Peroxy isomer	Peroxy conformer	Symmetry	Exp.	ROHF/ 6-31+G(d)	B3LYP/ 6-31+G(d)	G1/ 6-31+G(d)	G2MP2 ^a / 6-31G(d)	G2/ 6-31+G(d)	TDDFT ^b / 6-31+G(d)	CI ^c double ζ	EOMIP-CCSD/ DZP
methyl	T	C_s	7383	4321	7614	7257	7372	7375	9655	7267	7901
ethyl	T	C_s	7362	4332	7605	7247		7355			7938 ^d
ethyl	G	C_1	7592	4519	7808	7473	7590	7580			8059 ^d
1-propyl	T ₁ T ₂	C_s	7332	4313	7578	7221		7317			7920 ^e
1-propyl	T ₁ G ₂	C_1	7332	4312	7577 ^f	7204 ^f		7317 ^f			7932 ^e
1-propyl	G ₁ G ₂	C_1	7508	4446	7716 ^f	7364 ^f		7477 ^f			7970 ^e
1-propyl	G ₁ T ₂	C_1	7569	4523	7812 ^f	7465 ^f		7567 ^f			8057 ^e
1-propyl	G ₁ G ₂	C_1	7569	4610	7804 ^f	7555 ^f		7643 ^f			8091 ^e
2-propyl	G	C_1	7567	4524	7805	7467	7566	7566			8143 ^e
2-propyl	T	C_s	7701	4625	7912	7684		7771			8224 ^e
1-butyl	T ₁ T ₂ T ₃	C_s	7355	4314	7583	7225		7321			
isobutyl	T ₁ T ₂	C_s	7306	4302	7558	7188		7288			
1-pentyl	T ₁ T ₂ T ₃ T ₄	C_s	7351	4312	7581	7224		7321			
neopentyl	T ₁ T ₂	C_s	7267	4289	7524	7164		7252			
3-pentyl	T ₁ T ₂ T ₃	C_s	7643	4434	7701	7445		7532			

^a M. S. Stark, J. Am. Chem. Soc. **122**, 4162 (2000). ^b Vertical excitation, J. L. Weisman and M. Head-Gordon, J. Am. Chem. Soc. **123**, 11686 (2001). ^c J. A. Jafri and D. H. Phillips, J. Am. Chem. Soc. **112**, 2586 (1990). ^d P. Rupper, E. N. Sharp, G. Tarczay, and T. A. Miller, J. Phys. Chem. A **111**, 832 (2007), publication 3. ^e G. Tarczay, S. J. Zalyubovsky, and T. A. Miller, Chem. Phys. Lett. **406**, 81 (2005). ^f G. M. P. Just, P. Rupper, and T. A. Miller, to be published (2008).

tically to better understand the relationship between the observed spectra and the geometric and electronic structure of the radicals. Fig. 1 illustrates some of these structural/spectral relationships by plotting the experimental origin frequencies for various peroxy radicals vs number, n , of carbon atoms. Several trends are readily apparent from the figure. (i) The position of the O₂ substitution on the α carbon of the hydrocarbon provides the largest shift in origin frequencies with increasing frequency corresponding to the position order: primary, secondary, tertiary. (ii) Branching of the hydrocarbon at the β carbon generally decreases the frequency but the effect is significantly less pronounced than the branching at the α carbon. (iii) There is a small (non-monotonic) decrease with increasing number of carbon atoms.

Fig. 2 shows a similar plot of origin frequencies vs n , but now displays the differences among conformers. The T₁ conformers (OCC dihedral angle of 0°) have a significantly lower frequency than the G₁ or G₁' conformers (+120° or -120° OCC dihedral angle). The orientation of the OCC dihedral angle (T₂, G₂, or G₂') displaces by a smaller amount the G₁T₂ (and G₁G₂') conformer to a higher frequency than the G₁G₂ conformer.

The physical basis for these empirical structural/spectral relationships is not particularly obvious but most can be elucidated by some calculations using the density functional method, which as we know gives good predictions of the origin frequencies with modest expenditure of computer resources. Fig. 3 shows schematically a molecular orbital (MO) diagram for the bonds in the peroxy radicals. If one assumes the simplest one-electron-jump model for calculating the $\tilde{A}-\tilde{X}$ transition frequency, it is just the difference in energy between the singly occupied MO (SOMO) and the highest occupied MO (HOMO).

As an example of this approach we consider trend (iii), the general lowering of the $\tilde{A}-\tilde{X}$ origin transition

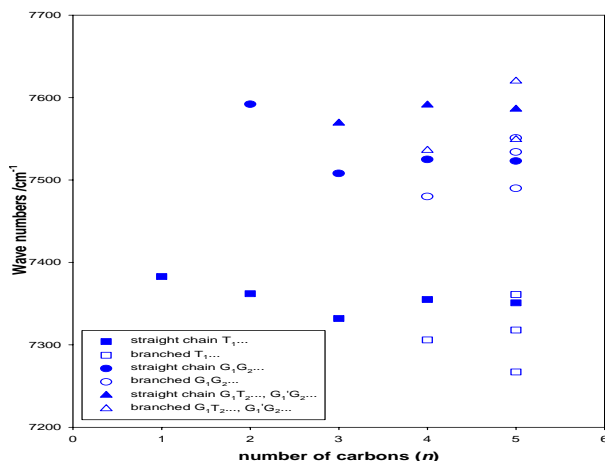


Figure 2: (Color on CD) Experimental $\tilde{A}-\tilde{X}$ origin frequencies of primary alkyl peroxy radical conformers. The squares correspond to T₁... conformers, the circles to G₁G₂... conformers, and the triangles to G₁T₂..., G₁'G₂'... conformers. The open symbols correspond to the branched peroxy isomers, while the filled symbols correspond to the straight chain peroxy isomers.

with increasing n , as discussed above and shown in Fig. 1. To rationalize the effect one can look at panel A of Fig. 4 which shows that both the HOMO and SOMO hydrocarbon radical orbitals are destabilized with increasing n . This causes a corresponding destabilization of the HOMO and SOMO of the peroxy radical (panel B). However from Fig. 3 it is clear that the HOMO is more delocalized onto the hydrocarbon fragment and hence should be de-stabilized more, resulting in the net decrease in transition frequency shown in panel C of Fig. 4. This result is consistent with experiment and the organic chemist’s simple picture of increased donation of electron density to the α carbon as the chain length increases, thereby de-stabilizing the electron rich HOMO, mostly localized on O_2 , but with a bonding lobe towards the α carbon. As detailed in publication 6, we have used similar arguments to successfully explain both trends (i) and (ii) discussed above, corresponding, respectively, to the effect on the origin frequency of α and β carbon branching.

It should be noted that while Fig. 4 is consistent with the general trend of decreasing origin frequency with increasing n , the simple model utilizing the BLYP density functional calculations fails to predict the experimental minimum at $n = 3$ seen in Fig. 1 for the primary peroxy radicals. However, referring to Table 1 one notes that the G2 calculations do predict a minimum at $n = 3$, which would suggest that it is due to higher order electron correlation effects.

The significant origin shifts between the $T_1\dots$ and $G_1\dots$ conformers seen experimentally in Fig. 2 can also be successfully explained by the model of a single-electron jump between the HOMO and SOMO orbitals. Fig. 5 gives a good physical picture of why the SOMO-HOMO gap is decreased in the T_1 conformer compared to the G_1 conformer. The SOMO is stabilized by the well-defined hyperconjugation in the T_1 conformer shown in panel Bii, but the opportunity for hyperconjugation is destroyed by the rotation of the OOC angle to the G_1 conformation (panel Cii).

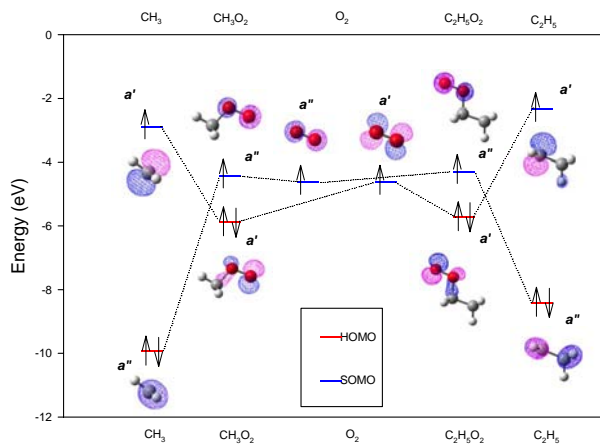


Figure 3: (Color on CD) The HOMO and SOMO of molecular oxygen, methyl and ethyl radicals, and methyl and ethyl peroxy (T) radicals. The pink and blue lobes of the molecular orbitals indicate different orbital phases. The orbitals are oriented such that the paper serves as the plane of symmetry, which determines the orbital’s symmetry designation of a' or a'' . The reaction path to form the peroxy radical from an alkyl radical and O_2 lies in this plane. Lobes that overlap in this orientation, particularly in the a'' orbitals, appear with overlapped pink and blue cross hashes, rendering them almost purple. The CH_3 radical has D_{3h} symmetry, so its HOMO and SOMO have e' and a_2'' symmetry, respectively, but they are a'' (for the linear combination chosen) and a' , respectively, with respect to the plane of the paper, which corresponds to a σ_v plane in D_{3h} .

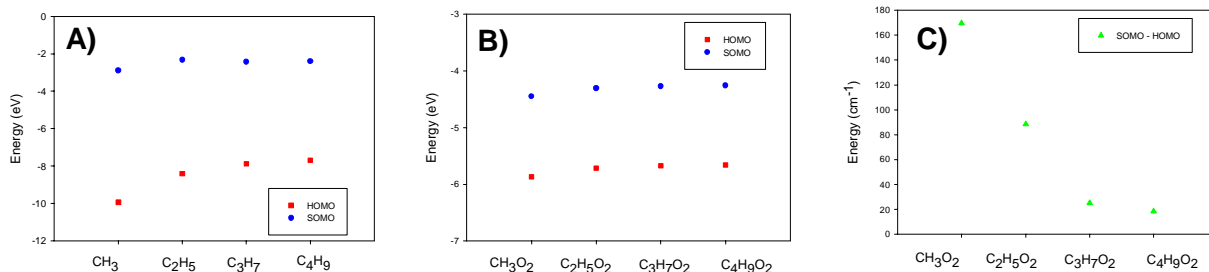


Figure 4: (Color on CD) HOMO and SOMO energies (red squares and blue circles respectively) for methyl through butyl radicals (Panel A), and for methyl through butyl peroxy radicals (Panel B), all calculated at the BLYP/6-31+G(d) level of theory. These calculations were carried out on the $T_1\dots$ conformers of the straight chain primary peroxy isomers. Panel C shows the SOMO-HOMO difference (with constant total energy offset) for methyl through butyl peroxy radicals.

3 Future Plans

Both the experimental spectroscopy and the corresponding computations are now well in hand for the saturated open-chain alkyl peroxy radicals. Accordingly we have recently turned our attention to unsaturated open-chain peroxy radicals, and both aromatic and non-aromatic cyclic peroxy radicals. Our first success with these species is reported in our recently published account of the NIR CRDS $\tilde{A} - \tilde{X}$ electronic spectrum

of phenyl peroxy.

Recently we have extended our investigations to open-chain unsaturated organic peroxy radicals, beginning with vinyl peroxy, $C_2H_3O_2$. *Ab initio* and density functional calculations predict that the $\tilde{A} - \tilde{X}$ transition of vinyl peroxy radical lies in the NIR, analogous to the $\tilde{A} - \tilde{X}$ systems of the previously-studied alkyl peroxies. The calculations indicate that the \tilde{X} state of vinyl peroxy is characterized by minima which are *cis* and *trans* conformers (OOCC dihedral angles of 0° and 180° , respectively). In the \tilde{A} state, a stable *cis* conformation has been located, with a geometry similar to that of the \tilde{X} state structure. By contrast, the *trans* geometry in the \tilde{A} state is found to be a transition state, separating two shallow *gauche* minima (OOCC dihedral angles of $\approx \pm 145^\circ$). We therefore expect to observe spectra corresponding to the $\tilde{A}(cis) - \tilde{X}(cis)$ and $\tilde{A}(gauche) - \tilde{X}(trans)$ transitions. Unfortunately both transitions have factors that could diminish their intensity. The *cis* conformer population in the \tilde{X} state is expected to be only $\approx 10\%$ of the *trans* conformer at room temperature based on its calculated energy above the *trans*. Due to the geometric differences, the $\tilde{A}(gauche) - \tilde{X}(trans)$ transition will likely have poor Franck-Condon factors.

Nonetheless using excimer photolysis of vinyl bromide in the presence of O_2 , we have observed a series of sharp bands near 7050 cm^{-1} with weaker, but similar sets of features found in the vicinities of 8000 cm^{-1} and 8900 cm^{-1} . The spacings between these bands are characteristic of the peroxy O-O stretching frequency. Photolysis of vinyl bromide- d_3 under identical conditions also yields a pattern of peaks at 7050 cm^{-1} which is replicated at 8000 cm^{-1} and 8900 cm^{-1} . Each of these band profiles exhibits marked similarity with, but also subtle differences from, those arising from photolysis of normal vinyl bromide.

In addition to the investigation of an increasing variety of organic peroxy radicals, we have begun work on a significant improvement to our CRDS experiment. The new apparatus will afford the possibility of performing CRDS experiments on the same sample with two probe beams of different wavelengths. This approach will allow the monitoring of two radical spectra simultaneously. Alternatively one reactive and one non-reactive product can be monitored, yielding the possibility of obtaining absolute absorption cross-sections for the former, utilizing the known cross-section of the latter.

Publications Supported by DOE (2006-2008)

- [1] "Cavity Ringdown Spectroscopy of the $\tilde{A} - \tilde{X}$ Electronic Transition of the Phenyl Peroxy Radical," G. M. P. Just, E. N. Sharp, S. J. Zalyubovsky, and T. A. Miller, *Chem. Phys. Lett.* **417**, 378 (2006).
- [2] "Spectroscopic Probing and Diagnostics of the Geometric Structure of the Alkoxy and Alkyl Peroxy Radical Intermediates," T. A. Miller, *Mol. Phys.* **104**, 2581 (2006).
- [3] "Investigation of Ethyl Peroxy Radical Conformers Via Cavity Ringdown Spectroscopy of the $\tilde{A} - \tilde{X}$ Electronic Transition," P. Rupper, E. N. Sharp, G. Tarczay, and T. A. Miller, *J. Phys. Chem. A* **111**, 832 (2007).
- [4] "Rovibronic Bands of the $\tilde{A} \leftarrow \tilde{X}$ Transition of CH_3OO and CD_3OO Detected with Cavity Ringdown Absorption Near $1.2\text{-}1.4\ \mu\text{m}$," C.-Y. Chung, C.-W. Cheng, Y.-P. Lee, H.-Y. Liao, E. N. Sharp, P. Rupper, and T. A. Miller, *J. Chem. Phys.*, **127**, 044311 (2007).
- [5] "Observation of the $\tilde{A} - \tilde{X}$ Electronic Transition of the Isomers and Conformers of Pentyl Peroxy Radical Using Cavity Ringdown Spectroscopy," E. N. Sharp, P. Rupper, and T. A. Miller, *J. Phys. Chem.*, **112**, 1445 (2008).
- [6] "Structure and Spectra of Organic Peroxy Radicals," E. N. Sharp, P. Rupper, and T. A. Miller, *Phys. Chem. Chem. Phys.* (invited perspective article, accepted).

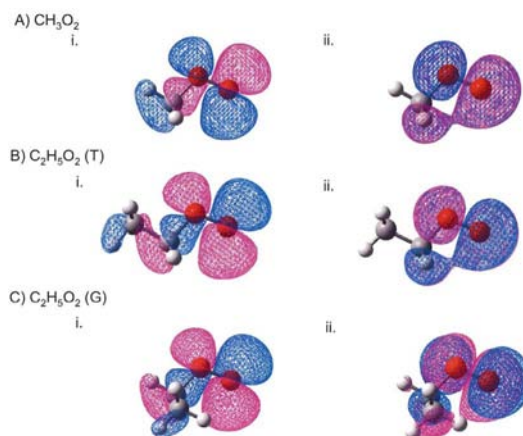


Figure 5: (Color on CD) Illustrations of electron density in the HOMO's (i.) and SOMO's (ii.) of CH_3O_2 , $C_2H_5O_2(T)$, and $C_2H_5O_2(G)$, calculated at the BLYP/6-31+G(d) level of theory. The pink and blue lobes indicate different orbital phases. The molecules have been oriented such that the C-O-O heavy atom frame lies in the plane of the paper.

Due to the geometric differences, the $\tilde{A}(gauche) - \tilde{X}(trans)$ transition will likely have poor Franck-Condon factors.

Probing Flame Chemistry with MBMS, Theory, and Modeling

T.J. Mountziaris, substitute PI for P. R. Westmoreland
Chemical Engineering Department, University of Massachusetts Amherst
Amherst, MA 01003-9330
tjm@ecs.umass.edu (westm@ecs.umass.edu)

I. Program Scope

Experimental and modeling research in this project is conducted by Prof. Phillip R. Westmoreland and his students. While he is on IPA leave from the university as an NSF program officer, I am his substitute PI, holding fiduciary responsibility during the period in which he is at NSF.

The objective of this research is obtaining kinetics of hydrocarbon combustion and molecular-weight growth in flames. Our approach combines molecular-beam mass spectrometry (MBMS) experiments on low-pressure flat flames; *ab initio* thermochemistry and transition-state structures; rate constants predicted by transition-state and chemical activation theories; and whole-flame modeling using mechanisms of elementary reactions.

MBMS is a particularly powerful technique because it can be used to measure a wide range of species quantitatively, including radicals, with minimal flame perturbation. By using two complementary instruments, we obtain remarkably complete sets of flame data that are useful for direct insights, testing of mechanistic models, and selected measurement of rate constants. Our electron-ionization quadrupole MS at UMass provides species profiles with high signal sensitivity and mass resolution. At the Advanced Light Source (ALS) at LBNL, we obtain species profiles with more precise isomer resolution and identification using time-of-flight MS with VUV photoionization. Professor Westmoreland co-developed this system with DOE-BES contractors Terry Cool, Andy McIlroy, Craig Taatjes, and Nils Hansen. Additional collaborators in making measurements include the group of Katharina Kohse-Höinghaus of Universität Bielefeld, while DOE-BES contractors Jim Miller, Stephen Klippenstein, Charlie Westbrook, and Fred Dryer have collaborated in modeling thermochemistry, kinetics, and flame structure.

II. Recent Progress

A. Data from the MBMS systems

Flames of a wide range of hydrocarbon and biomass-related fuels have been mapped by our team of researchers at the Advanced Light Source at Lawrence Berkeley National Laboratory in the past year:

- Methane ($\phi=1.0, 1.2, 1.4, 1.6$) to provide a reference set of data for model comparison and for use in direct calibration of signals for stable species and radicals;
- Acetylene, fuel-rich ($\phi=2.4$) for analysis of growth and oxidation chemistry by comparison to the literature results of Westmoreland *et al.* [i] and of Delfau and Vovelle [ii];
- trans-Dimethylbutene, stoichiometric and fuel-rich ($\phi=1.0$ and 1.7) for analysis of growth and oxidation chemistry with analogues to ethene and propene;
- 1,3-Butadiene, fuel-rich ($\phi=1.8$) because of its role in forming C_4H_x and C_3H_3 radicals;
- Toluene, lean and fuel-rich ($\phi=0.9$ and 1.9) for analysis of growth and oxidation chemistry including formation of indene and naphthalene;
- 1-Hexene and methylcyclopentene for comparison and contrast as cyclohexane isomers;
- Morpholine as a biofuel-related molecule having both ether and amine linkages;
- Tetrahydrofuran as a cyclooxigenate;
- Mixed ethanol / propene to study their flame interactions;
- Dimethylether ($\phi=1.00, 1.25, 1.50, 1.75, 2.00$) as a reference ether;
- Esters including methyl acetate, ethyl acetate, methyl propanoate, methyl propenoate, ethyl propanoate, methyl propanoate, methyl isobutanoate, methyl butyrate, methyl methacrylate, and methyl propionate as models for study of biofuel kinetics.

Temperature measurements for some of these flames were completed in our lab at UMass using Y_2O_3/BeO -coated, radiation-compensated Pt/Pt13%Rh thermocouples and by Tina Kasper at Sandia using LIF. Mole-fraction profiles of these and prior flames have been or are being analyzed in parallel at Cornell, Sandia, and UMass.

B. Morpholine chemistry appears analogous to cyclohexane chemistry.

Flame measurements for morpholine fuel, a compound that has heterocyclic ether and amine linkages observed in biomass, highlights the strengths of the ALS MBMS and the need for mechanistic interpretation. It has become clear that saturated alkanes initially are destroyed through H-abstraction by H, O, and OH, followed by a series of beta-scission steps to form alkenes. Morpholine (1-oxa-4-azacyclohexane or cyclo -O-CH₂CH₂-NH-CH₂CH₂-) has the same, fully saturated structure as cyclohexane but with ether and amine substitutions at the 1 and 4 positions, and it seemed reasonable to assume it would react like an alkane although having more varied products. The two heteroatoms lead to a richly diverse chemistry.

Dominant paths of this mechanism are shown in Fig. 1. Abstraction from C-H bonds in morpholine is favored kinetically because of bond energies and reaction path degeneracies. Ring-opening by beta-scission will dominate destruction of the morpholinyl radicals, although there will be small contributions from beta-scission of H's, making cyclohexene analogues, and radical disproportionation. The resulting radicals will likewise decompose mainly by beta-scission of heavy-heavy bonds where available. The result is rapid conversion to a mix of C₂H₄, CH₂=NH, CH₂O, C₂H₂, HCN, CO, and their combustion reaction intermediates, along with routes to analogues of cyclohexene, 1,5-hexadiene, and 1,3-butadiene.

Detection of intermediate species in a slightly fuel-rich flame ($\phi=1.3$) supports, clarifies, and extends this mechanism. At least two mass 86 species (2nd and 3rd rows) are in significant concentrations, as are mass 57 (probably the butadiene analogue NH=CH₂-CH=O) and mass 55 (probably CH₂=N-CH=CH₂), beta-scission products of row-4 species. All the molecular species in the bottom two rows are detected. In addition, NH₃, NO, and C₂NH_x species were detected that must be incorporated into the model. Modeling is in progress, including calculation of thermochemistry, kinetics, and ion energetics that are unavailable for many of the 2nd, 3rd, and 4th-row species.

C. Fuel decomposition can be more important in flame chemistry than previously thought.

Fuel destruction in flames is usually by fast radical abstraction and addition kinetics, but our recent work with 1,3-butadiene and 1-hexene flames shows how decomposition can be important.

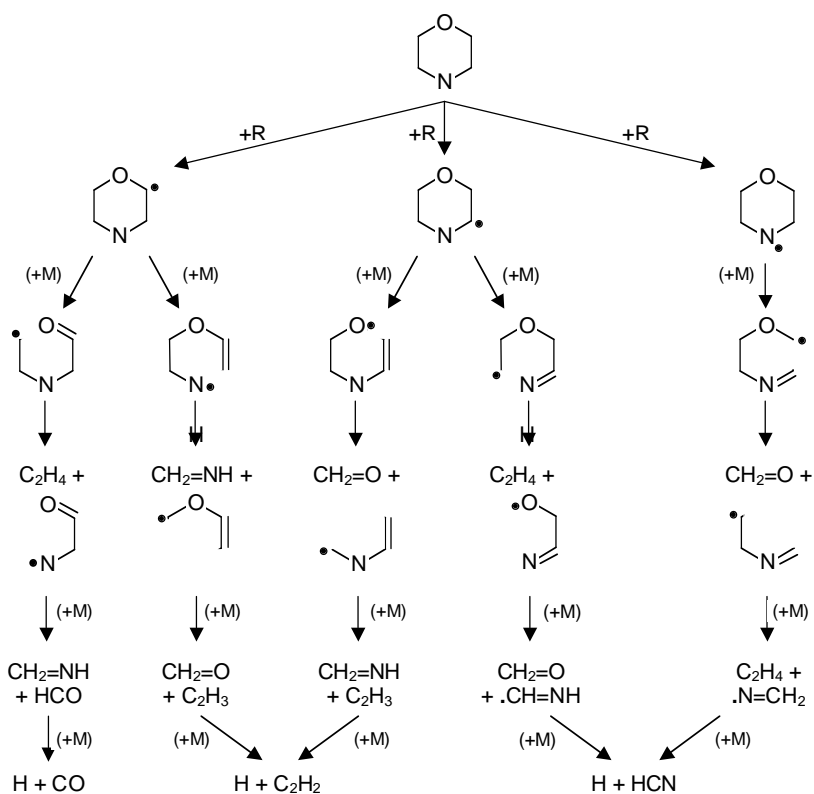


Figure 1. Basic abstraction-decomposition mechanism for morpholine combustion.

rows) are in significant concentrations, as are mass 57 (probably the butadiene analogue NH=CH₂-CH=O) and mass 55 (probably CH₂=N-CH=CH₂), beta-scission products of row-4 species. All the molecular species in the bottom two rows are detected. In addition, NH₃, NO, and C₂NH_x species were detected that must be incorporated into the model. Modeling is in progress, including calculation of thermochemistry, kinetics, and ion energetics that are unavailable for many of the 2nd, 3rd, and 4th-row species.

McEnally *et al.* [iii] noted that fuel dissociation can become important in flames for large fuel molecules, but the present work shows that even for a four-carbon species like butadiene it becomes significant.

In the butadiene study [Pub 16], we compared model predictions for the rich flame that we measured ($\phi=1.8$) and for the similar but richer ($\phi=2.4$) flame of Cole *et al.* [iv]. H-abstraction by H and OH dominates fuel destruction in the first flame, but butadiene dissociation to vinyls is significant and grows to become of equal importance in the $\phi=2.4$ flame.

Modeling of the 1-hexene flame shows fuel destruction is completely dominated by dissociation, forming allyl and n-propyl. We also calculated the pressure-dependence of 1-hexene's interesting chemically activated H-addition channels, which have facile isomerizations of the resulting radicals. However, these routes also were unable to compete with homolytic fission of the weak allylic C-C bond.

Routes to benzene formation in these flames were interesting as well. Butadiene flames should be the most favorable for any $C_4H_5+C_2H_2$ route, and the earlier MBMS study [iv] supported it. In both the Cole flame and the ALS flame, modeling showed that $C_3H_3 + C_3H_3$ and $i-C_4H_5 + C_2H_2$ reactions were roughly of equal importance. In the 1-hexene flame, initial modeling also shows that $C_3H_3 + C_3H_3$ contributes but does not appear sufficient to account for the benzene formation. Further modeling will examine possible $C_3H_3 + C_3H_5$ routes.

III. Future Work

We will conduct complementary experiments at UMass and at the ALS on flames of acetylene, benzene, toluene, and their mixtures along with modeling at UMass. The purpose is to establish formation and destruction chemistry of polycyclic aromatic hydrocarbons, using these fuels to focus on indene and naphthalene. The UMass system has a valuable role because it has higher signal sensitivity, especially for radicals, can be run at more fuel-rich conditions, and is more suitable for the thermocouple measurements. Professor Westmoreland will also continue to coordinate flame modeling for the research team, and we will participate in the team objectives of improving the mass and signal sensitivity of the ALS apparatus and of studying flame kinetics for other hydrocarbons, biofuel analogues, and amines.

IV. References

- i. Westmoreland, P.R., Howard, J.B., Longwell, J.P., *Proc. Combust. Inst.* **1986**, 31, 773.
- ii. Delfau, J.-L., Vovelle, C., *Combust. Sci. Tech.* **1984**, 41, 1; *J. Chim. Phys.* **1985**, 82, 747.
- iii. McEnally, C.S., Pfefferle, L.D., Atakan, B., Kohse-Höinghaus, K. *Prog. En. Comb. Sci.* **2006**, 32, 247.
- iv. Cole, J.A., Bittner, J.D., Howard, J.B., Longwell, J.P., *Combust. Flame* **1984**, 56, 51.

V. Publications and submitted journal articles supported by this project 2006-2008

1. N. Hansen, J.A. Miller, T.A. Cool, J. Wang, M.E. Law, P.R. Westmoreland, "Synchrotron Photoionization Measurements of Combustion Intermediates: Photoionization Efficiency of C_3H_2 Isomers," *Phys. Chem. Chem. Phys.* **7**, 806-813 (2005).
2. B. Ruscic, J. E. Boggs, A. Burcat, A. G. Czàszàr, J. Demaison, R. Janoschek, J. M. L. Martin, M. L. Morton, M. J. Rossi, J. F. Stanton, P. G. Szalay, P. R. Westmoreland, F. Zabel, T. Bérces, "IUPAC critical evaluation of thermochemical properties of selected radicals - Part I," *J. Phys. Chem. Ref. Data* **34**(2), 573-656 (2005).
3. C.A. Taatjes, N. Hansen, A. McIlroy, J.A. Miller, J.P. Senosiain, S.J. Klippenstein, F. Qi, L. Sheng, Y. Zhang, T.A. Cool, J. Wang, P.R. Westmoreland, M.E. Law, T. Kasper, K. Kohse-Höinghaus, "Enols Are Common Intermediates in Hydrocarbon Oxidation," *Science* **308**(5730), 1887-1889 (2005).
4. M. E. Law, *Molecular-Beam Mass Spectrometry of Ethylene and Cyclohexane Flames*, Ph.D. Dissertation, University of Massachusetts Amherst (2005).
5. T.A. Cool, A. McIlroy, F. Qi, P.R. Westmoreland, L. Poisson, D.S. Peterka, M. Ahmed, "A Photoionization Mass Spectrometer for Studies of Flame Chemistry with a Synchrotron Light Source," *Rev. Sci. Instr.* **76**, 094102-1 to 094102-7 (Sept 2005).

6. P. R. Westmoreland, M.E. Law, T.A. Cool, J. Wang, C.A. Taatjes, N. Hansen, T. Kasper. "Analysis of Flame Structure by Molecular-Beam Mass Spectrometry Using Electron-Impact and Synchrotron-Photon Ionization," *Fizika Goreniya i Vzryva* 42(6), 58–63, November–December, 2006. / *Combustion, Explosion and Shock Waves* (English) 42(6), 672-677 (2006).
7. C.A. Taatjes, N. Hansen, J.A. Miller, T.A. Cool, J. Wang, P.R. Westmoreland, M.E. Law, T. Kasper, K. Kohse-Höinghaus. "Combustion Chemistry of Enols: Possible Ethenol Precursors in Flames," *J. Phys. Chem. A* **110**(9), 3254-3260 (2006). DOI: 10.1021/jp0547313
8. N. Hansen, S.J. Klippenstein, C. A. Taatjes, J.A. Miller, J. Wang, T.A. Cool, B. Yang, R. Yang, L. Wei, C. Huang, J. Wang, F. Qi, M.E. Law, P.R. Westmoreland, T. Kasper, K. Kohse-Höinghaus. "Identification and Chemistry of C₄H₃ and C₄H₅ Isomers in Fuel-Rich Flames," *J. Phys. Chem. A* **110**(10), 3670-3678 (2006). DOI: 10.1021/jp0567691
9. N. Hansen, S.J. Klippenstein, J.A. Miller, J. Wang, T.A. Cool, M.E. Law, P.R. Westmoreland, T. Kasper, K. Kohse-Höinghaus, "Identification of C₅H_x Isomers in fuel-rich flames by photoionization mass spectrometry and electronic structure calculations", *J. Phys. Chem. A* **110**(13), 4376-4388 (2006). DOI: 10.1021/jp0569685.
10. M.E. Law, P.R. Westmoreland, T. A. Cool, J. Wang, N. Hansen, T. Kasper. "Benzene Precursors and Formation Routes in a Stoichiometric Cyclohexane Flame," *Proceedings of the Combustion Institute* **31**, 565-573 (2007); DOI: <http://dx.doi.org/10.1016/j.proci.2006.07.259>
11. T. A. Cool, J. Wang, N. Hansen, P. R. Westmoreland, F. L. Dryer, Z. Zhao, A. Kazakov, T. Kasper, K. Kohse-Höinghaus. "Photoionization mass spectrometry and modeling studies of the chemistry of fuel-rich dimethyl ether flames," *Proc. Combustion Institute* **31**, 285-293 (2007); DOI: <http://dx.doi.org/10.1016/j.proci.2006.08.044>
12. K. Kohse-Höinghaus, Patrick Obwald, Ulf Struckmeier, T. Kasper, N. Hansen, C. A. Taatjes, J. Wang, T.A. Cool, S. Gon, P.R. Westmoreland. "The influence of ethanol addition on a premixed fuel-rich propene-oxygen-argon flame," *Proceedings of the Combustion Institute* **31**, 1119-1127 (2007); DOI: <http://dx.doi.org/10.1016/j.proci.2006.07.007>
13. N. Hansen, J.A. Miller, C. A. Taatjes, J. Wang, T.A. Cool, M.E. Law, P.R. Westmoreland. "Photoionization Mass Spectrometric Studies and Modeling of Fuel-Rich Allene and Propyne Flames," *Proc Combust Inst* **31**, 1157-64 (2007); <http://dx.doi.org/10.1016/j.proci.2006.07.045>
14. N. Hansen, T. Kasper, S.J. Klippenstein, P.R. Westmoreland, M.E. Law, C.A. Taatjes, K. Kohse-Höinghaus, J. Wang, T.A. Cool, "Initial steps of aromatic ring formation in a laminar premixed fuel-rich cyclopentene flame", *J Phys Chem A* (accepted, 1/2007); DOI: 10.1021/jp0683317
15. P. Obwald, U. Struckmeier, T. Kasper, K. Kohse-Höinghaus, J. Wang, T.A. Cool, N. Hansen, P.R. Westmoreland, "Isomer-specific fuel destruction pathways in rich flames of methyl acetate and ethyl formate and consequences for the combustion chemistry of esters", *J. Phys. Chem. A* (accepted, 1/2007) ; DOI: 10.1021/jp068337w
16. N. Hansen, J. A. Miller, T. Kasper, K. Kohse-Höinghaus, P. R. Westmoreland, J. Wang, T. A. Cool, "Benzene Formation in Premixed Fuel-Rich 1,3-Butadiene Flames," *Proc. Combust. Inst.* **32** (accepted).

GAS-PHASE MOLECULAR DYNAMICS: THEORETICAL STUDIES IN SPECTROSCOPY AND CHEMICAL DYNAMICS

James T. Muckerman (muckerma@bnl.gov) and Hua-Gen Yu (hgy@bnl.gov)
Chemistry Department, Brookhaven National Laboratory, Upton, NY 11973-5000

Program Scope

The goal of this program is the development and application of computational methods for studying chemical reaction dynamics and molecular spectroscopy in the gas phase. We are interested in developing rigorous quantum dynamics algorithms for small polyatomic systems and in implementing approximate approaches for complex ones. Particular focus is on the dynamics and kinetics of chemical reactions and on the rovibrational spectra of species involved in combustion processes. This research also explores the potential energy surfaces of these systems of interest using state-of-the-art quantum chemistry methods.

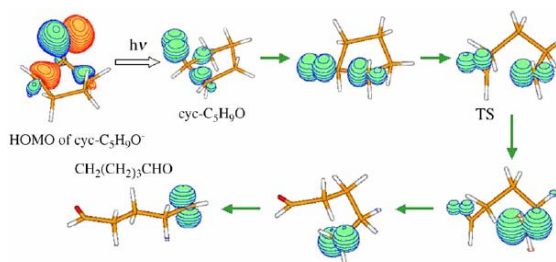
Recent Progress

Energetics and dynamics of the reaction of HOCO with O atoms

The important combustion reaction of O with HOCO has been studied using a direct *ab initio* dynamics method based on the scaling all correlation UCCD/D95(d,p) method. *Ab initio* calculations reveal two possible reaction mechanisms for the $O + HOCO \rightarrow OH + CO_2$ reaction. They are a direct hydrogen abstraction and an oxygen addition reaction through a short-lived HOC(O)O intermediate. The dynamics results show that only the addition mechanism is important at temperatures below 1000 K. The lifetime of the HOC(O)O complex is predicted to be 172 ± 15 fs. This is typical of a direct and fast radical-radical reaction. At room temperature, the calculated thermal rate coefficient is $1.44 \times 10^{-11} \text{ cm}^3 \text{ molec}^{-1} \text{ s}^{-1}$ and its temperature dependence is rather weak. Compared to the $O_2 + HOCO$ reaction, this reaction is about an order of magnitude faster. Trajectories also showed that a 1,3-H transfer reaction in the HOC(O)O intermediate complex could occur so that the oxygen atom in the OH product can be either the terminal oxygen in the reactant HOCO or the incident oxygen atom. In addition, our SAC UCCD method predicts a barrier height of 16.7 kcal/mol for the $HO_2 + CO \rightarrow OH + CO_2$ reaction.

Molecular dynamics simulation of photo-initiated reactions

The direct *ab initio* molecular dynamics program has been extended to study photo-initiated reactions through vibrational overtone excitations and photodetachment processes. The first example studied is the photodetachment reaction of cyclopentoxide since cyclopentoxy (cyc-C₅H₉O) radicals are important intermediates in combustion



The spin density evolution of the ring-opening reaction of cyclopentoxide produced from a photodetachment process of cyclopentoxide whose HOMO is also shown in the left-top corner.

environments and atmospheric chemistry. The molecular dynamics simulation is carried out using the HCTH/6-31G(d) DFT method. Here, the ring-opening reaction of

cyclopentoxo to the 5-oxo-pentan-1-yl radical has been the primary focus. The lifetime of cyclopentoxo is predicted to be 3.05 ± 0.07 ps. We have proposed a “post passive” scheme to include the nuclear dynamics effects for simulating the photoelectron kinetic energy (eKE) spectrum. The calculated eKE spectrum for the photodetachment reaction of cyclopentoxide is in good agreement with experimental results. It was also found that its ring-opening dynamics processes could be effectively investigated by using an atomic spin density technique as well as the traditional trajectory method.

Vibronic spectra of boron nitride nanotubes

Boron nitride nanotubes (BNNTs) are a potential material for hydrogen storage. In this work, radiative transitions of BNNTs in the energy range 1-6 eV have been studied using both experimental and theoretical approaches. In addition to the direct band-gap transition at 5.38 eV, diffuse structures near 4.09 eV were observed in the cathodoluminescences (CL) spectra for BNNTs. Our calculations suggested that these diffuse spectra could arise from a phonon-electron coupling mechanism *via* defects or impurities in the nanotubes. That is, they are typical vibronic spectra analogous to molecular electronic ones. For the ^{10}B N nanotubes, the phonon frequency was determined as 0.1752 eV (or 1413 cm^{-1}), and this mode produces a progression up to five phonon replicas which gives equally spaced peaks starting at 4.09 eV toward lower energies. The calculated frequency is in excellent agreement with the Raman value of 1390 cm^{-1} . It is assigned to a B-N bond stretching deformation mode. In addition, the DFT calculations with an oxygen atom-substituted BN(5,5) nanotube indicate that $\text{BN}_x\text{O}_{1-x}$ tubes are stable, which could substantially enhance the intensities of the vibronic spectra of BNNTs, together with excitons.

Future Plans

Kinetics and dynamics study of radical-radical reactions

We will continue to study some important combustion reactions using the direct *ab initio* molecular dynamics program. Of particular interest are fast radical-radical reactions such as the reactions of HOCO with H, HO_2 , CH_3 , Cl and HOCO radicals (collaboration with J. Francisco (Purdue)). We will address the energies, geometries, and vibrational frequencies of the stationary points, and the reaction mechanism by exploring the potential energy surfaces, and determine product branching ratios and rate coefficients of the reactions by carrying out molecular dynamics simulations.

Future development of the direct *ab initio* molecular dynamics program

Dissociative recombination (DR), in which a molecular ion recombines with a free electron and subsequently dissociates into neutral fragments, is a process of fundamental importance in ion and radical chemistry, including discharges and rocket and jet exhausts. Although DR rates can be well determined either experimentally or theoretically, it is still difficult to understand their product branching ratios. Recent heavy-ion storage ring experiments showed that the product distribution of a DR reaction is usually non-statistical. For polyatomic systems, the well-developed models such as the *R*-matrix method and multi-channel quantum defect theory (MQDT) for studying reaction cross sections are incapable of investigating product branching ratios. Therefore, it is desirable

to develop new techniques. In this proposal, we intend to extend our direct *ab initio* molecular dynamics program to study the DR reactions. Here, we only address the investigations of dissociation processes, but we have to deal properly with the quantum nature of the incoming electron and the non-adiabaticity of dissociation reactions of the energized neutral molecules. The latter could be treated by the “fewest switch” algorithm of Tully’s surface hopping method. In this work, we hope to figure out a classical analog to mimic the incident electron in the classical trajectory propagations.

Rovibrational spectroscopy of large amplitude molecule HO₃

HO₃ is an interesting molecule, which is an important intermediate in atmospheric chemistry. Its structure and stability has been the subject of longstanding debate. In 2005, a trans-HO₃ molecule was first observed by Endo et al. using Fourier-transform microwave (FTMW) spectroscopy. Surprisingly, they obtained a rather long central O-O bond length of 1.688 Å, which has not been predicted by most high level *ab initio* methods. The theoretical value is around 1.54 Å, which is substantially shorter than the experimental result. Recently, Lester and her co-workers measured a binding energy of 6.12 kcal/mol for this trans-HO₃ molecule with respect to the OH + O₂ limit. So it is a weakly bound molecule. We expect that this may explain the discrepancy in structure between theory and experiment. Theoretical results are the equilibrium values while the experimental ones are vibrationally averaged. A large amplitude motion of the floppy HO₃ molecule could give such a big difference. In order to verify our assumption, we are going to perform a full dimensionality quantum dynamics calculation using an accurate *ab initio* potential energy surface. The construction of the surface will be first priority in this work.

Publications since 2006

- H.-G. Yu, T.J. Sears and J.T. Muckerman, *Potential energy surfaces and vibrational energy levels of DCCL and HCCL in three low-lying states*, Mol. Phys. **104**, 47 (2006).
- G. E. Hall, T. J. Sears and H.-G. Yu, *Rotationally Resolved Spectrum of the A(060) --- X(000) Band of HCB_r*, J. Molec. Spectrosc. **235**, 125 (2006).
- Z. Wang, R.G. Bird, H.-G. Yu and T.J. Sears, *Hot bands in jet-cooled and ambient temperature spectra of chloromethylene*, J. Chem. Phys. **124**, 74314 (2006).
- H.-G. Yu, *A rigorous full-dimensional quantum dynamics calculation of the vibrational energies of H₃O₂⁻*, J. Chem. Phys., **125**, 204306 (2006).
- H.-G. Yu and T.J. Sears, *A clue to the diffuse structure in ultraviolet spectra of the GeCl₂ X-A transition*, J. Chem. Phys., **125**, 114316 (2006).
- H.-G. Yu, *Density functional theory study of ethylene partial oxidation on Ag₇ cluster*, Chem. Phys. Lett., **431**, 236 (2006).
- H.-G. Yu and J. T. Muckerman, *Quantum molecular dynamics study of the O₂ plus HOCO reaction*, J. Phys. Chem. A, **111**, 5312 (2006).
- H.-G. Yu, *Ab initio molecular dynamics simulation of photodetachment reaction of cyclopentoxide*, Chem. Phys. Lett, **441**, 20 (2007).
- H.-G. Yu, J. T. Muckerman and J.S. Francisco, *Quantum force molecular dynamics study of the O atoms with HOCO reaction*, J. Chem. Phys. **127**, 094302 (2007).

- W.-Q. Han, H.-G. Yu, C. Zhi, J. Wang, Z. Liu, T. Sekiguchi and Y. Bando, *Isotope effect on band gap and radiative transitions properties of boron nitride nanotubes*, Nano Lett. **10**, 491 (2008).
- B.J. Braams and H.-G. Yu, *Potential energy surface and quantum dynamics study of rovibrational states of $HO_3(X^2A'')$* , Phys. Chem. Chem. Phys. (accepted, 2008).
- H.-G. Yu, *A spherical electron cloud hopping model for studying product branching ratios of dissociative recombination*, J. Chem. Phys. (submitted, 2008).

Dynamics of Activated Molecules

Amy S. Mullin

Department of Chemistry and Biochemistry, University of Maryland
College Park, MD 20742
mullin@umd.edu

I. Program Scope

The focus of my research program is to investigate collisional energy transfer of molecules with large amounts of internal energy. Collisional energy transfer is ubiquitous in most gas-phase chemistry and it often controls overall reaction rates and branching ratios. However there are substantial challenges to making detailed experimental measurements of energy transfer at energies that are relevant to chemistry. High energy molecules contain extremely large densities of states, are of transient nature and have poorly understood interactions with other molecules. Currently, there are no first-principle theories of collisional energy transfer and the lack of fundamental knowledge often results in cursory and insufficient treatments in reactive models. A goal of my research is to gain new insights into the microscopic details of relatively large complex molecules at high energy as they undergo quenching collisions.

We use state-resolved transient IR absorption to characterize the energy transfer pathways that are responsible for the collisional cooling of high energy molecules. To overcome the inherent difficulties in developing a molecular level understanding of collisions involving high energy molecules, we use high-resolution IR probing to measure population changes in small collision partners that undergo collisions with high energy molecules. Using this technique, we have performed in-depth spectroscopic studies that provide a greater understanding of high energy molecules and their collisional energy transfer.

II. Recent Progress

A. State-resolved probes of low- ΔE energy transfer: Energy gain via “weak” collisions

Until recently, high-resolution probing of collisional energy transfer of high energy molecules has been limited to measuring large ΔE collisions that scattered bath molecules into previously unpopulated states. We have recently developed the experimental means to measure the outcome of small ΔE collisions for states of the bath gas that are thermally populated prior to collisions with high energy molecules. This breakthrough represents an important because it allows us to investigate for the first time the dynamics that are associated with so-called “weak” collisions. The terms “weak” and “strong” are qualitative descriptors that refer to collisions leading to small- ΔE and large- ΔE energy transfer, based historically on Hirschelwood’s strong collision assumption.

Collisions that induce small exchanges of energy make up the vast majority of energy transfer events but they are difficult to distinguish from the ambient background population in low-J states at 300 K. Parallel energy transfer processes that excite bath vibrational states (V-to-V energy transfer) interfere with high-resolution absorption measurements by moving population into upper states of the IR probe transitions. If this is the case, it is impossible to sort out how distinct processes contribute to the overall absorption signals. We overcome this problem by judiciously choosing probe transitions that have negligible cross sections for V-to-V energy transfer. For CO₂ probing, we use 00⁰→10⁰1 transitions near $\lambda=2.7 \mu\text{m}$. For HOD and DCl probing, we do not observe collisional transfer to the stretching modes and single quantum probe transitions are used at $\lambda=2.7 \mu\text{m}$ and $4.5 \mu\text{m}$, respectively.

To measure the transient populations from weak collisions, we collect transient Doppler-broadened IR line profiles for individual states of bath molecules immediately following single collisions with highly excited molecules. Representative line profiles for collisions of pyrazine (C₄H₄N₂, E=39700 cm⁻¹) with DCl and CO₂ are shown in Fig. 1. For low-J states of the bath molecule, such as shown in Fig. 1, signals are dominated by negative-going depletion of the initial population at the center frequency of the probe transition. In the Doppler-broadened wings, positive-going appearance signals correspond to the products of collisional energy transfer. The data are fit using a double Gaussian function that distinguish

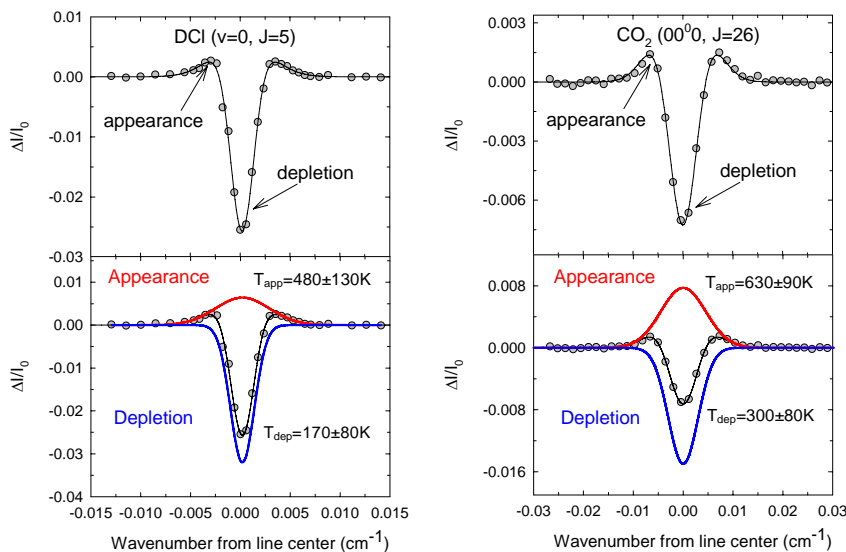


Figure 1. Transient absorption line profile of scattered DCl($v=0, J$) and CO₂($00^0_0, J$) in low- J states due to collisions with pyrazine(E). Negative-going signals are due to collisions that deplete thermally populated states. Positive-going appearance signals correspond to appearance of scattered molecules. Data are collected at $t=1 \mu\text{s}$ after UV excitation of pyrazine and correspond to single collisions under conditions ($P \sim 25 \text{ mTorr}$, $T=300\text{K}$) where the average time between collisions is $\tau_{\text{col}} \sim 4 \mu\text{s}$.

contributions of the appearance and depletion signals. Depletion line widths correspond to the initial distribution of collision velocities and appearance line widths directly yield the distribution of recoil velocities in the scattered molecules. The integrated area of the appearance component corresponds to the nascent population of bath molecules that are scattered into a final rotational state. In this way, we measure nascent rotational and translational energy distributions for the full range of rotational states of the scattered bath molecules.

B. Energy gain profiles of “weak” and “strong” collisions

We have measured the nascent appearance and depletion of individual rotational states of DCl($v=0, J=2-20$) and CO₂($0000, J=2-80$) following single collisions with pyrazine(E). The center-of-mass recoil energies of the scattered bath molecules are plotted in Fig.2 as a function of bath rotational state. Average recoil energies for appearance (in red) of low J -states are modest with $E_{\text{rel}} \sim 500 \text{ cm}^{-1}$ for DCl and $E_{\text{rel}} \sim 600 \text{ cm}^{-1}$ for CO₂. As the rotational quantum number of the bath increases, the recoil energy from collisions increases nonlinearly above a threshold bath state J_{th} . For DCl, the threshold is near $J_{\text{th}} \sim 16$ and for CO₂ the threshold is roughly near $J_{\text{th}} \sim 60$. The increase in recoil energy as a function of J is indicative of impulsive collisions. At higher J states, the recoil energies for CO₂ are significantly larger than those for DCl, consistent with angular momentum constraints and CO₂'s more closely-spaced rotational states. The threshold states for DCl and CO₂ have similar rotational energy with $E_{\text{rot}} \sim 1450 \text{ cm}^{-1}$. Interestingly, pyrazine has a number of vibrational modes in this region: the C–H bending modes at 1230 and 1350 cm^{-1} and ring stretching modes between 1410 and 1580 cm^{-1} . It is unlikely that our observations can be attributed to a single mode in the vibrationally excited donor, but it is interesting that thresholds are observed at similar rotational energies near vibrational frequencies that involve movement of heavy ring atoms. A number of trajectory studies indicate that ring stretches and out of plane bending modes are especially effective at imparting large energy changes in collisions.

The initial translational energies associated with depletion of low- J states of DCl and CO₂ are shown in blue in Fig. 2. These values are based on nascent depletion line width measurements. For DCl, the initial translational energies are slightly below the 300 K . This indicates that DCl molecules with slightly smaller velocities are undergoing the first set of collisions that quench pyrazine. This observation is consistent with the presence of attractive intermolecular forces that preferentially involve slower

molecules in collisions. For CO₂, the depletion line widths are all near 300 K. This is expected since pyrazine/CO₂ has much weaker intermolecular attraction.

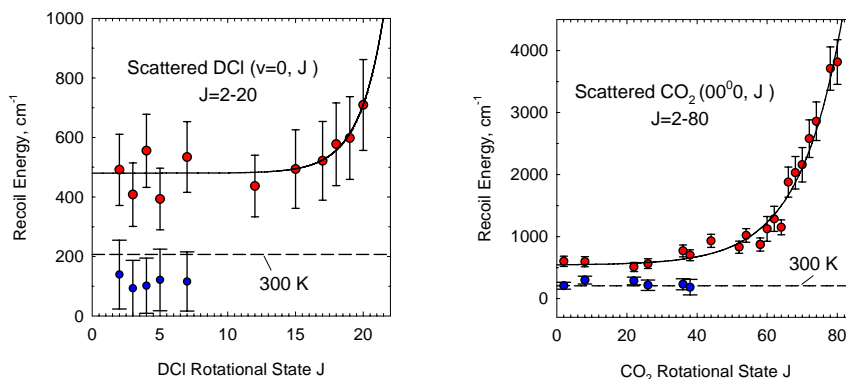


Figure 2. Recoil energy of individual rotational states of DCI and CO₂ following single collisions with highly excited pyrazine (red circles). The recoil energy of the scattered molecules (in the center-of-mass frame) increases as function of bath rotational state. Depletion measurements (blue circles) correspond to the translational energy of bath molecules prior to collisions with pyrazine(E). Depletion line widths for CO₂ correspond to a 300 K distribution, while those for DCI are closer to a 220 K distribution.

C. Direct measurements of collisions rates: When is Lennard-Jones trustworthy?

Transient IR data on the full range of ΔE collisions directly yields the full energy transfer distribution function $P(\Delta E)$ where ΔE is the amount of donor vibrational energy that is lost in collisions. ΔE includes the final bath energy and the recoil energy of the scattered molecules. In Fig. 3, $P(\Delta E)$ data for quenching pyrazine(E) with DCI and HOD using two different methods to get the collision rate. The probability is based on experimental measurements of the energy transfer rate which is scaled to a collision rate. The plot on the left uses a calculated collision rate. On the right, the collision rate is based on the sum of energy transfer rates. For pyrazine/DCI, the experimental collision rate is very close to the Lennard-Jones collision rate (within 90%). For pyrazine/HOD however, the experimental rate is nearly a factor of two larger than the Lennard-Jones rate. Using the Lennard-Jones rate artificially enhances the energy transfer efficiency for HOD because it underestimates the collision rate. When scaled to the experimental collision rate, the distributions for HOD and DCI have roughly similar intensities and integrate to unity. It is clear that the choice of collision rate has an important effect on the overall energy transfer results.

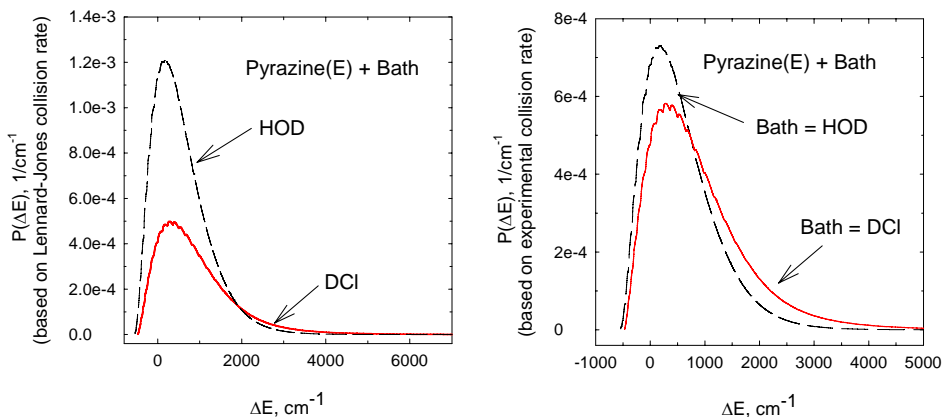


Figure 3. Energy transfer distribution functions $P(\Delta E)$ for pyrazine(E) quenching with HOD and DCI, based on transient IR absorption data. In the left-hand plot the energy transfer probability is determined by the ratio of measured energy transfer rates and the Lennard-Jones collision rate. In the right-hand plot, the collision rate is based on the sum of the measured energy transfer rates.

It is seen in Fig. 3 that the bulk of quenching collisions involve energy transfer with $\Delta E > 2000 \text{ cm}^{-1}$ for both HOD and DCl. DCl has a more pronounced strong collision component due to its larger rotational and translational energy gains. Water is a strongly interacting bath molecule and its rotational energy gain is sensitive to details of the intermolecular potential. Water is scattered with very little recoil energy for all donors we have studied. This is due to a combination of its light mass and its widely-spaced rotational levels.

D. Hydrogen-bonding effects in “strong” collisions

We have investigated whether strong collisions are sensitive to preferential orientations due to differences in the intermolecular potential between donor and acceptor. We used IR probing to measure the energy partitioning in water that results from strong collisions with vibrationally excited pyridine- h_5 (C_5H_5N), - d_5 and - f_5 . Energy minima of $\sim 700 \text{ cm}^{-1}$ exist for all three donors with water in two locations: a σ -type interaction of the nitrogen lone pair and a π -type interaction with the aromatic π -cloud. The lowest energy π -interaction of water with pyridine- h_5 and - d_5 occurs with water’s hydrogen atoms pointed toward the aromatic ring. In pyridine- f_5 , the opposite orientation of water is most stable due to the strong electronegativity of the fluorine atoms. We find that the amount of energy imparted to water in collisions with pyridine- h_5 and - d_5 is roughly twice that for pyridine- f_5 . The ability to impart rotational energy to water through close-range collisions is reduced when rocking motions of water on the surface of the donor are hindered.

III. Future Work

Experimental work is continuing on the low- ΔE collisions of vibrationally hot donor molecules with CO_2 . Future results will include information on the full energy gain distribution and the collision rates for relaxation. Other experiments are exploring whether collision rates are influenced by the amount of internal energy in the hot donor molecules and by the intermolecular potential. In the future, we plan to measure energy transfer dynamics for HCl as a collision partner. These studies along with those for DCl energy gain will provide a benchmark for testing how rotational and translational energy partitioning scales with angular momentum constraints for the same intermolecular potential energy surface.

IV. Publications and submitted journal articles supported by this project 2006-2008

1. “Relaxation dynamics of highly vibrationally excited picoline isomers ($E_{\text{vib}} = 38300 \text{ cm}^{-1}$) with CO_2 : The role of state density in impulsive collisions,” Elisa M. Miller, Liat Murat, Nicholas Bennette, Mitchell Hayes, and Amy S. Mullin, *J. Phys. Chem. A* **110**, 3266-3272 (2006).
2. “Direct determination of collision rates beyond the Lennard-Jones model through state-resolved measurements of strong and weak collisions,” Daniel K. Havey, Qingnan Liu, Ziman Li, Michael S. Elioff, Maosen Fang, Joshua Neudel and Amy S. Mullin, *J. Phys. Chem. A* **111**, 2458-2460 (2007).
3. Alkylation Effects on Strong Collisions of Highly Vibrationally Excited Alkylated Pyridines ($E_{\text{vib}} \sim 38800 \text{ cm}^{-1}$) with CO_2 ” by Qingnan Liu, Juan Du, Daniel K. Havey, Z. Li, Elisa M. Miller and Amy S. Mullin, *J. Phys. Chem. A* **111**, 4073-4080 (2007).
4. “Collisions of highly vibrationally excited pyrazine with HOD: State-resolved probing of strong and weak collisions,” D. K. Havey, Q. Liu, Z. Li, M. S. Elioff, and A. S. Mullin, *J. Phys. Chem. A* **111**, 13321-13329 (2007).
5. “State resolved strong collisions of vibrationally excited azulene ($E_{\text{vib}} = 20,100$ and $38,500 \text{ cm}^{-1}$) with CO_2 ,” L. Yuan, J. Du and A. S. Mullin, submitted to *J. Chem. Phys.*
6. “Energy transfer dynamics of weak and strong collisions between vibrationally excited pyrazine ($E_{\text{vib}} = 37900 \text{ cm}^{-1}$) + DCl,” J. Du, L. Yuan, Shizuka Hsieh, Felix Lin and Amy S. Mullin, submitted to *J. Phys. Chem.*
7. “Preferential Hydrogen Bonding Effects in Collisional Energy Transfer of Highly Excited Molecules with Water,” Daniel K. Havey, Qingnan Liu and Amy S. Mullin, submitted to *J. Phys. Chem.*

Reacting Flow Modeling with Detailed Chemical Kinetics

Habib N. Najm

Sandia National Laboratories
P.O. Box 969, MS 9051, Livermore, CA 94551
hnnajm@sandia.gov

1 Program Scope

The goal of this research program is to improve our fundamental understanding of reacting flow, thereby advancing the state of the art in predictive modeling of combustion. The work involves: (1) Using computations to investigate the structure and dynamics of flames in unsteady vortical flows; (2) Developing techniques for analysis of multi-dimensional reacting flow; (3) Developing numerical methods for discretizing reacting flow systems of equations with detailed kinetics and transport; (4) Developing massively parallel codes for computing large scale reacting flow with detailed kinetics; and (5) Developing means for uncertainty quantification in reacting flow computations, including Bayesian methods for construction of uncertain chemical models from experimental data.

2 Recent Progress

2.1 Reacting Flow Computations, Analysis, and Model Reduction

We studied methane-air edge flames stabilized against a uniform flow in a mixing layer between pure fuel and air streams. This investigation focused on the structure of NO chemistry in the edge flame, highlighting the NO structure in the two partially premixed flame branches and that in the trailing diffusion flame. Dominant NO production and consumption rates were evident behind the rich premixed flame branch. We identified the breakdown among the thermal, prompt, NO₂ and N₂O-mediated NO pathways in different regions of the edge flame. The thermal pathway exhibited dominant contribution to NO production, in a spatially integrated context over the edge flame tip. Both thermal and prompt NO were dominant locally in the flame. Comparisons with 1D premixed, diffusion, and triple flames, were investigated, exhibiting similarities as well as differences in specific features of NO_x structure.

We have also completed the development of a distributed parallel version of our existing uniform mesh low Mach number flow code, with adaptive mesh partitioning and dynamic load balancing. This capability enables our utilization of larger classes of machines than the shared-memory platforms we have hitherto used for low Mach number reacting flow studies with detailed kinetics. This will be necessary as we proceed to multidimensional reacting flow computations with more complex fuels.

We studied 1D premixed nHeptane-air flames using detailed and simplified mechanisms. The simplified mechanisms were developed using Computational Singular Perturbation (CSP) analysis of nHeptane-air ignition databases over ranges of stoichiometry and pressure. Two sets of simplified mechanisms, comprehensive over ranges of stoichiometry and pressure, were found to have good agreement with the detailed model in predicting global flame features, while significantly larger errors were observed for minor species. Examining the premixed flame structure in the low temperature region, we found a higher importance of low temperature chemistry under very lean/rich reactants mixture conditions. Using CSP analysis, we identified chemical and transport processes of high importance in the low temperature region. This analysis also revealed exceedingly small time scales of $O(10^{-15})$ sec in the detailed nHeptane chemical kinetic model. These time scales are smaller than collisional time scales under the conditions at hand, and are therefore non-physical. This observation highlights the need to pay attention to the aggregate dynamical character of complex chemical mechanisms. It also highlights the need for effective model reduction techniques that reduce both the size and stiffness of detailed chemical models.

We have also continued to advance the state of the art in the application of dynamical analysis techniques to chemical model reduction of complex fuels. We demonstrated utilization of CSP for analysis and reduction of kinetic models for the combustion of jet fuel surrogates. Specifically, we considered a well studied surrogate for Jet A-1, composed of mixture of n-Decane, n-Propyl-benzene, and n-Propyl-cyclohexane, with a “detailed” mechanism composed of 209 species and 1673 reactions. These studies were conducted in the context of homogeneous ignition, over a range of pressures from 1 to 40 atm, and the resulting simplified mechanisms were

comprehensive over ranges of stoichiometry and initial temperature. We examined and outlined *a posteriori* errors in the simplified models associated with different degrees of simplification, and the choice of target species in the simplification strategy. Consistent with the design of the reduction algorithm, we found smaller errors for target species, as compared to other species included in each simplified mechanism. Analysis results were also used to identify prevailing pathways of surrogate fuel oxidation for low and high temperature kinetics, comparing with observations in the literature.

2.2 Uncertainty Quantification

We have demonstrated the first use of intrusive polynomial chaos (PC) methods for uncertainty quantification (UQ) in realistic non-isothermal chemical ignition. This work utilized a multiwavelet-based Multi-Resolution Analysis (MRA) PC construction with adaptive block-decomposition in stochastic space. The block decomposition ensures robust representation of uncertain fields under conditions involving strong non-linearity, bifurcation, and bimodality. The numerical construction involved time integration of the MRA-PC reformulated governing equations for the PC mode strengths of species and temperature, using implicit high-order time integrators, on each stochastic block. Block refinement is applied on regular intervals to maintain accuracy and stability. We demonstrated the construction on homogeneous ignition of a methane-air mixture using a simple one-step irreversible global mechanism model of methane oxidation. Uncertainties were postulated in the pre-exponential rate constant A and activation energy E . The joint PDF for (A, E) was constructed using Bayesian inference methods, starting with simulated measurement data of species concentration with presumed experimental noise, and was found to exhibit strong correlation. This correlation was built into the PC UQ representation of these two uncertain parameters, and propagated through the ignition process. Despite the simplicity of the chemical model, significant care was required to maintain stability of the time integrator, because of the preponderance of fast active time scales over large time spans defined by the ranges of uncertainty in the parameters. Results demonstrated an unforeseen bimodality in the solution PDFs involving large probability mass centered around the pre and post-ignition states of the system. The initial probability distribution, centered on the state of the unburnt cold mixture, develops skewness and a long tail towards the burnt state, and “leaks” probability mass to the burnt state, where a new PDF peak is observed to grow in time, while the initial unburnt PDF peak diminishes in concert. This transfer leads eventually to a single peak centered on the burnt state. This bimodal behavior was also observed using random monte-carlo sampling of the uncertain parameters. It is primarily a consequence of the highly activated kinetics, where extreme sensitivity to temperature, strong nonlinearity, and fast ignition, lead to near-zero probability of being anywhere in the intermediate region between the unburnt and burnt states. To some extent, similar behavior is expected in premixed flames, although transport processes do lead to some amelioration of the gradients bridging the unburnt and burnt states.

2.3 High-Order Structured Adaptive Mesh Refinement

We have continued development of high-order structured adaptive mesh refinement (SAMR) algorithms and code components. We completed development of the fourth-order uniform mesh projection solver components for the momentum equations, and validated their order of accuracy. We coupled the pressure equation solver with the “Hypr” toolkit and tested scalability (up to 500 processors) for various Hypr solvers and pre-conditioners, including multigrid, conjugate gradient, and GMRES. We worked with the Hypr development team to enhance the convergence speed of high-order stencils (4^{th}) by allowing lower order (2^{nd}) pre-conditioners. We coupled the uniform-mesh momentum solver with the SAMR solvers for the species and energy equations, arriving at a full high-order construction for reacting flow computations employing the Common Component Architecture (CCA) software framework. We tested this construction in the context of transient chemically reacting flow in a rectangular channel with adaptive refinement of a 3-level mesh hierarchy, and are proceeding with further testing to validate the order of accuracy of the construction. We have also worked with the SciDAC APDEC center to implement the CHOMBO adaptive mesh library as a component under CCA. This development effort is now complete with validation testing underway. Completion of this testing will enable us to incorporate CHOMBO as an additional adaptive mesh component.

2.4 CSP Tabulation and Adaptive Chemistry

We have continued development of adaptive methods for tabulating low-dimensional chemical manifolds in high-dimensional spaces, identified via CSP analysis. The scheme facilitates time-scale splitting (as opposed to operator-splitting) for explicit time integration of reacting flows, by mitigating the stiffness of chemical source terms. The goal is to develop an adaptive tabulation scheme for efficient reuse of CSP quantities that (i) is scalable to high-dimensional chemical spaces typical of realistic and complex fuels, and (ii) operates within the existing modular CCA framework. The construction uses iterated CSP homogeneous corrections to identify slow manifolds. We tabulate components of a projection operator required to filter out fast processes. We take advantage of the low dimensionality of these manifolds, relative to the overall state space, to mitigate the curse of dimensionality associated with tabulated-chemistry. We are evaluating nonparametric and inherently adaptive tabulation methods. We are using data structures developed in machine learning and computational geometry (kd-trees and box-decomposition-trees) to enable efficient nearest-neighbor and approximate-nearest-neighbor queries in high dimensions. For each manifold, these queries support nonparametric regression of CSP quantities on the slow directions. Since regression is local, the geometry of the manifold is not limited to any simplistic (e.g., linear/quadratic) form. The scheme will also support "online" learning of the low dimensional manifolds in the state space.

3 Future Plans

3.1 Reacting Flow Computations, Analysis, and Model Reduction

We are working on extending the edge flame study to more complex fuels, specifically for nHeptane-air mixtures. This extension will make use of the distributed parallel version of the low Mach number uniform mesh code discussed above, on massively parallel computational platforms, given the steep rise in computational cost in going from methane-air ($O(50)$ species) to nHeptane-air ($O(500)$ species) computations. We will focus on the internal hydrocarbon and nitrogen chemical structure of nHeptane-air edge flames, and will study their dependence on mixing/shear layer details. The study will involve both detailed full chemical models, as well as CSP-simplified models capturing specific elements of the chemical systems with higher fidelity.

We will also further develop our uniform-mesh low Mach number code base towards a fourth-order axisymmetric construction. This has been planned to follow the above mentioned MPI-implementation of the present rectangular-geometry code. It will allow targeted investigation of laboratory scale axisymmetric flames, with associated comparisons to ongoing experiments. Specifically, axisymmetric lifted laminar jet flames, extending our above studies of edge flames with complex fuels, are of significant interest.

3.2 Uncertainty Quantification in Reacting Flow

There are numerous remaining challenges facing the routine implementation of intrusive MRA PC methods for UQ in chemical reacting flow systems. To begin with, efficient intrusive MRA PC UQ in ignition remains a work in progress. The preponderance of fast active timescales over "macroscopic" time intervals due to the spread of ignition times resulting from parametric uncertainty presents significant challenges to time integration, as excessively small time steps are required over long time intervals to maintain numerical accuracy. We will investigate time integration strategies targeted at these challenges, employing efficient patching between successive time intervals on given stochastic blocks. Moreover, effective block refinement and coarsening strategies require additional development. Another challenge pertains to the requirement for increased PC order and dimensionality in stochastic space to maintain accuracy in systems exhibiting oscillatory dynamics over long time horizons. Recently developed adaptive order strategies will be helpful in this context. Further, efficient parallelization and load balancing methods will be required to achieve fast and effective intrusive PC computations. At the same time, utilization of sparse quadrature non-intrusive methods coupled with the multi-block MRA PC representation requires further development. We plan to use these methods for improving our understanding of the predictability of chemical systems given uncertainties in chemical models and environmental conditions.

3.3 High-Order Structured Adaptive Mesh Refinement (SAMR)

We will conduct extensive testing and validation of the recently demonstrated SAMR reacting flow solver. Initial tests will address empirical demonstration of the order of convergence in multidimensional flame computations,

and detailed flame structure comparisons to solutions computed with other codes. This will be followed by studies of computational speedup dependence on mesh refinement parameters, and load partitioning/balancing strategies. We will also evaluate the performance of the CHOMBO mesh component, as coupled to the rest of our reacting flow components. We will examine scalability of the overall construction with large numbers of processors. We will use the resulting toolkit for studying canonical premixed/non-premixed flames in laminar unsteady flows, employing detailed kinetic models of complex fuels, in laboratory scale geometry.

3.4 CSP Tabulation and Adaptive Chemistry

Our ongoing work in this area will address initial demonstration of the tabulation algorithms coupled with CSP and computational reacting flow components in the homogeneous ignition of Hydrogen-air mixtures. Our hitherto demonstrations of CSP tabulation, in simple non-linear model systems, have provided ample testing of the efficacy and tradeoffs of the construction from an accuracy viewpoint. The key remaining challenge is ensuring scalability of the table construction and use algorithms in a general high-dimensional chemical system context. The algorithms under development have, as a strategic goal, a key feature where response surfaces and interpolations are employed exclusively in lower dimensional spaces, according to the local low-dimensional manifold evaluated with CSP. Only nearest/approximate-nearest neighbor searches, and not interpolations, are employed in the full dimensional context of the chemical system. The Hydrogen system is the first platform where these algorithms will be implemented and evaluated. It will be followed by demonstrations in higher dimensional systems, including Methane, Propane, and nHeptane fuels.

4 BES-Supported Published/In-Press Publications [2006-2008]

- [1] Najm, H.N., Uncertainty Propagation and Polynomial Chaos Techniques in CFD, *Annual Review of Fluid Mechanics* (2008) invited paper, in press.
- [2] Valorani, M., Creta, F., Li Brizzi, A., Najm, H.N., and Goussis, D.A., Surrogate Fuel Analysis and Reduction using Computational Singular Perturbation, *AIAA-2008-1009* (2008) AIAA 46th AIAA Aerospace Sciences Meeting and Exhibit, Reno, NV.
- [3] Marzouk, Y.M., Najm, H.N., and Rahn, L.A., Stochastic Spectral Methods for Efficient Bayesian Solution of Inverse Problems, *J. Comput. Phys.*, 224(2):560–586 (2007).
- [4] Le Maître, O.P., Najm, H.N., Pébay, P.P., Ghanem, R.G., and Knio, O.M., Multi-resolution-analysis scheme for uncertainty quantification in chemical systems, *SIAM J. Sci. Comput.*, 29(2):864–889 (2007).
- [5] Ray, J., Kennedy, C.A., Lefantzi, S., and Najm, H.N., Using High-Order Methods on Adaptively Refined Block-Structured Meshes, *SIAM J. Sci. Comp.*, 29(1):139–181 (2007).
- [6] Lee, J.C., Najm, H.N., Lefantzi, S., Ray, J., Frenklach, M., Valorani, M., and Goussis, D., A CSP and Tabulation Based Adaptive Chemistry Model, *Combustion Theory and Modeling*, 11(1):73–102 (2007).
- [7] Ortega, J.M., Najm, H.N., Ray, J., Valorani, M., Goussis, D.A., and Frenklach, M., Adaptive Chemistry Computations of Reacting Flow, *Journal of Physics: Conference Series*, 78:012054 (2007).
- [8] Valorani, M., Creta, F., Donato, F., Najm, H.N., and Goussis, D.A., Skeletal Mechanism Generation and Analysis for n-heptane with CSP, *Proc. Comb. Inst.*, 31:483–490 (2007).
- [9] Goussis, D.A., and Najm, H.N., Model Reduction and Physical Understanding of Slowly Oscillating Processes: The Circadian Cycle, *Multiscale Modeling and Simulation*, 5(4):1297–1332 (2006).
- [10] Valorani, M., Creta, F., Goussis, D.A., Lee, J.C., and Najm, H.N., Chemical Kinetics Simplification via CSP, *Combustion and Flame*, 146:29–51 (2006).
- [11] Singer, M.A., Pope, S.B., and Najm, H.N., Operator-Splitting with ISAT to Model Reacting Flow with Detailed Chemistry, *Combustion Theory and Modelling*, 10(2):199–217 (2006).
- [12] Singer, M.A., Pope, S.B., and Najm, H.N., Modeling Unsteady Reacting Flow with Operator-Splitting and ISAT, *Combustion and Flame* (2006).
- [13] Goussis, D.A., and Valorani, M., An Efficient Iterative Algorithm for the Approximation of the Fast and Slow Dynamics of Stiff Systems, *J. Comp. Phys.*, 214:316–346 (2006).

Spectroscopy, Kinetics and Dynamics of Combustion Radicals

David J. Nesbitt

*JILA, University of Colorado and National Institute of Standards and Technology, and
Department of Chemistry and Biochemistry, University of Colorado, Boulder, Colorado
29th Annual Combustion Research Conference, May 27-30, 2008*

Work over the past year has been directed toward high resolution IR spectroscopy of hydrocarbon transient species, exploiting i) intense slit discharge sources of jet cooled radicals, and ii) high sensitivity detection with direct IR laser absorption methods at the quantum shot noise limit. The high resolution laser spectrometer/slit modulation methods for probing transient species (developed under NSF support) have been taken over by the DOE program to focus exclusively on spectroscopy, kinetics and dynamics of jet cooled combustion radicals. The key advantage of this approach is that high concentrations of radicals can be formed under high pressure combustion conditions with the resulting species rapidly cooled ($T \approx 10\text{-}20\text{K}$) in the slit supersonic expansion. In conjunction with the generality of IR laser absorption methods, this combination offers prospects for first time spectral detection of many key combustion radicals. Highlights from this year's progress are summarized below.

I. Vinyl Radical: Tunneling, Spin Statistics and "Roaming" H atom Dynamics

Major progress has been made toward spectroscopic studies of vinyl radical ($\text{H}_2\text{C}=\text{CH}^\bullet$),¹ whose importance as a combustion intermediate has prompted many experimental²⁻⁸ and theoretical⁹ studies. Reactions of this prototypic open shell olefinic species with oxygen/hydrogen play an important role both in saturated and unsaturated hydrocarbon fuel/oxygen flames, and in the formation of polycyclic aromatic hydrocarbons (PAH) and soot.¹⁰ The radical center also provides a low energy pathway for in-plane motion of the lone α -CH bond from one side to the other, and therefore permitting large amplitude tunneling dynamics to be observable via high resolution rovibrational spectra. We have obtained and analyzed first high-resolution IR spectra of jet-cooled vinyl radical in the C-H stretch region,¹ with sample data and typical S/N demonstrated in Fig. 1. Detailed spectral assignments and least-squares fits to an A-reduction Watson asymmetric top Hamiltonian yield rotational constants and vibrational origins for two A-type bands, arising from single quantum excitation of the symmetric CH_2 stretch. By combination differences from previous CH_2 wagging and rotation-tunneling studies,^{2,5} the observed bands can be unambiguously assigned to vinyl radical, reflecting transitions out of symmetric (0^+) and antisymmetric (0^-) tunneling levels populated at 20 K slit jet expansion temperatures. The band origins for the lower-lower ($0^+ \leftarrow 0^+$) and upper-upper ($0^- \leftarrow 0^-$) transitions occur at $2901.8603(7)\text{ cm}^{-1}$ and $2901.9319(4)\text{ cm}^{-1}$, respectively, which indicates an *increase* in the tunneling splitting and therefore a

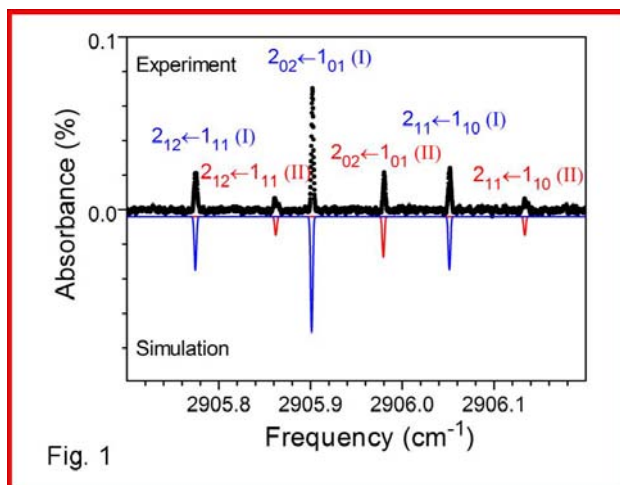


Fig. 1

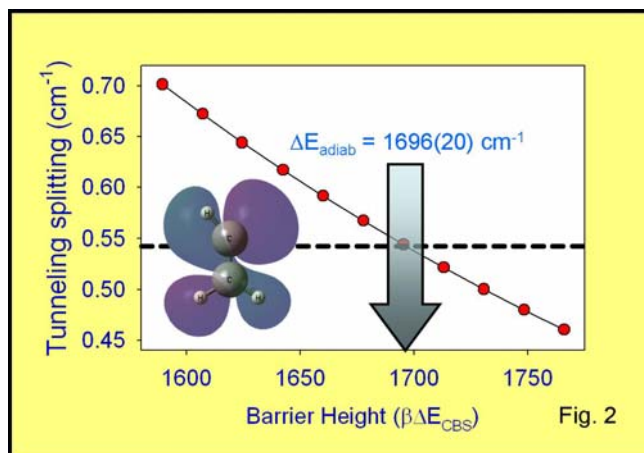
decrease in the effective tunneling barrier upon CH₂ symmetric stretch excitation. The observed CH₂ symmetric stretch bands are in excellent agreement with anharmonically scaled high level *ab initio* calculations, though red shifted from previous low resolution time resolved FTIR studies.³

Of special dynamical interest, Boltzmann analysis indicates that the 0⁺ and 0⁻ tunneling bands exhibit 1:1 nuclear spin statistics for K_a = even:odd states. This disagrees with the 3:1 ratio anticipated for feasible exchange of the *two methylenic H atoms* by tunneling of the α-CH followed by C₂ rotation. However, this is consistent with the 4:4 ratio predicted for feasible exchange of *all three H atoms*, with the 2³ = 8 nuclear spin states transforming as a $\Gamma = 4A_1' + 2E'$ irreducible representation. This observation suggests the possibility of large amplitude “roaming” of *all three H atoms* in vinyl radical at levels of excitation formed in the discharge source, consistent with the high vibrational excitation seen in photoelectron detachment studies of vinyl anion by Ervin, Ellison, Lineberger and coworkers.¹¹ This may not be so unexpected – clear precedent for such large amplitude “roaming” behavior has been well established in near threshold photolysis studies of H₂CO by Suits and coworkers,^{12,13} and acetaldehyde by Kable and Houston,¹⁴ as further explored by classical trajectory analysis of Bowman and coworkers.^{12,13,15} The issue of vibrationally mediated 1,2 intramolecular H atom shifts¹⁶ has long been of considerable importance in modeling complex combustion processes. Vibrationally excited vinyl radical appears to represent a possible benchmark system for such dynamics in a small open shell species, the elucidation of which will clearly require further experimental and theoretical exploration.

II. *Ab initio* Vibrationally Adiabatic Tunneling Dynamics in Vinyl Radical

In order to better understand these tunneling and spin statistical effects as well as corroborate our analysis of the high resolution CH₂ stretching spectra, a high level *ab initio* potential surface for *vinyl radical* has been calculated at the CCSD(T) level (AVnZ; n=2,3,4,5) for vibrationally adiabatic 1D motion along the planar CCH bending tunneling coordinate.¹⁷ This 1D tunneling potential is extrapolated to the complete basis set (CBS) limit, as well as corrected for harmonic/anharmonic zero point effects in the remaining 3N-7 = 8 coordinates. The dependence of these frequencies on the tunneling coordinate provides useful qualitative insights into the competition between sp² and sp³ hybridization for the radical C atom. In particular, this predicts an *increase* in the vibrationally adiabatic C_{2v} barrier height with symmetric CH₂ stretch excitation, which provides clear support of tunneling assignments given in analysis of the aforementioned high resolution spectra. This yields barriers to tunneling re-arrangement consistent with early *ab initio* treatments,¹⁸ yet appreciably higher than high resolution spectroscopic predictions of Kannamori et al.²

To explore this further, we have also implemented large amplitude quantum vibrational calculations for the tunneling dynamics, adiabatically corrected for rapid zero point motion in all other

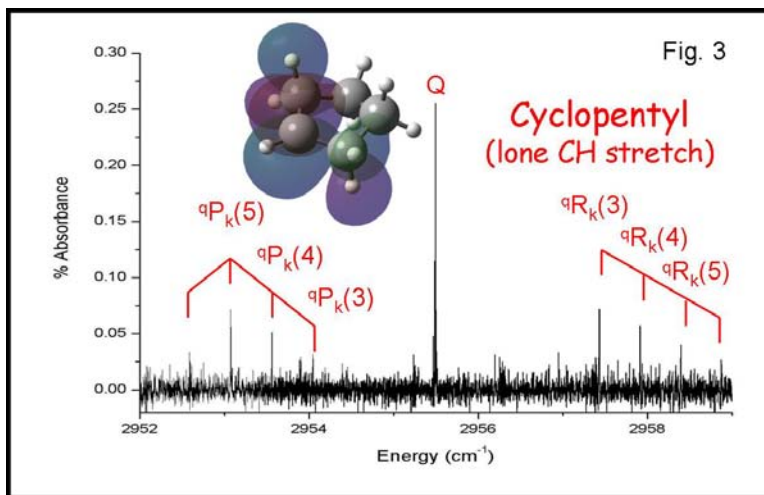


modes. Specifically, the polyatomic reduced moment of inertia is calculated explicitly as a function of tunneling coordinate, with eigenvalues and tunneling splittings obtained from numerical solution of the resulting 1D Schroedinger equation. Such an approach yields good first principles agreement with known tunneling splittings, and offers an empirically determined barrier height ($\Delta E_{\text{adiab}} = 1696(20) \text{ cm}^{-1}$) by linear scaling to match the ground state tunneling values⁵ (see Fig. 2). When corrected for zero point energy contributions, this translates into an effective barrier of $\Delta E_{\text{eff}} = 1602(20) \text{ cm}^{-1}$ which is consistent with estimates ($\Delta E = 1580(100) \text{ cm}^{-1}$) by Tanaka and coworkers.⁵ With this improved potential, the resulting $\Delta \nu_{\text{tun}} = 0.6177 \text{ cm}^{-1}$ value for the adiabatic potential is in excellent agreement with the experimentally observed value of $\Delta \nu_{\text{tun}} = 0.6144 \text{ cm}^{-1}$. Furthermore, excitation of the symmetric CH_2 stretch mode observed in previous studies¹ yield an *increase* (+14%) in the tunneling splitting. This predicts a $+0.0685 \text{ cm}^{-1}$ *blue* shift in the tunneling band origins, which agrees very well with the $+0.0716(5) \text{ cm}^{-1}$ shift observed experimentally.

III. High Resolution IR CH Stretching and Psuedorotation in Cyclopentyl Radical

Encouraged by previous success with cyclopropyl,¹⁹ we have recently undertaken efforts to extend our high resolution IR spectroscopic capabilities to even larger cycloalkyl species. This is stimulated by growing interest in alternative fuel sources from heavy oil and tar sand basins²⁰ known to have high concentration of cycloalkane species, specifically cyclopentanes and cyclohexanes. Chemical transformation pathways for such species are initiated by H atom removal to form highly reactive cycloalkyl radicals, about which very little is known spectroscopically.^{21,22} By way of starting point, we have performed B3LYP/6-311G⁺⁺(3pd,3df) calculations for the cyclopentyl species, yielding equilibrium structures and band origin predictions for the CH stretch manifold. Scanning has begun in the spectral region corresponding to the lone CH radical stretch, which is predicted to be $\approx 100 \text{ cm}^{-1}$ blue shifted from the alkylhalide precursor. With cyclopentyl iodide in the slit discharge, we have recently obtained first high resolution rovibrational spectra of jet cooled cyclopentyl radical.

Our initial scanning efforts have thus far revealed multiple bands, including a strong B-type band with clearly resolved P and R branch rotational progressions and a partially resolved Q branch progression (see Fig. 3). To our knowledge, this represents the first rovibrationally resolved IR spectra of such a large cycloalkyl open shell species. The pattern is clearly that of a near oblate symmetric top, as expected, with both C and $(A+B)/2$ constants in good agreement with *ab initio* predictions. However, of considerable dynamical interest, preliminary analysis of this band indicates the A and B constants to be essentially *equal*, even though the equilibrium geometry of the radical is predicted to be distinctly *puckered* and with



a high barrier for a planar C₅ ring. Such data represent the first gas phase high resolution structural information on this class of ring combustion radicals, which promises to be quite revealing.

Our spectroscopic analysis is still in early stages; however, the near equivalence of A and B strongly suggests “pseudorotation”,^{23,24} thereby averaging the moments of inertia around the A and B principle axes. This is in fact known to be the case in cyclopentane, when transverse displacements in nearly degenerate out of plane modes generate a low energy pathway for propagating a conformational distortion (e.g. “envelope” or “twist” forms of cyclopentane) around the ring. If correct, this would already imply that symmetry breaking of the sp² lone-CH radical center is insufficient to quench the large amplitude pseudorotation coordinate. Instead of a single band, we also see a progression of widely spaced subbands in a roughly uniform progression comparable to that observed in cyclopentane. This is indeed as predicted for a perpendicular band with an accompanying $\Delta\lambda = \pm 1$ change in pseudorotation quantum number, and additionally supports the presence of large amplitude “floppy” conformational dynamics in the cyclopentyl radical ring.

References

- ¹ F. Dong, M. Roberts, and D. J. Nesbitt, *J. Chem. Phys.* **128**, 044305 (2008).
- ² H. Kanamori, Y. Endo, and E. Hirota, *J. Chem. Phys.* **92**, 197 (1990).
- ³ L. Letendre, D. K. Liu, C. D. Pibel, J. B. Halpern, and H. L. Dai, *J. Chem. Phys.* **112**, 9209 (2000).
- ⁴ D. L. Osborn and J. H. Frank, *Chem. Phys. Lett.* **349**, 43 (2001).
- ⁵ K. Tanaka, M. Toshimitsu, K. Harada, and T. Tanaka, *J. Chem. Phys.* **120**, 3604 (2004).
- ⁶ A. Fahr, A. Laufer, R. Klein, and W. Braun, *J. Phys. Chem.* **95**, 3218 (1991).
- ⁷ A. Fahr, P. Hassanzadeh, and D. B. Atkinson, *Chem. Phys.* **236**, 43 (1998).
- ⁸ C. D. Pibel, A. McIlroy, C. A. Taatjes, S. Alfred, K. Patrick, and J. B. Halpern, *J. Chem. Phys.* **110**, 1841 (1999).
- ⁹ L. B. Harding, S. J. Klippenstein, and Y. Georgievskii, *Proc. Comb. Inst.* **30**, 985 (2005).
- ¹⁰ P. R. Westmoreland, A. M. Dean, J. B. Howard, and J. P. Longwell, *J. Phys. Chem.* **93**, 8171 (1989).
- ¹¹ K. M. Ervin, S. Gronert, S. E. Barlow, M. K. Gilles, A. G. Harrison, V. M. Bierbaum, C. H. Depuy, W. C. Lineberger, and G. B. Ellison, *J. Am. Chem. Soc.* **112**, 5750 (1990).
- ¹² S. A. Lahankar, S. D. Chambreau, D. Townsend, F. Suits, J. Farnum, X. B. Zhang, J. M. Bowman, and A. G. Suits, *J. Chem. Phys.* **125** (2006).
- ¹³ D. Townsend, S. A. Lahankar, S. K. Lee, S. D. Chambreau, A. G. Suits, X. Zhang, J. Rheinecker, L. B. Harding, and J. M. Bowman, *Science* **306**, 1158 (2004).
- ¹⁴ P. L. Houston and S. H. Kable, *Proc. Nat. Acad. Sciences* **103**, 16079 (2006).
- ¹⁵ X. B. Zhang, S. L. Zou, L. B. Harding, and J. M. Bowman, *J. Phys. Chem. A* **108**, 8980 (2004).
- ¹⁶ L. B. Harding, *J. Am. Chem. Soc.* **103**, 7469 (1981).
- ¹⁷ D. J. Nesbitt and F. Dong, *Phys. Chem. Chem. Phys.* **10**, 2113 (2008).
- ¹⁸ M. Dupuis and J. J. Wendoloski, *J. Chem. Phys.* **80**, 5696 (1984).
- ¹⁹ F. Dong, S. Davis, and D. J. Nesbitt, *J. Phys. Chem. A* **110**, 3059 (2006).
- ²⁰ O. P. Strausz, T. W. Mojelsky, J. D. Payzant, G. A. Olah, and G. K. S. Prakash, *Energy & Fuels* **13**, 558 (1999).
- ²¹ J. J. Orlando, L. T. Iraci, and G. S. Tyndall, *J. Phys. Chem. A* **104**, 5072 (2000).
- ²² D. M. Rowley, R. Lesclaux, P. D. Lightfoot, B. Noziere, T. J. Wallington, and M. D. Hurley, *J. Phys. Chem.* **96**, 4889 (1992).
- ²³ L. E. Bauman and J. Laane, *J. Phys. Chem.* **92**, 1040 (1988).
- ²⁴ H. L. Strauss, *Annu. Rev. Phys. Chem.* **34**, 301 (1983).

Radical Photochemistry and Photophysics

Daniel M. Neumark
Chemical Sciences Division
Lawrence Berkeley National Laboratory
Berkeley, CA 94720

The photodissociation dynamics of free radicals that play a key role in combustion are investigated. Experiments are carried out to determine the identity of the primary photoproducts and to measure their translational energy distributions. The experiments also probe the effects of starting with different structural isomers of the radicals. The overall goals are to determine bond dissociation energies and mechanisms for free radicals, in order to better understanding their chemistry and photochemistry.

The radical photochemistry and photophysics program is focused on fundamental studies of species and reactions relevant to combustion chemistry. This program is aimed at elucidating the photodissociation dynamics and bimolecular chemistry of free radicals and hydrocarbons. Although much time and effort has been invested in modeling combustion chemistry, the accuracy of these models depends on the primary chemistry of the reactions in the models and the thermochemistry of the species involved in these reactions. For example, it is difficult to assess the importance of a particular reaction in a combustion model without knowledge of its thermochemistry, and the direct determination of radical heats of formation via photodissociation can often provide the missing thermochemical link. Moreover, although the kinetics of many combustion reactions have been investigated, these studies often only measure the disappearance of reactants and yield relatively little about identity of the products. The photodissociation experiments described here offer a set of powerful experimental tools to probe product identity and energy disposal. The experiments yield primary chemistry and photochemistry, bond dissociation energies, heats of formation, photoionization cross sections, and excited state dynamics.

The program is focused on fundamental studies of species and reactions relevant to combustion chemistry. We have developed a state-of-the-art fast beam dissociation instrument for studying the photodissociation dynamics of free radicals and negative ions. In this experiment, radicals are generated by laser photodetachment of mass-selected negative ions, and the resulting fast radical beam is photodissociated with a second laser pulse. The installation of a photofragment coincident imaging detection system enables the study of three-body photodissociation events, and has facilitated the observation of photodissociation channels in which an H or D atom is ejected. A crossed molecular/laser beam instrument is used to investigate the primary chemistry and photochemistry of both closed-shell hydrocarbons and hydrocarbon radicals. Here, the radicals are formed by photolysis in the high pressure region of a pulsed free jet and are dissociated by a second laser, whereupon the photofragments are identified and analyzed with a rotating mass spectrometer detector. The instruments are highly complementary; the fast beam instrument is particularly well-suited to the study of radicals with high electron affinities

that dissociate to two heavy fragments, while the molecular beam instrument is more sensitive to H and H₂ loss channels.

Recent Results:

The photodissociation of DNCN following excitation of the $\tilde{C}^2A'' \leftarrow \tilde{X}^2A''$ electronic transition was studied using fast beam photofragment translational spectroscopy. Analysis of the time-of-flight distributions revealed a photodissociation channel leading to D + NCN competitive with the previously observed CD + N₂ product channel. The translational energy distributions describing the D + NCN channel were peaked at low energy, consistent with internal conversion to the ground state followed by statistical decay and the absence of an exit barrier. The results suggest a relatively facile pathway for the reaction CH + N₂ → H + NCN that proceeds through the HNCN intermediate and support a recently proposed mechanism for prompt NO production in flames.

Van der Waals clusters serve as prototypical systems for studying processes of energy transfer. The I₂·Ar system has attracted particular interest due to the wide array of decay processes occurring in competition with one another. We have carried out systematic dissociative photodetachment (DPD) studies of the I₂⁻ and I₂⁻·Ar anions in the region 4.24-4.78 eV. The resulting neutral fragments are detected by time- and position-sensitive (TPS) coincident imaging. Photofragment mass distributions and translational energy distributions from the DPD of I₂⁻ were determined to facilitate understanding of the I₂·Ar system. For the I₂·Ar complex, channels resulting from two-body dissociation leading to I₂ + Ar photoproducts were observed at all photon energies employed. We also reported the first direct observation of the previously-inferred three-body dissociation channel leading to I+I+Ar photoproducts. The relative intensities of each decay channel were investigated in relation to the electronic state being accessed. Translational energy distributions of the I₂·Ar complex lend further insight into the decay mechanism for each channel.

The photodissociation of propargyl radical, C₃H₃, and its perdeuterated isotopolog was investigated using photofragment translational spectroscopy. Propargyl radicals were produced by 193 nm photolysis of allene entrained in a molecular beam expansion, and then photodissociated at 248 nm. Photofragment time-of-flight spectra were measured at a series of laboratory angles using electron impact ionization coupled to a mass spectrometer. Data for ion masses corresponding to C₃H₂⁺, C₃H⁺, C₃⁺, and the analogous deuterated species show that both H and H₂ loss occur. The translational energy distributions for these processes have average values $\langle E_T \rangle = 5.7$ and 15.9 kcal/mol, respectively, and are consistent with dissociation on the ground state following internal conversion, with no exit barrier for H loss but a tight transition state for H₂ loss. Our translational energy distribution for H atom loss is similar to that in previous work on propargyl in which the H atom, rather than the heavy fragment, was detected, confirming that the earlier experiment was indeed performed on propargyl, in contrast to claims made in a recent theory paper. The branching ratio for H loss/H₂ loss was determined to be 97.6/2.4 ± 1.2, in good agreement with RRKM results.

Future Plans:

Following up on our study of propargyl photodissociation, we are investigating the photodissociation of the propynyl radical at 193 nm. Propynyl (H_3CCC) and propargyl (H_2CCCH) are C_3H_3 structural isomers, but propynyl is higher in energy by about 40 kcal/mol. While the propargyl radical can be generated by either photolysis or pyrolysis of a suitable precursor such as allene or propargyl chloride, no such route to the propynyl radical has been found. Instead, we will generate it by photodetachment of the propynyl anion and study its photodissociation dynamics on our fast beam radical dissociation instrument. At 193 nm, several dissociation channels are available, including H and H_2 loss, C-C bond fission to give $\text{CH}_3 + \text{C}_2$, and isomerization to propargyl followed by dissociation to give $\text{CH}_2 + \text{CH}$. We plan to determine which of these channels occur and measure their translational energy distributions, with the secondary goal of determining whether the 193 nm photodissociation of propynyl differs from that of propargyl. We will also investigate the photodissociation of ozone at 157 nm. At this wavelength, three-body dissociation is believed to be a major dissociation channel. We will be able to characterize this channel using the multi-particle detection capability of our coincidence imaging detector.

The photodissociation dynamics of the vinyl and phenyl radicals will be investigated on the molecular beam instrument. While the H atom loss channel from vinyl has been observed, H_2 loss is also accessible but has not been seen thus far, since the experimental techniques applied to date have been specific to H atom detection. The universal mass spectrometer detector on the molecular beam instrument is well-suited to the detection of H_2 loss and other channels. However, the electron impact ionizer in this detector results in considerable dissociative ionization, complicating the detection of radical photofragments. We plan to install a new ionizer that can operate at considerably lower electron energies (<15 eV) in order to minimize dissociative ionization. Such an ionizer has been used very effectively by Casavecchia and co-workers in reactive scattering experiments, and we expect similar advantages to arise in radical photodissociation studies.

Recent Publications:

"Photofragment translational spectroscopy of propargyl radicals at 248 nm" S. J. Goncher, D. T. Moore, N. E. Sveum, and D. M. Neumark, *J. Chem. Phys.* **128**, 114303 (2008).

"Dissociative photodetachment studies of $\text{I}_2^- \cdot \text{Ar}$: Coincident Imaging of two- and three-body product channels" K. E. Kautzman, P. E. Crider, D. E. Szpunar, and D. M. Neumark, *J. Phys. Chem. A* **111**, 12795 (2007).

"D atom loss in the photodissociation of the DNCN radical: Implications for prompt NO formation" D. E. Szpunar, A. E. Faulhaber, K. E. Kautzman, P. E. Crider II, and D. M. Neumark, *J. Chem. Phys.* **126**, 114311 (2007).

"Probing chemical dynamics with negative ions" D. M. Neumark, *J. Chem. Phys.* **125**, 132303 (2006).

"Photodissociation dynamics of the HCNN radical" A. E. Faulhaber, J. R. Gascooke, A. A. Hoops, and D. M. Neumark, *J. Chem. Phys.* **124**, 204303 (2006).

"Photofragment coincidence imaging of small Γ (H₂O)_n clusters excited to the charge-transfer-to-solvent state" D. E. Szpunar, K. E. Kautzman, A. E. Faulhaber, and D. M. Neumark, *J. Chem. Phys.* **124**, 054318 (2006).

"Photodissociation dynamics of the ethoxy radical investigated by photofragment coincidence imaging" A. E. Faulhaber, D. E. Szpunar, K. E. Kautzman, D. M. Neumark *J. Phys. Chem. A* **109**, 10239 (2005).

"Determination of absolute photoionization cross sections of the phenyl radical" N. E. Sveum, S. J. Goncher, and D. M. Neumark, *Phys. Chem. Chem. Phys.* **8**, 592 (2006).

Determination of Accurate Energetic Database for Combustion Chemistry by High-Resolution Photoionization and Photoelectron Methods

C. Y. Ng

Department of Chemistry, University of California, Davis, California 95616

E-mail Address: cyng@chem.ucdavis.edu

I. Program Scope:

The main goal of this research program is to obtain accurate thermochemical data, such as ionization energies (IEs), 0 K dissociative photoionization thresholds or appearance energies (AEs), 0 K bond dissociation energies (D_0 's), and 0 K heats of formation (ΔH_{f0}° 's) for small and medium sizes molecular species and their ions of relevance to combustion chemistry. Accurate thermochemical data determined by high-resolution photoionization and photoelectron studies for selected polyatomic neutrals and their ions are also useful for benchmarking the next generation of *ab initio* quantum computational procedures.

II. Recent Progress:

A. High-resolution pulsed field ionization photoelectron study of Allyl radical

Allyl radical (C_3H_5) plays an important role in fuel rich combustion by taking part in soot formation and the production of polyaromatic hydrocarbons. In collaboration with Dr. B. Ellison of the Univ. of Colorado, Boulder, and Dr. X. Zhang of the Jet Propulsion Lab., we have measured the vacuum ultraviolet (VUV) laser pulsed field ionization photoelectron (PFI-PE) spectra of C_3H_5 (see Publication 13). Based on the simulation of the rotational structures resolved in these vibrational bands of $C_3H_5^+(\tilde{X}^1A_1; 0^{0+}$ and $\nu_7^+=1)$, the IE values for $C_3H_5(\tilde{X}^2A_2; 0^0)$ to form $C_3H_5^+(\tilde{X}^1A_1; 0^{0+}$ and $\nu_7^+=1)$ are determined to be $65,584.6 \pm 2.0 \text{ cm}^{-1}$ ($8.13146 \pm 0.00025 \text{ eV}$) and $66,020.9 \pm 2.0 \text{ cm}^{-1}$ ($8.18556 \pm 0.00025 \text{ eV}$) respectively, where ν_7^+ is the symmetric C-C-C bending mode of $C_3H_5^+(\tilde{X}^1A_1)$. This measurement has resolved the inconsistency of previous experimental studies.

Table I. Comparison of experimental and CCSD(T)/CBS IE values in eV. $\Delta = \text{IE}(\text{theo}) - \text{IE}(\text{exp})$. (Publications 3 and 11)

Molecules or radicals	IE(exp)	IE(theo)	$\Delta(\text{eV})$
H ₂ O	12.6174±0.0003	12.617	-0.0004
D ₂ O	12.6360±0.0003	12.634	-0.002
NH ₃	10.1864±0.0001	10.185	-0.001
ND ₃	10.200±0.001	10.197	-0.003
CH ₄	12.618±0.004	12.617	-0.001
CD ₄	12.6708±0.0002	12.670	-0.0008
C ₂ H ₂	11.4006±0.0006	11.401	0.0004
C ₂ H ₄	10.51268±0.00003	10.514	0.0013
BCl ₃	11.6410±0.0002	11.606	-0.035
CH ₃ Br	10.5418±0.0002	10.548	0.006
CH ₃ I	9.5382±0.0002	9.523	-0.015
<i>cis</i> -butene	9.12462±0.00019	9.126	0.001
<i>trans</i> -butene	9.12837±0.00025	9.129	0.002
CH ₂ =C(CH ₃) ₂	9.22047±0.00025	9.222	0.002
<i>cis</i> -ClCH=CHCl	9.65815±0.00025	9.668	0.010
<i>trans</i> -ClCH=CHCl	9.63090±0.00025	9.642	0.011
CHCl=CCl ₂	9.4776±0.0002	9.484	0.006
CH ₂ =CHBr	9.8200±0.0015	9.841	-0.021
CH ₃ CH ₂ Br	10.307±0.002	10.320	0.013
<i>cis</i> -CH ₃ CH=CHBr	9.3162±0.0002	9.332	0.016
<i>trans</i> -CH ₃ CH=CHBr	9.2715±0.0002	9.289	0.017
OH	13.017±0.0003	13.014	-0.003
OD	13.0289±0.0003	13.024	-0.005
NH ₂	11.1633±0.0025	11.160	-0.003
ND ₂	11.1784±0.0025	11.182	0.004
CH ₂	10.3864±0.0004	10.382	-0.004
CH ₃	9.8380±0.0004	9.839	0.001
CD ₃	9.8303±0.0006	9.831	0.0007
C ₂ H	11.645±0.0014	11.650	0.005
C ₂ H ₃	8.468±0.029	8.485	0.017
C ₂ H ₅	8.117±0.008*	8.119	0.002
<i>c</i> -C ₃ H ₂	9.15±0.03*	9.164	0.014
HCCCH	8.96±0.04*	8.987	0.027
H ₂ CCC	10.43±0.02*	10.388	-0.042
C ₃ H ₃	8.673±0.001	8.679	0.006
C ₃ H ₅	8.13146±0.00025	8.142	0.004
2-C ₃ H ₇	7.430±0.027*	7.436	0.006
C ₆ H ₅	8.32±0.04*	8.261	-0.059
C ₆ H ₅ CH ₂	7.2491±0.0006	7.284	0.035

a) Values marked by * are not PFI values.

B. Benchmarking state-of-the-art *ab initio* quantum calculations

A main goal of this program is to benchmark state-of-the-art theoretical computational procedures by using highly precise energetic data obtained in photoionization and pulsed field ionization (PFI) measurements. Using the computational resources provided at the DOE National Energy Research Scientific Computing Center and the DOE's Molecular Science Computing Facility of the Pacific Northwest National Laboratory, we have also been performing state-of-the-art calculations on spectroscopic constants and energetic predictions for molecular species of interest to this project based on the high-level *ab initio* wavefunction based CCSD(T)/CBS procedures with high level corrections, including zero point vibrational energy, core-valence electrons correlation, scalar relativistic effect, and diagonal Born-Oppenheimer corrections. This CCSD(T)/CBS method combines the coupled cluster approach including single, double, and quasi-perturbative triple excitations [CCSD(T)] and the complete basis set (CBS) extrapolation approximation. Tables I, II, and III summarize the comparisons between PFI-PE and PFI-PE-photoion coincidence (PFI-PEPICO) measurements and CCSD(T)/CBS calculations for the IE, AE, and D_0 values, respectively, of selected neutrals species and cations (see Publications 3 and 11).

As shown in Table I, excellent agreement is observed between the theoretical and experimental IE values [IE(expt)'s] for the small hydrides and their deuterium substitutes including H_2O , D_2O , NH_3 , ND_3 , CH_4 , CD_4 , C_2H_2 , and C_2H_4 , as indicated by the small IE(theo) deviations (Δ) of 0.4-3.0 meV. The relative large deviation (35 meV) for the IE(theo) of BCl_3 is due to the existence of a low lying electronic state for BCl_3^+ . The IE(theo) values for unsaturated hydrocarbons are also in excellent accord with their IE(exp) values, with deviations of ≈ 2 meV. The deviations of the IE(theo) values increase to 6-11 meV for the chlorine-substituted ethenes, and to 16-21 meV for the bromine-substituted hydrocarbons. The increased errors for the IE(theo) values of larger molecules are to be expected and can be ascribed to insufficient correlation effects. This expectation is consistent with the increase in the IE(theo) deviation from 5 meV for CH_3Br to 15 meV for CH_3I . With the exception of the IE(theo) for $C_6H_5CH_2$, which has a deviation of 35 meV, the IE(theo) values for all these radicals are found to deviate by ≤ 10 meV. The CCSD(T)/CBS IE calculation for $C_6H_5CH_2$ represents the most time-consuming calculation. The comparison of the IE(theo) and IE(exp) for $C_6H_5CH_2$ can provide an idea of how the error limit of the CCSD(T)/CBS calculations "scales up" with molecular size. The large IE(theo) deviations are observed for radicals with large uncertainties in their IE(exp)'s, which were not determined by PFI measurements.

With exception to the PFI-PEPICO AEs of C_2H_5Br , $2-C_3H_7Cl$ and $2-C_3H_7Br$, which have the error limits of 5-10 meV, the PFI-PEPICO AEs of all the remaining molecules have precisions of 1-3 meV (see Table II). For H_2O , D_2O , NH_3 , ND_3 , CH_4 , CD_4 , and C_2H_2 , the deviations [Δ (theo-exp)'s] of the CCSD(T)/CBS AEs with respect to the PFI-PEPICO AEs are well within ± 4 meV. For the Cl- and Br-containing molecular systems, the

Table II. Comparison of AE values for the daughter ions formed from the corresponding parent neutrals determined by PFI-PEPICO measurements and CCSD(T)/CBS calculations. $\Delta = AE(PFI-PEPICO) - AE[CCSD(T)/CBS]$. (Publications 3 and 11)

Daughter ion/ Parent neutral	AE (eV)		Δ (eV)
	PFI-PEPICO	CCSD(T)/CBS	
N^+/N_2	24.2884 \pm 0.0010	24.276	-0.012
OH^+/H_2O	18.116 \pm 0.003	18.119	0.003
OD^+/D_2O	18.220 \pm 0.002	18.218	-0.002
NH_2^+/NH_3	15.765 \pm 0.001	15.762	-0.003
ND_2^+/ND_3	15.892 \pm 0.001	15.889	-0.003
CH_3^+/CH_4	14.323 \pm 0.001	14.323	0.000
CD_3^+/CD_4	14.418 \pm 0.001	14.420	0.002
C_2H^+/C_2H_2	17.357 \pm 0.001	17.353	-0.004
CH_3^+/CH_3Br	12.834 \pm 0.002	12.837	0.003
CH_3^+/CH_3I	12.269 \pm 0.003	12.230	-0.039
CHF_2^+/CHF_2Cl	12.415 \pm 0.001	12.412	-0.003
$CHFCI^+/CHFCI_2$	11.911 \pm 0.002	11.915	0.004
$CHCl_2^+/CHCl_3$	11.488 \pm 0.002	11.497	0.009
CH_2Cl^+/CH_2Cl_2	12.123 \pm 0.001	12.118	-0.005
CH_2Cl^+/CH_2ClBr	11.509 \pm 0.002	11.506	-0.003
BCl_2^+/BCl_3	12.495 \pm 0.002	12.492	-0.003
$C_2H_3^+/C_2H_3Br$	11.901 \pm 0.002	11.890	-0.011
$C_2H_5^+/C_2H_5Br$	11.130 \pm 0.005	11.141	0.011
$2-C_3H_7^+/2-C_3H_7Cl$	11.085 \pm 0.005	11.074	-0.011
$2-C_3H_7^+/2-C_3H_7Br$	10.455 \pm 0.010	10.474	-0.019

deviations for the CCSD(T)/CBS AE predictions are within ± 19 meV. The largest deviation (39 meV) is observed for the CCSD(T)/CBS AE(CH_3^+) from CH_3I .

As shown in Table III, the CCSD(T)/CBS D_0 values for all the neutral and ionic bonds are in excellent agreement with the corresponding experimental D_0 values with absolute deviations of ≤ 12 meV, except those for the Cl-BCl_2^+ , $\text{I-CH}_3/\text{I-CH}_3^+$, and $\text{Br-C}_2\text{H}_3/\text{Br-C}_2\text{H}_3^+$ bonds, where the deviations are found to be in the range of 24-40 meV.

Table III. Comparison of experimental and CCSD(T)/CBS D_0 values for neutrals and ions. $\Delta = D_0(\text{theo}) - D_0(\text{exp})$. (Publications 3 and 11)

Neutral/Ionic bonds	$D_0(\text{exp})$ (eV)	$D_0(\text{theo})$ (eV)	Δ (eV)
	Neutral/Ion	Neutral/Ion	Neutral/Ion
H-OH/H-OH ⁺	5.100 \pm 0.003/5.499 \pm 0.003	5.105/5.502	0.005/0.003
D-OD/D-OD ⁺	5.196 \pm 0.003/5.584 \pm 0.002	5.194/5.584	-0.002/0.000
H-NH ₂ /H-NH ₂ ⁺	4.6017 \pm 0.0025/5.579 \pm 0.001	4.602/5.577	0.000/-0.002
D-ND ₂ /D-ND ₂ ⁺	4.7126 \pm 0.0025/5.691 \pm 0.001	4.707/5.692	-0.0056/0.001
H-CH ₃ /H-CH ₃ ⁺	4.485 \pm 0.001/1.705 \pm 0.004	4.484/1.706	-0.001/0.001
D-CD ₃ /D-CD ₃ ⁺	4.588 \pm 0.001/1.748 \pm 0.001	4.589/1.749	0.001/0.001
H-C ₂ H/H-C ₂ H ⁺	5.7125 \pm 0.0010/5.957 \pm 0.001	5.703/5.952	-0.010/-0.005
Br-CH ₃ /Br-CH ₃ ⁺	2.996 \pm 0.002/2.291 \pm 0.002	2.998/2.289	0.002/-0.002
I-CH ₃ /I-CH ₃ ⁺	2.431 \pm 0.003/2.731 \pm 0.003	2.391/2.707	-0.040/-0.024
---/Cl-BCl ₂ ⁺	---/0.854 \pm 0.002	---/0.886	---/0.032
Br-C ₂ H ₃ /Br-C ₂ H ₃ ⁺	3.433 \pm 0.030/2.081 \pm 0.003	3.405/2.049	-0.026/-0.032
Br-C ₂ H ₅ /Br-C ₂ H ₅ ⁺	3.013 \pm 0.009/0.823 \pm 0.005	3.022/0.821	0.009/-0.002

III. Future Plans:

We are making excellent progress in photoionization efficiency (PIE) and PFI-PE measurements of small radicals using the VUV laser PFI apparatuses established in our laboratory. In collaboration with Xu Zhang (Jet propulsion Laboratory, NASA), Barney Eillison (Univ. of Colorado, Boulder), Ralf Kaiser (Univ. of Hawaii, Manoa) and Branko Ruscic (Argonne National Laboratory), we e plan to continue with the VUV-PFI-PE and VUV-PIE measurement of other selected hydrocarbon radicals including C_2H , C_3H , C_4H , C_3H_3 , C_3H_5 , $\text{HC}\equiv\text{C-CH}=\text{CH}$, $o\text{-C}_6\text{H}_4$, and C_6H_5 radicals in the coming years.

IV. Publications of DOE sponsored research (2006-present)

1. M.-K. Bahng, X. Xing, Sun Jong Baek, X.-M. Qian, and C. Y. Ng, "A combined VUV synchrotron pulsed field ionization-photoelectron and IR-VUV laser photoion depletion study of ammonia", *J. Phys. Chem. A*, **110**, 8488-8496 (2006).
2. Jingang Zhou, Kai-Chung Lau, Elsayed Hassanein, Haifeng Xu, Shan-Xi Tian, Brant Jones, and C. Y. Ng, "A photodissociation study of CH_2BrCl in the A-band using the time-sliced velocity ion imaging method", *J. Chem. Phys.* **124**, 034309 (2006).
3. K.-C. Lau and C. Y. Ng, "Accurate *ab initio* predictions of ionization energies and heats of formation for the $2\text{-C}_3\text{H}_7$, C_6H_5 , and C_7H_7 radicals", *J. Chem. Phys.* **124**, 044323 (2006).
4. P. Wang, H. K. Woo, K. C. Lau, X. Xing, C. Y. Ng, A. S. Zyubin, and A. M. Mebel, "Infrared vibrational spectroscopy of *cis*-dichloroethene in Rydberg states", *J. Chem. Phys.* **124**, 064310 (2006). Selected as the March 2006 issue of Virtual Journal of Ultrafast Science
5. T. Zhang, X. N. Tang, K.-C. Lau, C. Y. Ng, C. Nicolas, D. S. Peterka, M. Ahmed, M. L. Morton, B. Ruscic, R. Yang, L. X. Wei, C. Q. Huang, B. Yang, J. Wang, L. S. Sheng, Y. W. Zhang, and F. Qi, "Direct identification of propargyl radical in combustion flames by VUV photoionization mass spectrometry", *J. Chem. Phys.* **124**, 074302 (2006).
6. K.-C. Lau and C. Y. Ng, "Accurate *ab initio* predictions of ionization energies and heats of formation for the cyclopropenylidene, propargylene and propadienylidene radicals", *Chinese J. Chem. Phys.* (invited article), **19**, 29-38 (2006).
7. K. C. Lau, H. K. Woo, P. Wang, X. Xing, and C. Y. Ng, "Vacuum ultraviolet laser pulsed field ionization-photoelectron study of *cis*-dichloroethene", *J. Chem. Phys.* **124**, 224311 (2006).
8. Rainer A. Dressler, Y. Chiu, D. Lavandier, X. N. Tang, Y. Hou, C. Chang, C. Houchins, H. Xu, and Cheuk-Yiu Ng, "The Study of State-Selected Ion-Molecule Reactions using the Pulsed-Field Ionization-Photoion Technique", *J. Chem. Phys.* **125**, 132306 (2006)

9. Xi Xing, M.-K. Bahng, P. Wang, K. C. Lau, S.-J. Baek, and C. Y. Ng, "Rovibrationally selected and resolved state-to-state photoionization of ethylene using the infrared-vacuum ultraviolet pulsed field ionization-photoelectron method", *J. Chem. Phys.* **125**, 1333304 (2006).
10. Cheuk-Yiu Ng, "Introduction: Chemical Dynamics", *J. Chem. Phys.* **125**, 132201 (2006).
11. Kai-Chung Lau and Cheuk-Yiu Ng, "Benchmarking state-of-the-art *ab initio* thermochemical predictions with accurate pulsed-field ionization photoion-photoelectron measurements", *Accounts on Chemical Research*, **39**, 823-829 (2006).
12. S. Stimson, M. Evans, C.-W. Hsu, and C. Y. Ng, "Rotationally Resolved Vacuum Ultraviolet Pulsed Field Ionization-Photoelectron Bands for $\text{HD}^+(\text{X}^2\Sigma_g^+, v^+=0-20)$ ", *J. Chem. Phys.* **126**, 164303 (2007).
13. X. Xing, B. Reed, K.-C. Lau, C. Y. Ng, X. Zhang, G. B. Ellison, "Vacuum ultraviolet laser pulsed field ionization-photoelectron study of allyl radical CH_2CHCH_2 ", *J. Chem. Phys.* (communication), **126**, 171101 (2007).
14. J. Li, J. Yang, Y. Mo, K.-C. Lau, and C. Y. Ng, "A combined vacuum ultraviolet laser and synchrotron pulsed field ionization study of CH_2BrCl ", *J. Chem. Phys.* **126**, 184304 (2007). Selected for the May 28, 2007 issue of Virtual Journal of Nanoscale Science & Technology.
15. X. N. Tang, H. F. Xu, C. Houchins, C. Y. Ng, Y. Chiu, R. A. Dressler, and D. J. Levandier. "An experimental and quasi-classical trajectory study of the rovibrationally state-selected reactions: $\text{HD}^+(v=0-15, j=1) + \text{He} \rightarrow \text{HeH}^+(\text{HeD}^+) + \text{H}$ ", *J. Chem. Phys.* **126**, 234305 (2007).
16. X. Xing, B. Reed, K.-C. Lau, Sun-Jong Baek, Mi-Kyung Bahng, and C. Y. Ng, "Assignment of rovibrational transitions of propyne in the region of 2934-2952 cm^{-1} measured by the two-color IR-VUV laser Photoion and Photoelectron methods", *J. Chem. Phys.* **127**, 044313 (2007).
17. C. Chang, C. Y. Ng, S. Stimson, M. Evans, and C.-W. Hsu, "Rotationally Resolved Pulsed Field Ionization-Photoelectron Bands of $\text{H}_2^+(\text{X}^2\Sigma_g^+, v^+=0-18)$ ", *Chinese J. Chem. Phys.* (invited article), **20**, 352 (2007).
18. X. N. Tang, C. Houchins, Kai-Chung Lau, C. Y. Ng, R. A. Dressler, Yu-Hui Chiu, Tian-Shu Chu, and K.-L. Han, "A time-dependent wave packet quantum scattering study of the reaction $\text{HD}^+(v=0-3; j=1) + \text{He} \rightarrow \text{HeH}^+(\text{HeD}^+) + \text{D}(\text{H})$ ", *J. Chem. Phys.* **127**, 164318 (2007).
19. Jingang Zhou, Brant Jones, Xueliang Yang, W. M. Jackson, and C. Y. Ng, "A vacuum ultraviolet laser photoionization and pulsed field ionization study of nascent $\text{S}(\text{}^3P_{2,1,0}; \text{}^1D_2)$ formed in the 193.3 nm photodissociation of CS_2 ", *J. Chem. Phys.* **128**, 014305 (2008).
20. Mizuki Oku, Yu Hou, Xi Xing, Beth Reed, Hong Xu, C. Y. Ng, Kiyoshi Nishizawa, Keijihiro Ohshimo, and Toshinori Suzuki, "3s Rydberg and cationic states of pyrazine studied by photoelectron spectroscopy", *J. Phys. Chem. A*, in press.
21. X. Yang, J. Zhou, B. Jones, C. Y. Ng, and W. M. Jackson, "Single-photon vacuum ultraviolet excitation spectroscopy of autoionizing Rydberg states of atomic sulfur", *J. Chem. Phys.*, in press.
22. Jing Wang, Yuyang Li, Taichang Zhang, Zhenyu Tian, Bin Yang, Kuiwen Zhang, Fei Qi, Aiguo Zhu, Zhifeng Cui, and C. Y. Ng, "Interstellar Enols Are Formed in Plasma Discharge of Alcohols", *Astrophys. J.*, in press.
23. Xi Xing, Mi-Kyung Bahng, Beth Reed, C. S. Lam, Kai-Chung Lau, and C. Y. Ng, "Rovibrationally selected and resolved pulsed field ionization photoelectron study of propyne: Ionization energy and spin-orbit interaction in the propyne cation", *J. Chem. Phys.*, in press.
24. Xi Xing, Beth Reed, Mi-Kyung Bahng, and C. Y. Ng, "Infrared-vacuum ultraviolet pulsed field ionization-photoelectron study of C_2H_4^+ using a high-resolution infrared laser", *J. Phys. Chem. A*, in press.
25. X. Xing, B. Reed, M.-K. Bahng, P. Wang, H.-K. Woo, S.-J. Baek, C. S. Lam, and C. Y. Ng, "High-resolution infrared-vacuum ultraviolet photoion and pulsed field ionization-photoelectron methods for spectroscopic studies of neutrals and cations", *Chinese J. Chem. Phys.*, in press.
26. C. Y. Ng, "Spectroscopy and Dynamics of Neutrals and Ions by high-resolution infrared-vacuum ultraviolet and photoionization and photoelectron methods", in "Frontiers of Molecular Spectroscopy", edited by Jaan Laane, to be published by Elsevier.
27. Xi Xing, Beth Reed, Mi-Kyung Bahng, S. J. Baek, Peng Wang, and C. Y. Ng, "Infrared-vacuum ultraviolet pulsed field ionization-photoelectron study of CH_3I^+ using a high-resolution infrared laser", *J. Chem. Phys.*, in press.

Large Eddy Simulation of Turbulence-Chemistry Interactions in Reacting Multiphase Flows

Joseph C. Oefelein
Combustion Research Facility
Sandia National Laboratories, Livermore, CA 94551-9051
oefelei@sandia.gov

Program Scope

Application of the Large Eddy Simulation (*LES*) technique within the Diagnostics and Reacting Flows program is being conducted with two primary objectives. The first is to establish a set of high-fidelity, three-dimensional, computational benchmarks that identically match the geometry (i.e., experimental test section and burner) and operating conditions of selected experimental target flames. The second is to establish a scientific foundation for advanced model development. The goal is to provide direct one-to-one correspondence between measured and modeled results at conditions unattainable using Direct Numerical Simulation (*DNS*) by performing a series of calculations that progressively incorporate the fully coupled dynamic behavior of reacting flows with detailed chemistry and realistic levels of turbulence. Our focal point is the series of flames that have been studied as part of the Experimental Reacting Flow Research program. This represents a direct extension of joint activities being pursued as part of the International Workshop on Measurement and Computation of Turbulent Nonpremixed Flames (TNF Workshop).

Recent Progress

Given current research needs in the area of combustion, our goal is to be complementary, not redundant, and use the unique features of our theoretical-numerical framework to provide information that is not available elsewhere. To achieve this goal, we are investigating two new modeling approaches. The first employs a stochastic reconstruction methodology that treats detailed chemistry directly within the *LES* formalism. This model is “science-based” in that it incorporates turbulence-chemistry interactions and multiple-scalar mixing in a manner consistent with the application of *DNS*. The second is “engineering-based” and employs a tabulated combustion closure based on the Linear Eddy Model (*LEM*). Here we focus on progress with the tabulated *LEM* approach. Recently, the availability of space and time resolved Raman/Rayleigh/CO-LIF line-images of scalars in turbulent jet flames (*Combustion and Flame*, **135**, 185-190; *Combustion and Flame*, **148**, 62-75) has provided a new avenue to formulate subgrid-scale (*sgs*) models for *LES* of turbulent combustion. Conceptually, statistics conditioned on filtered quantities can be constructed more reliably from these data than was possible earlier. Interestingly, the fully-resolved one-dimensional “signal” provided by the experimental data is analogous to the signal obtained from *LEM* simulations. Both provide a local description of turbulent species and temperature evolution due to the resolved and the unresolved scales, albeit in one dimension. *LEM* provides a stochastic representation of scalar field evolution, whose statistical (higher order moments) and spectral properties are similar to experimental observations.

To investigate the prospect of using line-measurements and/or *LEM* as input for a tabulated combustion closure, we have adopted an approach that is superficially similar to a flamelet-based tabulation. In contrast

to the flamelet approximation, however, the relation between filtered and instantaneous quantities can be extracted directly from the one-dimensional signals and there is no need for *a posteriori* models that link these quantities. Instantaneous realizations can be processed directly as a function of pre-determined filter widths in space (and time) to obtain the conditional statistics of filtered scalars. If an appropriate state vector can be identified, key statistical quantities can be parameterized uniquely. Our primary goal has been to determine the degree to which such a parameterization can be achieved. To test the concept, we have conducted an *a priori* analysis of the proposed model for nonpremixed combustion using line measurements obtained from CH₄/H₂/N₂ jet flames at a Reynolds number of 15,200 (i.e., the “DLR-A” flame). This flame exhibits an interesting range of Damköhler and Schmidt numbers through local extinction, reignition, and differential diffusion. Instantaneous realizations were processed as a function of pre-determined filter widths in space to obtain the conditional statistics of filtered scalars. Key statistical quantities were then parameterized as a function of a filtered state vector. As a starting point, we use the filtered mixture fraction \tilde{Z} , filtered scalar dissipation rate $\tilde{\chi}$, and the subgrid Reynolds number Re_{Δ} . Using this state vector, conditional *PDF*'s of a scalar variable, ϕ , $P(\phi | \tilde{Z}, \tilde{\chi}, Re_{\Delta})$, and the corresponding thermodynamic and transport properties that depend on ϕ are tabulated.

The objective in the construction of the table is to build a distribution of the filtered thermochemical state using fully resolved line-image data obtained from the experiments and *LEM*. A unique feature of the approach is that we seek to tabulate conditional *PDF*'s of key scalar variables locally. This is equivalent to seeking a representation of the true “subgrid distribution” of respective scalars as a function of lower-order moments. Use of the filtered mixture fraction and filtered scalar dissipation rate follows directly from flamelet based approaches. The subgrid Reynolds number is used to characterize the effect of *sgs* turbulence on scalar evolution. Note that there is no need to model the subgrid distribution since it is available directly as a function of the instantaneous experimental or *LEM* profiles. To construct the table, an ensemble of instantaneous realizations of the scalar profiles is used. Conditional *PDF*'s of a scalar ϕ , $P(\phi | \tilde{Z}, \tilde{\chi}, Re_{\Delta})$, are constructed by (1) computing the mixture fraction Z from the instantaneous scalar profiles using Bilger's formula, (2) choosing a range of relevant filter sizes Δ , and (3) computing \tilde{Z} in a manner consistent with the definition of a filtered quantity. The filtered scalar dissipation, $\tilde{\chi} = |\nabla \tilde{Z}|^2$, is then calculated from \tilde{Z} along with the *sgs* Reynolds number. Instead of computing the filtered scalar dissipation by filtering the instantaneous scalar dissipation, we use the square of the gradient of filtered mixture fraction to be consistent with the *LES* evaluation of that quantity.

As a first step in validating this approach, we have performed a series of studies focused on three key issues. First, we establish the independence and relevance of Re_{Δ} as a tabulation parameter. Next, we use the experimental data acquired from the DLR-A flames to construct a table and demonstrate that the lower-order parameterization based on \tilde{Z} , $\tilde{\chi}$, and Re_{Δ} is capable of reproducing the measured experimental trends. Last, we demonstrate the analogy between the experimental line-images and *LEM* and show that simulations based on this approach can reproduce the experimental trends with the same level of accuracy. As one example, Fig. 1 shows scatter plots of the filtered CO mass fractions versus filtered mixture fraction obtained from the experiment and from the tabulated closure model. In Fig. 1, scatter plots corresponding to the experiments were obtained by directly filtering the ensemble of scalar profiles. On the other hand, the tabulated conditional *PDF*'s were integrated to yield the modeled filtered quantities shown. These plots incorporate data taken from the entire flow field. Comparisons between the actual and parametrized data are in good qualitative agreement with each other. Increased stretching of mixture fraction surfaces near the flame region can sometimes cause local extinction if the local scalar dissipation is above a threshold value. This leads to a sudden drop in the local temperature and a sudden increase in the mass fraction of temperature-dependent intermediate species such as CO. This effect is captured qualitatively by the current tabulation. To quantify the errors associated with the state vector approximation, we plot the conditional

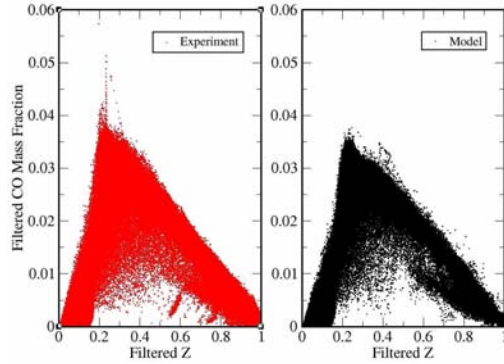


Figure 1: Scatter plots of filtered CO mass fraction versus filtered mixture fraction for DLR-A flame.

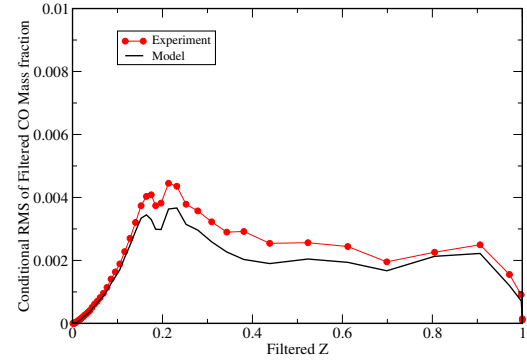


Figure 2: Conditional RMS of filtered CO mass fraction versus filtered mixture fraction for DLR-A flame.

RMS of the filtered temperature (not shown) and CO mass fraction versus filtered mixture fraction. A sample result is shown in Fig. 2. The agreement between the tabulated model and measurements is good, with errors in the predicted values of conditional RMS quantities less than 10 percent.

As a last test, we demonstrate the analogy between the experimental line-images and *LEM* and show that simulations based on this approach can reproduce the experimental trends with a high level of accuracy. Here, the length of the *LEM* domain is chosen to include the entire mean profile of the DLR-A flame. Resolution for the *LEM* simulations was chosen to resolve the Batchelor scale based on very accurate estimates provided by the experiments. This resolution was also adequate to fully resolve the Kolmogorov scale. A 16-species, 12-step reduced mechanism provided by J.Y.- Chen (UC Berkeley) was used for the *LEM* computations. Since the *LEM* domain extended well beyond the jet width, constant gradient boundary conditions were employed for the scalars. Transport properties such as viscosity and thermal conductivity were computed as a function of the local temperature. Figure 3 shows the mean profiles of temperature obtained from the experiments at $x/d = 20$, bounded by the RMS values of the temperature. Also shown in the figure are four instantaneous realizations obtained from the *LEM* simulations under similar conditions. As can be seen from the *LEM* solution, strong turbulence-chemistry interactions are present in the flow-field. The instantaneous *LEM* realizations look qualitatively similar to the line-images obtained from the experiments. Figure 4 shows scatter plots of temperature versus mixture fraction taken from the experiment, with corresponding plots obtained from *LEM* simulations. These data were plotted for a Reynolds number of $Re_{\Delta} = 360$. The agreement between the experiments and *LEM* is very good, indicating that the *LEM* simulation has the potential to generate data that is quantitatively similar to the line measurement data.

Future Plans

As our core effort, we plan to continue with the development of high-fidelity benchmark simulations in collaboration with the Experimental Flow Research program. Simulation of the DLR $\text{CH}_4/\text{H}_2/\text{N}_2$ jet flames will continue. Our goal as we progress will be to focus on the sequence of flames that are currently being studied under the TNF Workshop. We will continue to perform joint investigations of DLR flames with emphasis placed on the dynamics of scalar dissipation and provide a 3-D description of the related turbulence-chemistry interactions. We will also augment the experimental database by providing high-fidelity descriptions of turbulent boundary conditions that will be usable in a wide variety of engineering-based models. After establishing a good connection between the experimental and numerical data for the DLR flames, we will augment the effort by focusing on the series of piloted CH_4 -air jet flames. This series of flames exhibits

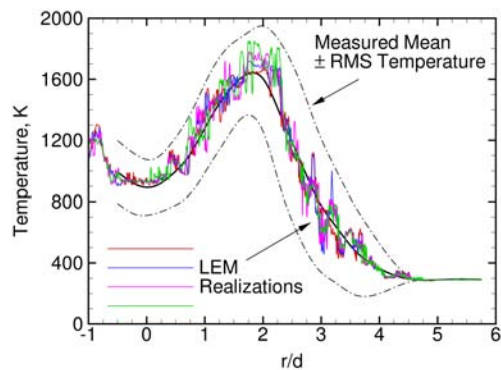


Figure 3: Experimental mean \pm RMS temperature at $x/d = 20$ with 4 superimposed instantaneous realizations from *LEM* for DLR-A flame.

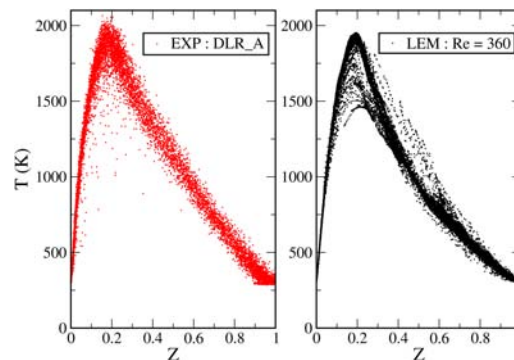


Figure 4: Scatter plots of temperature versus mixture fraction obtained from the experiments and corresponding *LEM* simulations.

increasing degrees of localized extinction due to strong interactions between turbulence and chemistry. The degree of extinction ranges from very low levels (the Sandia-D flame) to very high levels (Sandia-E and F flames) as the jet Reynolds number is progressively increased. Understanding and controlling local extinction is a leading research issue and has significant implications for a variety of applications. There is also a link between the dynamics of scalar dissipation and its effect on local extinction and reignition. This link is not yet fully understood. The third series of flames to be considered are the bluff-body configurations that have been studied jointly by researchers at the University of Sydney and Sandia. These configurations add fluid dynamic complexity by producing recirculation zones around a central jet that stabilizes the flames.

BES Sponsored Publications, 2006 - 2008

- Sankaran, V., Drozda, T. G. and Oefelein, J. C. (2008). A tabulated closure for turbulent nonpremixed combustion based on the Linear Eddy Model. *Proceedings of the Combustion Institute*, **32**: submitted.
- Drozda T. G., Wang G.-H., Sankaran, V., Mayo, J. R., Oefelein, J. C., and Barlow R. S. (2008). Scalar filtered mass density functions in non-premixed turbulent jet flames. *Combustion and Flame*, submitted.
- Williams, T. C., Schefer, R. W., Oefelein, J. C., and Shaddix C. R. (2007). Idealized gas turbine combustor for performance research and validation of large eddy simulations. *Review of Scientific Instruments*, **78**(3): 035114-1-9.
- Oefelein, J. C., Sankaran, V. and Drozda T. G. (2007). Large eddy simulation of swirling particle-laden flow in a model axisymmetric combustor, *Proceedings of the Combustion Institute*, **31**: 2291-2299.
- Oefelein, J. C., Drozda T. G. and Sankaran, V. (2006). Large Eddy Simulation of Turbulence-Chemistry Interactions in Reacting Flows: The Role of High-Performance Computing and Advanced Experimental Diagnostics. *Journal of Physics*, **46**: 16-27.
- Oefelein, J. C. (2006). Large eddy simulation of turbulent combustion processes in propulsion and power systems. *Progress in Aerospace Sciences*, **42**: 2-37.
- Oefelein, J. C., Schefer, R. W. and Barlow, R. S. (2006). Toward validation of large eddy simulation for turbulent combustion. *AIAA Journal*, **44**(3): 418-433.
- Oefelein, J. C. (2006). Mixing and combustion of cryogenic oxygen-hydrogen shear-coaxial jet flames at supercritical pressure. *Combustion Science and Technology*, **178**(1-3): 229-252.
- Special triple issue on Supercritical Fluid Transport and Combustion by J. C. Oefelein and V. Yang (guest editors). *Combustion Science and Technology*, **178**(1-3), 1-621 (20 topical papers), 2006.

KINETICS AND DYNAMICS OF COMBUSTION CHEMISTRY

David L. Osborn

Combustion Research Facility, Mail Stop 9055

Sandia National Laboratories

Livermore, CA 94551-0969

Telephone: (925) 294-4622

Email: dlosbor@sandia.gov

PROGRAM SCOPE

The goal of this program is to elucidate mechanisms of elementary combustion reactions through the use of multiplexed optical spectroscopy and mass spectrometry. We employ time-resolved Fourier transform spectroscopy (TR-FTS) to probe multiple reactants and products with broad spectral coverage ($> 1000 \text{ cm}^{-1}$), moderate spectral resolution (0.1 cm^{-1}), and a wide range of temporal resolution (ns – ms). The inherently multiplexed nature of TR-FTS makes it possible to simultaneously measure product branching ratios, internal energy distributions, energy transfer, and spectroscopy of radical intermediates. Together with total rate coefficients, this additional information provides further constraints upon and insights into the potential energy surfaces that control chemical reactivity. Because of its broadband nature, the TR-FTS technique provides a global view of chemical reactions and energy transfer processes that would be difficult to achieve with narrow-band, laser-based detection techniques.

Over the last three years, time-resolved photoionization mass spectrometry (PIMS) has become a much larger part of this program, and is used to sensitively and selectively probe unimolecular and bimolecular reactions. The Multiplexed Chemical Kinetics Photoionization Mass Spectrometer utilizes tunable vacuum ultraviolet light from the Advanced Light Source synchrotron at Lawrence Berkeley National Laboratory for sensitive, isomer-specific ionization of reactant and product molecules in chemical reactions.

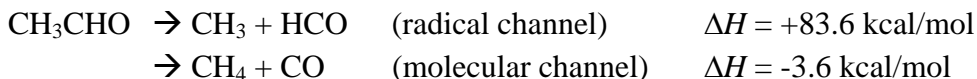
RECENT PROGRESS

Acetaldehyde photodissociation; contributions from roaming mechanisms

There is growing experimental and theoretical evidence that roaming mechanisms play a role in both unimolecular and bimolecular reactions.¹⁻³ A roaming mechanism is characterized by an activated complex in which an atom or functional group (such as CH_3) is loosely bound to the core of the complex by a potential that is quite flat in several dimensions. In this region of the potential, where forces are small, the roaming moiety may execute large amplitude motion until it finds an entrance valley on the potential surface that facilitates abstraction of part of the core.

In collaboration with Scott Kable, Meredith Jordan, and Joel Bowman, we have recently completed a study of the photodissociation of acetaldehyde (CH_3CHO), the largest molecule for which there is both experimental and theoretical evidence supporting a roaming mechanism. In analogy to its smaller cousin formaldehyde (H_2CO), acetaldehyde's photodissociation dynamics after $S_1 \leftarrow S_0$ excitation in the ultraviolet region are characterized by fast non-radiative decay to

the T_1 and S_0 electronic states. Two photodissociation channels have been observed with 308 nm ($h\nu = 92.8$ kcal/mol) excitation:



There is a well-defined transition state (TS) on the S_0 surface for the formation of the molecular channel. This TS is nearly isoenergetic with the $\text{CH}_3 + \text{HCO}$ asymptote.

Building on earlier VUV LIF measurements of CO by Kable and Houston, we have observed the CH_4 product of the molecular channel following 308 nm excitation in a time-resolved FTIR experiment. The CH_4 product has a very high degree of internal excitation, with a vibrational distribution peaked at $\sim 95\%$ of the available energy. The Emory and Sydney groups have performed quasiclassical trajectory calculations on both analytical PESs and via direct dynamics to predict the CH_4 vibrational energy distribution. Trajectories started from the TS on S_0 leading to $\text{CH}_4 + \text{CO}$ deposit much less energy into CH_4 vibration than the experimental result. By contrast, an ensemble of trajectories initiated from the CH_3CHO equilibrium geometry yields a CH_4 vibrational distribution in good agreement with experiment. Examination of these trajectories shows that the dominant mechanism for CH_4 formation is a CH_3 -roaming pathway, in which a methyl and formyl radical “orbit” each other before the methyl group abstracts the hydrogen atom from HCO forming the final products.

Comparing experiment to theory, we estimate the roaming dynamics represent 75 – 94% of the total CH_4 formation, a much larger fraction than in the case of $\text{H}_2\text{CO} \rightarrow \text{H}_2 + \text{CO}$. One reason roaming dynamics are more important in acetaldehyde is that the TS leading to molecular products is only 2 – 3 kcal mol⁻¹ lower than the $\text{CH}_3 + \text{HCO}$ asymptote, whereas the analogous energy gap in H_2CO is ~ 8 kcal mol⁻¹. This near degeneracy, coupled with the larger number of vibrational degrees of freedom in CH_3CHO vs. H_2CO , greatly increases the chance of sequestering sufficient energy in CH_3CHO vibrations so that it cannot quite dissociate to radical products, providing time for roaming dynamics that lead to molecular products. Roaming dynamics in larger molecules may affect the delicate balance of chain propagation, branching, and termination reactions in combustion and other high-energy environments.

Isomer-resolved mass spectrometry

The multiplexed chemical kinetics photoionization mass spectrometer operates both at Sandia National Laboratories (using a discharge lamp to create VUV radiation), and at the Chemical Dynamics Beamline of the Advanced Light Source (ALS) synchrotron of LBNL. The chemical reactor is based on the Gutman design,⁴ which allows the study of photodissociation and bimolecular reactions at pressures of 1 – 10 Torr. Recent changes to our reactor design now gives us routine access to temperatures of 300 – 1000 K.

While the study of chemical kinetics using PIMS is well-established, this apparatus has two unique features that make it especially powerful for chemical kinetics. First, the widely tunable, intense VUV radiation from the ALS enables isomer-specific ionization of product

species. As an example, we have recently studied the isomer-resolved products of the $C_2H + CH_2CCH_2$ reaction, measuring the branching ratios for three different C_5H_4 isomers.

The second unusual feature of this experiment is the mass spectrometer. We employ a small magnetic sector instrument coupled to a time- and position-sensitive single-ion counting detector. This approach creates a mass spectrometer with 100% duty cycle (like a quadrupole instrument) and the multiplex advantage of measuring a broad range of masses simultaneously (as in time-of-flight spectrometry). This detector also measures the time dependence of each observed reactant and product molecule, which provides kinetic information on the reaction.

The $C_3H_5 + C_3H_5 \rightarrow C_6H_{10}$ reaction

The reactions of resonance-stabilized radicals are key players in molecular weight growth chemistry leading to polycyclic aromatic hydrocarbons and eventually soot formation. As part of an ongoing study of such systems, we have recently completed work on the self reaction of allyl radicals (H_2CCHCH_2). All previous measurements of the kinetics of this reaction have been made with optical absorption spectroscopy of the allyl radical, and hence rely on the accuracy of the allyl radical absorption cross section. Our measurements by PIMS are independent of this value. Our derived rate coefficient $(2.7 \pm 0.7) \times 10^{-11} \text{ cm}^3 \text{ molecule}^{-1} \text{ s}^{-1}$ is in agreement with those of Tulloch *et al.*⁵ and Jenkin *et al.*,⁶ providing indirect support of the accepted absorption cross section of allyl radical at $\lambda = 223 \text{ nm}$.

We also analyzed the isomeric distribution of the C_6H_{10} product. The initial 1,5-hexadiene adduct, which intuitively should form upon reaction of two allyl radicals, is the only C_6H_{10} isomer observed at pressures of 1 – 6 Torr and temperatures from 300 – 500 K. Other acyclic and cyclic isomers are up to 20 kcal mol⁻¹ more stable than 1,5-hexadiene. Their absence implies that the barriers to these deeper wells on the potential energy surface are substantially higher than similar barriers in the $C_3H_3 + C_3H_3 \rightarrow C_6H_6$ reaction, where isomerization is facile at these pressures and temperatures. With only two π bonds in acyclic C_6H_{10} versus four in acyclic C_6H_6 , there are fewer opportunities to facilitate isomerization via uncoupling and recoupling of π bonds.

The $C_3H_3 + C_6H_5 \rightarrow C_9H_8$ reaction

The most important reaction in the formation of the first aromatic ring in combustion appears to be the propargyl (C_3H_3) self reaction. Propargyl radicals are resonance stabilized, leading to slow reactivity with closed-shell species, and can therefore attain concentrations much higher than most free radicals. By analogy, it seems probable that the next steps in soot formation, beyond the first aromatic ring, may involve reactions of propargyl with resonance-stabilized aromatic radicals, such as phenyl (C_6H_5). We have preliminary results on the isomer distributions of the C_9H_8 product from this reaction from 1 – 10 Torr and from 300 – 1000 K. The results show temperature-dependent isomerization of the C_9H_8 product. Analysis of these results is currently in progress.

Future Directions

Using TR-FTS, we will investigate reactions of the vinyl (C_2H_3) and propargyl (C_3H_3) radicals to determine product channel identities and energy disposal. We will employ higher spectral resolution to make more definitive measurements of the energy disposal in acetaldehyde photodissociation.

One interesting problem to explore using the multiplexed chemical kinetics mass spectrometer apparatus instrument is the reaction $C_3H_3 + C_2H_2$. Previous work by Knyazev and Slagle⁷ has shown that the initial product (C_5H_5) can react with excess acetylene to form C_7H_7 . This process continues to form C_9H_8 and perhaps larger species. Measuring the isomeric forms of these products will provide information critical to the reaction mechanism for this molecular weight growth process. We have preliminary data on this system, and will soon attempt to start the reaction with acetylene at the C_5H_5 or C_7H_7 points with isomerically-pure radical samples for comparison with the $C_3H_3 + C_2H_2$ data.

BES-sponsored publications, 2006 - present

- 1) "Ultraviolet photodissociation of vinyl iodide: understanding the halogen dependence of photodissociation mechanisms in vinyl halides" P. Zou, K. E. Strecker, J. Ramirez-Serrano, L. E. Jusinski, C. A. Taatjes, D. L. Osborn, *Physical Chemistry Chemical Physics*, 10, 713 (2008).
- 2) "Imaging combustion chemistry via multiplexed synchrotron-photoionization mass spectrometry" C. A. Taatjes, N. Hansen, D. L. Osborn, K. Koehse-Hoinghaus, T. A. Cool, P. R. Westmoreland, *Physical Chemistry Chemical Physics*, 10, 20 (2008).
- 3) "Photoionization of 1-alkenylperoxy and Alkylperoxy radicals and a general rule for the stability of their cations" G. Meloni, T. M. Selby, F. Goulay, S. R. Leone, D. L. Osborn, and C. A. Taatjes, *Journal of the American Chemical Society*, 129, 14019 (2007).
- 4) "Exploring multiple reaction paths to a single product channel" D. L. Osborn, *Advances in Chemical Physics*, in press (2007).
- 5) "Direct detection of polyynes formation from the reaction of ethynyl radical (C_2H) with propyne ($CH_3-C\equiv CH$) and allene ($CH_2=C=CH_2$)" F. Goulay, D. L. Osborn, C. A. Taatjes, P. Zou, G. Meloni, and S. R. Leone, *Physical Chemistry Chemical Physics*, 9, 4291 (2007).
- 6) "Energy-resolved photoionization of alkylperoxy radicals and the stability of their cations" G. Meloni, P. Zou, S. J. Klippenstein, M. Ahmed, S. R. Leone, C. A. Taatjes, and D. L. Osborn, *Journal of the American Chemical Society*, 128, 13559 (2006).
- 7) "Time-dependent infrared emission following photodissociation of nitromethane and chloropicrin" E. A. Wade, K. E. Reak, S. L. Li, S. M. Clegg, P. Zou, and D. L. Osborn, *Journal of Physical Chemistry A*, 110, 4405 (2006).
- 8) "Measurement of the sixth overtone band of nitric oxide, and its dipole moment function, using cavity-enhanced frequency modulation spectroscopy" J. Bood, A. McIlroy, and D. L. Osborn, *Journal of Chemical Physics*, 124, 084311 (2006).

References

- ¹ T. P. Marcy, R. R. Diaz, D. Heard, S. R. Leone, L. B. Harding, and S. J. Klippenstein, *J. Phys. Chem. A* **105**, 8361 (2001).
- ² D. Townsend, S. A. Lahankar, S. K. Lee, S. D. Chambreau, A. G. Suits, X. Zhang, J. Rheinecker, L. B. Harding, and J. M. Bowman, *Science* **306**, 1158 (2004).
- ³ P. L. Houston and S. H. Kable, *Proc. Nat. Acad. Sci.* **103**, 16079 (2006).
- ⁴ I. R. Slagle and D. Gutman, *J. Am. Chem. Soc.* **107**, 5342 (1985).
- ⁵ Tulloch, J. M.; Macpherron, M. T.; Morgan, C. A.; Pillng, M. J. *J. Phys. Chem.* **1982**, *86*, 3812.
- ⁶ Jenkin, M. E.; Murrells, T. P.; Shalliker, S. J.; Hayman, G. D. *J. Chem. Soc. Faraday Trans.* **1993**, *89*, 433.
- ⁷ V. D. Knyazev and I. R. Slagle, *J. Phys. Chem. A* **106**, 5613 (2002).

The dynamics of large-amplitude motion in energized molecules

David S. Perry, Principal Investigator
Department of Chemistry, The University of Akron
Akron OH 44325-3601
DPerry@UAkron.edu

Introduction

Most theories of reaction rely, either explicitly or implicitly, on a separation of the large-amplitude degrees of freedom from the other nuclear motions. For example, transition state theory (including its unimolecular variant RRKM theory) identifies a reaction coordinate and assumes thermal equilibrium among the other degrees of freedom. The transition state is a dividing hypersurface between reactants and products located at some point along the reaction coordinate so as to minimize recrossing. At high energies, particularly just below the threshold for a new fragmentation channel, there may be “roaming” trajectories, which may favor particular product channels and which clearly involve more than one large-amplitude degree of freedom. An alternative to transition state theory is the adiabatic channel model in which the excitation in one of more of the orthogonal degrees of freedom is assumed to be conserved as the system moves along the reaction coordinate. At the other end of the spectrum from statistical theories, close-coupled quantum scattering calculations are limited by practical considerations to a few degrees of freedom. Thus in systems larger than 3 or 4 atoms, one must define the active degrees of freedom and separate them in some way from the other degrees of freedom.

In this research, we test the limits of the adiabatic separation of different nuclear degrees of freedom, in particular, the separation of the large amplitude nuclear degrees of freedom (LADF) from the small amplitude vibrations (SAV). We will call this *vibrational adiabaticity* to distinguish it from *electronic adiabaticity*, that is, from the Born-Oppenheimer approximation. Nonadiabatic coupling terms scale as $(m/M)^{1/4}$ where m is the reduced mass for the fast degree of freedom and M is that for the slow degree of freedom. In the Born-Oppenheimer approximation, $m \ll M$, but in the vibrational case, often $m \approx M$. Therefore, the vibrational adiabatic approximation is on much more tenuous ground. The limits of its usefulness and the consequences of its failure are examined in this project.

While scattering systems are of primary interest in reactive chemistry, the collision complexes are relatively short lived and can rarely be probed directly. For this reason, we choose bound molecules, including methanol, nitromethane and methylamine, as our laboratory for studying adiabatic separations and consequent nonadiabatic effects. Bound systems are by definition long-lived, which means that we are able to use high-resolution spectroscopy to probe the interactions with a high level of precision and detail. In addition to experiments at the university of Akron, this project involves collaborative experiments with Brooks Pate at the University of Virginia (CD-FTMW-IR), Robert Sams at Pacific Northwest Labs (CW slit-jet IR), and Thomas Rizzo at the EPFL in Switzerland (IRLAPS).

A. Adiabatic and Diabatic Behaviors in the CH Stretch – Torsion Manifold of Methanol.

In previous work under this project, we discovered the inverted torsional tunneling splitting in the asymmetric CH stretch vibrational states ($\nu_2=1$ and $\nu_9=1$). These results were successfully explained by our 4-dimensional model calculation that included the three CH stretch coordinates and the torsion. Torsional motion interchanges the identities of the CH bonds *anti* and *gauche* to the OH, and the CH bonds in these positions have different force constants. A single lowest-order coupling term with the required symmetry (A_1 in G_6) was sufficient to reproduce the observed torsional structure. The inverted torsional structure is a general phenomenon that derives from molecular symmetry and the single coupling term results in many mixed vibrational states throughout the CH stretch-torsion manifold.

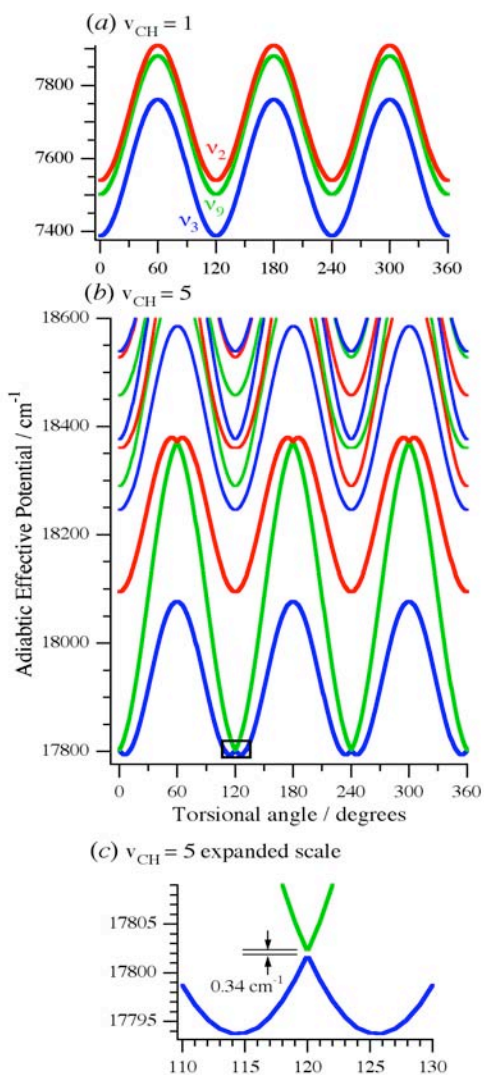
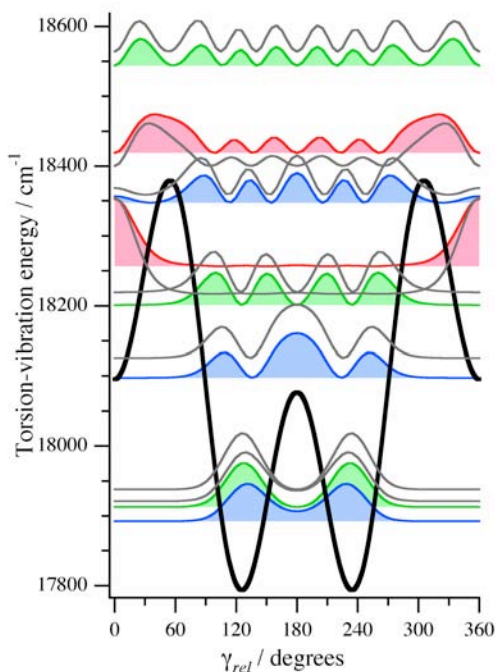


Fig. 1. (at left) Vibrationally adiabatic curves for the methanol torsional potential have very narrowly avoided crossings at high CH stretch excitation. The highlighted avoided crossing in (b) is shown on expanded scale in (c).

Fig. 2. (below) A diabatic effective torsional potential of the local $v_{\text{CH}}=5$ stretch of methanol is shown as the heavy black curve. The fully coupled torsional probability distributions (color) are compared with the approximate diabatic probability distributions (grey).



Subsequent spectroscopic reports¹ of other asymmetric vibrations have confirmed the generality of the effect, and a number of theoretical studies,² including the adiabatic treatment of Fehrensén et al.³ have contributed to our understanding. With the aid of our CH overtone data [1], we have been able to extend the model to treat the CH overtones and the torsional states built on them [4].

The model Hamiltonian was able to fit the ground state torsional structure up to energies well above the torsional barrier, the torsional tunneling splittings of the CH stretch fundamentals, and the frequencies of the CH overtone bands up to $v_{\text{CH}}=7$. The fully coupled solutions for the coupled CH stretch and torsional motion were obtained by diagonalizing the Hamiltonian in a free internal rotor – harmonic oscillator product basis. To diagnose the nature of the coupled eigenstates, an approximate adiabatic separation of the torsion from the three CH stretches was applied [2, 4]. Vibrationally adiabatic curves for the effective torsional potential are constructed (Fig. 1) by solving for the CH stretch vibrational energies at each torsional angle. At low CH stretch excitation (Fig. 1(a)), the effective torsional potentials are approximately parallel to each other, each having a similar shape to the ground state torsional potential. At high CH stretch excitation (Fig. 1(b)), the strength of the torsion-vibration coupling increases, leading to narrowly avoided crossings (Fig. 1(c)). The magnitude of the gap at the avoided crossing, decreases systematically with CH stretch excitation as the CH stretch vibrations approach the local mode limit.

The vibrations represented by the bold curves in Fig. 1(b, c) are local CH stretch vibrations in which the excitation is predominantly in one CH bond. As the torsional angle is varied through an avoided crossing, the CH stretch excitation jumps suddenly from one bond to the next. The presence of such narrowly avoided crossings indicates that a diabatic representation, in which the potential curves are allowed to cross, would likely yield a better approximation to the fully coupled dynamics. Fig. 2 show good qualitative agreement of the torsional energies and probability distributions from the full-coupled calculation with those calculated from the approximate diabatic potential. Thus we conclude that the dynamics undergo a transition from approximate adiabatic motion at low CH stretch excitation to approximate diabatic motion at high CH excitation.

B. Multistage Torsion-Vibration Coupling in the ν_3 CH Stretch Region of Methanol

When the adiabatic approximation is valid, the energy in each of the separated degrees of freedom is conserved. In this context, vibrational energy redistribution between the separated degrees of freedom (IVR) is a non-adiabatic effect. Whereas the discussion in the section above considered only the reduced-dimensional space of the torsion and the three CH stretches, we now turn to the coupling of the ν_3 symmetric CH stretch to all of the available degrees of freedom in the molecule. This experimental study is made possible by the development of a new experimental technique at the University of Virginia that makes it possible to record a greatly simplified infrared spectrum containing only transitions originating from a pair of coupled rotational levels. That technique, coherence-detected Fourier transform microwave – infrared spectroscopy (CD-FTMW-IR), is described below.

Population transfer induced by a pulsed IR laser is detected by FTMW spectroscopy using a sequence two microwave pulses. The first pulse converts the thermal population difference to a coherence using an approximate “ $\pi/2$ ” pulse. The pulsed IR laser interacts with the polarized sample. A second microwave pulse with a 180° phase shift interacts with the sample after a 100 ns delay to perform a “ $-\pi/2$ ” excitation. If the laser pulse does not induce population transfer, this second pulse cancels the microwave signal. For resonant IR excitation from either rotational level, the second pulse converts the laser-induced population transfer to a coherence, which is detected by the FTMW spectrometer. The phase of this FTMW signal determines which rotational level was excited by

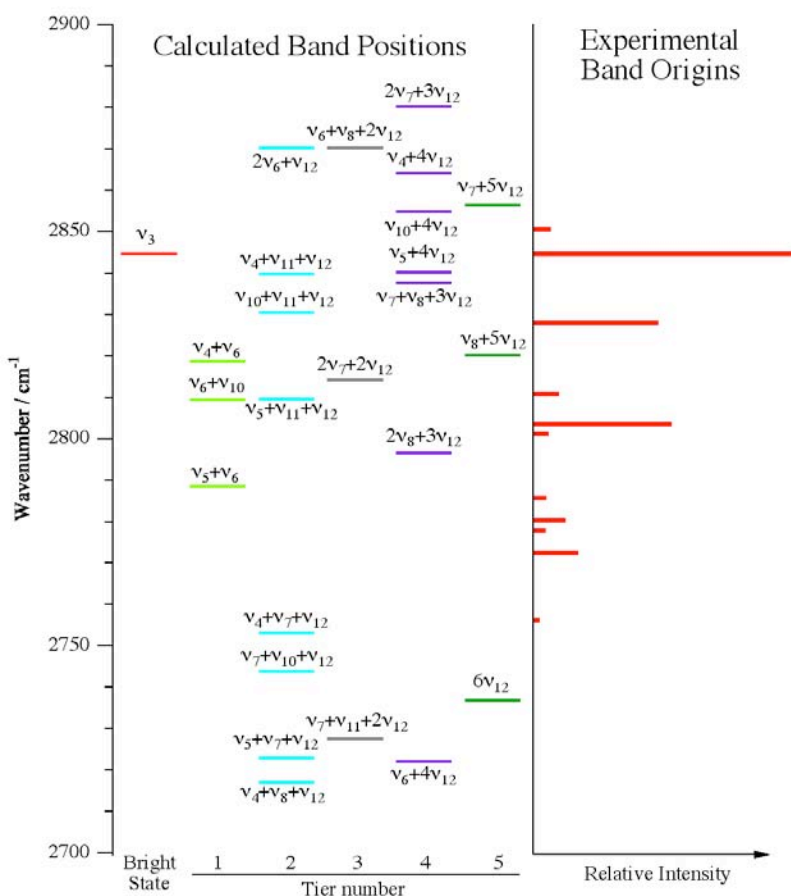


Fig. 3. At right are the vibrational band origins in the ν_3 symmetric CH stretch region of methanol that result from the analysis of CD-FTMW-IR experiments. The intensities remain to be confirmed. At left are the calculated zeroth-order band positions based on the fundamental frequencies.

the laser. In this experiment the microwave frequency was tuned to the $2_0 \leftarrow 3_{-1}$ and $2_1 \leftarrow 3_0$ transitions of the methanol E species.

Up to now, the only band in the region $2750\text{-}2900\text{ cm}^{-1}$ region with torsion-rotation assignments was the ν_3 fundamental at 2844 cm^{-1} . Ten additional vibrational band origins have now been identified in the interval $2755\text{-}2855\text{ cm}^{-1}$ along with their approximate relative intensities (Fig. 3). A direct state count in this interval gives a total of 14 vibrations arranged into 6 tiers of coupled states. The zeroth-order vibrational state energies are arranged into tiers in Fig. 3 according to the coupling order relative to the ν_3 bright state. Tier 1 represents a third-order coupling; tier 2 fourth order coupling etc. The pattern of the experimental spectrum with a relatively intense band at the ν_3 frequency with only a couple of relatively strong perturbing states to lower frequency is consistent with a primary interaction of ν_3 with the tier 1 states, which are combinations of the three HCH bends (ν_4 , ν_5 , and ν_{10}) with the COH bend ν_6 . It is known⁴ that the ν_6 fundamental mixes with the first torsionally excited state built on the methyl rock ($\nu_7 + \nu_{12}$), and for the E-species, we also anticipate interactions with the other methyl rock (ν_{11}). Together, this gives the following coupling pathway involving tiers 1 and 2:



This mechanism predicts a total of 8 vibrations in the range $2755 - 2855\text{ cm}^{-1}$ as compared to the 11 observed. To get 11 coupled states, it will likely be necessary to invoke coupling through at least tiers 3 and 4 and involving states with 3 or 4 quanta of torsional excitation.

Plans for the Next Year

The continuing development of our continuous-wave cavity ringdown technique (CW-CRDS) will be a priority in the coming year and experiments on the $2\nu_{\text{CH}}$ region of methanol and on methylamine will be undertaken. CD-FTMW-IR experiments are planned at the University of Virginia on isotopically labeled methanol. Extension of the CD-FTMW-IR technique to the 48 GHz range will allow improved sensitivity and access to the methanol A species.

Cited References

- ¹ R. M. Lees and L.-H. Xu, *Phys. Rev. Lett.* **84**, 3815 (2000).
- ² J. T. Hougen, *J. Mol. Spectrosc.* **181**, 287 (1997); J. T. Hougen, *J. Mol. Spectrosc.* **207**, 60 (2001); M. Abbouti Tamsamani, L.-H. Xu, and R. M. Lees, *Journal of Molecular Spectroscopy* **218**, 220 (2003); E. L. Sibert, III and J. Castillo-Chara, *J. Chem. Phys.* **122**, 194306/1 (2005); J. Castillo-Chara and E. L. Sibert, III, *J. Chem. Phys.* **119**, 11671 (2003).
- ³ B. Fehrensen, D. Luckhaus, M. Quack, M. Willeke, and T. R. Rizzo, *J. Chem. Phys.* **119**, 5534 (2003).
- ⁴ R. M. Lees, L.-H. Xu, J. W. C. Johns, Z. F. Lu, B. P. Winnewisser, M. Lock, and R. L. Sams, *J. Mol. Spectrosc.* **228**, 528 (2004).

Publications from this Project, 2005-2008

- [1] David Rueda, Oleg V. Boyarkin, Thomas R. Rizzo, Andrei Chirokolava and David S. Perry, Vibrational overtone spectroscopy of jet-cooled methanol from $5,000$ to $14,000\text{ cm}^{-1}$, *J. Chem. Phys.*, **122**, 044314 (2005). (8 pages)
- [2] Trocia N Clasp and David S Perry, Torsion-vibration coupling in methanol: The adiabatic approximation and IVR scaling, *J. Chem. Phys.*, **125**, 104313 (2006). (9 pages)
- [3] Pavel Maksyutenko, Oleg V. Boyarkin, Thomas R. Rizzo and David S. Perry, Conformational dependence of intramolecular vibrational redistribution in methanol, *J. Chem. Phys.*, **126**, 044311 (2007). (6 pages)
- [4] David S. Perry, Torsion-vibration coupling in methanol: Diabatic behavior in the CH overtone region, *J. Phys. Chem. A* **112**, 215-223 (2008). <http://dx.doi.org/10.1021/jp077269q>.

Chemical Kinetic Modeling of Combustion Chemistry

William J. Pitz and Charles K. Westbrook

Lawrence Livermore National Laboratory

Livermore, CA 94551

pitz1@llnl.gov

I. Program Scope

Our research project focuses on developing detailed chemical kinetic reaction mechanisms for the combustion of a wide variety of hydrocarbon, alternative fuels and other species. These reaction mechanisms are designed to be applicable over extended ranges of operating conditions, including temperature, pressure, and fuel/oxidizer ratio, making them so-called “comprehensive” reaction mechanisms. They can then be systematically reduced in size and complexity as needed for specific types of modeling applications. We also use these detailed kinetic mechanisms to carry out modeling studies of practical combustion systems, and we also contribute basic chemical information on thermochemical and kinetic data.

II. Recent Progress

During the past year, we have developed detailed kinetic mechanisms and carried out kinetic modeling studies in several areas including large n-alkanes, toluene and large methyl esters.

A. Large n-alkanes

Recently, much emphasis has been placed on extending chemical kinetic models to address large alkanes. Large n-alkanes are included in recommendations for components in surrogates for diesel and jet fuels. The recommendation for surrogates for diesel fuel includes n-hexadecane and for jet fuel includes n-decane and n-dodecane [3, 4]. Recently, we have developed a chemical kinetic model for all n-alkanes from n-octane to n-hexadecane [5]. This model allows the simulation of both low and high temperature chemistry of these n-alkanes. The simulation of low temperature combustion is important for new modes of combustion in engines such as homogeneous compression ignition (HCCI), premixed compression ignition (PCCI), and smokeless rich combustion. Figure 1 shows comparison of results from the detailed chemical kinetic model for n-hexadecane [5] and measurements made in a stirred reactor [1]. The agreement between the model and the experiments are good. n-Hexadecane is an important component for consideration for a diesel surrogate because it is a primary reference fuel for diesel engines. However, there is little experimental data in the literature on n-hexadecane. Our detailed chemical kinetic model [5] includes chemistry for all the n-alkanes up to C16. There is experimental data on ignition of n-decane,

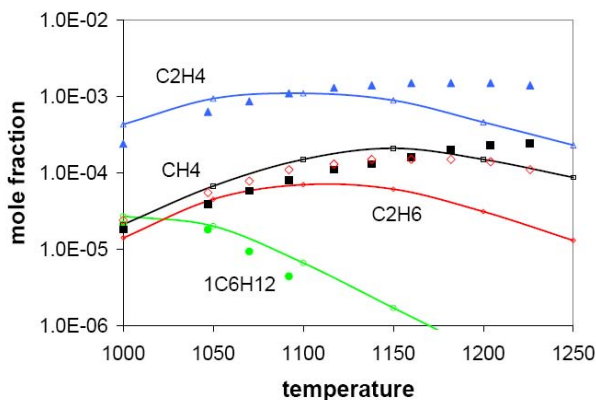


Fig. 1 Intermediate species for n-hexadecane oxidation in a stirred reactor [1]. Symbols are from the experiment and curves are from the model. (stoichiometric, 1 atm, 70 ms residence time)

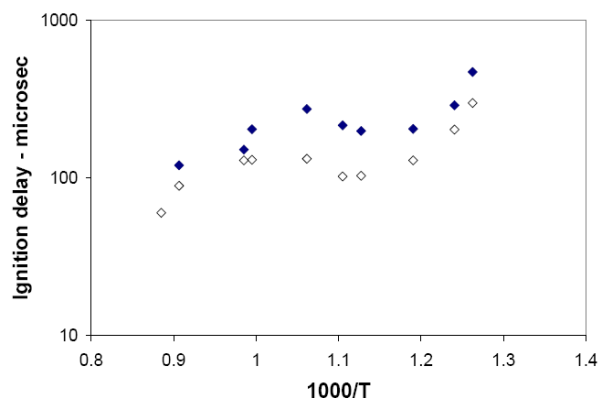


Fig. 2 n-Decane ignition in a shock tube (stoichiometric, 80 bar). Model: filled symbols, Experiments [2]: open symbols.

another large n-alkane (Fig. 2). The experiments were performed at engine-like conditions of 80 bar and covered the low to high temperature region of 800 to 1100 K including the negative temperature coefficient region [2]. The comparison of model predictions with the experimental measurements shows good agreement (Fig. 2). The development of a chemical kinetic model for all n-alkanes up to n-hexadecane allows a broad choice of surrogate fuel components in this chemical class for use in surrogate fuels.

B. Toluene

Toluene is an important component in gasoline. It is the most common aromatic in gasoline and it can reach levels up to 35% [P8, “P” refers to our publication list at the end of the abstract]. Toluene is recommended as a component in gasoline surrogates in recent review by a surrogate fuel working group [P8]. Recently, there have been significant improvements in the ability to simulate toluene oxidation [P5, P6]. Many of the reactions of toluene have been updated in the present work with rate constants recently reported in the literature. These include toluene decomposition reactions [6], and reactions of toluene with OH, H, and O₂ [7]. Abstraction of phenyl H’s on toluene is also now included in the mechanism from Bounaceur et al. [8]. The updated mechanism has led to improved agreement with toluene ignition delay times at shock tube conditions [P6].

C. Methyl esters

One of the important renewable fuels is biodiesel. Biodiesel is frequently derived from vegetable oils from soy beans, canola (rapeseed), and other plants. These vegetable oils are usually converted into methyl esters so that they can be easily blended with conventional diesel fuel. Much of the methyl esters are derived from soybeans and canola and these fuels consist of only five components (Fig. 3). As a starting point, we have used methyl butanoate, a large methyl ester, as a surrogate for the methyl esters in soy bean and rapeseed derived biodiesel. Methyl decanoate has a long n-alkane chain like in methyl palmitate in soy and rapeseed derived methyl esters (Fig. 3). The n-alkane chain in methyl decanoate is shorter than methyl palmitate and may lead to a lower reactivity than biodiesel. However, this effect can be compensated for by adding a large n-alkane to the methyl decanoate if needed to increase the reactivity.

Recently, we have developed a chemical kinetic mechanism for the low and high temperature oxidation methyl decanoate [P1]. This development significantly enhances the capability for modeling biodiesel fuels. The results of the methyl decanoate model [P1] are compared to rapeseed oxidation

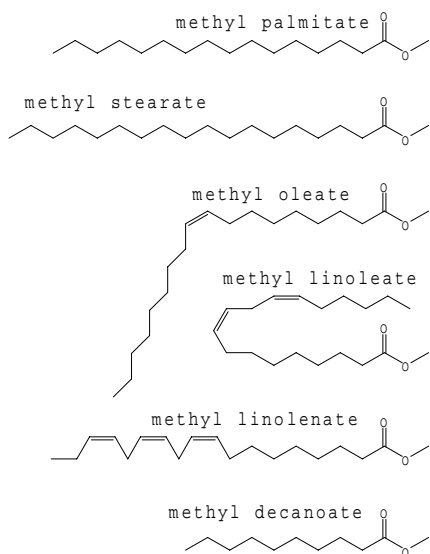


Fig. 3 Molecular structure of the main components found in soybean and rapeseed oils methyl esters and of methyl decanoate [P1].

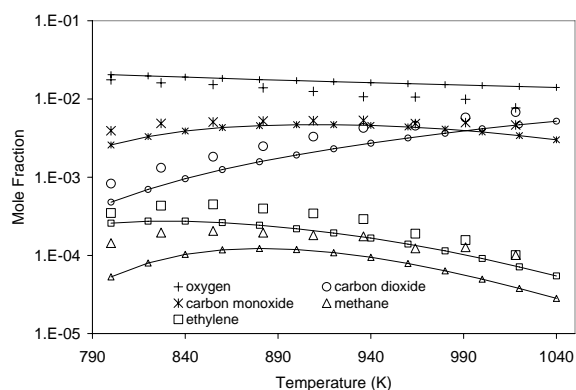


Fig. 4. Comparison of model predictions (methyl decanoate) with experimental measurements [9](rapeseed-based methyl esters) in a jet stirred reactor at 10 atm (equivalence ratio = 0.5, fuel/O₂/N₂ mixtures, residence time 1.0 sec).

experiments in a jet stirred reactor (Fig. 4). The experiments were performed at 10 atm so that they are relevant to pressure found in internal combustion (IC) engines. It can be seen from the results that methyl decanoate is quite a good surrogate for rapeseed derived methyl esters.

Methyl esters form carbon dioxide at low temperatures directly from the methyl ester structure [10, 11] [P1]. The methyl decanoate model simulated the formation of CO₂ [P1] at low temperature quite well (Fig. 4). When methyl esters are used as biodiesel, this direct formation of CO₂ wastes some of the oxygen in the fuel that can otherwise be used to prevent carbon in the fuel from leading to soot formation [10, 12].

In other related work on esters, a detailed chemical kinetic reaction mechanism has been developed for a group of four small alkyl ester fuels, consisting of methyl formate, methyl acetate, ethyl formate and ethyl acetate [13]. This mechanism was validated by comparisons between computed results and recently measured intermediate species mole fractions in fuel-rich, low pressure, premixed laminar flames. The model development employed a principle of similarity of functional groups in constraining the H atom abstraction and unimolecular decomposition reactions in each of these fuels. As a result, the reaction mechanism and formalism for mechanism development are suitable for extension to larger oxygenated hydrocarbon fuels, together with an improved kinetic understanding of the structure and chemical kinetics of alkyl ester fuels that can be extended to biodiesel fuels. Variations in concentrations of intermediate species levels in these flames were traced to differences in the molecular structure of the fuel molecules.

III. Future Work

We plan to develop a detailed chemical kinetic mechanism for 2,2,4,4,6,8,8-heptamethylnonane which is a primary reference fuel used to determine the ignition quality (Cetane Number) for diesel fuel and a recommended component in a diesel fuel surrogate [3]. This is a very ambitious undertaking because the branched molecular structure of the hydrocarbon and large number of carbon atoms leads to a detailed chemical kinetic model with a large number of species and reactions that are needed to address low and high temperature reactions that are important in combustion in internal combustion engines.

This work performed under the auspices of the U.S. Department of Energy by Lawrence Livermore National Laboratory under Contract DE-AC52-07NA27344.

IV. References

1. A. Ristori, P. Dagaut and M. Cathonnet, "The oxidation of n-Hexadecane: experimental and detailed kinetic modeling," *Combust. Flame* **125**, 1128-1137 (2001).
2. V. P. Zhukov, V. A. Sechenov and A. Y. Starikovskii, "Autoignition of n-decane at high pressure," *Combust. Flame*, in press (2008).
3. J. T. Farrell, N. P. Cernansky, F. L. Dryer, D. G. Friend, C. A. Hergart, C. K. Law, R. McDavid, C. J. Mueller and H. Pitsch, "Development of an experimental database and kinetic models for surrogate diesel fuels," *SAE Paper 2007-01-0201, 2007 SAE World Congress*, Detroit, MI, 2007.
4. M. Colket, T. Edwards, S. Williams, N. P. Cernansky, D. L. Miller, F. N. Egolfopoulos, F. L. Dryer, J. Bellan, P. Lindstedt, K. Seshadri, H. Pitsch, A. Sarofim, M. Smooke and W. Tsang, "Identification of Target Validation Data for Development of Surrogate Jet Fuels," *46th AIAA Aerospace Sciences Meeting and Exhibit*, Reno, Nevada, paper no. AIAA-2008-0972, 2008.
5. C. K. Westbrook, W. J. Pitz, O. Herbinet, H. J. Curran and E. J. Silke, "A Detailed Chemical Kinetic Reaction Mechanism for n-Alkane Hydrocarbons from n-Octane to n-Hexadecane," *Combust. Flame*, Submitted (2008).
6. M. A. Oehlschlaeger, D. F. Davidson and R. K. Hanson, "Thermal decomposition of toluene: Overall rate and branching ratio," *Proc. Combust. Inst.* **31**, 211-219 (2007).
7. T. Seta, M. Nakajima and A. Miyoshi, "High-temperature reactions of OH radicals with benzene and toluene," *J. Phys. Chem. A* **110**, 5081-5090 (2006).

8. R. Bounaceur, I. D. Costa, R. Fournet, F. Billaud and F. Battin-Leclerc, "Experimental and modeling study of the oxidation of toluene," *Int. J. Chem. Kinet.* **37**, 25-49 (2005).
9. P. Dagaut, S. Gail and M. Sahasrabudhe, "Rapeseed oil methyl ester oxidation over extended ranges of pressure, temperature, and equivalence ratio: Experimental and modeling kinetic study," *Proc. Combust. Inst.* **31**, 2955-2961 (2007).
10. C. J. Mueller, W. J. Pitz, L. M. Pickett, G. C. Martin, D. L. Siebers and C. K. Westbrook, "Effects of Oxygenates on Soot Processes in DI Diesel Engines: Experiments and Numerical Simulations," SAE 2003-01-1791, 2003 Arch T. Colwell Merit Award Paper, (2003).
11. P. A. Glaude, W. J. Pitz and M. J. Thomson, "Chemical Kinetic Modeling of Dimethyl Carbonate in an Opposed-Flow Diffusion Flame," *Proc. Combust. Inst.*, 2004.
12. C. K. Westbrook, W. J. Pitz and H. J. Curran, "Chemical kinetic modeling study of the effects of oxygenated hydrocarbons on soot emissions from diesel engines," *J. Phys. Chem. A* **110**, 6912-6922 (2006).
13. C. K. Westbrook, W. J. Pitz, P. R. Westmoreland, F. L. Dryer, M. Chaos, P. Osswald, K. Kohse-Hoinghaus, T. A. Cool, J. Wang, B. Yang, N. Hansen and T. Kasper, "A Detailed Chemical Kinetic Reaction Mechanism for Oxidation of Four Small Alkyl Esters in Laminar Premixed Flames," *Proc. Combust. Inst.*, Montreal, Canada, submitted, 2008.

V. Publications and submitted journal articles supported by this project 2006-2008

1. O. Herbinet, W. J. Pitz and C. K. Westbrook, "Detailed chemical kinetic oxidation mechanism for a biodiesel surrogate," *Combust. Flame*, in press (2008).
2. H. R. Zhang, E. G. Eddings, A. F. Sarofim and C. K. Westbrook, "Mechanism Reduction and Generation Using Analysis of Major Fuel Consumption Pathways for n-Heptane in Premixed and Diffusion Flames," *Energy Fuels* **21**, 1967-1976 (2007).
3. E. J. Silke, W. J. Pitz, C. K. Westbrook and M. Ribaucour, "Detailed Chemical Kinetic Modeling of Cyclohexane Oxidation," *J. Phys. Chem. A* **111**, 3761-3775 (2007).
4. A. Saylam, M. Ribaucour, W. J. Pitz and R. Minetti, "Reduction of large detailed chemical kinetic mechanisms for autoignition using joint analyses of reaction rates and sensitivities," *Int. J. Chem. Kinet.* **39**, 181-196 (2007).
5. Y. Sakai, H. Ozawa, T. Ogura, A. Miyoshi, M. Koshi and W. J. Pitz, "Effects of Toluene Addition to the Primary Reference Fuel at High Temperature," *SAE Commercial Vehicle Engineering Congress & Exhibition*, Chicago, IL, 2007.
6. Y. Sakai, T. Inamura, T. Ogura, M. Koshi and W. J. Pitz, "Detailed Kinetic Modeling of Toluene Combustion over a Wide Range of Temperature and Pressure," 2007 JSAE/SAE International Fuels and Lubricants Meeting, Kyoto TERRSA, Japan, SAE 2007-01-1885, 2007.
7. W. J. Pitz, C. V. Naik, T. N. Mhaolduin, C. K. Westbrook, H. J. Curran, J. P. Orme and J. M. Simmie, "Modeling and experimental investigation of methylcyclohexane ignition in a rapid compression machine," *Proc. Combust. Inst.* **31**, 267-275 (2007).
8. W. J. Pitz, N. P. Cernansky, F. L. Dryer, F. Egolfopoulos, J. T. Farrell, D. G. Friend and H. Pitsch, "Development of an Experimental Database and Kinetic Models for Surrogate Gasoline Fuels," SAE 2007 Transactions Journal of Passenger Cars - Mechanical Systems, SAE Paper 2007-01-0175, 2007.
9. W. J. Pitz and C. K. Westbrook, "A detailed chemical kinetic model for gas phase combustion of TNT," *Proc. Combust. Inst.* **31**, 2343-2351 (2007).
10. W. K. Metcalfe, W. J. Pitz, H. J. Curran, J. M. Simmie and C. K. Westbrook, "The development of a detailed chemical kinetic mechanism for diisobutylene and comparison to shock tube ignition times," *Proc. Combust. Inst.* **31**, 377-384 (2007).
11. C. K. Westbrook, W. J. Pitz and H. J. Curran, "Chemical kinetic modeling study of the effects of oxygenated hydrocarbons on soot emissions from diesel engines," *J. Phys. Chem. A* **110**, 6912-6922 (2006).

INVESTIGATION OF NON-PREMIXED TURBULENT COMBUSTION

Grant: DE-FG02-90ER14128

Stephen B. Pope
Sibley School of Mechanical & Aerospace Engineering
Cornell University
Ithaca, NY 14853
s.b.pope@cornell.edu

1 Scope of the Research Program

The focus of the current work is on the development of computational approaches which allow our detailed knowledge of the chemical kinetics of combustion to be applied to the modeling and simulation of combustion devices. In the past year, the work has been focused in three general areas: Lagrangian investigations of the competition between mixing and reaction in turbulent non-premixed flames (Wang & Pope 2008); the development and application of a methodology for sensitivity analysis in PDF methods for turbulent combustion (Ren & Pope 2007, 2008); and, a fundamental investigation of the modeling of turbulent mixing (Viswanathan & Pope 2008). The latter two topics are described further below.

2 Recent Progress

The principal research results from this program are described in the publications listed in Section 4. Some of these results are highlighted in the following subsections.

2.1 Sensitivity calculations in PDF methods

Modeling combustion phenomena requires the knowledge of chemical kinetics, transport properties and turbulence/combustion model coefficients as input parameters, and produces predictions (such as species concentration profiles) as the output, with the input and output being connected by the governing model equations. Often it is desirable to know how sensitive the predictions are to certain parameters in the model formulation. In the fields of chemical kinetics and laminar flames, sensitivity analysis [1] has been widely used to examine quantitatively the relationship between the parameters and the output of the model. In contrast, sensitivity analysis in turbulent combustion calculations is less well developed. For example, in the past, in modeling turbulent reactive flows based on PDF methods, somewhat crude global sensitivity analyses have been performed by repeating a calculation with a single parameter changed by a small amount. This divided difference technique has been used to show the strong sensitivity of some PDF calculations of turbulent flames to the temperature of a pilot stream [2, 3], to a reaction rate [4], and to the mixing model constant C_ϕ governing the rate of turbulent mixing [2, 5, 6]. However, using divided differences in PDF particle methods is costly and inefficient, as the statistical errors need to be reduced so as to be small compared to the differences in the two calculations.

In Ren & Pope (2007), we have developed a method for the accurate calculation of sensitivities in PDF modeling of turbulent combustion. It enables the calculation of sensitivities (to model

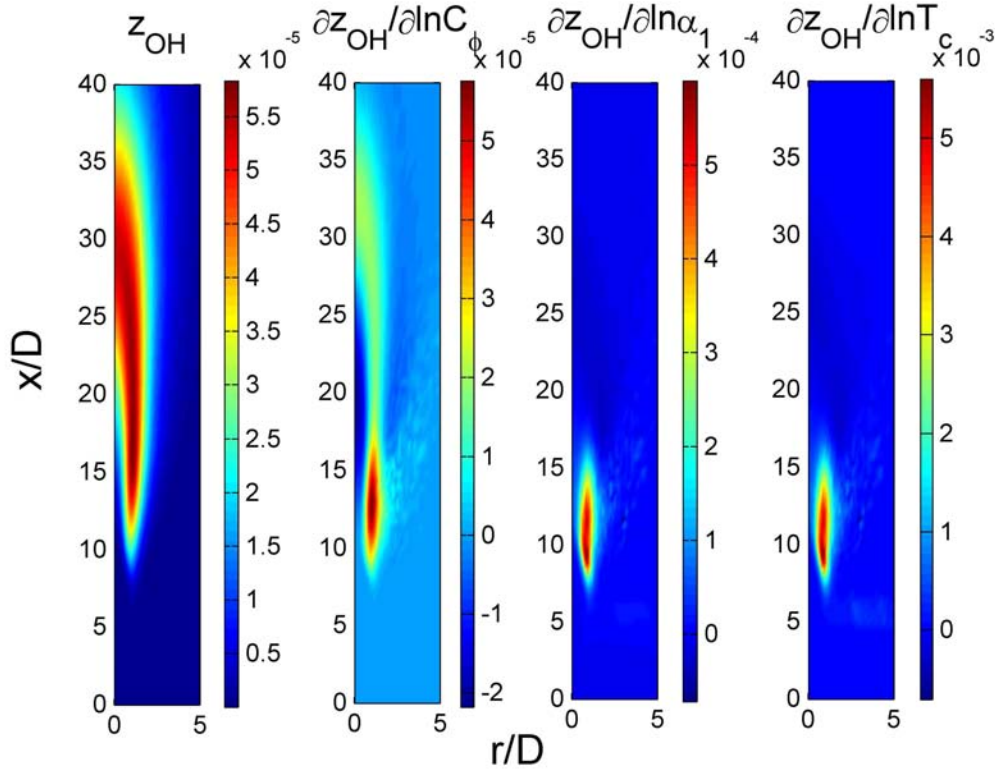


Figure 1: For the Cabra flame, contour plots of the mean specific moles of OH and its semi-logarithmic sensitivities to the mixing model constant C_ϕ , the pre-exponential factor α_1 , and the coflow temperature T_c . (Note that in the four plots the upper limits of the color scales are approximately 5×10^{-5} , 5×10^{-5} , 5×10^{-4} and 5×10^{-3} , respectively.)

parameters of interest) for each particle in the PDF particle method. These particle-level sensitivities are revealing: they allow one to examine the particles with the largest sensitivities, and the corresponding compositions reveal the sensitive regions in the composition and physical spaces. Moreover sensitivities of mean (and conditional mean) quantities can be extracted by ensemble averaging the particle sensitivities.

In Ren & Pope (2008), a further significant contribution is the development and application of a methodology for the efficient calculation of these particle-level sensitivities via the *in situ* adaptive tabulation (ISAT) algorithm [7]. This study, for the first time, investigates the sensitivities (including the particle-level sensitivities) in the PDF calculations of turbulent flames. The flame considered is the Cabra H_2/N_2 jet flame [8], which is a turbulent jet flame of H_2/N_2 issuing into a wide co-flow of lean combustion products and is designed to simulate conditions, albeit with simple flows, that are encountered in gas turbine combustors and furnaces where there is a recirculation of hot combustion products. Measurement shows that the liftoff height of this flame is very sensitive to the coflow temperature T_c , such that a decrease of 10 K in T_c can double the liftoff height. By employing the new sensitivity methodology, Ren & Pope (2008) compute the particle-level sensitivities to the mixing model constant C_ϕ , the coflow temperature T_c , and the pre-exponential factor α_1 of the chain reaction: $R1 : O_2 + H \rightleftharpoons OH + O$.

In physical space (normalized by the jet diameter D), Fig. 1 shows the contour plots of the specific moles of OH and its semi-logarithmic sensitivities to C_ϕ , α_1 and T_c . As may be seen, the most sensitive parameter for this flame is the coflow temperature T_c . The calculation is extremely sensitive to T_c with the normalized sensitivity ($\partial \ln \tilde{z}_{OH} / \partial \ln T_c$) being of order 100. The sensitivity to T_c is about 10 times larger than the sensitivity to α_1 , and about 100 times larger than that to C_ϕ . For species OH , the maximum sensitivity to α_1 and T_c occurs around the axial location $x/D = 9 - 10$ and radial location $r/D \approx 1$, whereas the maximum sensitivity to C_ϕ occurs around $x/D = 11.5 - 14.5$ and $r/D \approx 1$.

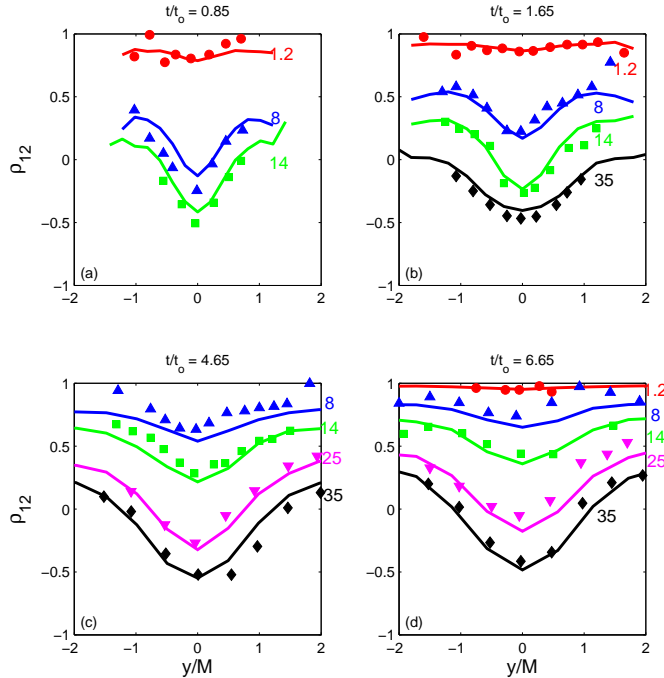


Figure 2: Radial profiles of the cross-correlation coefficient, ρ_{12} between the sources 1 and 2, for different spacings between the two sources, d_o . The sources are positioned at $x_o/M = 20$ from the turbulence generating grid. (a) : $t/t_o = 0.85$; (b) : $t/t_o = 1.65$; (c) : $t/t_o = 4.65$; (d) : $t/t_o = 6.65$; Present model calculations (solid line); Warhaft data: $d_o = 1.2 \text{ mm}$, \bullet ; $d_o = 8 \text{ mm}$, \blacktriangle ; $d_o = 14 \text{ mm}$, \blacksquare ; $d_o = 25 \text{ mm}$, \blacktriangledown ; $d_o = 35 \text{ mm}$, \blacklozenge ;

2.2 Modeling turbulent mixing from line sources

Following a fluid particle in a gaseous turbulent reactive flow, the chemical composition is affected by just two processes: chemical reactions, and mixing due to molecular diffusion. In PDF methods, reaction is treated exactly — without turbulence modeling approximations — and hence the modeling of mixing is crucial.

In Viswanathan & Pope (2008) we have made a significant advance in the modeling of turbulent mixing in a canonical flow: the dispersion from a pair of line sources in grid turbulence. In 1984 Warhaft made measurements in this flow [9] which have provided a challenge to models ever since. The results shown in Fig. 2 demonstrate that we have now met this challenge. The plots show the correlation coefficient between the scalars from the two line sources as a function of downstream distance (indicated by t/t_o), lateral distance (y/M) and source separation distance (d_o). As may be seen, the PDF calculations (lines) accurately represent all aspects of the experimental observations (symbols).

Compared to the previous modeling, the advances arise from the use of the “interaction by exchange with the conditional mean” (IECM) mixing model [10, 11, 12], and correctly accounting for the direct effects of molecular diffusion at very early times.

3 Future Plans

The focus of current and future work is on the development of a computationally-efficient implementation of “local” turbulent mixing models. The IECM mixing model considered in the previous section is an example of such a local mixing model, in this case local in physical and velocity spaces. Another important example arises in Multiple Mapping Conditioning (MMC) [13]. While localness is highly desirable on physical grounds, such models are difficult to implement numerically. Current and future work is aimed at developing efficient and accurate numerical implementations, and using these in computations of turbulent flames, both using PDF and LES/FDF methodologies.

4 Publications from DOE Research 2005-2007

1. R.R. Cao, H. Wang and S.B. Pope (2007) “The effect of mixing models in PDF calculations of piloted jet flames,” Proceedings of the Combustion Institute, **31**, 1543–1550.
2. Z. Ren and S.B. Pope (2007) “Sensitivity calculations in PDF particle methods,” Combustion and Flame, **153**, 202–215.
3. Z. Ren and S.B. Pope (2006) “The geometry of reaction trajectories and attracting manifolds in composition space,” Combustion Theory and Modelling, **10**, 361–388.
4. Z. Ren and S.B. Pope (2008) “Sensitivity calculations in PDF modelling of turbulent flames,” Proceedings of the Combustion Institute, **32**, (submitted).
5. M.A. Singer, S.B. Pope and H.N. Najm (2006a) “Operator-Splitting with ISAT to Model Reacting Flow with Detailed Chemistry,” Combustion, Theory & Modelling, **10**, 199–217.
6. M.A. Singer, S.B. Pope and H.N. Najm (2006b) “Modeling unsteady reacting flow with operator-splitting and ISAT,” Combustion and Flame, **147**, 150–162.
7. S. Viswanathan and S.B. Pope (2008) “Turbulent dispersion behind line sources in grid turbulence,” Physics of Fluids (to be published).
8. H. Wang and S.B. Pope (2008) “Lagrangian investigation of local extinction, re-ignition and auto-ignition in turbulent flames,” Combustion Theory and Modelling (to be published).

References

- [1] A.E. Lutz, R.J. Kee, J.A. Miller, SENKIN: A Fortran program for predicting homogeneous gas phase chemical kinetics with sensitivity analysis, Technical Report SAND87-8248, Sandia National Laboratories, 1987.
- [2] Q. Tang, J. Xu, S.B. Pope, Proc. Combust. Inst. 28 (2000) 133-139.
- [3] R. Cao, S.B. Pope, A.R. Masri, Combust. Flame 142 (2005) 438-453.
- [4] A.R. Masri, R. Cao, S.B. Pope, G.M. Goldin, Combust. Theory Modelling 8 (2004) 1-22.
- [5] R.P. Lindstedt, S.A. Louloudi, E.M. Váos, Proc. Combust. Inst. 28 (2000) 149-156.
- [6] R. Cao, H. Wang, S.B. Pope, Proc. Combust. Inst. 31 (2007) 1543-1550.
- [7] S.B. Pope, Combust. Theory Modelling 1 (1997) 41-63.
- [8] R. Cabra, T. Myrvold, J.Y. Chen, R.W. Dibble, A.N. Karpetis, R.S. Barlow, Proc. Combust. Inst. 29 (2002) 1881-1888.
- [9] Warhaft, Z., J. Fluid Mech. 144 (1984) 363-387.
- [10] Pope, S.B., Phys. Fluids 6 (1994) 973-985.
- [11] Fox, R.O., Phys. Fluids 8 (1996) 2678-2691.
- [12] Sawford, B., Flow, Turb. Combust. 72 (2004) 133-160.
- [13] Klimenko, A.Y. and Pope, S.B., Phys. Fluids 15 (2003) 1907–1925.

OPTICAL PROBES OF ATOMIC AND MOLECULAR DECAY PROCESSES

S.T. Pratt
Building 200, B-125
Argonne National Laboratory
9700 South Cass Avenue
Argonne, Illinois 60439
E-mail: spratt@anl.gov

PROJECT SCOPE

Molecular photoionization and photodissociation dynamics can provide considerable insight into how energy and angular momentum flow among the electronic, vibrational, and rotational degrees of freedom in isolated, highly energized molecules. This project involves the study of these dynamics in small polyatomic molecules, with an emphasis on understanding the mechanisms of intramolecular energy flow and determining how these mechanisms influence decay rates and product branching ratios. It is also aimed at understanding how internal energy can influence photoionization cross sections and dissociative ionization processes. The experimental approach combines double-resonance laser techniques, which are used to prepare selected highly excited species, with mass spectrometry, ion-imaging, and high-resolution photoelectron spectroscopy, which are used to characterize the decay of the selected species. Four-wave mixing techniques to generate vacuum ultraviolet (vuv) light for single-photon ionization studies are also employed.

RECENT PROGRESS

We have continued to focus on using a combination of ion imaging and vuv single-photon ionization to probe the photodissociation of halogenated hydrocarbons, the secondary decomposition of the resulting hydrocarbon radicals, and the internal energy dependence of the relative photoionization cross sections and dissociative ionization of these radicals. In the past year, studies were completed and published on the dissociative ionization of allyl and 2-propenyl radicals, and on the secondary decomposition of 2-propenyl radicals produced by the photodissociation of 2-bromopropene. The latter study was of particular interest because the time-dependence of the C_3H_5 decomposition to $C_3H_4 + H$ could be observed by monitoring the $C_3H_5^+$ and $C_3H_4^+$ images as a function of the delay between the photodissociation and photoionization pulses. While this approach is fairly general, the unknown branching of internal energy between the rotational and vibrational degrees of freedom in the radical makes it difficult to study the vibrational energy dependence of the decomposition rates. This approach should have significantly more utility if a cold radical source is used and the radicals are prepared in an energy selective manner by photoexcitation. Modifications to the apparatus to allow such studies are currently in progress.

In the past year, a new approach to determine absolute photoionization cross sections of radicals and other reactive species was developed. One difficulty in determining the absolute photoionization cross sections of radicals is getting a handle on the absolute concentration of radicals. One way to circumvent this issue is to use photodissociation of a suitable precursor to produce the desired radical in conjunction with a species of known cross section. For example, Neumark and coworkers have developed an approach based on translational spectroscopy and

the photoionization of momentum-matched fragments produced by photodissociation. By using radical-chloride precursors, the known absolute photoionization cross section of Cl is used to extract the absolute cross section of the radical. Our approach is closely related to that of Neumark and coworkers,¹⁻³ but the translational spectroscopy apparatus has been replaced by an ion-imaging apparatus, and the synchrotron vacuum-ultraviolet (vuv) light source has been replaced by a laser-based vuv source. This approach has its roots in the ion-imaging work of Gross et al. on the internal energy dependence of radical cross sections.⁴ Ion-imaging results in a considerable simplification of the experiment, and the improved resolution of the translational energy distributions provides information on the internal state dependence of the radical cross sections. The laser-based vuv source has the advantage of considerably higher resolution than the synchrotron-based source, and the disadvantages of being more difficult to tune over large energy regions and to calibrate with respect to photon flux. We have applied this approach to the determination of the absolute photoionization cross section of the methyl radical, using the photodissociation of methyl iodide as a precursor. Although the absolute photoionization cross section of iodine has not been measured experimentally, theoretical calculations by Robicheaux and Greene⁵ allow the calibration of the experimental relative photoionization cross section⁶ of I $^2P_{3/2}$ and thus the relative ionization signals and translational energy distributions obtained from the I⁺ and CH₃⁺ images can be calibrated to give the absolute cross section for the CH₃. Using this approach, we have determined $\sigma_{\text{abs}}^{\text{CH}_3}(\lambda) = 5.4 \pm 2.0 \text{ Mb}, 5.5 \pm 2.0 \text{ Mb}, \text{ and } 4.9 \pm 2.0 \text{ Mb}$ at 10.460 eV, 10.466 eV, and 10.471 eV, respectively. The error bars reflect not only the measurement statistics but also the estimated error in the I $^2P_{3/2}$ cross section and the mass-dependent detector gain, and we believe that these can be improved considerably by referencing the I cross section to that of Cl. The results for the CH₃ cross section are in excellent agreement with those determined by Craig Taatjes and coworkers (Sandia National Laboratory) using an entirely different technique, and a joint paper has been submitted on this work.⁷ We believe that both approaches should be applicable to a significant number of other radicals.

I am continuing my collaboration with Christian Jungen (Laboratoire Aimé Cotton) on the development of simple models for vibrational autoionization in polyatomic molecules. We have adapted the three-state model of the Renner-Teller interaction developed by Gauyacq and Jungen⁸ for use in a multichannel quantum defect theory treatment, and have shown how spectroscopic parameters extracted from an analysis of the Renner-Teller interaction in low-lying Rydberg states can be used to calculate the vibrational autoionization rates for these modes. These rates can be significantly larger than expected for modes that are Renner-Teller inactive. We have also shown that one can use the rates derived by this approach to calculate the electron capture cross section of the corresponding ionic state, and to estimate the dissociative recombination cross section. The dissociative recombination cross section calculated for HCO⁺ X $^1\Sigma^+$ using this simple model and only a small number of channels is in good agreement with the experimental values for these cross sections. Interestingly, the spectroscopic parameter g_K , which reflects the dipole component of the Renner-Teller interaction and characterizes the deviation of Λ from an integer value, plays a key role in the equations describing the autoionization and recombination rates. This observation once again illustrates the close connection between spectroscopy and dynamics.

Finally, I was involved in experimental studies using x-ray probes of laser aligned molecules. In collaboration with the Atomic, Molecular, and Optical Physics Group at Argonne, we used a

stretched ps laser pulse to adiabatically align gas-phase CF_3Br molecules and then probed the aligned molecules using a σ^* resonance near the Br K-edge. We were able to demonstrate that aligning the molecules parallel to the polarization axis of the laser resulted in an increase in x-ray absorption, and that aligning them perpendicular to the polarization axis led to a decrease in absorption. This work has implications for studies using free-electron x-ray lasers for single-shot and serial crystallography of single molecules.

FUTURE PLANS

We plan on continuing our studies of the photodissociation and photoionization of combustion-relevant radicals by using ion-imaging techniques and vacuum-ultraviolet single photon ionization. In particular, in the near future we hope to complete some studies of the 1-propenyl radical that were initiated in 2007. In collaboration with Laurie Butler (University of Chicago), we are beginning to study the photodissociation of the halogenated ethanol molecules, $\text{XC}_2\text{H}_4\text{OH}$, with $\text{X} = \text{Cl}, \text{Br}, \text{and I}$. Single-photon ionization should allow the direct detection of $\text{C}_2\text{H}_4\text{OH}$ and its secondary decomposition products. In this manner, we hope to gain insight into the mechanism of the $\text{OH} + \text{C}_2\text{H}_4$ reaction. Using a new imaging apparatus, we hope to begin studies on the photodissociation of cold radicals prepared by using a jet-cooled photolysis or pyrolysis source to produce cold radicals. We plan on extending our time-resolved studies to these systems to understand some of the questions raised about the unimolecular decomposition mechanisms in the studies of allyl and propargyl radicals by Chen and co-workers^{9,10} Because our approach for determining absolute photoionization cross sections of radicals is relatively simple, these measurements can be performed simultaneously with other imaging studies, and we plan to perform such measurements to a number of other systems, including CF_3 , C_2H_5 , the different isomers of C_3H_5 and C_3H_7 , and $\text{C}_2\text{H}_4\text{OH}$.

Finally, I will continue to collaborate with Christian Jungen on theoretical models of vibrational autoionization in polyatomic molecules. Following the completion of our work on autoionization enhanced by Renner-Teller interactions, we plan on extending this approach to include autoionization via Jahn-Teller interactions in symmetric nonlinear molecules, and we believe that our approach for calculating dissociative recombination cross sections will also be applicable in this case. The work on vibrational autoionization has suggested a number of new experimental studies. In particular, new studies using photoelectron imaging are planned to look at the photoelectron angular distributions for autoionizing resonances as a function of the decay process. Significant effects are expected for autoionization via non-totally symmetric vibrations, and the angular distribution measurements should provide new insight into the autoionization mechanisms.

This work was supported by the U.S. Department of Energy, Office of Science, Office of Basic Energy Sciences, Division of Chemical Sciences, Geosciences, and Biological Sciences under contract No. DE-AC02-06CH11357.

References

1. J. C. Robinson, N. E. Sveum, and D. M. Neumark, *J. Chem. Phys.* **119**, 5311 (2003).
2. J. C. Robinson, N. E. Sveum, and D. M. Neumark, *Chem. Phys. Lett.* **383**, 601 (2004).
3. N. E. Sveum, S. J. Goncher, D. M. Neumark, *Phys. Chem. Chem. Phys.* **8**, 592 (2006).
4. R. L. Gross, X. Liu, and A. G. Suits, *Chem. Phys. Lett.* **36**, 229 (2002).

5. J. Berkowitz, C. H. Batson, and G. L. Goodman, *Phys. Rev. A* **24**, 149 (1981).
6. F. Robicheaux and C. H. Greene, *Phys. Rev. A* **46**, 3821 (1992).
7. C. A. Taatjes, D. L. Osborn, T. Selby, G. Meloni, H. Fan, and S. T. Pratt, submitted to *J. Phys. Chem. A*.
8. D. Gauyacq and Ch. Jungen, *Mol. Phys.* **41**, 383 (1980).
9. H. J. Deyerl, I. Fischer, and P. Chen, *J. Chem. Phys.* **110**, 1450 (1999).
10. H. J. Deyerl, I. Fischer, and P. Chen, *J. Chem. Phys.* **111**, 3441 (1999).

DOE-SPONSORED PUBLICATIONS SINCE 2006

1. L. R. McCunn, D. I. G. Bennett, L. J. Butler, H. Fan, F. Aguirre, and S. T. Pratt
PHOTODISSOCIATION OF PROPARGYL CHLORIDE AT 193 NM
J. Phys. Chem. A. **110**, 843-850 (2006).
2. Haiyan Fan and S. T. Pratt
NEAR THRESHOLD PHOTOIONIZATION OF HOT ISOPROPYL RADICALS
J. Chem. Phys. **124**, 114312 (2006).
3. Haiyan Fan and S. T. Pratt
PHOTODISSOCIATION OF PROPARGYL BROMIDE AND PHOTOIONIZATION OF
PROPARGYL RADICALS
J. Chem. Phys. **124**, 144313 (2006).
4. Haiyan Fan and S. T. Pratt
THE STABILITY OF ALLYL RADICALS FOLLOWING THE PHOTODISSOCIATION
OF ALLYL IODIDE AT 193 NM
J. Chem. Phys. **125**, 144302 (2006).
5. Haiyan Fan and S. T. Pratt
DETERMINATION OF SPIN-ORBIT BRANCHING FRACTIONS IN THE
PHOTODISSOCIATION OF HALOGENATED HYDROCARBONS
J. Phys. Chem. A, **111**, 3901-3906 (2007).
6. H. Fan, L. B. Harding, and S. T. Pratt
DISSOCIATIVE IONIZATION OF HOT C₃H₅ RADICALS
Mol. Phys., **105**, 1517-1534 (2007).
7. H. Fan, S. T. Pratt, and J. A. Miller
SECONDARY DECOMPOSITION OF C₃H₅ RADICALS FORMED BY THE
PHOTODISSOCIATION OF 2-BROMOPROPENE
J. Chem. Phys., **127**, 144301 (2007).
8. E. R. Peterson, C. Buth, D. A. Arms, R. W. Dunford, E. P. Kanter, B. Krässig, E. C.
Landahl, S. T. Pratt, R. Santra, S. H. Southworth, and L. Young
X-RAY ABSORPTION BY LASER-ALIGNED MOLECULES
Appl. Phys. Lett. **92**, 094106 (2008).

Photoinitiated Reactions of Radicals and Diradicals in Molecular Beams

Hanna Reisler

Department of Chemistry, University of Southern California

Los Angeles, CA 90089-0482

reisler@usc.edu

Program Scope

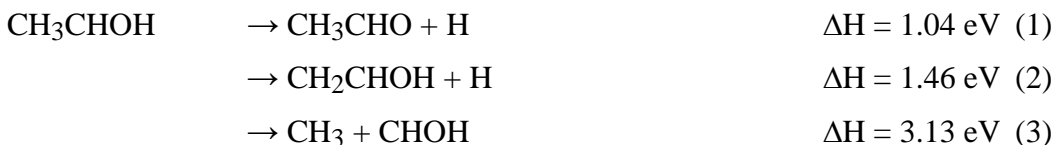
Open shell species such as radicals and diradicals are central to reactive processes in combustion and environmental chemistry. Our program is concerned with photoinitiated reactions of hydroxyalkyl radicals and carbenes. The goal is to investigate the detailed dynamics of dissociation of free radicals and diradicals for which multiple pathways including molecular rearrangements compete, and compare them with high level calculations. Studies include unimolecular reactions on the ground state of CH_2OH initiated by overtone excitation to above the barriers to dissociation and isomerization. The photochemistry of the 2-hydroxyethyl radical, a primary intermediate in the $\text{OH} + \text{C}_2\text{H}_4$ reaction, will be elucidated with special emphasis on the vinyl alcohol (enol) channel. The photodissociation of triplet methylene, the prototypical carbene, exhibits conical intersections and experiments will be compared with high-level electronic structure calculations. The detailed measurements on simple systems will serve as benchmarks for homologous series.

Recent Progress

Electronic spectroscopy and photodissociation dynamics of the 1-Hydroxyethyl radical, CH_3CHOH

The photodissociation of the hydroxyethyl radical has not been studied before. It is an isomer of the ethoxy radical ($\text{CH}_3\text{CH}_2\text{O}$), and it has been implicated in a series of intermediates in the $\text{OH} + \text{C}_2\text{H}_4$ reaction.

There are no theoretical papers on the excited states of the hydroxyethyl radical. However, there are several *ab initio* calculations of the geometry of the ground state and the ion as well as barriers to isomerization and dissociation on the ground-state potential energy surface (PES). The lowest barrier channels calculated for the ground state PES are:¹



In particular, we note that channel (2), the formation of vinyl alcohol following terminal C-H bond breaking, is not available in CH_2OH and can lead to a formation of enol at low excitation energies.² The molecular elimination channels, $\text{CH}_3\text{CO} + \text{H}_2$ and $\text{CH}_3 + \text{CO} + \text{H}_2$, involve high barriers and tight TS's and, as in CH_2OH , are not competitive with simple bond fission channels. In addition, The $\text{CH}_3\text{CH}_2\text{O} \leftrightarrow \text{CH}_3\text{CHOH}$ isomerization can lead to $\text{CH}_2\text{O} + \text{CH}_3$ ($\Delta H = 0.85 \text{ eV}$) and $\text{CH}_3\text{CHO} + \text{H}$.¹ The barrier to isomerization is calculated at 1.61 eV from the hydroxyethyl side.¹

The experience gained in our work on CH_2OH work served us well in producing molecular beams of CH_3CHOH , though beam intensities were lower.³ Cold radicals (10-15 K) were generated by reaction of Cl atoms (from 355 nm photolysis of Cl_2) with $\text{CH}_3\text{CH}_2\text{OH}$ in a quartz tube attached to the pulsed nozzle.

(a) Electronic Spectroscopy -- In analogy with CH_2OH ,³ we expected Rydberg states to be the lowest excited electronic states of CH_3CHOH , whose ionization energy (IE) is lower than that of CH_2OH (6.64 vs. 7.50 eV). Drawing upon the analogy with CH_2OH , we used the Rydberg formula ($h\nu = \varepsilon_1 - R_{\text{yd}}/(n-\delta)^2$, where R_{yd} is the Rydberg Constant) with similar quantum defects δ to predict the threshold energies for transitions to the $3s$ and $3p$ Rydberg states.

REMPI and H-photofragment yield spectroscopy were used to assign the electronic spectrum. Using 2+2 REMPI, we identified a progression of broad bands ($\sim 100 \text{ cm}^{-1}$) separated by $\sim 1600 \text{ cm}^{-1}$, which in analogy with the narrower bands observed in the hydroxymethyl radical, were assigned to a CO-stretch progression. The band origin was at $32\,360 \text{ cm}^{-1}$ (4.01 eV), close to the value predicted by the Rydberg formula for the $3p_z$ state. Thus, the upper state was assigned as the $3p_z$ state. As no REMPI spectrum was observed for other Rydberg states, H-photofragment yield spectroscopy was used.

H- and D-photofragment yield spectra were obtained for $\text{CH}_3\text{CHOH(D)}$ in the wavelength region where Rydberg transitions were expected. The $3s$ state is predicted to lie around $18,530 \text{ cm}^{-1}$ and the onset of absorption was indeed found at $19,600 \text{ cm}^{-1}$ (2.43 eV). We expected the $3p_x$ state to have a quantum defect of 0.94, similar to CH_2OH , and lie around 3.42 eV or $\sim 27,700 \text{ cm}^{-1}$. However, no REMPI spectrum and no vibronic structure were observed in this region, indicating that dissociation from $3p_x$ is very fast. The spectroscopic results show that the couplings of the Rydberg states to the ground state are much stronger in CH_3CHOH than in CH_2OH .

(b) Photodissociation dynamics: acetaldehyde and vinyl alcohol channels -- We obtained TOF spectra of H and D atoms from $\text{CH}_3\text{CHOH(D)}$ with 520-300 nm photolysis and derived kinetic energy distributions (KED's) and recoil anisotropy parameters β . When exciting CH_3CHOH near the onset of the $3s$ state, we observe one peak, centered close to the maximum of the allowed kinetic energy, from which we have determined the O-H bond energy: $D_0 = 1.1 \text{ eV} \pm 0.1 \text{ eV}$. In this region, the recoil anisotropy parameter, $\beta = -0.7 \pm 0.1$, is typical of a perpendicular transition. At excitation energies $> 31,200 \text{ cm}^{-1}$ (3.87 eV), another peak appears at low E_t , with an isotropic recoil distribution (Fig. 1). Its relative intensity increases with excitation energy but its β value does not change. In contrast, the β value of the higher E_t peak becomes monotonically less negative at higher excitation energies, decreasing to -0.2 at 4.4 eV . We also note that whereas we observe a REMPI spectrum from $3p_z$ at $> 4.00 \text{ eV}$, the H and D photofragment yield spectra remain unstructured. These results indicate that (i) throughout the 520-300 nm region, the strongest absorption is to the $3s$ state; and (ii) there are two distinct product channels that yield H atoms.

To identify these channels, TOF spectra of D-photofragments were recorded with CH_3CHOD and CD_3CHOH . Photodissociation of the former shows only the fast component (high E_t) in the TOF and KED spectra (Fig. 1), while the latter exhibits only the slow peak. We conclude therefore that both reactions (1) and (2) contribute. Simulations of the bimodal KED's of the H photofragments from CH_3CHOH (Fig. 1) by two gaussians, show that the channel represented by the low E_t peak [channel (2)] must have dissociation energy smaller than 2.7 eV . This value is much larger than the calculated 1.46 eV dissociation threshold of the C-H bond in the terminal carbon, but is below the energy required to break the C-H bond closest to OH (the 1-position), which is estimated at 3.37 eV .⁴ Breaking the latter bond also does not agree with our isotope experiments.

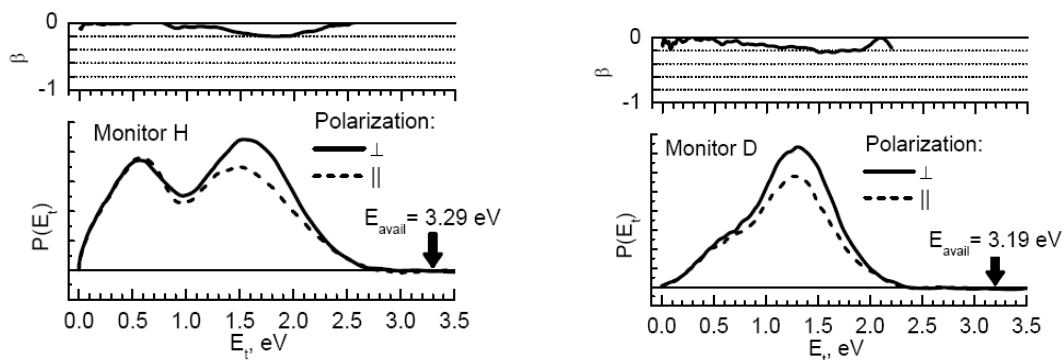


Fig. 1: H (left) and D (right) signals from CH_3CHOH and CH_3CHOD , respectively.

Another notable feature of the dissociation is the increasing amount of internal energy in the acetaldehyde product [reaction (1)] as the excitation energy increases. The less negative values of β of the fast peak at higher excitation energies may result from out-of-plane motions during dissociation of vibrationally excited molecules required to reach the conical intersection seam with the ground electronic state. As the excitation energy increases in the ground state PES following internal conversion, an increasing fraction of the parent vibrational energy is deposited in modes that appear eventually as internal modes (vibration and rotation) of the acetaldehyde fragment. This is manifested in the broadening of the high energy peak in the E_t distributions and the increasing value of $E_{\text{avail}} - E_{t,\text{max}}$, where $E_{t,\text{max}}$ is the maximum observed translational energy. The latter is especially pronounced in CH_3CHOD . The slow vinyl alcohol product from channel (2) also has a broad internal energy distribution. These results reflect the dynamics both in the regions of the conical intersections and in the exit channel

The variation of β with excitation energy is much less noticeable in $\text{CH}_2\text{OH(D)}$ where the β parameter is nearly constant over the entire range of perpendicular transitions to $3s$ and $3p_x$, and a sudden change in anisotropy occurs only at the onset of the parallel transition to the Rydberg $3p_z$ state.

In addition to experiments, we have just completed a collaborative electronic structure study with the group of Prof. Anna Krylov on the ionization of CH_3CHOH and CH_2OH ,⁵ in order to understand why the ionization energy (IE) of the former is lower by almost 1 eV than the latter. Our results show that the decrease in IE of CH_3CHOH results from hyperconjugation involving the methyl group, which destabilizes the SOMO in the neutral and stabilizes the cation.

In summary, we assigned transitions to the lowest Rydberg states of CH_3CHOH and observed structureless electronic absorption originating mainly from transition to the $3s$ state that extends from the visible to the UV and makes this radical unstable in visible light. We identified two independent dissociation channels, one leading to acetaldehyde and the other to vinyl alcohol. No CH_3 products from channel (3) or via isomerization to ethoxy were detected. We suggest that conical intersections with the ground state lead to O-H bond fission [channel (1)] from the onset of absorption to $3s$. However, the pathway leading to reaction (2) has a minimum energy much above the thermochemical threshold for this channel. The dynamics in the conical intersection regions deposit much of the available energy as internal energy of the molecular fragments. From experiment and theory we conclude that the Rydberg formula should hold rather well in the homologous series of CH_2OH , serving as a guide to the absorption spectra of higher hydroxyalkyl radicals whose radical centers are in the 1-position (C adjacent to OH).

References

1. Senosiain, J. P.; Klippenstein, S. J.; Miller, J. A. *J. Phys. Chem. A* **2006**, *110*, 6960.
2. Taatjes, C. A.; Hansen, N.; McIlroy, A.; Miller, J. A.; Senosiain, J. P.; Klippenstein, S. J.; Qi, F.; Sheng, L. S.; Zhang, Y. W.; Cool, T. A.; Wang, J.; Westmoreland, P. R.; Law, M. E.; Kasper, T.; Kohse-Hoinghaus, K. *Science* **2005**, *308*, 1887.
3. Feng, L.; Huang, X.; Reisler, H. *J. Chem. Phys.* **2002**, *117*, 4820.
4. Klippenstein, S. J.; private communication.
5. B. Karpichev, K. Diri, H. Reisler and A.I. Krylov, to be published.

Future Work

Our immediate goals are to study the photodissociation of the 2-hydroxyethyl radical, $\text{CH}_2\text{CH}_2\text{OH}$, and the triplet methylene radical. The latter is being produced efficiently by the pyrolysis of diazomethane, and preliminary results on its REMPI spectrum via Rydberg states have been obtained. The $\text{CH}_2\text{CH}_2\text{OH}$ isomer does not belong to the homologous series of hydroxymethyl radical and is more similar to a substituted ethyl radical. Very little is currently known about its photophysics and photochemistry. It is being produced in our lab by the photolysis of bromo- or iodo- ethanol in a newly constructed molecular beam source. Studies will include the dynamics of "hot" radicals produced by the initial photolysis in the interaction region of the molecular beam apparatus, and photodissociation dynamics of cold radicals generated in the source region and supersonically cooled.

Recent Publications

Unimolecular processes in CH_2OH below the dissociation barrier: O-H stretch overtone excitation and dissociation, J. Wei, B. Karpichev, and H. Reisler, *J. Chem. Phys.* **125**, 34303, (2006).

Theoretical and experimental investigations of the electronic rydberg States of diazomethane: assignments and state Interactions, I. Fedorov, L. Koziol, G. Li, J. A. Parr, A. I. Krylov, and H. Reisler, *J. Phys. Chem. A*, **111**, 4557 (2007).

Vibronic structure and ion core interactions in Rydberg states of diazomethane: An experimental and theoretical investigation, I. Fedorov, L. Koziol, G. Li, H. Reisler, and A. I. Krylov, *J. Phys. Chem. A*, **111**, 13,347 (2007).

Electronic spectroscopy and photodissociation dynamics of the 1-hydroxyethyl radical CH_3CHOH , B. Karpichev, L.W. Edwards, J. Wei, and H. Reisler, *J. Phys. Chem. A*, **112**, 412 (2008).

Accurate Calculations and Analyses of Electronic Structure, Molecular Bonding and Potential Energy Surfaces

Klaus Ruedenberg

Ames Laboratory USDOE, Iowa State University, Ames, Iowa, 50011
ruedenberg@iastate.edu

Scope

Essential for the theoretical treatment of molecular reactions, dynamics, kinetics, spectra etc is an accurate knowledge of potential energy surfaces, not only at equilibrium geometries but also in other coordinate space regions that are traversed during reactive geometry changes. A major difficulty is the sufficiently accurate description of non-relativistic electron correlations because the effectiveness of most methods is tied to the dominance of a single configuration in the wavefunction, a feature that does not carry over to most reaction paths and transition states. A substantive advance in dealing with this problem has been the correlation energy extrapolation by intrinsic scaling (CEEIS) developed and pursued in this group.

The complexity of accurate ab-initio electronic wavefunctions presents a challenge to extracting legitimate identifications of physical reasons for calculated structure rearrangements and energy changes. Substantive advances in dealing with this conceptual problem have been made by rigorously expressing ab initio molecular wavefunctions in terms of intrinsic atomic constituents in the context of the variation principle.

Recent Work

(1) The recently introduced method of *correlation energy extrapolation by intrinsic scaling (CEEIS)*, made it possible to calculate the first full potential energy curve of any 18-electron system, accurate enough for theoretically recovering the ro-vibrational spectrum with wave-number accuracy. Specifically, the $^1\Sigma_g^+$ ground state potential energy curve of the F_2 molecule has been obtained with an accuracy of about 0.2 millihartree from about 1.1 Å to 3 Å (the equilibrium distance being near 1.4 Å). Full configuration interaction energies were determined for the non-relativistic correlated wavefunctions, extrapolated to the complete basis set limits, and complemented by the contributions due to spin-orbit coupling and scalar relativistic effects. Using a new type of analytical fit, the vibration-rotation spectrum was calculated. The full experimental spectrum of 22 vibrational levels is recovered with a mean absolute deviation of about 5 cm^{-1} . The rotational constants are recovered within 0.002 cm^{-1} . The dissociation energy is obtained within 30 cm^{-1} of the experimental value of 12953 cm^{-1} . The experimental spectrum had been reported by Colbourn, Dagenais, Douglas, Raymonda from the Herzberg Institute at the National Research Council in Ottawa [Can. J. Phys. 54, 1343 (1976)].

(2) A further study of this potential for internuclear distances beyond 3Å has shown that its decay to zero exhibits some unexpected features. It proved possible to express the potential energy as the sum of the energy of the uncorrelated, but properly dissociating wavefunction and the correlation energy. At long ranges, the former was shown to become exactly identical with the interaction between the quadrupoles of the fluorine atoms, whose alignment in the $^1\Sigma_g^+$ is such as to yield *repulsion*. The correlation energy,

on the other hand, was shown to become exactly identical with the *attractive* dispersion energy. Since the former goes like $(+r^{-5})$ while the latter goes like $(-r^{-6})$, the potential energy curve *must* have a hump. This slightly positive maximum (at about 3.5 Å) is moreover re-enforced by a repulsive contribution of the spin-orbital coupling, the repulsion being a consequence of the fact that an energy-lowering spin-orbit coupling exists in the atomic 2P ground states, but not in the molecular $^1\Sigma_g^+$ ground state.

As a result of these mutually antagonistic long-range contributions, the descent of the potential energy towards the minimum, when the atoms approach each other from infinity, begins only at internuclear distances less than 3Å (about twice the equilibrium distance) and is then much steeper than the conventionally presumed exponential decay. Nor does the total potential exhibit a dispersion-type (r^{-6}) behavior anywhere.

In addition, there exist several Π states that lie a few tenths of a millihartree *below* the $^1\Sigma_g^+$ state in the long-range region. This is because, in Π states, the quadrupoles of the two fluorine atoms are aligned in such a manner as to yield an *attraction*. These Π states are repulsive at short range and therefore cross the $^1\Sigma_g^+$ state at about 3Å. A spin-orbit-coupling-assisted non-adiabatic mixing, of the Π and $^1\Sigma_g^+$ states is therefore required for the correct calculation of the three highest “vibrational” levels of the ground state.

The inclusion of these highest levels in a one-state RKR procedure, as was done by the experimentalists, therefore seems unjustified. So is also their assumption of a long-range dispersion-type (r^{-6}) decay for the determination of the dissociation energy, as mentioned above. The uncertainty in the “experimental value” of the dissociation energy of F_2 may therefore be considerably larger than the claimed 8 cm^{-1} .

(3) In order to clarify the connection between ab-initio correlation energy and dispersion energy, an accurate potential energy curve of the neon dimer was obtained by coupled-cluster calculations using correlation-consistent basis sets and complementing them by extrapolation to the complete basis set limit. The deviation from the experiment-based empirical potential is found to be less than a microhartree. The potential energy was then resolved into the self-consistent-field Hartree-Fock contribution and the correlation contribution. A least-mean-squares fit of the latter to a three-term dispersion expansion in the long-range region yielded dispersion coefficients C_6 , C_8 , and C_{10} in close agreement with the empirical values. It was furthermore proven that only a certain linear combination of C_8 and C_{10} can be determined by LMSQ fitting to a long-range potential whose values can have errors of up to 0.01 microhartree, which is in fact the case for all available empirical and theoretical potentials. Any choice of C_8 and C_{10} that leaves the mentioned linear combination invariant, including the option $C_{10}=0$, yields an equally good fit.

(4) It has been shown that conventional physical rationalizations of electronic energy changes on potential energy surfaces and along reaction paths in fact represent interpretations of the *minimization process in the context of the variation principle* in terms of physical attributes of the kinetic and the potential energy functionals. It has been shown that shifts in the variational energy minimum, e.g. those caused by deformations of nuclear geometries, can be the result of kinetic energy functional changes as well as potential energy functional changes. Therefore, both contributions must always be taken into account. For instance, the energy lowering that electron sharing contributes to the

formation of a covalent bond is the result of *kinetic* energy functional changes due to delocalization in the variational process. In this context, it has also been shown that, contrary to a widespread lore, the virial theorem provides no information whatsoever regarding whether it is the kinetic or the potential energy functional that causes the variationally optimized energy to change when the geometry changes.

Future Work

The CEEIS method will be applied to reaction paths of other dissociations and reactions, most likely to O₂ and O₃. The method will be adapted to the treatment of core correlations. The use of localized orbitals will be developed for the treatment of larger reactive systems. The rigorous ab initio energy analyses of chemical binding will be further extended.

Publications in 2006, 2007, 2008

Correlation Energy Extrapolation Through Intrinsic Scaling. V. Electronic Energy, Atomization Energy and Enthalpy of Formation of Water.

L. Bytautas and K. Ruedenberg
J. Chem. Phys., **124**, 174304 (2006)

Scalable Correlated Electronic Structure Theory.

Mark S. Gordon, Klaus Ruedenberg, Michael W. Schmidt, Laimis Bytautas,
Timothy J. Dudley, Takeshi Nagata, Ryan Olson, Sergey Varganov,
J. of Physics: Conference Series 46, 229-233 (2006).

Why Does Electron Sharing Lead to Covalent Bonding? A Variational Analysis.

Klaus Ruedenberg and Michael W. Schmidt.
J. Comp. Chem., 28, 391-410 (2007).

Toward a Physical Understanding of Electron-Sharing Two-Center Bonds. I.

T. Bitter, K. Ruedenberg, W.H.E. Schwarz,
J. Comp. Chem., 28, 411-422 (2007).

Economical Description of Electron Correlation,

L. Bytautas and K. Ruedenberg,
Advances in Electron Correlation Methodology (A. K. Wilson and K. A. Peterson
Edtrs), ACS Symposium Series Volume 958, p. 103-124 (2007).

Accurate Ab Initio Potential Energy Curve of F₂. I. Non-Relativistic Full Valence CI Energies by the CEEIS Method.

L. Bytautas, T. Nagata, M. S. Gordon, K. Ruedenberg,
J. Chem. Phys. 127, 164317, 1-20 (2007).

Accurate Ab Initio Potential Energy Curve of F₂. II. Core-Valence Correlations, Relativistic Contributions and Long-Range Interactions.

L. Bytautas, N. Matsunaga, T. Nagata, M. S. Gordon, K. Ruedenberg,
J. Chem. Phys. 127, 204301, 1-12 (2007).

Accurate Ab Initio Potential Energy Curve of F₂. III. The Vibration Rotation Spectrum.

L. Bytautas, N. Matsunaga, T. Nagata, M. S. Gordon, K. Ruedenberg,
J. Chem. Phys. 127, 204313 1-19 (2007)

Intrinsic Local Constituents of Molecular Electronic Wave Functions. I. Exact Representation of the Density Matrix in terms of Chemically Deformed and Oriented Atomic Minimal Basis Set orbitals.

J. Ivanic, G. J. Atchity and K. Ruedenberg,

Theor. Chem. Acc, 119, May (2008); published on line May 8, 2007

Intrinsic Local Constituents of Molecular Electronic Wave Functions. II. Electronic Structure Analyses in terms of Intrinsic Oriented Quasi-Atomic Molecular Orbitals for the Molecules FOOH, H₂BH₂BH₂, H₂CO and the Isomerization HNO → NOH.

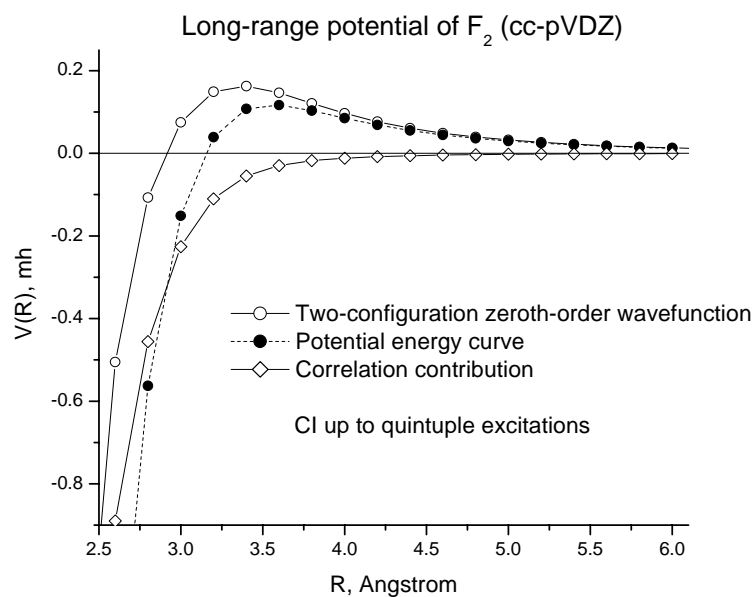
J. Ivanic and K. Ruedenberg,

Theor. Chem. Acc, 119, May (2008); published on line May 22, 2007.

Correlation Energy and Dispersion Interaction in the ab initio Potential Energy Curve of the Neon Dimer.

Laimutis Bytautas and Klaus Ruedenberg

J. Chem. Phys., submitted



Quadrupole-quadrupole repulsion *versus* dispersion attraction
in the long range region of the dissociation curve of F₂

Open circles: Potential energy without correlation
= $[C_5/r^{-5}]$ beyond 5Å.

Open diamonds: Correlation energy
= $[C_6/r^{-6}] + (C_8/r^{-8})$ beyond 5Å.

Full circles: Total potential energy curve

Active Thermochemical Tables – Progress Report

Branko Ruscic

Chemical Sciences and Engineering Division, Argonne National Laboratory,
9700 South Cass Avenue, Argonne, IL 60439
ruscic@anl.gov

Program Scope

The *spiritus movens* of this program is the need to provide the scientific community with accurate and reliable thermochemical, spectroscopic, and structural information on chemical species that are relevant in combustion, or play prominent roles in related post-combustion environmental chemistry, thus contributing to the global comprehension of the underlying chemical reactions and/or providing reliable benchmark values for development and testing of state-of-the-art theoretical approaches. In particular, thermochemistry is one of the essential underpinning scientific blocks that is enabling DOE to understand and successfully model energy-producing chemical reactions and thus fulfill its mission, and is, as such, a long-term component of the DOE BES research program. The current focal point of this program is to bring substantial innovations to the field of thermochemistry through the development of new tools and methodologies, and utilize these new approaches to systematically improve the quality of relevant thermochemical data. In order to accomplish the stated goal, this program has recently developed a novel approach centered on the idea of optimally extracting the knowledge content from thermochemically relevant measurements, and hence producing not only *the best currently possible* thermochemical parameters for the target chemical species, but also providing *critical tests of new experimental or theoretical data*, developing *pointers to future determinations that will most efficiently improve the thermochemical knowledge base*, and allowing efficient updates with new knowledge, instantly propagating its consequences through all affected chemical species. The effort of this program is synergistically coordinated with related experimental and theoretical efforts within the Argonne Chemical Dynamics Group to provide a broad perspective of this area of science.

Recent Progress

Development of Active Thermochemical Tables and the Core (Argonne) Thermochemical Network

Active Thermochemical Tables (ATcT) are a new paradigm of how to derive accurate, reliable, and internally consistent thermochemical values for stable, reactive, and transient chemical species. Availability of high-quality thermochemical values for a broad range of species, accompanied by properly quantified uncertainties, is central to chemistry, and critical in many areas of physical chemistry and chemical engineering, including, for example, experimental and computational chemical kinetics and dynamics, development of credible chemical reaction mechanisms, and formulation of realistic and predictive multi-scale models for complex chemical environments such as flames or the atmosphere. In addition, the availability of accurate and reliable thermochemical benchmarks has been historically the strongest *spiritus movens* for the advancement of sophisticated electronic structure theories. The success of ATcT is rooted in its Thermochemical Network (TN) approach. As opposed to the legacy sequential approach to thermochemistry, which has serious limitations in how the underlying thermochemical data can be utilized, the TN approach provides a simultaneous solution for all target species and thus furnishes consistent and accurate thermochemistry that leverages the entire knowledge content of the TN. The TN Graph is constructed by incorporating all available thermochemically-relevant experimental determinations, and further complemented both by existing and new (custom-computed) high-quality theoretical results, as well as new (custom-conducted) experiments. The TN Graph explicitly exposes to analysis the maze of inherent thermochemical interdependencies between various chemical species, and allows, *inter alia*, a thorough statistical analysis of the individual experimental and theoretical measurements that define

the TN, the goal of which is to isolate “optimistic” uncertainties that invariably occur with some of the original determinations (both experimental and theoretical), and which, if left unchecked, would adversely affect the quality of the resulting knowledge. The end result is the extraction of *best possible thermochemical values* for all chemical species described by the TN, based on optimal use of *all the available knowledge*, hence making conventional tabulations of thermochemical values obsolete.

The current Core (Argonne) TN encompasses ~850 chemical species intertwined by ~10,000 thermochemically-relevant determinations, and is an *ab ovo* TN. (As opposed to *localized* networks, which we use extensively during the development process, an *ab ovo* network does not contain any species constrained to an externally selected or imposed value of enthalpy of formation.) The current network contains a significant number of sections that are essentially completely mature, spanning a substantial number of “key” species whose interdependencies are by now so richly and thoroughly developed, that the related thermochemical properties are unlikely to be seriously affected by expansions of the TN toward additional species. Thus, while we are constantly expanding the TN, the current focus is on finalizing the thermochemistry of species that are of near-release quality.

One of the prime near-release candidates is OH, together with most of the other H_nO_m species and their ions. Almost all neutral species in the O/H group play prominent roles both in combustion and atmospheric chemistry, and are thus of immediate interest to many researchers. Furthermore, several of the O/H species are “key” thermochemical pegs that would normally define the static foundation of traditional thermochemistry, and their ions are crucial in determining such important properties as proton affinities and gas-phase acidities. All of the O/H species described by the C(A)TN are currently being prepared for final release, with the exception of species with cumulative oxygen bonds, such as HOOO and HOOOH. While these were until recently deemed to be somewhat exotic, they recently gained interest as potential intermediates in important atmospheric processes. HOOO is known spectroscopically, but its very scant thermochemically-relevant experimental and theoretical data displays a huge degree of inconsistency and most definitely requires additional experimental and theoretical work. M. I. Lester, U. Pennsylvania, is currently pursuing some extremely interesting experimental measurements, and J. Stanton, UT Austin, is pursuing related theoretical work.

Another near-release candidate that is in the final stages of preparation is the revised “key” value for C atom, whose ATcT solution has finally begun displaying the desired stability on account of the “critical mass” of dependencies across the C(A)TN that now help anchor its value, further amplified by the latest experimental photoionization data obtained by C.-Y. Ng (UC Davis). Together, these very recent developments indicate that we have also probably correctly resolved the remaining problem that was flagged by prior ATcT analyses (an experimental inconsistency in the spectroscopic data for ^{12}CO and ^{13}CO , preventing a unique reinterpretation in terms of thermochemical parameters). Finalization of the revised thermochemistry of C atom (which is a quantity deeply relevant, *inter alia*, to all electronic structure methods that use computed atomization enthalpies to produce enthalpies of formation, and is an important peg in defining many other values across the TN) will also allow us to promptly release the thermochemistry of a sequence of small carbon-containing species, such as CH_n , C_2H_n , COH_n , etc. (Preliminary results for the latter three groups of species, in a form independent of the final value for C atom, have been recently utilized in several collaborative efforts, involving S. J. Klippenstein, L. B. Harding, and J. Michael, ANL, W. Klopper, U. Karlsruhe, J. F. Stanton, UT Austin, J. M. L. Martin, Weizmann.) An almost parallel situation exists for the thermochemistry of N atom, where again the resolution of the inconsistencies flagged by the ATcT analysis were crucially helped by new photoionization measurements obtained in a collaborative effort with C.-Y. Ng. The thermochemistry of N atom, also deeply relevant in connecting theoretical results to practical thermochemical values, is a “key” to successfully defining the thermochemistry of NO_x and NO_y , as well as the thermochemistry of a number of small C/N containing species, including HCN and CN.

As we are finalizing the thermochemistry of prominent C/N/O/H species, we are also preparing the release of a highly accurate benchmark set of TAE_0 for a number of basic species involving first-row elements. Portions of this thermochemical dataset were recently successfully utilized in collaborative

efforts that led to the development of two highly-accurate electronic structure approaches: W4 (J. M. L. Martin, Weizmann) and HEAT 3 (J. Stanton, UT Austin). The two approaches bear very interesting similarities in the underpinning computational sequences, and both are capable of producing confidently thermochemistry accurate to $\pm 1 \text{ kJ mol}^{-1}$ or better. Though rather expensive, and thus at present not suited for routine computations of large chemical species, we expect that tailored results from both methods will valuably complement some of the interdependencies across the existing ATcT C(A)TN and help converge the thermochemistry of additional species toward near-release status.

In response to popular demand, we have recently started clearing the way to make ATcT results available over the web to all interested parties. The dedicated web site that we are developing will contain the latest ATcT/C(A)TN results that are of 'release' on 'near-release' quality, while also archiving all prior versions of web-exposed ATcT results. We are currently developing the templates and the external codes, and will start shortly amending the ATcT kernel code in an effort to implement an additional post-processing step that will generate the counterpart codes and dump the pertinent data. Together, these tools will result in an automatically generated web site content, which will be updated by ATcT after every successful run that produces new information. Once this *prima facie* web-exposure is accomplished, we will implement the second developmental phase, which is geared toward expanding the templates and amending the codes with additional post-processing steps that will encapsulate the pertinent information in xml format, which will then be coupled to templates of web pages using Ajax technologies. The latter approach will have the advantage of making the ATcT results available not only in html format (for human consumption), but also in xml (readily utilized by software, such as modeling applications, data depositories, etc.) Once the full automation is completed, we plan on enhancing the ATcT website by constructing – based on previous successful tests and experiences gained during the CMCS Collaboratory effort – the necessary infrastructure that will fully expose other prominent ATcT capabilities, such as solving user-created TNs, executing user-initiated “what if” scenarios, etc. These developments, particularly during the second (xml and Ajax) and third (exposure via web-services) phase, have important components that should – with some token additional cyberinfrastructure – allow transparent access to the most current ATcT data and capabilities within the PrImE initiative of M. Frenklach and his collaborators.

We have also numerous ongoing collaborations with members of the Argonne Chemical Dynamics Group, where we are developing and providing ATcT thermochemistry that is crucial in evaluating and correcting the computed potential energy surfaces, or is needed as reliable thermochemical data in interpreting current experimental results.

Other progress

As part of the IUPAC Task Group on Thermochemistry of Radicals (where the Argonne effort is central to the success of the project), we are in the process of performing critical and meticulous evaluations of the thermochemistry of a number of small radicals and intermediate species that are important in combustion and atmospheric chemistry. The resulting “IUPAC recommended values” are being published in a series of papers. On the experimental arena, we have ongoing long-term collaborations with C.-Y. Ng (UC Davis) and T. Baer (UNC Chapel Hill) to perform thermochemically relevant photoionization measurements, which are driven by deficiencies or inconsistencies that are being uncovered as we are building and analyzing the Core (Argonne) Thermochemical Network. On the theoretical arena, we have ongoing long-term collaborations with J. Stanton and J. Boggs (UT Austin), A. Császár (Eötvös U. Budapest), and J. M. L. Martin (Weizmann) on developing new and improved high-fidelity theoretical methods (where the benchmark data is developed via ATcT), as well as on computing critical thermochemistry for small radicals via state-of-the-art theory (where the selection of targets is via ATcT). We have also an ongoing collaboration with the group of T. Turányi (Eötvös U. Budapest) on extending the ATcT approach toward Monte Carlo analysis of reaction mechanisms, and with A. Burcat (Technion) in refining the largest existing polynomialized thermochemical database and coupling it to ATcT. We are also developing a number

of additional *ad hoc* collaborations with prominent scientists that are interested in the thermochemistry of particular target species, such as, for example, M. I. Lester (U. Pennsylvania), B. J. McCall, S. Widicus Weaver, and D. Woon (UI Urbana-Champaign), J. Aguilera-Iparraguirre, A. D. Boese, and W. Klopper (U. Karlsruhe and FZ Karlsruhe), etc.

Future Plans

Future plans of this program pivot around further developments and expansive use of Active Thermochemical Tables, providing accurate thermochemistry, and driving targeted theoretical and laboratory experimental investigation of radicals and transient species that are intimately related to combustion processes. The final goal is to achieve a reliable thermochemical characterization of chemical species that are crucial in understanding and modeling the combustion processes of alternative (as well as conventional) fuels, or are implicated in subsequent atmospheric chemistry.

This work is supported by the U.S. Department of Energy, Office of Basic Energy Sciences, Division of Chemical Sciences, Geosciences, and Biosciences, under Contract No. DE-AC02-06CH11357.

Publications resulting from DOE sponsored research (2006 - present)

- *Active Thermochemical Tables: Accurate Enthalpy of Formation of Hydroperoxyl Radical, HO₂*, B. Ruscic, R. E. Pinzon, M. L. Morton, N. K. Srinivasan, M.-C. Su, J. W. Sutherland, and J. V. Michael, *J. Phys. Chem.* **110**, 6592–6601 (2006).
- *Reflected Shock Tube Studies of High-Temperature Rate Constants for OH + NO₂ → HO₂ + NO and OH + HO₂ → H₂O + O₂*, N. K. Srinivasan, M.-C. Su, J. W. Sutherland, J. V. Michael, and B. Ruscic, *J. Phys. Chem.* **110**, 6602-6607 (2006).
- *Direct Identification of Propargyl Radical in Combustion Flames by VUV Photoionization Mass Spectrometry*, T. Zhang, X. N. Tang, K.-C. Lau, C. Y. Ng, C. Nicolas, D. S. Peterka, M. Ahmed, M. L. Morton, B. Ruscic, R. Yang, L. X. Wei, C. Q. Huang, B. Yang, L. S. Sheng, Y. W. Zhang, and F. Qi, *J. Chem. Phys.* **124**, 074302/1-8 (2006).
- *The Origin of Systematic Error in the Standard Enthalpies of Formation of Hydrocarbons Computed via Atomization Schemes*, G. Tasi, R. Izsak, G. Matisz, A. G. Császár, M. Kállay, B. Ruscic, and J. F. Stanton, *Chem. Phys. Chem.* **7**, 1664-1667 (2006).
- *W4 Theory for Computational Thermochemistry: In Pursuit of Confident sub-kJ/mol Predictions*, A. Karton, E. Rabinovich, J. M. L. Martin, and B. Ruscic, *J. Chem. Phys.* **125**, 144108/1-17 (2006).
- *Unimolecular Thermal Fragmentation of ortho-Benzynes*, X. Zhang, A. T. Maccarone, M. R. Nimlos, S. Kato, V. M. Bierbaum, B. K. Carpenter, G. B. Ellison, B. Ruscic, A. C. Simmonett, W. D. Allen, and H. F. Schaefer III, *J. Chem. Phys.* **126**, 044312/1-20 (2007).
- *Benchmark Atomization Energy of Ethane: Importance of Accurate Zero-point Vibrational Energies and Diagonal Born-Oppenheimer Corrections for a 'Simple' Organic Molecule*, A. Karton, B. Ruscic, and J. M. L. Martin, *J. Mol. Struct. (Theochem)* **811**, 345-353 (2007)
- *Kinetics of the Reaction of Methyl Radical with Hydroxyl Radical and Methanol Decomposition*, A. W. Jasper, S. J. Klippenstein, L. B. Harding, and B. Ruscic, *J. Phys. Chem. A* **111**, 3932-3950 (2007)
- *Portal-based Knowledge Environment for Collaborative Science*, K. Schuchardt, C. Pancerella, L. A. Rahn, B. Didier, D. Kodeboyina, D. Leahy, J. D. Myers, O. O. Oluwole, W. Pitz, B. Ruscic, J. Song, G. von Laszewski, and C. Yang, *Concurrency Computat.: Pract. Exper.* **19**, 1703-1716 (2007)
- *HEAT: High Accuracy Extrapolated ab initio Thermochemistry. III. Additional Improvements and Overview*, M. E. Harding, J. Vazquez, B. Ruscic, A. K. Wilson, J. Gauss, and J. F. Stanton, *J. Chem. Phys.* **128**, 114111/1-15 (2008)
- *Accurate ab initio Computation of Thermochemical Data for C₃H_x (x = 0,...,4) Species*, J. Aguilera-Iparraguirre, A. D. Boese, W. Klopper, and B. Ruscic, *Chem. Phys.* in press (2008)

Theoretical Studies of Elementary Hydrocarbon Species and Their Reactions

Henry F. Schaefer III and Wesley D. Allen
Center for Computational Chemistry
University of Georgia, Athens, GA 30602-2525
E-mail: hfs@uga.edu and wdallen@uga.edu; Phone: (706) 542-2067

Next-generation, explicitly-correlated electronic structure methods

All common wave function methods of electronic structure theory have a fundamental and troublesome flaw: the inability to correctly describe the exact mathematical cusp behavior of many-electron wave functions in the vicinity of coalescence points (Coulomb singularities), and hence to fully account for instantaneous, short-range correlation among electrons. To achieve high thermochemical accuracy, next-generation methodologies are needed that solve the electron cusp problem by explicitly incorporating interelectronic variables (r_{12}) into molecular wave functions. We are pursuing a long-term research program to develop practical explicitly-correlated methods, to create attendant, freely available computer codes, and to undertake chemical applications of unprecedented size.

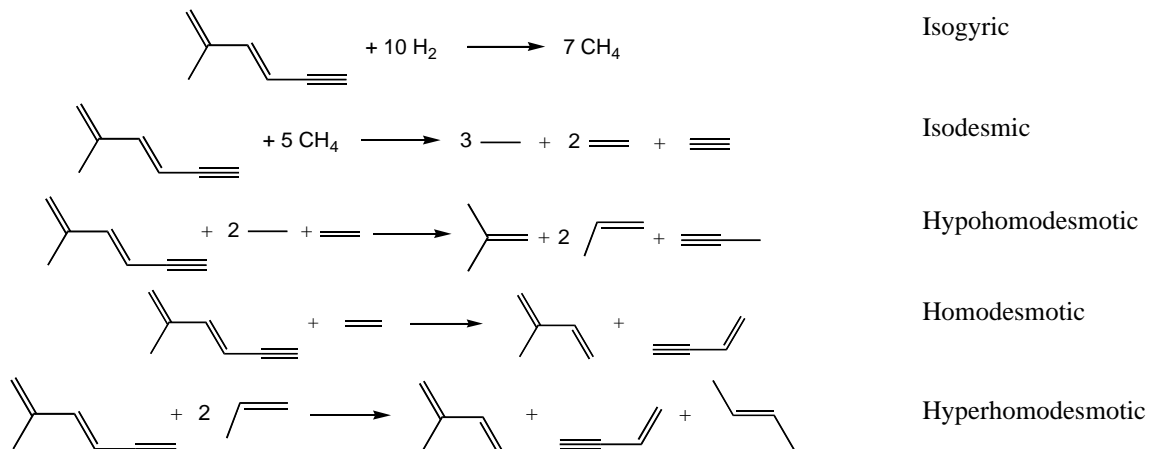
Most recently we have developed new explicitly-correlated methods for open-shell molecules, an area critical for studying the free-radical chemistry of combustion processes but whose development has lagged far behind closed-shell formulations. A key advance within the past year is our derivation and implementation of ZAPT2-F12 theory within the Massively Parallel Quantum Chemistry (MPQC) package. Our new capabilities include both linear r_{12} and effective Slater correlation factors, the latest auxiliary basis set (ABS) techniques for computing many-electron integrals, as well as the A, A', and B variants of F12 methodologies. We have demonstrated the effectiveness of our ZAPT2-F12 theory for numerous open-shell systems, promising impressive future applications to combustion problems. For OH, CN, and O₂, ZAPT2-R12 with an aug-cc-pVQZ basis obtains 99.44%, 99.58%, and 99.38%, respectively, of the exact second-order correlation energy; in contrast, the corresponding conventional computations recover less than 98.8% of this quantity even with a massive aug-cc-pV6Z basis set.

In comparison with its competitors, ZAPT (Z-averaged perturbation theory) is the only open-shell approach that possesses rigorous size extensivity, orbital invariance, and a Koopmans zeroth-order eigenspectrum while achieving computational efficiency by averting different orbitals for different spins (DODS). Despite its desirable attributes, ZAPT has not been widely utilized. To advance the understanding of ZAPT and promote its use, we executed the first analysis¹¹ of high-order ZAPT series of energies, equilibrium bond lengths, and harmonic vibrational frequencies for a number of challenging test molecules. For the high-spin $X^4\Sigma_g^- C_2^+$ case, all properties converge rapidly to the full configuration interaction (FCI) limit. The $b^2\Delta_g C_2^+$ species places severe demands on any single-reference theory because there are two equivalent determinants that predominate. Nonetheless, the ZAPT n energy, r_e , and ω_e series all converge to the proper FCI limit, albeit very slowly. We tracked the energy series out to ZAPT1000 and found a spectacular ringing pattern with a period of about 300 in the order of the perturbation. For NO, CN, and O₂, the ZAPT2 and ZAPT4 r_e and ω_e results with a TZ2P basis set are in close agreement with corresponding data from second- and fourth-order ROMP and RMP theory for the first two species and substantially better in the third case. Feenberg transformation of the ZAPT/TZ2P series with a fixed parameter $\lambda = 0.4$ for the NO, CN, and O₂ molecules yields striking overall improvements in the r_e and ω_e predictions, even at second order. Given its comparable or higher accuracy relative to other ROHF-based perturbation theories and its superior mathematical characteristics, ZAPT is the perturbation method of choice for open-shell systems.

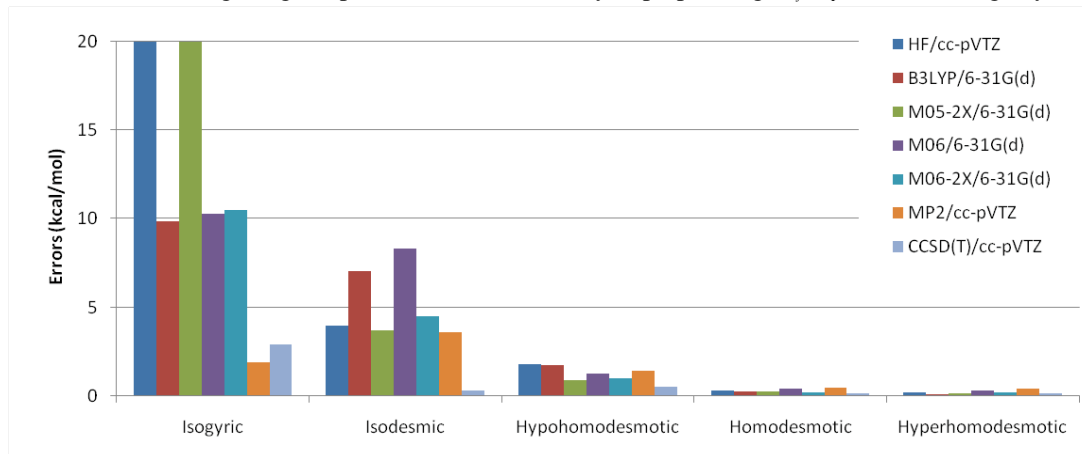
A Hierarchy of Homodesmotic Reactions

Balanced reactions such as isodesmic and homodesmotic transformations are often used for both chemical interpretation and error cancellation in computational chemistry; however, confusion abounds over the definitions of such reaction classes. In our recent comprehensive analysis of this problem,¹⁹ we proved that the two most prevalent definitions of homodesmotic reactions are inconsistent. By setting forth canonical criteria, we constructed a new hierarchy of reaction classes that conserves successively larger groups of atoms: isogyric \supseteq isodesmic \supseteq hypohomodesmotic \supseteq homodesmotic \supseteq hyperhomodesmotic. This hierarchy leads to a highly effective scheme

for computing hydrocarbon enthalpies of formation by means of *generalized bond separation reactions*, in which the target compound is uniquely decomposed into *elemental molecular products* via reactions with *elemental molecular reactants*. To illustrate this concept, the bond separation reactions for 2-methylhexa-1,3-diene-5-yne are:

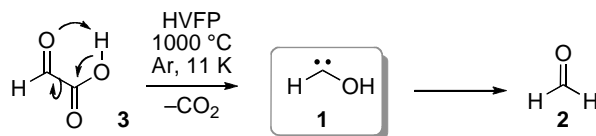


We worked out the complete set of elemental molecules for each reaction class: the count of (reactant, product) species being isogyric (1,1), isodesmic (1,3), hypohomodesmotic (3,7), homodesmotic (6,13), and hyperhomodesmotic (9,26). Establishing precise $\Delta_f H_T^\circ$ values just for the molecules in these limited sets will allow enthalpies for general hydrocarbons to be computed by well-defined and error-balanced procedures, yielding high accuracy even with modest levels of theory. The following figure shows average errors in the enthalpies of bond separation reactions for a group of 22 five- and six-carbon species, as computed across a wide range of theoretical approaches. The errors in the homodesmotic and hyperhomodesmotic reaction energies are consistently smaller than $0.4 \text{ kcal mol}^{-1}$, showing the great potential of the hierarchy in pinpointing $\Delta_f H_T^\circ$ values for large hydrocarbons.



Capture of Elusive Hydroxymethylene, a Tunneling Marvel

Hydroxymethylene (**1**, H-C-OH), the archetypical donor-substituted carbene, was posited as the “activated formaldehyde” in the photocatalytic formation of simple carbohydrates as early as 1921, and hydroxycarbenes have been implicated as key reactive intermediates in the high-energy chemistry of carbonyl compounds. Nonetheless, H-C-OH escaped isolation and direct spectroscopic characterization despite repeated efforts over many years. In our 2008 article in *Nature*,¹⁷ we report the successful preparation of **1** by means of a novel route, the extrusion of CO₂ from glyoxylic acid (**3**) via high-vacuum flash pyrolysis (HVFP) followed by immediate matrix isolation:



A definitive characterization of both H–C–OH and H–C–OD was achieved by a confluence of careful IR and UV measurements and high-level *ab initio* theory, including variational vibrational computations on an all-electron (AE) CCSD(T)/cc-pCVQZ anharmonic force field, and a rigorous multireference Mk-MRCCSD study of the low-lying electronic states. For 13 of the 15 assigned IR bands of H–C–OH and H–C–OD, the (mean, std. dev.) of the residual between pure (unscaled) theory and experiment is only (6.0, 3.3) cm⁻¹. Particularly impressive is the match for $\nu_3+\nu_4$ of H–C–OH, $2\nu_3$ of H–C–OD, and the Fermi resonance pair ($\nu_3+\nu_4, \nu_1$) of H–C–OD. Our Mk-MRCCSD computations conclusively assign the recorded UV/Vis absorptions between 500 and 380 nm to the expected lowest-lying open-shell singlet excited electronic state (S_1) of H–C–OH. Upon geometry optimization, the S_1 state relaxes to a nonplanar structure with a widened $\angle(\text{H–C–O}) = 127.4^\circ$ and a dihedral angle of 108.4° , consistent with the extensive vibrational progression observed in the electronic absorption spectrum. We optimized all singlet structures surrounding **1** at the AE-CCSD(T)/cc-pCVQZ level and determined the energetics to around 0.1 kcal mol⁻¹ by means of exhaustive focal-point analyses. Ground-state H–C–OH has a *trans*-planar geometric structure lying 51.9 kcal mol⁻¹ above formaldehyde (**2**), with barriers of 29.7 and 26.8 kcal mol⁻¹ for isomerization to **2** and the *cis* conformer of **1**, respectively.

Despite the high surrounding barriers, matrix-isolated H–C–OH disappears quickly with a half-life ($t_{1/2}$) of ca. 2 hr. in Ar, Kr, and Xe matrices, virtually independent of temperature in the 11–20 K range. However, H–C–OD is completely stable under identical conditions. After carefully excluding other mechanisms, quantum mechanical tunneling becomes the most viable explanation for these observations. To obtain a theoretical tunneling rate for **1** → **2**, we mapped out the AE-CCSD(T)/cc-pCVQZ potential energy curve along the intrinsic reaction path (IRP) for the isomerization. The quantum dynamics was treated within a reaction-path Hamiltonian model with tunneling probabilities given by the WKB method in terms of barrier penetration integrals, which we computed numerically from our electronic structure data. Our tunneling analysis yields $t_{1/2} = 2.1$ hr. for *trans*-H–C–OH in its ground vibrational level, and $t_{1/2} > 1200$ years for *trans*-H–C–OD, in remarkable accord with experiment. Pending more rigorous quantum dynamics computations, we conclude that the disappearance of H–C–OH is attributable to pure quantum mechanical tunneling under a large barrier of about 30 kcal mol⁻¹. The occurrence of such an event near 0 K on a tangible time scale of a few hours is a striking chemical phenomenon with little precedent.

Diverse Combustion Applications

The celebrated C₂H₅ + O₂ reaction is an archetype for hydrocarbon combustion, and the critical step in the process is the concerted elimination of HO₂ from the ethylperoxy intermediate (C₂H₅O₂). Master equation kinetic models fitted to measured reaction rates have placed the concerted elimination transition state (**TS1**) 3.0 kcal mol⁻¹ below the C₂H₅ + O₂ reactants, whereas the best previous electronic structure computations gave a barrier more than 2.0 kcal mol⁻¹ higher. This is a serious disparity, engendering seven-fold changes in the branching fractions for the ethyl + O₂ reaction. Our recent investigation¹² resolved to this long-standing problem by converging on the *ab initio* limit via focal point computations of the highest possible quality. Arduous geometry optimization and evaluation of **TS1** at the CCSD(T)/cc-pVQZ level does not appreciably change the best earlier electronic structure predictions. Two improvements past CCSD(T)/cc-pVQZ prove essential: first, a 1.2 kcal mol⁻¹ lowering of **TS1** by extrapolation to the complete basis set limit of CCSD(T), and second, an additional 0.9 kcal mol⁻¹ reduction by incorporation of quadruple excitations via the CCSDT(Q) method. The final predicted barrier is -3.0 kcal mol⁻¹, bringing the concerted elimination mechanism into precise agreement with experiment.

Previous attempts to detect the NCCO radical in combustion environments have failed, in part because of uncertainty in the IR signatures of this species. Our recent AE-CCSD(T)/cc-pCVQZ anharmonic vibrational study⁹ gave a characteristic stretching frequency $\nu_2 = 1898$ cm⁻¹, in stark contrast to the earlier experimentally-derived value of 1774 cm⁻¹. The high-quality computations stimulated a collaboration with the Schreiner laboratory in Giessen, Germany. Within the past few months, a novel strategy has been employed to generate NCCO by a microwave discharge technique, followed by immediate matrix isolation at 15 K. Analysis of the matrix IR spectrum yields the critical assignment $\nu_2 = 1889.2$ cm⁻¹, within 9 cm⁻¹ of our prediction. Our work establishes indisputable thermochemistry and spectroscopic signatures for the elusive NCCO radical.

The pyrolysis of aromatic fuels generates substantial quantities of diacetylene. Previous estimates of the enthalpy of formation of this important compound range from 102 to 113 kcal mol⁻¹. By a focal point investigation¹⁸

employing basis sets as large as cc-pV6Z and correlation treatments as extensive as CCSDT(Q), we have converged on $\Delta_f H^\circ$ for the reaction $2 \text{H-C}\equiv\text{C-H} \rightarrow \text{H-C}\equiv\text{C-C}\equiv\text{C-H} + \text{H}_2$. With the precisely established $\Delta_f H^\circ$ of acetylene, we thus obtain $\Delta_f H^\circ(\text{C}_4\text{H}_2) = (109.4, 109.7) \pm 0.3 \text{ kcal mol}^{-1}$ at (0, 298.15) K. We have also determined the first full quartic force field of diacetylene at the AE-CCSD(T)/cc-pCVQZ level, which yields VPT2 fundamental vibrational frequencies differing by no more than 7 cm^{-1} from experiment, without any empirical adjustments.

Publications Supported by DOE: 2006, 2007, 2008

1. B. N. Papas and H. F. Schaefer, "Concerning the Precision of Standard Density Functional Programs: GAUSSIAN, MOLPRO, NWCHEM, QCHEM, and GAMESS," *J. Mol. Struct.* **768**, 175-181 (2006).
2. X. Zhang, Q. Li, J. B. Ingels, A. C. Simmonett, S. E. Wheeler, Y. Xie, R. B. King, H. F. Schaefer, and F. A. Cotton, "Remarkable Electron Accepting Properties of the Simplest Benzenoid Cyanocarbons: Hexacyanobenzene, Octacyanonaphthalene, and Decacyanoanthracene," *J. Chem. Soc. (London) Chem. Comm.* **758** (2006).
3. N. C. Handy, S. Carter, Y. Yamaguchi, S. Li, and H. F. Schaefer, "Rovibrational Energy Levels for the Electronic Ground State of AlOH," *Chem. Phys. Lett.* **427**, 14-17 (2006).
4. D. Moran, A. C. Simmonett, F. E. Leach III, W. D. Allen, P. v. R. Schleyer, and H. F. Schaefer, "Popular Theoretical Methods Predict Benzene and Arenes to be Nonplanar," *J. Am. Chem. Soc.* **128**, 9342-9343 (2006), communication. See highlight in Editor's Choice, *Science* **313**, 149 (July 14, 2006 issue).
5. V. Kasalová, W. D. Allen, H. F. Schaefer, E. D. Pillai, and M. A. Duncan, "Model Systems for Probing Metal Cation Hydration," Roger E. Miller Memorial Issue, *J. Phys. Chem. A* **111**, 7599-7610 (2007).
6. X. Zhang, A. T. Maccaroni, M. R. Nimlos, S. Kato, V. M. Bierbaum, G. B. Ellison, B. Ruscic, A. C. Simmonett, W. D. Allen, and H. F. Schaefer, "Unimolecular thermal fragmentation of *ortho*-benzynes," *J. Chem. Phys.* **126**, 044312: 1-20 (2007).
7. S. E. Wheeler, K. A. Robertson, W. D. Allen, H. F. Schaefer, Y. J. Bomble, and J. F. Stanton, "Thermochemistry of Key Soot Formation Intermediates: C_3H_3 Isomers," *Jim Miller Festschrift, J. Phys. Chem. A* **111**, 3819-3830 (2007).
8. P. Bera, Y. Yamaguchi, and H. F. Schaefer, "The Low-Lying Quartet Electronic States of Nitrogen Dioxide," *J. Chem. Phys.* **127**, 174303: 1-12 (2007).
9. A. C. Simmonett, F. A. Evangelista, W. D. Allen, and H. F. Schaefer, "In Search of Definitive Signatures of the Elusive NCCO Radical," *J. Chem. Phys.* **127**, 014306: 1-9 (2007).
10. L. Belau, S. E. Wheeler, B. W. Ticknor, M. Ahmed, S. R. Leone, W. D. Allen, H. F. Schaefer, and M. A. Duncan, "Ionization Thresholds of Small Carbon Clusters: Tunable VUV Experiments and Theory," *J. Am. Chem. Soc.* **129**, 10229-10243 (2007).
11. S. E. Wheeler, W. D. Allen, and H. F. Schaefer, "On the Convergence of Z-Averaged Perturbation Theory (ZAPT)," *J. Chem. Phys.* **128**, 074107: 1-11 (2008).
12. J. J. Wilke, W. D. Allen, and H. F. Schaefer, "Establishment of the $\text{C}_2\text{H}_3 + \text{O}_2$ Reaction Mechanism: A Combustion Archetype," *J. Chem. Phys.* **128**, 074308: 1-9 (2008).
13. P. P. Bera, Y. Yamaguchi, H. F. Schaefer, and T. D. Crawford, "Born-Oppenheimer Symmetry Breaking in the \tilde{C} State of NO_2 : Importance of Static and Dynamic Correlation Effects," *J. Phys. Chem. A* **112**, 2669-2676 (2008).
14. R. K. Sreeruttan, P. Ramasami, C. S. Wannere, A. C. Simmonett, and H. F. Schaefer, " π - and σ -Phenylethynyl Radicals and Their Isomers *o*-, *m*-, and *p*-Ethynylphenyl: Structures, Energetics, and Electron Affinities," *J. Phys. Chem. A* **112**, 2838-2845 (2008).
15. S. Carter, N. C. Handy, Y. Yamaguchi, J. M. Turney, and H. F. Schaefer, "Vibrational Energy Levels for the Electronic Ground State of the Diazocarbene (CNN) Molecule," *Raphael D. Levine Special Issue, Molecular Physics*, in press (2008).
16. L. D. Speakman, J. M. Turney, and H. F. Schaefer, "Toward the Experimental Observation of Quartet States of the Ozone Radical Cation: Insights from Coupled Cluster Theory," *J. Chem. Phys.*, in press (2008).
17. P. R. Schreiner, H. P. Reisenauer, F. C. Pickard, A. C. Simmonett, W. D. Allen, E. Máttyus, and A. G. Császár, "Capture of Hydroxymethylene and Its Fast Disappearance through Tunnelling," *Nature*, in press (2008).
18. A. C. Simmonett, H. F. Schaefer, and W. D. Allen, "The Enthalpy of Formation and Anharmonic Force Field of Diacetylene," *J. Phys. Chem. A.*, submitted (2008).
19. S. E. Wheeler, K. N. Houk, W. D. Allen, and P. v. R. Schleyer, "A Hierarchy of Homodesmotic Reactions," *J. Am. Chem. Soc.*, submitted (2008).
20. N. J. Stibrich, A. C. Simmonett, B. N. Papas, W. D. Allen, and H. F. Schaefer, "Composite CCSDT(Q) Investigation of the Ketenyl Radical," *J. Chem. Phys.*, submitted (2008).

Picosecond Nonlinear Optical Diagnostics

Thomas B. Settersten
Combustion Research Facility, Sandia National Laboratories
P.O. Box 969, MS 9056
Livermore, CA 94551-0969
tbsette@sandia.gov

Program Scope

This program focuses on the development of innovative laser-based detection strategies for important combustion radicals and the investigation of the fundamental physical and chemical processes that directly affect quantitative application of these techniques. These investigations include the study of fundamental spectroscopy, energy transfer, and photochemical processes. This aspect of the research is essential for the correct interpretation of diagnostic signals, enabling reliable comparisons of experimental data and detailed combustion models. Many of these investigations use custom-built tunable picosecond (ps) lasers, which enable efficient nonlinear excitation, provide high temporal resolution for pump/probe studies of collisional processes, and are amenable to detailed physical models of laser-molecule interactions.

Recent Progress

Two-photon ps-LIF detection of atomic hydrogen. Atomic hydrogen plays a key role in ignition, flame propagation, and heat release in hydrocarbon combustion because of its high reactivity and diffusivity. Multi-photon laser-induced fluorescence (LIF) can be used for sensitive, spatially resolved detection of H in flames. In the current work, we focus on the two-photon LIF scheme using two 205-nm photons to excite $3s\ ^2S, 3d\ ^2D \leftarrow 1s\ ^2S$ transitions, which produces fluorescence emission at 656 nm ($n=3 \rightarrow n=2$). In comparison to other multi-photon LIF schemes, this approach is the simplest, requiring a single laser beam for the two-photon-resonant step. Prior work, however, demonstrates that this approach is prone to photolytic interference because two-photon-resonant excitation requires high-intensity UV laser pulses, which can readily photodissociate H_2O and CH_x to produce H. A similar process had hindered two-photon LIF imaging of atomic oxygen in flames, but we previously demonstrated that excitation with ps pulses can substantially reduce interference due to single-photon photolysis by allowing the use of reduced laser energy.¹ In the current work, we collaborate with J. H. Frank (Sandia) to demonstrate a similar advantage for H imaging.

LIF line images were recorded in a series of methane flames (equivalence ratios ranging from 0.5–1.8) using a range of laser fluences for 50-ps and 3.5-ns pulses. Photolytic interference is evidenced by the change of the shape of the peak-normalized LIF profiles as the pulse fluence is increased (Fig. 1a). *Interference-free* signal was defined as that which can be produced without measurable distortion of the LIF line profile. Except for the richest flame investigated ($\Phi=1.8$), ps excitation produced 1 to 2 orders of magnitude higher interference-free LIF signals.² A series of pump-probe experiments were conducted to further understand the photolytic processes. A detuned, ns-duration, laser pulse photolytically produced atomic hydrogen under different flame conditions,

and the photoproduct was probed using a weak, nonperturbing ps pulse and directly compared to nascent H in each flame. Further, time- and spatially-resolved spectrograph images were used to identify the photolytic production of electronically excited flame radicals. Based on our previous results, we used a ps laser sheet to produce interference-free, 2-D LIF images of H (Fig. 1b).³ The high-quality images enable the observation of increased signal at the flame tip, consistent with diffusional focusing of H where the flame front has a sharp curvature. Motivated by these results, we plan to use ps two-photon LIF imaging to investigate the influence of preferential diffusion of atomic hydrogen on ignition and flame propagation in collaboration with J.H. Frank (Sandia).

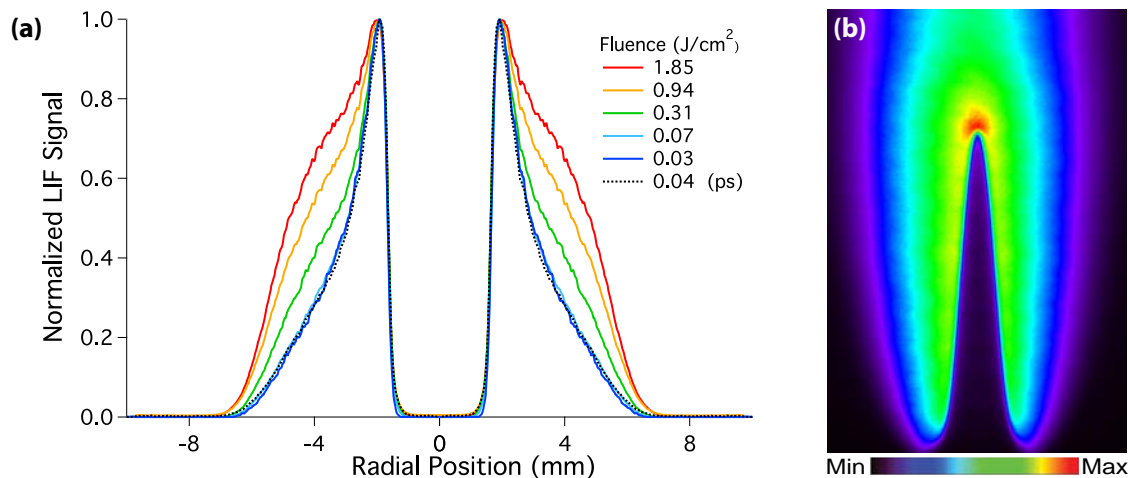


Figure 1: (a) Photolytic interference observed in atomic hydrogen LIF line profiles recorded in a $\phi=0.70$ $\text{CH}_4/\text{O}_2/\text{N}_2$ flame. Interference-free profiles are evident for ns fluences ≤ 0.07 J/cm^2 and ps fluences ≤ 0.04 J/cm^2 . (b) Interference-free two-dimensional PLIF image of H in $\phi=1.20$ $\text{CH}_4/\text{O}_2/\text{N}_2$ flame.

Time-Resolved ps-LIF. Using ps lasers and fast electronics for time-resolved LIF, we previously measured precisely the temperature ($300 \text{ K} \leq T \leq 1300 \text{ K}$) and species dependence of fluorescence quenching cross sections (thermally averaged) of $\text{CO B } ^1\Sigma^+(v=0)$ ⁴ and $\text{NO A } ^2\Sigma^+(v=0)$,⁵ which are the excited states that are commonly used for fluorescence detection of these species. The precision of our data for quenching of $\text{NO A } ^2\Sigma^+(v=0)$ enables, for the first time, the observation of subtle temperature dependencies in quenching cross sections, which provide new scientific insight into the mechanisms responsible for the quenching.⁵ Near room-temperature, the cross sections for the most significant colliders exhibit a negative temperature dependence, indicative of the importance of an attractive potential. At the low temperatures characteristic of hypersonic flow conditions ($T \approx 150 \text{ K}$), quenching is expected to be facile and very sensitive to temperature changes. In collaborative work with Campbell Carter (AFRL), we extend our precise characterization of $\text{NO A } ^2\Sigma^+(v=0)$ to the low temperature range ($150 \text{ K} < T < 300 \text{ K}$). Experiments were conducted in a liquid- N_2 -cooled cryostat, which has been custom-fitted with a vacuum fluorescence cell that is immersed in N_2 vapor. Our work extends the pioneering measurements of Zhang and Crosley,⁶ who measured quenching cross sections between 215 and 300 K. We have completed characterization of the temperature dependent quenching by O_2 , and experiments characterizing temperature dependence of self quenching and N_2 quenching are nearing completion. In this low-temperature range, attractive intermolecular force lead to large cross sections with strong temperature dependence. We expect that new high-precision results over a large temperature range will help elucidate the details of long-range intermolecular potentials involving $\text{NO A } ^2\Sigma^+$ and other small molecules.

Photofragment-LIF detection of H_2O_2 . The decomposition of H_2O_2 is the critical chain branching step in the intermediate-temperature (800–1100 K) ignition chemistry. An imaging technique for H_2O_2 will be extremely valuable for ignition research in homogeneous charge compression ignition (HCCI) and rapid compression machines. Imaging directly with LIF is not possible because the UV absorption of H_2O_2 , which is featureless and monotonically decreases with increasing wavelength, results in excitation to repulsive Rydberg states that promptly produce two hydroxyl radicals. Single-photon absorption produces two OH(X) fragments, while multi-photon absorption can produce electronically excited OH. We can exploit these processes in a photofragment-LIF scheme to image the parent H_2O_2 molecules, and we have very recently started experiments to characterize these processes and to determine optimum detection strategies. In one approach, a 70-ps pulse at either 266 or 355 nm photodissociates H_2O_2 via multi-photon absorption, leading to OH(X)+OH(A). In this single-laser scheme, the prompt OH fluorescence is directly related to the H_2O_2 number density. In the second detection scheme, an UV laser sheet photodissociates H_2O_2 , and the product OH(X) radicals are imaged via OH LIF using a second overlapped laser sheet.

In our initial experiments in an atmospheric-pressure flow cell, we used ps laser pulses at either 266 nm or 355 nm to excite OH(A) fluorescence directly via multi-photon absorption by H_2O_2 . Spectrally resolved measurements clearly identified OH A-X fluorescence resulting directly from either 266- or 355-nm excitation. Because fluorescence was observed both from N_2/H_2O and $N_2/H_2O/H_2O_2$ flows, H_2O represents a potential interference to this approach. Preliminary measurements at 266 nm, however, indicate that the fluorescence yield per precursor molecule is approximately two-orders of magnitude greater for H_2O_2 than for H_2O . Power-law scans confirmed that excitation of OH(A) results from 2-photon absorption at 266 nm by either H_2O or H_2O_2 . On the other hand, it appears that the OH (A) fluorescence produced by 355-nm excitation results from 3-photon excitation for both species. Further experiments are ongoing.

Future Plans

Ignition Experiments using ps H-atom LIF. Based on the success of our ps two-photon LIF imaging of H, we plan to continue collaboration with J. H. Frank to apply this technique to study preferential diffusion in edge flames during extinction and re-ignition in pulsed counterflows. Studies of H-atom preferential diffusion in flames with different Lewis numbers are also envisioned.

Photofragment-LIF detection of H_2O_2 . We will continue experiments aimed at developing an imaging diagnostic for H_2O_2 at elevated pressures. We will directly compare single-step and two-step approaches as described in the previous section for pressures up to 10 bar. Immediate work will quantify OH(A) yields using multi-photon excitation at 266 and 355 nm. Because excitation at 355 nm will simultaneously excite H_2O_2 photofragment LIF and LIF from CH_2O , we will investigate the possibility of a two-detector, single-laser, imaging diagnostic for these two species, which are important in low- and intermediate-temperature combustion chemistry. Subsequent experiments will investigate the two-laser, two-step process. Because ps photodissociation of H_2O_2 results in vibrationless products in a rotationally hot distribution, we will evaluate the efficacy of probing the prompt rotationally hot product distribution with a short pulse laser to discriminate against any background (thermalized) OH in the sample. A further refinement of the technique uses a dual-image camera and two OH lasers to measure both the nascent OH before the photodissociation pulse and the nascent-plus-photoproduct OH following the photodissociation pulse.

Picosecond Pure Rotational CARS. Coherent Anti-Stokes Raman Spectroscopy (CARS) is a well developed technique, but line-mixing and non-resonant background can restrict its utility at high pressures. We propose to address both issues using pure rotational CARS with a time-delayed ps probe pulse. Pure rotational CARS is significantly less affected by line mixing than the more commonly used vibrational CARS. A time-delayed probe pulse can significantly suppress the non-resonant background.⁷ Broadband detection will enable single-shot temperature determination and possibly mixture determination in high-pressure systems. In initial experiments in collaboration with T. Seeger (Erlangen), we will excite pure rotational Raman coherences using a broadband ps pulse, and the CARS signal will be generated by a time-delayed, transform-limited ps pulse. We will characterize dependence of CARS spectra on pressure (up to 10 bar), probe delay, and resonance enhancement. Model development will be based on a mature code at Erlangen. Subsequent experiments will characterize the pure rotational linewidths in the time domain, and polarization studies should enable detailed characterization of anisotropy decay.⁸ Narrowband pump and probe pulses will excite single rotational (J) R-branch Raman resonances, and a delayed probe pulse will measure the coherence decay as a function of J , temperature, and colliding species.

References

- [1] T. B. Settersten, A. Dreizler, B. D. Patterson, P. E. Schrader, R. L. Farrow, *Appl. Phys. B* **76**, 479 (2003); J. H. Frank, X. Chen, B. D. Patterson, T. B. Settersten, *Appl. Opt.* **43**, 2588 (2004); J. H. Frank, T. B. Settersten, *Proc. Combust. Instit.* **30**, 1527 (2005).
- [2] W. D. Kulatilaka, B. D. Patterson, J. H. Frank, T. B. Settersten, "Investigation of photolytic interferences in nanosecond and picosecond excitation schemes for two-photon laser-induced fluorescence detection of atomic hydrogen in flames," *Appl. Opt.*, submitted (2008).
- [3] W. D. Kulatilaka, B. D. Patterson, J. H. Frank, T. B. Settersten, "Interference-free two-photon LIF imaging of atomic hydrogen in flames using picosecond excitation," *Proc. Comb. Instit.*, submitted (2008).
- [4] T. B. Settersten, A. Dreizler, R. L. Farrow, *J. Chem. Phys.* **117**, 3173 (2002).
- [5] T. B. Settersten, B. D. Patterson, J. A. Gray, *J. Chem. Phys.* **124**, 234308 (2006).
- [6] R. Zhang, D. R. Crosley, *J. Chem. Phys.* **102**, 7418 (1995).
- [7] S. Roy, T. R. Meyer, J. R. Gord, *Appl. Phys. Lett.* **87**, 264103 (2005).
- [8] X. Chen, T. B. Settersten, *Appl. Opt.* **46**(19), 3911 (2007).

BES-Supported Publications (2006-present)

- T. B. Settersten, B. D. Patterson, J. A. Gray, "Temperature- and species-dependent quenching of NO $A^2\Sigma^+(v'=0)$ probed by two-photon laser-induced fluorescence using a picosecond laser," *J. Chem. Phys.*, **124**, 234308 (2006).
- T. B. Settersten, B. D. Patterson, H. Kronemayer, V. Sick, C. Schulz, J. Daily, "Branching ratios for quenching of nitric oxide $A^2\Sigma^+(v'=0)$ to $X^2\Pi(v''=0)$," *Phys. Chem. Chem. Phys.* **8**, 5328 (2006).
- X. Chen, T. B. Settersten, "Investigation of OH $X^2\Pi$ collisional kinetics in a flame using picosecond two-color resonant four-wave-mixing spectroscopy," *Appl. Opt.* **46**(19), 3911 (2007).
- W. D. Kulatilaka, R. P. Lucht, S. Roy, J. R. Gord, T. B. Settersten, "Detection of atomic hydrogen in flames using picosecond two-color two-photon-resonant six-wave-mixing spectroscopy," *Appl. Opt.* **46**(19), 3921 (2007).
- C. A. Bauer, T. V. Timofeeva, T. B. Settersten, B. D. Patterson, V. H. Liu, B. A. Simmons, M. D. Allendorf, "Influence of Connectivity and Porosity on Ligand-Based Luminescence in Zinc Metal-Organic Frameworks," *J. Am. Chem. Soc.* **129**(22), 7136 (2007).

Theoretical Studies of Potential Energy Surfaces and Computational Methods

Ron Shepard

Chemical Sciences and Engineering Division,
Argonne National Laboratory, Argonne, IL 60439
[email: shepard@tcg.anl.gov]

Program Scope: This project involves the development, implementation, and application of theoretical methods for the calculation and characterization of potential energy surfaces (PES) involving molecular species that occur in hydrocarbon combustion. These potential energy surfaces require an accurate and balanced treatment of reactants, intermediates, and products. This difficult challenge is met with general multiconfiguration self-consistent-field (MCSCF) and multireference single- and double-excitation configuration interaction (MR-SDCI) methods. In contrast to the more common single-reference electronic structure methods, this approach is capable of describing accurately molecular systems that are highly distorted away from their equilibrium geometries, including reactant, fragment, and transition-state geometries, and of describing regions of the potential surface that are associated with electronic wave functions of widely varying nature. The MCSCF reference wave functions are designed to be sufficiently flexible to describe qualitatively the changes in the electronic structure over the broad range of molecular geometries of interest. The necessary mixing of ionic, covalent, and Rydberg contributions, along with the appropriate treatment of the different electron-spin components (e.g. closed shell, high-spin open-shell, low-spin open shell, radical, diradical, etc.) of the wave functions are treated correctly at this level. Further treatment of electron correlation effects is included using large scale multireference CI wave functions, particularly including the single and double excitations relative to the MCSCF reference space. This leads to the most flexible and accurate large-scale MR-SDCI wave functions that have been used to date in global PES studies.

Recent Progress: ELECTRONIC STRUCTURE CODE MAINTENANCE, DEVELOPMENT, AND APPLICATIONS: A major component of this project is the development and maintenance of the COLUMBUS Program System. The COLUMBUS Program System computes MCSCF and MR-CI(SD) wave functions, MR-ACPF (averaged coupled-pair functional) energies, MR-AQCC (averaged quadratic coupled cluster) energies, spin-orbit CI energies, analytic energy gradients, and nonadiabatic coupling. Geometry optimizations to equilibrium and saddle-point structures can be done automatically for both ground and excited electronic states. The COLUMBUS Program System is maintained and developed collaboratively with several researchers including Isaiah Shavitt (University of Illinois), Russell M. Pitzer (Ohio State University), Thomas Mueller (Central Institute for Applied Mathematics, Juelich, Germany), and Hans Lischka (University of Vienna, Austria). The nonadiabatic coupling and geometry optimizations for conical intersections is done in collaboration with David R. Yarkony (Johns Hopkins). The distributed development effort and software coordination uses a cvs repository of source code. The COLUMBUS Program System of electronic structure codes is maintained on the various machines used for production calculations by the Argonne group, including Macintosh personal computers, IBM RS6000 workstations, the parallel IBM SP at NERSC, the Group's 96-CPU Linux cluster, the 320-CPU JAZZ Teraflop facility at Argonne, and more recently ports to the Cray X1 and to the IBM BG/L and BG/P machines have been initiated. The parallel sections of the code are based on the single-program multiple-data (SPMD) programming model with explicit message passing using the portable MPI library, and the portable Global Array Library (distributed from PNNL) is used for data distribution. These computer codes are used in the production-level molecular applications by members and visitors of the Argonne

This work was performed under the auspices of the Office of Basic Energy Sciences, Division of Chemical Sciences, Geosciences, and Biosciences, U.S. Department of Energy, under contract number DE-AC02-06CH11357.

Theoretical Chemistry Group. The next major release of the COLUMBUS codes will begin to incorporate the newer language features of F90/F95. This will facilitate future development and maintenance effort.

ANALYSIS OF THE DIIS METHOD: The direct inversion in the iterative subspace (DIIS) method of Pulay is used commonly as a convergence acceleration technique. It consists of two steps, a least-squares condition imposed on a set of error vectors, followed by an interpolation of the associated input vectors. Traditionally, the solution of the DIIS equations has been formulated almost always in terms of the augmented normal equations. Over twenty other ways to solve the DIIS equations have been analyzed, many of them introduced for the first time in this work. Some of these solution methods are inherently inaccurate and are never recommended, others have some efficiency or accuracy advantages that may be exploited in different situations. Two of these ways, linear least squares with substitution and elimination, and linear least squares with equality constraint, have the potential to produce solutions that are significantly more accurate than the traditional normal equation solutions. The advantage of one of these methods has been demonstrated on model problems for which the exact solutions may be determined from simple closed-form expressions.

LINEAR COMBINATION OF PRODUCT WAVEFUNCTIONS: We have recently developed a novel expansion basis for electronic wave functions [*J. Phys. Chem. A* **109**, 11629 (2005)]. In this approach, the wave function is written as a linear combination of *product basis functions*, and each product basis function in turn is formally equivalent to a linear combination of configuration state functions (CSFs) that comprise an underlying linear expansion space of dimension N_{csf} . The CSF coefficients that define the basis functions are nonlinear functions of a smaller number of variables $N_{\varphi} \ll N_{\text{csf}}$. The method is formulated in terms of spin-eigenfunctions using the Graphical Unitary Group Approach (GUGA) of Shavitt, and consequently it does not suffer from spin contamination or spin instability.

Our new method is characterized by several important features. First, open-shell spin-eigenfunctions are included in our expansions. This allows our new method to be used for the reactions that are important to combustion chemistry (i.e. involving radicals and other open-shell electronic states) without introducing spin contamination. Second, we place no intrinsic restrictions on the orbital occupations, so our product functions are not restricted to only geminals or to other preselected molecular fragments, and there are no artificial excitation-level or occupation restrictions with respect to a reference function or reference space. Third, we use linear combinations of N_{α} product wave functions rather than a single expansion term. This allows our method to be used for both ground and excited electronic states, the increased wave function flexibility leads to more accurate wave functions, and it will allow the computation of transition moments, nonadiabatic coupling, and other properties that at present can only be computed reliably with MCSCF and MRCI approaches.

Efficient procedures to compute hamiltonian matrix elements and reduced one- and two-particle density matrices for this nonlinear expansion have been developed [Shepard-2006]. The effort required to construct an individual hamiltonian matrix element between two product basis functions

$H_{MN} = \langle M | \hat{H} | N \rangle$ scales as $\mathcal{O}(\beta n^4)$ for a wave function expanded in n molecular orbitals. The prefactor β itself scales between N^0 and N^2 , for N

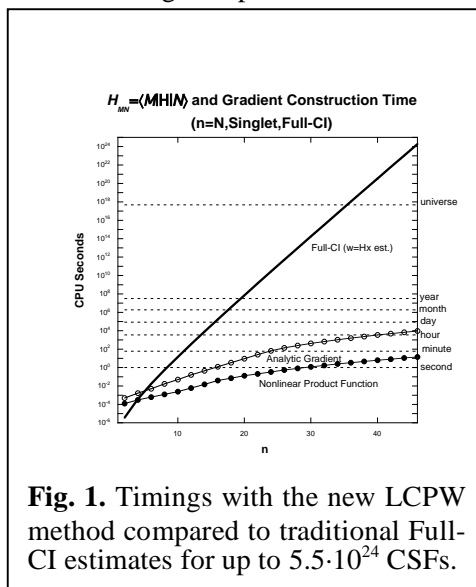


Fig. 1. Timings with the new LCPW method compared to traditional Full-CI estimates for up to $5.5 \cdot 10^{24}$ CSFs.

electrons, depending on the complexity of the underlying Shavitt Graph. The corresponding metric matrix element $S_{MN}=\langle M|N\rangle$ requires effort that scales as $\mathcal{O}(\beta n)$, the one-particle transition density \mathbf{D}^{MN} requires $\mathcal{O}(\beta n^2)$ effort, the two-particle density \mathbf{d}^{MN} requires $\mathcal{O}(\beta n^4)$ effort, and the gradient of the energy with respect to the nonlinear parameters requires $\mathcal{O}(\beta n^5)$ effort. There is no component of the effort or storage for matrix element computation or wave function optimization that scales as N_{csf} . Timings with our initial implementation of this method are very promising (see Fig. 1). A hamiltonian matrix element involving product basis functions corresponding to an underlying linear expansion space dimension $N_{\text{csf}}\approx 5.5\cdot 10^{24}$ requires only 10 to 15 seconds on a typical laptop or desktop computer. The computation of this same matrix element would require over a million times the age of the universe using traditional full-CI technology. An energy-based optimization approach has been developed and applied to the nonlinear wave function parameters; this exploits *partially contracted functions* in order to reduce the dimensionality of the optimization problem at each step and to minimize the number of expensive gradients that must be computed.

We have applied this new method to the dissociation of the $\text{N}\equiv\text{N}$ triple bond using the full-valence 6^6 Shavitt graph. It is seen that even the $N_\alpha=1$ wave function does a good job of describing the bond-breaking and spin-recoupling involved in the dissociation to the high-spin ^4S ground state atom fragments. The $N_\alpha=2$ curve is only slightly above the CASSCF curve, and the $N_\alpha=3$ curve is indistinguishable from the converged CASSCF curve. We have also applied this new method to the atomization of H_2O using a DZ basis using the full-CI 14^{10} Shavitt graph. Results for product wave function expansions with $N_\alpha=1$ to 16 are shown in Fig. 2 at four points along the symmetric dissociation path. The LCPW energies are lower than the MR-SDCI values at all geometries with $N_\alpha=12$. 99% or greater of the correlation energy is attained at all geometries also with $N_\alpha=12$. Compared to the full-CI energies, convergence to within 1 kcal/mole is attained with $N_\alpha=13$, and convergence to within 1 mE_h is attained with $N_\alpha=16$. Nonparallelity errors (NPE) less than 1 kcal/mole are attained with $N_\alpha=13$, and NPE errors less 1 mE_h are attained with $N_\alpha=16$. It is encouraging that chemical accuracy can be attained with relatively modest expansion dimensions with our new method.

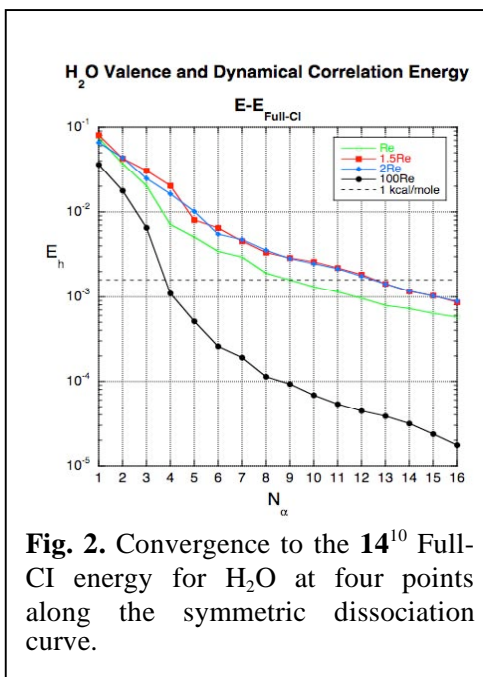


Fig. 2. Convergence to the 14^{10} Full-CI energy for H_2O at four points along the symmetric dissociation curve.

MOLECULAR BOND LENGTHS USING MULTIREFERENCE METHODS: Experimental and computed R_e values are compared for 20 molecules using three multireference electronic structure methods, MCSCF, MR-SDCI, and MR-AQCC. Three correlation-consistent orbital basis sets are used, along with complete basis set extrapolations, for all of the molecules. These data complement those computed previously with single-reference methods. Several trends are observed. The SCF R_e values tend to be shorter than the experimental values, and the MCSCF values tend to be longer than the experimental values. We attribute these trends to the ionic contamination of the SCF wave function and to the corresponding systematic distortion of the potential energy curve. For the individual bonds, the MR-SDCI R_e values tend to be shorter than the MR-AQCC values, which in turn tend to be shorter than the MCSCF values. Compared to the previous single-reference results, the MCSCF values are roughly comparable to the MP4 and CCSD methods, which is more accurate than might be expected due to the fact that these MCSCF

wave functions include no extra-valence electron correlation effects. This suggests that static valence correlation effects, such as near-degeneracies and the ability to dissociate correctly to neutral fragments, play an important role in determining the shape of the potential energy surface, even near equilibrium structures. The MR-SDCI and MR-AQCC methods predict R_e values with an accuracy comparable to, or better than, the best single-reference methods (MP4, CCSD, and CCSD(T)), despite the fact that triple and higher excitations into the extra-valence orbital space are included in the single-reference methods but are absent in the multireference wave functions. The computed R_e values using the multireference methods tend to be smooth and monotonic with basis set improvement. The molecular structures are optimized using analytic energy gradients, and the timings for these calculations show the practical advantage of using variational wave functions for which the Hellmann-Feynman theorem can be exploited.

Future Plans: LINEAR COMBINATION OF PRODUCT WAVEFUNCTIONS: Our applications have so far used single-headed Shavitt graphs appropriate for describing individual molecular states with a given number of electrons, with a particular spin state, and that belong to a particular irreducible representation (irrep). We will generalize this in several respects. First, we will introduce state averaging over several irreps. This will allow the computation of several molecular states with essentially no additional effort over single-irrep calculations. Second, we will employ multi-headed Shavitt graphs into the state-averaging procedure. This will allow the computation of hamiltonian matrix elements corresponding to states with different numbers of electrons, different spin values, and different irreps simultaneously with only a relatively small increase in effort over the current single-state approach.

Publications:

- “Hamiltonian Matrix and Reduced Density Matrix Construction with Nonlinear Wave Functions,” R. Shepard, *J. Phys. Chem. A* **110**, 8880-8892 (2006).
- “Optimization of Nonlinear Wave Function Parameters,” R. Shepard and M. Minkoff, *Int. J. Quantum Chem.* **106**, 3190-3207 (2006).
- “Advanced Software for The Calculation of Thermochemistry, Kinetics, and Dynamics,” R. Shepard, A. F. Wagner, and S. K. Gray, *J. Physics: Conference Series* **46**, 239-243 (2006).
- “Nonlinear Wave Function Expansions: A Progress Report,” R. Shepard, M. Minkoff, and S. R. Brozell, *Int. J. Quantum Chem.* **107**, 3203-3218 (2007).
- “Spin-Orbit Interaction with Nonlinear Wave Functions,” S. R. Brozell, R. Shepard and Z. Zhang, *Int. J. Quantum Chem.* **107**, 3191-3202 (2007).
- “Some Comments on the DIIS Method,” R. Shepard and M. Minkoff, *Molecular Physics* **105**, 2839-2848 (2007).
- “Advanced Software for The Calculation of Thermochemistry, Kinetics, and Dynamics,” R. Shepard, *J. Physics: Conference Series* **78**, 012067 (2007).
<http://www.iop.org/EJ/abstract/1742-6596/78/1/012067>
- “The Accuracy of Molecular Bond Lengths Computed by Multireference Electronic Structure Methods”, R. Shepard, G. S. Kedziora, H. Lischka, I. Shavitt, T. Müller, P. G. Szalay, M. Kállay, M. Seth, *Chemical Physics (in press)* (2008).

COMPUTATIONAL AND EXPERIMENTAL STUDY OF LAMINAR FLAMES

M. D. Smooke and M. B. Long
Department of Mechanical Engineering
Yale University
New Haven, CT 06520
mitchell.smooke@yale.edu

Program Scope

Our research has centered on an investigation of the effects of complex chemistry and detailed transport on the structure and extinction of hydrocarbon flames in coflowing axisymmetric configurations. We have pursued both computational and experimental aspects of the research in parallel. The computational work has focused on the application of accurate and efficient numerical methods for the solution of the boundary value problems describing the various reacting systems. Detailed experimental measurements were performed on axisymmetric coflow flames using two-dimensional imaging techniques. Spontaneous Raman scattering and laser-induced fluorescence were used to measure the temperature, and major and minor species profiles. Laser-induced incandescence has been used to measure soot volume fractions. A new approach to optical pyrometry has been developed to measure temperatures where the other techniques fail due to the presence of soot. Our goal has been to obtain a more fundamental understanding of the important fluid dynamic and chemical interactions in these flames so that this information can be used effectively in combustion modeling.

Recent Progress

Measurements of Soot and NO: Experimentally, the soot volume fraction field is determined by several different techniques. Laser extinction measurements are being coupled with laser-induced incandescence (LII) measurements in order to obtain the calibrated the soot volume fraction, and can be used as an independent measurement of the soot volume fraction profile in the future. Three-color optical pyrometry [1,2], using a color digital camera, is used to determine soot surface temperatures and also soot volume fractions. The use of the built-in color filter array (CFA) of a digital camera allows for two-dimensional imaging of flame emission at the wavelengths of the color filters. The camera was calibrated in two independent ways. Peak soot volume fractions, as well as variations in concentration across our target flames, show excellent agreement between both LII and soot pyrometry. The use of multiple measurement techniques should improve our overall confidence in the results as well as provide better estimates of the accuracy of the measurements.

For measurements of NO, the output of a dye laser is doubled, producing an ultraviolet (UV) beam near 225.8 nm that is used to excite transitions in the NO $A^2\Sigma^+ - X^2\Pi$ (0,0) band. The $Q_1(18)$ transition is selected because it is reasonably well separated from neighboring transitions, has significant population from room temperature to the flame temperatures investigated, and causes minimal spectral interferences from other species such as O_2 [3]. Spectrally resolved fluorescence emission from NO in our target ethylene diffusion flames is imaged onto a spectrograph coupled to an intensified CCD camera. When taking data in sooty regions within the flame, a colored glass filter (Corning 7-54) is placed between the two collection lenses in order to suppress the Rayleigh scattering by the soot, which would otherwise saturate the detector. Radial images of the (0,2) vibrational band are acquired at varying axial heights, by moving the burner vertically in 0.5 mm steps, to create a two-dimensional fluorescence image. Changes in the laser energy and any slight drift of the laser wavelength are normalized using the averaged output of the NO

fluorescence from a premixed reference burner, detected by a PMT. Calibration of the experiment is obtained by imaging a nonreacting flow of 45.2 ppm NO in N₂, mixed with 3% O₂ by volume, through the burner's coflow.

The presence of soot complicates the LIF experiment. The colored glass filter, used to remove scattering from the soot, makes it possible to make measurements in the sooty regions, but does not remove all interferences present in the measurement. A broadband background interference is observed, which is found to be primarily composed of C₂ fluorescence from laser vaporization of the soot, as well as from LII and PAH fluorescence. A background correction is applied using data taken with the excitation laser tuned off-peak of an NO resonance. Due to the heavy sooting within the target flames, it is difficult to characterize the flame temperature and major species and to provide an accurate quenching correction for quantitative results. Instead, a reverse-quenching correction [4] and Boltzmann correction are applied to the computational results to determine an expected fluorescence signal for comparison with experimental results. A comparison of experimental and computational results shows good qualitative agreement of the profiles of the fluorescence signal [5]. The fairly constant signal level in the regions above the flame, and the lower signal inside the flame/sooty areas, for example, are captured. Quantitatively, computational results are approximately 30% lower than the experimental results overall.

Comparison of Experiments and Computations: We have recently begun investigating a different approach to comparing experimental data and numerically computed data through simulation of expected signals. The more traditional approach of measuring fundamental quantities (e.g., mole fractions) often requires measurement of many variables to arrive at the desired quantity, and uncertainty may accumulate with each additional measurement. Because recent advances in computational resources have led to more detailed numerical models, more complete information is available within simulations. This allows for the possibility of using simulation results to derive predictions of measured signals (i.e., “computed signals”) rather than measuring many quantities to derive a single fundamental quantity. The main premise of this “paradigm shift” is that, in designing experiments and choosing diagnostics, experimentalists should consider the accurate measurement of signals that can be calculated with little uncertainty as well as the more conventional approach of making direct comparison with computed results. It may be that deriving predictions of signals from numerical results is better than measuring the fundamental quantities that are normally output by simulations. Quantitative comparisons can easily be obtained by using appropriate calibration on both sides of the comparison. In a recently submitted paper [6], we present three examples of comparing measured and computed signals: NO laser-induced fluorescence (LIF) in both non-sooting and sooting diffusion flames, and luminosity images of sooting diffusion flames, where computational results are used to simulate an image taken by a digital camera.

Sooting Time-Varying Flames: Quantitative soot volume fraction measurements in time-varying diffusion flames have shown that peak soot volume fractions can increase by factors of four to five over peak values in the equivalent steady flame [7,8]. In an effort to predict soot volume fractions and NO_x as a function of time, we have started to incorporate the soot model into our time-dependent flame calculations. Given the size of the system of partial differential equations that must be solved (upwards of 100 chemical species and 20 soot sectional classes), the number of cycles that must be computed to eliminate start-up transients [9], and the fact that, even with a fully implicit algorithm, time steps will be in the 10⁻⁵ – 10⁻⁴ range, parallel computation is essential in the research program.

Although previous time-dependent flame computations [9] have not included soot modeling, analysis of these results can be helpful in understanding why these time varying flames produce

more soot than their steady counterparts. As a fluid parcel in a steady flame moves upwards from the fuel nozzle it moves into a region of chemical reactivity ($T > 1300\text{K}$) that contains relatively high concentrations of species necessary for PAH growth and particle nucleation (notably acetylene and hydrogen atoms). Further along the streamline, the fluid passes into flame regions where particle oxidation will occur, near the stoichiometric surface. In this region of growth ($0.1 < \text{Mixture Fraction} < 0.15$), the residence time is less than 7 msec. For an equivalent fluid parcel in a forced flame, the residence time in the soot growth region exceeds 8 msec. For some streamlines that originate further from the flame centerline, the increase in residence time in particle growth regions may be even more pronounced. Analysis of this type of data for different fuel concentrations, forcing amplitudes and frequencies will be useful to determine the optimum conditions under which to study molecular growth processes in these systems.

Because the study of sooting time-varying flames is computationally intensive it is important to determine which flow conditions will provide the most information. For this reason, an effort to map out the parameter space of sooting tendencies for various fuel dilutions and forcing levels has been carried out experimentally. A fast, interline transfer camera is used to acquire 1-ms exposure, phase-locked, images at 10 phases of sooting flames forced at 20 Hz. Soot luminosity images are taken separately through two interference filters, and the results are used to determine soot volume fraction using optical pyrometry as a function of fuel dilution and forcing amplitude. Preliminary results indicate an increase in peak soot levels as well as sooting over a much wider spatial area. Regions of higher fluid velocity drive the soot-containing areas outward, producing a narrow region of soot separating the unburned fuel from the air coflow and the burned gases over the flame. As the forcing level is increased, this sooting region becomes thinner and the peak soot volume fraction increases. Further above the burner, the soot pinches off from the flame closer to the burner, and fuel remaining inside this sooting region is burned inward, causing a decrease in diameter. The quantitative results from this exploration will be used to determine the ideal cases for further study both computationally and experimentally. The goal is to study cases where there is a pronounced increase in soot, without exceeding levels that would challenge the optically-thin approximation made in the computations.

Future Plans

During the next year we will continue our study of sooting hydrocarbon flames with the goal of understanding the development of soot formation in time varying flames. Experimentally we will continue our work on improving the accuracy of our soot volume fraction measurements, as well as applying other diagnostic techniques that can provide information on the soot such as primary particle size and aggregation. Finally, using the same techniques that we have developed for the steady sooting flames, we will perform phase-averaged measurements in the time-varying flames.

References

1. Y.A. Levendis, K.R. Estrada, H.C. Hottel, *Rev. Sci. Instrum.*, **63** (1992) 3608-3622.
2. F. Cignoli, S. De Iuliis, V. Manta, G. Zizak, *App. Opt.*, **40** (2001) 5370-5378
3. C.D. Carter and R.S. Barlow, "Simultaneous Measurements of NO, OH, and the Major Species in Turbulent Flames," *Optics Letters*, **19**, 299-301 (1994).
4. T.B. Settersten, B.D. Patterson and J.A. Gray, "Temperature-and species-dependent quenching of NO A (2) $\Sigma^+(\nu'=0)$ probed by two-photon laser-induced fluorescence using a picosecond laser," *Journal of Chemical Physics*, **124** (2006).
5. B.C. Connelly, M.B. Long, M.D. Smooke, R.J. Hall and M.B. Colket, "Computational and Experimental Investigation of the Interaction of Soot and NOx in Coflow Diffusion Flames," accepted to the *Proceedings of the Combustion Institute* (2008).

6. B.C. Connelly, B.A.V. Bennett, M.D. Smooke and M.B. Long, "A Paradigm Shift in the Interaction of Experiments and Computations in Combustion Research," accepted to the *Proceedings of the Combustion Institute* (2008).
7. J.E. Harrington, C.R. Shaddix and K.C. Smyth, "Laser imaging of chemistry-flowfield interactions: enhanced soot formation in time-varying diffusion flames," *Proceedings of SPIE-The International Society for Optical Engineering*, **2124**, 278-91 (1994).
8. K.C. Smyth, J.E. Harrington, C.R. Shaddix, W.M. Pitts and E.L. Johnsson, *Flickering Flames as Testing Grounds for Reliable Models of Gas Combustion*. 1994. NIST, Gaithersburg, MD.
9. S.B. Dworkin, B.C. Connelly, A.M. Schaffer, M.B. Long and M.D. Smooke, "Computational and Experimental Study of a Forced, Time-Dependent, Methane-Air Coflow Diffusion Flame," *Proceedings of the Combustion Institute*, **31**, (2006).

DOE Sponsored Publications since 2006

1. M. Noskov, M. Benzi and M. D. Smooke, "An Implicit Compact Scheme Solver for Two-Dimensional Multicomponent Flows," *Comp. and Fluids*, **36**, (2006).
2. S. B. Dworkin, B. C. Connelly, A. M. Schaffer, M. B. Long and M. D. Smooke, "Computational and Experimental Study of a Forced, Time-Dependent, Methane-Air Coflow Diffusion Flame," *Proceedings of the Combustion Institute*, **31**, (2006).
3. A. V. Mokhov, B. A. V. Bennett, H. B. Levinsky and M. D. Smooke, "Experimental and Computational Study of C₂H₂ and CO in a Laminar Axisymmetric Methane-Air Diffusion Flame," *Proceedings of the Combustion Institute*, **31**, (2006).
4. S. Hu, P. Wang, R. W. Pitz and M. D. Smooke, "Experimental and Numerical Investigation of Non-Premixed Tubular Flames," *Proceedings of the Combustion Institute*, **31**, (2006).
5. V. Giovangigli, N. Meynet and M. D. Smooke, "Application of Continuation Techniques to Ammonium Perchlorate Plane Flames," **10**, *Comb. Theory and Modelling*, (2006).
6. G. Amantini, J. H. Frank, A. Gomez and M.D. Smooke, "Computational and Experimental Study of Standing Methane Edge Flames in the Two-Dimensional Axisymmetric Counterflow Geometry," *Comb. and Flame*, **147**, (2007).
7. G. Amantini, J. H. Frank, A. Gomez and M.D. Smooke, "Computational and Experimental Study of Steady Two-Dimensional Axisymmetric Non-Premixed Methane Counterflow Flames," *Comb. Theory and Modelling*, **11**, (2007).
8. G. Amantini, B. A. V. Bennett, J. H. Frank, A. Gomez and M. D. Smooke, "Comprehensive Study of Extinction, Re-ignition, and the Evolution of an Annular Edge Flame in a Counterflow Flame Perturbed by Vortices," *Comb. and Flame*, **150**, (2007).
9. B. A. V. Bennett, M. D. Smooke, R. J. Osborne and R. W. Pitz, "Computational and Experimental Study of Oxy-Fuel Diffusion Flames," in press *Comb. Theory and Modelling*, (2008).
10. B. C. Connell, B. A. V. Bennett, M. D. Smooke, M. B. Long, "A Paradigm Shift in the Interaction of Experiments and Computations in Combustion Research," accepted to the *Proceedings of the Combustion Institute*, **32**, (2008).
11. B. C. Connelly, M. B. Long, M. D. Smooke, R. J. Hall and M. B. Colket, "Computational and Experimental Investigation of the Interaction of Soot and NO_x in Coflow Diffusion Flames," accepted to the *Proceedings of the Combustion Institute*, **32**, (2008).
12. S. B. Dworkin, M. D. Smooke and V. Giovangigli, "The Impact of Detailed Multicomponent Transport and Thermal Diffusion Effects on Soot Formation in Ethylene/Air Flames," accepted to the *Proceedings of the Combustion Institute*, **32**, (2008).
13. J. H. Miller, B. McAndrew, M. P. Puccio, S. B. Dworkin, A. M. Schaffer, B. C. Connelly, M. B. Long and M. D. Smooke, "Measurements and Calculations of Formaldehyde Concentrations in a Methane/N₂/Air, Non-Premixed Flames," accepted to the *Proceedings of the Combustion Institute*, **32**, (2008).

Quantum Chemistry of Radicals and Reactive Intermediates

John F. Stanton
Department of Chemistry
And
Institute for Theoretical Chemistry
University of Texas at Austin
Austin, TX 78712
jfstanton@mail.utexas.edu

I. Program Scope

My group and its collaborators study the chemical physics of individual molecules. Our work, much of which is done in collaboration with experimentalists, applies various theoretical approaches to issues associated with molecular properties, spectroscopy and reactivity. Our research encompasses both theoretical method development and applications; the former focus is on both quantum chemistry and model Hamiltonian approaches, and the latter is largely associated with applications to molecular spectroscopy, thermochemistry and reactivity of small molecules.

II. Recent Progress

A. Explorations in the area of high-accuracy theoretical thermochemistry

Our research group, together with collaborators in Europe, has developed the so-called HEAT (High-accuracy Extrapolated *Ab initio* Thermochemistry) in the current decade. This approach, which has much in common with the Wn hierarchy of Martin and coworkers and the focal point approach of Allen and coworkers, joins these other well-defined methods in giving molecular heats of formation (more correctly, bond energies) to an accuracy of $< 1.0 \text{ kJ mol}^{-1}$. The design feature of HEAT is such that the method is intended to explore the limits of accuracy attainable by quantum chemistry, rather than to be routinely applicable to “large” molecules (see Future Work section, however). Specifically, HEAT attempts to estimate the exact ground state energy of a molecule within the adiabatic approximation. Much has been learned in these investigations, principally: 1) the separation of core and valence electron correlation, commonly assumed in virtually all other theoretical model chemistries, imposes an effective limit on accuracy of *ca.* 0.5 kJ mol^{-1} ; effects of electron correlation beyond the CCSD(T) treatment are vital if one strives for an accuracy of better than 1 kJ mol^{-1} ; zero-point energies calculated in the harmonic approximation impose a similarly limitation on accuracy. These findings were discovered in parallel or subsequently confirmed by many others, and plans are in the work to write a definitive review on the area of high-accuracy *ab initio* thermochemistry with the other leaders in the field in the next few years.

B. Studies in the perturbation treatment of nuclear motion

We have recently been working on two different applications of fourth-order vibrational perturbation theory: the first treatment of vibration-rotation interaction in polyatomic molecules beyond the (leading-order) “alphas” that relate rotational constants in the vibrationally excited state $|n\rangle$ to the rigid-rotor constants (B_e) that are inversely proportional to the principal moments of inertia associated with the equilibrium structure. The vibrational dependence of rotational constants can be written, empirically, as the Taylor series

$$\mathbf{B}_v^\alpha = \mathbf{B}_e^\alpha - \sum_{i=1}^{3N-6} \alpha_i^\alpha \left(\nu_i + \frac{1}{2} \right) + \sum_{i \leq j}^{3N-6} \gamma_{ij}^\alpha \left(\nu_i + \frac{1}{2} \right) \left(\nu_j + \frac{1}{2} \right) + \dots$$

In which the linear and quadratic coefficients of $(\nu+1/2)$ are called the first and second vibration-rotation constants respectively. These can be related to parameters of the molecular force field and simple geometrical considerations, using second- and fourth-order perturbation theory, respectively. That the

latter are of some numerical importance was recently pointed out by Csaszar and collaborators, who showed that the truncation of the equation above to linear terms does a rather poor job of predicting rotational constants of water. We have implemented a program for full fourth-order vibrational perturbation theory (within the Rayleigh-Schrödinger formalism) that allows the calculation of both second rotation-vibration constants as well as fourth-order energy levels. This also permits the zero-point energy to be improved, given a particular polynomial force field. This work, together with the theoretical and computational work on vibrational resonances done by a remarkable undergraduate prodigy in my group (D.A. Matthews) has also assisted us in some collaborative work dealing with vibrational spectroscopy of methyl nitrate and the water dimer, as well as an investigation of the hydroxyperoxy radical (HO_3), where thermodynamics are both presently unclear and very important.

III. Future Work

Some of the ongoing and near-future work in the areas mentioned above include:

1. HEAT calculations are currently underway for several isomers of benzene that have been implicated and/or suggested as intermediates in the important dimerization of propargyl in flames. This has been made possible by recent advances by M.E. Harding (Mainz, soon to be a postdoc in Austin), who has managed to parallelize the ACES II program system developed by myself and collaborators over the year. Calculations with as many as 1500 basis functions at the CCSD(T) level are now possible, and a HEAT calculation for benzene itself has recently been completed and is currently being prepared for publication.

2. Together with a collaborator within the combustion program (Krylov, USC) we intend to investigate the oxidation of the vinyl radical. A previous study on this problem by Carpenter showed the extreme difficulty of this for some standard quantum chemical methods. It seems, however, that the equation-of-motion coupled-cluster approaches favored here and in Los Angeles are well-suited to this task, and it is our attention to bring them to bear on the reaction between O_2 and vinyl. If this is successful, it would be interesting to extend these to the allyl radical and perhaps larger resonance-stabilized radicals.

3. Together with the Field group at MIT, we are currently using the EOMIP-CCSDT method to analyze the potential energy surface of the first excited state of acetylene. This represents what is, to date, the most advanced quantum chemical method brought to bear on this problem. The S_1 state of acetylene is a highly anharmonic system – it supports two distinct minima, both *trans*- and *cis*-bent – and the anharmonic coupling is such that the usual second-order perturbation theory (as extended for Darling-Dennison coupling) is inadequate. Our work is intended to sort out the anharmonicity on this surface, and to assist the Field group with assigning levels in the S_1 state. Together with the discrete-variable representation, the initial calculations have already been successful in identifying several eigenstates as belonging to the previously unobserved *cis* conformer. Eventually, we plan to carry out full-scale variational calculations using the EOMIP-CCSDT potential surface.

IV. References

- i. A. Csaszar, W.D. Allen and H.F. Schaefer *J. Chem. Phys.* 108, 9571 (1998), and references therein.
- ii. Carton, A, Taylor, P.R. and Martin, J.M.L. *J. Chem. Phys.* 127, 064104 (2007), and references therein
- iii. Harding, M.E., Metzroth, T., Gauss, J. and Auer, A.A. *J. Theor. Comput. Chem.* 4, 64 (2008).
- iv. Carpenter, B.K. *J. Phys. Chem.* 99, 9801 (1995).
- v. Murray, C., Derro, E.L., Sechler, T.D. and Lester, M.I. *J. Phys. Chem.* 111, 4727 (2007).
- vi. Feller, D., Peterson, K.A., de Jong, W.A. and Dixon, D.A. *J. Chem. Phys.* 118, 3510 (2003), and references therein.

V. Publications and submitted journal articles supported by this project 2007-2008

1. M.E. Harding, J. Vazquez, B. Ruscic, A.K. Wilson, J. Gauss and J.F Stanton "High-accuracy extrapolated ab initio thermochemistry. III. Additional improvements and overview" *J. Chem. Phys.* 128, 114111 (2008).
2. M.E. Varner, M.E. Harding, J. Gauss and J.F. Stanton "On the Geometry of the HO₃ Radical" *Chem. Phys.* 346, 53 (2008).
3. J.F. Stanton, D.A. Matthews, A.F. Ware, B.A. Flowers and G.B. Ellison "Gas-phase Infrared Spectrum of Methyl Nitrate" *J. Mol. Spect.*, in press.
4. H.G. Kjaergaard, A.L. Garden, C. Chaban, R.B. Gerber, D.A. Matthews, J.F. Stanton "Calculation of Vibrational Transition Frequencies and Intensities in Water Dimer: Comparison of Different Vibrational Approaches" *J. Phys. Chem.*, in press.

Universal and State-Resolved Imaging Studies of Chemical Dynamics

Arthur G. Suits
Department of Chemistry, Wayne State University
5101 Cass Ave
Detroit, MI 48202
asuits@chem.wayne.edu

Program Scope

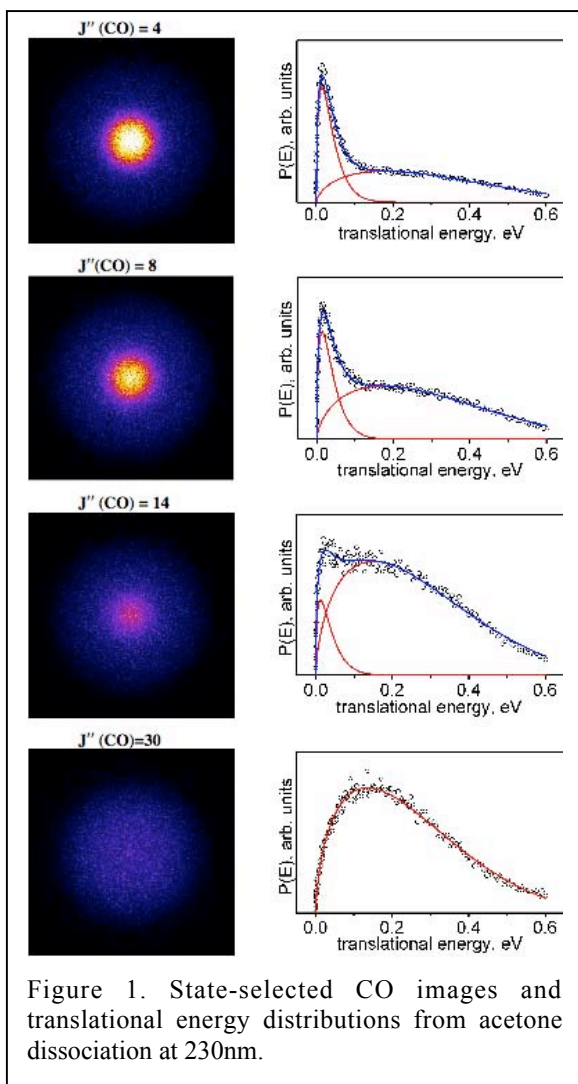
The focus of this program is on combining universal ion imaging probes providing global insight, with high-resolution state-resolved probes providing quantum mechanical detail, to study elementary reactions under collisionsless conditions. The goal of these investigations is to develop a molecular-level understanding of chemical phenomena. Particular emphasis is placed upon reactions important in understanding and predicting combustion chemistry. This research is conducted using state-of-the-art molecular beam machines, photodissociation, reactive scattering, and vacuum ultraviolet lasers in conjunction with ion imaging techniques. An ongoing parallel effort is made to develop new tools and experimental methods with which to achieve these goals.

Recent Progress

Roaming atoms in formaldehyde dissociation. We have continued our focused examination of the “roaming atom” mechanism in formaldehyde dissociation. In studies in collaboration with Joel Bowman’s group, we showed dramatic evidence of a novel pathway in formaldehyde ground state dissociation that avoids the region of the familiar transition state entirely. Our original report showed high-resolution state-resolved CO velocity measurements that revealed the correlated H₂ internal state distribution. Low rotational levels of CO were correlated with highly vibrationally excited H₂, demonstrating this “roaming” intramolecular abstraction mechanism. Three major publications in the *Journal of Chemical Physics* and a paper currently in the Domcke festschrift issue of *Chemical Physics* have followed our initial report in *Science*. In the initial effort, we explored the dynamics of the intramolecular H abstraction mechanism in great detail, building on the potential surface and dynamics from the Bowman group. The second paper in this series exploited the remarkable resolution of the slice imaging technique to provide fully correlated product state distributions for H₂ and CO for the “conventional” molecular channel. The photolysis energy ranged from 1800 to 4100 cm⁻¹ above the molecular elimination threshold, and included the 2¹4¹, 2¹4³, 2²4¹, 2²4³, and 2³4¹ transitions to S₁. These detailed measurements allowed determination of the ν_{H_2} -specific CO rotational distributions even though the data was obtained in an orthogonal dimension, and afforded a new level of detail in understanding the dissociation via the conventional transition state. We then documented the detailed energy dependent dynamics and branching for the roaming channel relative to the conventional molecular channel, and combined this with theoretical calculations to develop a qualitative picture of the multichannel branching in this system, a key issue in understanding the implications of the roaming mechanism for modeling combustion chemistry. In the most recent paper on this subject, we found evidence for roaming dynamics down to ~100 cm⁻¹ below the threshold for the radical channel in photofragment excitation spectra. This was understood on the basis of a very flat

transition state “region” reported for roaming by Klippenstein and Harding at a similar energy. The TS configuration essentially consists of a loosely bound hydrogen atom at 7-8 bohr and a free HCO molecule. Furthermore, this picture allowed us to understand the nearly flat energy dependent branching to roaming, as each product HCO state could support a similar roaming TS, so that a “roaming continuum” must exist. We expect some fluctuations in the roaming rate vs. energy should exist, corresponding to regions of sparse HCO product state density. However, the S_1 levels we use to excite formaldehyde do not access these, so that we have not been able to examine this issue experimentally.

Roaming dynamics in acetone photodissociation. The photochemistry of acetone is among the most thoroughly studied of any polyatomic molecule, with hundreds of studies ranging from classical flash photolysis to nanosecond laser studies to a dizzying array of recent femtosecond studies as well as extensive theoretical work. It is perhaps surprising that a unified picture of its dissociation dynamics have not yet emerged and some controversies persist. This is likely a testament to the complexity of the problem and the changing dynamics with excitation energy as key surface crossings are accessed.



We have recently employed DC slice imaging to study the photodissociation dynamics of acetone at 230 nm, with detection of the CO photoproduct via the $B(v'=0) \ ^1\Sigma^+ \leftarrow X(v''=0) \ ^1\Sigma^+$ transition. A bimodal translational energy distribution observed in the CO fragments (Fig. 1) points to two distinct dissociation pathways in the 230 nm photolysis of acetone. One pathway results in substantial translational energy release ($E_{ave} \approx 0.3$ eV) along with rather high rotational excitation (up to $J''=50$) of CO, and is attributed to the thoroughly investigated stepwise mechanism of bond cleavage in acetone. The other dissociation pathway leads to rotationally cold CO ($J''=0-20$) with very little energy partitioned into translation ($E_{ave} \approx 0.04$ eV) and in this way it is dynamically similar to the recently reported roaming mechanism found in formaldehyde and acetaldehyde dissociation. We ascribe the second dissociation pathway to an analogous roaming dissociation mechanism taking place on the ground electronic state following internal conversion. We estimate that about 15% of the total CO fragments are produced through the roaming pathway. Rotational populations were obtained using a new Doppler-free method that simply

relies on externally masking the phosphor screen under velocity map conditions in such a way that only the products with no velocity component along the laser propagation direction are detected.

State-correlated photochemistry of HCCO. We have recently reported the first state-selected detection of HCCO radical dissociation to CH and CO at 230 nm. The measurements were made using a two-color reduced Doppler probe strategy. The CO rotational distribution was consistent with a Boltzmann distribution at 3500 K. Using the DC slice ion imaging approach, and two color reduced-Doppler probe, we obtained CO REMPI spectra and CO product images for various rotational levels of CO ($v=0$). The results are largely consistent with earlier work from Neumark and Osborn, albeit with a significant 0.9 eV peak seen previously in the translational energy distributions absent in our state-selected imaging study.

DC sliced imaging of CN radical reactions. We have recently completed a study of CN radical reaction dynamics with a variety of alkane targets. We studied the reaction at 7.5 kcal/mol for all systems, but added 10.8 kcal/mol for the n-butane system to gain additional insight into the dynamics. The product alkyl radical images were obtained via single photon ionization at 157 nm for the reactions of CN ($X^2\Sigma^+$) with n-butane, n-pentane, n-hexane, and cyclohexane. Based on the image analyses, we obtained the center-of-mass frame product angular distributions and translational energy distributions directly. The images show predominately backward scattered distributions, although forward peaking is also seen to a lesser extent. However, photochemical background compromises our ability to see the forward scattering for some systems. The translational energy distributions show that most of the available energy (~80%) goes to the internal energy of the products. We examine the reaction dynamics in light of results from our studies and from Nesbitt and coworkers for related halogen atom reactions.

Selected Future Plans

Roaming reaction dynamics. We will continue to study systems showing roaming dynamics. We will extend our studies in acetone, and examine deuterated formaldehyde. We will also pursue the use of vector correlations as a general probe of roaming dynamics.

Crossed-beam imaging. We plan to extend our crossed-beam imaging studies to include $^1\text{CH}_2$ reactions. This should allow for “chemical activation” production of energized ground state molecules as suggested by Floyd Davis. In our experiments we will be looking for likely prospects for roaming dynamics. We also plan to extend our CN studies to look at reaction with methane, in this case with state-selective detection of the methyl radical product.

Correlated state photochemistry. We will continue our studies of HCCO radical dissociation dynamics, looking to regions at lower energy where the absorption is structured and the spin-forbidden products dominate, as well as to high energy to try to understand the differences between our results and the Neumark study.

DOE Publications 2006-present

1. S. D. Chambreau, D. Townsend, S. A. Lahankar, S. K. Lee and A. G. Suits, "Novel molecular elimination mechanism in formaldehyde photodissociation: The roaming H atom pathway," *Phys. Scr.* **73** C89-C93 (2006).
2. W. Li, C. Huang, M. Patel, D. Wilson and A. G. Suits, "State-Resolved Reactive Scattering by Slice Imaging: A New View of the Cl+C₂H₆ Reaction," *J. Chem. Phys.* **124**, 011102 (2006).
3. A. Komissarov, M. Minitti, A. G. Suits and G. E. Hall, "Correlated product distributions from ketene dissociation measured by dc sliced ion imaging" *J. Chem. Phys.* **124**, 014303 (2006).
4. S. D. Chambreau, S. A. Lahankar, and A. G. Suits, "Correlated v_{H_2} and j_{CO} product states from formaldehyde photodissociation: Dynamics of molecular elimination," *J. Chem. Phys.* **125** 044303 (2006).
5. C. Huang, W. Li and A. G. Suits, "Rotationally-Resolved Reactive Scattering: Imaging Detailed Cl + C₂H₆ Reaction Dynamics," *J. Chem. Phys.* **125**, 133107 (2006).
6. S. A. Lahankar, S. D. Chambreau, F. Suits, J. Farnum, X. Zhang, J. M. Bowman and A. G. Suits, "The roaming atom mechanism in formaldehyde decomposition," *J. Chem. Phys.* **125**, 044302 (2006).
7. C. Huang, W. Li, M. H. Kim, and A. G. Suits, "Two-color Reduced Doppler Ion Imaging," *J. Chem. Phys.* **125**, 121101 (2006).
8. S. A. Lahankar, S. D. Chambreau, X. Zhang, J. M. Bowman and A. G. Suits, "Energy dependence of the roaming atom mechanism in formaldehyde decomposition," *J. Chem. Phys.* **126**, 044314 (2007).
9. A. G. Suits, S. D. Chambreau, S. A. Lahankar, "State-correlated DC slice imaging of formaldehyde photodissociation: roaming atoms and multichannel branching," *Int. Rev. Phys. Chem.* **26**, 585 (2007).
10. S.A. Lahankar, V. Goncharov, F. Suits, J.D. Farnum, J.M. Bowman and A. G. Suits. "Further aspects of the roaming mechanism in formaldehyde dissociation," *Chem. Phys.* (in press).
11. C. Huang, A. D. Estillore and A. G. Suits, "State-selected imaging of HCCO radical photodissociation dynamics," *J. Chem. Phys.* (in press).
12. V. Goncharov, N. Herath and A. G. Suits, "Roaming dynamics in acetone dissociation," *J. Phys. Chem. A* (submitted).
13. C. Huang, A. Estillore, and A. G. Suits, "Crossed-beam CN ($X^2\Sigma^+$) + alkane reactions by DC slice imaging," *Phys. Chem. Chem. Phys.* (submitted).

Elementary Reaction Kinetics of Combustion Species

Craig A. Taatjes

*Combustion Research Facility, Mail Stop 9055, Sandia National Laboratories,
Livermore, CA 94551-0969*

cataatj@sandia.gov www.ca.sandia.gov/CRF/staff/taatjes.html

SCOPE OF THE PROGRAM

This program aims to develop new methods for studying chemical kinetics and to apply these methods to the investigation of fundamental chemistry relevant to combustion science. One central goal is to perform accurate measurements of the rates at which important free radicals react with each other and with stable molecules. Another goal is to characterize complex reactions that occur via multiple potential wells by investigating the formation of products. Increasingly, these investigations are moving towards simultaneous time-resolved detection of multiple species in well-characterized photolytically-initiated reaction systems where multiple consecutive and competing reactions may occur. Understanding the reactions in as much detail as possible under accessible experimental conditions increases the confidence with which modelers can treat the inevitable extrapolation to the conditions of real-world devices. Another area of research is the investigation and application of new detection methods for precise and accurate kinetics measurements. Absorption-based techniques and mass-spectrometric methods have been emphasized, because many radicals critical to combustion are not amenable to fluorescence detection.

An important part of our strategy, especially for complex reaction systems, is using experimental data to test and refine detailed calculations (working in close cooperation with Stephen Klippenstein at Argonne and Jim Miller at Sandia), where the calculational results offer insight into the interpretation of experimental results and to guide new measurements that will probe key aspects of potential energy surfaces. This methodology has been applied in our investigations of the reactions of alkyl radicals with O₂, where the combination of rigorous theory and validation by detailed experiments has made great strides toward a general quantitative model for alkyl oxidation.

PROGRESS REPORT

We continue to apply frequency-modulation and direct absorption spectroscopy to measurements of product formation in reactions of alkyl radicals with O₂ and kinetics of unsaturated hydrocarbon radicals. However, the multiplexed photoionization mass spectrometric reactor at the Advanced Light Source, operated in collaboration with David Osborn, has become a major part of our investigations of low-temperature hydrocarbon oxidation chemistry. Several highlights of the recent work are described briefly below.

Photoionization of Alkenyl Radicals. The photoionization of 1-alkenylperoxy radicals, which are peroxy radicals where the OO moiety is bonded to an sp^2 -hybridized carbon, was studied by experimental and computational methods and compared to the similar alkylperoxy systems. Experimental measurements of 1-cyclopentenylperoxy (1-*c*-C₅H₇OO) and propargylperoxy (CH₂=C=CHOO) photoionization are used as examples. Electronic structure calculations are employed to give structural parameters and energetics that are used in a Franck-Condon (FC) spectral simulation of the photoionization efficiency (PIE) curves. Adiabatic ionization energies (AIE) of 1-*c*-C₅H₇OO ((8.70±0.05) eV) and CH₂=C=CHOO ((9.32±0.05) eV) are derived from fits to the experimental PIE curves. From consideration of the relevant molecular orbitals, the ionization behavior of alkyl- and alkenylperoxy radicals can be generalized with a simple rule: Alkylperoxy radicals dissociatively ionize, with the exception of methylperoxy, whereas alkenylperoxy radicals have stable singlet ground electronic state cations.

Photoionization Cross Section of Methyl Radical. The absolute photoionization cross section of the methyl radical has been measured relative to that of acetone and methyl vinyl ketone in the ALS kinetics machine. Comparison of the initial methyl signal with the decrease in precursor signal yields the absolute photoionization cross section of the methyl radical; $\sigma_{\text{CH}_3}(10.2 \text{ eV}) = (5.9 \pm 1.4) \times 10^{-18} \text{ cm}^2$ and $\sigma_{\text{CH}_3}(11.0 \text{ eV}) = (6.0 \pm 2.0) \times 10^{-18} \text{ cm}^2$. The photoionization cross section for vinyl radical determined by photolysis of methyl vinyl ketone is in good agreement with previous measurements. Completely independent measurements from Stephen Pratt (Argonne) using molecular-beam photodissociation of CH₃I with laser-ionization velocity-map imaging detection, agree well with these cross section determinations. The measurements allow relative photoionization efficiency spectra of methyl radical to be placed on an absolute scale, and will facilitate quantitative measurements of methyl concentrations by photoionization mass spectrometry.

Photoionization of Cyclopentenol. Cyclopentenol (1-*c*-C₅H₇OH) and two other isomers, 2-hydroxycyclopentene (2-*c*-C₅H₇OH) and cyclopentanone (*c*-C₅H₈=O), were observed in OH-initiated cyclopentene oxidation. Electronic structure calculations (CBS-QB3 at B3LYP/6-311+G** optimized geometries) are used in a Franck-Condon (FC) spectral simulation of the photoionization efficiency curves (PIE). The measured adiabatic ionization energy (AIE) of 1-*c*-C₅H₇OH is (8.42 ± 0.06) eV, and that of 2-*c*-C₅H₇OH is (9.39 ± 0.08) eV. The CBS-QB3 calculated AIE of the *cis*-1,2-epoxycyclopentane and 2-3-epoxycyclopentanol (other possible products in cyclopentene oxidation) are 9.97 eV and 9.44 eV, respectively.

Product Formation in OH-initiated Oxidation of 2,5-Dimethylfuran. Production of 2,5-dimethylfuran (DMF) has been proposed as a means to derive renewable fuels from biomass (Román-Leshkov, Barrett et al. 2007). However, neither atmospheric reactions nor the combustion behavior of DMF have yet been investigated.

The first step in either process is likely to be attack by a radical species, and OH radical is one of the most prominent radicals in combustion. We have evidence that the OH-initiated oxidation of DMF proceeds partially by ring-opening, yielding one oxygenated product molecule (ketene or acetic acid) along with a C₄H₅ radical. The formation of unsaturated species in the initial oxidation steps could affect soot formation in DMF combustion.

Kinetics of C₂H₃ Self-Reaction. In collaboration with Bill Green's group at MIT, we have carried out an extensive investigation of the kinetics of the vinyl radical self-reaction. Laser-Photolysis / Laser-Absorption measurements at MIT and at Sandia are in agreement that the rate constant is substantially (approximately a factor of 2) smaller than that reported in the literature, $(6.4 \pm 0.7) \times 10^{-11} \text{ cm}^3 \text{ molecule}^{-1} \text{ s}^{-1}$ at room temperature. In addition, measurements in the ALS kinetics machine have demonstrated that methyl + propargyl is a prominent product channel in the reaction. As several literature studies deduced the vinyl radical concentration by measurements of the butadiene product in conjunction with a product branching fraction that neglected methyl + propargyl, substantial branching to this channel may be responsible for the disagreement with the earlier measurements.

FUTURE DIRECTIONS

Characterization of R + O₂ reactions will continue, both in the laser absorption work and in the ALS kinetics machine. The ability to simultaneously probe various reactants and products will play a key role in extending these measurements. One important extension of the alkane oxidation work will be to probe OD formation. Because the reaction coordinate for the internal isomerization to QOOH (the precursor to OH formation) involves a large degree of H-atom motion, the deuterium kinetic isotope effect may be larger for OH formation than for HO₂ formation. Further in the future, oxidation of selectively deuterated alkanes may make it possible to distinguish among different internal abstraction pathways in R + O₂ reactions.

The application of synchrotron photoionization mass spectrometry to chemical kinetics will continue. The ready tunability of the ALS photon energy permits isotopic discrimination, and the kinetics measurements will continue to exploit this capability. Further characterization of enol formation in reactions of OH with alkenes, kinetics of reactions of combustion radicals with ethenol, addition reactions of propargyl radicals with unsaturated hydrocarbons, and oxidation of other cycloalkyl radicals are possible targets of future investigations.

References:

Román-Leshkov, Y., C. J. Barrett, et al. (2007). "Production of dimethylfuran for liquid fuels: biomass-derived carbohydrates." *Nature* **447**: 982-986.

Publications acknowledging BES support 2006-present

1. Craig A. Taatjes, Nils Hansen, James A. Miller, Terrill A. Cool, Juan Wang, Phillip R. Westmoreland, Matthew E. Law, Tina Kasper, Katharina Kohse-Höinghaus, "Combustion Chemistry of Enols: Possible Ethenol Precursors in Flames," *J. Phys. Chem. A* **110**, 3254-3260 (2006).
2. Nils Hansen, Stephen J. Klippenstein, Craig A. Taatjes, James A. Miller, Juan Wang, Terrill A. Cool, Bin Yang, Rui Yang, Lixia Wei, Chaoqun Huang, Jing Wang, Fei Qi, Matthew E. Law and Phillip R. Westmoreland, "The Identification and Chemistry of C₄H₃ and C₄H₅ Isomers in Fuel-Rich Flames," *J. Phys. Chem. A* **110**, 3670- (2006).
3. Craig A. Taatjes, "Uncovering the Fundamental Chemistry of Alkyl + O₂ Reactions via Measurements of Product Formation," *J. Phys. Chem. A* **110**, 4299-4312 (2006).
4. John D. DeSain, Leonard E. Jusinski, and Craig A. Taatjes, "Ultraviolet Absorption Cross Section of Vinyl Trichlorosilane and Allyl Trichlorosilane and the Branching Fraction of the Vinyl Radical and Allyl Radical Channels in 193 nm Photolysis," *Phys. Chem. Chem. Phys.* **8**, 2240-2248 (2006).
5. Eric R. Hudson, Christopher Ticknor, Brian Sawyer, Craig A. Taatjes, Heather J. Lewandowski, Jason Bochinski, John Bohn, and Jun Ye, "Stark-deceleration of formaldehyde molecules for high resolution studies of hydrogen atom abstraction reaction dynamics," *Phys. Rev. A* **73**, 063404 (2006).
6. Arjan Gijsbertsen, Harold V. Linnartz, Craig A. Taatjes and Steven Stolte, "Quantum Interference as the Source of Steric Asymmetry and Parity Propensity Rules in NO-Rare Gas Inelastic Scattering," *J. Am. Chem. Soc.* **128**, 8777-8789 (2006).
7. Giovanni Meloni, Peng Zou, Stephen J. Klippenstein, Musahid Ahmed, Stephen R. Leone, Craig A. Taatjes, and David L. Osborn, "Energy-resolved photoionization of alkylperoxy radicals and the stability of their cations," *J. Am. Chem. Soc.* **128**, 13559-13567 (2006).
8. John D. DeSain, Linda Valachovic, Leonard E. Jusinski and Craig A. Taatjes, "The Reaction of Chlorine Atom with Trichlorosilane from 296 K to 473 K," *J. Chem. Phys.*, **124**, 224308 (2006).
9. Ph. R. Westmoreland, M. E. Law, T. A. Cool, J. Wang, A. McIlroy, C. A. Taatjes, and N. Hansen, "Analysis of Flame Structure by Molecular-Beam Mass Spectrometry Using Electron-Impact and Synchrotron-Photon Ionization," *Combustion, Explosion, and Shock Waves* **42**, 672-677 (*Fizika Goreniya i Vzryva* **42**, 58-63) (2006).
10. Matthew E. Law, Phillip R. Westmoreland, Terrill A. Cool, Juan Wang, Nils Hansen, Craig A. Taatjes, and Tina Kasper, "Benzene Precursors and Formation Routes in a Stoichiometric Cyclohexane Flame," *Proc. Combust. Inst.* **31**, 565-573 (2007).
11. Katharina Kohse-Höinghaus, Patrick Obwald, Ulf Struckmeier, Tina Kasper, Nils Hansen, Craig A. Taatjes, Juan Wang, Terrill A. Cool, Saugata Gon and Phillip R. Westmoreland, "The influence of ethanol addition on a premixed fuel-rich propene-oxygen-argon flame," *Proc. Combust. Inst.* **31**, 1119-1127 (2007).
12. Nils Hansen, James A. Miller, Craig A. Taatjes, Juan Wang, Terrill A. Cool, Matthew E. Law, Phillip R. Westmoreland, Tina Kasper and Katharina Kohse-Höinghaus, "Photoionization Mass Spectrometric Studies and Modeling of Fuel-Rich Allene and Propyne Flames," *Proc. Combust. Inst.* **31**, 1157-1164 (2007).
13. Sarah V. Petway, Huzeifa Ismail, William H. Green Jr., Edgar G. Estupiñán, Leonard E. Jusinski, and Craig A. Taatjes, "Measurements and Automated Mechanism Generation Modeling of OH Production in Photolytically-Initiated Oxidation of the Neopentyl Radical," *J. Phys. Chem. A* **111**, 3891-3900 (2007) (J. A. Miller festschrift).
14. Edgar G. Estupiñán, Jared D. Smith, Atsumu Tezaki, Stephen J. Klippenstein, and Craig A. Taatjes, "Measurements and Modeling of DO₂ Formation in the Reactions of C₂D₃ and C₃D₇ Radicals with O₂," *J. Phys. Chem. A* **111**, 4015-4030 (2007) (J. A. Miller festschrift).
15. N. Hansen, T. Kasper, S. J. Klippenstein, P. R. Westmoreland, M. E. Law, C. A. Taatjes, K. Kohse-Höinghaus, J. Wang, and T. A. Cool, "Initial Steps of Aromatic Ring Formation in a Laminar Premixed Fuel-Rich Cyclopentene Flame," *J. Phys. Chem. A* **111**, 4081-4092 (2007) (J. A. Miller festschrift).
16. Huzeifa Ismail, C. Franklin Goldsmith, Paul R. Abel, Pui-Teng Howe, Askar Fahr, Joshua B. Halpern, Leonard E. Jusinski, Yuri Georgievski, Craig A. Taatjes, and William H. Green, "Temperature and Pressure Dependence of the Reaction of Vinyl Radical (C₂H₃) with Ethylene," *J. Phys. Chem. A* **111**, 6843-6851 (2007) (M.C. Lin festschrift).
17. Craig A. Taatjes, "How Does the Molecular Velocity Distribution Affect Kinetics Measurements by Time-Resolved Mass Spectrometry?," *Int. J. Chem. Kinet.*, **39**, 565-570 (2007).
18. Craig A. Taatjes, Arjan Gijsbertsen, Marc J. L. de Lange, and Steven Stolte, "Measurements and Quasi-Quantum Modeling of the Steric Asymmetry and Parity Propensities in State-to-State Rotationally Inelastic Scattering of NO (²Π_{1/2}) with D₂," *J. Phys. Chem. A* **111**, 7631-7639 (2007) (R. E. Miller festschrift).
19. Adam M. Knepp, Giovanni Meloni, Leonard E. Jusinski, Craig A. Taatjes, Carlo Cavallotti, and Stephen J. Klippenstein, "Theory, Measurements and Modeling of OH and HO₂ Formation in the Cl-Initiated Oxidation of Cyclohexane," *Phys. Chem. Chem. Phys.* **9**, 4315 - 4331 (2007).
20. Fabien Goulay, David L. Osborn, Craig A. Taatjes, Peng Zou, Giovanni Meloni and Stephen R. Leone, "Direct detection of Polyynes Formation from the Reaction of Ethynyl Radical (C₂H) with Methylacetylene (CH₃-C≡CH) and Allene (CH₂=C=CH₂)," *Phys. Chem. Chem. Phys.* **9**, 4291-4300 (2007).
21. A. Ballast, A. Gijsbertsen, H. Linnartz, C. A. Taatjes, and S. Stolte, "A Quasi-Quantum Treatment of Inelastic Molecular Collisions," in *Rarefied Gas Dynamics: 25th International Symposium*, ed. M. S. Ivanov and A. K. Rebrov, Russian Academy of Sciences, Novosibirsk, 2007, pp. 1263-1272.
22. Alex T. Archibald, Max R. McGillen, Craig A. Taatjes, Carl J. Percival, Dudley E. Shallcross, "The atmospheric transformation of enols: a potential secondary source of carboxylic acids in the urban troposphere," *Geophys. Res. Lett.* **34**, L21801 (2007) DOI:10.1029/2007GL031032.
23. Giovanni Meloni, Talitha M. Selby, Fabien Goulay, Stephen R. Leone, David L. Osborn, and Craig A. Taatjes, "Photoionization of 1-alkenylperoxy and alkylperoxy radicals and a general rule for the stability of their cations," *J. Am. Chem. Soc.* **129**, 14019-14025 (2007) DOI: 10.1021/ja075130n.
24. Craig A. Taatjes, Nils Hansen, David L. Osborn, Katharina Kohse-Höinghaus, Terrill A. Cool, Phillip R. Westmoreland, "'Imaging' Combustion Chemistry with Multiplex Synchrotron Photoionization Mass Spectrometry," *Phys. Chem. Chem. Phys.* **10**, 20-34 (2008) DOI: 10.1039/b713460f.
25. Peng Zou, Kevin E. Strecker, Jaime Ramirez-Serrano, Leonard E. Jusinski, Craig A. Taatjes, and David L. Osborn, "Ultraviolet photodissociation of vinyl iodide: understanding the halogen dependence of photodissociation mechanisms in vinyl halides," *Phys. Chem. Chem. Phys.* **10**, 713-728 (2008) DOI: 10.1039/b712117b.
26. Craig A. Taatjes, "Recent developments in the coupling of theory and experiment to study the elementary chemistry of autoignition," *J. Combust. Soc. Japan* **50**, 29-38 (2008).

Theoretical Chemical Dynamics Studies of Elementary Combustion Reactions

Donald L. Thompson

Department of Chemistry, University of Missouri, Columbia, MO 65211
thompsondon@missouri.edu

Program Scope

Our research has focused on developing efficient, robust methods for fitting *ab initio* potential energy surfaces (PESs). Our goal has been to take greater advantage of high-level quantum chemistry calculations and high performance computing to make global *ab initio* PES fitting and the direct use of *ab initio* forces in MD simulations feasible. One of the problems we address stems from the fact that high-level quantum calculations are often too costly in computer time for practical applications and the levels of theory that must be used are often inadequate for reactions. A particularly important objective was to develop more efficient ways for expensive high-level quantum chemistry methods, which often do not directly provide gradients. A critical part of the solution was to develop better methods for fitting global PESs and performing direct dynamics more efficient by reducing the number of *ab initio* points that must be computed. Thus, we and others have focused on local fitting schemes. The first attempts at developing these approaches were based on cubic splines,^{1,2} but have proven not to be the best approach, and thus various other approaches are being vigorously investigated. Those attracting most of the effort are modified-Shepard (MS)³⁻⁵ interpolating moving least-squares (IMLS),⁶⁻¹⁶ distributed approximating functionals (DAF),¹⁷⁻²⁰ and neural networks (NN).²¹⁻²⁵ We have focused on higher-order IMLS, which does not require derivatives but can benefit from them if available, and thus can be used with the highest-level quantum chemistry methods. The emphasis has been on efficient methods for PESs in high dimensions. To a large extent this has now been achieved. Using our methods in which software for rate calculations directs quantum chemistry codes to produce *ab initio* predictions of reaction rates and related dynamics quantities, we are now poised to address specific systems and dynamical processes.

Recent Progress

The IMLS method is based on weighted least-squares fits to *ab initio* points. The weight function is peaked about the evaluation point such that only local *ab initio* points strongly influence the value of the fit. The fact that the weights vary with the evaluation point also implies that every fit evaluation involves a least squares fit. In our initial studies,⁸⁻¹³ we explored the basic properties of IMLS fits of energy values alone to generate PESs of qualitative chemical accuracy (rms fitting errors of ~1 kcal/mol). This includes automatically growing a PES with no human intervention from an initial small number of seed points. We found that fitting basis sets of relatively low degree (second or third degree) could achieve this accuracy over a large dynamic range (~100 kcal/mol) with a few hundred points for triatomic PESs and 1000-2000 points for simple tetra-atomic PESs. After a PES has been fit using N *ab initio* points, the cost of evaluating the IMLS fit goes as NM^2 , where M is the number of basis functions. We explored cutoff strategies that reduce the effective value of N and the selective elimination of basis function cross terms that reduce the value of M (HDMR basis).¹⁶

More recently, we have:

- Extended our IMLS fits down to spectroscopic accuracy (rms fitting errors of ~1 cm⁻¹) by using much larger basis sets.

- Incorporated gradients and Hessians into the IMLS formalism and observed a more rapid convergence of the PES fitting error with the number of *ab initio* points.^{15,16} Typically we find gradients more cost-effective than Hessians.
- Overcome the NM^2 cost by storing local expansions at the data points (L-IMLS).^{16,26,27} L-IMLS is a variant of a local approximates method of evaluating a fit.⁷ The evaluation of L-IMLS goes approximately as NM , the same cost as a modified Shepard approach if M were that for a second-order basis set. However, M can be much larger, with generally a decrease in the effective N , and no higher order derivatives are required.

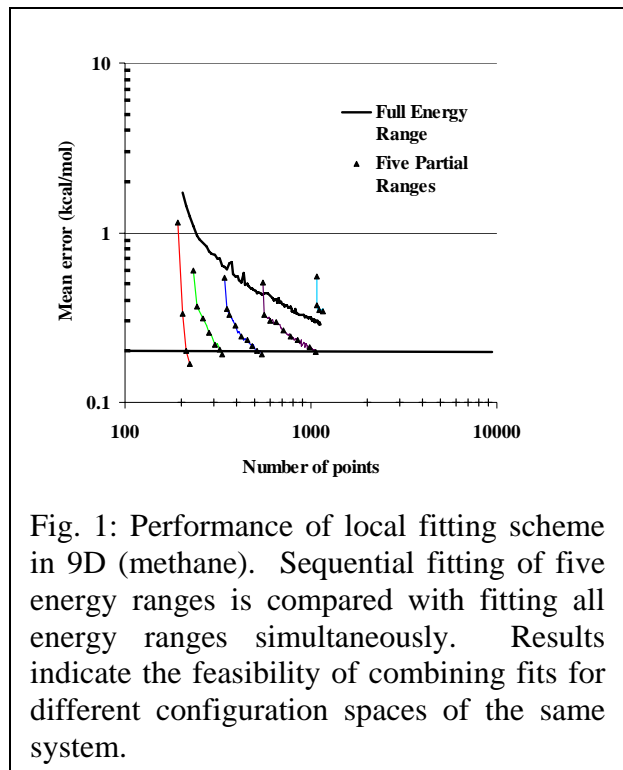
Most recently, we have:

- Expanded (in terms of dimensionality) the range of systems for which high quality PESs can be fit.²⁶ Figure 1 shows how fits to portions of configuration space in 9-D (defined by energy ranges) can be efficiently combined.
- Interfaced our global surface generator with three popular *ab initio* codes: Gaussian, Molpro, and Aces II. An input file specifies the number of atoms and their types, choice of coordinates and their ranges, desired energy range, fitting accuracy, choice of quantum chemistry code, and method. The code then runs in parallel using multiple processors to choose the data point placement as well as to perform the *ab initio* calculations and update the fit. Once the desired accuracy target is met, the code automatically outputs a standard format subroutine, which provides 3 useful PES functions: (1) fitted energy value, (2) analytic gradients (required by dynamics codes), and (3) a geometry dependent fitting error estimate.
- Interfaced our IMLS fitting method to a classical trajectory code.²⁸ This allows us to fit the dynamically accessible configuration space “on the fly.” The required number of calls to a quantum chemistry code is greatly reduced. This allows one to consider both larger systems and to use higher levels of *ab initio* theory than would otherwise be feasible. Recently, Harding *et al.*²⁹ found that in the combustion reaction of $CH+N_2$, higher level *ab initio* calculations predict a qualitatively different reaction mechanism since competing rates were affected by an order of magnitude (based on barrier heights). We are presently applying our approach to this system in order to describe the complete dynamics at this high level.

Future Work

We are pursuing the following avenues for applications to combustion chemistry:

- We are extending our “on the fly” fitting method (in which the fitting method is directly coupled to a trajectories code) to high dimensions. This will allow trajectory studies of dynamical processes in large systems for which it is not practical (or necessary) to produce a



global PES. The advantages in efficiency over direct dynamics methods will permit the use of high-levels of *ab initio* necessary for realistic results.

- We intend to perform a series of trajectory and spectroscopic studies involving the reactions of propargyl radicals with atomic, diatomic, triatomic, and polyatomic radicals and molecules. We will use classical trajectories with these PESs to study important dynamical issues and improve the understanding of precursor reactions to soot formation. We also plan to compute spectroscopic signatures of reaction products and postulated intermediates to aid in their identification in flames.
- Given that multi-reference methods are critical at some configurations but seldom necessary at all configurations, and that their cost is much higher than single-reference methods, we are now exploring a strategy in which the two methods can be combined within the context of an IMLS fit. A test calculation known as the T1-diagnostic is commonly used to determine the necessity of multi-reference methods. Our approach involves fitting the T1-diagnostic as a global property surface prior to fitting the PES. The PES fit can then automatically select the appropriate electronic structure method at any given point (relying on fitted values of the T1-diagnostic). The derived surfaces will be useful for many types of calculations such as spectroscopy, quantum scattering, or trajectories.

This work is being done in collaboration with Drs. A. Wagner and M. Minkoff at ANL.

References

- ¹ D. L. Thompson and D. R. McLaughlin, *J. Chem. Phys.* **62**, 4284 (1975).
- ² N. Sathyamurthy, R. Rangarajan, and L. M. Raff, *J. Chem. Phys.* **64**, 4606 (1976).
- ³ J. Ischtwan and M. A. Collins, *J. Chem. Phys.* **100**, 8080 (1994).
- ⁴ T. Ishida and G. C. Schatz, *Chem. Phys. Lett.* **314**, 369 (1999).
- ⁵ M. Yang, D. H. Zhang, M. A. Collins, and S.-Y. Lee, *J. Chem. Phys.* **114**, 4759 (2001).
- ⁶ D. H. McLain, *Comput. J.* **17**, 318 (1974).
- ⁷ R. Farwig, in *Algorithms for Approximation*, edited by J. C. Mason and M. G. Cox (Clarendon, Oxford, 1987).
- ⁸ G. G. Maisuradze and D. L. Thompson, *J. Phys. Chem. A* **107**, 7118 (2003).
- ⁹ G. G. Maisuradze, D. L. Thompson, A. F. Wagner, and M. Minkoff, *J. Chem. Phys.* **119**, 10002 (2003).
- ¹⁰ A. Kawano, Y. Guo, D. L. Thompson, A. F. Wagner, and M. Minkoff, *J. Chem. Phys.* **120**, 6414 (2004).
- ¹¹ Y. Guo, A. Kawano, D. L. Thompson, A. F. Wagner, and M. Minkoff, *J. Chem. Phys.* **121** (11), 5091 (2004).
- ¹² G. G. Maisuradze, A. Kawano, D. L. Thompson, A. F. Wagner, and M. Minkoff, *J. Chem. Phys.* **121**, 10329 (2004).
- ¹³ A. Kawano, I.V. Tokmakov, D. L. Thompson, A. F. Wagner, and M. Minkoff, *J. Chem. Phys.* **124**, 54105 (2006).
- ¹⁴ Y. Guo, L. B. Harding, A. F. Wagner, M. Minkoff, and D. L. Thompson, *J. Chem. Phys.* **126**, 104105 (2007).
- ¹⁵ I. Tokmakov, A. F. Wagner, M. Minkoff, and D. L. Thompson, "Interpolating Moving Least-Squares Methods for Fitting Potential Energy Surfaces: Gradient Incorporation in One-Dimensional Applications," *J. Theor. Chem. Accts.*, in press.
- ¹⁶ R. Dawes, D. L. Thompson, Y. Guo, A. F. Wagner, and M. Minkoff, *J. Chem. Phys.*, **126**, 184108 (2007)
- ¹⁷ A. M. Frishman, D. K. Hoffman, R. J. Rakauskas, and D. J. Kouri, *Chem. Phys. Lett.* **252**, 62 (1996).
- ¹⁸ D. K. Hoffman, A. M. Frishman, and D. J. Kouri, *Chem. Phys. Lett.* **262**, 393 (1996).
- ¹⁹ A. M. Frishman, D. K. Hoffman, and D. J. Kouri, *J. Chem. Phys.* **107**, 804 (1997).

-
- ²⁰ V. Szalav, *J. Chem. Phys.* **111**, 8804 (1999).
²¹ B. G. Sumpter and D. W. Noid, *Chem. Phys. Lett.* **192**, 455 (1992).
²² T. B. Blank, S. D. Brown, A. W. Calhoun, and D. J. Doren, *J. Chem. Phys.* **103**, 4129 (1994).
²³ D. F. R. Brown, M. N. Gibbs, and D. C. Clary, *J. Chem. Phys.* **105**, 7497 (1996).
²⁴ D. I. Doughan, L. M. Raff, M. G. Rockley, H. Hagan, P. M. Agrawal, and R. Komanduri, *J. Chem. Phys.* **124** 054321 (2006); *ibid.* 125, 079901 (2006).
²⁵ S. Manzhos, X. Wang, R. Dawes, and T. Carrington, Jr., *J. Phys. Chem. A* **110**, 5295 (2006).
²⁶ R. Dawes, D. L. Thompson, A. F. Wagner, and M. Minkoff, *J. Chem. Phys.*, **128**, 084107 (2008)
²⁷ Y. Guo, I. Tokmakov, A. F. Wagner, M. Minkoff, and D. L. Thompson, *J. Chem. Phys.* **127**, 214106 (2007)
²⁸ R. Dawes, D. L. Thompson, A. F. Wagner, and M. Minkoff, *J. Chem. Phys.* (in prep)
²⁹ L. B. Harding, S. J. Klippenstein and J. A. Miller, *J. Phys. Chem. A* **112**, 522 (2008)

Publications (2005-present):

- (1) D. M. Medvedev, S. K. Gray, A. F. Wagner, M. Minkoff, and R. Shepard, "Advanced Software for the Calculation of Thermochemistry, Kinetics, and Dynamics," *J. Physics: Conference Series* **16**, 247-251 (2005).
- (2) D. L. Thompson, A. F. Wagner, and M. Minkoff, "Advanced Computational Methods for Simulating Chemical Reactions," *J. Physics: Conference Series* **16**, 252-256 (2005).
- (3) A. Kawano, I. V. Tokmakov, D. L. Thompson, A. F. Wagner, and M. Minkoff, "Interpolating Moving Least-Squares Methods for Fitting Potential-Energy Surfaces: Further Improvement of Efficiency via Cutoff Strategies," *J. Chem. Phys.* **124**, 54105 (2006).
- (4) D. L. Thompson, A. F. Wagner, and M. Minkoff, "Advanced Computational Methods for Simulating Chemical Reactions," *Journal of Physics: Conference Series* **46**, 234-238 (2006).
- (5) Y. Guo, L. B. Harding, A. F. Wagner, M. Minkoff, and D. L. Thompson, "Interpolating Moving Least-Squares Methods for Fitting Potential Energy Surfaces: An Application to the H₂CN Unimolecular Reaction," *J. Chem. Phys.* 126, 104105(1-9) (2007).
- (6) I. Tokmakov, A. F. Wagner, M. Minkoff, and D. L. Thompson, "Interpolating Moving Least-Squares Methods for Fitting Potential Energy Surfaces: Gradient Incorporation in One-Dimensional Applications," *J. Theor. Chem. Accts.*, in press.
- (7) R. Dawes, D. L. Thompson, Y. Guo, A. F. Wagner, and M. Minkoff, "Interpolating Moving Least-Squares Methods for Fitting Potential Energy Surfaces: Computing High-Density PES Data from Low-Density *Ab Initio* Data Points," *J. Chem. Phys.*, **126**, 184108 (2007).
- (8) Y. Guo, I. Tokmakov, A. F. Wagner, M. Minkoff, and D. L. Thompson, "Interpolating moving least-squares methods for fitting potential energy surfaces: Improving efficiency via local approximants," *J. Chem. Phys.* **127**, 214106 (2007)
- (9) R. Dawes, D. L. Thompson, A. F. Wagner, and M. Minkoff, "Interpolating moving least-squares methods for fitting potential energy surfaces: A strategy for efficient automatic data point placement in high dimensions," *J. Chem. Phys.*, **128**, 084107 (2008)
- (10) R. Dawes, D. L. Thompson, A. F. Wagner, and M. Minkoff, "Interpolating moving least-squares methods for fitting potential energy surfaces: Classical trajectory studies using "on the fly" fitted dynamics," *J. Chem. Phys.*, (in preparation)

Elementary Reactions of PAH Formation

Robert S. Tranter
C.S.E. Division
Argonne National Laboratory
Argonne, IL-60439
tranter@anl.gov

Program scope

This program is focused on the experimental determination of kinetic and mechanistic parameters of elementary reactions, in particular those involved in the formation and destruction of the building blocks for aromatic species. The approach involves the development of a low pressure, fast flow, reactor equipped with a quadrupole MS and a shock tube (ST) equipped with laser schlieren (LS) and a time-of-flight mass spectrometer (TOF-MS). The combination of these techniques permit a wide range of reaction temperatures and pressures to be accessed.

A newly developed diaphragm free driver section has been installed on the shock tube (DFST). The control available with the DFST has given rise to reproducible shock wave experiments and fine control over the post shock conditions obtained. Improvements to the TOF-MS include the installation of micro channel plates with a much wider dynamic range that reduce the tendency of the detector to saturate. Recently, the nozzle/skimmer interface between the DFST and TOF-MS has been redesigned and the new interface greatly simplifies the alignment of the nozzle/skimmer and moves the skimmer exit closer to the ion source of the TOF-MS.

Recent Progress

DFST/TOF-MS: In a conventional chemical kinetics shock tube the driver and driven sections are separated by a diaphragm which when burst, either mechanically or spontaneously, releases the high pressure driver gas resulting in the development of a shock wave in the driven gas. It is well known that the way each diaphragm ruptures has a large effect on the development of the shock wave and hence the reaction conditions that are obtained behind the shock wave. Thus for experiments with identical initial conditions and apparently identical diaphragms it is unlikely that the same post shock conditions will be obtained. Normally, this variation is not a problem however it prevents the use of techniques such as signal averaging over consecutive experiments with the TOF-MS. Furthermore, with a conventional ST the diaphragm has to be changed every experiment which can be time consuming, relatively expensive and prevents automation of the apparatus. It is also not unusual for a bursting diaphragm to generate fragments which can block sampling ports and damage sensors. To address these problems, particularly reproducibility, a diaphragm free driver section has been developed which replaces the conventional driver section previously used with the ST/TOF-MS.

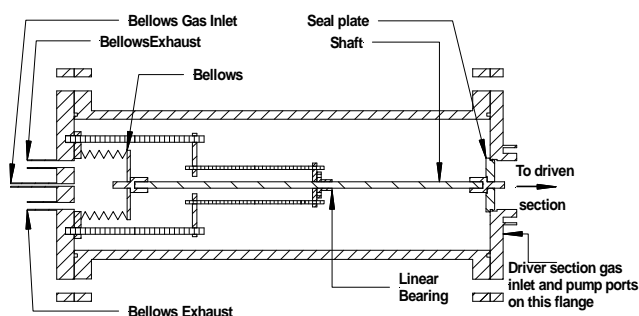


Figure 1: Schematic of the DFST driver section. The linear bearing supports the shaft and ensures that it runs parallel to the driver section.

The driver section of the DFST, Fig. 1, is essentially a fast opening valve consisting of a seal plate attached to a bellows by a shaft encapsulated in the original driver section. To close the valve the interior of the bellows is pressurized and the expanding bellows pushes the seal plate into the throat of the driven section. The driver and driven sections are then filled to pressures P_1 and P_4 respectively, $P_1 \ll P_4$. The bellows is rapidly evacuated and the pressure in the driver section collapses the bellows pulling the seal plate away from the driven section

allowing the driver gas to expand and generate a shock wave in the driven gas.

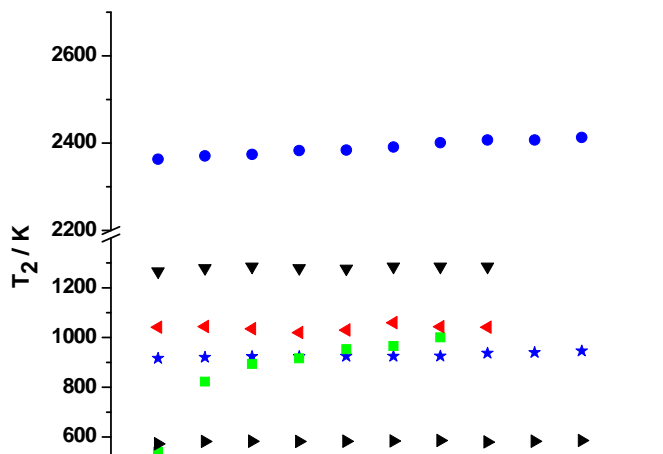


Figure 2: Comparison of incident shock temperatures, T_2 , obtained in the DFST with different bath gases, loading pressures and the effect of the mass of the shaft on T_2 . Squares show typical variations in T_2 obtained in a shock tube with diaphragms and constant P_4 and P_1 . DFST Krypton [●] = 3/8" o.d. shaft, $P_4=30$ psi, $P_1=5$ torr; [▼] = 3/8" o.d. shaft, $P_4=30$ psi, $P_1=30$ torr; [▲] = 1" o.d. shaft, $P_4=30$ psi, $P_1=30$ torr; DFST Argon [★] = 1" o.d. shaft, $P_4=45$ psi, $P_1=20$ torr; DFST Neon [▶] = 1" o.d. shaft, $P_4=30$ psi, $P_1=30$ torr; [■] = 0.004" Al diaphragms.

slower opening and weaker shock waves. In each experimental set P_4 and P_1 were kept constant and within a set T_2 varies by <1% which is about the accuracy with which T_2 can be determined in the current apparatus. Thus reproducible shocks can be generated with the DFST. For comparison a set of experiments using diaphragms is also shown in Fig. 2. Even if the first point is discarded T_2 varies by about 10%. A further benefit of the DFST is that the turn around time is considerably shorter than with the conventional shock tube and when fully automated should be about 1-2 minutes compared to the 15-20 minutes required with the diaphragmed tube.

One purpose in building the DFST was to produce sufficiently reproducible experiments that mass spectra obtained in consecutive DFST/TOF-MS experiments could be averaged to improve S/N and peak shapes. Fig. 3a shows a concentration/ time profile derived from a single DFST/TOF-MS experiment, $T_5=1397$ K, $P_5=582$ torr, on the dissociation of 1-fluoroethane (FE) dilute in neon. As usual with TOF-MS experiments argon is used as an internal standard. A similar concentration time profile is shown in Fig. 3b, $T_5=1393 \pm 11$ K, $P_5=579 \pm 6$ torr, where mass spectra from 6 experiments have been averaged. Fig. 3b clearly shows considerably less scatter than Fig. 3a which simplifies the identification of the start of reaction and reduces the error in simulation. The extracted rate coefficients from Figs. 3a and b are in excellent agreement with each other and the results of an extensive set of ST/TOF-MS experiments.

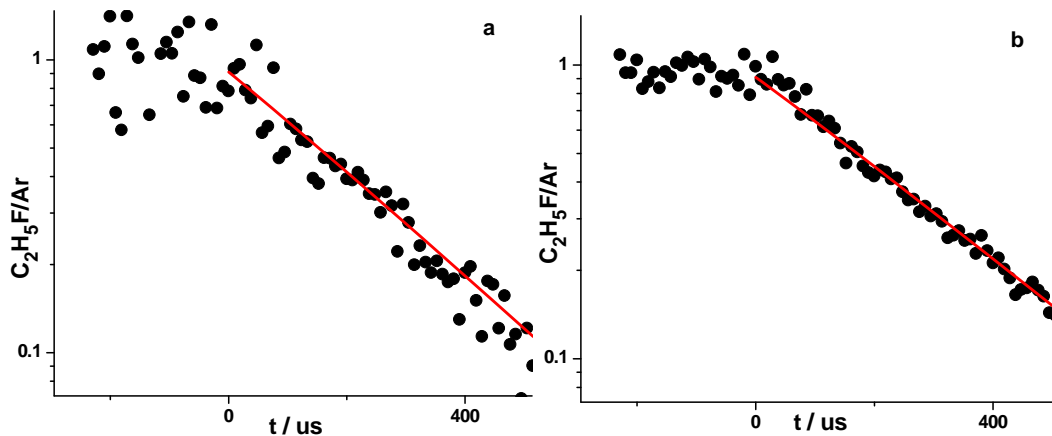


Figure 3: DFST/TOF-MS dissociation of fluorine ethane. Solid points represent experimental data and red lines represent the results of simulations. a) Individual experiment $T_5=1397$ K, $P_5=582$ torr; b) Concentration profile derived from averaged mass spectra from 6 experiments $T_5=1393 \pm 11$ K, $P_5=579 \pm 6$ torr

The DFST is intended for use both in TOF-MS and LS experiments. Typical reaction conditions in the TOF-MS experiments are $P_5=200-3000$ torr, $T_5 < 2200$ K and in LS experiments $P_2=30-500$ torr, $T_2 < 3000$ K where the subscripts 5 and 2 denote reflected and incident shock conditions respectively. In TOF-MS experiments neon is normally the bath gas whereas argon and krypton are preferred for LS work. Thus, the DFST has to reproducibly produce a wide range of shock strengths in a variety of bath gases. The range and reproducibility of the DFST is demonstrated in Fig. 2 where the T_2 is shown for several experiments with different bath gases and two different shaft diameters. Altering the shaft diameter effectively changes the mass that has to be accelerated to open the valve and increased mass results in

Fluoroethanes: An ongoing project with John Kiefer, UIC, has been the elimination of HF from fluorinated ethanes which was stimulated by a series of LS experiments on 1,1,1-trifluoroethane (TFE) dissociation. In previous work we have applied the ST/TOF-MS technique to TFE and vinyl fluoride (VF) dissociation and the ST/LS method to these molecules and 1,1-difluoroethane (DFE) dissociation. The results of the ST/TOF-MS and ST/LS techniques overlap and provide a more extensive dataset than can be obtained by either experiment individually. ST/LS has also been used to investigate vibrational relaxation in these species.

The final member of the sequence is 1-fluoroethane, FE. The enthalpy of reaction for the dissociation of FE is too small to produce density gradients from which rate coefficients can be reliably extracted rendering LS effectively blind to the dissociation reaction, although vibrational relaxation can still be resolved. Consequently, only the ST/TOF-MS method has been applied to the dissociation of 1-fluoroethane ($T_5=1207$ to 1711 K, $P_5 = 500$ and 1200 torr). The results of these experiments are in good agreement with the results of Master Equation and VTST calculations by Stephen Klippenstein. Both DFE and FE show strong falloff with a small pressure dependency that can be simulated with a standard RRKM formulation. Thus of the fluoroethanes that we have studied, the only one showing an anomalous fall-off behavior is TFE.

Phenyl Iodide: The thermal decomposition of phenyl iodide has been used as precursor for phenyl radicals in shock tube experiments and at sufficiently high temperatures decomposition of phenyl may be significant. Many of the experiments planned for the DFST/TOF-MS will also use phenyl iodide as source of phenyl radicals. Consequently, the dissociation of C₆H₅I has been studied in the fall off region over the temperature range $1350 - 1888$ K at 60 ± 10 torr and 129 ± 6 torr. Initial rate coefficients for phenyl iodide dissociation were extracted from the LS density gradient profiles and simulated with a restricted rotor Gorin model [S. S. Kumaran, M.-C. Su, J. V. Michael, Chem. Phys. Lett. 269, 99-106, 1997], Fig. 4. The results of the LS experiments are about a factor 1.5 higher at 1400 K and 130 torr than those of

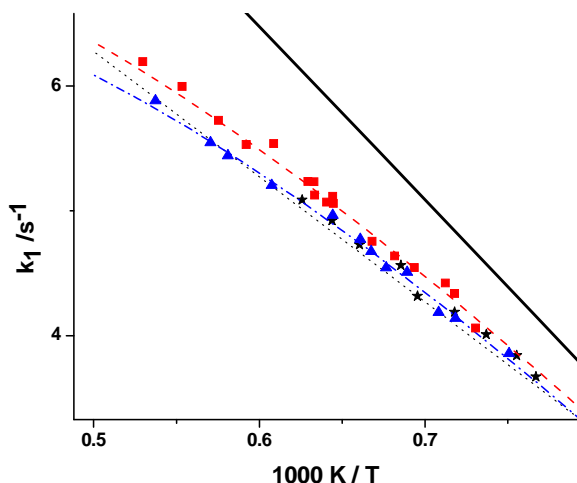


Figure 4: Initial rate coefficients derived from density gradient profiles for 2% C₆H₅I in Kr and the results of Gorin model calculations. Experimental Data: [■] $P_2=130 \pm 6$ torr; [▲] $P_2=60 \pm 10$ torr; [★] $P_2=75-129$ torr; Calculations: - - -, Gorin 130 torr, - · -, Gorin 60 torr, — k_∞ ; ··· 103-731 torr, Kumaran et al.

Kumaran et al. and support a higher $\langle \Delta E_{down} \rangle$ of 1300 cm^{-1} with all other parameters unchanged in the Gorin model. An interesting point to note is that with the control available with the DFST the post shock conditions have been confined to two very narrow pressure ranges by varying both P_4 and P_1 rather than the broader pressure range that is obtained by fixing P_4 as in a classical ST experiment (black stars Fig. 4). The results of the Gorin calculations are in excellent agreement with the experimental data and the small difference between the two pressure ranges is clearly resolved. In addition to the rate of dissociation of phenyl iodide the LS profiles are also yielding information about the dissociation and recombination of phenyl radicals. While interpretation of these data is still in the early stages it appears to indicate that under the experimental conditions of the LS work dissociation of the phenyl radical is not significant below about 1600 K.

Future Plans

Several studies are planned for the DFST/TOF-MS now that it is producing reliable data. These include investigation of HF elimination in the remaining fluoroethanes that cannot be studied with LS and planned improvements to the apparatus should increase the upper limit of rate coefficients that can be

measured in these systems. Along with the characterization of phenyl iodide as a source of phenyl radicals the dissociation of propargyl iodide as a source of propargyl radicals will be studied. Both of these investigations will be extended to the DFST/TOF-MS. Following successful characterization of the radical sources a series of experiments including reactions of the propargyl and phenyl radicals with other molecules and radicals will be started to investigate high temperature routes to larger aromatic species.. Additionally, experiments will be completed on the dissociation of oxygenated cyclic species including 1,4-dioxane and 1,3-dioxane.

In addition to the chemical studies effort will also be devoted to completing the low pressure, fast flow reactor which is particularly valuable for radical/molecule studies. On going improvements to the DFST/TOF-MS will include the implementation of ion gating to improve signal quality by preventing unwanted ions from reaching the detector and the examination of ways to increase the sampling frequency to obtain better definition of the concentration time profiles for faster reactions than can currently be studied.

Publications

1. Xu H., Kiefer J. H., Sivaramakrishnan R., Giri B.R. and Tranter R. S., "Shock tube study of dissociation and relaxation in 1,1-difluoroethane and vinylfluoride", *Phys. Chem. Chem. Phys.*, 9, 4164-4176, 2007.
2. Saxena S., Kiefer J. H. and Tranter R. S., "Relaxation, Incubation, and Dissociation in CO₂", *J. Phys. Chem. A*, 111, 3884 - 3890, 2007.
3. Tranter R. S., Giri B. G. and Kiefer J. H., "Coupling of a Shock Tube to a Time-of-Flight Mass Spectrometer for High Temperature Kinetic Studies" *Rev. Sci. Instrum.*, 78, 034101, 2007.
4. Giri B.R. and Tranter R. S., "Dissociation of 1,1,1-Trifluoroethane Behind Reflected Shock Waves: Shock Tube/Time-of-Flight Mass Spectrometry Experiments" *J. Phys. Chem. A*, 111(9), 1585 – 1592, 2007.
5. Sivaramakrishnan R, Comandini A, Tranter R. S., Brezinsky K., Davis S. G. and Wang H., "Combustion of CO/H₂ Mixtures at Elevated Pressures", *Proc. Combust. Inst.*, 31, 167-174, 2007
6. Sivaramakrishnan R., Tranter R. S. and Brezinsky K., "High Pressure Pyrolysis of Toluene. 2. Modeling Benzyl Decomposition and Formation of Soot Precursors", *J. Phys. Chem. A* 110(30), 9400-9404, 2006
7. Sivaramakrishnan R., Tranter R. S., Brezinsky K., "High Pressure Pyrolysis of Toluene. 1. Experiments and Modeling of Toluene Decomposition", *J. Phys. Chem. A* 110(30), 9388-9399, 2006
8. Gupte K. S., Kiefer J. H., Tranter R.S., Klippenstein S. J. and Harding L. B., "Decomposition of Acetaldehyde: Experiment and Detailed Theory", *Proc. Combust. Inst.* 31, 429-437, 2007
9. Miller, C. H., Tang W., Tranter R.S. and Brezinsky K., "Shock tube pyrolysis of 1,2,4,5-hexatetraene", *J. Phys. Chem. A* 110, 3605-3613, 2006.
10. Sivaramakrishnan R., Vasudevan H., Tranter R. S. and Brezinsky K., "A Shock Tube Study of the High Pressure Thermal Decomposition of Benzene", *Combustion Science and Technology*, 178, 285-305, 2006
11. Tang W., Tranter R. S. and Brezinsky K., "An optimized semi-detailed sub-mechanism of benzene formation from propargyl recombination", *J. Phys. Chem. A*, 110, 2165-2175, 2006.

Variational Transition State Theory

Donald G. Truhlar

Department of Chemistry, University of Minnesota
207 Pleasant Street SE, Minneapolis, Minnesota 55455
truhlar@umn.edu

Program scope

This project involves the development of variational transition state theory (VTST) with optimized multidimensional tunneling (OMT) contributions and its application to gas-phase reactions. For overbarrier processes, we are employing both methods suitable for tight transition states, employing isoinertial minimum energy paths, variational reaction paths, and curvilinear generalized normal mode coordinates (Garrett and Truhlar 1979; Isaacson and Truhlar 1982, Jackels, Gu, and Truhlar 1995, Fast and Truhlar 1998), and methods suitable for loose transition states, employing multifaceted dividing surfaces and Monte Carlo integration over transition modes (Georgievskii and Klippenstein 2003). For optimized multidimensional tunneling, we employ small curvature tunneling (Skodje, Truhlar, and Garrett 1981; Liu, Lynch, Truong, Lu, Truhlar, and Garrett 1993) and large curvature tunneling (Garrett, Truhlar, Wagner, and Dunning 1983; Fernandez and Truhlar 2001).

The further development of VTST/OMT as a useful tool for combustion kinetics also involves developing and applying new methods of electronic structure calculations for the input potential energy surface, which is typically an implicit surface defined by a level of electronic structure theory (direct dynamics: Baldrige, Gordon, Steckler, and Truhlar, 1989; González-Lafont, Truong, and Truhlar 1991) and methods to interface reaction-path and reaction-swath dynamics calculations with electronic structure theory, for example, interpolated variational transition state theory with mapping (Corchado, Coitiño, Chuang, Fast, and Truhlar 1998) and multiconfiguration molecular mechanics (Kim, Corchado, Villà, Xing, and Truhlar 2000). Electronic structure developments include both wave function theory and density functional theory.

The project also involves the development and implementation of practical techniques and software for applying the theoretical methods to various classes of reactions and transition states and applications to specific reactions, with special emphasis on combustion reactions and reactions that provide good test cases for methods needed to study combustion reactions.

Recent progress

A theme that runs through our current work is the development of improved electronic structure methods and their use for rate constant calculations. One class of new methods involves wave function theory, especially generally defined electronic wave function methods with empirical elements ("semiempirical model chemistries," in the language of Pople), such as methods based on extrapolating the correlation energy to complete configuration interaction; another class of methods is based on new density functionals. These methods are then used in direct dynamics calculations or with efficient interpolation schemes. Direct dynamics denotes that, instead of using a pre-defined potential energy function, all required energies and forces for each geometry that is important for evaluating dynamical properties are obtained directly from electronic structure calculations. Density functional theory is very attractive as an electronic structure method for direct dynamics because of its relatively low cost and the availability of analytic gradients and Hessians. Development of improved exchange and correlation functionals is an active research area in theoretical chemistry and physics, but most of this research has

neglected the important issues of barrier height prediction and noncovalent interactions, and as a consequence the functionals have not been accurate for quantitative kinetics. We have now developed new functionals, especially the M06-2X functional (Minnesota 2006 functional with double nonlocal exchange), that are quite accurate for these properties, and we have also developed multi-coefficient correlation methods for using wave function theory for these properties. A recent test of the M06-2X functional on a diverse database of reaction barrier heights (for primarily single-reference systems) yielded a mean unsigned error of only 0.5 kcal/mol, comparable to the accuracy of CCSD(T). A key advantage of M05-2X as compared to other density functionals is the improved accuracy for attractive noncovalent interactions. This is important for barrierless reactions and for reactions with low, early saddle points (like OH + H₂S), where it is necessary to have a consistent treatment of the energy along the reactant approach coordinate.

In order to generate reactive potential energy surfaces with minimal computational effort, we have introduced an algorithm called multiconfiguration molecular mechanics (MCMM). MCMM describes polyatomic potential energy surfaces by interacting molecular mechanics (MM) configurations (each of which is the analog of a valence bond configuration) and can thus be viewed as an extension of standard MM to chemical reactions or as an extension of semiempirical valence bond theory to be systematically improvable. MCMM fitting is accomplished by combining molecular mechanics potentials for the reactant and product wells with electronic structure data (energy, gradient, and Hessian) at the saddle point and a small number of non-stationary points. We developed a general strategy for placement of the non-stationary points for fitting potential energy surfaces in the kinetically important regions and for calculating rate constants for atom transfer reactions by variational transition state theory with multidimensional tunneling. Then we improved the efficiency of the MCMM method by using electronic structure calculations only for certain critical elements of the Hessians at the non-stationary points and by using interpolation for the other elements at the non-stationary points. We tested this new MCMM strategy for a diverse test suite of reactions involving hydrogen-atom transfer. The new method yields quite accurate rate constants as compared to straight (uninterpolated) direct dynamics calculations at the same electronic structure level.

Software distribution

We have developed several software packages for applying variational transition state theory with optimized multidimensional tunneling coefficients to chemical reactions and for carrying out MCCM calculations, density functional theory calculations with new density functionals, direct dynamics, and MCMM applications. The URL of our software distribution site is comp.chem.umn.edu/Truhlar. The license requests that we fulfilled during the period Jan. 1, 2006–Mar. 30, 2008 for software packages developed wholly or partially under DOE support is as follows:

	<i>Total</i>	<i>academic</i>	<i>government/DoD</i>	<i>industry</i>
POLYRATE	189	168	11	10
GAUSSRATE	77	72	2	3
GAMESSPLUS	38	30	5	3
HONDOPLUS	28	22	5	1
MULTILEVEL	20	19	1	0
8 others	53	48	5	0

Future plans

We have several objectives for the next few years: (1) complete the incorporation of dividing surfaces appropriate for association reactions into POLYRATE, and integrate of these methods with master equation solvers to treat the stabilization of intermediate complexes by energy transfer collisions; (2) integrate the above methods with tight transition state methods to treat multiwell reactions and reactions with inner and outer dynamical bottlenecks; (3) further improve our density functionals and multi-coefficient correlation methods for potential energy surfaces, especially for saddle point geometries, barrier heights, and vibrational frequencies at saddle points; (5) develop model chemistries based on multireference methods; (5) further develop the multi-configuration molecular mechanics approach as an efficient tool for the semiautomatic fitting of complex-system potential energy surfaces; (6) develop more reliable methods for including anharmonicity at variational transition states, especially for torsions and mode-mode coupling; (7) continue our calculations of reaction rates of peroxides and enols; (8) enhance our user-friendly computer program packages to allow more researchers to carry out calculations conveniently by the new methods.

Publications, 2006-present

Journal articles

1. "Combined Valence Bond-Molecular Mechanics Potential Energy Surface and Direct Dynamics Study of Rate Constants and Kinetic Isotope Effects for the $\text{H} + \text{C}_2\text{H}_6$ Reaction," A. Chakraborty, Y. Zhao, H. Lin, D. G. Truhlar, *Journal of Chemical Physics* **124**, 044315/1-044315/14 (2006).
2. "Design of Density Functionals by Combining the Method of Constraint Satisfaction with Parametrization for Thermochemistry, Thermochemical Kinetics, and Noncovalent Interactions," Y. Zhao, N. E. Schultz, D. G. Truhlar, *Journal of Chemical Theory and Computation* **2**, 364-382 (2006).
3. "Searching for Saddle Points by Using the Nudged Elastic Band Method: An Implementation for Application to Gas-Phase Systems," N. Gonzalez-Garcia, J. Pu, A. Gonzalez-Lafont, J. M. Lluch, D. G. Truhlar, *Journal of Chemical Theory and Computation* **2**, 895-904 (2006).
4. "Modeling of Bimolecular Reactions," A. Fernández-Ramos, J. A. Miller, S. J. Klippenstein, D. G. Truhlar, *Chemical Reviews* **106**, 4518-4584 (2006).
5. "Statistical Thermodynamics of Bond Torsional Modes. Tests of Separable and Almost-Separable Approximations Applied to H_2O_2 , HOOD, D_2O_2 , $\text{H}_2^{18}\text{O}_2$, H^{18}OOH , D^{18}OOH , and H^{18}OOD ," B. A. Ellingson, V. A. Lynch, B. A. Ellingson, S. L. Mielke, and D. G. Truhlar, *Journal of Chemical Physics* **125**, 84305/1-17 (2006).
6. "Assessment of Density Functionals for π Systems: Energy Differences Between Cumulenes and Polyynes and Proton Affinities, Bond Length Alternation, and Torsional Potentials of Conjugated Polyenes, and Proton Affinities of Conjugated Schiff Bases," Y. Zhao and D. G. Truhlar, *Journal of Physical Chemistry A* **110**, 10478-10486 (2006).
7. "Optimizing the Performance of the Multiconfiguration Molecular Mechanics Method," O. Tishchenko and D. G. Truhlar, *Journal of Physical Chemistry A* **110**, 13530-13536 (2006).
8. "A New Local Density Functional for Main Group Thermochemistry, Transition Metal Bonding, Thermochemical Kinetics, and Noncovalent Interactions," Y. Zhao and D. G. Truhlar, *Journal of Chemical Physics* **125**, 194101/1-18 (2006).
9. "Representative Benchmark Suites for Barrier Heights of Diverse Reaction Types and Assessment of Electronic Structure Methods for Thermochemical Kinetics," J. Zheng, Y. Zhao, and D. G. Truhlar, *Journal of Chemical Theory and Computation* **3**, 569-582 (2007).
10. "Global Potential Energy Surfaces with Correct Permutation Symmetry by Multi-Configuration Molecular Mechanics," O. Tishchenko and D. G. Truhlar, *Journal of Chemical Theory and Computation* **3**, 938-948 (2007).

11. "The M06 Suite of Density Functionals for Main Group Thermochemistry, Thermochemical Kinetics, Noncovalent Interactions, Excited States, and Transition Elements: Two New Functionals and Systematic Testing of Four M06 Functionals and Twelve Other Functionals," Y. Zhao and D. G. Truhlar, *Theoretical Chemistry Accounts*, accepted Feb. 13, 2007. (Mark S. Gordon 65th Birthday Issue)
12. "Thermochemical Kinetics of Hydrogen-Atom Transfers Between Methyl, Methane, Ethynyl, Ethyne, and Hydrogen," J. Zheng, Y. Zhao, and D. G. Truhlar, *Journal of Physical Chemistry A* **111**, 4632-4642 (2007).
13. "Symmetry Numbers and Chemical Reaction Rates," A. Fernández-Ramos, B. A. Ellingson, R. Meana-Pañeda, J. M. C. Marques and D. G. Truhlar, *Theoretical Chemistry Accounts* **118**, 813-826 (2007).
14. "Multi-Coefficient Gaussian-3 Calculation of the Rate Constant for the OH + CH₄ Reaction and its ¹²C/¹³C Kinetic Isotope Effect with Emphasis on the Effects of Coordinate System and Torsional Treatment," B. A. Ellingson, J. Pu, H. Lin, Y. Zhao, and D. G. Truhlar, *Journal of Physical Chemistry A* **111**, 11706-11717 (2007).
15. "Explanation of the Unusual Temperature Dependence of the Atmospherically Important OH + H₂S → H₂O + SH Reaction and Prediction of the Rate Constant at Combustion Temperatures," B. A. Ellingson and D. G. Truhlar, *Journal of the American Chemical Society* **129**, 12765-12771 (2007).
16. "Computational Chemistry of Polyatomic Reaction Kinetics and Dynamics: The Quest for an Accurate CH₅ Potential Energy Surface," Titus V. Albu, J. Espinosa-García, D. G. Truhlar, *Chemical Reviews* **107**, 5101-5132 (2007).
17. "Reactions of Hydrogen Atom with Hydrogen Peroxide," B. A. Ellingson, D. P. Theis, O. Tishchenko, J. Zheng, and D. G. Truhlar, *Journal of Physical Chemistry A* **111**, 13554-13566 (2007).
18. "Non-Born–Oppenheimer Molecular Dynamics of Na...FH Photodissociation," A. W. Jasper and D. G. Truhlar, *Journal of Chemical Physics* **127**, 194306/1-7 (2007).
19. "A Comparative Assessment of the Perturbative and Renormalized Coupled Cluster Theories with a Non-iterative Treatment of Triple Excitations for Thermochemical Kinetics, Including a Study of Basis Set and Core Correlation Effects," J. Zheng, J. R. Gour, J. J. Lutz, M. Włoch, P. Piecuch, and D. G. Truhlar, *Journal of Chemical Physics* **128**, 44108/1-7 (2008).
20. "How Well Can New-Generation Density Functionals Describe the Energetics of Bond Dissociation Reactions Producing Radicals?" Y. Zhao and D. G. Truhlar, *Journal of Physical Chemistry A* **112**, 1095-1099 (2008).

Book chapters

1. "Variational Transition State Theory and Multidimensional Tunneling for Simple and Complex Reactions in the Gas Phase, Solids, Liquids, and Enzymes," D. G. Truhlar, in *Isotope Effects in Chemistry and Biology*, edited by A. Kohen and H.-H. Limbach (Marcel Dekker, New York, 2006), pp. 579-620.
2. "Multilevel Methods for Thermochemistry and Thermochemical Kinetics," B. J. Lynch, D. G. Truhlar, in *Recent Advances in Electron Correlation Methodology*, edited by A. K. Wilson and K. A. Peterson (American Chemical Society Symposium Series Volume 958, Washington, DC, 2007), pp. 153-167.
3. "Variational Transition State Theory in the Treatment of Hydrogen Transfer Reactions," D. G. Truhlar and B. C. Garrett, in *Hydrogen Transfer Reactions*, edited by J. T. Hynes, J. P. Klinman, H.-H. Limbach, and R. L. Schowen (Wiley-VCH, Weinheim, Germany, 2007), Vol. 2, pp. 833-874.
4. "Variational Transition State Theory," B. C. Garrett, D. G. Truhlar, in *Theory and Applications of Computational Chemistry: The First Forty Years*, edited by C. E. Dykstra, G. Frenking, K. Kim, and G. Scuseria (Elsevier, Amsterdam, 2005), pp. 67-87.
5. "Variational Transition State Theory with Multidimensional Tunneling," A. Fernandez-Ramos, B. A. Ellingson, B. C. Garrett, D. G. Truhlar, in *Reviews in Computational Chemistry*, Vol. 23, edited by K. B. Lipkowitz and T. R. Cundari (Wiley-VCH, Hoboken, NJ, 2007), pp. 125-232.

Chemical Kinetic Data Base for Combustion Modeling

Wing Tsang
National Institute of Standards and Technology
Gaithersburg, MD 20899
Wing.tsang@nist.gov

Program Scope and Definition: There has been much recent interest in the computer simulation the combustion of real fuels in real devices. This is due to progress in Computational Fluid Dynamics Codes[1,2] that has led to the possibility of combining detailed chemistry with fluid dynamics. In addition, the increasing price of oil has led to renewed interest in improving energy efficiency without degrading emission limits and the use of alternative fuels. Simulations offer a means of answering many of these issues without the need of an extensive program of expensive and uncertain physical testing.

This program has its aim the development of an information base on the conversion of real fuels to their thermodynamic end points or water and carbon dioxide for lean mixtures and hydrogen and carbon for rich mixtures in real devices.. There are two basic problems in working with real fuels. The first has to do with the definition of fuel composition. Recent work on the selection of surrogates[3] as representative of real fuels has now made it possible to carry out molecule based simulations. The second barrier is due to the relatively large molecular size of real fuels. They range from eight (for gasoline) to ten for (aviation fuel) to sixteen (diesels) carbon atom hydrocarbons. It is understood that the numbers given above are merely in the mid-range of the distribution of hydrocarbons. Until recently there have been no mechanistically clean experimental kinetic data on these molecules and the associated radicals..

The focus of this program is on the unimolecular breakdown of the fuel radicals generated from the fuel during combustion. This is the key step in the pyrolytic breakdown of fuel molecules. It reduces the size of the fuel to the small unsaturates and fragments that are the precursors for PAH/SOOT formation. The mechanism and rate constants for radical attack on the fuel molecule itself is well established. Practically all the existing fuel combustion models are for single component fuels and fitted to global results near stoichiometric conditions. The present work extends the range of existing models to cover richer systems and mixtures. An interesting issue is how purely pyrolytic reactions effect PAH/SOOT formation propensities.

Since it involves only the fuel molecule and radicals (C and H), pyrolytic systems represent the logical first step in any chemical kinetic approach to unraveling the detailed chemistry of combustion of real fuels.. Indeed, it sets the stage to determining the nature of the oxidation process by treating the oxygen induced reaction as a perturbation on the pyrolytic situation.

Recent Progress: With AFOSR support we have been filling the serious experimental gap on the decomposition of larger and intermediate size fuel radicals through studies in a single pulse . shock tube. For most of these studies we have found that the alkyl iodide is a very good source for the fuel radicals of interest. The very weak C-I bond readily releases the 1-fuel radical into the system. Conditions are set so that only unimolecular reactions can occur The isomerization reactions creates other possible fuel radicals, while the competitive beta bond scission processes

Five carbon	Six carbon	Seven carbon	Eight carbon
1-pentyl (a)	1-hexyl (c)	1-heptyl (f)	1-octyl (h)
2-pentyl (a)	2-hexyl (c)	2-heptyl (f)	2-octyl (h)
Cyclopentyl (b)	3-hexyl (c)	3-heptyl (f)	3-octyl (h)
1-pentenyl-5 (b)	4-methylpentyl-1 (d)	4-heptyl (f)	4-octyl (h)
	2-methylpentyl-1 (d)	5-methylhexyl-1 (g)	
	4-methylpentyl-2 (d)	2-methylhexyl-1 (g)	
	2-methylpentyl-2 (d)	2-methylhexyl-2 (g)	
	Cyclohexyl (e)	2-methylhexyl-3 (g)	
	1-hexenyl-6 (e)	2-methylhexyl-4 (g)	
	1-hexenyl-3 (e)	2-methylhexyl-5 (g)	
	Cyclopentyl-methyl (e)		
	2-hexenyl-1 (e)		
	3-methylcyclopentyl-1 (e)		
	5-hexenyl-2 (e)		
	2-methyl-4-pentenyl-1 (e)		

Table 1: Radicals for which experimental data on olefin branching ratios have been determined. The letters refer to precursors (a) 1-iodopentane (b) 1-7-octadiene (c) 1-iodohexane, (d) 1-iodo-methylpentane (e) tert-butylcyclohexane, 1,8 nonadiene (f) 1-iodoheptane (g) 1-iodo-5-methylhexane (h) 1-iodo-octane

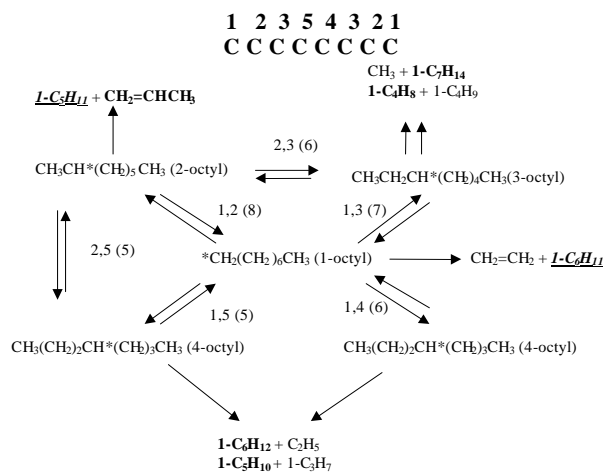


Figure 1: Mechanism for octyl radical decomposition and isomerization. The numbers at the top of the figure refers to the convention used in describing the process

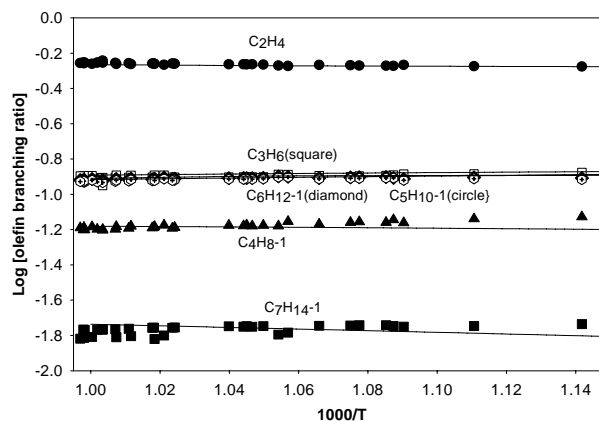


Figure 2: Olefin branching ratios for the production of the olefins from 1-octyl radical decomposition as a function of temperature

leads to the formation of the small unsaturated olefins of interest. Table 1 is a listing of the radicals for which experimental data have been obtained. The main task is the interpretation of these results in terms of rate expressions for the various decomposition and isomerization processes. For this purpose molecular and thermodynamic properties have to be estimated. In addition use is made of earlier results on smaller alkyl radicals. Thus the rate constants as a

	A: Reaction	Log A	n	E/R	Log (k [1000])
1	1-octyl = ethene + 1-hexyl	11.96	.31	13708	6.93
2	2-octyl = propene + 1-pentyl	10.78	.84	14001	7.24
3	3-octyl = 1-butene + 1-butyl	13.31	.04	14340	7.21
4	3-octyl = 1-heptene + methyl	9.98	1.08	14790	6.78
5	4-octyl = 1-pentene + 1-propyl	11.74	.55	14134	7.26
6	4-octyl = 1-hexene + ethyl	9.83	1.11	13600	7.25
7	1-octyl = 4-octyl (1-4-H trans)	.71	3.23	8479	6.72
8	1-octyl = 4-octyl (1-5-Htrans)	1.36	2.82	5413	7.46
9	1-octyl = 3-octyl	.47	3.08	5544	7.29
10	4-octyl = 1 octyl 1-4-H trans	-.38	3.57	9532	6.20
11	4-octyl = 1-octyl 1-5-H trans	.27	3.16	6466	6.94
12	3-octyl = 1-octyl	.52	3.11	6579	6.99
13	2-octyl = 3-octyl	.27	3.27	6642	7.20
14	2-octyl = 4-octyl	.15	3.32	8125	6.60
15	3-octyl = 2-octyl	1.33	2.96	6625	7.34
16	4-octyl = 2-octyl	.071	3.32	8128	6.52

Table 2: High pressure rate expressions for reactions involved in octyl radical decomposition and isomerization. 1-7 Hydrogen transfer is not included. Results are not sensitive to this process

function of temperature and pressure is a reflection of all the existing information.

The most recent results are for the octyl radicals generated from 1-iodo-octane and is typical of the high quality data used for the analysis. The general mechanism is outlined in Figure 1. It can be seen that there are 6 beta bond scission reactions and 6 reversible isomerization. For most of the reactions the rate constants can be directly carried over from the smaller fuel compounds [4-6]. The larger size of the octyl radicals makes contributions from secondary to secondary radical isomerization increasingly important. On the basis of reasonable assumptions the present results indicate, as in the case for heptyl radicals, that the 1-3 H-transfer process (involving a seven member cyclic transition state) have rate constants that are within a factor of 2 of those for the 1-5 process (six member cyclic transition state). Similarly, it appears that rate constants for 1-2 H-transfer isomerization, involving an eight member cyclic transition state is unimportant in comparison to contributions from secondary to secondary H-transfer processes. The strain energy does not appear to play an important role for these larger transition states. These results have important implications on the prediction of isomerization rate constants for larger fuel radicals. It means that transition states with larger than seven member ring structures need not be considered for larger fuel radicals. It should be possible to estimate rate constants and olefin branching ratios for any linear fuel radical. The resulting fit of the experimental results can be seen in Figure 2 on the basis of the solution of the master equation. The high pressure rate expressions used to make this fit can be found in Table 2. Having made this fit these rate expressions can be used to determine rate constants over all combustion conditions. These rate constants have a pressure dependence that for 1 bar pressure can be as large as an order of magnitude at temperatures in excess of 1000 K.

Future Work: The remaining issue is the determination of the rate constants for the full range of possible hydrogen atom transfer processes. The data of Hardwidge et al[7] on the chemically activated decomposition of fuel radicals generated by the hydrogen atom addition to the appropriate olefin will be analyzed and new rate expressions derived. One of the larger aims of this work is to demonstrate the quantitative compatibility of chemical and thermal activation results. This will bring into the kinetics database the large volume of chemically activated results derived by Rabinovitch and coworkers. The earlier work was used to demonstrate the validity of RRKM theory. Unfortunately, the thermodynamic properties used are now known to be in error. It is expected that the new values of the rate parameters will be equally valid with respect to RRKM theory but also provide insights into the reactions of large fuel radicals.. Experimental results on the decomposition on 2,2 dimethylbutyl-1 radicals will be analyzed and should yield information of primary to primary H-atom transfer. Together with the results on the branched radicals this will substantially complete work on the decomposition of fuel radicals.

Publications 2006-2008

1. Tsang, W, Walker, J. A. and Manion, J. A., Proc. Comb. Institute, 31, 141-148, 207
2. Tsang, W., Awan, I., McGovern, S., Manion, J. A., "Soot Precursors from Real Fuels: The Unimolecular Reactions of Fuel Radicals" in "Combustion Generated Fine Carbon Particles" (A. Sarofim, ed) in press
3. Tsang, W., McGovern, S., Manion, J. A., "Multichannel Decomposition and Isomerization of Octyl Radicals Proc Comb. Institute 32, submitted
4. Tsang, W., "Mechanism and Rate Constants for the Decomposition of 1-Pentenyl Radicals", J. Phys. Chem., A 110 27: 8501-8509 2006
5. McGovern, S., Manion, J. A., and Tsang, W., "Kinetics and Thermal Decomposition of t-butyl-1,3, cyclopentadiene, J. Phys. Chem., A 110(47) 12822-12831, 2006

References

1. Kee, R. J., Coltrin, M. E. and Glarborg, P., "Chemically Reacting Flow" Theory and Practice, Wiley, Interscience, New York, 2003
2. Maas, U. and Pope, S. B., Comb. Flame 88, 2391, 1992
3. Colket M., Edward, C. T., Williams, S., Cernansky, N. P., Miller, D. L., Egolfopoulos, F., Lindstedt, P., Seshadri, K., Dryer F. L., Law, C. K., Friend, D., Lenhart, D. B., Pitsc, H., Sarofim, A, Smooke, M., Tsang, W., "Development of an Experimental Database and Kinetic Models for Surrogate Fuels", 45th AIAA Aerospace Sciences Meeting and Exhibit, Reno, Nevada, January 9, 2007
4. Tsang, W, Walker, J. A. and Manion, J. A., Proc. Comb. Institute, 31, 141-148, 207
5. Tsang, W., Awan, I., McGovern, S., Manion, J. A., "Soot Precursors from Real Fuels: The Unimolecular Reactions of Fuel Radicals" in "Combustion Generated Fine Carbon Particles" (A. Sarofim, ed) in press
6. Tsang, W., McGovern, S., Manion, J. A., "Multichannel Decomposition and Isomerization of Octyl Radicals Proc Comb. Institute 32, submitted
7. Hardwidge, E. A. . Larson, C. W. And Rabinovityh, B. S., J. Amer. Chem. Soc., 92, 3278, 1970

Dynamics on Multiple and Single Electronic Surfaces: Isomerization and Conformerization

Peter M. Weber
Department of Chemistry
Brown University, Providence, Rhode Island 02912
Peter_Weber@brown.edu

1. Program Scope

Structural probes of molecular reaction dynamics with ultrafast time resolution remain at the center of our research progress. Current efforts are directed toward developing time-resolved Rydberg ionization spectroscopy, a method that we found to have many compelling advantages.

In our recent work we have discovered that the binding energies of electrons in Rydberg states are very sensitive toward molecular structures. The structure specificity arises from the phase shift that the Rydberg electron encounters when passing the molecular ion core. The phase shifts are spectrally observed as deviations of the Rydberg electron binding energies from the corresponding energies in hydrogen atoms. This leads to a method to characterize molecular structures by using Rydberg binding energy spectra as fingerprints.

The photoionization from Rydberg states offers several unique attributes. First, the spectra are purely electronic in nature, meaning that the entire Franck-Condon envelope is enclosed in a narrow band. This implies that the spectra are entirely insensitive toward internal energy. The method can therefore be used to explore molecules at high temperatures, or those undergoing chemical dynamics. Secondly, the complexity of the spectra does not scale with the size of the molecule: the number of Rydberg states a molecule has equals the number of hydrogen atom orbitals, as determined by the radial and angular momentum quantum numbers. As a result, the method can be applied to large molecules. Finally, the Rydberg electron encompasses the entire molecule, so that the shape specificity covers the global molecular structure. Consequently, it is possible to distinguish isomeric and even conformeric forms of large molecules.

To implement Rydberg ionization spectroscopy in a time-resolved mode to observe molecular dynamics, we use a pump-probe multi-photon ionization/photoelectron experiment: a first laser pulse excites the molecule to a Rydberg state in a one-photon or multiphoton process, and a time-delayed probe pulse ionizes the molecule. The photoelectron spectrum provides the binding energy of the electron, and thereby reveals the molecule's time-dependent structural fingerprint. The ultimate time resolution of the technique is given by the duration of the laser pulses, while the spectral resolution is limited by the bandwidth of the laser and/or the spectral resolution of the photoelectron spectrometer.

2. Recent Progress

Conformer dynamics of hydrocarbon chains

We have completed our studies of the time-dependent conformational dynamics of aliphatic hydrocarbons decorated with tertiary amine groups. In these molecules, the amine serves as a chromophore that is ionized; the Rydberg state, which is generated in the initial photoexcitation step, spans the entire aliphatic chain. The conformational forms are therefore reflected in the Rydberg photoelectron spectrum. This work is now published in reference 2. In summary, we were able to observe the spectral signatures of the conformeric forms; assign the spectral features to specific conformers; measure equilibrium parameters for the conformers in their ground state; perturb the equilibrium by electronic excitation to the Rydberg state; and completely map the conformational dynamics. Importantly, this work resulted in the first ever time-resolved conformeric dynamic determination of all relevant reaction rates of flexible molecules at very high temperatures.

Ongoing work continues to explore the time-dependent conformer dynamics of hydrocarbons. We have now completed the data acquisition for the conformeric folding of tetramethyl-ethane-diamine (TMEDA).

Figure 1 shows the time resolved Rydberg photoionization spectrum of TMEDA, on a picosecond time scale. Upon excitation to 3p, the molecule rapidly converts to 3s. While a full data analysis is still in progress, we can already conclude that the molecule folds on a time scale of tens of picoseconds. It appears that the attraction between the newly created positive charge and the negative nonbonding electrons on the second amine causes a cyclization of the molecule. The cyclic structure has a smaller structural dispersion, explaining the reduced linewidth of the Rydberg spectrum.

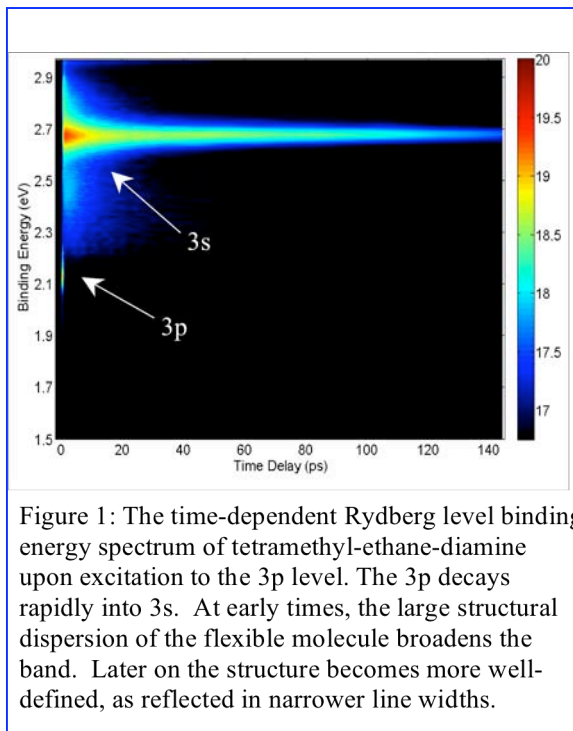


Figure 1: The time-dependent Rydberg level binding energy spectrum of tetramethyl-ethane-diamine upon excitation to the 3p level. The 3p decays rapidly into 3s. At early times, the large structural dispersion of the flexible molecule broadens the band. Later on the structure becomes more well-defined, as reflected in narrower line widths.

Curve crossing dynamics – leading to ground state isomerization?

Cyclic unsaturated hydrocarbons, such as 1,3-cyclohexadiene and 1,3 cyclopentadiene have long been known to undergo ultrafast curve crossing dynamics upon electronic excitation. The molecules quickly cross to a 2A state, which brings them through a conical intersection to the ground state. Following this pathway, from the initial through the intermediate all the way to the ground state, has posed a tremendous experimental challenge because the processes are very fast, and because spectroscopic techniques have not been available to follow the molecule through all these stages. Also unknown was whether the molecules open the ring upon crossing to the ground state, or whether they

remain closed and later on cross thermally. Also unclear is if and how any other isomeric cyclic forms of the molecules are generated as part of the electronic reaction pathway.

We have applied the ionization via Rydberg states, coupled with photoelectron spectroscopy to probe the reaction sequence in 1,3-cyclohexadiene, tetramethyl-1,3-cyclopentadiene, pentamethyl 1,3-cyclopentadiene, 2-(trimethylsiloxy) 1,3-cyclopentadiene, and thiophene. The Rydberg spectra are obtained through 1-photon, 2-photon, and 3-photon

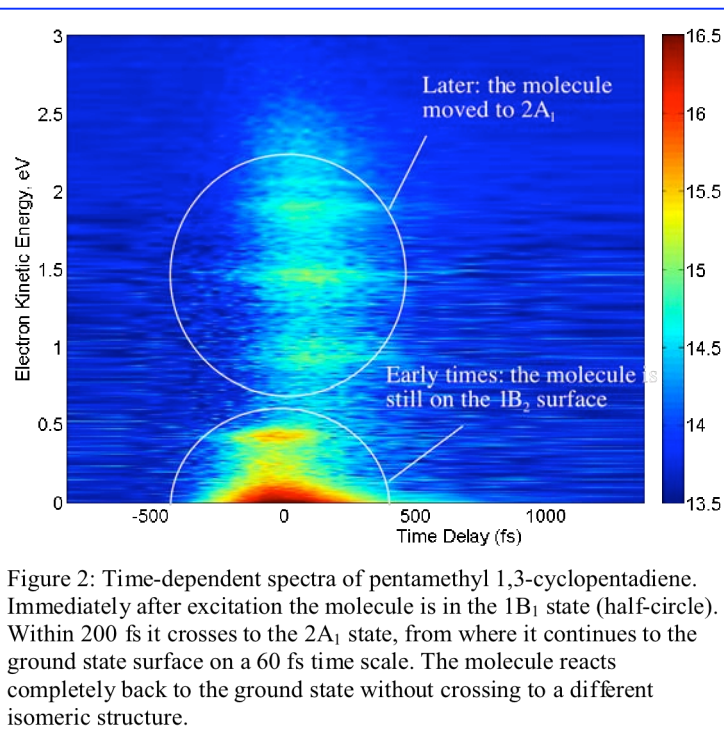
ionization respectively, depending on the electronic state occupied at any particular time. The Rydberg resonances appear as well-defined peaks in the photoelectron spectra and reveal the structural identity and the time scale of any dynamic processes.

Importantly, we observe the spectral signatures after the molecules cross to the ground electronic state. In 1,3-cyclohexadiene we observe a depletion of the original ground state structure: apparently the ring opens up to 1,3 hexatriene, which has no particular structure as its energy is above the threshold to isomerization. In contrast, all derivatives of 1,3-cyclopentadiene react back to their original ground state structure completely, see figure 2. There is no depletion of the original Rydberg peak, and no new peak that would arise from a new structure. We can therefore positively exclude the possibility that the curve crossing dynamics in the pentadiene derivatives leads directly to new molecular structures. Of course, a later, thermal isomerization may be possible.

3. Future Plans

Rydberg states turn out to be exceedingly valuable tools in the exploration of chemical reaction dynamics, as they enable us to solve problems that up to now could not be approached. The spectroscopic method has numerous features that set it apart from others: it works for all molecules, including large molecules; the complexity of the spectra does not scale with the size of the molecule; high internal energies do not materially affect the spectra; and the technique can be done with ultrafast time resolution. In combination these features make the Rydberg method is a superb tool in the study of chemical dynamics.

We will continue our explorations on the reaction dynamics of isomeric systems, including conformers. Ongoing work on the diamines probes the condensation into a



well that presumably belongs to a fairly rigid cyclic structure. Our work also continues on the curve crossing dynamics of conjugated, cyclic hydrocarbons, as they are important components in the formation of soot.

4. Publications resulting from DOE sponsored research (2005 - 2008)

1. “Resolved: Electronic states underneath broad absorptions,” J. D. Cardoza and P. M. Weber, *J. Chem. Phys.* **127**, 036101 (2007).
2. “Ultrafast conformational dynamics in hydrocarbon chains,” Michael P. Minitti and Peter M. Weber, *Phys. Rev. Lett.*, **98**, 253004 (2007).
3. “Spectroscopy and femtosecond dynamics of the ring-opening reaction of 1,3-cyclohexadiene,” N. Kuthirummal, F. M. Rudakov, C. Evans, and P. M. Weber, *J. Chem. Phys.* **125**, 133307 (2006).
4. “Ultrafast time-resolved electron diffraction with megavolt electron beams,” J. B. Hastings, F. M. Rudakov, D. H. Dowell, J. F. Schmerge, J. Cardoza, J.M. Castro, S.M. Gierman, H. Loos, and P. M. Weber, *Appl. Phys. Lett.* **89**, 184109 (2006).
5. “Rydberg Fingerprint Spectroscopy of Hot Molecules: Structural Dispersion in Flexible Hydrocarbons” M.P. Minitti, J.D. Cardoza and P.M. Weber, *J. Phys. Chem. A* **2006**, *110*, 10212-10218.
6. “The Ultrafast Photofragmentation Pathway of N,N-Dimethylisopropylamine,” M.P. Minitti, J.L. Gosselin, T.I. Sølling and P.M. Weber, *FemtoChemistry VII*, Ed. A. W. Castleman Jr & M. L. Kimble, Elsevier (2006) p. 44 - 48.
7. “Megavolt electron beams for ultrafast time-resolved electron diffraction,” F. M. Rudakov, J. B. Hastings, D. H. Dowell, J. F. Schmerge, and P. M. Weber, In “Shock Compression of Condensed Matter – 2005,” ed. M. D. Furnish, M. Elert, T. P. Russel, and C. T. White, American Institute of Physics (2006).
8. “Structure sensitive photoionization via Rydberg levels,” N. Kuthirummal and P. M. Weber, *J. Mol. Structure*, **787**, 163 – 166 (2006).
9. “Energy Flow and Fragmentation Dynamics of N, N, Dimethyl-isopropyl amine,” Jaimie L. Gosselin, Michael P. Minitti, Fedor M. Rudakov, Theis I. Sølling and Peter M. Weber, *Journal of Physical Chemistry A*, **2006**, *110*, 4251-4255.
10. “Ultrafast Electron Microscopy in Materials Science, Biology, and Chemistry,” Wayne E. King, Geoffrey H. Campbell, Alan Frank, Bryan Reed, John Schmerge, Bradley J. Siwick, Brent C. Stuart, and Peter M. Weber, *Journal of Applied Physics*, **97**, 111101 (2005).
11. “Rydberg Fingerprint Spectroscopy: A New Spectroscopic Tool With Local And Global Structural Sensitivity,” J. L. Gosselin and Peter M. Weber, *J. Phys. Chem. A*, **109**, pp 4899 – 4904 (2005).
12. “Control of local ionization and charge transfer in the bifunctional molecule 2-phenylethyl-N,N-dimethylamine using Rydberg fingerprint spectroscopy,” W. Cheng, N. Kuthirummal, J. Gosselin, T. I. Sølling, R. Weinkauf, and P. M. Weber, *Journal of Physical Chemistry*, *109*, pp 1920 – 1925 (2005).

Photoinitiated Processes in Small Hydrides

Curt Wittig
Department of Chemistry
University of Southern California
Los Angeles, CA 90089
213-740-7368
wittig@usc.edu

Program Scope

At long last our heavy atom hydride project is drawing to a close. The past year witnessed very good progress. This followed, and stands in sharp contrast to, the seemingly endless string of difficulties that plagued us the year before. The past year began with promising results for AsH_3 that indicated that this system would finally succumb to our efforts. Indeed, the experimental part of this project is now finished [1]. In addition, we have mastered (to a reasonable extent) a tricky SbH_3 synthesis, and experiments with this molecule will be carried out in the very near future. Because the experimental difficulties were ironed out with AsH_3 , the SbH_3 experiments will be routine except for the synthesis. In parallel, our collaboration with Aleksey Alekseyev (Wuppertal, Germany) on the theoretical front is alive and well. Data are being sent to him with suggestions and guesses about mechanisms. This work proceeds more quickly than the experimental part, and it is extremely valuable.

Two Ph.D. students have been supported on this project. Lee-Ann Smith-Freeman is the senior graduate student. She is working extremely hard and will graduate with a Ph.D. this summer. She is inclined to go into teaching. Jessica Quinn left with an MA about 8 months ago. Bill Schroeder passed the Ph.D. qualifying exam a little less than a year ago. He is an excellent experimentalist, and I had hoped that he would complete his Ph.D. research by carrying out detailed studies of non-adiabatic processes in $\text{C}_2\text{H}(\text{D})$. Both the heavy atom hydride and $\text{C}_2\text{H}(\text{D})$ systems have numerous surface crossings. Non-adiabatic processes have been central to our research program; it is the common ingredient that ties such systems together and provides much of the intellectual content of theses that are forthcoming from this work. Unfortunately my DOE renewal proposal, which was focused on the complex set of non-adiabatic processes that transpire in $\text{C}_2\text{H}(\text{D})$, was declined, despite strongly supportive reviews. So much for the peer review process! If it is not reinstated in the next round, Bill Schroeder will move to a different project.

Recent Progress

In this annual report, I will present some of the AsH_3 data that have been collected during the past year, with qualitative comments about what they reflect insofar as mechanisms are concerned. The experimental method is high- n Rydberg time-of-flight (HRTOF) spectroscopy, which by now is a well-known diagnostic. We have used it for a long time and it is described in our previous reports and publications. Consequently, a description of the HRTOF method is not given here. It goes without saying that non-trivial safety measures have been enlisted in all experiments that involve heavy metal hydrides.

Figure 1 shows a time-of-flight spectrum that was acquired using 193 nm photolysis and 10% AsH_3 in H_2 expanded at 1 atm. Results from 1.2×10^5 laser firings were added. The

vertical red line indicates the arrival time (17.7 μs) that is predicted on the basis of the AsH_2 product formed in its ground rovibronic state and $D_0(\text{H-AsH}_2) = 3.26 \text{ eV}$ [2]. This is the shortest time that can be reconciled by one-photon AsH_3 photolysis. In other words, signals at $t < 17.7 \mu\text{s}$ must arise from secondary photolysis. In separate experiments (not discussed here), secondary photolysis was examined and found to be efficient. By increasing the 193 nm fluence, it was possible to increase the relative size of the $t < 17.7 \mu\text{s}$ contribution to the point where it is as high as the peak at 25 μs . Alternatively, by lowering the fluence it was possible to reduce the $t < 17.7 \mu\text{s}$ contribution such that it is $\sim 1/3$ as large as that shown in Fig. 1. The data shown in Fig. 1 are a compromise: there is enough secondary photolysis present for us to identify it as such, and say something about the origin of the long series of peaks seen at the shorter times.

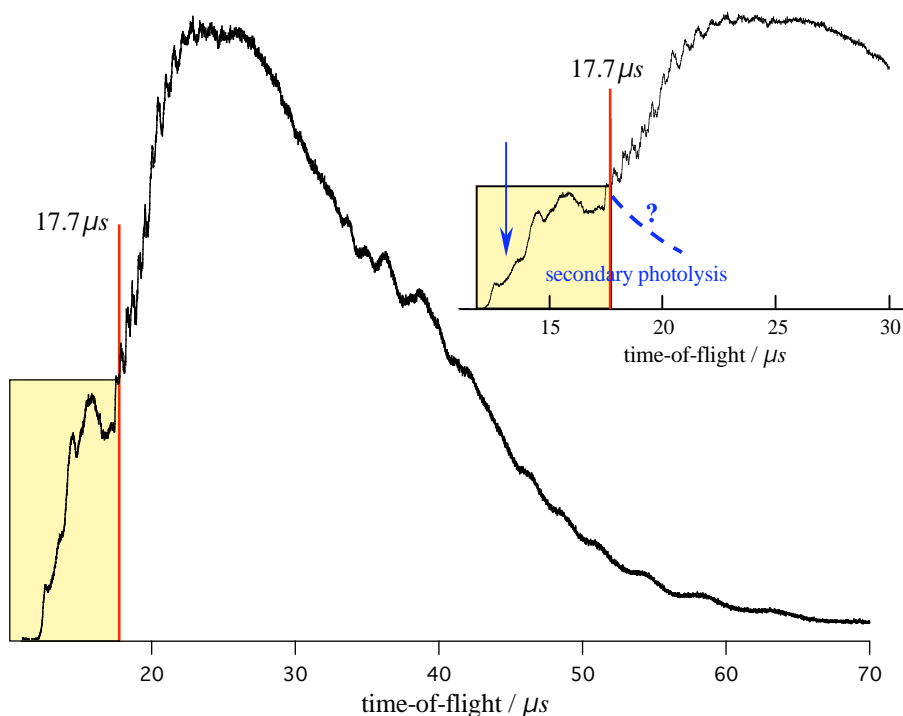


Figure 1. One-photon photodissociation of AsH_3 yields arrival times $> 17.7 \mu\text{s}$. Arrival times shorter than this (signals in the boxes) must be due to secondary photolysis. It is assumed that secondary photolysis also yields products at $t > 17.7 \mu\text{s}$, e.g., giving rise to the peaks atop the broad structure-less feature.

Referring to Fig. 1, note that the signal rises abruptly at 12.5 μs . The c.m. translational energy that corresponds to 12.5 μs is large: 6.3 eV. As mentioned above, the earliest signals are due to AsH_2 photolysis, and the fact that so high a c.m. translational energy is observed indicates that AsH_2 is formed with internal energies extending almost up to its bond dissociation energy. To see how this follows from the data, consider the energy balance for AsH_2 photolysis:

$$h\nu + E_{\text{int}}^{\text{AsH}_2} - D_0(\text{H-AsH}) = E_{\text{cm}} + E_{\text{int}}^{\text{AsH}} \quad (1)$$

Putting the photon energy of $h\nu = 6.42 \text{ eV}$ and $D_0(\text{H-AsH}) = 2.89 \text{ eV}$ [3] into eqn (1) gives:

$$E_{\text{cm}} = 3.53 \text{ eV} + E_{\text{int}}^{\text{AsH}_2} - E_{\text{int}}^{\text{AsH}} \quad (2)$$

The amount of AsH internal excitation is expected to be small. Specifically, vibrational excitation is expected to be modest because As-H bond lengths do not differ significantly for the species and electronic states involved, and AsH₂ *a*-axis rotation correlates more to product translation than to AsH rotation.

The largest value that E_{cm} can achieve via secondary photolysis is when $E_{int}^{AsH} = 0$ and $E_{int}^{AsH_2} = D_0(H-AsH) = 2.89$ eV. In this case, the 6.42 eV photon energy is converted entirely into c.m. translational energy. If $E_{int}^{AsH_2}$ exceeds 2.89 eV by more than just a little, dissociation occurs, and this will be rapid on the timescale of the laser pulse duration. Putting these numbers into eqn (2) yields $E_{cm}^{max} = 6.42$ eV, i.e., the photon energy, as expected. This corresponds to an arrival time of 12.4 μ s, which is very close to the earliest peak seen in Fig. 1. Note that these are very fast hydrogen atoms: they travel **1 Å in slightly less than 3 fs**.

It is not possible at this time to determine quantitatively the extent to which the AsH₂ \tilde{A}^2A_1 state participates in secondary photolysis. Its energy is ~ 2.3 eV above the \tilde{X}^2B_1 ground state [4], and the c.m. translational energy corresponding to an $E_{int}^{AsH_2}$ value that is equal to the $\tilde{A}^2A_1 - \tilde{X}^2B_1$ energy difference is indicated in Fig. 1 with a vertical blue arrow. Consequently, the participation of the \tilde{A}^2A_1 state is expected to be minor.

From the above, it follows that it is AsH₂ *rovibrational* energy that extends almost up to $D_0(H-AsH)$. When an E_{cm} value of 6.3 eV is used in eqn (2), the value of $E_{int}^{AsH_2} - E_{int}^{AsH}$ that is obtained is 2.77 eV, which is only slightly smaller than $D_0(H-AsH) = 2.89$ eV! Indeed, some of the nascent AsH₂ contains energies just below D_0 .

Figure 2 shows the data in Fig. 1 converted to c.m. translational energy. Note the amusing resemblance between Figs. 1 and 2. Of course, long times are low energies and *vice versa*. The data shown in Figs. 1 and 2 reveal a small amount of structure atop a broad featureless distribution. The integrated area of the structured part is much smaller ($< 10^{-2}$) than that of the underlying featureless distribution. Nonetheless, it invites speculation about mechanism, as discussed below. For example, the low energy peaks correspond to highly excited AsH₂, and the spacing between peaks can be reconciled as due mainly to bending and *a*-axis rotation.

Figure 3. The high-energy peaks shown do not include the data in the yellow boxes in Fig. 1. These high-energy features are more easily seen in Fig. 1.

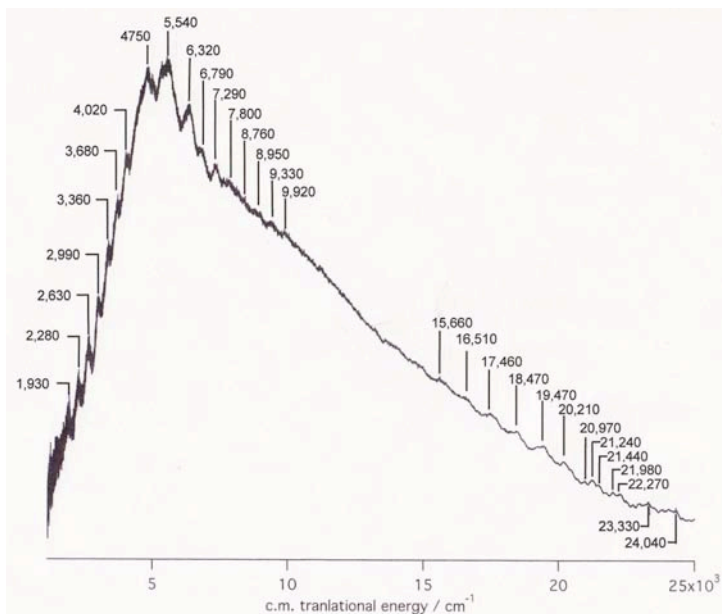
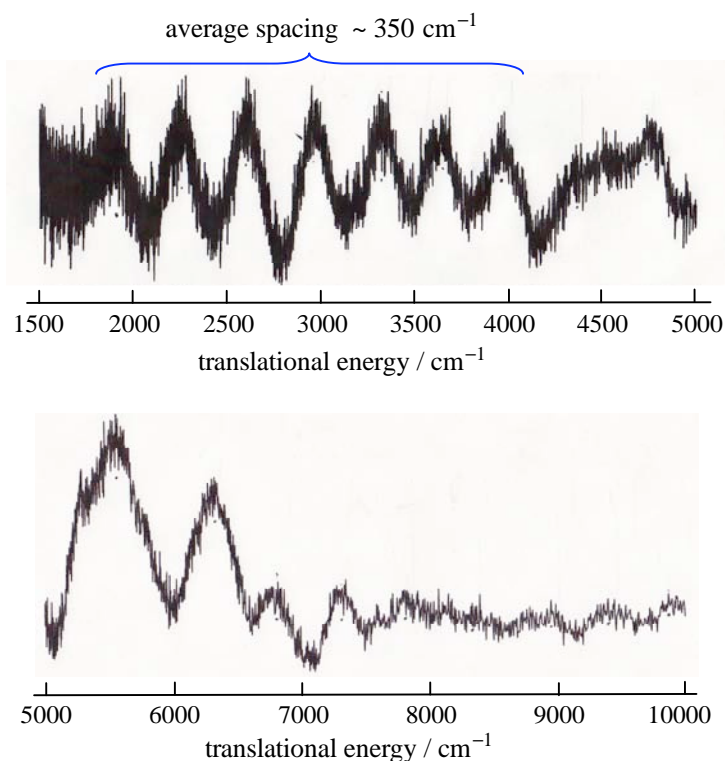


Figure 3 displays the low c.m. translational energy peaks much more clearly than Figs. 1 and 2. By using Fourier-transform filtering, it was possible to remove the broad structure-less feature and leave the relatively sharp peaks, which for all practical purposes are unaffected. These data are of low S/N despite averaging results from 1.2×10^5 laser firings. Resolution is not limited by the apparatus but by the complex molecular dynamics. Despite the crude appearance of the data, a pattern emerges.

Figure 3. These peaks probably arise from the photodissociation of highly excited AsH_2 . The two degrees of freedom that are most likely to play a role are a -axis rotation and the bend.



There can be no doubt that there is a large amount of a -axis rotational excitation, but if this does not change much from one vibrational level to the next, the peak vibrational levels will still resolve. Our tentative explanation of the peaks shown in Fig. 3 is that they reflect a tremendous amount of a -axis rotation.

References

1. We are just now beginning to publish this work. An experimental paper on the AsH_3 system is in preparation. A second paper based on the theoretical modeling will probably take 4-6 months. I assume that at least one additional paper will be written, e.g., on the SbH_3 system, including a grand summary of the photophysics of the Group VI hydrides.
2. J. Berkowitz, *J. Chem. Phys.* **89**, 7065 (1988).
3. D. Dai and K. Balasubramanian, *J. Chem. Phys.* **93**, 1837 (1990).
4. T. Ni, Q. Lu, X. Ma, S. Yu, and F. Kong, *Chem. Phys. Lett.* **126**, 417 (1986).

THEORETICAL STUDIES OF THE REACTIONS AND SPECTROSCOPY OF RADICAL SPECIES RELEVANT
TO COMBUSTION REACTIONS AND DIAGNOSTICS

DAVID R. YARKONY

DEPARTMENT OF CHEMISTRY, JOHNS HOPKINS UNIVERSITY, BALTIMORE, MD 21218
yarkony@jhu.edu

Electron spectroscopies including photoelectron (PE), slow electron velocity-map imaging (SEVI), mass-analyzed threshold ionization (MATI) and photoinduced Rydberg ionization (PIRI) are powerful tools for describing the spectra of combustion intermediates. However, the spectra become difficult to assign when they arise from states that are strongly coupled by conical intersections. The spin-orbit interaction further complicates matters. We are currently working on simulations of the photoelectron spectra of the anion precursors of the ethoxy, isopropoxy, and 1-propynyl radicals. In each case the observed spectrum, that of the neutral radical, is expected or suspected to be affected by nonadiabatic interactions induced by conical intersections. The ethoxy^{1,2} and isopropoxy¹ radicals, whose spectra have been measured, are expected to exhibit nonadiabatic effects due to a low-lying conical intersection seam analogous to that in the well-studied methoxy³ radical. The 1-propynyl radical, whose spectrum has been measured by SEVI and analyzed in Neumark's laboratory,⁴ has not been the subject of a full nonadiabatic analysis.

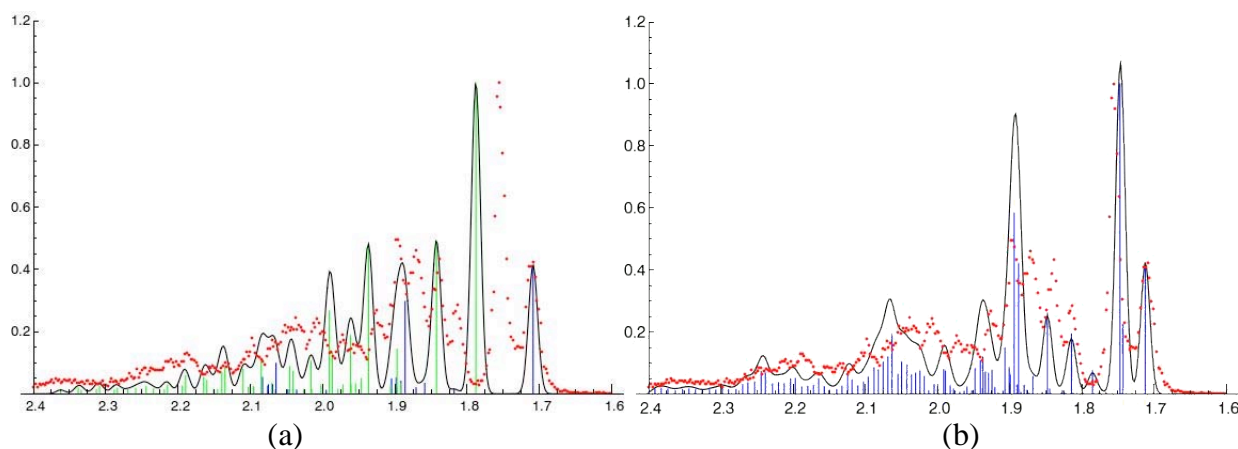
The approach of choice for the calculation of these complex nonadiabatic spectra is the multimode vibronic coupling method.⁵ In order to treat the above molecules we have found it necessary to develop a series of algorithms that greatly extend the range of the multimode vibronic coupling method.⁶⁻¹⁰ (i) We have developed a method for determining $\mathbf{H}^{(d)}$ the requisite diabatic Hamiltonian^{6,8} – the Hamiltonian modeling the electronic structure problem, that includes all second order terms in both the diagonal and all the coupling blocks. Ours is the only method that routinely determines all quadratic terms. $\mathbf{H}^{(d)}$ may be expanded about any point in nuclear coordinate space. Furthermore, this Hamiltonian may be optimized to better reproduce key stationary points on the *ab initio* surfaces without sacrificing an accurate description of the nonadiabatic coupling or the conical intersection seams. (ii) We have incorporated the ability to choose a vibronic basis that is optimized for the description of the observed states.¹⁰ This is to be contrasted with the usual approach that requires the basis to be the normal modes of the precursor (the anion) state. This requisite choice can dramatically increase the size of the vibronic expansion, which is already the limiting aspect of this method. (iii) We have developed an open-ended fine-grained parallel algorithm that can efficiently handle expansions in excess of 1 billion vibronic basis functions, over an order of magnitude larger than previous implementations.⁷

Photoelectron Spectrum of the Ethoxy anion

The ethoxy results obtained to date strongly support the utility of the methodology we have developed. For ethoxy a quasi diabatic Hamiltonian incorporating all 18 internal coordinates was determined using *ab initio* data at only 37 nuclear configurations. The origin was the minimum energy conical intersection.⁶ $\mathbf{H}^{(d)}$ constructed with our new approach, reproduces the *ab initio* electronic structure data quite well.^{6,7} We obtained the spectrum using a comparative compact vibronic basis. Each vibronic basis function consists of a product of N^{int} harmonic oscillator functions (one for each mode). Thus if N_i is the number of harmonic oscillator functions in the i^{th} mode, the vibronic basis, for N^{state} coupled electronic states, consists of $D=N^{\text{state}}N^{\text{vib}}$ basis functions where $N^{\text{vib}} = \prod_{i=1}^{N^{\text{int}}} N_i$. In the standard approach, in which a precursor or anion biased basis is used, $D^H=2N^{\text{vib}}=1.15 \times 10^9$. However with our new approach¹⁰ in which an observed state or neutral biased basis is used $D^H=2N^{\text{vib}}=31.8 \times 10^6$, that is $\sim 1/36$ the size of the anion biased basis.

We have determined a photoelectron detachment spectrum of $\text{C}_2\text{H}_5\text{O}^-$. The figure below compares the adiabatic spectrum, an uncoupled union of the ${}^2\text{A}''$ and ${}^2\text{A}'$ state spectra (scaled so that the first two peaks match the experimental intensities), with the results of the full nonadiabatic simulation, and with Lineberger's¹ experiment, (red) dots.

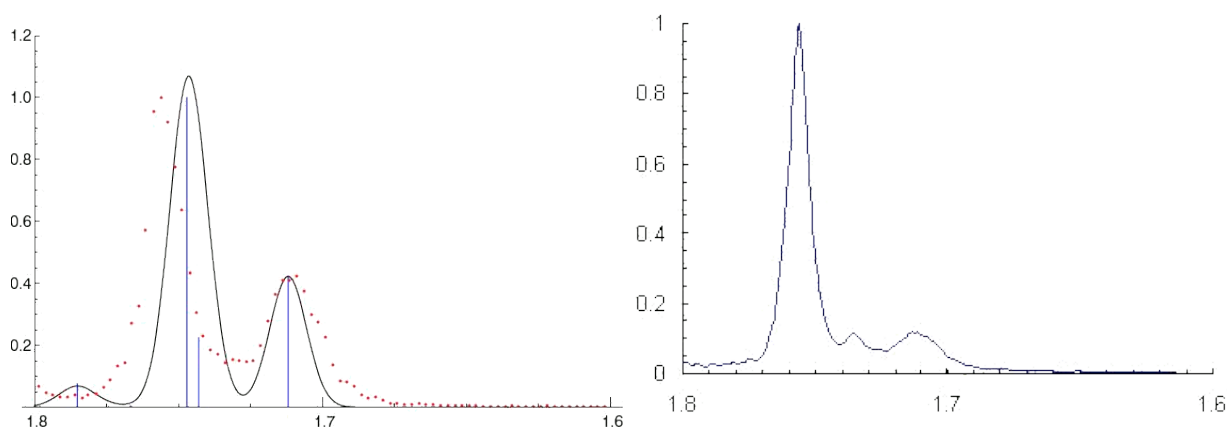
Figure 1; Photoelectron spectrum of the ethoxy anion (a) Adiabatic spectrum from synthesis of ${}^2\text{A}''$ and ${}^2\text{A}'$ adiabatic state results and (b) 2 state nonadiabatic multimode vibronic coupling treatment.



While the agreement between the full 2 state nonadiabatic spectrum (plate (b)) and the experimental result¹ is not perfect, the improvement over the adiabatic simulation (plate (a)) is stunning. The separation of the two principal lines is well reproduced by the coupled state representation but not by the adiabatic result. The positions and intensity ratios of the higher

energy peaks, are reproduced, semi-quantitatively in the coupled state picture but much less so in the adiabatic picture. While agreement with the (low resolution) photoelectron spectrum is good, the unpublished SEVI spectrum of Neumark² raises interesting issues. In particular we note that in the nonadiabatic simulation (but not in the adiabatic spectrum) the brightest line is actually a convolution of two lines, giving a total of three lines in this near threshold region. The SEVI spectrum also finds three lines in this region but the positions differ from our predictions

Figure 2:(left) Blow up of near threshold region of nonadiabatic computed spectrum,(right) near threshold portion of Neumark's SEVI spectrum



We are currently testing the sensitivity of our spectra to the details of the *ab initio* electronic structure treatment.

Photoelectron Spectrum of the Isopropoxy anion

We are currently generating the entire quadratic quasi diabatic $\mathbf{H}^{(d)}$ for the full 27 internal coordinates (over 1200 parameters if spatial symmetry is ignored) using data at 55 nuclear configurations. A flexible aug-cc-TZP basis on the carbons and oxygen and a cc-DZP basis on the hydrogens is being used.

Photoelectron Spectrum of the 1-Propynyl anion

For 1-propynyl we are concerned about the affect nonadiabatic interactions between the ground 2A_1 state and excited 2E state have on the spectral intensity of the 2E state in the 1-propynyl anion photoelectron spectrum. We have obtained a 3-state (2A_1 , 2E) quasi diabatic Hamiltonian, $\mathbf{H}^{(d)}$ including all second order terms involving the 12 internal coordinates. This treatment used an aug-cc-TZP basis on the carbons and a cc-DZP basis on the hydrogens. Multireference configuration interaction wave functions comprised of 186 million configuration state functions were used at only 13 nuclear configurations to obtain $\mathbf{H}^{(d)}$. This $\mathbf{H}^{(d)}$ is currently being reshaped to optimize agreement with the *ab initio* data. Interestingly, *ab initio* calculations (and the $\mathbf{H}^{(d)}$) exhibit an accidental same symmetry conical intersection of the $1,2{}^2A'$ states for C_s

symmetry nuclear configurations, near the Jahn-Teller (C_s symmetry) minimum of the 2E state. These intersecting states correlate with the 2A_1 and 2E_x states as C_{3v} symmetry is restored. This conical intersection seam could contribute to a reduction of the spectral intensity of the 2E state. To assess the diminution of the E state intensity due to nonadiabatic effects we will compare the spectrum obtained from an “adiabatic” treatment in which the two components of the 2E state are uncoupled from the 2A_1 state, with that obtained from the full three state nonadiabatic simulation.

References

- ¹ T. M. Ramond, G. E. Davico, R. L. Schwartz, and W. C. Lineberger, *J. Chem. Phys.* **112**, 1158 (2000).
- ² D. Neumark, private communication.
- ³ S. C. Foster, P. Misra, T.-Y. D. Lin, C. P. Damo, C. C. Carter, and T. A. Miller, *J. Phys. Chem.* **92**, 5914 (1988); A. V. Marenich and J. E. Boggs, *J. Chem. Phys.* **122**, 024308 (2005).
- ⁴ J. Zhou, E. Garand, W. Eisfeld, and D. M. Neumark, *J. Chem. Phys.* **127**, 034304(7 pages) (2007).
- ⁵ H. Köppel, W. Domcke, and L. S. Cederbaum, in *Conical Intersections*, edited by W. Domcke, D. R. Yarkony, and H. Köppel (World Scientific, New Jersey, 2004), Vol. 15, pp. 323.
- ⁶ R. A. Young Jr and D. R. Yarkony, *J. Chem. Phys.* **125**, 234301(14) (2006).
- ⁷ M. S. Schuurman, R. A. Young, and D. R. Yarkony, *Chem. Phys.*, available on line (2007).
- ⁸ M. S. Schuurman and D. R. Yarkony, *J. Chem. Phys.* **127**, 094104(9 pages) (2007).
- ⁹ M. S. Schuurman, D. E. Weinberg, and D. R. Yarkony, *J. Chem. Phys.* **127**, 104309(12 pages) (2007).
- ¹⁰ M. S. Schuurman and D. R. Yarkony, *J. Chem. Phys.* **128**, 044119(9) (2008).

PUBLICATIONS SUPPORTED BY DE-FG02-91ER14189: 2005-present

1. *Statistical and Nonstatistical Nonadiabatic Photodissociation from the first excited state of the hydroxymethyl radical*
David R. Yarkony, *J. Chem. Phys.* **112**, 084316 (2005)
2. *A Novel Conical Intersection Topography and its Consequences. The 1, 2²A Conical Intersection Seam of the Vinyloxy Radical*
R. Andrew Young, Jr. and David R. Yarkony, *J. Chem. Phys.* **123**, 084315(2005).
3. *Towards a Highly Efficient Theoretical Treatment of Jahn-Teller Effects in Molecular Spectra: The 1²A, 2²A Electronic States of the Ethoxy Radical*
R. Andrew Young, Jr. and David R. Yarkony, *J. Chem. Phys.* **125**, 234301 (2006).
4. *On the simulation of photoelectron spectra in molecules with conical intersections and spin-orbit coupling: The vibronic spectrum of CH₃S.*
Michael S. Schuurman, Daniel E. Weinberg and David R. Yarkony, *J. Chem. Phys.* **127**, 104309,(12 pages)(2007)

Experimental Characterization of the Potential Energy Surfaces for Conformational and Structural Isomerization in Aromatic Fuels

Timothy S. Zwier

Department of Chemistry, Purdue University, West Lafayette, IN 47907-2084
zwier@purdue.edu

Program Definition and Scope

Gasoline and diesel fuels are complicated mixtures containing about 30% aromatics, including alkylbenzene, alkenylbenzene, and alkynylbenzenes of various chain lengths. The combustion of these molecules is influenced by their structural and conformational make-up, and by the rates of isomerization between them. The objective of this research program is to develop and utilize laser-based methods to characterize the spectroscopy and isomerization dynamics of conformational isomers of aromatic derivatives that play a role in soot formation. As a first step in all these studies, UV-UV hole-burning and resonant ion-dip infrared (RIDIR) spectroscopy are being used to determine the number and identity of the conformations present, based on their ultraviolet and infrared spectral signatures. These structural studies then serve as a foundation for studies of the dynamics of conformational isomerization using stimulated emission pumping-population transfer (SEP-PT) spectroscopy or infrared population transfer (IR-PT) spectroscopy (Figure 1). SEP is used to selectively excite a single conformation of the molecule of interest to a well-defined vibrational energy early in the supersonic expansion. If the excited molecules have sufficient energy, they can isomerize before being re-cooled in the expansion to allow isomer-specific detection via laser-induced fluorescence. By tuning the SEP dump laser in a 20-10-20 Hz laser configuration, it is possible to directly measure the energy thresholds separating individual A→B reactant-product isomer pairs, thereby mapping out key stationary points on the multi-dimensional potential energy surface for isomerization. We are using these methods to study conformational isomerization in substituted benzenes spanning a range of types and degrees of conformational flexibility. From near-threshold intensity measurements we hope to explore the rate of isomerization relative to collisional cooling as a function of energy above threshold. These results can provide new tests of RRKM descriptions of isomerization in large molecules.

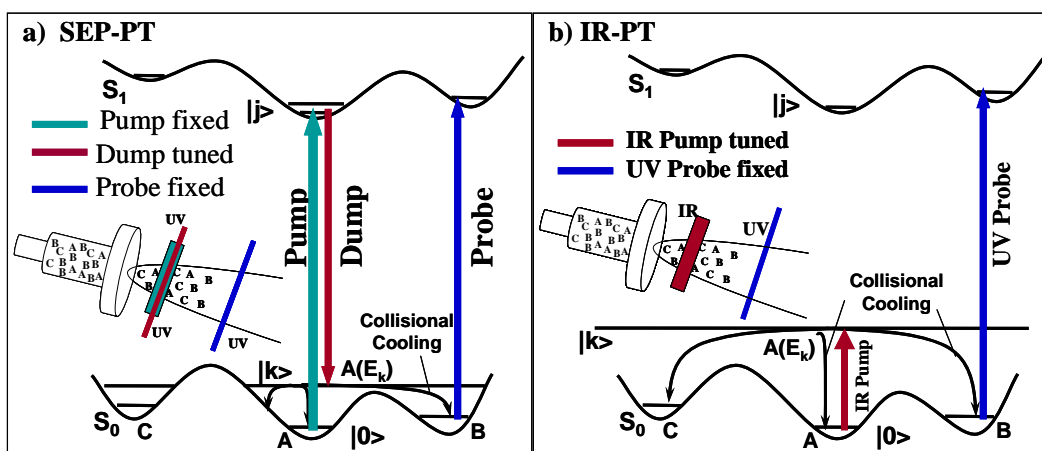


Figure 1: Schematic diagrams for SEP-PT and IR-PT spectroscopy.

Recent Progress

Over the past year, we have expanded our studies of the spectroscopy and the conformational isomerization dynamics of a series of aromatic derivatives of increasing conformational and structural complexity. Many of these studies have employed our new fluorescence-based chamber, which is pumped by a roots blower and thus is capable of the high gas throughput needed for hole-filling studies of conformational isomerization dynamics.

A. Spectroscopy and Dynamics of *o*-, *m*-, and *p*-divinylbenzene

We have now completed and published studies of the spectroscopy and isomerization dynamics of the three structural isomers of divinylbenzene (*ortho*-, *meta*-, and *para*-). Building on previous work from the Pratt group (T. V. Nguyen, J. W. Ribblett, D. W. Pratt, *Chem. Phys.* **283**, 279-287 (2002)) we have identified and assigned spectra due to all three conformational isomers of *meta*-DVB (*cis-cis*, *cis-trans*, and *trans-trans*) and both isomers of *para*-DVB. Stimulated emission pumping-population transfer (SEP-PT) spectroscopy has been employed to study the pathways, energy thresholds, and isomerization dynamics in *meta*-DVB, which occurs on a prototypical two-dimensional torsional surface. These studies established that the isomerization pathway between *cis-cis* and *trans-trans* traverses through the *cis-trans* and *trans-cis* wells rather than occurring in a concerted fashion.

B. Internal State mixing in Diphenylmethane

After intensive effort, we are finally gaining a more firm understanding of the vibronic spectroscopy of diphenylmethane ($C_6H_5-CH_2-C_6H_5$, DPM), a prototypical flexible bichromophore with fascinating vibronic coupling resulting from the close proximity of its first two excited electronic states, which are separated from one another by only 123 cm^{-1} . The ground state and S_1 state are firmly established as C_2 symmetry based on the rotational constants and transition dipole moment direction for the S_0-S_1 transition extracted from the high resolution ultraviolet spectrum, recorded in collaboration with David Plusquellic of NIST. Assignments for the symmetric and antisymmetric torsional vibrations in S_0 , S_1 , and S_2 states have been made. Dispersed fluorescence from the S_2 origin reveals a mixed S_2/S_1 character to its wave function, with components to the emission clearly assignable to each. The $S_1(v)$ emission has imprinted upon it the vibrational character of the S_1 levels that are mixed with the S_2 zero-point level, providing what we believe to be the first state-selected view of internal conversion, a process of considerable importance in photophysics. The S_1 vibrational levels which are mixed with the S_2 0^0 level have an odd number of quanta of the antisymmetric torsion (b symmetry), as required for coupling to the S_2 origin (A). Four S_1 vibrational levels are tentatively assigned as contributing to the mixed character. These levels are those closest in energy to the S_2 origin (within $\sim 10\text{ cm}^{-1}$) with the correct symmetry to couple to S_2 . As such, they break the conventional rules of vibronic coupling by having large quantum number changes of $\Delta v > 1$ in the coupling mode. We are presently preparing two manuscripts based on this work.

We are presently in the midst of a study of the vibronic spectroscopy and high resolution UV spectroscopy of DPM- d_5 . This is once again a collaborative effort, this time with both John Cable (BGSU) and David Plusquellic (NIST). By deuterating one of the phenyl rings, we partially localize the electronic excitation in S_1 and S_2 . This changes both the vibronic intensities and rotational structure of the bands. The dispersed emission from the $S_2(v)$ levels again show mixed excited state character, which we hope to analyze in some detail.

C. Isomerization and vibrational cooling in bis-(2-hydroxyphenyl)methane

We have completed our experimental work on the spectroscopy and conformational isomerization of bis-(2-hydroxyphenyl)methane. This analog of DPM has four flexible coordinates, two phenyl torsions and the two OH torsions. Two conformational isomers are observed, one that possesses an OH \cdots OH H-bond between the two rings, and the other two OH \cdots π H-bonds in which the OH group on one ring H-bonds to the π cloud on the other ring. High resolution UV spectra and dispersed fluorescence spectra have also been recorded in order to better understand the effects of large-amplitude torsional motion on the transition moment and vibronic intensities.

SEP-PT spectroscopy has also been used to measure the barriers to isomerization between these two isomers in both directions ($E_{\text{thresh}} \sim 1400 \text{ cm}^{-1}$), thereby determining the relative energies of the two minima. The π -bound conformer is slightly lower in energy than the OH \cdots O conformer ($\Delta E = 14-123 \text{ cm}^{-1}$). The long Franck-Condon progressions present in the OH \cdots O conformer have been used to measure the per-collision efficiencies for vibrational cooling as a function of internal energy in the range from 30-1200 cm^{-1} .

D. Isomerization in 5-phenyl-1-pentene

In preparation for a study of its conformational isomerization dynamics, we have completed and are preparing a manuscript describing a systematic study of the ultraviolet spectroscopy of 5-phenyl-1-pentene (5PPE), including assignment of its 5 conformational isomers based on rotational band contour and vibronic analysis.

We are currently carrying out a comprehensive SEP-PT study of conformational isomerization in 5PPE. When completed, we will have directly measured the energy thresholds for all but a few of the 30 X \rightarrow Y conformer pairs, providing barrier heights and relative energies of the minima, providing an unprecedented level of characterization of a potential energy surface of this complexity. For the most part, the potential energy surface appears to be well described by three seemingly independent barrier heights associated with hindered rotation about the three flexible C-C bonds in the chain.

E. Intersystem crossing in cyclopentenone

Finally, in collaboration with Steve Drucker (UW-Eau Claire) and Richard Judge (UW-Parkside), we have completed and published our study of the jet-cooled phosphorescence excitation spectrum of the spin-forbidden $S_0 \rightarrow T_1$ transition of cyclopentenone, including a rotationally-resolved spectrum of the S_0 - T_1 origin transition. This triplet excited state is known to be responsible for much of the photochemistry of the molecule. We observe a steep decrease in the triplet lifetime with increasing energy above the T_1 origin.

Publications acknowledging DOE support, 2006-present

1. Timothy S. Zwier, "Laser probes of Conformational Isomerization in Flexible Molecules and Complexes", *J. Phys. Chem. A* **110**(12) 4133-4150 (2006). Feature article.
2. Talitha M. Selby, W. Leo Meerts, and Timothy S. Zwier, "Isomer-specific Ultraviolet Spectroscopy of *meta*- and *para*-divinylbenzene", *J. Phys. Chem. A* **111**, 3697-3709 (2007).
3. Talitha M. Selby and Timothy S. Zwier, "Flexing the muscles of Divinylbenzene: Direct measurement of the barriers to conformational isomerization", *J. Phys. Chem. A* **111**, 3710-3718 (2007).
4. Nathan R. Pillsbury, Timothy S. Zwier, Richard H. Judge, Stephen Drucker, "Jet-cooled phosphorescence excitation spectrum of the $T_1(n,\pi^*) \leftarrow S_0$ transition of 2-cyclopenten-1-one", *J. Phys. Chem. A* **111**, 8357-8366 (2007).

Participant List

29th Annual Combustion Research Conference Participant List

Lastname	Firstname	Organization	Email
Allen	Wesley	University of Georgia	wdallen@uga.edu
Baer	Tomas	University of North Carolina	baer@unc.edu
Barlow	Robert	Sandia National Laboratories	barlow@sandia.gov
Bowman	Joel	Emory University	jmbowma@emory.edu
Braams	Bastiaan	Emory University	bbraams@emory.edu
Brown	Nancy	Lawrence Berkeley National Laboratory	NJBrown@lbl.gov
Butler	Laurie	The University of Chicago	L-Butler@uchicago.edu
Casassa	Michael	U.S. Department of Energy	michael.casassa@science.doe.gov
Chandler	David	Sandia National Laboratories	chand@sandia.gov
Chaos	Marcos	Princeton University	mchaos@princeton.edu
Chen	Jacqueline	Sandia National Laboratories	jhchen@sandia.gov
Continetti	Robert	University of California, San Diego	rcontinetti@ucsd.edu
Cool	Terrill	Cornell University	tac13@cornell.edu
Davis	Floyd	Cornell University	hfd1@cornell.edu
Davis	Michael	Argonne National Laboratory	davis@tcg.anl.gov
Dryer	Frederick	Princeton University	fdryer@princeton.edu
Ervin	Kent	University of Nevada, Reno	ervin@unr.edu
Field	Robert	Massachusetts Institute of Technology	rwfield@mit.edu
Flynn	George	Columbia University	gwf1@columbia.edu
Frank	Jonathan	Sandia National Laboratories	jhfrank@sandia.gov
Frenklach	Michael	University of California, Berkeley	myf@me.berkeley.edu
Gray	Stephen	Argonne National Laboratory	gray@tcg.anl.gov
Green, Jr.	William	Massachusetts Institute of Technology	whgreen@mit.edu
Guo	Hua	University of New Mexico	hguo@unm.edu

29th Annual Combustion Research Conference Participant List

Hall	Gregory	Brookhaven National Lab	gehall@bnl.gov
Hansen	Nils	Sandia National Laboratories	nhansen@sandia.gov
Hanson	Ronald	Stanford University	rkhanson@stanford.edu
Harding	Lawrence	Argonne National Laboratory	harding@anl.gov
Head-Gordon	Martin	Lawrence Berkeley National Laboratory	mhg@cchem.berkeley.edu
Heaven	Michael	Emory University	mheaven@emory.edu
Hershberger	John	North Dakota State University	john.hershberger@ndsu.edu
Jasper	Ahren	Sandia National Laboratories	ajasper@sandia.gov
Johnson	Philip	Stony Brook University	philip.johnson@sunysb.edu
Kaiser	Ralf	University of Hawaii	ralfk@hawaii.edu
Kellman	Michael	University of Oregon	kellman@uoregon.edu
Kerstein	Alan	Sandia National Laboratories	arkerst@sandia.gov
Kiefer	John	University of Illinois, Chicago	kiefer@uic.edu
Klippenstein	Stephen	Argonne National Laboratory	sjk@anl.gov
Krylov	Anna	University of Southern California	krylov@usc.edu
Laufer	Allan	National Institute of Standards and Technology	allan.laufer@nist.gov
Leone	Stephen	Lawrence Berkeley National Laboratory and University of California	srl@berkeley.edu
Lester	Marsha	University of Pennsylvania	milester@sas.upenn.edu
Lester, Jr.	William	Lawrence Berkeley National Laboratory	walester@lbl.gov
Linne	Mark	Sandia National Laboratories	mlinne@sandia.gov
Long	Marshall	Yale University	marshall.long@yale.edu
Lucht	Robert	Purdue University	lucht@purdue.edu
Macdonald	Robert	Argonne National Laboratory	rgmacdonald@anl.gov
Manley	Dawn	Sandia National Laboratories	dmanley@sandia.gov
Marceau	Diane	U.S. Department of Energy	diane.marceau@science.doe.gov

29th Annual Combustion Research Conference Participant List

Marzouk	Youssef	Sandia National Laboratories	ymarzou@sandia.gov
McIlroy	Andrew	Sandia National Laboratories	amcrlr@sandia.gov
Mebel	Alexander	Florida International University	mebela@fiu.edu
Michael	Joe	Argonne National Laboratory	jmichael@anl.gov
Michelsen	Hope	Sandia National Laboratories	hamiche@sandia.gov
Miller	Terry	Ohio State University	tamiller@chemistry.ohio-stte.edu
Miller	James	Sandia National Laboratories	jamille@sandia.gov
Ming	Lin	Emory University	chemmcl@emory.edu
Muckerman	James	Brookhaven National Laboratory	muckerma@bnl.gov
Mullin	Amy	University of Maryland	mullin@umd.edu
Najm	Habib	Sandia National Laboratories	hnnajm@sandia.gov
Nesbitt	David	University of Colorado	djn@jila.colorado.edu
Neumark	Daniel	Lawrence Berkeley Laboratory	dneumark@berkeley.edu
Ng	Cheuk-Yiu	University of California, Davis	cyng@chem.ucdavis.edu
Oefelein	Joseph	Sandia National Laboratories	oefelei@sandia.gov
Osborn	David	Sandia National Laboratories	dlosbor@sandia.gov
Perry	David	The University of Akron	dperry@uakron.edu
Pitz	William	Lawrence Livermore National Laboratory	pitz1@llnl.gov
Polansky	Walter	U.S. Department of Energy	amy.clark@science.doe.gov
Pope	Stephen	Cornell University	s.b.pope@cornell.edu
Pratt	Stephen	Argonne National Laboratory	stpratt@anl.gov
Rahn	Larry	U.S. Department of Energy	Larry.Rahn@science.doe.gov
Reisler	Hanna	University of Southern California	reisler@usc.edu
Ruscic	Branko	Argonne National Laboratory	ruscic@anl.gov
Schaefer	Henry	University of Georgia	hfs@uga.edu
Sears	Trevor	Brookhaven National Laboratory	sears@bnl.gov

29th Annual Combustion Research Conference Participant List

Settersten	Thomas	Sandia National Laboratories	tbsette@sandia.gov
Shepard	Ron	Argonne National Laboratory	shepard@tcg.anl.gov
Singer	Marvin	U.S. Department of Energy	marvin.singer@science.doe.gov
Sisk	Wade	U.S. Department of Energy	wade.sisk@science@doe.gov
Smooke	Mitchell	Yale University	mitchell.smooke@yale.edu
Stanton	John	University of Texas	jfstanton@mail.utexas.edu
Suits	Arthur	Wayne State University	asuits@chem.wayne.edu
Taatjes	Craig	Sandia National Laboratories	cataatj@sandia.gov
Thompson	Donald	University of Missouri-Columbia	thompsondon@missouri.edu
Tishkoff	Julian	Air Force Office of Scientific Research	julian.tishkoff@afosr.af.mil
Tranter	Robert	Argonne National Laboratory	tranter@anl.gov
Truhlar	Donald	University of Minnesota	truhlar@umn.edu
Tsang	Wing	National Institute of Standards and Technology	wing.tsang@nist.gov
Wagner	Albert	Argonne National Laboratory	wagner@anl.gov
Weber	Peter	Brown University	Peter_Weber@brown.edu
Westmoreland	Phillip	National Science Foundation	pwestmor@nsf.gov
Wilson	Kevin	Lawrence Berkeley National Laboratory	krwilson@lbl.gov
Wittig	Curt	University of Southern California	wittig@usc.edu
Yarkony	David	Johns Hopkins University	yarkony@jhu.edu
Yu	Hua-Gen	Brookhaven National Laboratory	hgy@bnl.gov
Zare	Richard	Stanford University	zare@stanford.edu
Zwier	Timothy	Purdue University	zwier@purdue.edu